PETROLOGY, DIAGENESIS AND RESERVOIR POTENTIAL OF NARRABEEN GROUP SANDSTONES, SYDNEY BASIN, N. S. W.

GUO PING BAI

A thesis submitted in fulfilment
of the requirement for the degree of
Doctor of Philosophy

Department of Geology and Geophysics University of Sydney

June, 1991

STATEMENT

All results and interpretation reported in this thesis are the original work of the author except where otherwise acknowledged. This work has not been submitted previously to this or any other University.

GUO PING BAI

ACKNOWLEDGEMENT

This project was supervised by Dr Jock Keene. I would like to express my deep gratitude for his help and encouragement throughout my candidature and for the many hours he devoted to discussion and review of my work.

I would like to especially thank Dr Joe Hamilton for his supervision since July, 1989 and the time he devoted to discussion and review of my work.

I would like to thank Dr Peter Eadington for his guidance with the fluid inclusion investigation. I also thank Mr Gabor Foldvary for his assistance with the development of photographs, Mr Tony Romeo for his assistance with the SEM / EDX, Mr Hugh Simmons for his assistance with the microprobe, Mr Andrew Bryce for his assistance with the mass spectrometer, Dr Ian Threadgold for his assistance and guidance with the X-ray diffractometer.

I am grateful to the staff at the Londondary Core Library of the New South Wales Department of Mineral Resources for their assistance with the geological logging and sampling of bore cores.

I am grateful to Associate Professor Don Emerson for allowing me to use the facilities of the Department of Geology and Geophysics.

I would like to thank Chinese Ministry of Education for my living allowance for four years. I also thank AGL for its research grant which made it possible for me to undertake the isotope and fluid inclusion investigation.

Finally, I would like to thank my wife, Yu Ping, for her support and encouragement throughout my candidature and for drafting some of the diagrams and compiling the thesis.

ABSTRACT

The reservoir potential of sandstones in the Narrabeen Group (excluding Garie and Newport Formations), which ranges in age from Late Permian to Early Triassic, in the Sydney Basin varies considerably, depending on a combination of depositional and diagenetic factors. The determination of the factors affecting reservoir quality is important in predicting the distribution of high quality reservoirs.

The aims of this study are to carry out facies analyses; to document petrological characteristics of the sandstones and deduce the sandstone provenance; to identify authigenic minerals and establish their paragenetic sequence; to analyse stable isotopes of diagenetic minerals and determine K-Ar ages of authigenic illite; to measure homogenisation and ice melting point temperatures of aqueous fluid inclusions in quartz overgrowths; to reconstruct chemical evolution of pore fluids with time and temperature; and to discuss the factors affecting reservoir quality and assess the distribution of high quality reservoirs.

A total of 7648.5 meters of cores from 26 boreholes, which cover an area of about 80 km x 240 km, were geologically logged. Of the boreholes penetrating the whole Narrabeen Group, a maximum thickness of 716 m of the group (excluding Garie and Newport Formations) was recorded with an average thickness of about 433 m. Based on the logging, 417 sandstone samples were collected for various laboratory studies. Of them, 324 were selected for quantitative evaluation of composition and visible porosity under a petrological microscope, 167 for SEM/EDX examinations, 63 for XRD studies, 20 for microprobe analyses, 9 for isotope measurements, 4 for fluid inclusion investigations, and 175 for porosity and permeability measurements.

Using gamma ray and neutron logs, the Narrabeen Group (excluding Garie and Newport Formations) is subdivided into five operational units. From bottom to top,

they are Wombarra (WO), Scarborough (SC), Lower Bulgo (LB), Upper Bulgo (UB), and Bald Hill (BH) Operational Units (Galloway and Hamilton, 1988). They are regarded as time stratigraphic units. The thickness of these units range from 11 to 193 m for the WO unit, from 20 to 181 m for the SC unit, from 10 to 149 m for the LB unit, from 16 to 185 m for the UB unit and from 12 to 76 m for the BH unit. The group was deposited in fluvial / lacustrine depositional systems. Channel fill, inter-channel floodplain / lacustrine and channel margin are the principal facies recognised with the channel margin facies being of minor volumetric importance. Medium to very coarse sandstones and conglomerates are the principal lithological components of the channel fill facies with sandstone being of much more quantitative importance. The floodplain / lacustrine facies consists largely of shales / mudstones and very fine sandstones. The channel margin facies is represented lithologically by silty shale, very fine and fine sandstones.

The sandstones in the Narrabeen Group consist largely of detrital quartz grains with a range of 5-80 % of the total sandstone and lithics (including chert) with a range of 0-75 %, which vary inversely with each other. Detrital feldspar is a minor component (0-15 %). Detrital clasts are consolidated by clays (both detrital and diagenetic) (0-32 %) and carbonate cements (0-49 %), which are inversely related to each other. Quartz cement is less important as it accounts for less than 2 % of the total sandstone in the majority of sandstones studied. Visual primary porosity varies from 1 to 17 % and secondary porosity from 0 to 11 %.

The percentage of detrital quartz generally increases upwards from 20-40 % of the total detrital clasts at the basal part of the group to 80-95 % in the BH unit and that of detrital lithics decreases from 60-85 % to 20-40 %, particularly in the boreholes in the southern Sydney Basin. However, these changes do not proceed at a uniform rate. Depending upon the borehole location, one to three distinctive boundaries, across which the detrital composition has a sudden and significant change, and / or one abnormally lithic-rich interval can be recognised in different

boreholes. The lowermost boundary is defined as DB3, the middle one as DB2, and the uppermost one as DB1 with DB2 being the most obvious. Across DB2 upwards, a sudden 20-35 % increase of detrital quartz clasts and a sudden 20-35 % decrease of detrital lithics occur.

Regionally, the average percentage of detrital quartz clasts in the sandstones of a given stratigraphic horizon decreases and that of detrital lithics increases eastwards and less obviously northwards. The variations in detrital compositions of sandstones were used for deduction of detrital sources and source changes.

During deposition of the Narrabeen Group, there existed three sources: the Lachlan Fold Belt supplying detrital quartz clasts, the New England Fold Belt supplying detrital lithics as well as detrital quartz clasts, and an eastern volcanic source lying east of present day coast line offshore from Cape Banks 1 borehole (Borehole J). The first two were more important quantitatively than the latter. The existence of the third source (the eastern volcanic source) was recognised by the abundance of volcanic lithics in sandstones from the boreholes in the southern east coast zone and petrological evidence. The lithics from this source seem to be intermediate volcanic clasts, which are different from the acidic volcanic rock fragments from the New England Fold Belt. The eastern volcanic source supplied detritus to the basin from middle WO time and seemed to be very active only during two periods: early SC time and early and middle UB time. The presence of the abnormally lithic-rich interval correlating with the lower part of the SC unit is directly related to this volcanic source.

The New England Fold Belt was the major source during early WO time. As sedimentation proceeded, its influence gradually decreased. The Lachlan Fold Belt played a more and more important role in supplying detritus to the basin and finally replaced the New England Fold Belt as the major source. However, this replacement did not take place uniformly throughout the whole basin. It happened

in the early period of WO time in the west margin, in the middle period of WO time in the western portion of the southern region, at the end of WO time in the central part of basin, and in the late period of SC time in the southwestern portion of the northern region. In the northeastern portion of the northern region, the source change did not take place until the end of UB time.

There are three principal types of diagenetic minerals in the Narrabeen Group sandstones: carbonates, clay minerals, and quartz. Carbonates consist of calcite, dolomite, ankerite, and siderite with siderite being the most common. Clay minerals include kaolin (kaolinite and dickite), illite, mixed-layer illite / smectite, and chlorite with kaolin being the most common. Micro-quartz, mega-quartz and quartz overgrowths comprise quartz cements with quartz overgrowths being the most common and abundant. In addition, authigenic albite was commonly found in the sandstones containing detrital plagioclase. A minor amount of haematite, pyrite, apatite, anatase, analcime, and dawsonite were also found.

Based on petrological observations, a paragenetic sequence of these diagenetic minerals was established. Diagenesis of the Narrabeen Group sandstones began with the formation of rare grain coating haematite and early clays including kaolin, grain coating mixed-layer illite / smectite and chlorite. Following the formation of these early clays, major carbonate cementation took place. Among the diagenetic carbonates, calcite coating detrital grains was the first to crystallise and was succeeded by siderite coating detrital grains, pore filling calcite, pore filling siderite, and pore filing ferroan calcite and pore filling ankerite. After the major carbonate cementation, kaolin, quartz overgrowth and filamentous pore-bridging illite crystallised. The last cements to form were minor amounts of calcite and ankerite.

The formation of early authigenic clay minerals was mainly controlled by physico-chemical conditions of pore waters. The early mixed-layer illite / smectite coating detrital grains and early kaolin (generation I) were precipitated in sands with

oxygenated and mildly acidic pore waters whereas the chlorite crystallised in sands with anoxic and neutral to mildly alkaline pore waters. The formation of chlorites was also controlled by the detrital composition of sandstones, as suggested by the close association of the occurrence of authigenic chlorite with abundant volcanic rock fragments.

The type of carbonate formed during carbonate cementation was controlled by the relative concentration of Ca^{2+}, Fe^{2+}, Mg^{2+} and Mn^{2+} and physico-chemical conditions in pore waters. Non-ferroan calcite crystallised in pore waters where Fe^{2+} was virtually absent. The extensive presence of Fe^{2+} in pore waters during the carbonate cementation determined the limited formation of non-ferroan calcite. Non-ferroan calcite coating detrital grains was found in only two samples, which are from the west margin. Pore filling non-ferroan calcite is restricted to some volcanic lithic-rich sandstones in the east coast zone and northern region of the basin. In the presence of a high concentration of Fe^{2+}, Fe calcite, or dolomite, or ankerite, or siderite could have crystallised depending upon the concentrations of other cations and physico-chemical conditions in pore waters.

The Fe^{2+} used in forming Fe bearing carbonates was derived from reduction of Fe_2O_3, alteration of volcanic rock fragments and organic matter in that order of importance. The Ca^{2+} used in forming Ca bearing carbonates was largely derived from the initial hydration of volcanic rock fragments. The Ca^{2+} produced was incorporated with HCO_3^- at or near where it was produced so that pore filling calcite and ankerite are restricted to the lower Narrabeen Group sandstones, which are generally rich in detrital volcanic lithics.

Kaolins were formed by direct precipitation from migrating pore waters and alteration of volcanic rock fragments, feldspar and mica. They are more common and abundant in the sandstones rich in quartz.

Quartz overgrowths developed in two ways and / or a combination of them: overlap and / or emergence of the initial micro-quartz crystals and envelopment of earlier multiple overgrowths by an outer shell. They are more common and abundant in quartz-rich sandstones than in lithic-rich sandstones. The silica used for the overgrowths was largely derived from pressure solution.

Precipitation of post quartz overgrowth illite was related to the build up of K^+ in pore waters following quartz overgrowths. Cessation of illitisation of smectite was probably the principal contributing factor for the build up of K^+.

The data from stable isotope analyses suggest that the diagenesis of the Narrabeen Group sandstones proceeded in two different fluid flow regimes: early dynamic fluid flow regime and late slow flow / static fluid regime. The former was characterised by a slight increase of the $\delta^{18}O$ of pore waters from the estimated initial value of -15 ‰ to -12 ‰ with the temperature increasing from ~ 10 °C to 80-85 °C. During early diagenesis, early clays and pore filling carbonates were precipitated from the pore waters. The late slow flow / static fluid regime was characterised by a rapid ^{18}O-enrichment process. The $\delta^{18}O$ of pore waters increased from -12 ‰ to -3 ‰ with the temperature increasing from 85 °C to 110-135 °C. During late diagenesis, kaolin (generation II), quartz, and illite crystallised.

Means of measured homogenisation temperatures of aqueous fluid inclusions in quartz overgrowths are 45 to 60 °C higher than the current formation temperatures at the sample depths of 500-600 m. The high fluid inclusion temperature, together with vitrinite reflectance data, imply that a section with a thickness of *ca* 1600 to 2200 m was eroded away in the southern basin. The heat flow varied with time. A peak of the heat flow of 2.1 HFU relatively to the current values of 1.7-1.9 HFU was

reached in late Cretaceous time (~ 90 Ma BP), which is coincident with the youngest dated illite age of 90.5 Ma.

Chemical kinetic modelling suggests that significant volumes of oil were generated (~ 400 bbls/10^4m^3) in, and expelled from, the Illawarra Coal Measures. Oil migrated through the sandstones of the Scarborough and Lower Bulgo Operational Units during and probably after precipitation of quartz overgrowth, as indicated by the presence of liquid hydrocarbon inclusion in quartz overgrowths and fractures. Oil migration probably occurred at a time of 190 Ma to 170 Ma BP. There may have been oil columns at that time.

Porosity and permeability of the Narrabeen Group sandstones are controlled by a combination of depositional and diagenetic factors. The former include detrital composition of sandstones and texture of sandstones (grain size, sorting, and clay matrix) and the latter mechanical compaction, cementation by diagenetic minerals and dissolution. Sandstones with a porosity of > 15 % and permeability > 50 md have the following three general features: (1) a high percentage of detrital quartz clasts, (2) medium to coarse grain size (better if moderately to well sorted), (3) quartz overgrowths and siderite as the principal cements. Quartz-rich sandstones with grain coating siderite / calcite are high quality reservoirs. The potential of the Narrabeen Group sandstones as hydrocarbon reservoirs can be summarised as: (1) In terms of stratigraphy, the BH unit has the highest potential, which is succeeded in order by the LB unit, UB unit, SC unit and WO unit; (2) Geographically, the west margin has the highest potential, followed by the southern region, northern region and the east coast zone.

TABLE OF CONTENTS

LIST OF FIGURES

LIST OF TABLES

CHAPTER ONE

SYDNEY BASIN: STRATIGRAPHY AND DEPOSITIONAL ENVIRONMENT

1.1 INTRODUCTION

1.1.1 GENERAL STATEMENT

W.B. Clark, who is credited to be the first trained geologist to work in Australia, was the first to recognise the Sydney Basin as a geological entity. In 1847, he predicted the coal seams present at the basin margins occurred at depth in the basin (Mayne et al., 1974). Since then, abundant literature on the Sydney Basin has accumulated.

Previous work has been discussed by Carne (1903), Vallance and Branagan (1968), Packham (1969), Mayne et al. (1974), Menzies (1974), Branagan et al. (1976), and Herbert and Helby (1980). The most recent comprehensive study of the Narrabeen Group in the Sydney Basin was undertaken by Galloway and Hamilton (1988) and Hamilton and Galloway (1989).

1.1.2 DEFINITION OF THE SYDNEY BASIN

The Sydney Basin (Fig 1-1) is the southern part of the Sydney-Bowen Basin (Bembrick et al., 1973). It is bounded to the northeast by the Hunter Thrust System, which developed at the Middle Permian time (Leitch, 1974). To the west, the Permo-Triassic sequences of the basin thin and onlap the Lachlan Fold Belt. Thus the western boundary is depositional or erosional, rather than structural. The basin is separated from the Gunnedah Basin by the Mount Coricudgy Anticline in the northwest (Stuntz, 1969). The southeastern margin is a rifted margin and its exact location is still to be determined. However, Mayne et al. (1974) defined the edge of the continental shelf as the probable southeastern boundary, but the tectonic boundary is more likely to be the base of the continental slope adjacent to the oldest magnetic anomaly. The Sydney Basin covers an area of about 52,000 km^2,

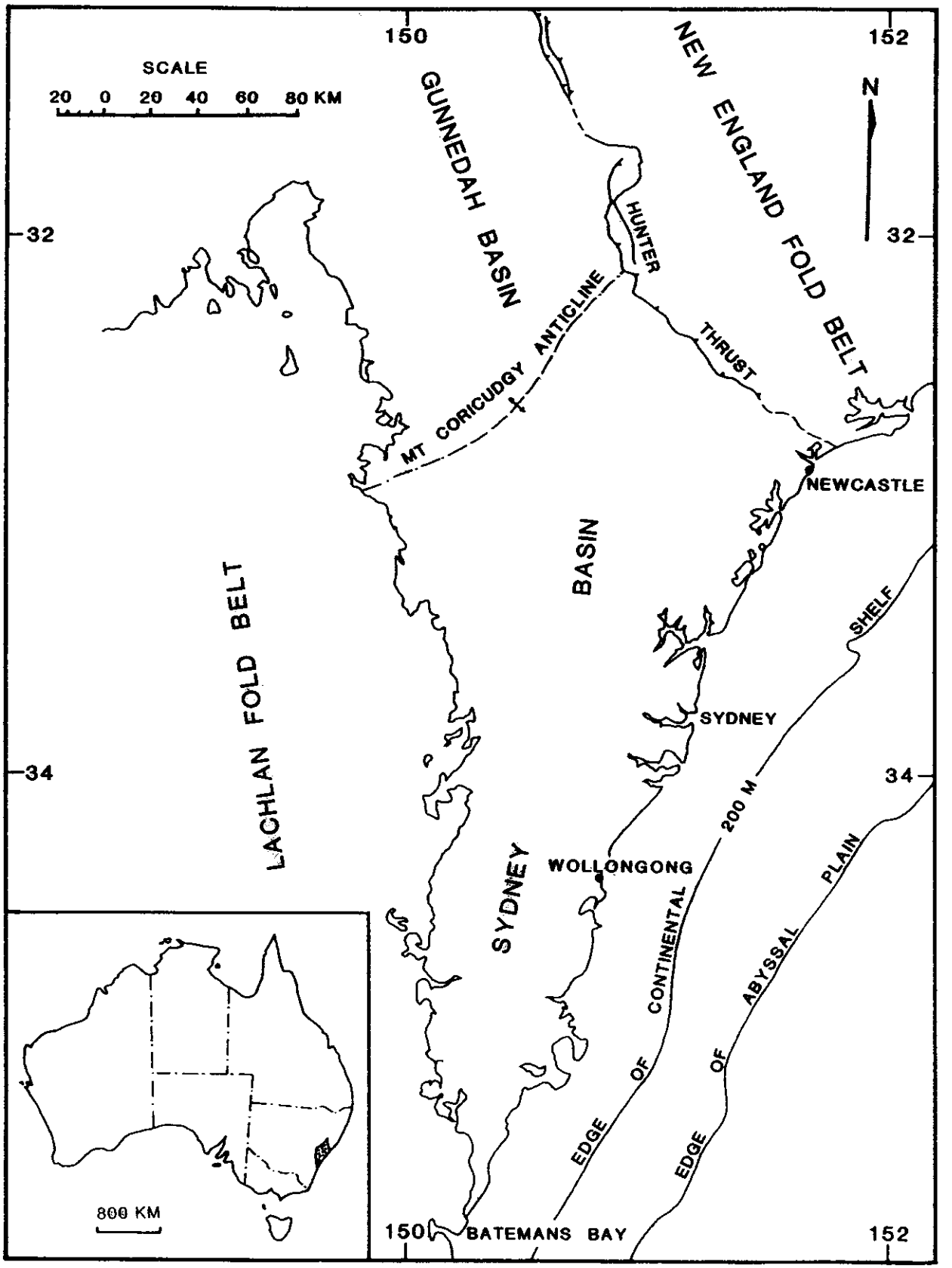

Fig 1-1 Location and present day boundaries of the Sydney Basin.

of which 6, 000 km^2 is offshore, if the edge of the continental shelf is taken as the southeastern boundary of the basin (Mayne et al., 1974).

The onset of sedimentation in the basin is not defined here. In fact, most definitions are vague in terms of the onset of sedimentation in the basin (Herbert, 1980a). According to Herbert, the Upper Carboniferous and Lower Permian sediments are included in the sediments of the basin even though the Sydney Basin took shape only from the mid-Permian. The Carboniferous to Triassic sediments were deposited in an alternating marine and non-marine environment. Of them, the Carboniferous and Triassic sediments were largely laid down in non-marine environment.

1.1.3 NOMENCLATURE AND CORRELATION OF STRATIGRAPHY

Sediments contained in the Sydney Basin range in age from Late Carboniferous to Middle Triassic (Fig 1-2). However, Devonian sediments, which lie beneath Carboniferous sediments in the northeast margin of the basin, may occur at depth in the basin, especially in the Hunter Valley area (Bembrick et al., 1973). Carboniferous sediments are mostly absent in the more southerly areas where Permo-Triassic sequences rest directly on a Palaeozoic basement of granitic and metamorphic rocks and Upper Devonian sediments. Permian sediments outcrop in separated areas along the margins of the basin. Triassic sediments are exposed over a great part of the central area of the basin.

The way in which the sediments contained in the basin crop out complicates the nomenclatures for the stratigraphy, particularly for the Permian sediments. Three different nomenclature schemes have evolved for the western area, northern area, and central and southern areas (Fig 1-3).

Mayne et al. (1974) made a correlation of the stratigraphy in different areas of the

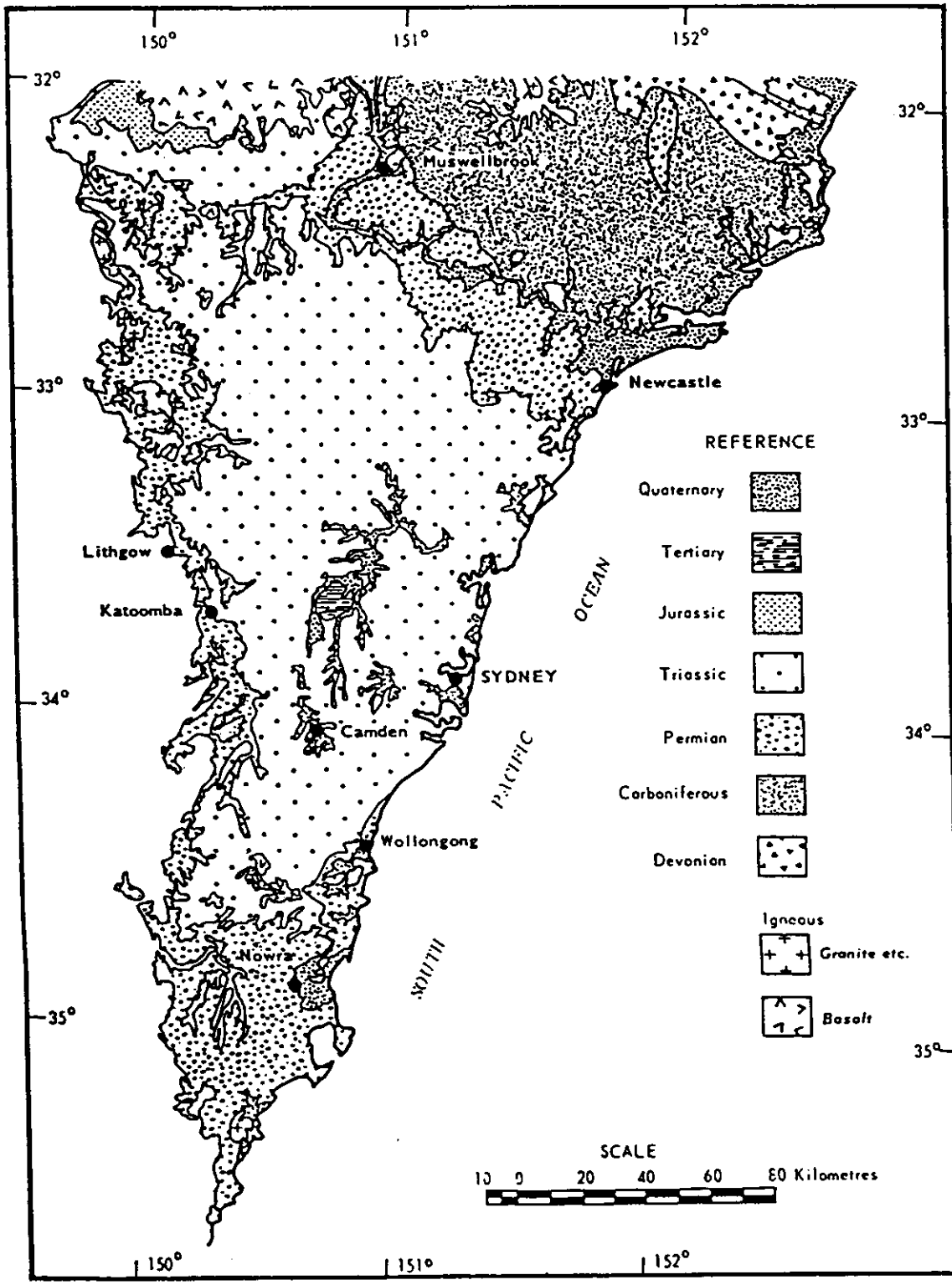

Fig 1-2 Generalised geology of the Sydney Basin.
(After Bembrick and Lonergan, 1976)

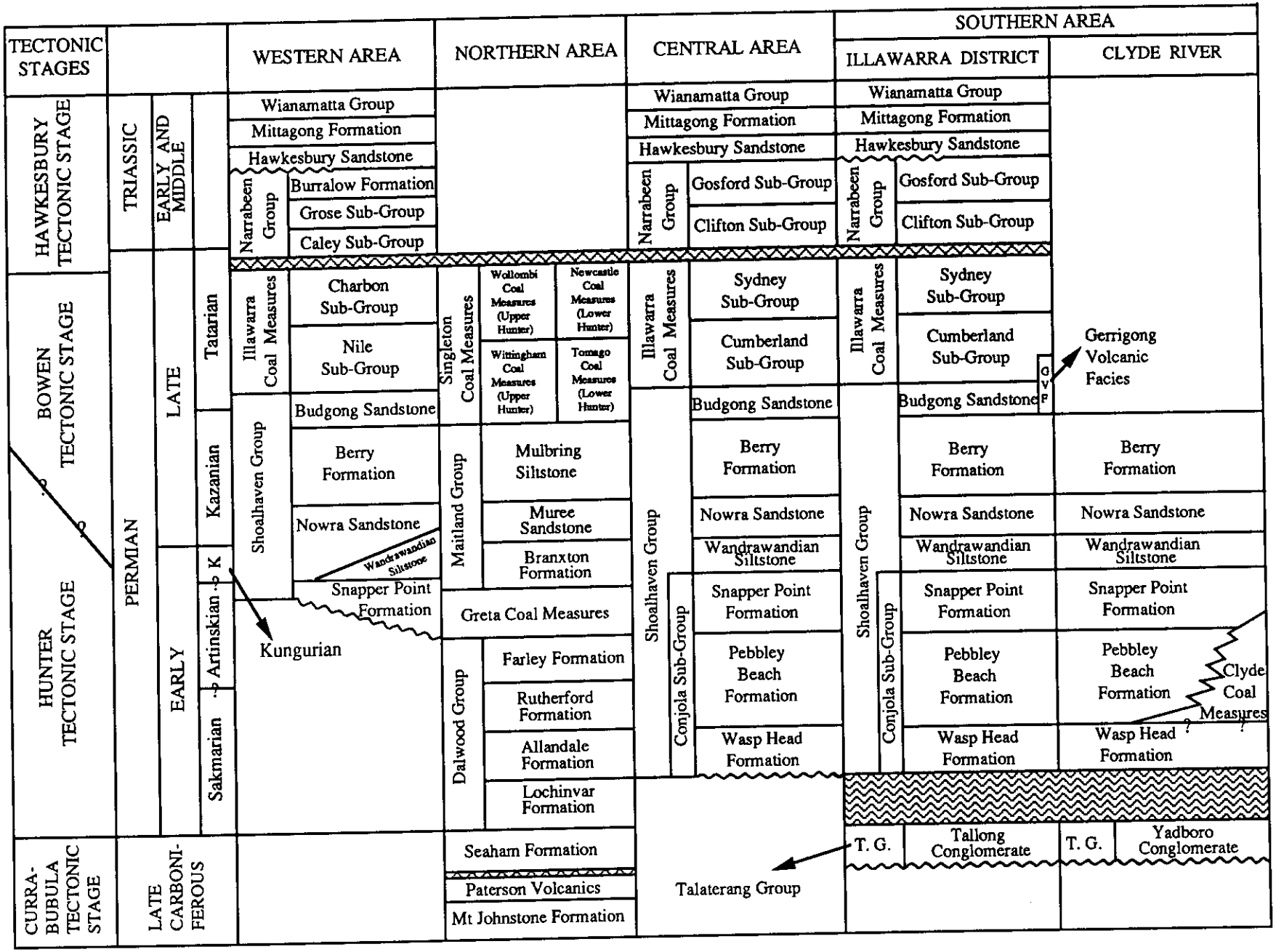

Fig 1-3 Stratigraphic nomenclature - Sydney Basin (Modified from Branagan et al., 1976).

basin. They divided the Permo-Triassic sequence into fourteen sedimentary subdivisions, which were defined as "intervals". Based on a combination of paleontological evidence, lithology, order of stratigraphic superposition and evidence from seismic reflection sections, they correlated the fourteen sedimentary intervals throughout the whole basin. According to them, however, the precision of the paleontological age dating throughout the basin is not accurate enough to prove the temporal equivalence of each interval over a long distance. The correlation schemes by Bembrick and Lonergan (1976) and Branagan et al. (1976) incorporate Upper Carboniferous sediments. Except for this, both schemes are similar to that by Mayne et al. (1974).

The correlation scheme used in the thesis (Fig 1-3) largely follows that by Branagan et al. (1976) with minor modifications using the correlation scheme by Bembrick and Lonergan (1976) and other recent literature. Although recent deep drilling and geophysical studies have aided correlations within the basin, some problems still remain to be resolved.

1.2 STRATIGRAPHY AND DEPOSITIONAL ENVIRONMENT

A comprehensive discussion of the topic was made by Packham (1969), Mayne et al. (1974), and Herbert and Helby (1980). The following general discussion is summarised mainly from the publications by these authors.

In their study of the Sydney Basin, Mayne et al. (1974) adopted the "interval" concept. The interval was defined as an informal interval subdivision of the rocks into wide-spread units that have genetic significance. Its boundaries were taken at lithological changes in a sequence in such a way that they approximate time lines as close as possible. Due to the limited paleontological dating data, however, the age accuracy of an interval is still to be determined. Using the "interval" concept, Mayne et al. divided the Permo-Triassic sequence of the Sydney Basin into 14 intervals.

Herbert (1980a) developed the "depositional episode" concept in his discussion of the sedimentation in the Sydney Basin. This term is not the same as the "depositional episode" used by Frazier (1974) in his description of the stratigraphy of the Gulf Basin. Herbert (1980a, p.19) defined his depositional episode thus: "A DEPOSITIONAL EPISODE is envisaged herein as a period of continuous deposition during a relatively major regression or transgression which is now represented by a more or less conformable stratigraphic sequence of sediments. All sediments deposited during a single depositional episode may not be of equivalent age because sediments become progressively younger in the direction of progradation. Also, part of one depositional episode may co-exist in time with another." Using his depositional episode concept Herbert, following a system of tectonic stages proposed by Scheibner (1976), grouped the Late Carboniferous to Middle Triassic sedimentary sequence of the basin into 13 different depositional episodes. They took place in four different tectonic stages.

Herbert's "depositional episode" had no certain relationship with Mayne et al.'s "interval". In terms of the components of rock units, one depositional episode can include several intervals and vice versa. (e.g. The Greta Depositional Episode includes Intervals 1 and 2; Interval 12 includes the Lower, Middle and Upper Narrabeen Depositional Episodes.) In other cases, one depositional episode is the equivalent of one interval. (e.g. Interval 14 and the Wianamatta Depositional Episode are equivalents.)

1.2.1 TALATERANG GROUP AND CORRELATIVE SEAHAM FORMATION

In the southern area of the Sydney Basin, the oldest sediments, whose age is determined to be Late Carboniferous by spores (Helby and Herbert, 1971), rest unconformably on much older strongly folded Palaeozoic rocks. These sediments comprise the Talaterang Group (Gostin and Herbert, 1973). The group is represented only in two narrow east-west trending palaeo-valleys and was laid

down in a glacial-fluvial environment (Herbert, 1972; 1980b). In the northern area of the Sydney Basin, its correlative, the Seaham Formation, experienced a similar depositional environment (Bembrick and Lonergan, 1976).

1.2.2 LOCHINVAR FORMATION; ALLANDALE FORMATION AND ITS CORRELATIVE WASP HEAD FORMATION

The Lochinvar and Allandale Formations consist of shale to conglomerate and interbedded pyroclastics. The Lochinvar Formation is restricted to the northern area of the basin. It has a thickness of 835 m in the Lochinvar area but is poorly exposed (Osborne, 1949). Mayne et al. (1974) attributed the two formations to marine deposition in a northwesterly trending trough in the northern Sydney Basin. Sea water invaded the trough from both the northwest and southeast. The marine sedimentation was accompanied by intrusive and extrusive basic to intermediate volcanism.

The Allandale Formation represents a sublittoral sandstone and conglomerate facies. Its correlative to the south, the Wasp Head Formation, has similar lithologies and consist largely of sandstones, pebbly sandstones and conglomerates. It is restricted to a small area at Durras on the south coast and was deposited in a littoral to nearshore environment (Runnegar, 1980).

1.2.3 RUTHERFORD AND FARLEY FORMATIONS AND THEIR CORRELATIVE PEBBLY BEACH FORMATION

The Rutherford Formation is composed of shale and siltstone with thin limestones and marls occurring in the Pokolbin area (McClung, 1980). The formation crops out so poorly that no type section has been established. However, a 384 m section was intersected in the Sunwell No.1 borehole (McClung, 1980). The overlying Farley Formation is 300 m thick in its type section at Farley Railway Station where it consists of fine to medium grained, moderately fossiliferous, silty sandstone (Osborne, 1949). The sandstone becomes coarse towards both the top and the

northern source area. The two formations together have been correlated with the Pebbly Beach Formation in the central and southern areas of the basin (Fig 1-3), whose lithology is dominated by siltstones, silty fine and very fine sandstones.

The sediments of the Rutherford and Farley Formations were deposited during a marine transgression, which began in Lochinvar Formation time (Mayne et al., 1974). According to McClung (1980), however, most of the sediments of the two formations were laid down during a slow marine regression after an initial marine transgression.

The silty sediments of the Pebbly Beach Formation were laid down in a tidal flat environment (Gostin and Herbert, 1973). Landward of the tidal flat, peat accumulated in isolated swampy coastal plains, which resulted in the deposition of the Clyde Coal Measures in part of the Clyde River area.

The Lochinvar, Allandale, Rutherford, and Farley Formations discussed above comprise the Dalwood Group in the northern area of the Sydney Basin (Fig 1-3). It is generally the product of marine sedimentation, which was accompanied by active volcanism (McClung, 1980).

1.2.4 GRETA COAL MEASURES AND CORRELATIVE SNAPPER POINT FORMATION

The Greta Coal Measures consist of conglomerates and sandstones with subordinate siltstones and mudstones. Several coal seams, of which the Greta Coal Member is the most important, are interbedded with these sediments. The Greta Coal Measures have a thickness of 242 ft in their type section near Greta (Raggatt, 1938). They have a transitional relationship with the underlying Farley Formation in the Lochinvar Anticline area. The relationship implies a gradual shallowing, which led to deposition of non-marine sediments. Facies relationships and current directions in the Greta Coal Measures suggest a northerly source area

(Rattigan and McKenzie, 1969), which is also supported by the southward thinning of the unit in the subsurface (Mayne et al., 1974; McClung, 1980). The Greta Coal Measures resulted from a marine regression.

The correlative of the Greta Coal Measures in other areas of the basin, the Snapper Point Formation, has a similar lithology but is lack of coal seams. The formation thins eastwards (Herbert, 1980b). In outcrops, which are extensive in the southwestern area of the basin, it is a sublittoral sand. The sand coarsens westwards where beach and even fluvial facies may occur (Runnegar, 1980). The formation exists in most parts of the southern, western and central areas of the basin. In fact, the Snapper Point Formation marks the first of the two major transgressions which invaded to the western margin of the basin (Runnegar, 1980).

As indicated above, the Greta Coal Measures are the product of a marine regression whereas the Snapper Point Formation resulted from a marine transgression. Thus it seems unreasonable that the Greta Coal Measures correlate with the Snapper Point Formation. Runnegar (1980) attempted to resolve this troublesome correlation problem. According to him, the Snapper Point Formation appears more likely to be the southern expression of a major transgression which followed the brief Greta regression. The major transgression also resulted in the deposition of the basal part of the Branxton Formation in the northern area of the Sydney Basin. However, Runnegar did not discuss which rock units correlate with the Greta Coal Measures.

The Wasp Head, Pebbly Beach, and Snapper Point Formations discussed above comprise the Conjola Sub-Group. It is the basal part of the Shoalhaven Group in the southern and central areas of the basin (Fig 1-3).

1.2.5 WANDRAWANDIAN SILTSTONE AND CORRELATIVE BRANXTON FORMATION (EXCLUDING BASAL PART)

The Wandrawandian Siltstone is dominated by siltstones. It contains dispersed clasts and megaclasts, which are also common in the underlying Conjola Sub-Group. It thins westwards from about 250 m at the coast to its disappearance on the western margin of the basin where the overlying Nowra Sandstone rests directly on the Snapper Point Formation (Runnegar, 1980). It correlates with the Branxton Formation (excluding the basal part) to the north. The basal part of the Branxton Formation correlates with the top part of the Snapper Point Formation and consists of sandstones and conglomerates. However, towards the top the Branxton Formation is dominated by silty sandstones and siltstones.

The Wandrawandian Siltstone was laid down in a quiet shallow shelf environment below wave base. The dispersed clasts and megaclasts contained in the unit were probably transported to the quiet marine environment by ice rafts and icebergs from the south (Herbert, 1980b). To the north, the Branxton Formation resulted from a steady marine transgression following the Greta regression (McClung, 1980).

1.2.6 NOWRA SANDSTONE AND CORRELATIVE MUREE SANDSTONE

The Nowra Sandstone and its correlative to the north, the Muree Sandstone, consist of quartzose to lithic quartzose sandstones with some interbedded siltstones. They show well-developed cross-stratification. Thickness reaches up to 80-90 m but commonly is less than 50 m (Bembrick and Lonergan, 1976).

The sediments of the Nowra and Muree Sandstones were laid down in a nearshore marine environment during a brief regression followed by a major transgression (Mayne et al., 1974). However, Runnegar (1980) thought the deposition took place well out on the Permian continental shelf. McKelvey et al. (1971) suggested that the Nowra Sandstone resulted from northerly flowing longshore currents during transgression. It was derived from the south while the Muree Sandstone had its source in the north.

1.2.7 BERRY FORMATION AND CORRELATIVE MULBRING SILTSTONE

The Berry Formation consists of dark to mid-grey siltstones. It is recorded to have a maximum thickness of 550 m in the Stockyard Mountain No.1 borehole (Bowman, 1980) and thins westwards. Its correlative to the north, the Mulbring Siltstone is also dominated by siltstones. It reaches a thickness of 330 m at its type section near Mulbring (McKellar, 1969).

The sediments of the Berry Formation were deposited in the distal to prodelta fringe of Visher's (1965) delta classification (Bowman, 1980). The Mulbring Siltstone was laid down in deeper quiet water during and after the transgression that began with the deposition of the Nowra and Muree Sandstones (Mayne et al., 1974).

The Branxton Formation, the Muree Sandstone and the Mulbring Siltstone discussed in above three sections comprise the Maitland Group in the northern area of the Sydney Basin (Fig 1-3).

1.2.8 BUDGONG SANDSTONE

The Budgong Sandstone conformably overlies the Berry Formation. It consists of quartzose sandstones although to the east altered volcanic rock fragments are increasingly common. It has a thickness of 370 m at Saddleback Mountain area (Bowman, 1980). To the north it correlates with the basal part of the Singleton Coal Measures.

The Budgong Sandstone represents a nearshore sand, which was deposited during a regression. The regression produced the overlying Illawarra Coal Measures (Bowman, 1970). In a later publication Bowman (1980) concluded that the lower part of the Budgong Sandstone was deposited below wave base while the rest of the unit was laid down above wave base.

The Conjola Sub-Group, the Wandrawandian Siltstone, the Nowra Sandstone, the

Berry Formation and the Budgong Sandstone together comprise the Shoalhaven Group in the central, western and southern areas of the Sydney Basin (Fig 1-3). The group and its correlative in the northern area of the basin are dominated by marine sediments which were deposited as a result of alternating marine transgressions and regressions.

Of those transgressions taking place during the Shoalhaven Group time, the transgression during the deposition of the Snapper Point Formation and the one during the deposition of the Mulbring Siltstone are the two major ones. The earlier one resulted in the marine deposition of the Snapper Point Formation in the western area of the basin for the first time (Bembrick and Lonergan, 1976). The later one is the most widespread in the Sydney Basin (Mayne et al., 1974). Faunal evidence (Dickins, 1968) suggests that the sea was connected with the Bowen Basin at this time. The situation lasted until the end of Budgong Sandstone deposition when a regression occurred and resulted in the end of the dominant marine sedimentation in the Sydney Basin.

1.2.9 SINGLETON COAL MEASURES (EXCLUDING BASAL PART) AND CORRELATIVE ILLAWARRA COAL MEASURES

A widespread regression throughout the whole Sydney Basin took place at the end of Budgong Sandstone deposition and led to the formation of extensive coal swamps and associated sediments. In the northern basin, the regression ended marine sedimentation and produced a sequence of thick coal measures of fluvial origin - the Singleton Coal Measures (Conolly and Ferm, 1971). Further south towards the basin centre, terrestrial sedimentation at this time was interrupted by several brief marine transgressions. The deposition of the Kulnura Marine Tongue and equivalents within the Tomago Coal Measures recorded one of these brief transgressions.

The Singleton Coal Measures are divided into the Wittingham Coal Measures and

the overlying Wollombi Coal Measures in the Upper Hunter Valley and the Tomago and the overlying Newcastle Coal Measures in the Lower Hunter Valley where the Singleton Coal Measures consist of some 1200 m of predominantly terrestrial sediments (Diessel, 1980).

The Tomago Coal Measures were deposited on tidal mud flats. Throughout its deposition, marine or at least brackish influence remained. The overlying Newcastle Coal Measures represent the product of a high energy terrestrial setting (Diessel, 1980), which is shown by the substantial increase of coarse sediments.

The Singleton Coal Measures (excluding the basal part) correlate with the Illawarra Coal Measures in other areas of the basin. The Illawarra Coal Measures are divided into the Cumberland Sub-Group and overlying Sydney Sub-Group in the central and southern areas of the basin, and the Nile Sub-Group and the Charbon Sub-Group in the western area of the basin (Fig 1-3).

The Cumberland Sub-Group consists of the Pheasants Nest Formation and the overlying Erins Vale Formation. The Pheasants Nest Formation represents deltaic plain sediments grading from coarse sandstone at the base of the sequence to siltstone and coal at the top. It has a general thickness of about 75 m with a maximum thickness being up to 185 m (Bowman, 1980). The overlying Erins Vale Formation consists of poorly sorted, often bioturbated volcaniclastic sandstone and is the product of a marine transgression.

The Sydney Sub-Group is separated from the underlying Cumberland Sub-Group by a marked erosion surface. The sub-group consists of lithic sandstone, laminite, siltstone, mudrock, and coal with minor amounts of tuff. Its thickness reaches up to 165 m. It was deposited in a lower deltaic plain environment (Bowman, 1980). The sediments of the sub-group seemed to have been derived from a southern andesitic source while those of the Sydney Sub-Group from a northern quartz-lithic

source.

In the western area of the basin, the Nile Sub-Group represents the transition from marine siltstones and sandstones of the Berry Siltstone to delta sandstones and top-delta coals. The overlying Charbon Sub-Group is composed of fluvial point bar sandstones, with floodplain siltstones, claystones, and coals (Bembrick, 1980).

1.2.10 NARRABEEN GROUP

The Narrabeen Group (excluding Newport and Garie Formations) is the stratigraphic unit studied in this project. The stratigraphy and depositional environment of the group will be discussed in more detail.

In 1887, Wilkinson first applied "Narrabeen" to a rock unit in the Sydney Basin (Hanlon et al., 1953). After the pioneering work of Raggatt (1938), the Permo-Triassic "Narrabeen Beds" of the Sydney Basin were eventually defined as the Narrabeen Group by Hanlon et al. (1953).

Historically the Narrabeen Group was considered to be the lowermost part of the Triassic rock units in the Sydney Basin. However, further palynological evidence (Balme and Helby, 1973) suggested that the Permo-Triassic boundary does not correlate with the base of the Narrabeen Group but lies within the fluvial sediments of the Narrabeen Group (i.e. in the upper part of the Caley Formation). Therefore, the Narrabeen Group ranges in age from Late Permian to Early Triassic. The Group has a variable thickness in different parts of the basin. It varies from 90 m on the basin edge, 90 to 510 m on the basin slope, to 510 to 700 m on the basin floor (Mayne et al., 1974).

The formal stratigraphic nomenclature for the Narrabeen Group was described by Hanlon et al. (1953) in coastal regions and by Crook (1956) in western districts. Crook's nomenclature was later applied over a wide area from the Burragorang

Valley (Helby, 1961) to Glen Davies district (Goldbery, 1970) and the upper Colo-St Albans region (Galloway, 1967). However, the subdivision scheme for the group introduced by Hanlon et al. (1953) was modified as a result of further studies by Stuntz (1961, cited in Ward, 1971b) and Bradley (1964, cited in Ward, 1971b). The history of nomenclature modification prior to 1970 has been summarised by Herbert (1970). Ward (1971b) gave a lithological correlation of the rock units of the Narrabeen Group (Fig 1-4).

Galloway and Hamilton (1988) proposed a new subdivision scheme for the Narrabeen Group. Based on all available geophysical log data, principally gamma and neutron logs, they established a correlation framework throughout the whole Sydney Basin and subdivided the Narrabeen Group into five operational units, which will be discussed in Chapter 4.

Following the study of the sedimentation of the Narrabeen Group by Ward (1971a, 1972), further details were discussed by Bembrick (1980), Conaghan et al. (1982), Hamilton et al. (1987) and Galloway and Hamilton (1988). The Narrabeen Group is generally considered to be derived from fluvial / lacustrine depositional systems. As deposition proceeded, the energy of the depositional system declined (Ward, 1972). The following general discussion reviews the views from these authors.

(i) Caley Formation and Wombarra Shale

These two stratigraphic units consist largely of shaly sediments. To the north and northwest, they become interbedded with conglomeratic units, the Munmorah Conglomerate in the east and the Widdin Brook Conglomerate in the northwest (Goldbery, 1970). Palaeocurrent data from the overlying Grose Sandstone in the western district show that the mean direction of the palaeocurrent is 155° (Ward, 1972). The lateral relationship and palaeocurrent data led Ward to the conclusion that the two units were deposited at the outwash end of a southeast flowing alluvial

<table>
<tr><th>NORTH COAST
(Bradley, 1964)</th><th colspan="2">SOUTH COAST
(Incl. Collaroy-palm bch)</th><th colspan="2">WESTERN DISTRICT
(Goldbery, 1966)</th></tr>
<tr><td rowspan="4">Gosford Formation</td><td colspan="2">Newport Formation</td><td rowspan="3" colspan="2">Burralow Formation</td></tr>
<tr><td colspan="2">Garie Formation</td></tr>
<tr><td colspan="2">Bald Hill Claystone</td></tr>
<tr><td rowspan="2">Shaley facies</td><td rowspan="6">Bulgo Sandstone</td><td rowspan="8">Grose Sandstone</td><td rowspan="4">Banks Walls Sandstone Member</td></tr>
<tr><td rowspan="2">Patonga Claystone</td></tr>
<tr><td rowspan="2">Volcanic facies</td></tr>
<tr><td rowspan="2">Tuggerah Formation</td></tr>
<tr><td>Menai Claystone Member</td><td>Mt York Claystone Member</td></tr>
<tr><td rowspan="9">Munmorah Conglomerate</td><td>Pebbly facies</td><td rowspan="3">Burra Moko Head Sandstone Member</td></tr>
<tr><td colspan="2">Stanwell Park Claystone</td></tr>
<tr><td colspan="2">Scarborough Sandstone</td></tr>
<tr><td rowspan="4" colspan="2">Wombarra Shale (Incl. Otford Sandstone Member)</td><td rowspan="6">Caley Formation</td><td>Martley Vale Claystone Member</td></tr>
<tr><td>Govett's Leap Claystone Member</td></tr>
<tr><td>Victoria Pass Claystone Member</td></tr>
<tr><td rowspan="2">Clwydd Sandstone Member</td></tr>
<tr><td rowspan="2" colspan="2">Coal Cliff Sandstone</td></tr>
<tr><td>Beauchamp Falls Shale Member</td></tr>
</table>

Fig 1-4 Rock units of the Narrabeen Group showing lithological correlation. (After Ward, 1972)

system, which also produced the Munmorah Conglomerate in the north. The basal part of the Caley Formation was deposited in a lacustrine environment and represents swampy facies (Galloway and Hamilton, 1988; Chapter 4).

(ii) Coal Cliff, Scarborough, Bulgo and Grose Sandstones

The Coal Cliff, Scarborough, Bulgo and Grose Sandstones are the sandy units of the Narrabeen Group. They are from different parts of the basin and are of different age (Fig 1-4). Despite the differences, these sandy units have many sedimentological features in common (Ward, 1972). Ward ascribed these sandstones to a fluvial deposition. The fluvial depositional system changed during sedimentation. The Coal Cliff, Scarborough Sandstones and the lower part of the Grose and Bulgo Sandstones were laid down in a braided fluvial system. By contrast, the upper parts of the Grose and Bulgo Sandstones represent the point bar sediments of a meandering fluvial system.

In his discussion of the Blue Mountains geology, Bembrick (1980) increased the rank of the stratigraphy. He defined the Grose units as the Grose Sub-Group instead of the Grose Sandstone. Thus the Banks Wall Sandstone Member becomes the Banks Wall Sandstone. Bembrick indicated that marine incursions had been found in the basal part of the Grose Sub-Group (Burra-Moko Head Sandstone). Following the suggestion of Conolly (1969) that the Grose Sub-Group was deposited in a fluvial environment, he proposed that marine incursions should become evident in the lower deltaic plain environment from outcrops in the lower Blue Mountains and eastwards.

(iii) Stanwell Park Formation

The Stanwell Park Formation consists largely of red-brown and grey-green laminated claystones with minor friable conglomerates. Like the Caley Formation and Wombarra Shale, it is also interbedded with conglomeratic sediments to the northwest. Conolly (1969) indicated that the shaly sequence might represent a

marine transgression into the basin. In contrast, Ward (1972) thought the unit was the product of a sub-aerial accumulation derived from a newly exposed volcanic source east of present coastline. It represents inter-channel floodplain / lacustrine facies (Chapter 4).

(iv) Burralow Formation

The Burralow Formation is the uppermost part of the Narrabeen Group in the Blue Mountains area. It consists largely of fine grained micaceous sandstones which are quartzose and quartz-lithic, with minor interbedded claystones and siltstones. The formation was deposited in a fluvial to fluvial-deltaic environment in the Blue Mountains (Bembrick, 1980). To the east the formation merges progressively with the Newport Formation, which was deposited in a shallow estuarine environment (Bunny and Herbert, 1971).

(v) Gosford Formation

The Gosford Formation, which was recently named as the Terrigal Formation by McDonnell (1980), is the uppermost part of the Narrabeen Group along the north coast. It is composed of sandstones and siltstones. McDonnell (1974) ascribed the Gosford Formation to deposition in an alluvial inchannel and floodplain environment. Later he developed this interpretation and divided the formation into seven fine grained and six coarse grained subdivisions. In the Terrigal area, the Gosford Formation is the product of at least six stages of fluvial deposition (McDonnell, 1980).

(vi) Bald Hill Claystone

The Bald Hill Claystone is the most important stratigraphic marker in the Sydney Basin. It has a distinctive red-brown or chocolate colour. The Wentworth Falls Claystone Member, which is within the Banks Wall Sandstone in the Blue Mountains area, correlates with part of the Bald Hill Claystone in the southern and central areas of the basin (Goldbery and Holland, 1973). To the north, the Bald Hill

Claystone interfingers with the Gosford Formation. However, the distinctive chocolate beds disappear from the sequence completely. The Bald Hill Claystone has a unique mineralogy (Loughnan, 1963). It consists almost entirely of haematite (locally siderite) and well-ordered kaolinite. Quartz and any unstable minerals such as feldspar and mica are virtually absent.

The origin of the chocolate beds within the Bald Hill Claystone and the Wentworth Falls Claystone Member is highly controversial (Goldbery and Holland, 1973). Two different interpretations have been proposed for the origin of haematite in the red beds. One is that the haematite is produced by laterization and then transported to an oxidising environment to be deposited. The other is that haematite results from in situ diagenetic breakdown of iron-rich minerals. Both modes of origin require a combination of particular climatic conditions, source materials and oxidising environment.

Based on the single clay mineralogy, high concentration of haematite, and relative absence of quartz, Loughnan et al. (1964) postulated that the Bald Hill Claystone resulted from lateritic weathering of a basic to intermediate volcanic source. This interpretation was later followed and developed by Ward (1972) and Goldbery and Holland (1973). However, with regard to the source area, differences appeared between them. Ward thought that the Bald Hill Claystone was derived from the same exposed volcanic source to the east of the present coastline as the Stanwell Park Claystone. It perhaps represents a terrestrial accumulation which occurred on the flank of the delta, in an area free of other clastic influx. Goldbery and Holland (1973) ascribed the Bald Hill Claystone to a newly developed northerly drainage system and was derived from a southern source and deposited in a piedmont environment. They also suggested that chocolate beds in the Blue Mountains area were derived from western and southern sources and deposited in a floodplain environment. The source for the Bald Hill Claystone at Long Reef north of Sydney was uncertain (Goldbery and Holland, 1973). However, they suggested that the

sediments might also come from the southern source.

(vii) Garie and Newport Formations

The Garie Formation, formerly known as Garie Member, has a mineralogy similar to that of the underlying Bald Hill Claystone except that the iron-bearing mineral is siderite instead of haematite. It is composed of sideritic flint or kaolinite claystone and also contains abundant pisolitic and brecciated clasts. The formation correlates with the flint clays which lie about 9 m above the Wentworth Falls Claystone Member of the Banks Wall Sandstone (Goldbery and Holland, 1973).

The origin of the Garie Formation was discussed by Loughnan (1962, 1970) and Goldbery and Holland (1973). Loughnan thought the formation was produced by silicification of transported bauxitic minerals, which were laid down in reducing low-lying vegetated swamps. This interpretation was later modified by Goldbery and Holland. They ascribed the formation to the rapid deposition of bauxitic materials on the flanks of exposed bauxitized area on the eastern and southern margins of the basin.

In the Garie Formation, Bunny and Herbert (1971) recognised the presence of root remains in leached shales, which led them to the conclusion that a depositional break existed at the top of the Bald Hill Claystone. This was supported by Goldbery and Holland (1973). They thought that the depositional break was consistent with the final bauxitization introduced by them in their discussion of the Garie Formation.

The Newport Formation overlies the Garie Formation. It consists of shaly sediments in the lower part and sandy sediments in the upper part. The lower part was deposited in a combined deltaic, interdistributary bay and sub-aerial levee environment and the upper part in a fluvial environment (Bunny and Herbert, 1971). The upper part contains a number of point bar or fining upwards sequences. By considering the persistence of beds and laminations, Ward (1972) suggested

that many beds within the Newport Formation represented distributary mouth bar deposits, or the product of a similar environment which involved wide, but shallow water under mild current activity.

1.2.11 HAWKESBURY SANDSTONE

The Hawkesbury Sandstone has an extensive exposure. It dominates the landscape within 100 km of Sydney and has a maximum thickness of 250 m (Conaghan, 1980). The stratigraphic unit consists of quartzose sandstones with minor thin-layered claystones and siltstones. It was deposited in a braided fluvial depositional system, which led to the paucity of claystones and siltstones within the unit (Conaghan and Jones, 1975; Conaghan, 1980).

1.2.12 MITTAGONG FORMATION

The Mittagong Formation, previously known as the "Passage Beds" (Lovering, 1954), was included within the base of the Wianamatta Group by Bryan et al. (1967), and Lovering and McElroy (1969). However, Herbert (1980c) showed that the formation was related genetically to the underlying Hawkesbury Sandstone rather than the overlying Ashfield Shale. Thus he agreed with Lovering (1954) and excluded the Mittagong Formation from the Wianamatta Group.

The Mittagong Formation consists of fine to medium grained quartzose sandstones identical to the underlying Hawkesbury Sandstone in terms of mineral composition. It has a thickness of 15 m at its type section in Gib Tunnel, but is usually less than 10 m. In some areas, it is absent (Herbert, 1980c). According to Herbert, the Mittagong Formation represents an overbank complex of levee, abandoned channel, and swamp sediments. It is actually the preserved floodplain sediments of the palaeo-Hawkesbury Sandstone river.

1.2.13 WIANAMATTA GROUP

The Wianamatta Group is the uppermost part of the Permo-Triassic sequence in

the Sydney Basin. It consists largely of shales with minor sandstones. It reaches a thickness of 304 m at Razorback Range (recorded in the DM Razorback DDH 1 borehole, Herbert, 1976, cited in Herbert, 1980c).

The group was divided into three subdivisions by Herbert (1980c). From bottom to top they are the Ashfield Shale, the Minchinbury Sandstone, and the Bringelly Shale. The Wianamatta Group experienced a single regressive episode after the inundation of the Hawkesbury Sandstone - Mittagong Formation alluvial plain. The regression resulted in the deposition of the Wianamatta Group which graded upwards from lacustrine to brackish or shallow marine deposits at the base, through a shoreline sand, and finally into alluvial sediments at the top (Herbert, 1980c).

1.3 DEPOSITIONAL HISTORY SUMMARY

The depositional development of the Sydney Basin has been comprehensively discussed by Herbert (1980a). The following general discussion is required to give the setting for the core samples analysed in this thesis.

Sedimentation in the Sydney Basin was both initiated and controlled by tectonism and can thus be discussed within a tectonic framework (Herbert, 1980a). During its development, the Sydney Basin experienced four tectonic stages. They are the Late Carboniferous Currabubula Tectonic Stage, the Early Permian Hunter Tectonic Stage, the Late Permian Bowen Tectonic Stage, and the Early to Middle Triassic Hawkesbury Tectonic Stage (Fig 1-3).

During the Currabubula Tectonic Stage, the Sydney Basin did not yet exist as a structural entity. The incipient Sydney Basin (the eastern part of the Lachlan Fold Belt) experienced fluvial-glacial conglomerate sedimentation (Talaterang Group and correlatives). These conglomerates are restricted to valleys surrounded by highlands of moderate elevation.

Up to the beginning of Early Permian times, the New England Fold Belt and the eastern margin of the Lachlan Fold Belt slowly subsided so that a broad continental shelf was created. During the Hunter Tectonic Stage, the lower Shoalhaven, the Dalwood and the lower Maitland Groups were deposited on the inner continental shelf during extensive marine transgressions. Incipient orogenic movement, which occurred within the New England Fold Belt, interrupted the shelf sedimentation and resulted in the deposition of the Greta Coal Measures with a wedge shape in the northern part of the developing Sydney Basin. The deposition of the overlying Branxton Formation and the Muree Sandstones and their correlatives also took place during this tectonic stage.

Mid-Permian diastrophism (Leitch, 1974) led to the development of the Hunter-Mooki Thrust System, which is defined as the northeastern boundary of the present day Sydney-Gunnedah Basin. At this time, the Sydney Basin began to take shape and persisted as a structural entity until the end of the Middle Triassic time.

The mid-Permian diastrophism (Hunter Orogeny) resulted in the uplift of the New England Fold Belt and the rapid subsidence of the adjacent Sydney Basin. Thus in terms of plate tectonics, the Sydney basin is a foreland basin. During the Bowen Tectonic Stage, most sediments were derived from the uplifted New England Fold Belt and minor, intermittent sediment inputs from the southwestern margin. These sediments (Singleton Coal Measures, their correlatives - Illawarra Coal Measures and Budgong Sandstone) were deposited in a newly formed foredeep (the Sydney Basin) during three major regressive depositional episodes: Lower, Upper Tomago Depositional Episodes, and Newcastle Depositional Episode. Terrestrial sediments of this tectonic stage contain the most important coals in the Sydney Basin. They are named in different areas as the Illawarra, Newcastle / Tomago Coal Measures.

All three regressive depositional episodes are characterised by repeated

progradation of depositional environments. Close to the northeastern source area, coarse conglomerates were deposited in alluvial fan and alluvial plain environments. To the southwest, finer sandstones, siltstones and shales were laid down in deltaic, marine deltaic front, and prodelta environments. Peat swamps formed in all the major terrestrial environments.

During the Hawkesbury Tectonic Stage, four major lithological stratigraphic units were deposited. They are the Narrabeen Group, the Hawkesbury Sandstone, the Mittagong Formation, and the Wianamatta Group. It is generally considered that these units were deposited in a fluvial-deltaic system. At different times, the New England Fold Belt and the Lachlan Fold Belt acted as the major source which supplied sediments to the basin. Deposition ceased at the end of Middle Triassic.

After a Late Triassic depositional hiatus, Lower Jurassic sediments with an unknown thickness were deposited unconformably over the Middle Triassic sediments of the Sydney Basin. According to Herbert (1980a), these sediments are more likely to be related to the developments of the Great Australian Basin than to the tectonically extinct Sydney Basin.

1.4 STRUCTURE

The structural subdivision of the Sydney Basin was discussed first by Bembrick et al. (1973). This discussion was later summarised by Bembrick and Lonergan (1976) and Bembrick et al. (1980) . The following discussion is largely based on the three papers by these authors.

The Sydney Basin, which is the southern part of the Sydney-Bowen Basin, can be further divided into lower category structural units. They include six plateaus, one belt of folds and one secondary category basin (Fig 1-5).

The Hunter Valley Dome Belt ("Dome Belt" of Voisey, 1959), lies in the most

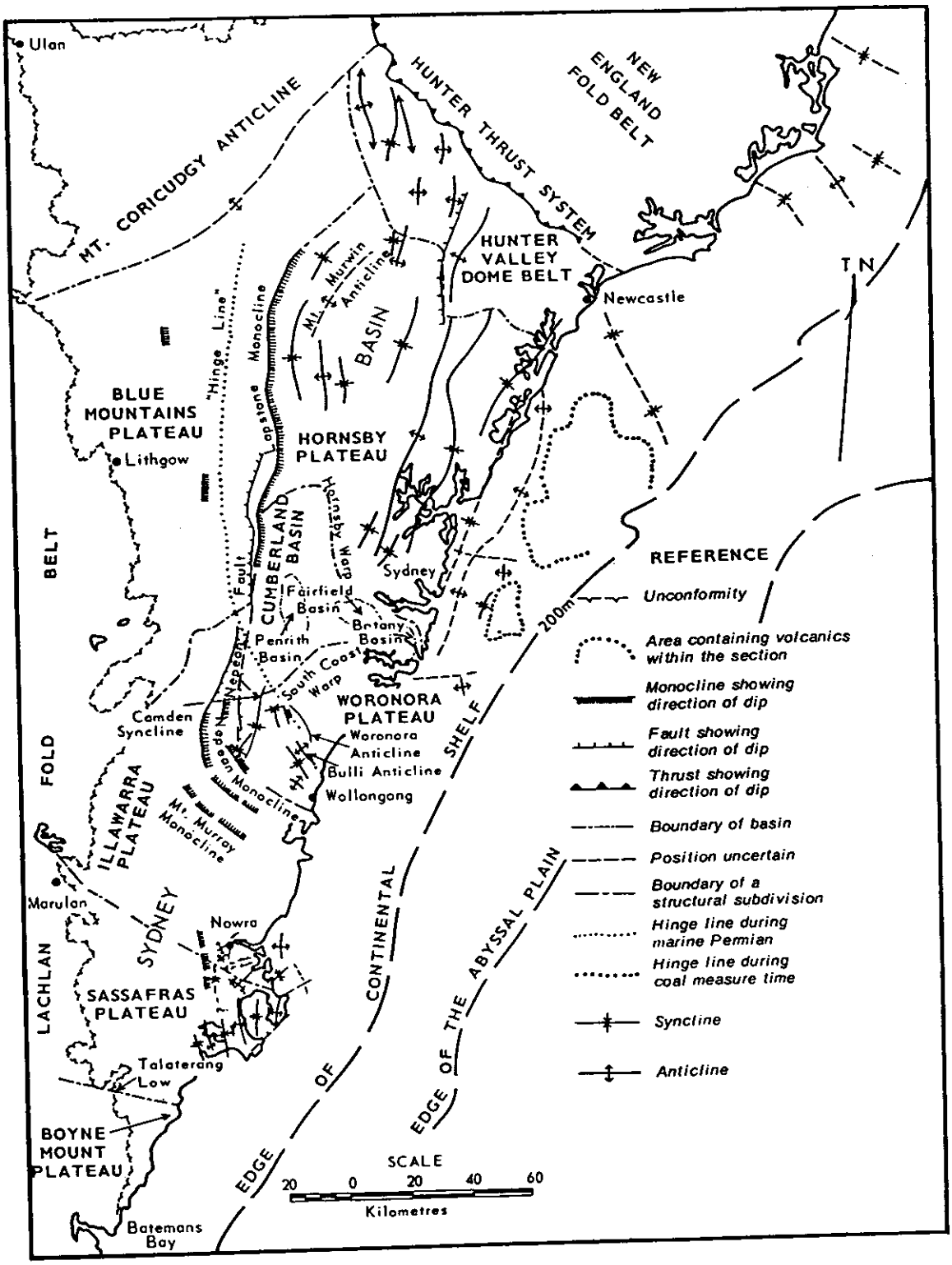

Fig 1-5 Structure subdivision of the Sydney Basin.
(After Bembrick and Lonergan, 1976)

northeastern part of the basin. It is bounded by the Hunter Thrust to the northeast, and by a less distinctive basement fault - possibly a thrust - to the southwest (Fig 1-5). The basement fault is parallel to the escarpment of Triassic rocks, which forms the southern side of the Hunter Valley. The dome belt is characterised by a series of approximately north-trending folds of varying amplitudes, of which the Lochinvar Anticline and the Muswellbrook Anticline are the most prominent. Two distinctive sets of faults exist in the dome belt. The first set of faults are parallel to the Hunter Thrust System. The other set of faults trend north-south and are associated with folding. They are predominantly normal faults with displacement of up to 300 m (Mayne et al., 1974).

The Blue Mountains Plateau lies in the western part of the Sydney Basin. It is bounded to the north by the Mount Coricudgy Anticline and the basement fault mentioned above. To the east the Lapstone Monocline-Nepean Fault complex forms the boundary. The western boundary is a regional unconformity along the edge of the Sydney Basin. To the south, the plateau merges with the Illawarra Plateau.

The Illawarra Plateau lies south of the Blue Mountains Plateau. It is bounded to the northeast by the Nepean Fault and associated minor faults, and then by the Nepean Monocline and its projection to the coast south of Wollongong (Fig 1-5). To the south, a basement low, which is a Carboniferous to Early Permian river channel, is taken as the boundary with the Sasafras Plateau. To the west, the plateau is bounded by a regional unconformity along the edge of the Sydney Basin.

The Sassafras Plateau lies south of the Illawarra Plateau and is also delineated on the west by the regional unconformity. To the south, it is separated from the Boyne Mount Plateau by the east-west oriented Talaterang Low (McElroy and Rose, 1962), in which sudden thickening of Permian sediments has been observed (Fig

1-5). The thick sequence indicates the existence of some sort of basement discontinuity. The presence of the Milton Monzonite along the Talaterang Low further supports this idea.

The Boyne Mount Plateau lies immediately south of the Sassafras Plateau. It is the southernmost structural subdivision of the Sydney Basin. The regional unconformity forms its southwestern boundary (Fig 1-5).

The Hornsby Plateau lies south of the Hunter Valley Dome Belt and east of the Blue Mountains Plateau (Fig 1-5). To the south, it is separated from the Cumberland Basin by the Hornsby Warp. Large scale low amplitude, north-north-easterly trending folds are present over most of the plateau.

The Woronora Plateau lies northeast of the Illawarra Plateau. To the north, it is separated from the Cumberland Basin by the South Coast Warp. The boundary with the Illawarra Plateau is well defined as a series of tensional structures, which are reflected in variations of sedimentary facies and thickness. The Camden Syncline is the most prominent structure in the Woronora Plateau. The Bulli Anticline and its north-westerly bifurcation, the Woronora Anticline (Fig 1-5), are the most significant structures related to the deposition. However, the whole area within the plateau is gently deformed.

The Cumberland Basin is the only secondary structural low recognised in the Sydney Basin. As shown in Fig 1-5, it lies east of the Lapstone Monocline and is bounded by the Hornsby Warp to the north, and by the South Coast Warp to the south. The axis of the Cumberland Basin is considered to be identical with that of the Sydney Basin, further lower category structural lows such as the Penrith, Fairfield and Botany Basins are also recognised. They are located in an undistinctive trough (Bryan et al., 1967).

Bembrick et al. (1973, 1980) and Bembrick and Lonergan (1976) did not mention when and how these lower category structural units developed. However, Mayne et al. (1974) made a brief discussion of the timing for prominent structures in the basin in their review of Sydney Basin geology. According to them, most of the folding and faulting of the two prominent Lochinvar and Muswellbrook Anticlines and other structures in the Hunter Valley Dome Belt developed during the Tatarian (late Permian) and all other prominent structures in the basin formed during the Late Tertiary Kosciusko Uplift of the eastern Australia. The uplift led to the development of the Blue Mountains, Hornsby and Woronora Plateaus and the Cumberland Basin. However, recent studies (e.g. Schmidt and Embleton, 1981, Middleton and Schmidt, 1982) and fission track analyses of basement apatites between Wollongong and Melbourne (Moore et al., 1986) and this study (see Chapter 7) all indicate thermal uplift and erosion in the mid Cretaceous just prior to the onset of Tasman Sea spreading. This uplift must have contributed to the development of lower category structural units in the basin to some extent. In his discussion of eastern highlands of Australia, Wellman (1987) proposed that the tectonic uplift of the highlands took place throughout the late Cretaceous and Cainozoic. This implies that the uplift initiated at mid Cretaceous probably persisted throughout this period in plateau areas of the basin. Thus, the lower category structural units in the basin was most likely to have developed from mid Cretaceous to late Cainozoic.

CHAPTER TWO

SANDSTONE DIAGENESIS REVIEW

2.1 INTRODUCTION

The term "diagenesis" was first introduced to geological literature by Von Guembels in 1868 (Chilingarian, 1983). However, it did not receive much attention until the 1950's and it is only recently that it has been discussed in much more detail. Following the book edited by Larsen and Chilingar (1967), which summarised the previous work on diagenesis, a number of monographs on diagenesis have been published. Among them, "Diagenesis in Sediments and Sedimentary Rocks" by Larsen and Chilingar (1979a, 1983), "Aspects of Diagenesis" by Scholle and Schluger (1979), "Sediment Diagenesis" by Parker and Sellwood (1983), "Clastic Diagenesis" by McDonald and Surdam (1984), "Roles of Organic matter in Sediment diagenesis" by Gautier (1986), and "Diagenesis of sedimentary sequence" by Marshall (1987) are the most important.

Diagenesis is defined as all the processes that begin to operate from the moment of sediment deposition and cease at the moment when solid rocks go into the realms of metamorphism or weathering (Larsen and Chilingar, 1979b). But not everyone agrees with this definition. Some authors (e.g. Chilingarian, 1983) define it as the processes that turn sediments into solid rocks and exclude the later processes from diagenesis. A more detailed discussion of this topic was made by Larsen and Chilingar (1979b). Authigenesis is one aspect of diagenesis. It refers to the formation of new or secondary minerals within enclosing sediments or sedimentary rocks (Fairbridge, 1983).

The classification of diagenesis into several phases by Russian authors was quite confusing in the 1950's and 1960's. This resulted in different schemes by different authors and different meaning of the same term introduced by different authors. Larsen and Chilingar (1979b) quoted a summary of different classification by

Soviet authors by Vassoevich (1971, p.14) in which classifications were discussed. They also mentioned a quite confusing term "metagenesis" in Soviet literature. According to them, the term was almost simultaneously introduced to literature in three different published works in 1957. However, the definition of the term was quite different. "Vassoevich (1957), in using it, referred to metamorphism, whereas A.G. Kossovslaya, N.V. Logvinenko and V.D. Shutovc in Vassoevich (1971, p.14) defined metagenesis as early metamorphism prior to regional metamorphism. Strakhav (1957 in Vassoevich 1971, p.14) agreed with the later authors as far as the lower boundary of metamorphism is concerned, but included catagenesis in this term." (Larsen and Chilingar, 1979b, p.5)

In the English speaking world, the subdivision of diagenesis is generally consistent. Fairbridge (1967) classified diagenesis into three phases: syndiagenesis, anadiagenesis, and epidiagenesis. Syndiagenesis includes the initial stage and the biological activity. Anadiagenesis includes the compaction and maturation stages of diagenesis and it is characterised by long duration. Epidiagenesis is not undergone by solid rocks in every sedimentary basin. In some sedimentary basins, the strata are uplifted to the surface and exposed to the ground water zone (fresh water). This phase is the so called epidiagenesis.

In their study of carbonate porosity, Choquette and Pray (1970) proposed three diagenetic stages: eogenesis (early), mesogenesis (middle), and telogenesis (late). The three stages are slightly different from those of Fairbridge (1967) in emphasising the temporal sequence. Schmidt and McDonald (1979a) thought that the classification scheme by Choquette and Pray (1970) was appropriate for study of secondary porosity in sandstones and so they adopted the scheme. Eodiagenesis takes place at or near the surface and it is characterised by the surface environment controlling the properties of interstitial fluids prior to effective burial (the burial under strata which shields the sediment from the impact from the surface environment and thus the chemistry of interstitial fluids is not controlled by

it.). Mesodiagenesis is defined as the subsurface regime under effective burial. Telodiagenesis is the regime at or near the surface after effective burial when the rocks have been exposed. The scheme of Choquette and Pray (1970) was used by Kantorowicz (1985) in his case study of diagenesis of Middle Jurassic sediments, Ravenscar Group, Yorkshire (U.K.).

There are other classification schemes (e.g. Bjørlykke, 1983) which do not take the last stage of Schmidt and McDonald (1979a) into account. Bjørlykke subdivided the diagenetic reactions in sandstones into only two stages: early diagenesis and burial diagenesis. In this scheme, the burial depth is taken as the major factor defining diagenetic stages. By comparing the scheme with the one by Schmidt and McDonald (1979a), it can be found that the early diagenesis of Bjørlykke generally corresponds to the eodiagenesis, and that the burial diagenesis to the mesodiagenesis. Therefore, no significant difference exists between the two schemes except for the lack of counterpart for the last stage – telodiagenesis of Schmidt and McDonald's scheme in Bjørlykke's scheme.

2.2 FACTORS AFFECTING SANDSTONE DIAGENESIS

There are a number of factors affecting sandstone diagenesis depending on the history of the sedimentary basin. The five most important are described below.

2.2.1 PORE WATER CHEMISTRY

The influences of pore water chemistry on sandstone diagenesis have been discussed by a number of authors. They include Almon et al. (1976), Davies et al. (1979), Bjørlykke (1983), Burley (1984), and Kantorowicz (1985).

In their study area, Almon et al. (1976) found two distinct cement assemblages: corrensite ± calcite ± dolomite and montmorillonite ± calcite. They recognised three characteristic features in the cements: (1) The former assemblage is only found in

samples from delta distributary channel and distributary mouth bar environments while the latter assemblage occurs only in samples from bay-beach, crevasse splay, lagoon, barrier island and shallow subtidal environments. (2) Each assemblage is uniminerallic with regard to clay minerals. (3) The corrensite and the montmorillonite are mutually exclusive. All the evidence supports the conclusion that the formation of authigenic clay minerals was controlled by original pore fluid chemistry.

Davies et al. (1979) considered the pore water chemistry to be the most important control on diagenesis of Tertiary-Holocene volcaniclastics in their case study. The formation of three successive cements, haematite-geothite; montmorillonite plus haematite; montmorillonite plus heulandite, was mainly controlled by pore water chemistry.

Bjørlykke (1983) contributed a general discussion of the initial pore water chemistry and cement precipitation in different types of pore water. He divided initial pore water into three different types: sea water, evaporitic water and meteoric water. Sea water is present in marine environment and it is characterised by constant composition. Upward moving pore sea water due to compaction precipitates carbonates, iron and manganese oxides. Of them, carbonates are the most important. In addition, pyrite, iron-rich chlorite and glauconite may also precipitate from sea water. In suitable conditions, silica can also be precipitated as a less stable phase and later change to quartz.

Evaporitic pore water occurs in both marine and continental evaporitic basins. It is characterised by high concentrations of ions. In addition to carbonates and sulphates, zeolites are common early diagenetic minerals in this environment. Furthermore, the special conditions of the environment stabilise the smectite. In the vadose zone of arid environments, early calcite and also iron and manganese oxides are common cements.

Meteoric water occurs in continental environments. It is characterised by low ion concentration and variable pH values. It is initially undersaturated with respect to most minerals. However, as it leaches unstable particles, it becomes saturated with some minerals such as gypsum and carbonates and precipitates them. Silica, illite, montmorillonite, and kaolinite can be produced by dissolution of feldspar and other silicate minerals.

Burley (1984) thought the overall chemistry of the near-surface pore waters and the interaction of unstable minerals with the pore waters largely controlled the eodiagenetic minerals of the Sherwood Sandstone Group, a conclusion supported by Kantorowicz (1985). According to Kantorowicz, during the eodiagenetic stage quartz overgrowths and vermiform kaolinites were precipitated in sandstones with oxygenated and mildly acidic pore water while chlorites and quartz overgrowths were restricted to sandstones with anoxic and neutral pore water in the Middle Jurassic Ravenscar Group of Yorkshire (U.K.).

All the discussions made above show that pore water chemistry has an effect on sandstone diagenesis. However, due to the complexity of pore water chemistry, the influence of pore water chemistry on sandstone diagenesis is not the same at different areas. In addition, the chemistry changes with time.

2.2.2 DETRITAL MINERALOGY

(i) Volcanic Lithic Sandstone

Clearly, detrital minerals affect sandstone diagenesis. A number of papers on diagenesis of volcanic lithic sandstones have been published (e.g. Galloway, 1974, 1979; Davies et al., 1979; Surdam and Boles, 1979). Galloway (1974) indicated that the formation of calcite cement is the common reaction in volcanic lithic sandstone. During diagenesis, the unstable particles such as pyroxene and volcanic glass are dissolved and thus pore water chemistry is changed (Davies et

al., 1979). In regard to the porosity characteristics of the volcanic lithic sandstone, Surdam and Boles (1979) concluded that the diagenesis of volcanic glass and volcanic rock fragments can greatly reduce or even completely destroy the original primary porosity, but later diagenesis may create secondary porosity through dissolution of unstable components.

(ii) Feldspathic Sandstone

The most characteristic feature of diagenesis in feldspathic sandstones is the dissolution of feldspars and the replacement of them by clay minerals and / or carbonates. In very acidic environments (pH < 5), the rate of feldspar dissolution is determined by activity of hydrogen ions whereas it is independent of pH when pH value is more than 5 (Bjørlykke, 1983). Feldspars are stable in basic solutions of high alkali and silica concentrations. The alteration of feldspars to clay minerals was described by Hawkins (1978). According to him, kaolinite replaced feldspars in coarse grained sandstones whereas illite replaced feldspars in fine grained sandstones in Upper Carboniferous sandstones in Bothamasall Oilfield (U.K.).

(iii) Quartzose Sandstone

Quartzose sandstones are stable and simple in terms of their detrital compositions. Thus their diagenesis is relatively simple compared with that of feldspathic and volcanic lithic sandstones. Schmidt and McDonald (1979a) described a number of models of quartzose sandstone diagenesis from a purely theoretical viewpoint. The model is a function of the source of silica cement, the type of carbonate cement and the content of detrital carbonate fragments. The most common features of quartzose sandstone diagenesis are pressure solution and quartz overgrowth. Authigenic clay minerals and / or carbonates may also be precipitated in quartzose sandstones.

2.2.3 DEPOSITIONAL ENVIRONMENT

Depositional environment controls initial pore water chemistry and detrital

mineralogy composition of sandstones to a certain extent. Therefore it must have an influence on sandstone diagenesis. It is only during early diagenesis that it greatly affects diagenesis (Fuchtbauer, 1983). Since the role of initial pore water in sandstone diagenesis has been discussed above, a discussion of depositional environments on sandstone diagenesis is omitted here. A comprehensive discussion of the topic was made by Fuchtbauer (1983).

2.2.4 HEAT FLOW (TEMPERATURE)

The influence of temperature on sandstone diagenesis has been discussed by a number of authors (e.g. Galloway, 1974, 1979; Bjørlykke, 1983; Loucks et al., 1984). Bjørlykke (1983) summarised the impact of temperature on sandstone diagenesis in four ways: (1) temperature affects the solubilities of minerals; (2) the effect of hydration of ions will be reduced by increasing temperature so that the ions such as Fe^{2+}, Mg^{2+} which are easily hydrated at surface temperature are more available to get into mineral phases; (3) increasing temperature makes hydrous minerals (e.g. montmorillonite and kaolinite) become unstable and transform to less hydrous mineral phases. This process also releases water; (4) pore water will expand with increasing temperature so that fluid pressure will increase if the pore fluid cannot escape.

Based on his study of diagenesis of sandstones in northwest Pacific arc-related basins, Galloway (1974, 1979) concluded that temperature had a great impact on diagenesis of some sandstone suits. Therefore, the preservation of porosity in these sandstones was mainly controlled by temperature. The correlation between temperature and porosity was also shown by Loucks et al. (1984) in their study of diagenesis of lower Tertiary sandstones along the Texas Gulf Coast. In the Wilcox Group and Frio Formation, porosity decreases with increasing temperature. This relationship is not only shown in a vertical profile but also more significantly in an areal sense: at the same burial depth, the sandstones in the inland area with a

higher temperature have a lower porosity than those in the area along the coast with a lower temperature.

A discussion of the paleothermometry of the Sydney Basin has been made by Schmidt and Elmleton (1981) and Middleton and Schmidt (1982). Schmidt and Elmleton (1981) concluded with confidence that the rocks present at the surface throughout much of the coastal areas of the Sydney Basin were elevated to temperatures of at least 100 ° to 200 °C at some time prior to 80 m.y. This conclusion was supported by Middleton and Schmidt (1982) based on overprinting of magnetisations of Upper Permian and Mesozoic rocks and the rank of Permian Coals and Mesozoic phystoclasts (coal particles). They proposed that the rocks exposed at the surface of the Sydney Basin might have been raised to temperatures of 200 °C or even higher. Both Schmidt and Embleton (1981) and Middleton and Schmidt (1982) attributed the high temperatures to a thick sediment sequence, which overlay the current surface rocks and was later eroded away. A sediment sequence with a thickness of between 1 and 2 km was regionally lost and locally a 3 km thick sediment sequence was probably lost (Middleton and Schmidt, 1982). However, this conclusion was disputed by Branagan (1983). He thought that the evidence for a thick cover, which was eroded away, was poor. The thickness of sediments eroded was much less than 1 km. He attributed the high vitrinite reflectance to heat flow resulting from volcanic intrusion rather than deep burial. The heat flow history model of the basin will be discussed in detail in Chapter 7.

2.2.5 PRESSURE

The solid rocks at subsurface undergo pressure from overburden materials. This pressure is called confining pressure (P_o) (North, 1985). It comprises the fluid pressure (P_f) and the effective pressure or grain to grain pressure (∂p). The effective pressure can be expressed in the following formula:

$$\partial p = P_o - P_f \text{ (North, 1985, p.219)}$$

Obviously it is the effective pressure that controls the mechanical deformation and pressure solution. The influence of the effective pressure on sandstone diagenesis is shown by the Brent Sandstone of Viking Graben in the North Sea (Chiarelli and Duffaud, 1980). They showed that the sandstone, now at 2.5-3.0 km, was in an overpressure zone (where the fluid pressure is more than the normal hydrostatic pressure) and remained loose and friable.

In addition to the factors discussed above: pore water chemistry, detrital mineralogy, depositional environment, heat flow, and pressure, there are several other factors affecting sandstone diagenesis such as texture, tectonics, and subsidence history and rate. The texture factor was discussed by Fuchtbauer (1983) and Stonecipher et al. (1984) and the latter factors by Bjørlykke (1983). However, these factors are generally less important than the ones mentioned above.

2.3 POROSITY

2.3.1 GENERAL STATEMENT

Porosity is defined as the ratio of pore space to the total rock volume and it is usually expressed as a percentage. It includes two types: effective and absolute porosity. The former is the percentage of inter-connected pore space in the total rock volume. The latter is the percentage of total pore space in the total rock volume. The porosity can be primary, secondary or a combination of the two. Primary porosity is that which the rock possesses at the end of its depositional phase. Secondary porosity is additional void space due to post-depositional or diagenetic processes.

2.3.2 POROSITY REDUCTION

Hayes (1979) classified porosity reduction processes into three types: (1) chemical (cementation, replacement and recrystallisation), (2) mechanical (compaction by deformation and fracture of detrital grains), and (3) combination of the above (alteration of a detrital grain accompanied by compaction). Bjørlykke (1983) thought there were four processes responsible for porosity reduction. They were (1) mechanical compaction of the grains, (2) precipitation of cement in the primary pore space, (3) mineral reaction forming expanded hydrous minerals, and (4) pressure solution. The two schemes are similar. The (2) and (3) of Bjørlykke can be classified into (1) of Hayes. The (1) and (4) of Bjørlykke correspond to the (2) and (3) of Hayes respectively.

Cementation is obviously a porosity reduction process. A lot of minerals have been noted as cements in sandstones. A summary of these minerals was made by Hayes (1979, p.128). Mechanical compaction includes particle rearrangement, plastic deformation and particle breakage. Chilingarian (1983) had a lengthy discussion of this topic. Biotite alteration and pressure solution belong to the combination of chemical and mechanical porosity reduction processes (Hayes, 1979).

2.3.3 POROSITY ENHANCEMENT (SECONDARY POROSITY)

Although several processes reduce porosity or even completely destroy it, sandstones at deep burial may still have a quite high porosity. The porosity is either a combination of primary and secondary or nearly totally secondary. In fact, the high porosity of many oil reservoirs results from the formation of secondary porosity (Hayes, 1979).

Secondary porosity may occur in any sandstone of Phanerozoic age (Schmidt and McDonald, 1979a). Its recognition was a great advance in the study of sandstone diagenesis. A discussion of secondary porosity in sandstones was already made in the literature quite a long time ago such as Phipps (1969), Morgan and Gordon

(1970), and Heald and Larese (1973). Recently numerous articles have been published on this topic. They mainly deal with the origin and recognition of secondary porosity in a general sense (e.g. Hayes, 1979; Schmidt and McDonald, 1979a, b; Bjørlykke, 1983, 1984; Surdam et al., 1984) and the formation and recognition of secondary porosity in a particular formation in a sedimentary basin (e.g. Lindquist, 1977; McBride, 1977; Boles, 1984; Crossey et al., 1984; Moncure et al., 1984).

Of the criteria for recognition of secondary porosity in thin sections proposed by these authors, those proposed by Schmidt and McDonald (1979b), are perhaps the most complete and valuable. These useful criteria include (1) partial solution, (2) moulds, (3) inhomogeneity of packing, (4) oversized pores, (5) elongate pores, (6) corroded grains, (7) intra-constituent pores, and (8) fractured grains. The origin of secondary porosity was attributed by Schmidt and McDonald (1979b) to five different processes. They are (1) fracturing , (2) shrinkage, (3) dissolution of sedimentary grains and matrix, (4) dissolution of authigenic pore-filling cement, and (5) dissolution of authigenic replacive minerals. Of them, dissolution is the most important process.

The formation of secondary porosity was also discussed by Surdam et al. (1984) and Bjørlykke (1984). The former mainly discussed the secondary porosity from chemical viewpoints. Like Schmidt and McDonald (1979b), Bjørlykke also considered dissolution as the major process of porosity enhancement. In the dissolution process CO_2 plays a very important role. Unstable particles are dissolved by meteoric water at initial burial or by formation water rich in CO_2 at deeper burial. But according to Bjørlykke, CO_2, which is released from decarboxylation of kerogen at deeper burial, is not enough to produce the observed leaching of feldspar and carbonates in some sedimentary basins. Thus he proposed two alternative processes to explain large scale leaching of carbonates and feldspars. One is the clay reactions including the transformation of

kaolinite and smectite to illite releasing H^+ and the other is the reactions between clay and carbonates releasing CO_2.

The dissolution process generally creates the majority of secondary porosity. It can take place both at shallow depth and at deep burial. However, Schmidt and McDonald (1979a, b) discounted the shallow dissolution process by meteoric water rich in CO_2 as being important. Their interpretation that the secondary porosity in the Jurassic Brent sandstones of the North Sea resulted from later formed CO_2 by kerogen maturation was challenged by Bjørlykke et al. (1979) who interpreted that the leaching process, which may have taken place early, was responsible for the formation of secondary porosity in these sandstones.

2.4 PERMEABILITY

It is defined as the property of a medium of allowing fluids to pass through it without change in the structure of the medium or displacement of its parts (North, 1985, p.121). Porosity and permeability comprise the two most important criteria for measuring the quality of oil reservoirs.

Factors affecting permeability may be different from those affecting porosity. For example, a few percent of authigenic clay minerals can greatly reduce permeability of a sandstone but it has little influence on porosity (Almon and Davies, 1979). Thus permeability does not have a definite relationship with porosity. However, higher permeability generally corresponds to higher porosity in sandstones. Permeability and porosity data from the Wilcox Group of the Gulf Coast shows that permeability generally increases with porosity (Loucks et al., 1984). This is also the case for the Narrabeen Group sandstones (see Chapter 8).

CHAPTER THREE

STUDY AIMS, DATA BASE AND METHODOLOGY

3.1 STUDY AIMS

The main aims of this study are to discuss petrology and diagenesis of the Narrabeen Group sandstones and to assess the potential of these sandstones as hydrocarbon reservoirs. More specifically, they can be stated as seven points.

1) Basic facies analyses of the Narrabeen Group based on the geological logging and available geophysical logs.

2) Quantitative analyses of petrology of the Narrabeen Group sandstones in the whole Sydney Basin to establish compositional variations of these sandstones vertically from the bottom to the top of the group and regionally across the basin, and to deduce the detrital sources for the sediments.

3) Identification of authigenic minerals, establishment of paragenetic sequence for authigenic minerals and discussion of diagenetic history.

4) Stable isotope (oxygen, carbon and deuterium) analyses of diagenetic clays, carbonates and quartz overgrowths, and potassium / argon age dating of authigenic illites in the Narrabeen Group sandstones to constrain temperature and pore water chemistry.

5) Homogenisation temperature and ice melting point temperature measurements of aqueous fluid inclusions within quartz overgrowths to constrain formation temperatures of quartz overgrowths, to deduce heat flow history, and to carry out kinetic chemical modelling of hydrocarbon generation.

6) Combining petrological observation data with stable isotope and fluid inclusion

data to construct pore fluid chemical evolution with time and temperature.

7) Laboratory measurement of porosity and permeability of selected sandstones of the Narrabeen Group. Integrating these data with all other data to discuss the potential of the Narrabeen Group sandstones as hydrocarbon reservoirs.

3.2 DATA BASE

In the Sydney Basin there are plenty of boreholes from coal and petroleum exploration activities. For the current study, 26 boreholes (represented by 26 capital letters, Table 3-1) are selected. They were selected to allow study of both the regional and local variation in the basin (Boreholes K and V are in the adjacent Gunnedah Basin but near the border of the two basins) (Fig 3-1).

Detailed 1:100 geological logging of 7648.5 meters of cores from the 26 boreholes, which cover an area of about 80 km x 240 km, was made. The logging includes detailed basic lithological description and sedimentological analyses (colour, grain size estimation, sedimentary structure, upper and lower contacts, vertical texture profile and a preliminary interpretation of the genetic facies associations). It forms the major basis for selecting sandstone samples used in various laboratory studies and facies interpretation. The interval logged in each borehole is listed in Table 3-1.

Based on the geological logging, a total of 417 sandstone samples were collected for detailed analyses. The sampling principle was to take samples from every significant change of sandstone lithology. Samples vary from very fine sandstones to very coarse sandstones. The sampling interval is about 15-20 meters. However, more samples were selected from relatively porous sandstone intervals of Boreholes W and X. The sample taken from the drill core is about 8 cm long, which supplies enough materials for thin section, SEM/EDX, XRD, microprobe, isotope, fluid inclusion studies and porosity and permeability measurements. Sample no. is

Table 3-1 List of boreholes used in this project, their symbols, position (latitude and longitude), elevation relative to sea level, and interval logged in each borehole.

Symbol	Borehole Name	Latitude	Longitude	Elevation to Sea Level (m)	Logging Interval (m)
A*	DM Wollongong 45	34°16'55"	150°51'13"	308.00	110.00 – 366.80
B*	Coal Cliff DDH 17	34°11'00"	151°02'25"	217.32	85.00 – 418.00
C*	Coal Cliff DDH 13	34°13'29"	150°59'49"	187.80	13.00 – 269.00
D	DM Jilliby CK DDH 1	33°06'	151°21'	51.82	40.00 – 308.00
E	DM Brush CK DDH 1	33°09'	151°16'	41.12	98.00 – 397.00
F	DM Murrays Run DDH 1	33°06'	151°11'	134.51	40.00 – 759.00
G	AOG Higher MacDonald 1	33°13'	150°56'	17.70	533.50 – 600.00
H*	MIH ST Albans DDH 1	33°21'27"	150°58'39"	7.62	304.00 – 710.00
I	NW Oil Longley DDH 1	33°21'	151°17'	276.70	294.00 – 905.00
J*	DM Cape Banks DDH 1	33°59'26"	151°14'59"	21.50	448.40 – 688.00
K	DM Doyles CK DDH 10	32°16'	150°38"	140.00	23.00 – 120.00
L*	DM Liverpool DDH 91	33°59'59"	150°59'47"	85.00	260.00 – 765 .00
M	Stevens Cape Three Pts	33°29'	151°26'	67.00	91.50 – 609.70
N*	Armco Illawarra DDH 8	34°37'46"	150°32'1"	701.12	152.00 – 201.00
O	South Colah DDH 1	n.a.	n.a.	147.00	278.00 – 760.00
P*	Moonshine DDH 9	34°14'07"	150°40'10"	208.79	420.00 – 470.00
Q	Victoria Park 1	n.a.	n.a.	n.a.	415.00 – 462.50
R*	DM Never Never DDH 1	32°45'52"	150°14'47"	n.a.	3.00 – 128.00
S	DM Howes Valley DDH	32°52'	150°48'	155.92	446.00 – 657.00

Symbol	Borehole Name	Latitude	Longitude	Elevation to Sea Level (m)	Logging Interval (m)
T*	Wancol Mt Tomah DDH 1	33°29'21"	150°29'02"	460.00	307.70 – 449.00
U*	DM Coolamin DDH 1	32°52'10"	151°04'38"	99.50	112.00 – 371.00
V	DM Doyles CK DDH 4	32°32'	150°56'	177.10	9.00 – 68.00
W*	Weromba 2	33°59'47"	150°33'25"	301.00	175.00 – 534.50
X*	Cobbitty 3	34°00'15"	150°39'01"	78.70	273.50 – 692.60
Y*	Campbelltown 5	34°01'14"	150°45'31"	94.80	343.00 – 778.00
Z*	Campbelltown 2	34°03'43"	150°47'07"	121.80	340.00 – 776.00

* Latitude and longitude are converted from co-ordinates in the ISG grid.
n.a. = not available.

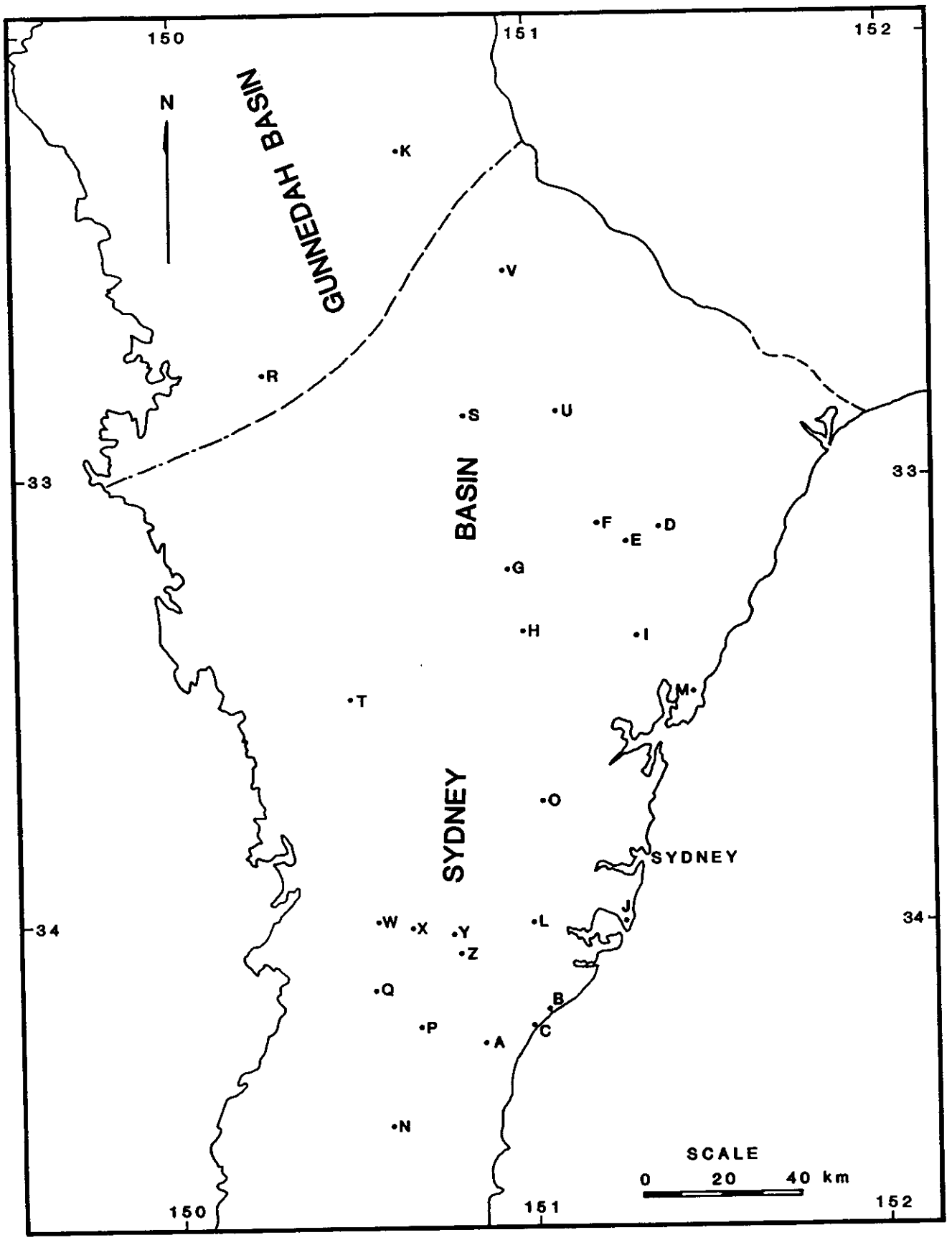

Fig 3-1 Locations of boreholes used in this study.
(Modified from Galloway and Hamilton, 1988)

named by the borehole letter and then drilling depth (in meters) at which the sample was selected. For example, X531.9 means that the sample is from Borehole X (Cobbitty 3) at a drilling depth of 531.9 m.

Thin sections were cut for all the 417 sandstone samples and examined under a petrological microscope. Of the 417 samples, 324 were selected for quantitative evaluation of composition and visible porosity (point counting), 167 for SEM/EDX examinations, 63 for XRD studies, 20 for microprobe analyses, 9 for isotope measurements, 4 for fluid inclusion investigations, and 175 for porosity and permeability measurements. The majority of the samples subject to SEM/EDX examinations and / or porosity and permeability measurements are from the 324 samples which underwent point counting. The samples studied by XRD and / or microprobe were selected from the 167 samples examined under the SEM/EDX. The 9 samples for isotope measurements were chosen from those subject to both point counting and SEM/EDX examinations. The 4 samples for fluid inclusion investigations were selected from these 9 samples. The samples used in this project, together with a list of the analyses performed, are presented in Appendix I.

Geophysical data are also available for the study. They are wireline logs, which include spontaneous potential, conventional resistivity, gamma ray and neutron logs with the latter two being more useful. For the current study these wireline logs are used to confine the geological logging and aid facies analyses.

3.3 METHODOLOGY

Bjørlykke (1983) made a summary of the principal means used in the study of sandstone diagenesis. They include the petrologic microscope, the porecast, the scanning electron microscopy (SEM), the microprobe, cathodoluminescence, X-ray diffraction (XRD), and stable isotope. The petrological microscope is still the most useful tool in the study of sandstone diagenesis. SEM has become the most useful tool in delineating the delicate features of sandstones (e.g. microporosity and

authigenic clay minerals). XRD is of much value in correctly identifying clay minerals and semi-quantitatively studying them.

In this project, a number of techniques are used. They range from the petrological microscope to the more recently developed technique - stable isotope / K-Ar age dating of illite and fluid inclusion investigations. In addition to these, other techniques include X-ray diffraction (XRD), scanning electron microscope (SEM) and energy dispersive X-ray analyses (EDX), microprobe, and porosity and permeability measurement.

Sample preparation and methodology for each of these techniques will be described in the relevant chapter, Namely, Chapter 5 - petrological microscope studies, Chapter 6 - SEM/EDX, XRD and microprobe analyses, Chapter 7 - isotope geochemistry analyses and fluid inclusion investigations, and Chapter 8 - porosity and permeability measurements.

CHAPTER FOUR

STRATIGRAPHIC UNITS AND FACIES ANALYSES OF THE NARRABEEN GROUP

4.1 STRATIGRAPHIC UNITS

A complex variety of lithological and paleoenvironmental facies within the Narrabeen Group have resulted in a complex and bewildering stratigraphic nomenclature for the group (Herbert, 1980a). In different areas of the basin, different nomenclatures were proposed (see Fig 1-4). In their recent Sydney Basin reservoir studies, Galloway and Hamilton (1988) established a new subdivision scheme for the Narrabeen Group. Using neutron and gamma ray geophysical logs, they subdivided this group (excluding Garie and Newport Formations) into five operational units: Wombarra (WO), Scarborough (SC), Lower Bulgo (LB), Upper Bulgo (UB), and Bald Hill (BH) Operational Units (Fig 4-1). Each unit is defined by characteristic depositional style and geophysical log pattern (Fig 4-2). The boundaries of the units are marked by the characteristic peaks or lows in the neutron and gamma ray logs. The defined operational units can be regarded as time - stratigraphic units (Galloway and Hamilton, 1988). Their correlation with the conventional stratigraphic units introduced by previous researchers is shown in Fig 4-3. This subdivision scheme is followed in this thesis for its nomenclature consistence throughout the basin. Petrology and reservoir potential of the Narrabeen Group sandstones will be described under this stratigraphic subdivision framework. The following description of the five operational units is summarised from Hamilton et al. (1987) and Galloway and Hamilton (1988).

4.1.1 WOMBARRA OPERATIONAL UNIT

This operational unit is the lowermost part of the Narrabeen Group and conformably overlies the Permian Coal Measures. In the geophysical logs, the base of the unit is marked by a strong low on both the gamma ray and neutron logs (Fig 4-1). In bore cores, it was recognised by the sudden absence of coal seams from the Permian Coal Measures to the Narrabeen group. The informally known

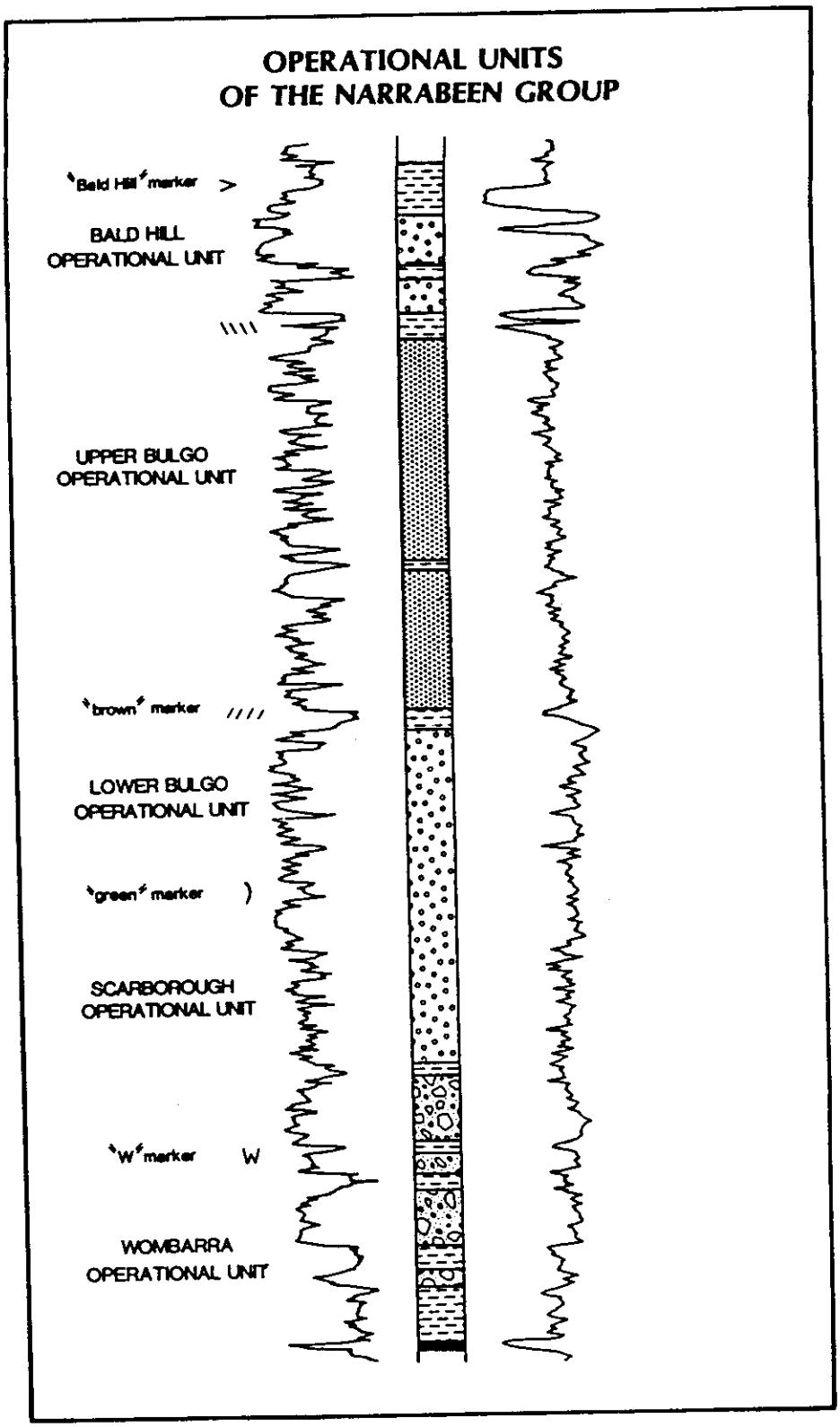

Fig 4-1 Operational units and their bounding correlation markers for the Narrabeen Group. The left hand log is Gamma Ray and the right hand log is Neutron. (After Galloway and Hamilton, 1988)

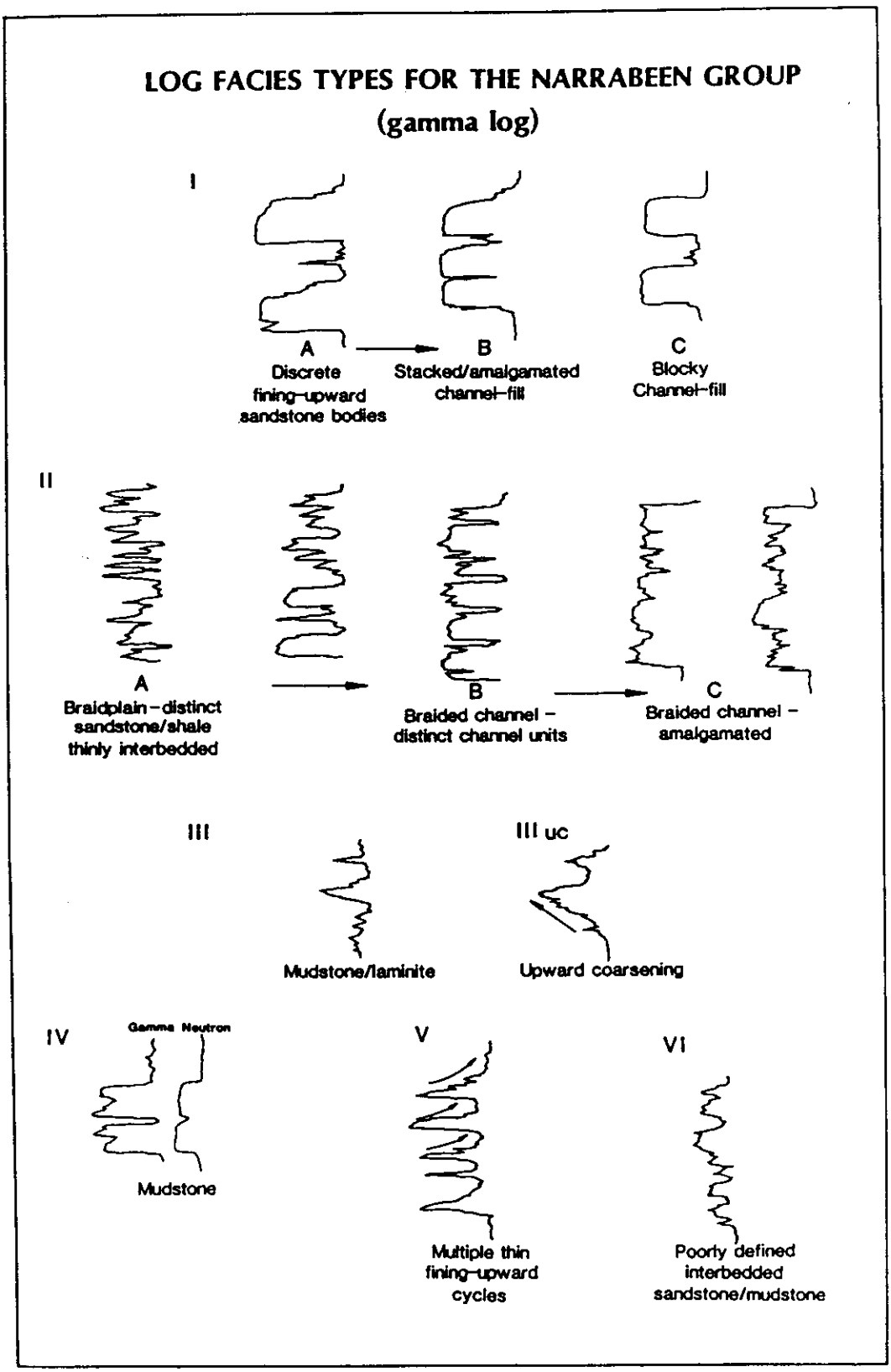

Fig 4-2 Log facies types for the Narrabeen Group.
(After Galloway and Hamilton, 1988)

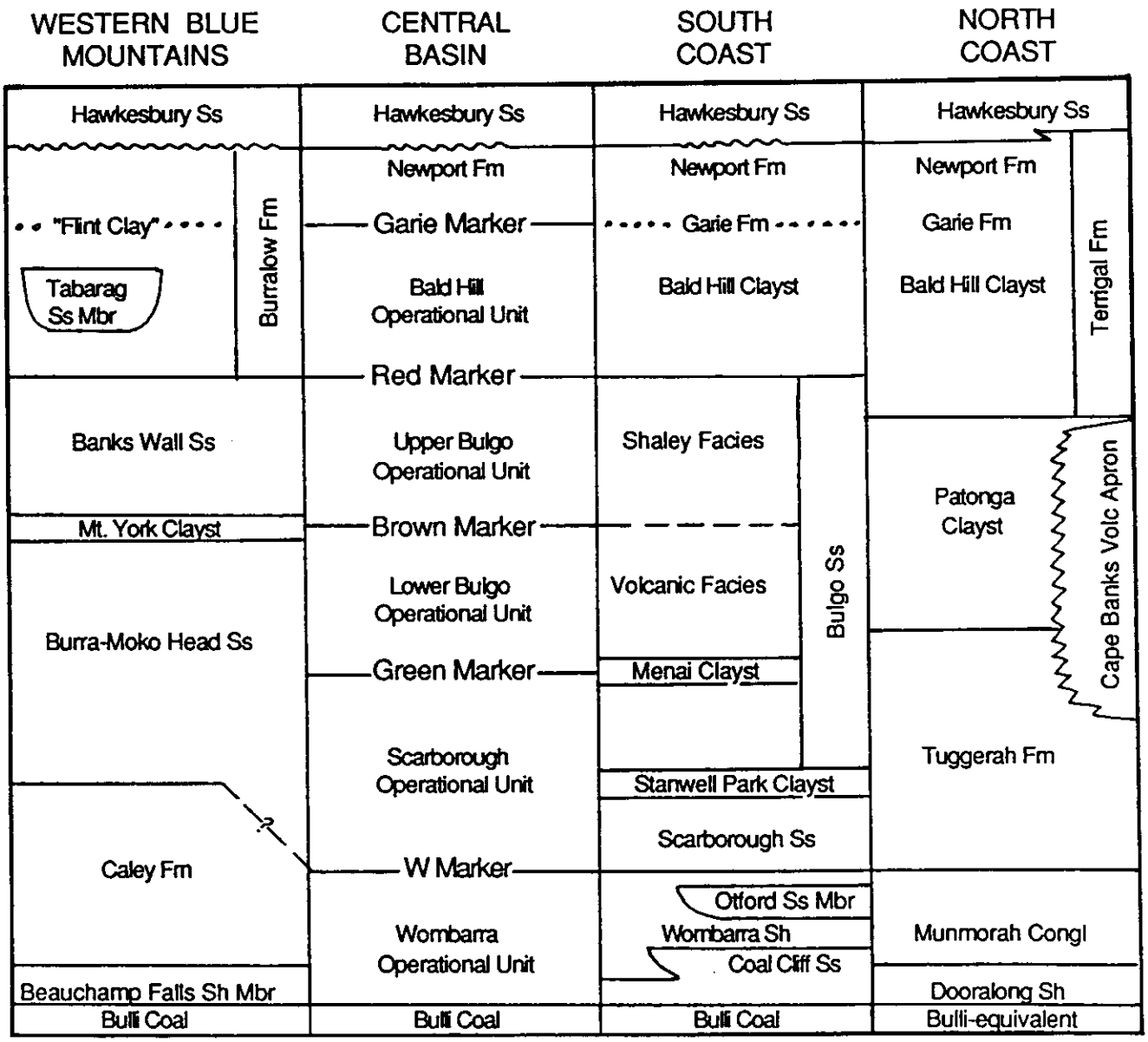

Fig 4-3 Correlation chart for uppermost Permian and Triassic strata of the Sydney Basin (After Galloway and Hamilton, 1988).

"W" marker is taken as the top of the unit. It generally represents a thick shaly break in the sequence. It also marks the log pattern change from type I log facies to type II log facies (Figs 4-1 & 4-2).

4.1.2 SCARBOROUGH OPERATIONAL UNIT

This operational unit overlies the Wombarra Operational Unit and is separated from the overlying Lower Bulgo Operational Unit by the informally known "green marker", which corresponds to a strong peak in the gamma ray log (Fig 4-1). It generally represents a shaly horizon. However, the marker is not lithologically controlled. For example, in Borehole W, it represents a very fine sandstone horizon. Hamilton et al. (1987) attributed the anomaly to a contemporaneous scattering of radioactive material, which is probably caused by a volcanic eruption or similar event.

4.1.3 LOWER BULGO OPERATIONAL UNIT

This unit includes the strata overlying the "green marker' up to the informally termed "brown marker", which is a regionally persist marker and represents a shaly horizon in the sequence. In geophysical logs, it corresponds to a gamma peak within the highly serrate log package (Fig 4-1). The marker does not have any depositional meaning since the depositional style above and below it is essentially the same (Hamilton et al., 1987).

4.1.4 UPPER BULGO OPERATIONAL UNIT

This operational unit includes the strata extending from the "brown marker" to the base of the overlying Bald Hill Operational Unit, which marks the sudden change of log facies from the highly serrate type to the blocky motif of the Bald Hill Operational Unit.

4.1.5 BALD HILL OPERATIONAL UNIT

This unit is characterised by the chocolate coloured claystones within it. It overlies

the Upper Bulgo Operational Unit and its top is marked by the informally known "Bald Hill" marker. The marker is recognised on geophysical logs by a low on the neutron log and strong gamma spike (Fig 4-1). Lithologically it correlates to a distinctive pelletoidal claystone horizon.

4.2 FACIES ANALYSES

4.2.1 STRATIGRAPHIC CORRELATION

In this study, twenty-six boreholes are selected with 24 in the Sydney Basin and the other 2 in the adjacent Gunnedah Basin (Fig 4-4). Five of the 26 boreholes (Boreholes C, K, L, R, and V) were not used by Galloway and Hamilton (1988). Of the other 21 boreholes, nine (Boreholes A, B, D, E, F, H, I, J, and S) are from the 15 key boreholes used by them. Detailed 1:100 geological logging of each of the 26 boreholes was made. The logging includes basic lithological description and detailed sedimentological analyses (colour, grain size estimation, sedimentary structure, upper and lower contacts, vertical texture and a preliminary interpretation of the genetic facies associations). The geological logging, together with available geophysical logs, form the bases for facies analyses. Also based on the geological logging, two west - east and three north - south stratigraphy correlation sections were drawn, as shown in Figs 4-5 to 4-9 (enclosures). The legends for Figs 4-5 to 4-9 are shown in Fig 4-10. For the 21 boreholes also used by Galloway and Hamilton (1988), the boundaries of the five operational units are taken from their correlation results with those in the other five boreholes being correlated with adjacent boreholes by this author. These boundaries are presented in Table 4-1.

4.2.2 TERMINOLOGY

The classification and systematic description of the clastic rocks are based on the Wentworth - Udden Grade Scale (Wentworth, 1922), which provides a three - fold subdivision of sediments into gravel, sand and mud (silt and clay), as shown in Appendix II. The definition of every term used is given in the book - A GUILD TO

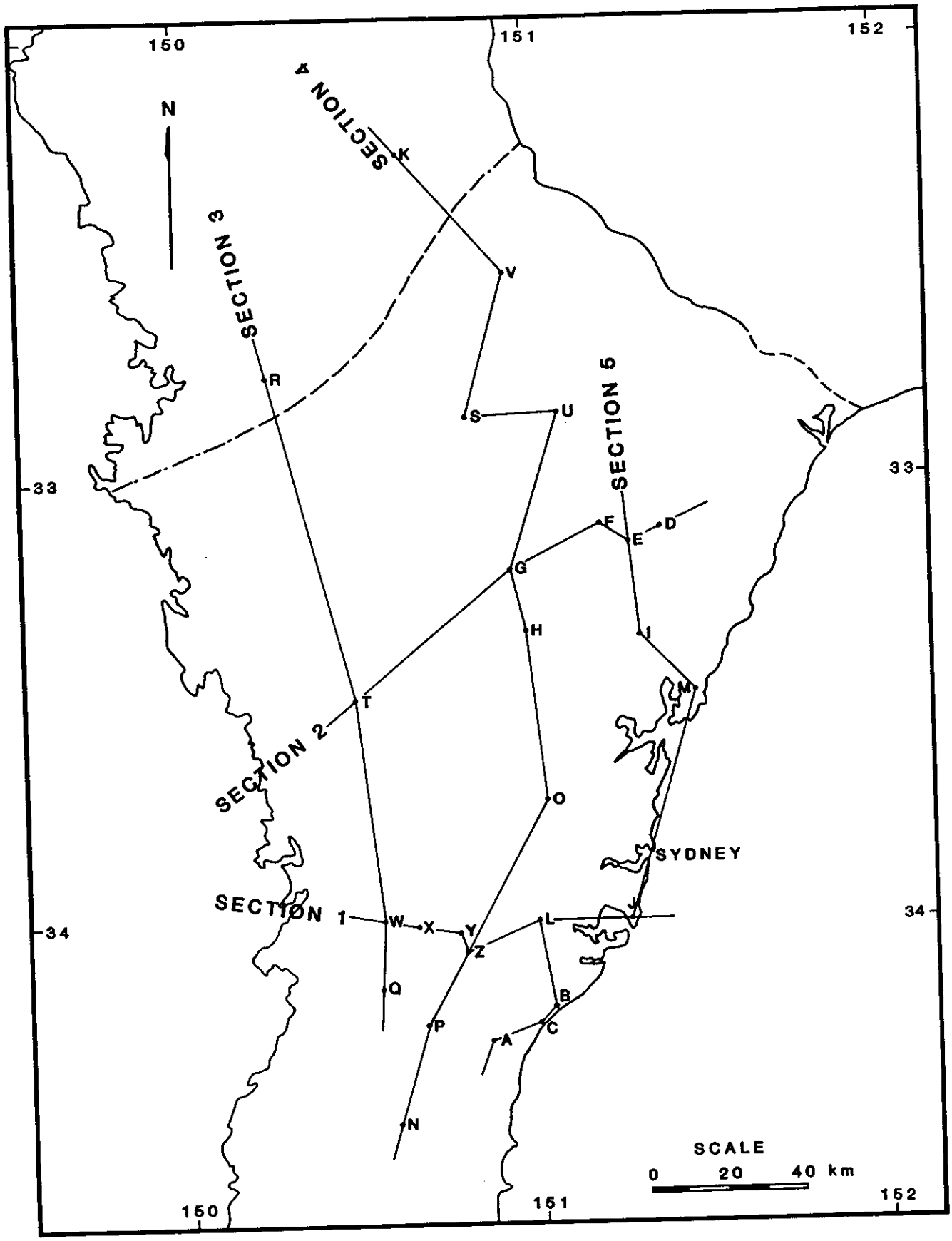

Fig 4-4 Borehole locations and cross sections.

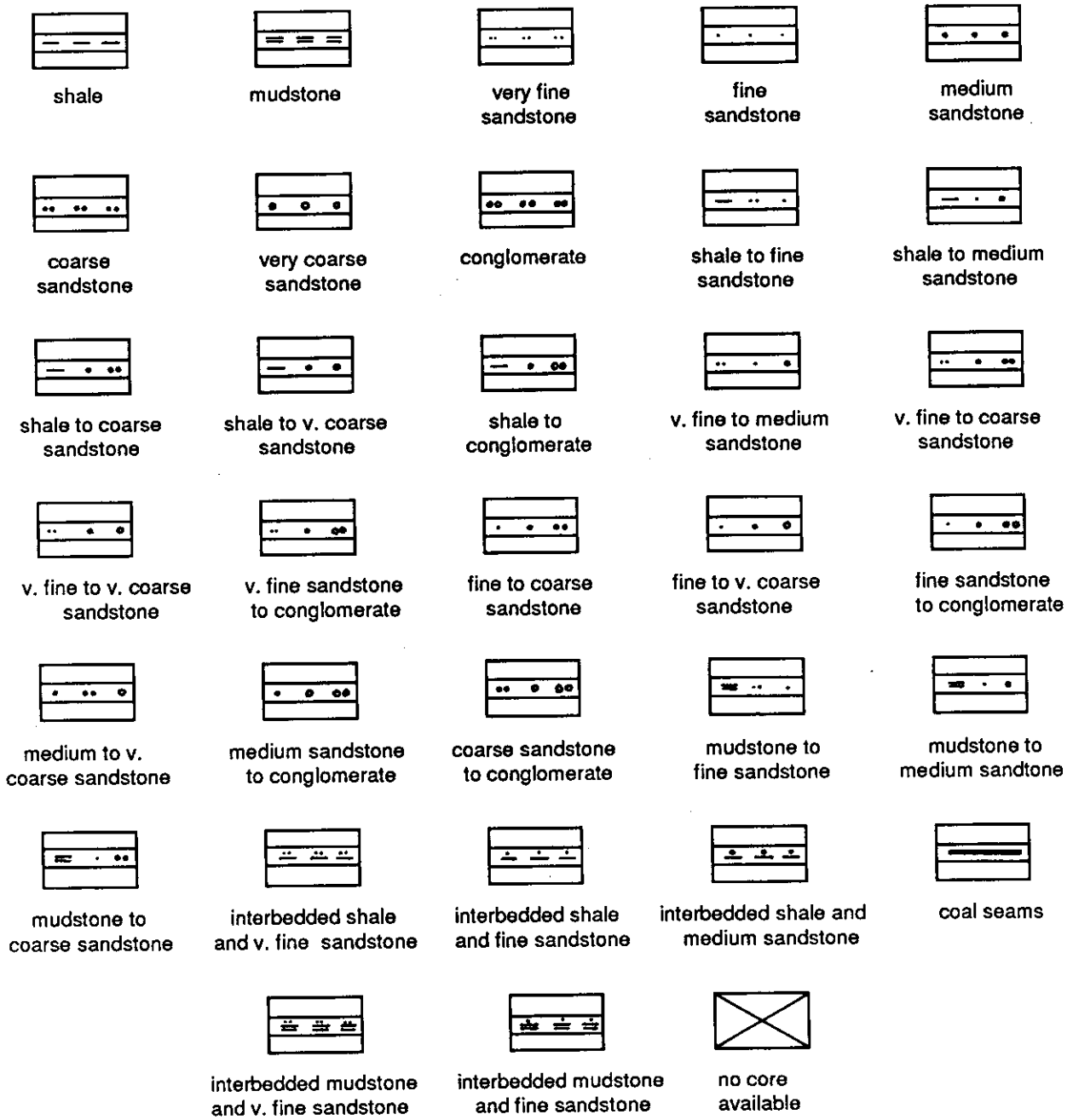

Fig 4-10 Legends for Figs 4-5 to 4-9.

Table 4-1 Boundaries of operational units in the 26 boreholes.

Borehole	Depth (measured in metres) interval of operational units									
A#	113.33	BH	131.72	UB	207.58	LB	244.55	SC 328.13	WO	366.80
B#	99.00	BH	119.28	UB	215.00	LB	279.00	SC 345.00	WO	415.00
C*			<13.00	UB	74.20	LB	132.40	SC 205.25	WO	264.50
D#							<41.00	SC 189.00	WO	308.00
E#							<100.00	SC 252.00	WO	392.00
F#	42.00	BH	106.00	UB	263.00	LB	412.00	SC 566.00	WO	758.00
G								<533.50	WO	595.00
H#	62.00	BH	138.00	UB	322.52	LB	429.00	SC 581.05	WO	703.79
I#	315.16	BH	376.61	UB	491.00	LB	619.20	SC 756.00	WO	902.82
J#					390.00	LB	463.00	SC 597.00	WO	683.50
L*	269.70	BH	308.00	UB	442.00	LB	524.50	SC 656.50	WO	762.00
M	33.53	BH	98.75	UB	220.83	LB	331.85	SC 468.25	WO	609.70
N	131.00	BH	143.00	UB	159.35	LB	169.56	SC 189.25	WO	200.46
O	289.25	BH	322.84	UB	481.89	LB	545.90	SC 637.87	WO	755.90
P	147.00	BH	195.00	UB	216.00	LB	300.00	SC 404.00	WO	457.80
Q							368.00	SC 420.31	WO	456.14
R*								3.00	WO	120.20
S#							370.00	SC 551.00	WO	657.00
T							186.00	SC 326.00	WO	449.00
U							59.45	SC 192.00	WO	354.85
V*								<9.00	WO	67.40
W	175.00	BH	237.00	UB	352.00	LB	400.00	SC 477.00	WO	530.00
X	275.79	BH	330.91	UB	448.69	LB	513.53	SC 606.52	WO	692.60
Y	350.00	BH	387.00	UB	506.00	LB	583.00	SC 668.00	WO	776.00
Z	347.46	BH	390.70	UB	500.14	LB	569.27	SC 672.68	WO	776.00

BH = Bald Hill, UB = Upper Bulgo, LB = Lower Bulgo, SC = Scarborough
WO = Wombarra Operational Unit.

Key boreholes used by Galloway and Hamilton (1988).

* Boreholes not used by Galloway and Hamilton (1988).

CORED ROCKS IN THE SYDNEY BASIN by Ward et al. (1986). The following terms are defined here.

Siltstone: a rock in which more than 75% of the framework particles are of silt size (0.06 to 0.004 mm). The rock may be stratified (laminated) or massive. Although silt - sized particles can be differentiated from very fine sand by techniques such as the use of hand lens with a graticule scale, it is very difficulty to distinguish siltstone from very fine sandstone by visual examination. Therefore, siltstones are classified into very fine sandstones during geological logging of these boreholes.

Claystone: It is a general term defined here. It refers to all rocks in which more than 75 % of the particles are of clay size (less than 0.004 mm). It includes mudstone and shale. The former refers to the claystone which has a massive structure. The latter refers to the claystone which has a laminated structure. The claystone which has an observed amount of silts (less than 25 %) is called silty mudstone or silty shale. The definition of the three terms are slightly different from those given by Ward et al. (1986).

4.2.3 FACIES ANALYSES

A facies is a body of rock with specified characteristics (Reading, 1986). It can be used in a strictly observational sense, e.g. "cross-bedded sandstone facies" and "green mudstone facies". It can also be used in an interpretive sense, e.g. "turbidite facies" for a rock or a suite of rocks which are thought to have resulted from turbidity currents, and "fluvial facies" for a rock or a suite of mixed rocks which are thought to have formed in a fluvial environment. Obviously facies analyses should be approached by observing facies relationships both laterally and vertically.

The importance of facies relationships was recognised first by Walther in 1894 and emphasised by Walker (1984) and Reading (1986). Walther's Law of Facies (1894) states that "It is a basic statement of far-reaching significance that only those facies

and facies areas can be superimposed primarily which can be observed beside each other at the present time." As Middleton (1973) has pointed out, Walther stressed the law was applicable only to succession without major breaks.

The introduction of the concept of a depositional system is a major advance in the study of facies and facies relationships since it provides a genetic basis for facies analyses. This concept was first introduced by Fisher and McGowen (1967) in their study of Tertiary Wilcox Group of Texas. A depositional system is a three dimensional assemblage of sedimentary facies linked genetically by inferred sedimentary environments and depositional processes (Fisher and Brown, 1984, cited in Hamilton, 1991).

A detailed study of sedimentary facies of the Narrabeen Group was undertaken recently by Galloway and Hamilton (1988). On the basis of lithofacies maps, cross sections, core descriptions, outcrop analyses, and key summary papers (Bembrick, 1980; Herbert, 1980a), they recognised five principal depositional systems within the Narrabeen Group (excluding Garie and Newport Formations): Wombarra lacustrine system, Munmorah fluvial system, Bulgo braidplain system, Patonga fluvial / lacustrine system, and Bald Hill fluvial system, which are named informally after the outcrop stratigraphic units displaying typical aspects of each depositional system. Figs 4-11 and 4-12 show the five depositional systems and their spatial relationships. As illustrated in these figures, two different depositional systems can interfinger at any one time. This reflects the evolving importance of the New England Fold Belt provenance (Munmorah, Patonga) and the Lachlan Fold Belt provenance (Bulgo, Bald Hill). The provenance changes will be discussed in detail on the basis of sandstone petrology data in the next chapter. From isopach, net sandstone, percentage sandstone, and net conglomerate maps drawn for each operational unit of the Narrabeen Group, Galloway and Hamilton (1988) reconstructed the paleogeographic environment for each of the five units and the resultant maps are also published in a separate paper (Hamilton et al., 1987).

Fig 4-11 East-west correlation cross section showing boundaries (dashed lines) of the operational units and boundaries (solid lines) of the principal depositional systems. The section follows regional section 1.

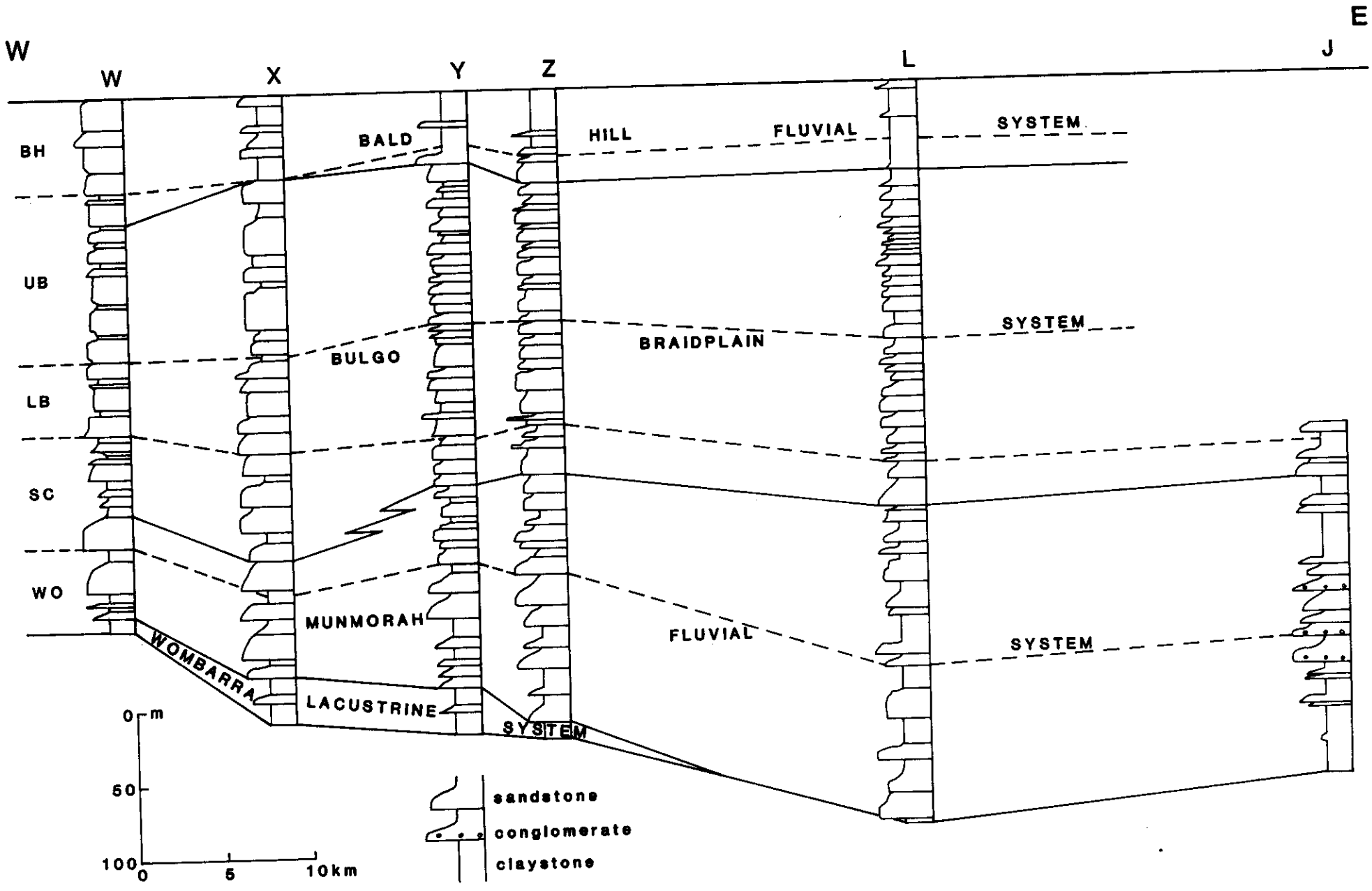
W
E
W
X
Y
Z
L
J
BH
UB
LB
SC
WO
BALD
HILL
FLUVIAL
SYSTEM
BULGO
BRAIDPLAIN
SYSTEM
MUNMORAH
FLUVIAL
SYSTEM
WOMBARRA
LACUSTRINE
SYSTEM
0
m
50
100
0
5
10km
sandstone
conglomerate
claystone

Fig 4-12 North-south correlation cross section showing boundaries (dashed lines) of the operational units and boundaries (solid lines) of the principal depositional systems. The section follows regional section 5 with Borehole C being excluded.

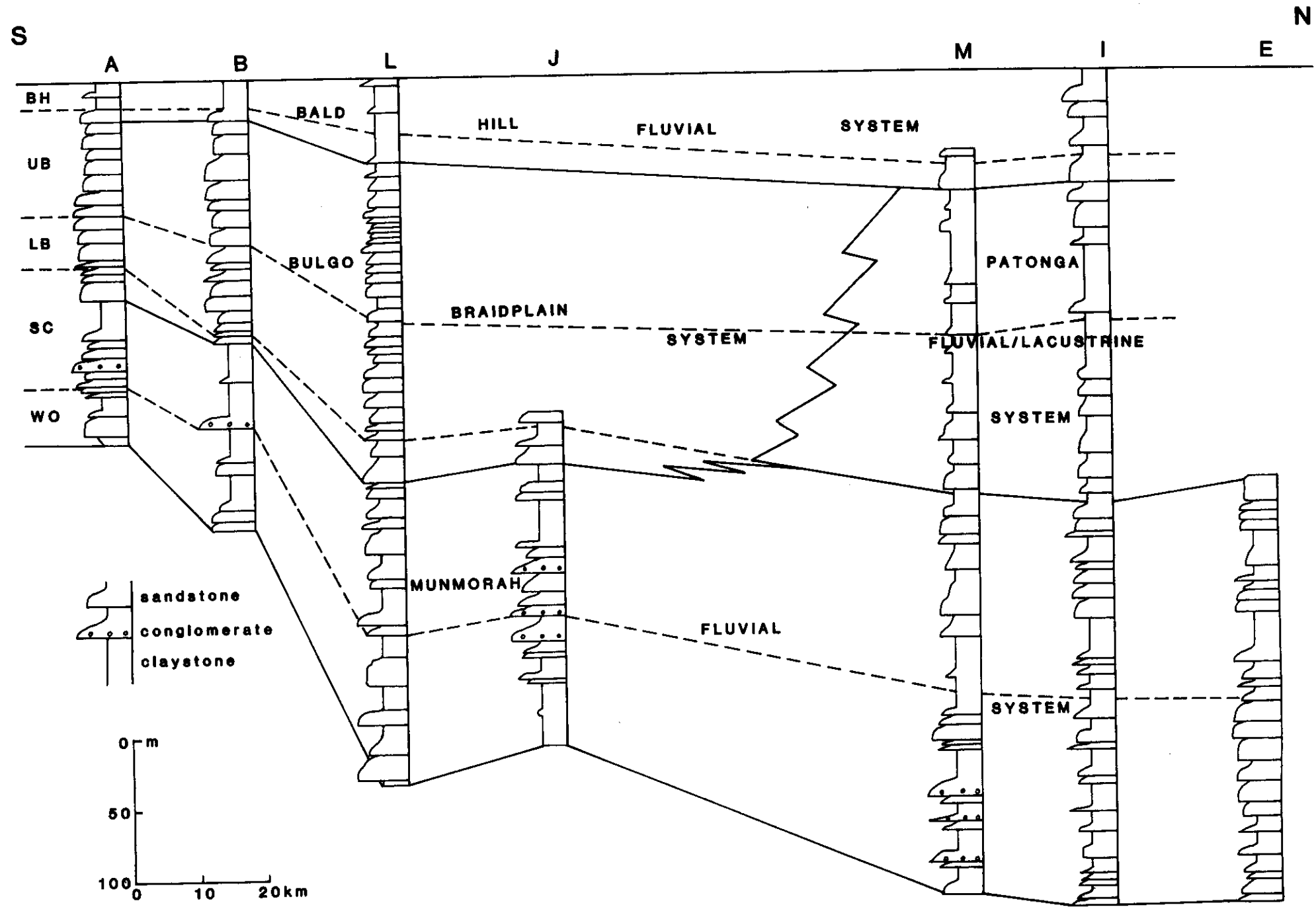
S
N
A
B
L
J
M
I
E
BH
UB
LB
SC
WO
BALD
HILL
FLUVIAL
SYSTEM
BULGO
PATONGA
BRAIDPLAIN
SYSTEM
FLUVIAL/LACUSTRINE
SYSTEM
MUNMORAH
FLUVIAL
SYSTEM
sandstone
conglomerate
claystone
0 m
50
100
0
10
20km

The WO unit, which ranges in thickness from 11 to 192 m, was the product of a bed-load to mixed-load fluvial system (Munmorah fluvial system) with low to moderate sinuosity (Figs 4-11 & 4-12). Sediments were principally deposited in southwesterly flowing tributary streams emanating from the New England Fold Belt (Herbert, 1980a) and a trunk complex flowing south and southeasterly along the basin axis (Galloway and Hamilton, 1988). The slight dominance of detrital quartz over lithics in the sandstones in the upper part of the unit in Boreholes W and X along the western margin of the basin (refer to Fig 5-41) suggests that the Lachlan Fold Belt supply quartzose detritus to this part of the basin during the deposition of the upper WO unit.

The WO unit consists of sandstones and shales / mudstones with conglomerates occurring locally. The ratio of sandstones to shales / mudstones varies from one borehole to another. In Borehole O, shales / mudstones dominate the WO unit whereas in Boreholes D, E, K, and V, this unit consists largely of sandstones as well as conglomerates.

The sandstones in this unit are dominated by medium to very coarse, volcanic lithic - rich sandstones. They are massive or cross bedded. Some of them show undistinctive cross bedding. A sandstone facies shows upward decrease in grain size. It may be overlain by claystone facies. This vertical texture variation of sandstones is typical of channel fill deposits in a meandering fluvial channel. Thus sandstones in this unit are interpreted to be upward fining channel fill or amalgamated channel fill deposits (Figs 4-13 & 4-14).

In the southern and western parts of the basin, the basal part of this unit consists of dark grey to black shales and interbedded very fine sandstones (Fig 4-15). Some of the shales have lenticular bedding. The interbedded very fine sandstones show flaser bedding and / or ripple cross-lamination. The shales / mudstones and

Fig 4-13 Amalgamated upward-fining channel-fill sandstone facies (centre of photograph) and inter-channel floodplain / lacustrine mudstone / shale facies (left and right of photograph) in the WO unit in Borehole Z. Each core length is approximately 1.1 m. The number on the wood block is the drilling depth in feet.

Fig 4-14 One complete upward fining sequence (centre of photograph) with conglomerate and sandstone representing channel fill (point bar) facies and green mudstone inter-channel floodplain facies. Conglomerate and sandstone overlying the sequence (right of photograph) are channel fill facies and silty mudstone and very fine sandstone underlying it (left of photograph) inter-channel floodplain facies. From the WO unit in Borehole M. Each core length is approximately 1.1 m. The number on the wood block is the drilling depth in feet.

Fig 4-15 Dark grey silty shale and interbedded very fine sandstone and shale in the basal part of the WO unit in Borehole Z. The shaly sedimentary sequence is interpreted to be the product of swampy deposition. The overlying light grey lithic sandstones represent channel fill deposits. Each core length is approximately 1.1 m. The number on the wood block is the drilling depth in feet.

Fig 4-16 Green mudstone / shale in the basal part of the WO unit in Borehole G. The mudstone / shale is interpreted to be the product of inter-channel floodplain / lacustrine deposition. The overlying light grey sandstone and conglomerate represent amalgamated channel fill facies. Each core length is approximately 1.1 m. The number on the wood block is the drilling depth in feet.

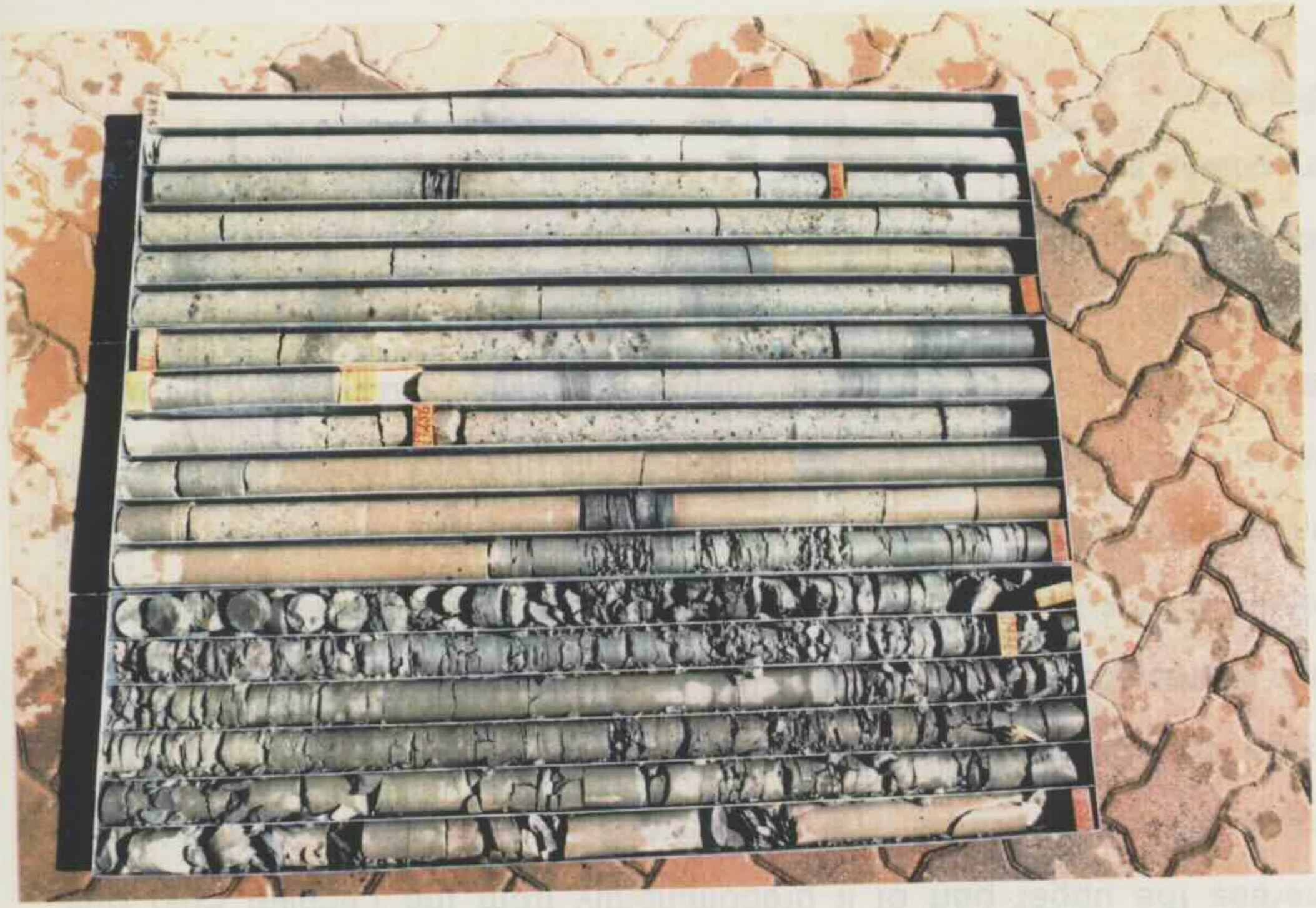

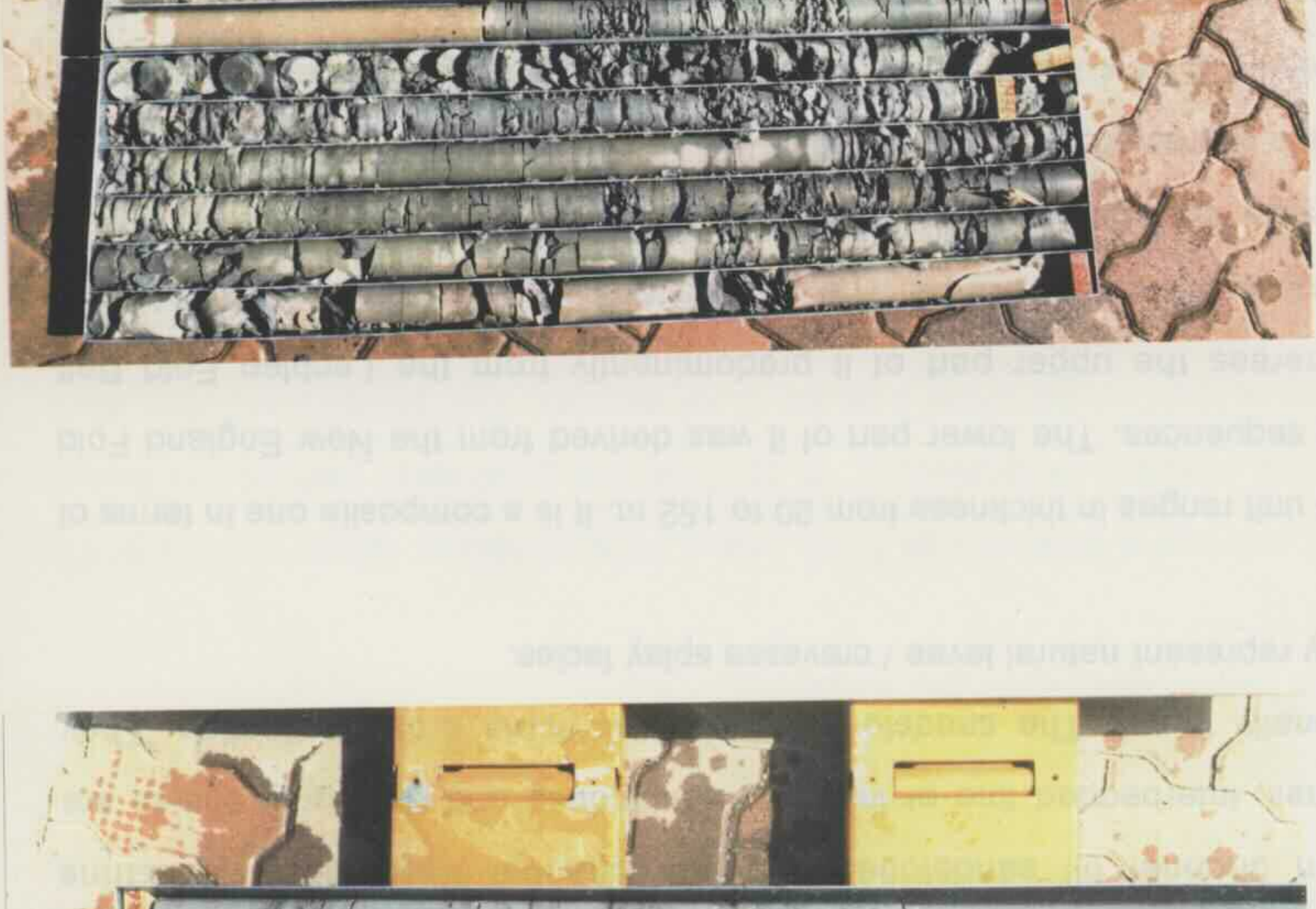

interbedded very fine sandstones in the basal part of the unit are interpreted to be products of a swamp / lacustrine environment, deposited in the Wombarra lacustrine system (Galloway and Hamilton, 1988) (Fig 4-11). The dark colour resulted from the preserved organic matter in these shales / mudstones.

Grey to green shales / mudstones within this unit (Figs 4-13 & 4-16) overlying and / or underlying upward fining channel fill facies represent inter-channel floodplain / lacustrine deposits. The green to grey colour of the shales / mudstones was related to the paucity of preserved organic matter in them.

Between channel fill sandstones and inter-channel floodplain / lacustrine claystones, interbedded fine or very fine sandstones and dark grey shales are occasionally found. The sandstones may show ripple cross-lamination. They probably represent natural levee / crevasse splay facies.

The SC unit ranges in thickness from 20 to 152 m. It is a composite one in terms of genetic sequences. The lower part of it was derived from the New England Fold Belt whereas the upper part of it predominantly from the Lachlan Fold Belt (Galloway and Hamilton, 1988). The composite character is also reflected by the geophysical log facies in the southern basin. In Boreholes W to Z, the lower part of this unit is characterised by log facies IA, IB, and IC whereas the upper part of it by log facies IIB (Figs 4-2 & 4-5). The sandstone petrology data of this author suggests that the composite feature of this unit in the southern basin is probably more related to an eastern volcanic source. The lower part of this unit was largely derived from this eastern volcanic source rather than the New England Fold Belt and the upper part of it from the Lachlan Fold Belt in the southern basin (see next chapter). The presence of this source is also supported by the occurrence of lithic conglomerate and very coarse sandstones in the lower SC unit in the boreholes along the south coast (Fig 4-12).

Principal facies recognised in the lower SC unit include upward fining channel fill, amalgamated and inter-channel floodplain / lacustrine facies (Figs 4-17 & 4-18). Channel margin (levee and crevasse splay) facies developed but were not common. Braided channel fill and amalgamated braided channel fill quartzose sandstones (Fig 4-19) comprise the bulk of the upper SC unit. Inter-channel floodplain / lacustrine facies rarely developed due to erosion by the lateral migration of braid channels, as indicated by Walker and Cant (1984).

To the far northeast part of the basin, the whole unit was deposited in the Munmorah fluvial system with sediments largely derived from the New England Fold Belt (Galloway and Hamilton, 1988). Upward fining channel fill, amalgamated channel fill facies and inter-channel floodplain / lacustrine deposits are the principal facies recognised (Fig 4-20).

The LB unit has a thickness of 10 to 149 m. It is extremely sandy in most of the boreholes studied. In Boreholes W to Z of the southwest part of the basin, sandstones account for more than 85 % of the unit. The majority of them show cross bedding with the remainder being massive. Galloway and Hamilton (1988) concluded that this unit was deposited in a major easterly and southeasterly flowing fluvial apron of the lower Bulgo braidplain system with sediments derived from the Lachlan Fold Belt. This conclusion is supported by the petrology data of sandstones of the unit (see Fig 5-52). Principal component facies includes braided channel-fill (log facies IIB) and amalgamated braided channel fill (log facies IIC) (Fig 4-21). Inter-channel floodplain / lacustrine facies was rarely found except in the northeast part of the basin near the New England Fold Belt. In this part of the basin, mudstones / shales dominate the unit in Boreholes F, I, and M. Sandstones of this unit in these boreholes contain roughly equal amounts of detrital quartz and lithics (see Figs 5-44 & 5-45), suggesting that the New England Fold Belt continued to supply sediments to this part of the basin during the deposition of the LB unit. In the northeast part of the basin, the unit was the products of the lower Patonga fluvial /

Fig 4-17 Amalgamated channel fill sandstone facies in the lower part of the SC unit in Borehole Z. Channel lag deposits, which consist of intrabasinal mudflakes, can be recognised at the base of channel fill facies (centre of photograph). Each core length is approximately 1.1 m. The number on the wood block is the drilling depth in feet.

Fig 4-18 Upward fining sequence (central left of photograph) with sandstone representing channel fill (point bar) facies and shales inter-channel floodplain facies. Sandstones overlying the sequence are interpreted to be amalgamated channel fill facies. From the lower part of the SC unit in Borehole J. Each core length is approximately 1.1 m. The number on the wood block is the drilling depth in feet or meters.


1824.2
5787
1911 11


2002.6
2002.7
2003.1

Fig 4-19 Amalgamated braided channel fill sandstone facies (left and centre of photograph). Dark grey silty shales within the facies are interpreted to be inter-channel floodplain facies. Dark grey silty shales and light grey very fine to fine sandstones (right of photograph) also represent inter-channel floodplain facies. From the upper part of the SC unit in Borehole Y. Each core length is approximately 1.1 m. The number on the wood block is the drilling depth in feet or meters.

Fig 4-20 Upward fining sequences in the SC unit in Borehole I. Sandstones are interpreted to be channel fill (point bar) facies and mudstones inter-channel floodplain facies. Each core length is approximately 1.1 m. The number on the wood block is the drilling depth in feet.


2394.9
2391
2406.6
134
1414.5
2418.7
2428.6
1402
2435.7
1424


CAM
5
1111.5
1115.2
1355.5

Fig 4-21 Amalgamated braided channel fill sandstone facies. The rare silty shales intercalculated within the facies represent inter-channel floodplain facies. From the UB unit in Borehole Y. Each core length is approximately 1.1 m. The number on the wood block is the drilling depth in feet or meters.

Fig 4-22 Amalgamated braided channel fill sandstone facies. The rare silty shales intercalculated with the facies represent inter-channel floodplain facies. From the UB unit in Borehole Z. Each core length is approximately 1.1 m. The number on the wood block is the drilling depth in feet.

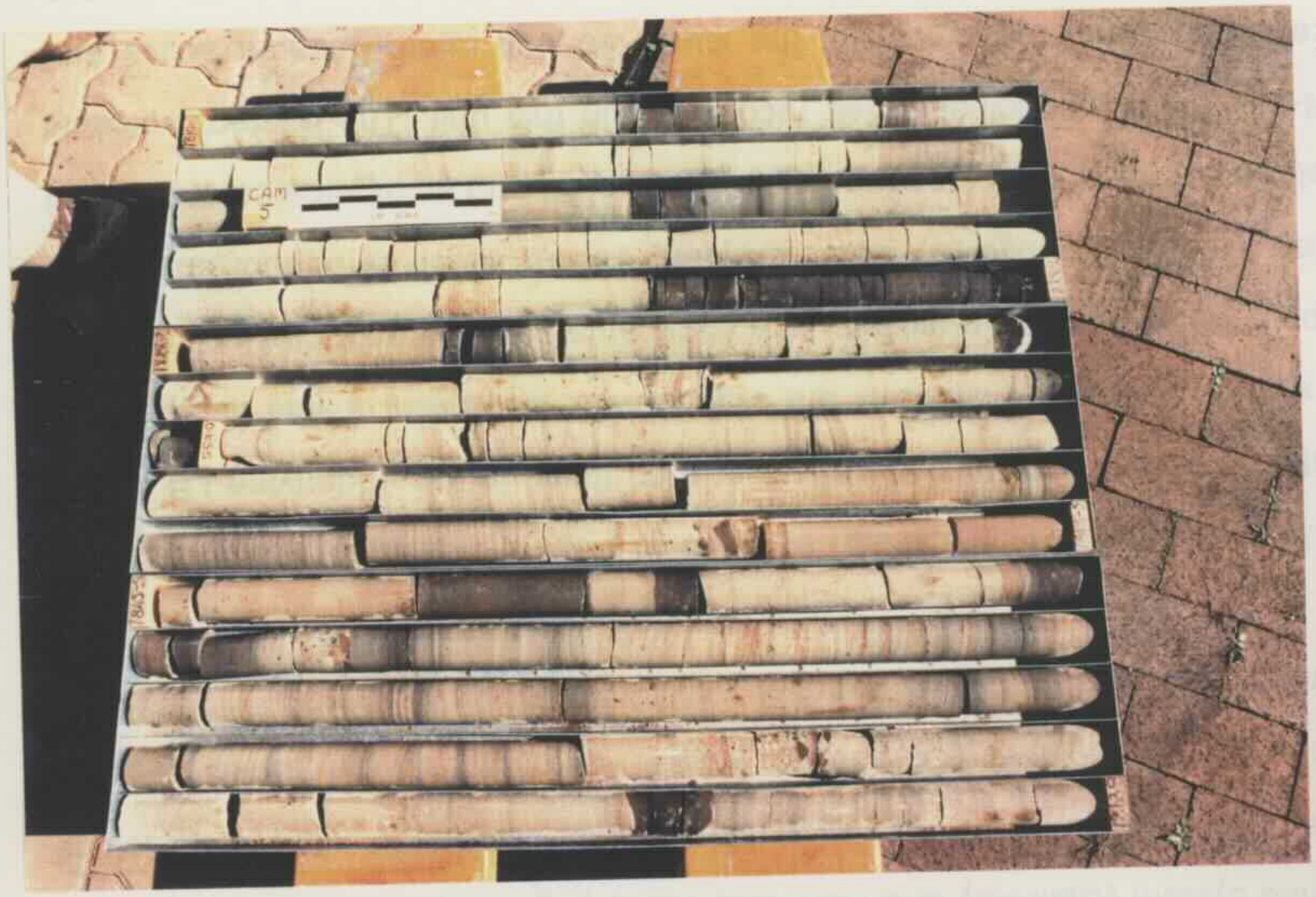

lacustrine system (Galloway and Hamilton, 1988) (Fig 4-12). In Boreholes F, I, and M, upward fining channel fill (log facies IIA) and inter-channel floodplain / lacustrine facies are the principal component facies. Channel margin facies is also recognised and consists of fine, very fine sandstones and silty shales.

The UB unit ranging in thickness from 16 to 185 m is also a sandy unit, but sandstones in this unit are generally finer than those in the underlying LB unit in grain size and shales / mudstone are slightly more abundant. It was deposited in the upper Bulgo braidplain system with sediments being largely derived from the Lachlan Fold Belt (Galloway and Hamilton, 1988), which is supported by the sandstone petrology data (see Fig 5-52). Channel fill and amalgamated channel fill (Fig 4-22) are the principal facies recognised in this unit. The eastern volcanic source active during deposition of the lower SC unit again became active and supplied sediments to the southern basin during the deposition of the lower UB unit, as supported by the occurrence of conglomerates and very coarse sandstones in the lower UB unit in Boreholes A, B, and C along the south coast and the vertical variation of detrital composition of sandstones in these boreholes (see Fig 5-47). These conglomerates and sandstones consist largely of intermediate volcanic clasts, which are different from the silicic volcanic clasts derived from the New England Fold Belt. The similarity of detrital compositions of sandstones in the top part of the UB unit and the overlying BH unit (see next Chapter) implies that the top part of the UB unit was more likely to be deposited in the Bald Hill fluvial system (Figs 4-11 & 4-12).

To the northeast part of the basin, in Borehole F, the UB unit is dominated by sandstones, which are interpreted to be upward fining channel fill deposits. In Boreholes M and I, shales / mudstones dominate the unit particularly the lower part of it. Sandstones of the unit in the two boreholes are upward fining channel fill deposits and shales / mudstones represent inter-channel floodplain / lacustrine deposits (Fig 4-23). Channel margin facies, which consist of fine sandstones and

Fig 4-23 Inter-channel floodplain chocolate mudstone facies (left and right of photograph) and amalgamated channel fill sandstone facies (centre of photograph) in the UB unit in Borehole I. Each core length is approximately 1.1 m. The number on the wood block is the drilling depth in feet.

Fig 4-24 Amalgamated braided channel fill sandstone facies. The sign "+" marks the top of the Bald Hill Operational Unit. From the BH unit in Borehole W. Each core length is approximately 1.1 m. The number on the wood block is the drilling depth in metres.

interbedded very fine sandstones and shales, are also recognisable. The quartz-rich composition of sandstones in the top part of this unit in the three boreholes (see Figs 5-44 & 5-45) suggests that sediments were largely derived from the Lachlan Fold Belt and deposited in the Bald Hill fluvial system (Fig 4-12). The Lachlan Fold Belt finally replaced the New England Fold Belt as the major source for this part of the basin.

Geological logging data of the BH unit, which ranges in thickness from 12 to 76 m, show that grain size and percentage of sandstones generally decreases from west to east (from Borehole W to Borehole L, Fig 4-5). These changes, together with the eastward decrease of detrital quartz in sandstones (see Fig 5-53), imply that the detritus was largely derived from a western source. During the deposition of the BH unit, the Lachlan Fold Belt was the major source. This is consistent with the conclusion that this unit was deposited in an easterly to southeasterly flowing mixed - load system (Bald Hill fluvial system) (Galloway and Hamilton, 1988). An eastern volcanic source also contributed sediments, mainly clays, to the basin during deposition of Bald Hill Claystone - equivalent of this unit (Ward, 1972).

The depositional style of the BH unit seems to vary from one location to another. In Borehole W in the west margin of the basin, the operational unit is dominated by medium and coarse sandstones. The sandstones are massive (in the lower part, 237.5-200.5 m) or cross-bedded (Fig 4-24) (the upper part, 200.5-175.00 m). The paucity of vertical accretion deposits (claystones and very fine sandstones) and the absence of parallel lamination in the sandstones are characteristics similar to those found in the Battery Point section (Cant and Walker, 1976). Thus it is interpreted that the operational unit in Borehole W was deposited in a braided fluvial environment. Braided channel fill and amalgamated channel fill (Fig 4-24) are the principal facies.

In Borehole X, the operational unit is dominated by mudstones and interbedded

very fine sandstones and shales. The sandstones account for about 20 % of the unit. Sandstones vary in grain size from fine to coarse grained. The thick mudstones characterised by log facies IV (Fig 4-2) are interpreted to be the product of inter-channel floodplain / lacustrine deposition. In the unit, two distinctive upward-fining sections (log facies IA, Fig 4-2) can be recognised (311.0-297 m and 317-311 m). The upper section consists of massive and cross-bedded medium sandstones at the base then parallel laminated fine, very fine sandstones, interbedded very fine sandstones and shales and finally mudstones. The lower section grades upwards from cross-bedded medium sandstones, to ripple cross-bedded fine sandstones and finally to shales. Thus the sandstones in the two sections are of channel fill origin, representing point bar deposits and shales / mudstones are products of inter-channel floodplain deposition.

In Boreholes Y, Z and L, the operational unit consists largely of mudstones and shales. The sandstones account for less than 10 % of the total unit. In the shales or mudstones, root structures are recognised (Fig 4-25). The mudstones and shales vary from dark-grey, grey to green, white, mixture of grey and chocolate colour, to chocolate in colour (Fig 4-26). The shales / mudstones of the unit in the three wells is considered to be deposited in a floodplain environment. The medium to very coarse sandstones within it represent upward fining channel fill and amalgamated channel fill deposits and ripple cross laminated fine and very fine sandstones channel margin (levee and crevasse splay) deposits.

Similarly in other boreholes, the sandy beds are the products of channel fill deposition. The claystones and the interbedded very fine sandstones and mudstones / shales resulted from the floodplain / lacustrine deposition. Ripple cross laminated fine and very fine sandstones, which occur between upward fining channel fill sandstones and inter-channel floodplain / lacustrine shales / mudstones and / or within the floodplain facies, represent channel margin deposits.

Fig 4-25 Root structures within shales of the BH unit. From Borehole Y at drilling depth of 382.1 m.

Fig 4-26 Inter-channel floodplain claystone facies in the BH unit in Borehole Z. The white claystone is of pyroclastic origin. Chocolate claystone was deposited in oxidising environments and dark grey claystone in reducing environments. Each core length is approximately 1.1 m. The number on the wood block is the drilling depth in feet.

4.2.4 FACIES DESCRIPTION

Channel fill, inter-channel floodplain / lacustrine and channel margin are the three principal component facies recognised in the Narrabeen Group. They have already been mentioned in the previous section. In this section, the individual component facies will be described in some detail.

(i) Channel Fill Facies

Channel fill facies consists of coarse sediments retained in the fluvial system. Conglomerate and sandstone are the lithological components of the channel fill deposits in the Narrabeen Group with sandstone being of much more volumetric importance.

Conglomerates in the channel fill facies generally show massive structure and occasionally flat - bedded structure. They may themselves comprise the bulk of channel fill facies or the entire facies (Fig 4-14), but this is rare in the boreholes studied in this project. More commonly conglomerates occur as thin beds on the scoured base of the channel. In these cases, they are interpreted to represent channel lag deposits, which could be transported only during peak periods of flooding. Fig 4-27 shows an example of channel lag deposits. The deposit is 8 cm thick and lies on the eroded surface of the underlying cross bedded fine sandstone. The lag pebbles consist of intrabasinal chocolate mudflakes, which were derived from erosion of inter-channel floodplain mudstones, and extrabasinal volcanic lithic clasts, which were transported there from source areas. The subrounded feature of the mudflakes reflects rolling around by strong currents and slow sedimentation.

Sandstones commonly comprise the entire channel fill facies by themselves although in some cases sandstones, together with channel lag conglomerates, make up channel fill deposits. Channel fill sandstones vary in colour from offwhite, light grey, mid grey to green, depending on the composition of the sandstones. Quartz - rich sandstones generally show offwhite colour whereas lithic - rich

Fig 4-27 Channel lag deposits on the eroded surface of underlying fine sandstones. From Borehole Z at drilling depth of 725.8 m.

Fig 4-28 Cross bedding shown by grain size variation of sandstones. From Borehole Z at drilling depth of 609.8 m.


MADE IN CANADA
LUFKIN


LUFKIN

sandstones show light to mid grey colour. Sandstones with chlorite, which is identified with SEM/EDX analyses, generally show green colour. In terms of structure, four principal types of facies can be distinguished for channel fill sandstones. They include cross - bedded, massive, ripple - cross laminated, and parallel laminated sandstone facies.

Cross Bedded Sandstone Facies: Cross bedding is the most common structure recognised in the channel fill sandstones of the Narrabeen Group. It includes two major types: planar - tabular cross bedding and trough cross bedding. The narrow core width limits the distinction of the two types. The type of cross bedding cannot always be identified in cores. Cross bedding is illustrated by variations of grain sizes of sandstones (Fig 4-28), sideritic laminae (Fig 4-29), and grey silty clay laminae (Fig 4-30). It commonly occurs in medium to very coarse sandstones. In Fig 4-30, the silty clay laminae represent settling of suspended fine material during low river stage. The medium to coarse sandstones, showing planar - tabular cross bedding, were transported at high river stage and deposited in the low flow regime during falling river stage. Cross bedding was produced by migration of megaripples and sand dunes.

Massive Sandstone Facies: Sandstones are more or less homogeneous. No internal lamination / bedding can be seen with naked eyes. Massive structure occurs from fine to very coarse sandstones. Reineck and Singh (1980) mentioned several modes of origin for the massive structure. It can be the result of strong bioturbation activity. Organism bioturbation can lead to complete destruction of primary layers, producing homogeneous mass. It can also be created by inorganic process, e.g. water draining out of sediments during compaction. Massive structure can be primary in origin. In the case of rapid sedimentation, sediments are deposited as a massive homogeneous mass. The massive sandstone facies of the Narrabeen Group is most likely to be primary in origin and is the product of rapid deposition.

Fig 4-29 Cross bedding shown by sideritic laminae. From Borehole X at drilling depth of 427.9 m.

Fig 4-30 Cross bedding shown by clay laminae. From Borehole X at drilling depth of 456.7 m.

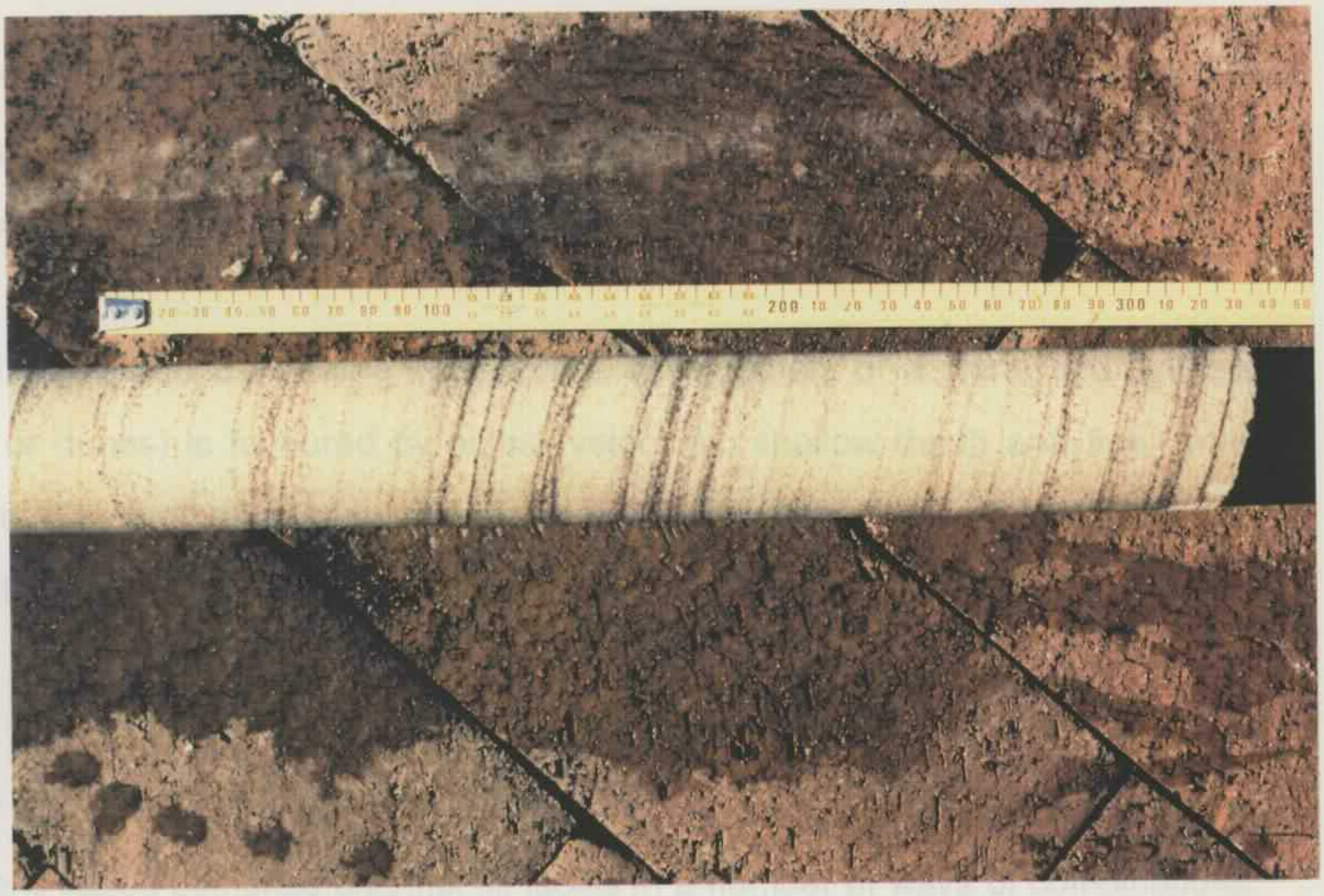

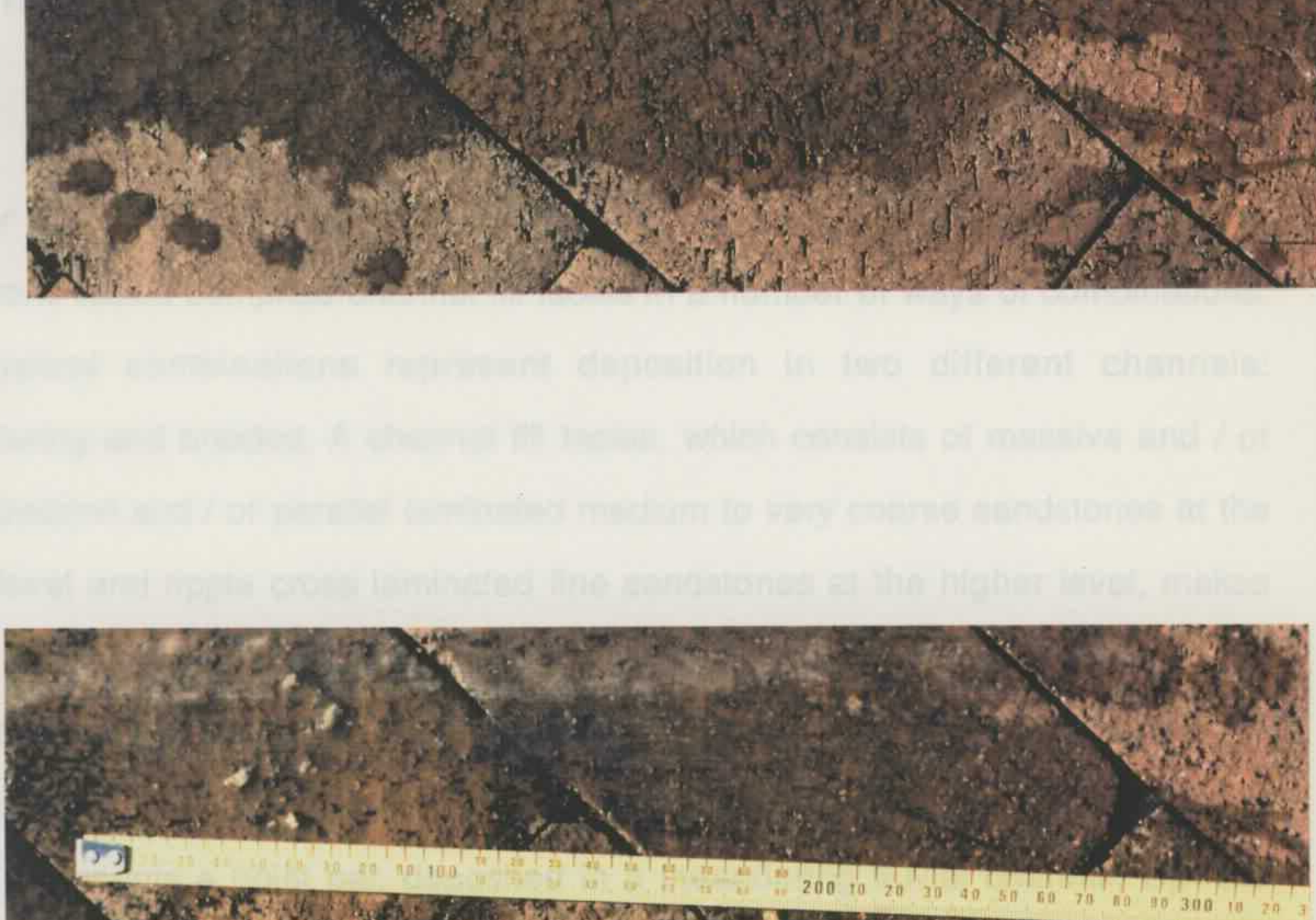

Ripple Cross Laminated Sandstone Facies: Ripple cross lamination is generally restricted to fine sandstones in the top level of channel fill deposits. It is illustrated by carbonaceous (Fig 4-31) or sideritic laminae (Fig 4-32).

Parallel Laminated Sandstone Facies: The development of a plane bed (without ripples or dunes) is favoured by higher velocities, shallow depth and finer grain size. Parallel lamination results from deposition on the plane bed (Walker and Cant, 1984). It was found in all levels of the upward fining channel fill (point bar) facies.

With or without conglomerates as channel lag deposits, the four principal types of sandstone facies comprise channel fill facies in a number of ways of combinations. Two typical combinations represent deposition in two different channels: meandering and braided. A channel fill facies, which consists of massive and / or cross bedded and / or parallel laminated medium to very coarse sandstones at the lower level and ripple cross laminated fine sandstones at the higher level, makes up an upward fining sandstone sequence with a thickness of around 2 m. The sandstone sequence, which was deposited by lateral accretion of sediments, is often overlain by inter-channel floodplain shales / mudstones. The channel fill facies represents a point par, deposited in a meandering fluvial channel. Upward fining sandstone facies can be stacked together to form a multistory amalgamated channel fill facies (Figs 4-13 & 4-16), which can be up to 15 m or more thick.

The other typical combination of sandstone facies is that massive and / or cross bedded sandstones comprise the bulk of the channel fill facies with ripple cross laminated fine sandstones occurring in the top part. The grain size of the channel fill sandstones does not show any characteristic vertical variations. The channel fill sandstones are overlain by inter - channel flood plain shales / mudstones, which are much thinner than the sandstones. This sort of channel fill facies was deposited

Fig 4-31 Ripple cross lamination shown by carbonaceous laminae. From Borehole Y at drilling depth of 685.7 m.

Fig 4-32 Ripple cross lamination shown by sideritic laminae. From Borehole Z at drilling depth of 756.7 m.

by vertical aggradation of sediments and is interpreted to represent braided channel fill deposits. Braided channel fill facies can be stacked together to form amalgamated braided channel fill facies.

(ii) Inter - Channel Floodplain / Lacustrine Facies

The facies consists of fine suspended load sediments, which are deposited in the flood basin during flood stage. Shales / mudstones and very fine sandstones are the principal lithological components for this facies in the Narrabeen Group. Some of the shales show lenticular bedding and the very fine sandstones often show parallel lamination and / or ripple cross lamination, illustrated by carbonaceous or sideritic laminae. In terms of colour, the claystones (shales and mudstones) can be divided into four facies: chocolate, green, grey to black, and white facies. Chocolate claystone facies is interpreted to result from deposition in oxidising environments. By contrast, green and grey to black claystone facies resulted from deposition in reducing environments. The dark grey and black colours are related to the preserved organic matter in the claystone. White claystone facies is of pyroclastic origin.

(iii) Channel Margin Facies

The facies includes natural levee and crevasse splay facies. The former bounds the channel and the latter extends into floodbasin from breaches or low areas of the levees. In the Narrabeen Group, the facies is of minor volumetric importance and consists of silty shales, very fine and fine sandstones. Fig 4-33 shows an example of channel margin facies. It consists of interbedded silty shales, very fine and fine sandstones. The interbedding of shales and sandstones suggests periodic flooding with sandstones being deposited during flood periods and shales during waning periods. The parallel lamination of the sandstones resulted from settling of suspended fine material and ripple cross lamination from migration of bed load sediments in the lower flow regime.

Fig 4-33 Crevasse splay facies consisting of interbedded silty shale and very fine to fine sandstones, which is marked at its top and bottom by the sign "+". The overlying green mudstone is interpreted to be inter-channel floodplain facies. Offwhite medium to very coarse sandstones (left and right of photograph) are channel fill facies. From the SC unit in Borehole Z. Each core length is approximately 1.1 m. The number on the wood block is the drilling depth in feet.


1854-3
1854-4

CHAPTER FIVE

PETROLOGY OF THE NARRABEEN GROUP SANDSTONES

5.1 INTRODUCTION

McElroy (1954) was the first to study the composition and texture of the Narrabeen Group sediments in a systematic manner. Later Loughnan (1963) made a petrological study of a vertical section in the Narrabeen Group at Helensburgh. The most comprehensive petrological studies of the Narrabeen Group sediments in the southern Sydney Basin were undertaken by Ward (1971a, b). All the studies show that the content of detrital quartz grains generally increases toward the top of the group and that of detrital lithic fragments generally decreases.

The aims of this petrological study are to determine the variation of detrital composition of sandstones, to deduce their detrital sources, and to assess the effects of the detrital composition on diagenesis and the quality of sandstones as hydrocarbon reservoirs. The influence of detrital composition of sandstones on diagenesis and reservoir quality will be discussed in Chapters 6 and 8.

5.2 METHODOLOGY

Thin sections were cut for all the 417 sandstone samples collected from the 26 boreholes subject to geological logging. They were impregnated with a blue dye to facilitate observation of porosity in thin sections. All thin sections were examined under a Leitz - Wetzlar petrological microscope to observe grain size, framework mineralogy, texture, porosity, dissolution features and cementation history. Some samples are altered to such an extent that the detrital lithics cannot be distinguished from the clay matrix and are considered to be unsuitable for reliable point counting. Of the 417 samples, a total of 324 thin sections were selected for point counting. Photomicrographs were taken of selected thin sections using an Olympus (Model BHSP) camera with 100 ASA film.

There are two different point counting methods for modal analyses of sandstones: traditional point counting method and the so called Gazzi-Dickinson point counting method (Ingersoll et al., 1984; Zuffa, 1985). The key difference between the two methods lies in the treatment of rock fragments. In the traditional point counting method, all rock fragments are included in the lithic pole. By contrast, the lithic pole in the Gazzi-Dickinson method includes only the fine grained lithic fragments in which no individual crystal or grain is larger than 0.0625 mm in size (the lower limit of sand size). For the coarse grained lithics, which are composed of crystals or grains larger than 0.0625 mm in size, the sand sized crystal or grain is counted into the category of the crystal or grain rather than that of the lithic fragment.

The traditional point counting method is generally applied to the study of sandstone diagenesis (e.g. Burns and Ethridge, 1979; Loucks et al., 1984; Kantorowicz, 1985). The Gazzi-Dickinson point counting method is widely used by workers who put greater emphasis on using petrographic techniques to deduce the provenances of arenites in areas of active tectonism / magmatism (e.g. Ingersoll, 1978; Dickinson et al., 1982; Jett and Heller, 1988).

For this project, the traditional point counting method has been used (the rare presence of coarse grained lithics in the Narrabeen Group sandstones ensures that selection of point counting method makes little difference to the results of modal analyses). The quantitative evaluation of composition and visible porosity of the sandstones was carried out using a Swift Automatic Point Counter (Model F 415 C) and counting 500 points per thin section under the cross hairs at the maximum grid spacing, which resulted in coverage of the entire thin section. The results of point counting are presented in Appendix III.

Carbonates were counted into two categories "carbonate cement" filling pore

spaces and "replacement carbonate" replacing partly or completely detrital grains for samples from Boreholes A to V. However, for samples from Boreholes W to Z, which were counted during early stage of the modal analyses, carbonates were counted under the term "carbonates".

Grain size was measured directly under the petrological microscope by means of a micrometer eyepiece. The measurement was carried out by 1) randomly select ten detrital grains (not necessarily the same type of detrital grains), 2) measure the longest intercept across the grain in the X axis without rotating the microscope stage, and 3) average the values of the ten measurements.

Sorting and rounding were estimated from thin section examinations. The degree of sorting ranges from very poorly, through poorly and moderately to well sorted. The degree of rounding ranges from angular, through subangular and subrounded to well rounded.

Even though porosity characteristics were examined under the petrological microscope, the study of porosity characteristics is not an easy task since the blue dye penetration is not always complete in every thin section and the inadequate grinding of thin sections can create artificial pore spaces. In some thin sections, the determination of porosity and its origin by this method is very subjective.

As indicated by Ingersoll (1978) and Moore (1979), the uncertainty of identifying detrital clasts is only one of the sources of counting errors. This means that the counting error purely due to the statistical variation is the minimum estimate of the total errors. At the 95 % confidence level (2∂) and counting 500 points, 4.6 % is the maximum counting error wholly resulting from the statistical variation (Van Der Plas and Tobi, 1965)

5.3 DESCRIPTION OF COMPONENTS AND POROSITY

5.3.1 QUARTZ

The detrital quartz grains recognised consist of three types: (1) unstrained monocrystalline grains displaying uniform extinction (Figs 5-1 & 5-2), (2) strained monocrystalline grains displaying undulatory extinction (Fig 5-3), and (3) polycrystalline grains. In addition, a trace amount of chalcedony was also recognised in a few thin sections. Types (1) and (2) were counted under the term "monocrystalline quartz" whereas type (3) as well as chalcedony were counted under the term "polycrystalline quartz".

The highest detrital monocrystalline quartz content is recorded in samples X281.3 and X297.7 (the letter prefix of sample numbers refers to the borehole location shown in Fig 5-4, the following number is the drilling depth in meters from which the sample was taken) in which it accounts for 73.2 % of the total sandstone (Appendix III). Samples K030.7 and K057.3 have the lowest detrital monocrystalline quartz content of 3.4 % of the total sandstone. In other samples, the content varies between the two extremes, largely depending upon the stratigraphic horizon from which the sample was selected, which will be discussed later.

As indicated by Pettijohn et al. (1987), it is commonly impossible to assign special grains in a sandstone to one or another source even though there may be differences in the statistical average for several different source rock types. This is considered to be true for most of the detrital monocrystalline quartz grains in the Narrabeen Group sandstones. For some of the monocrystalline quartz grains, however, they do show the characteristics typical of one particular source rock as proposed by Blatt et al. (1980).

The high proportion of coarse grained monocrystalline quartz grains in some coarse quartz rich sandstones in the Bald Hill, Upper and Lower Bulgo Operational

Fig 5-1 Unstrained monocrystalline quartz grains (Q) with overgrowths (O). Note: one of the detrital quartz grains (centre of photograph) contains many fluid inclusions. This may imply that the detrital quartz grain is of hydrothermal vein origin. Top - plane polarised light, bottom - crossed nicols. From Brush CK 1 at drilling depth of 128.0 m (sample E128.0). Scale bar is 0.125 mm.

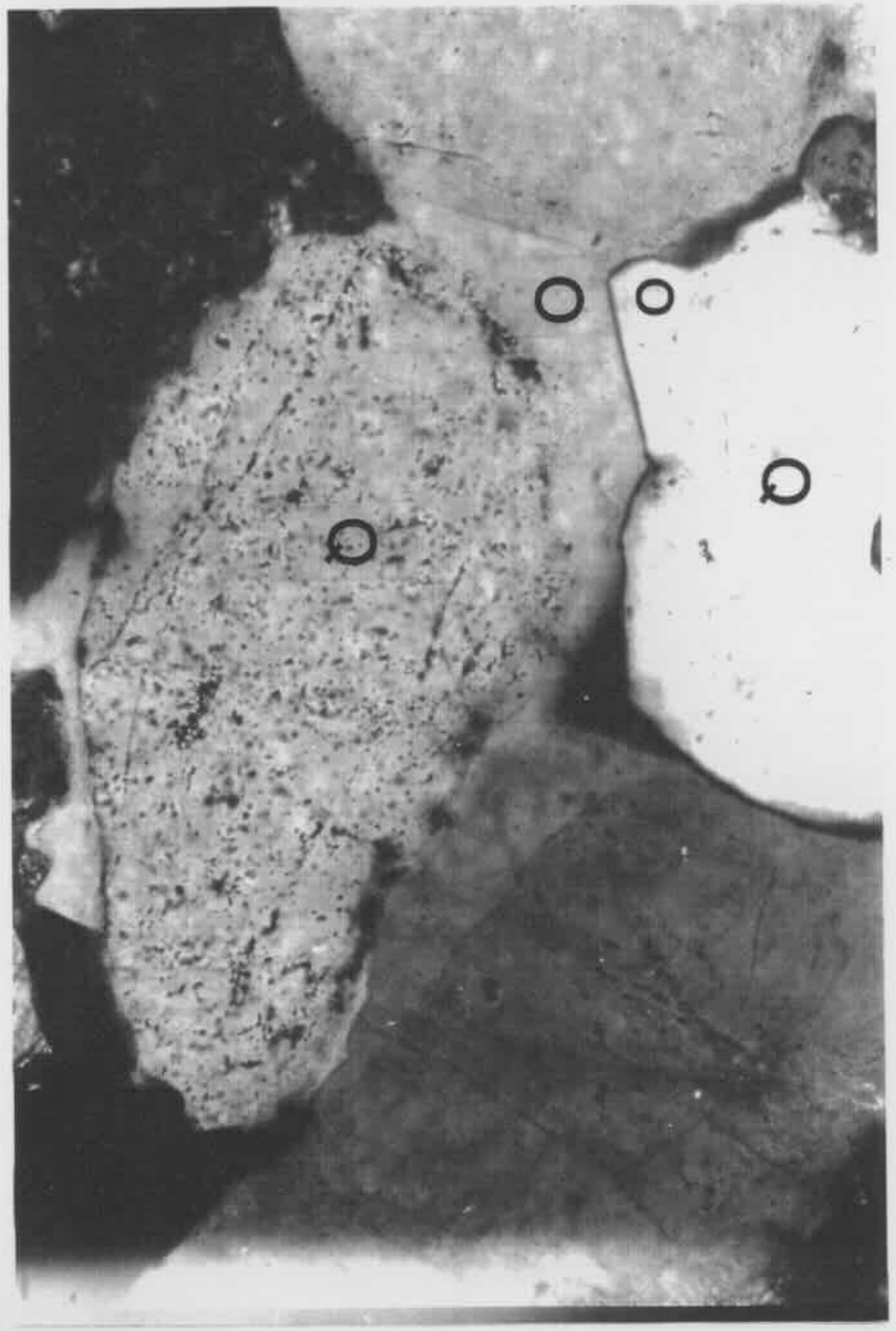

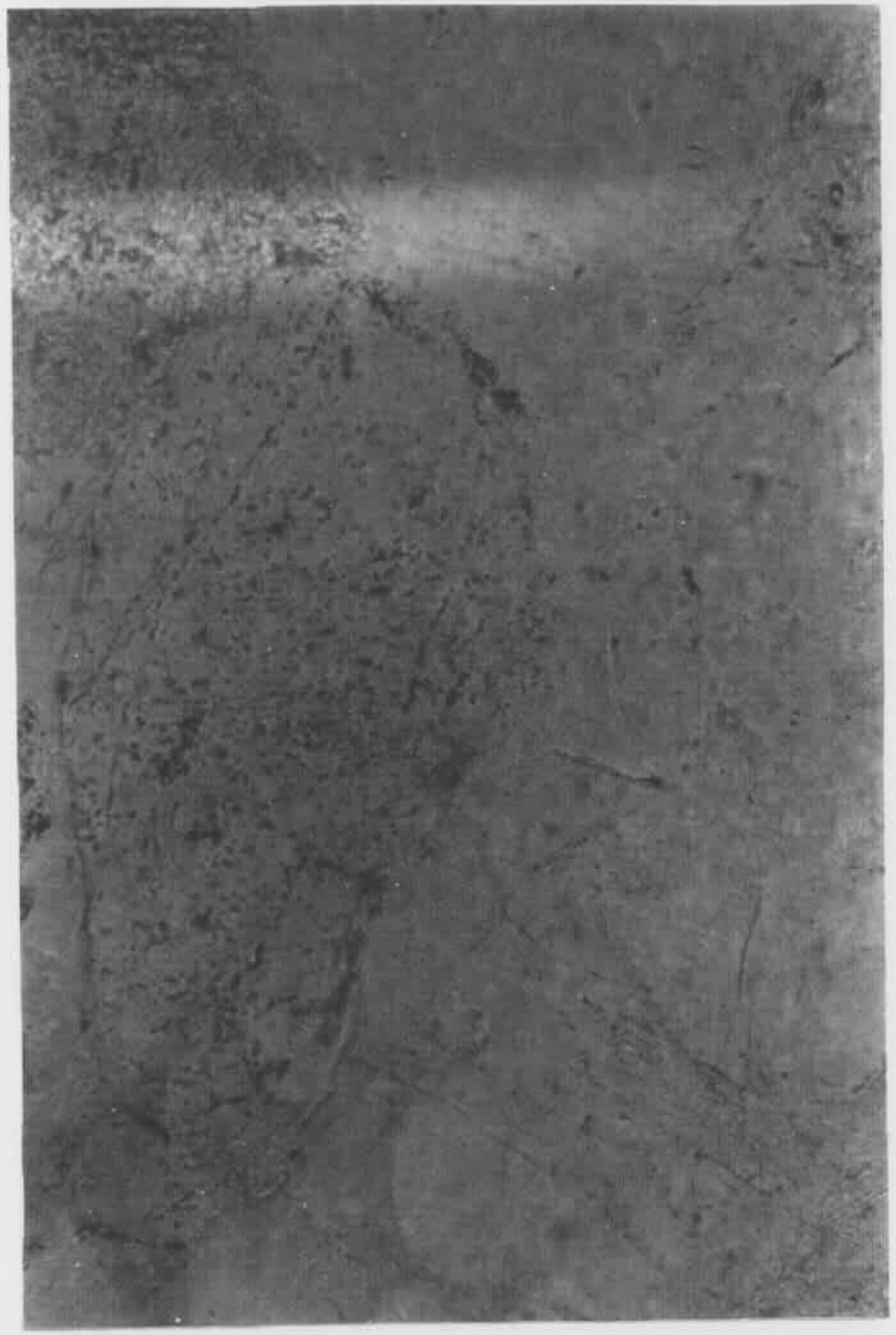

Fig 5-2 Unstrained monocrystalline quartz grains (Q) with overgrowths (O). C marks single carbonate crystals. Top - plane polarised light, bottom - crossed nicols. From Cobbitty 3 at drilling depth of 490.9 m (sample X490.9). Scale bar is 0.25 mm.

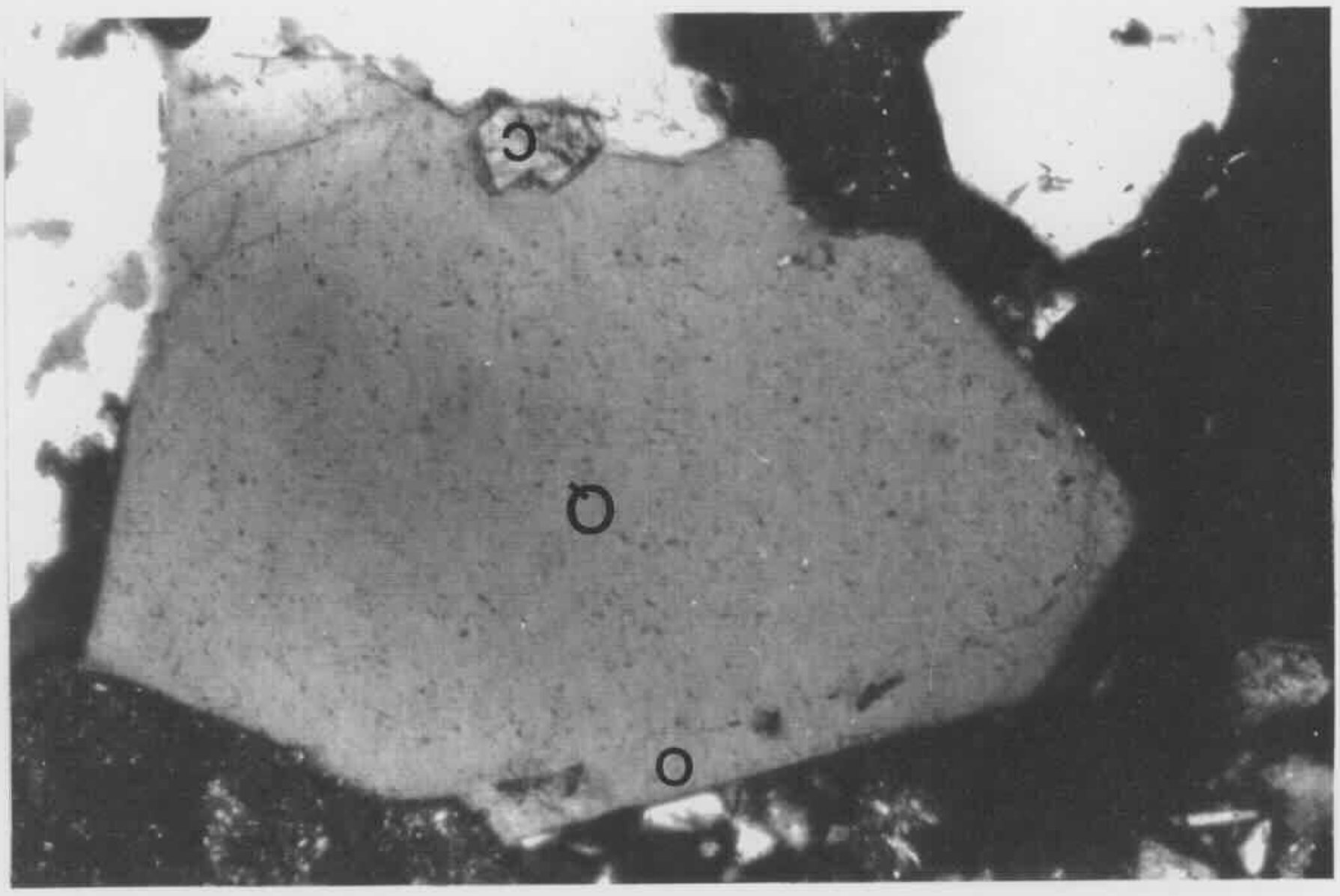

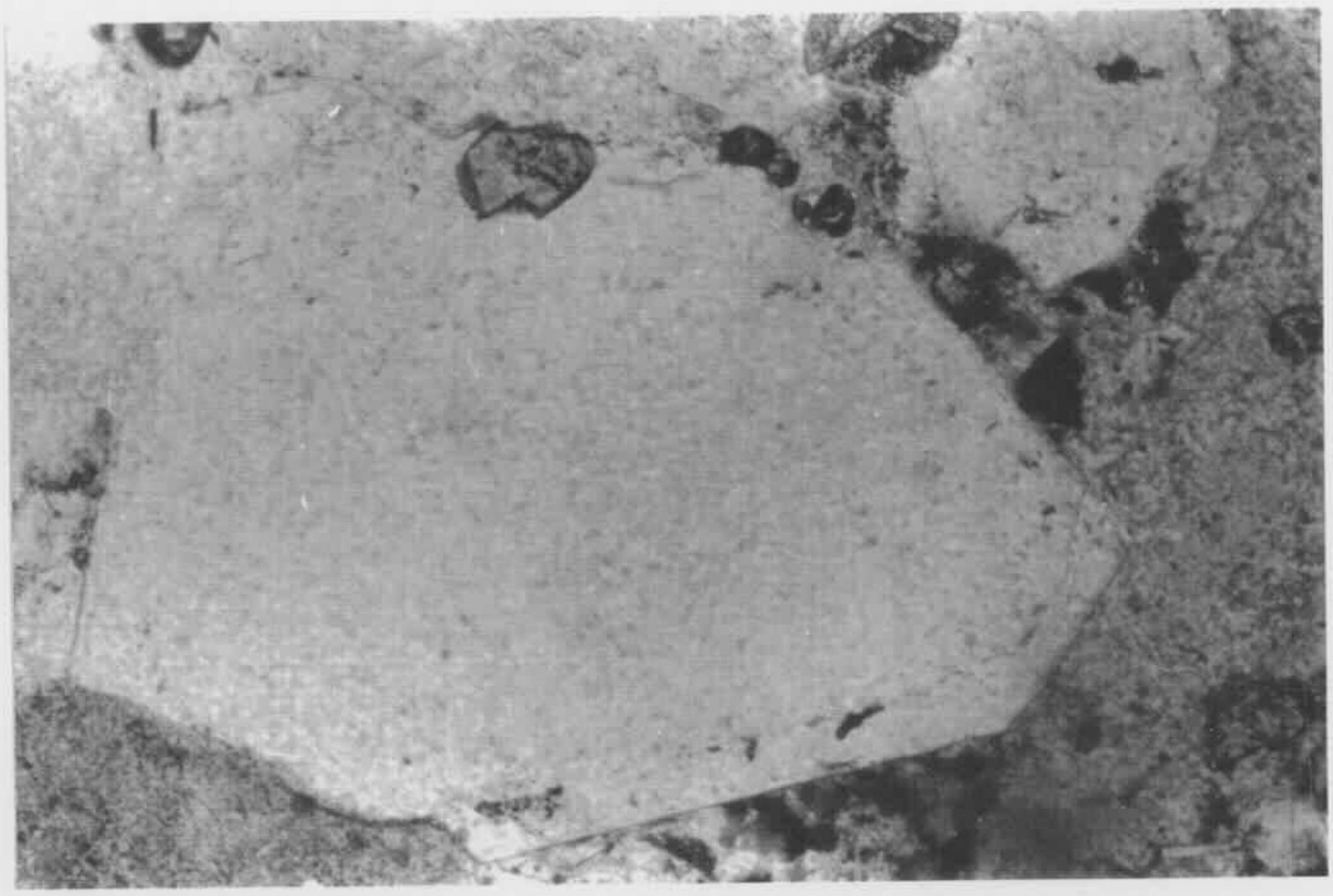

Fig 5-3 Strained monocrystalline quartz grain (Q), deformed muscovite (M), argillized volcanic rock fragments (V), and chert (C). Top - plane polarised light, bottom - crossed nicols. From Coal Cliff 17 at drilling depth of 234.7 m (sample B234.7). Scale bar is 0.25 mm.

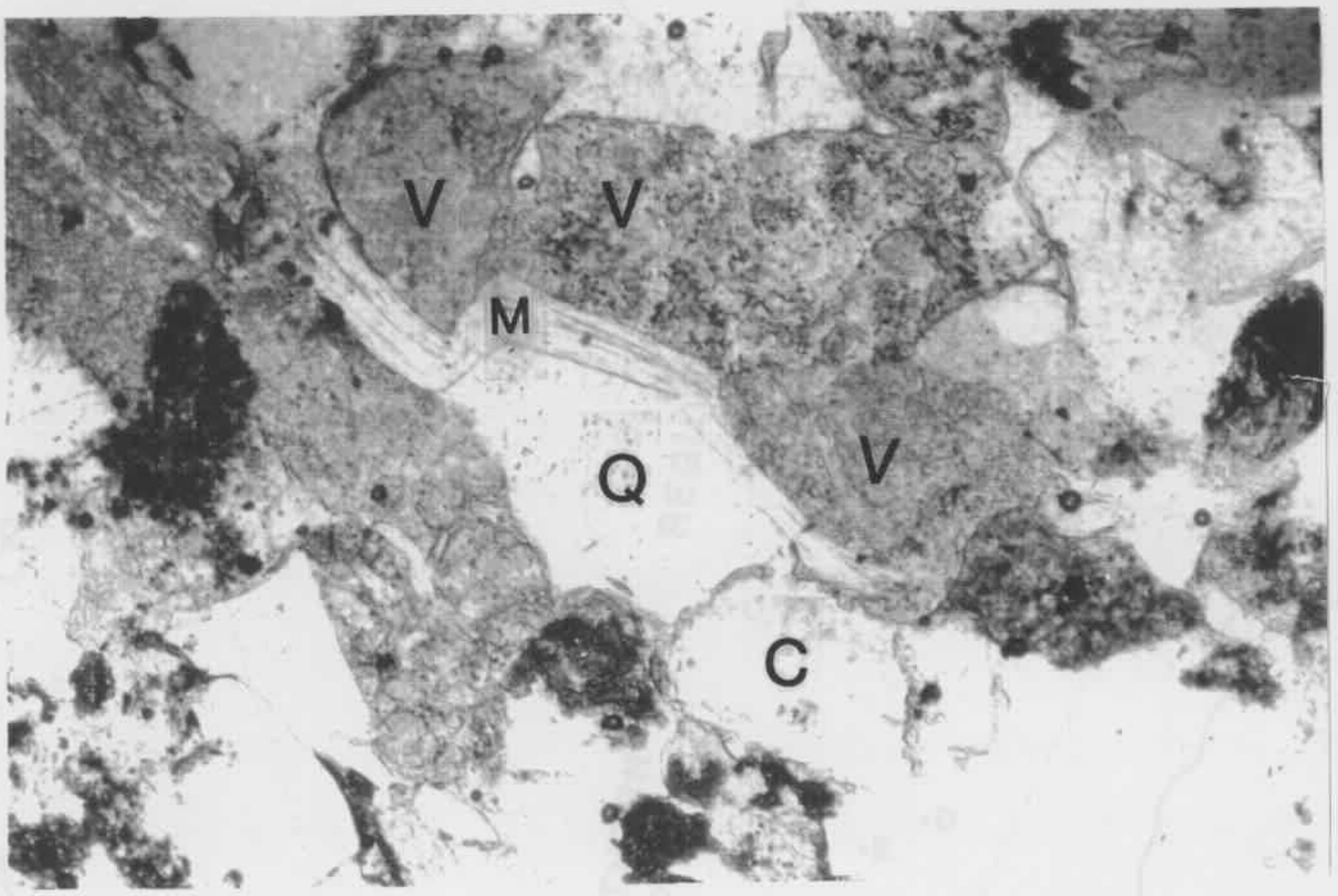
V
V
M
Q
V
C

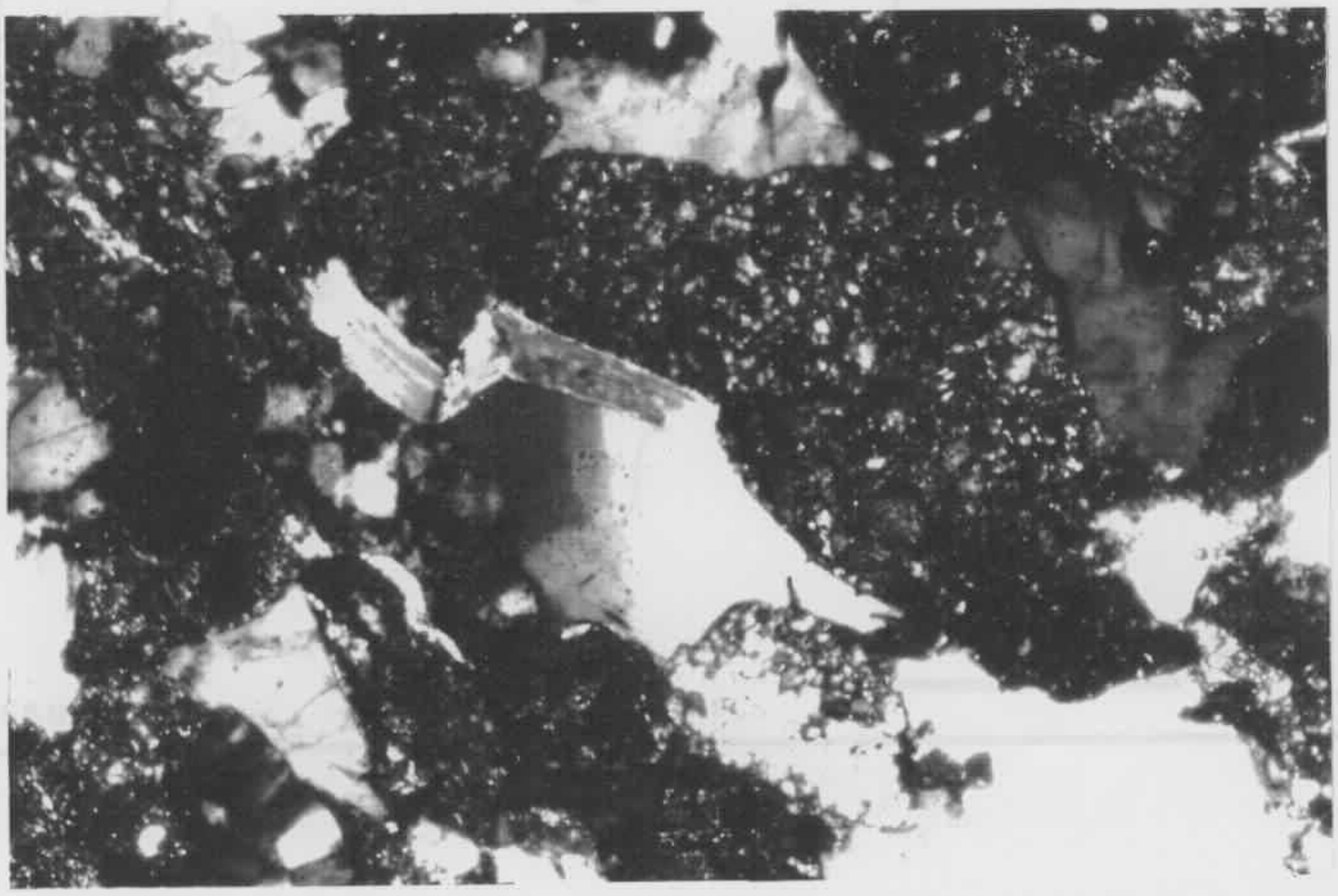

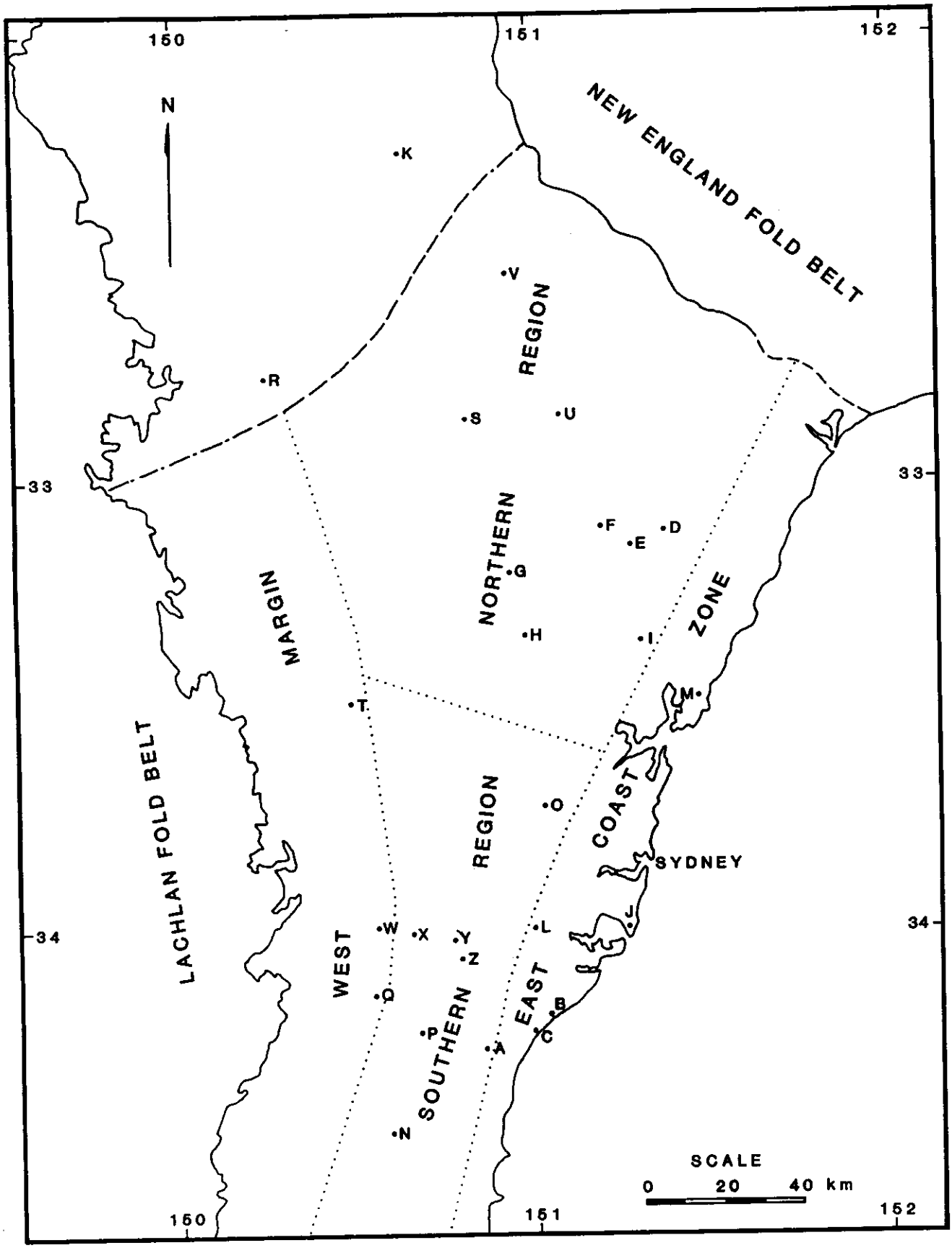

Fig 5-4 Borehole locations and regional subdivisions of the Sydney Basin.

Units in the west margin and western portion of the southern region of the basin (Fig 5-4) implies that at least some of the quartz grains were derived from granites (cf. Blatt et al., 1980). Some of the quartz grains in sandstones, which are from the Wombarra and Scarborough Operational Units in the northern region and the east coast zone of the basin (Fig 5-4), show an originally euhedral crystal form, sometimes with exsolved boundaries. This indicates that they are volcanic derived quartz. Some of the detrital monocrystalline quartz grains contain many fluid inclusions and have a very cloudy appearance under plane polarised light (Fig 5-1). They are most likely derived from hydrothermal vein sources.

Detrital polycrystalline quartz grains are present in three different forms: (1) composite consisting of uniformly sized crystals, which have mostly straight or sutured contacts (Fig 5-5). (2) composite consisting of different sized crystals (Fig 5-6), and (3) composite with preferred orientation of elongate crystals, of which some have sutured contacts (Fig 5-7). Type (3) is the least abundant.

The highest content of detrital polycrystalline quartz grains is recorded in sample X476.2 as 23.2 % of the total sandstone. In sample W334.9, no detrital polycrystalline quartz grains were recognised. In most other samples, the content ranges from 2.0 % to 7.0 %. The abundance of detrital polycrystalline quartz grains in sandstones is controlled by the grain size and the detrital source. This will be discussed later in some detail.

The detrital polycrystalline quartz grains are considered to be largely derived from metamorphic rocks including quartzites as most of them contain more than 5 monocrystalline crystals, sutured contacts (Fig 5-5) and / or preferred orientation (Fig 5-7) (cf. Blatt et al., 1980). In addition, a small number of the polycrystalline quartz grains show a cloudy appearance under plane light, which is caused by abundant fluid inclusions (Fig 5-6). Like the detrital monocrystalline quartz grains

Fig 5-5 Polycrystalline quartz grain (PQ), monocrystalline quartz grain (Q), silicified volcanic rock fragment (V), and carbonate cement (C). Top - plane polarised light, bottom - crossed nicols. From Cobbitty 3 at drilling depth of 490.9 m (sample X490.9). Scale bar is 0.25 mm.

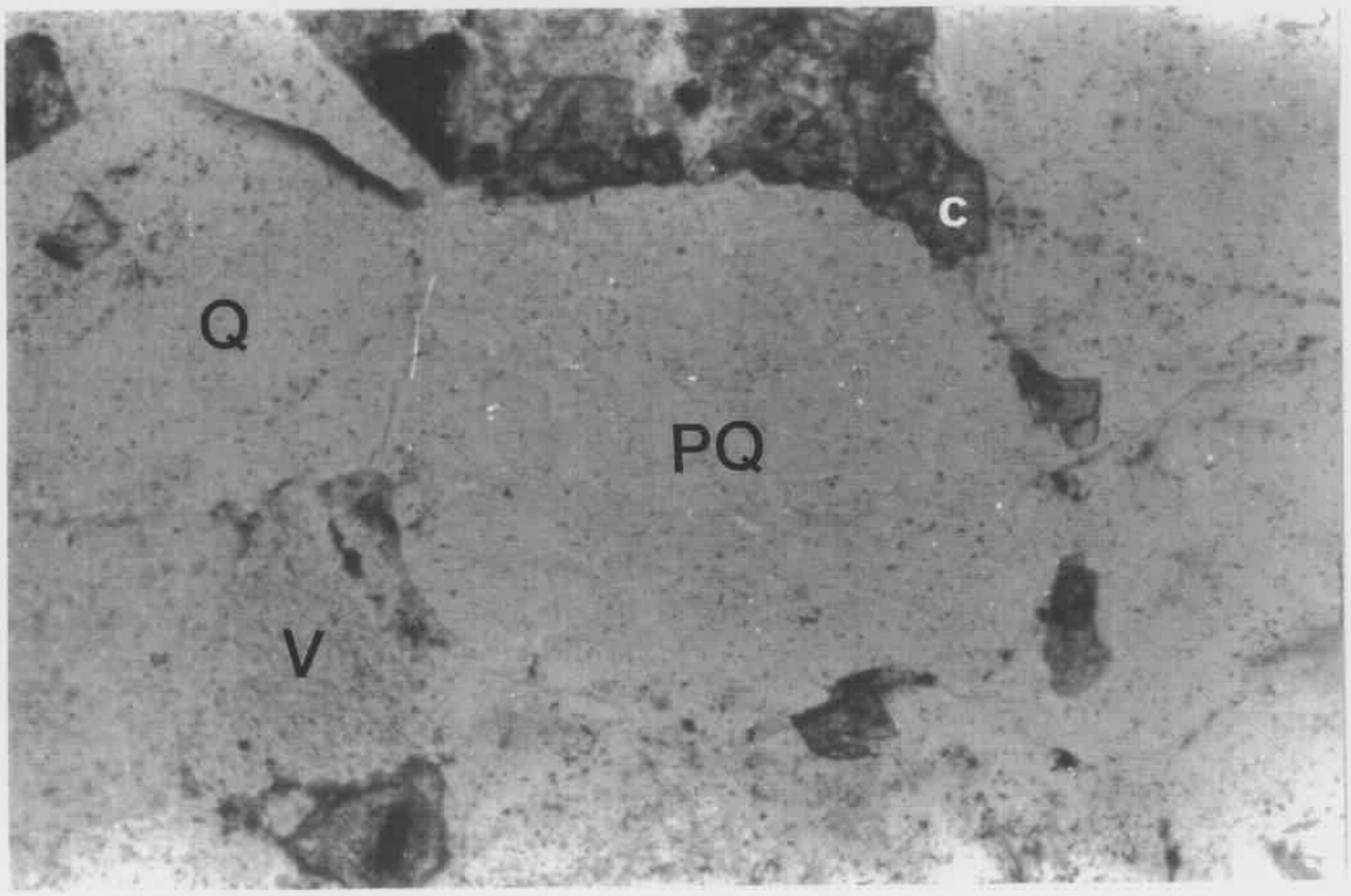
C
Q
PQ
V

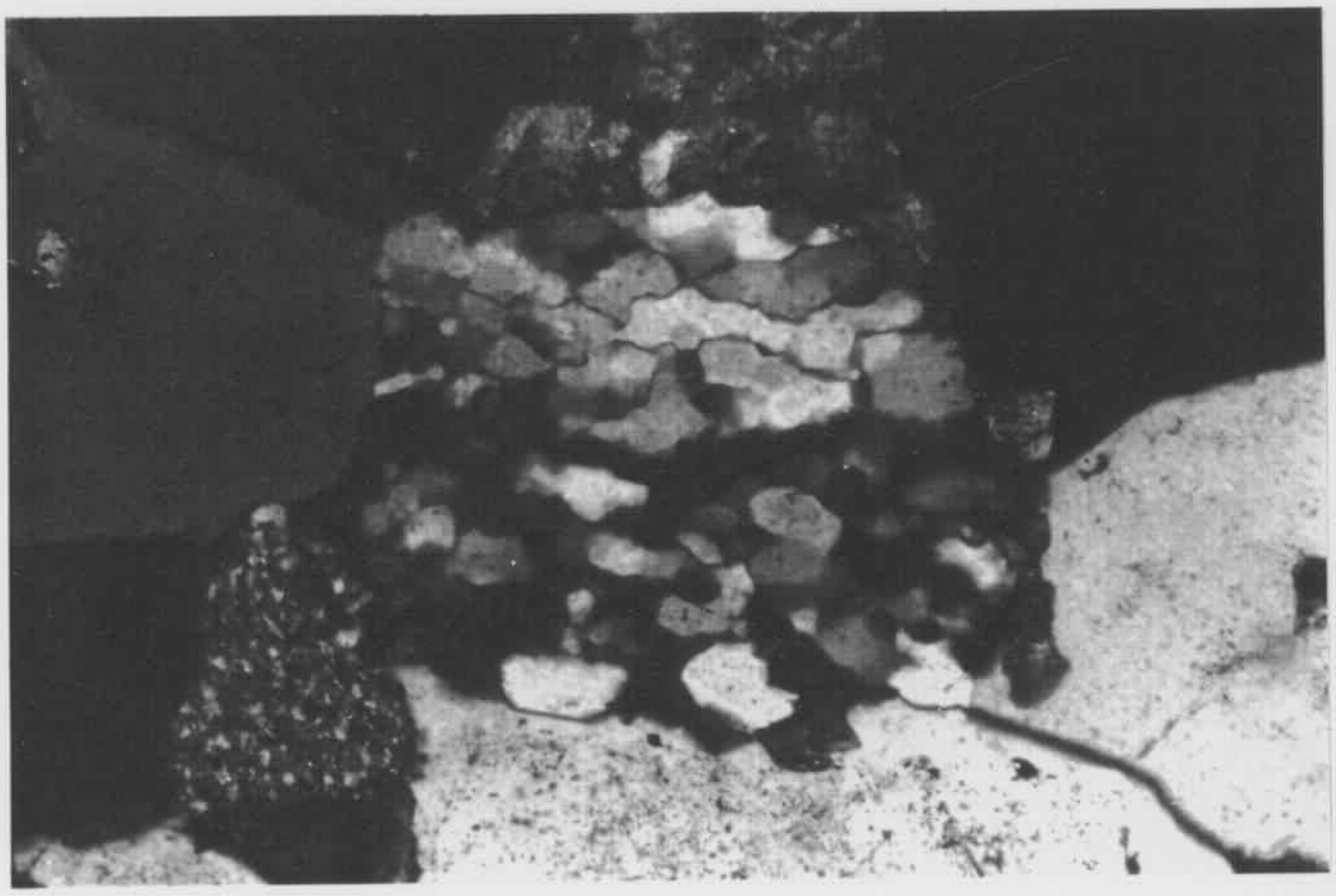

Fig 5-6 Polycrystalline quartz grain (PQ) and monocrystalline quartz grain (Q). Note: the polycrystalline quartz and the monocrystalline quartz marked with Q contain many fluid inclusions. This may imply that they are of hydrothermal vein origin. Top - plane polarised light, bottom - crossed nicols. From Cobbitty 3 at drilling depth of 508.2 m (sample X508.2). Scale bar is 0.25 mm.

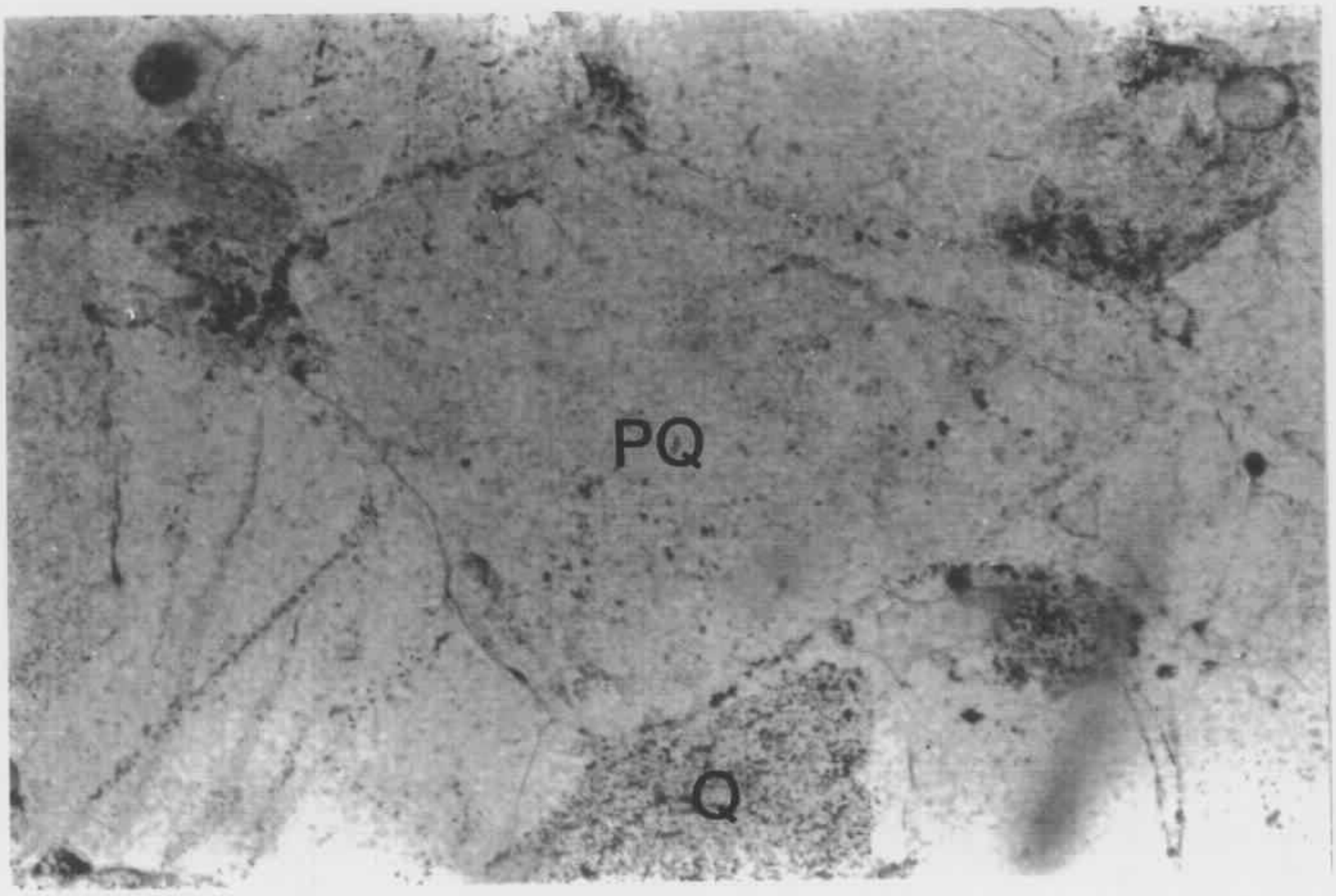
PQ
Q

Fig 5-7 Zoned polycrystalline quartz grain (PQ) and monocrystalline quartz grains (Q). Top - plane polarised light, bottom - crossed nicols. From Weromba 2 at drilling depth of 289.8 m (sample W289.8). Scale bar is 0.625 mm.

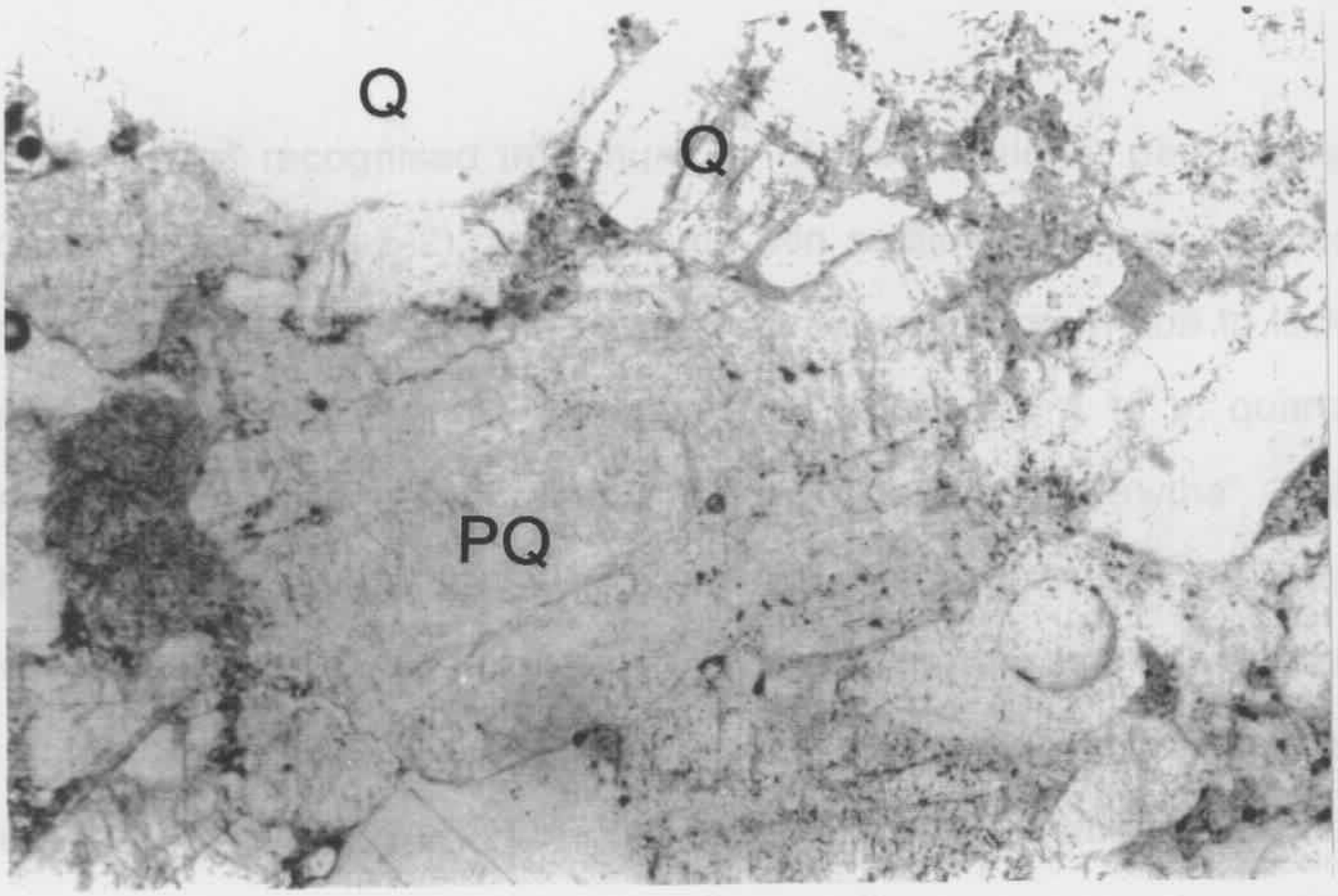
Q
Q
PQ

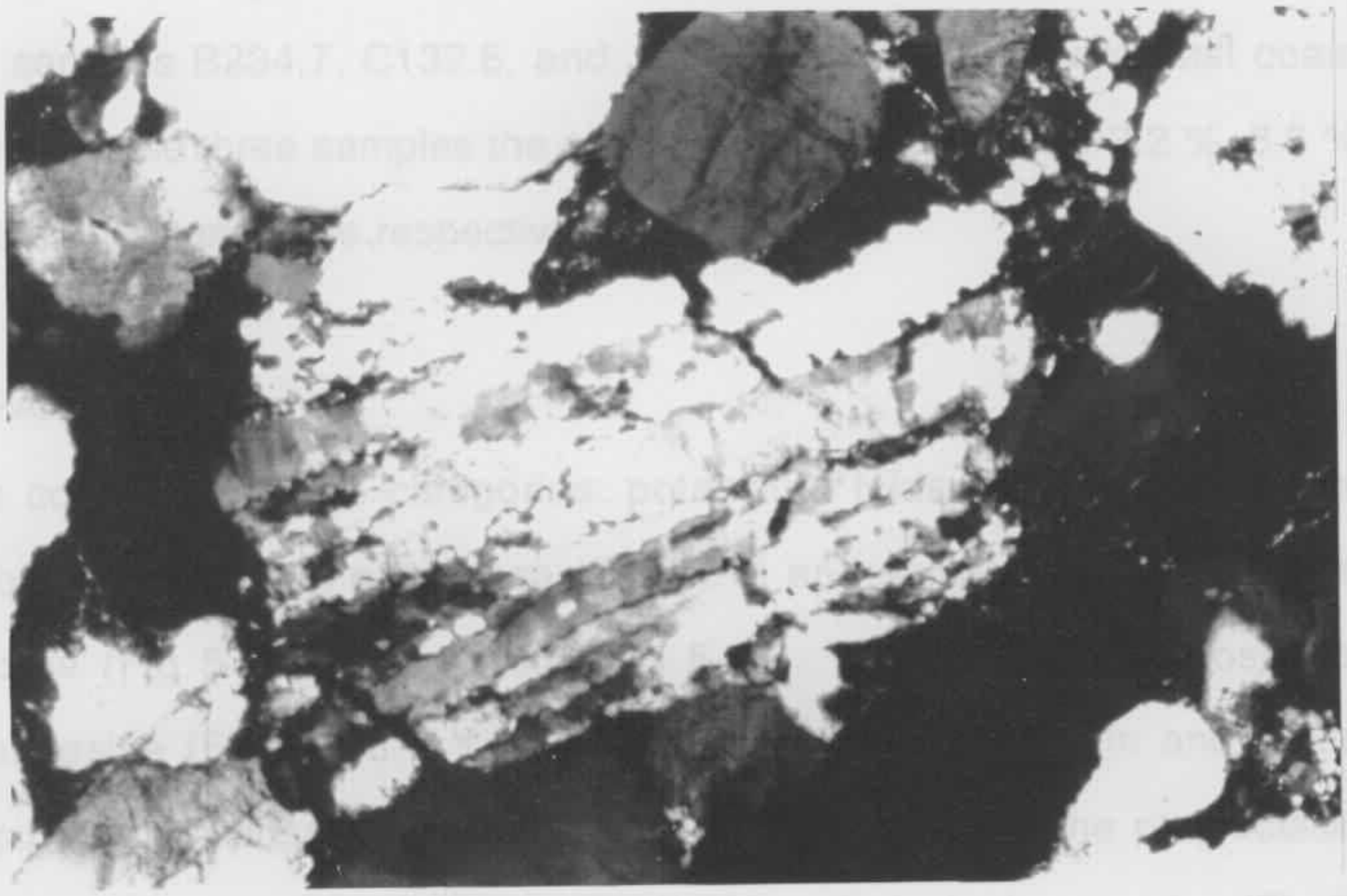

with a cloudy appearance, they were probably derived from hydrothermal vein sources.

Quartz overgrowths were recognised in a number of thin sections, particularly those rich in quartz (Figs 5-1 & 5-2), and in some thin sections it is not easy or possible to distinguish quartz overgrowth from the detrital quartz grain due to lack of a clear boundary (Fig 5-8). For the samples from Boreholes A to V, quartz overgrowths were counted into a separated category "quartz overgrowths". The counting results show that quartz overgrowths are rarely more than 2.0 % of the total sandstone. No quantitative evaluation of quartz overgrowths was made for the samples from Boreholes W to Z. In these samples, quartz overgrowths on detrital monocrystalline quartz grains were counted under "monocrystalline quartz" whereas those rare occurrences on detrital polycrystalline quartz grains were counted under "polycrystalline quartz". In the majority of these sandstones, however, the content of quartz overgrowths was estimated to be less than 2 % of the total sandstone.

In addition to quartz overgrowths, quartz cement (Fig 5-9) as mega-quartz was seen in three samples B234.7, C132.6, and J514.8 from the southern east coast zone (Fig 5-4). In these three samples the quartz cement accounts for 3.2 %, 8.8 % and 8.8 % of the total sandstone respectively.

5.3.2 FELDSPAR

Feldspar was counted into two categories: potassium feldspar and plagioclase. The former consists largely of orthoclase (Fig 5-10) and sanidine and to a lesser extent microcline (Fig 5-11) and perthite (Fig 5-12). The latter is composed of oligoclase - andesine (Figs 5-13 & 14), as also recognised by Martin and Baker (1987). The potassium feldspar is generally more abundant than the plagioclase. Feldspar overgrowths on both orthoclase (Fig 5-10) and plagioclase grains (Fig 5-

Fig 5-8 Carbonate cement (C) postdating quartz overgrowths (O). Note: quartz overgrowths are corroded by the carbonate cement (arrow). The boundary between the detrital quartz grain and the overgrowths is not clear. V marks the argillized volcanic rock fragment. Top - plane polarised light, bottom - crossed nicols. From Oil Longley 1 at drilling depth of 781.5 m (sample I781.5). Scale bar is 0.25 mm.

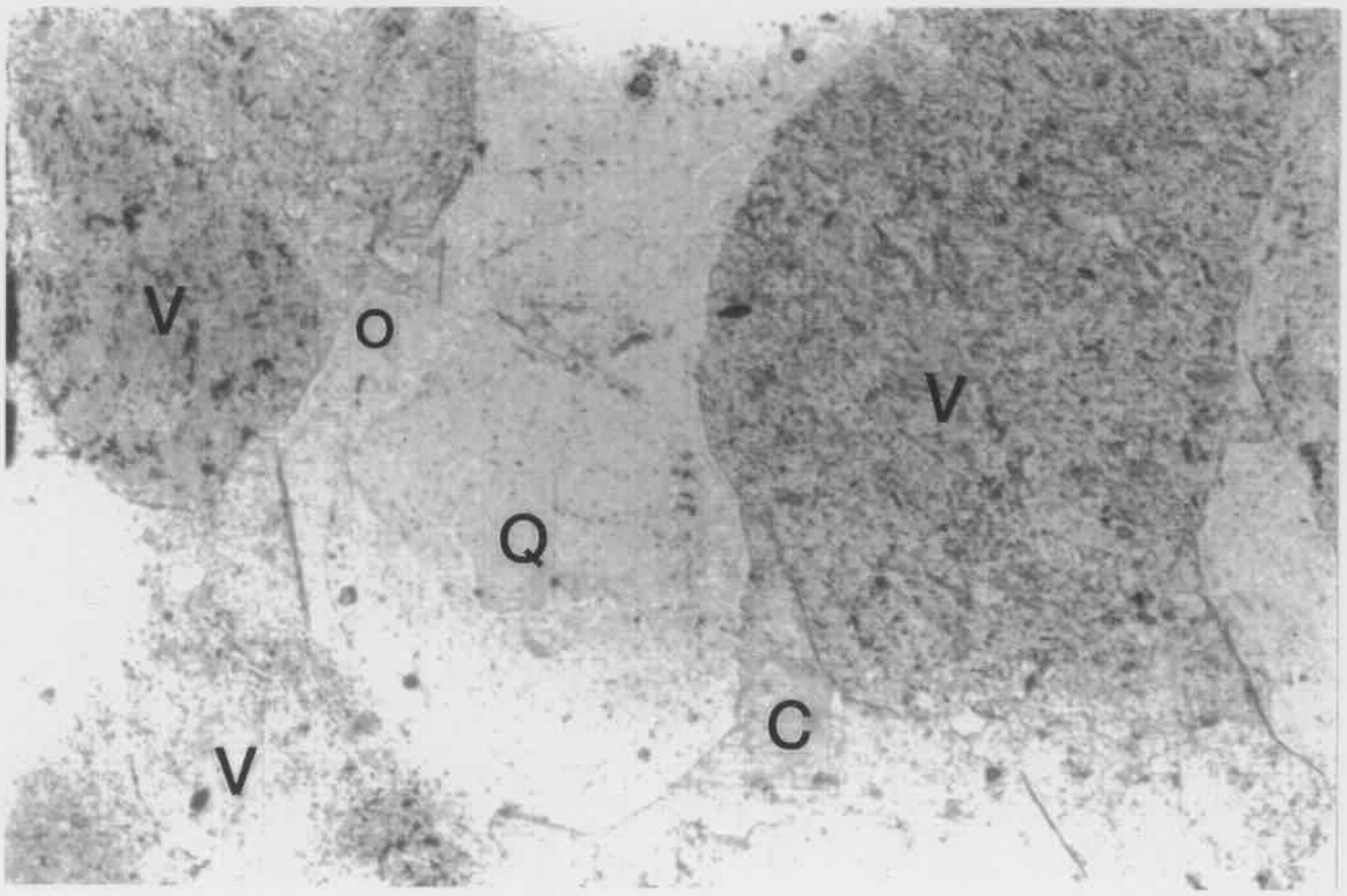
V
O
Q
V
V
C

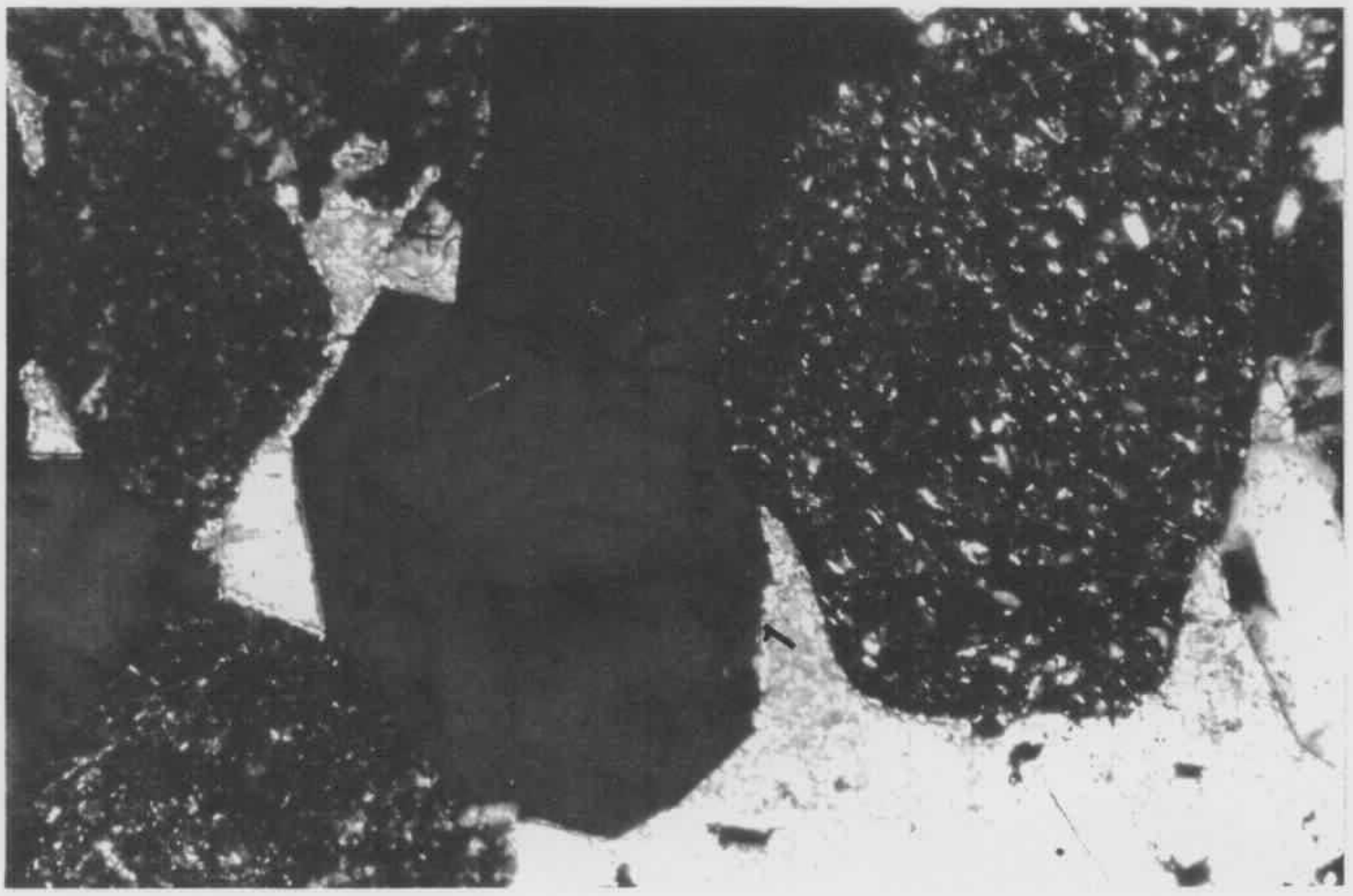

Fig 5-9 Later formed quartz cement (mega-quartz crystals) marked by MQ and earlier formed chlorite coating detrital grains (arrows). Top - plane polarised light, bottom - crossed nicols. From Coal Cliff 13 at drilling depth of 132.6 m (sample C132.6). Scale bar is 0.125 mm.

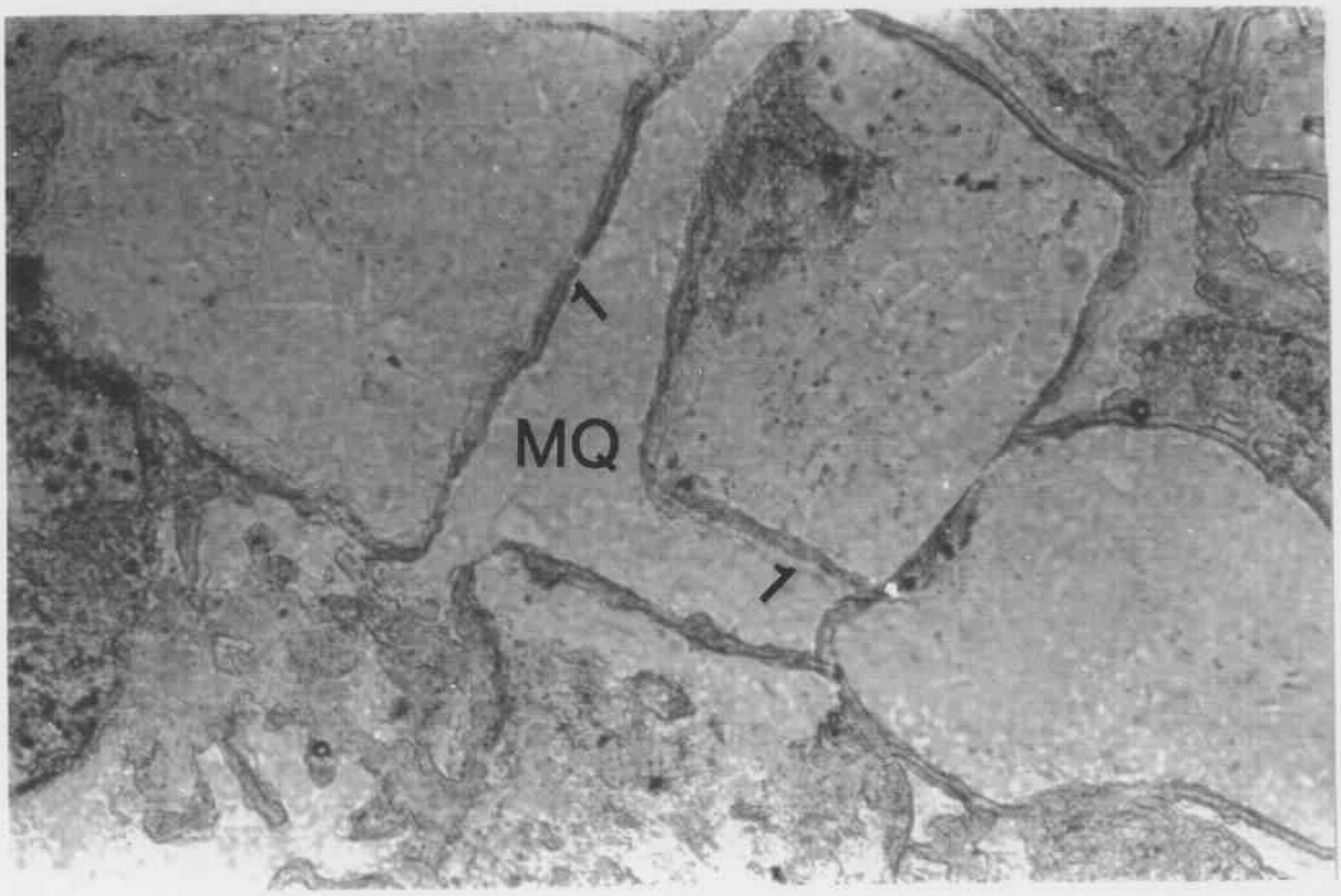
MQ

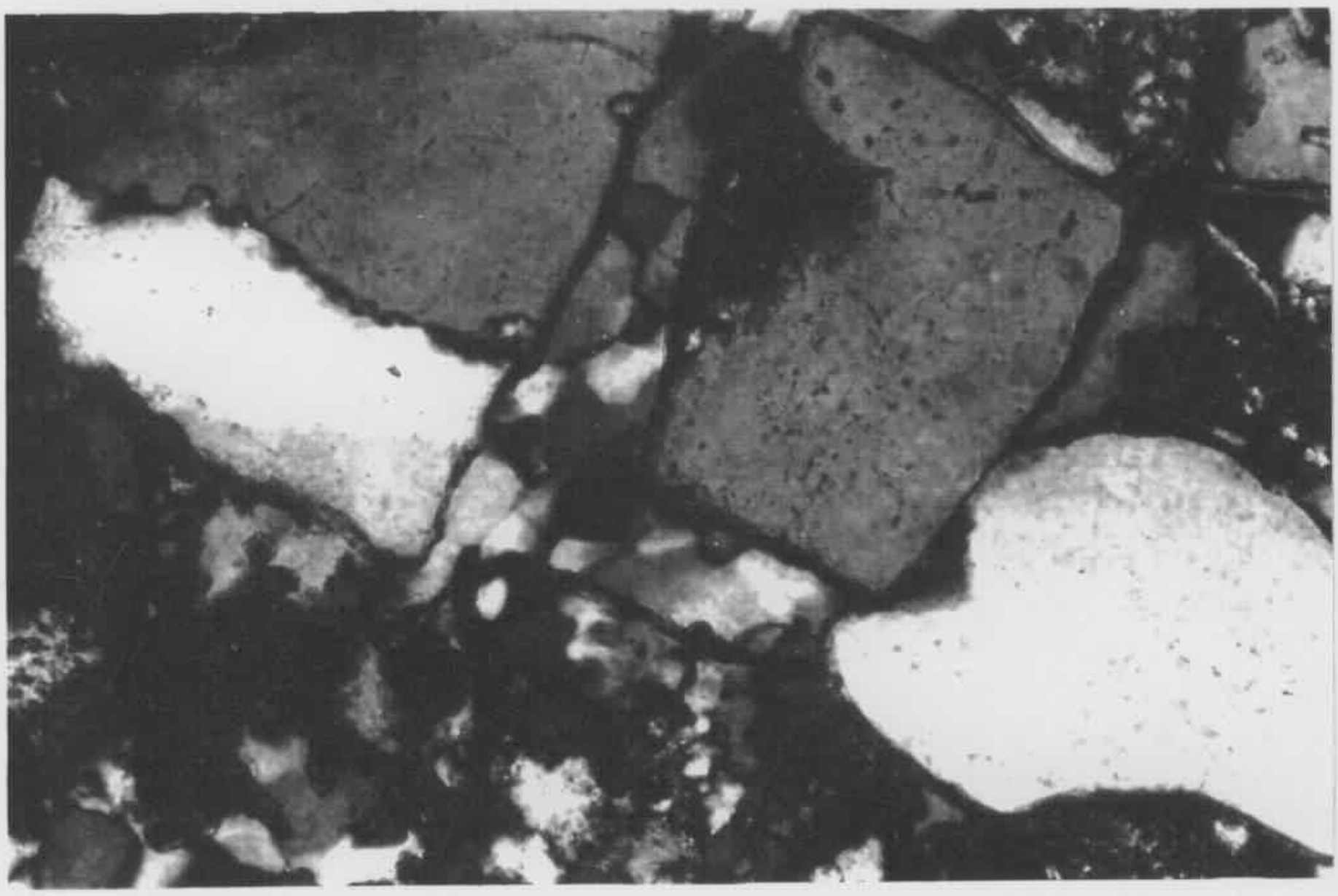

Fig 5-10 Orthoclase (Or) with overgrowths (O). Top - plane polarised light, bottom - crossed nicols. From Brush CK 1 at drilling depth of 128.0 m (sample E128.0). Scale bar is 0.25 mm.

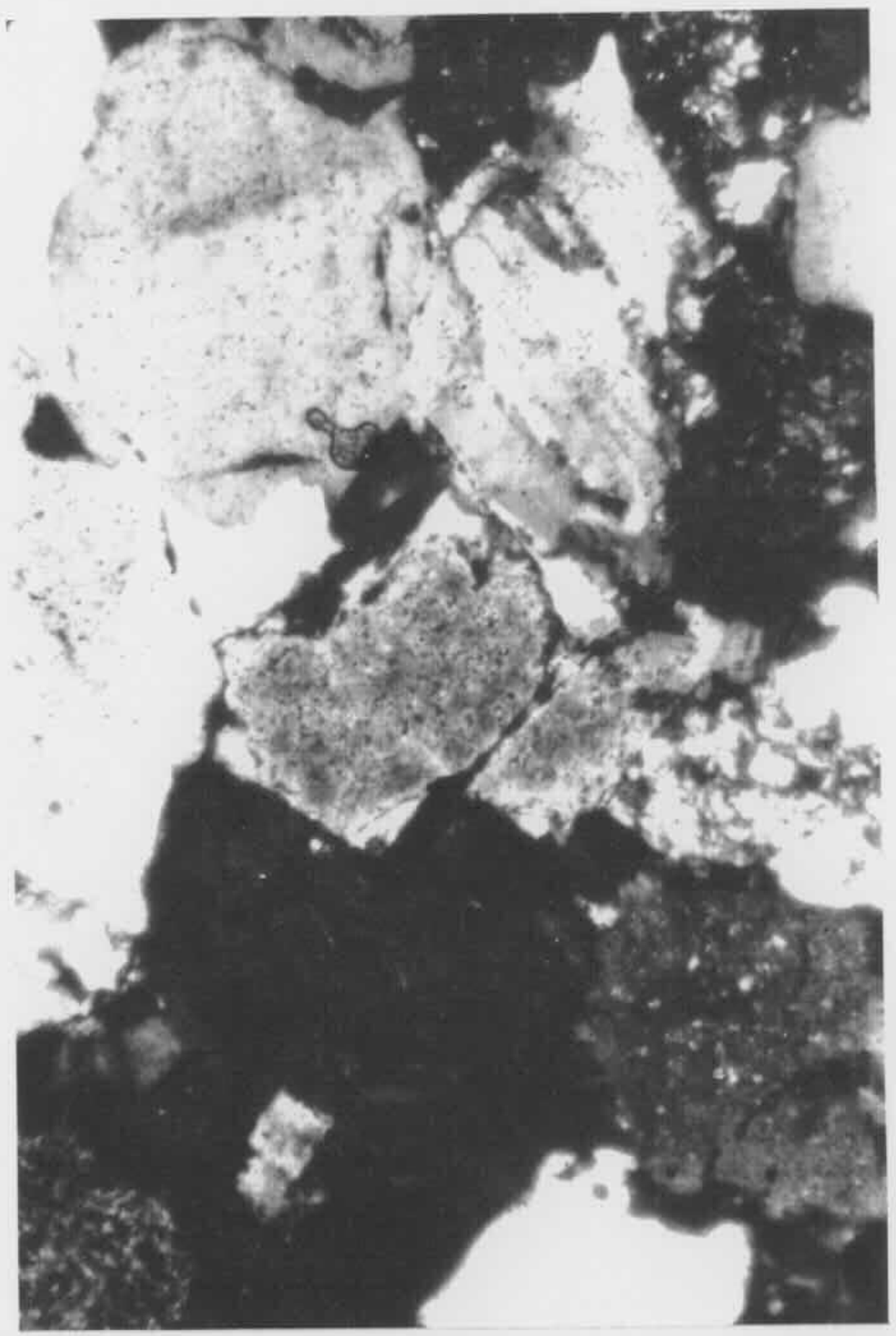


Or
O

Fig 5-11 Microcline (M) partly replaced by carbonate. Carbonate also replaces volcanic rock fragments (R). C marks carbonate cement, V argillized volcanic rock fragments, Q monocrystalline quartz, and CH chert. Crossed nicols. From Liverpool 91 at drilling depth of 595.2 m (sample L595.2). Scale bar is 0.25 mm.

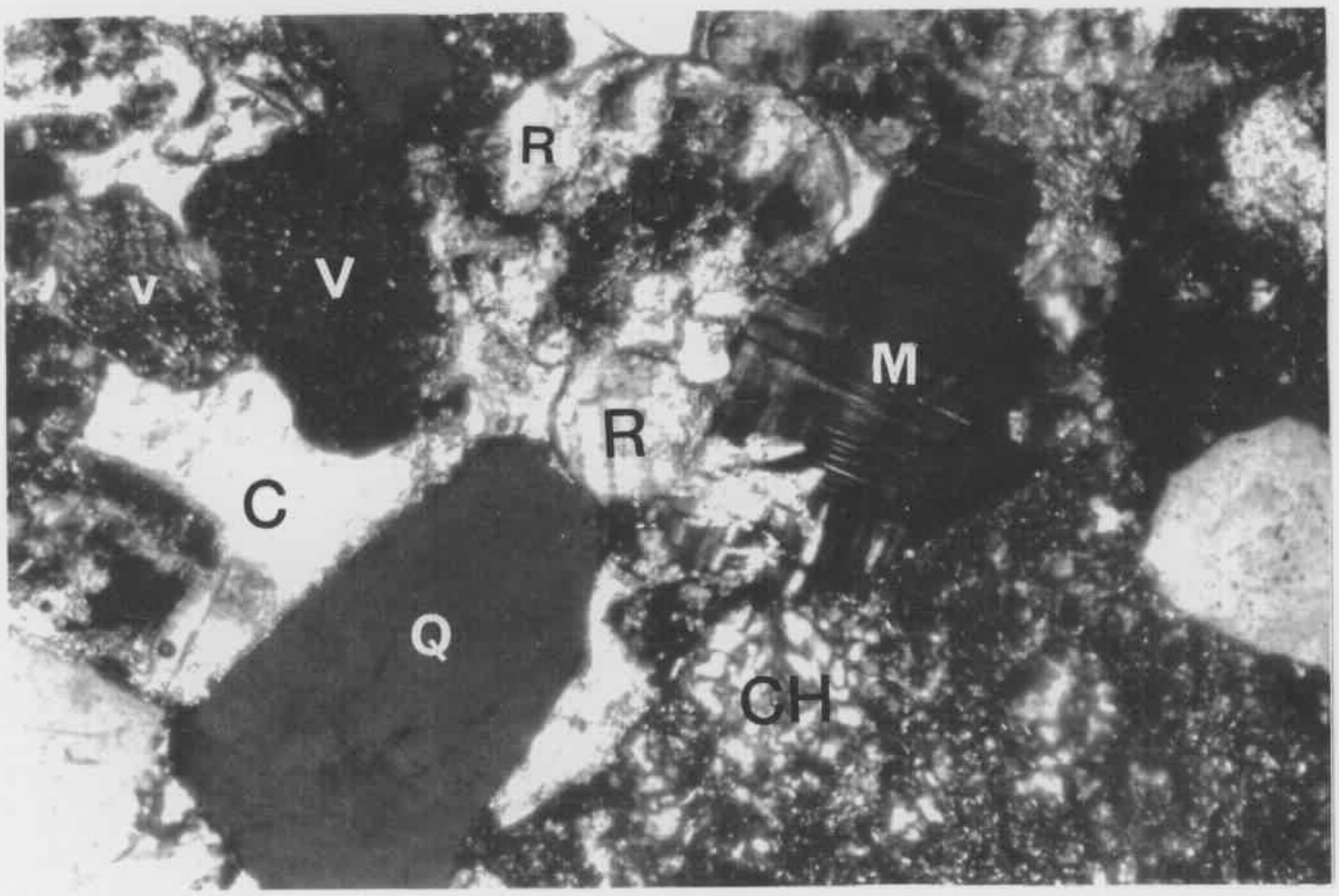
R
V
V
M
R
C
Q
CH

Fig 5-12 Perthite (P), silicified volcanic rock fragment (V), chert (C), and monocrystalline quartz (Q). Top - plane polarised light, bottom - crossed nicols. From Oil Longley 1 at drilling depth of 629.3 m (sample I629.3). Scale bar is 0.25 mm.

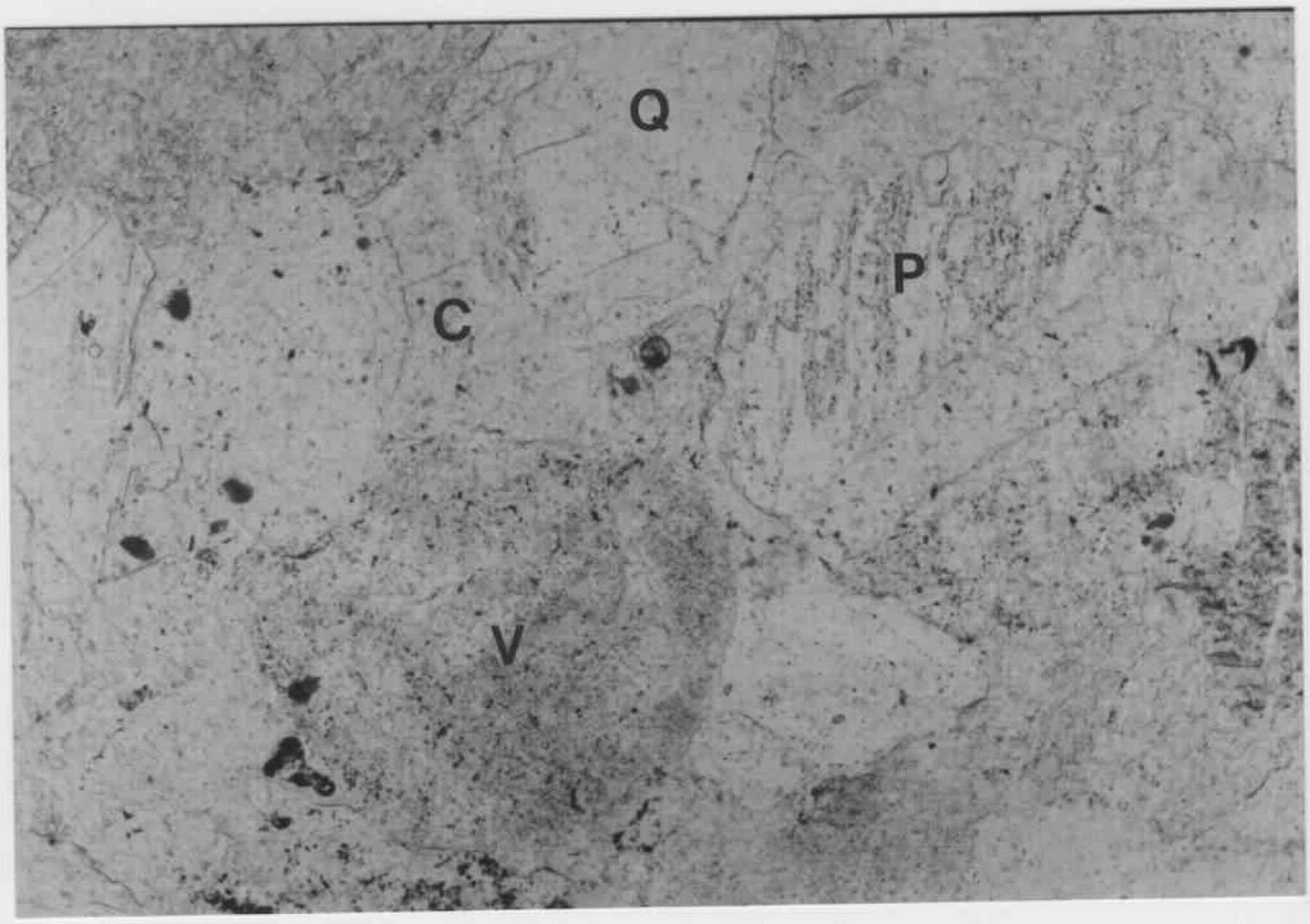
Q
P
C
V

Fig 5-13 Plagioclase (P) with overgrowths (albite ?) (O). Crossed nicols. From Brush CK at drilling depth of 128.0 m (sample E128.0). Scale bar is 0.25 mm.

Fig 5-14 Plagioclase (P) corroded by carbonate cement (C). Carbonate (R) also partly replaces volcanic rock fragment (upper right corner of microphotograph). Crossed nicols. From Cape Banks 1 at drilling depth of 650.3 m (sample J650.3). Scale bar is 0.125 mm.

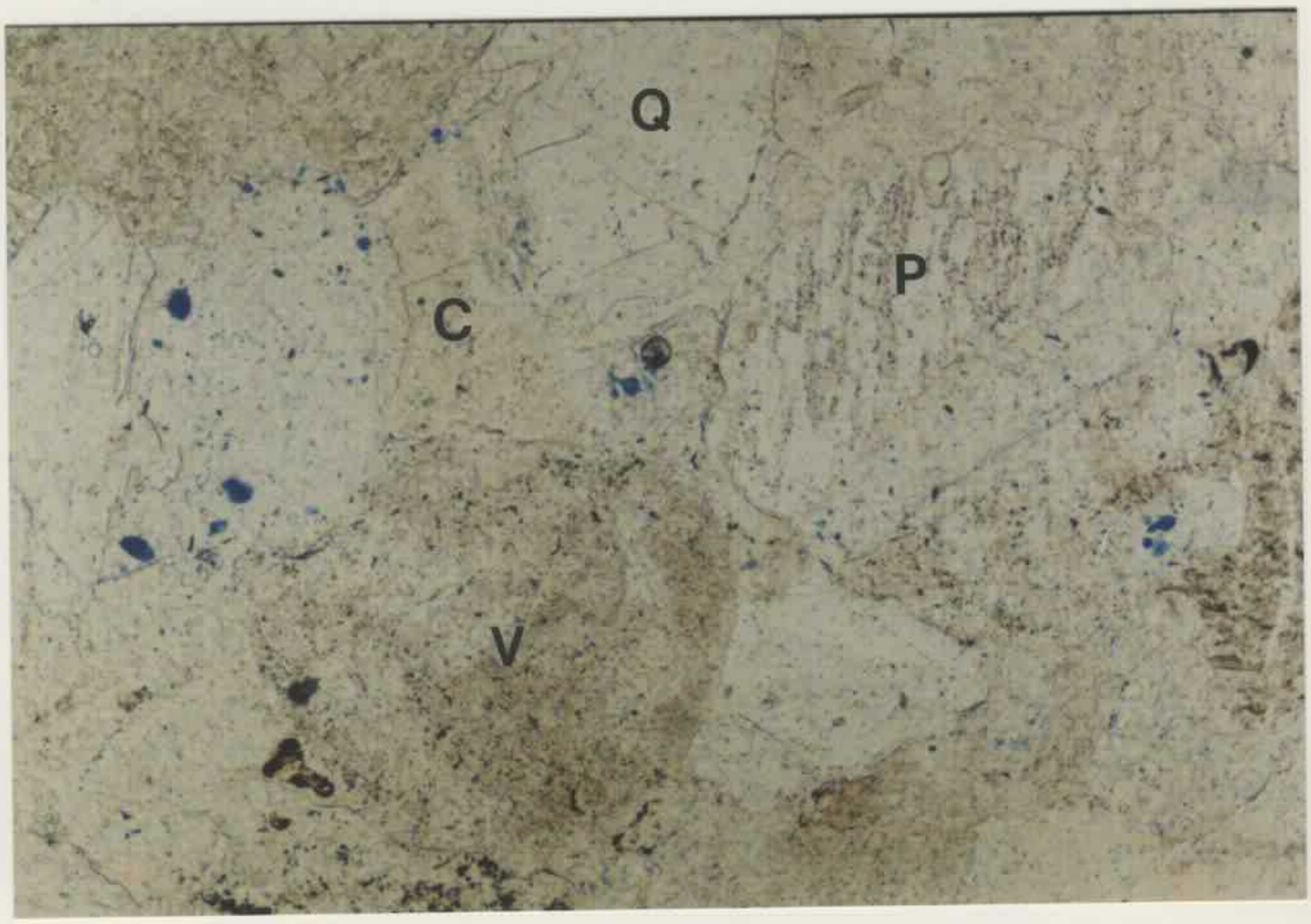
Q
P
C
V

Fig 5-13 Plagioclase (P) with overgrowths (albite ?) (O). Crossed nicols. From Brush CK at drilling depth of 128.0 m (sample E128.0). Scale bar is 0.25 mm.

Fig 5-14 Plagioclase (P) corroded by carbonate cement (C). Carbonate (R) also partly replaces volcanic rock fragment (upper right corner of microphotograph). Crossed nicols. From Cape Banks 1 at drilling depth of 650.3 m (sample J650.3). Scale bar is 0.125 mm.

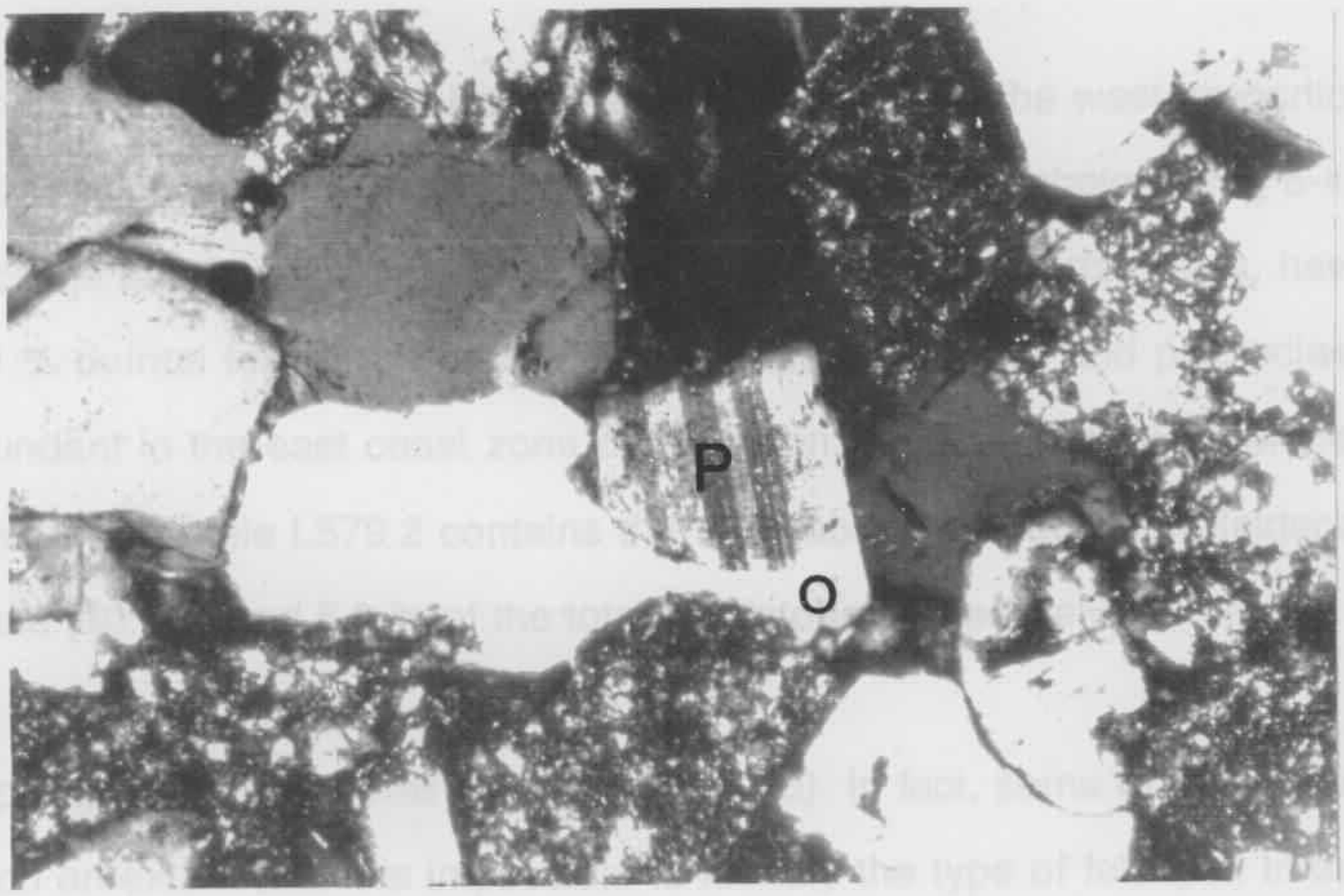
P
O

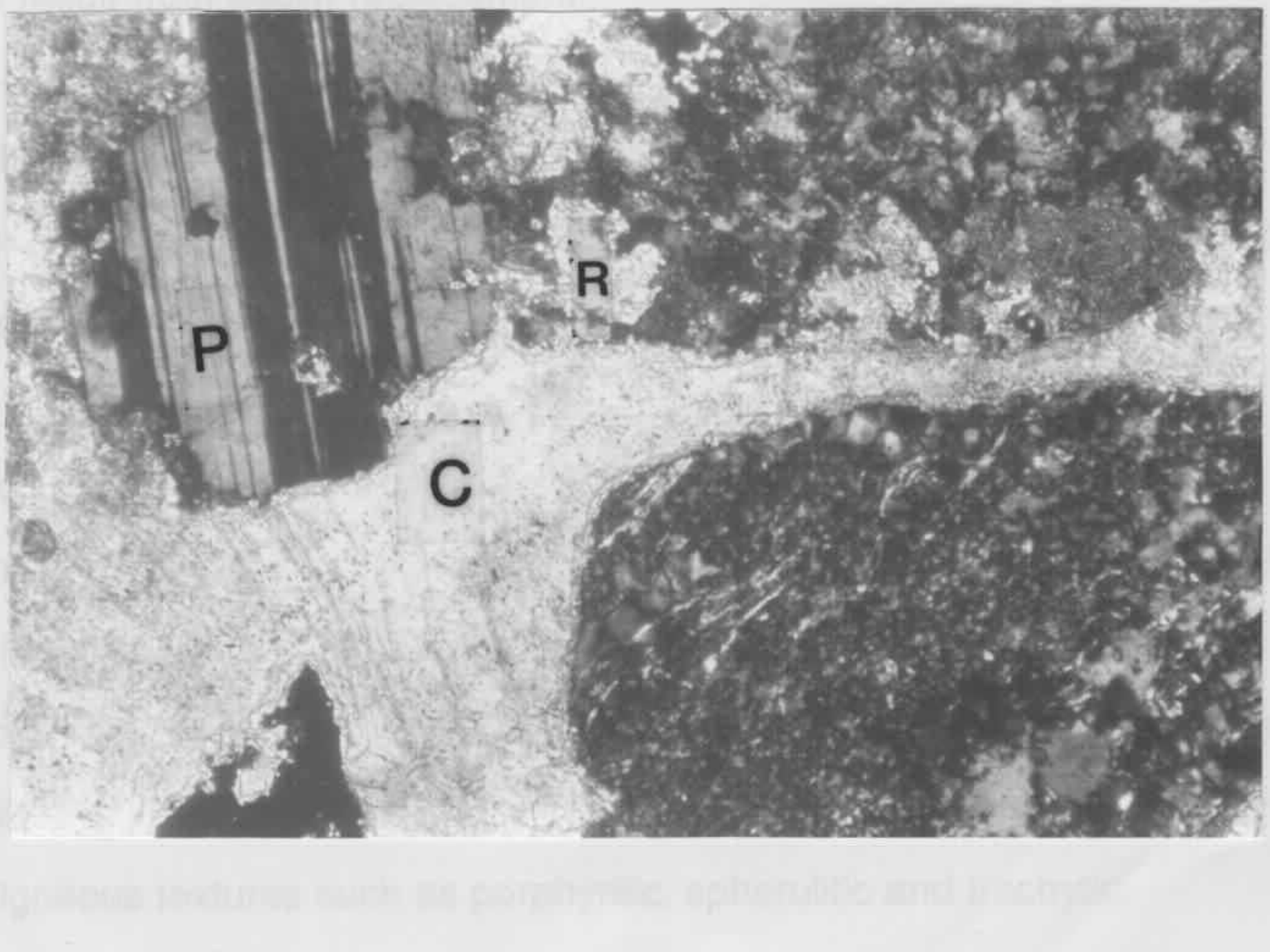
P
R
C

13) were seen, but they are very rare.

In the west margin (represented by Boreholes Q, T, W, and R), the western portion of the southern region (represented by Boreholes X to Z) and Borehole K (Fig 5-4), the majority of the sandstones, especially those rich in detrital quartz grains, have less than 2.0 % detrital feldspar. Both detrital potassium feldspar and plagioclase are more abundant in the east coast zone of the basin (represented by Boreholes B, C, L, J, and M). Sample L579.2 contains the most abundant potassium feldspar and plagioclase (10.0 % and 5.0 % of the total sandstone respectively).

Detrital feldspar grains are generally altered (Fig 5-10). In fact, some of them have altered to such an extent that it is impossible to identify the type of feldspar. In this case, the grains were counted as detrital potassium feldspar. In addition detrital feldspar grains are easy targets for carbonate replacement. Some have been partly or completely replaced by carbonates (Figs 5-11 & 14) and some of the secondary pore spaces seen in thin sections are created by the dissolution of detrital feldspar grains. Patchy kaolin flakes with the outline of detrital K-feldspar grains are considered to result from kaolin replacement.

5.3.3 LITHIC FRAGMENTS

Rock fragments are dominated by volcanic rock clasts with a trace amount of granitic, metamorphic and sedimentary rock fragments.

(i) Igneous Rock Fragments

In the Narrabeen Group sandstones, igneous rock fragments are overwhelmingly composed of volcanic lithics. They were mainly derived from silicic (rhyolite - dacite) and to lesser extent intermediate flows and tuffs. They show a wide range of textural variations, as also recognised by Martin and Baker (1987). Many grains show typical igneous textures such as porphyritic, spherulitic and trachytic.

The detrital volcanic lithics consist of two major groups: felsitic (silicified) and vitric (argillized) types of Dickinson (1970, 1985). The former broadly resemble the detrital chert grains (Fig 5-12) and were derived from silicic volcanic rocks or flows and tuffs which have been silicified. Their distinction from detrital chert grains is very difficult and even impossible in some thin sections. The distinction can be made with confidence only if they contain microphenocrysts, or have groundmasses coarse enough to show the contrast in RI between quartz and feldspar crystallites or if the detrital chert grains contain radiolaria. The argillized lithics are largely composed of clays, together with feldspar and quartz (Figs 5-3 & 5-8). They originated from glassy flows and tuffs which have been devitrified and altered to illite / smectite during diagenesis. All argillized volcanic lithics tend to have a dirty surface under plane polarised light due to alteration. This feature, together with texture characteristics, was used to distinguish them from detrital chert grains and other fine grained rock fragments.

In addition to these two major groups, microlithic (Dickinson, 1970; 1985) volcanic rock fragments were occasionally seen under the microscope (Figs 5-15 & 5-16), and a trace amount of granitic rock fragments were identified in a few samples.

The highest content of igneous rock fragments reaches 64.0 % of the total sandstone in sample K030.7. Sample W209.8 has the lowest content of igneous rock fragments of 0.4 %.

(ii) Sedimentary Rock Fragments

Sedimentary clasts consist of mudstone, shale (Fig 5-17) and siltstone (Fig 5-18) fragments. Some of the mudstone / shale fragments are intrabasinal mud clasts derived from inter-channel floodplain deposits. The mudstone and shale fragments were recognised by several characteristics: much larger than surrounding detrital

Fig 5-15 Volcanic rock fragment (V) with feldspar lathworks and silicified volcanic rock fragment (V1). Top - plane polarised light, bottom - crossed nicols. From Brush CK 1 at drilling depth of 243.6 m (sample E243.6). Scale bar is 0.25 mm.


V
V1

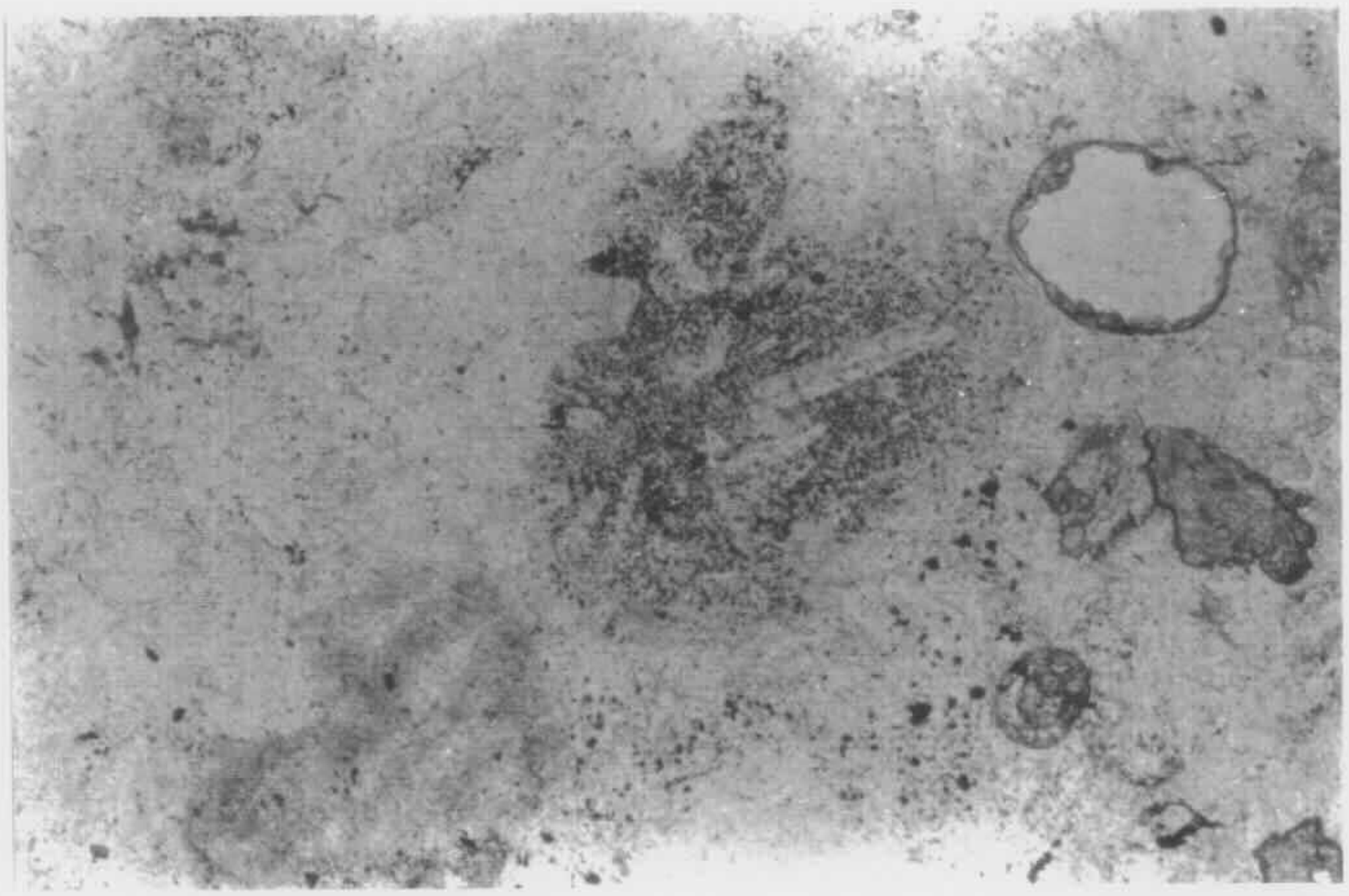

Fig 5-16 Volcanic rock fragment with feldspar lathworks (V). Top - plane polarised light, bottom - crossed nicols. From Brush CK 1 at drilling depth of 128.0 m (sample E128.0). Scale bar is 0.25 mm.

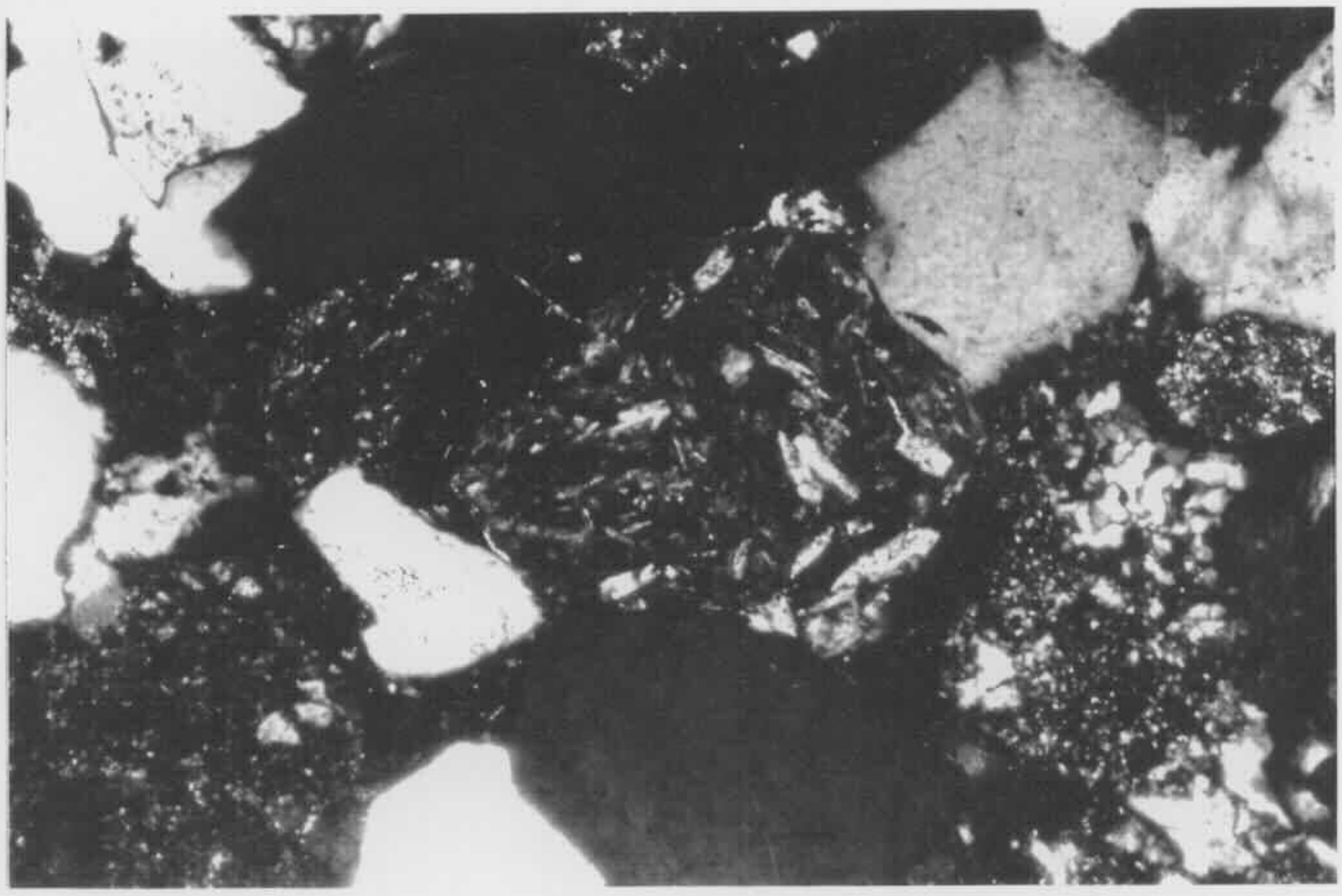

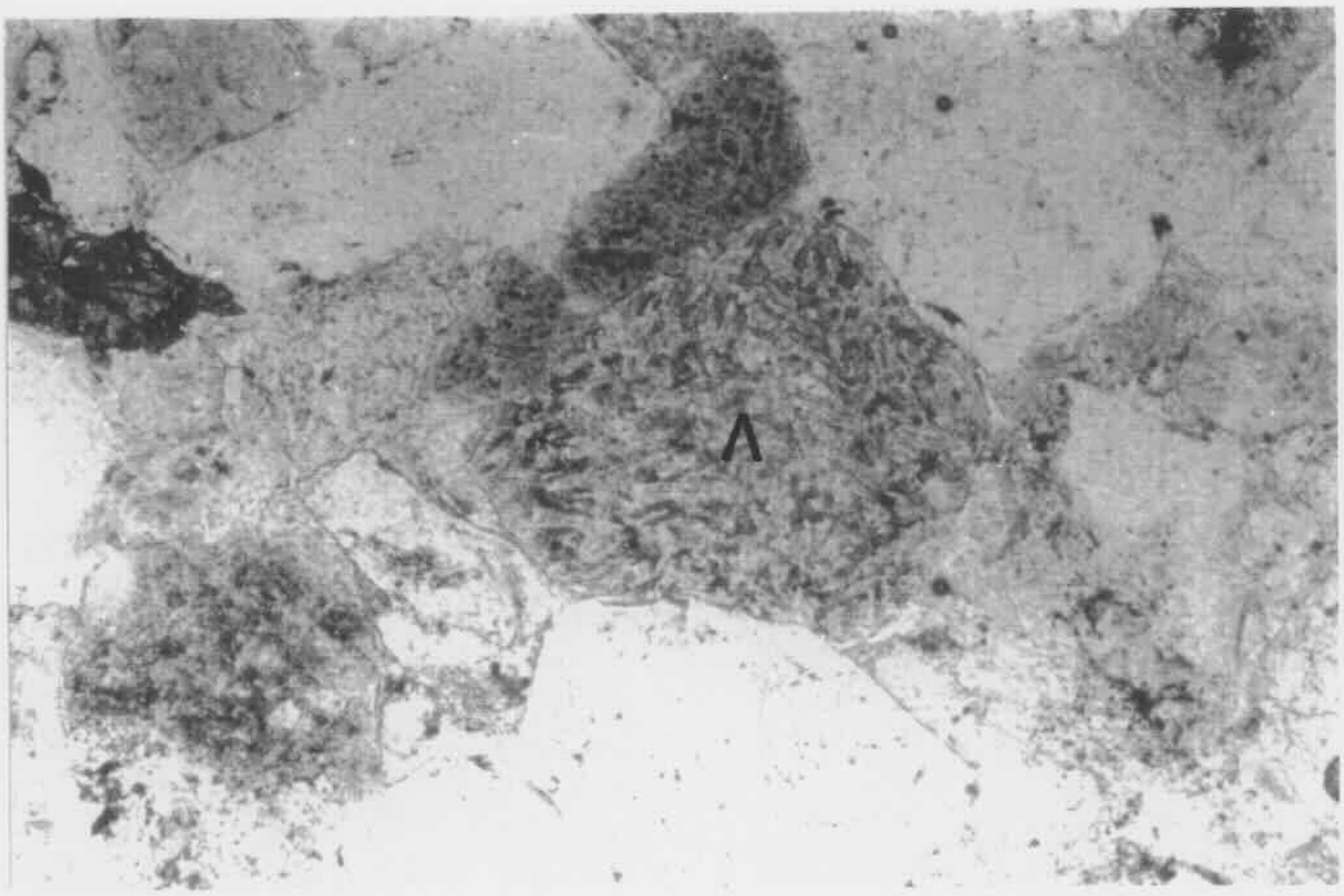

Fig 5-17 Shale fragment (S) deformed by adjacent quartz grains. Top - plane polarised light, bottom - crossed nicols. From Liverpool 91 at drilling depth of 595.2 m (sample L595.2). Scale bar is 0.25 mm.

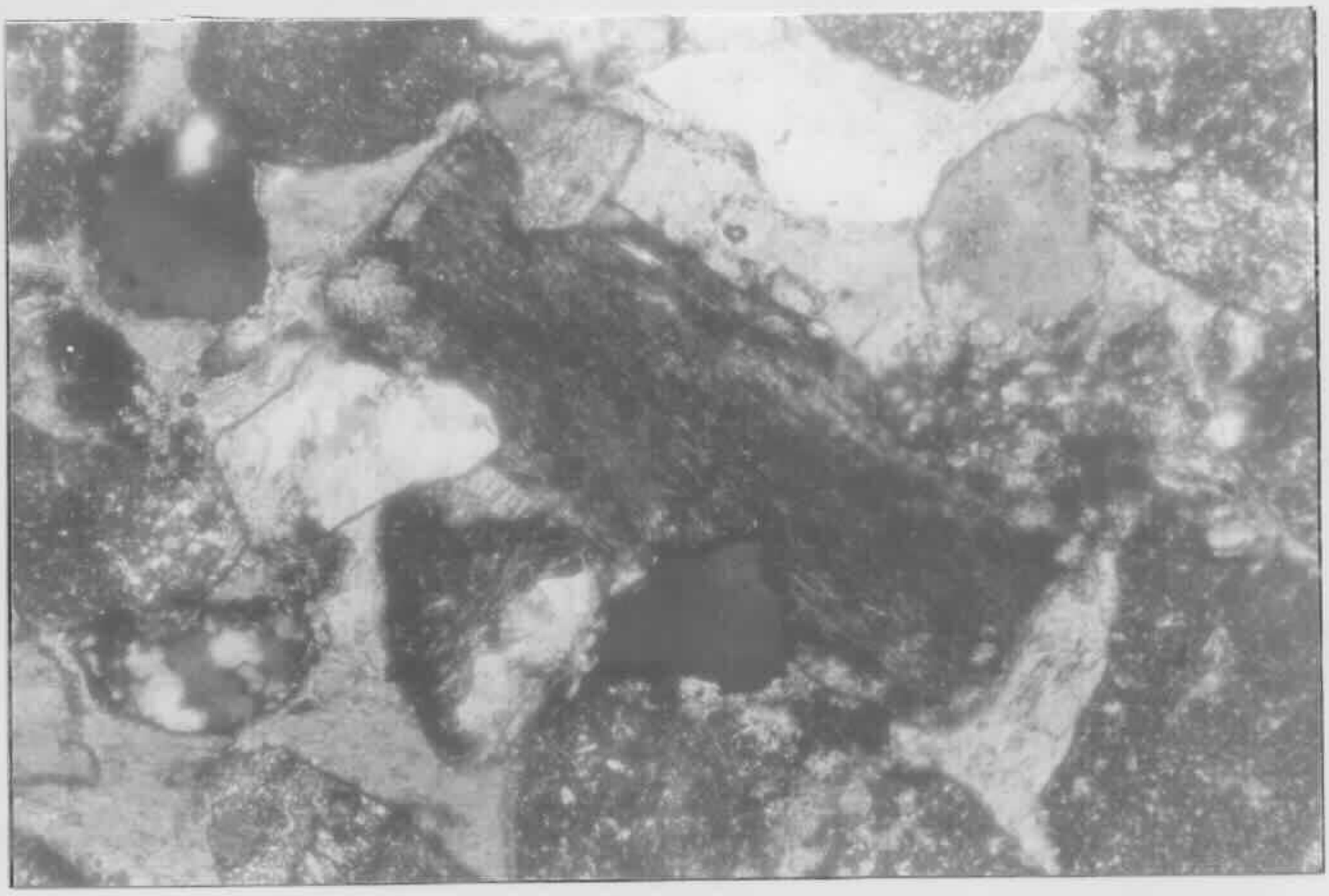

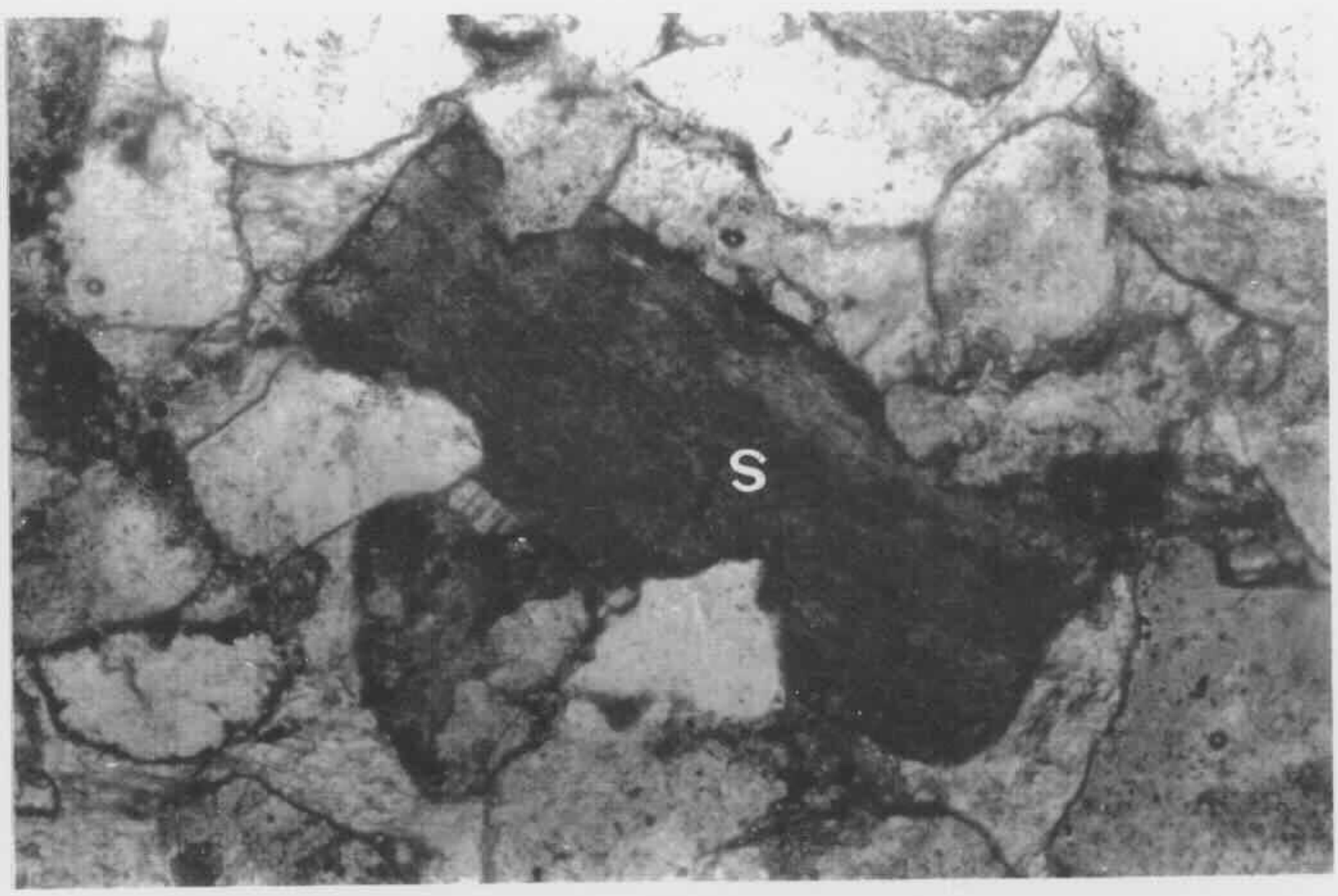
S

Fig 5-18 Siltstone fragment (S), crossed nicols. From Oil Longley 1 at drilling depth of 830.4 m (sample l830.4). Scale bar is 0.625 mm.

Fig 5-19 Chert grain (C) with radiolaria, which appear as spherulitic bodies consisting of chalcedony. Crossed nicols. From Weromba 2 at drilling depth of 430.8 m (sample W430.8). Scale bar is 0.625 mm.

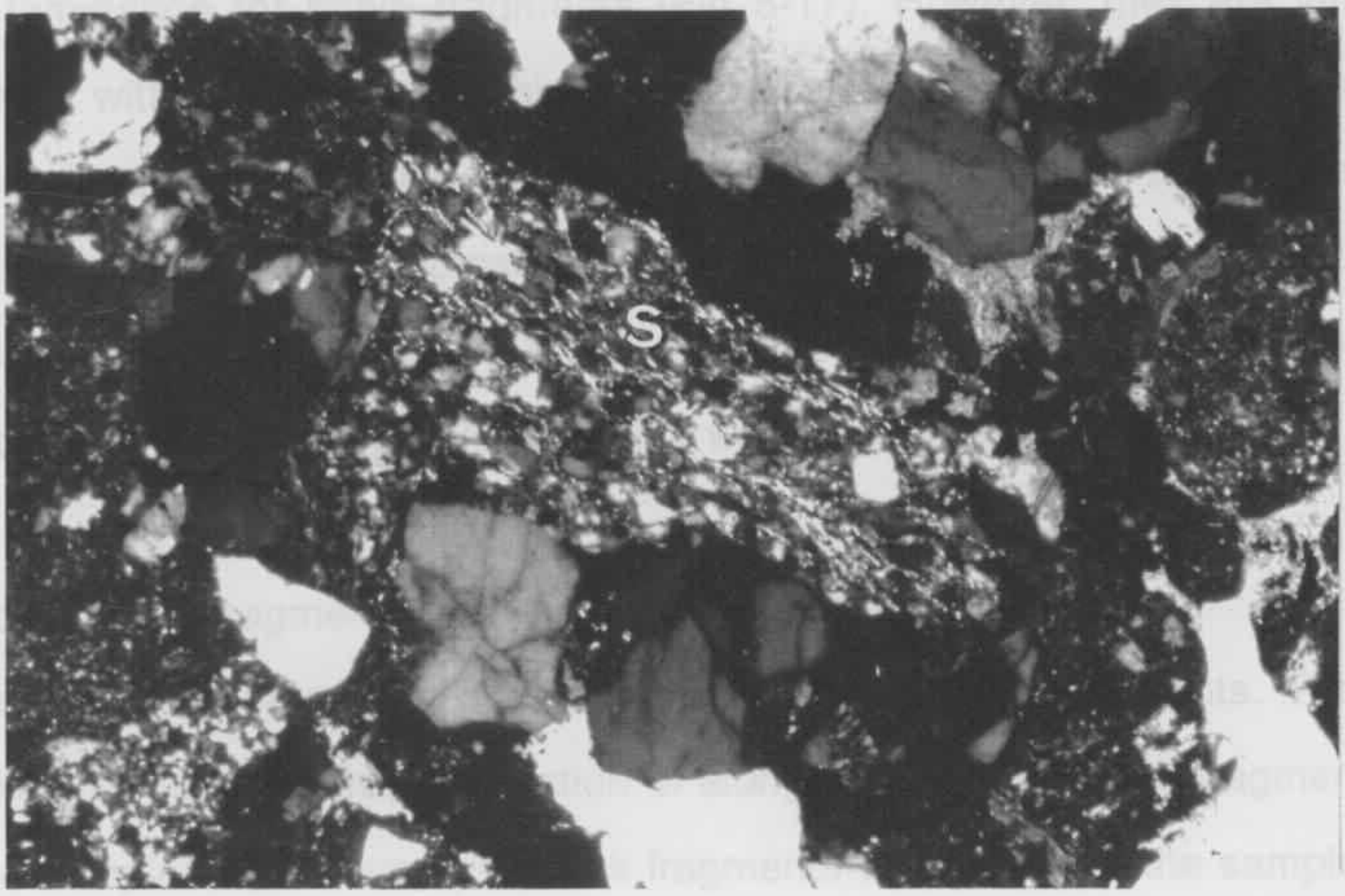
S

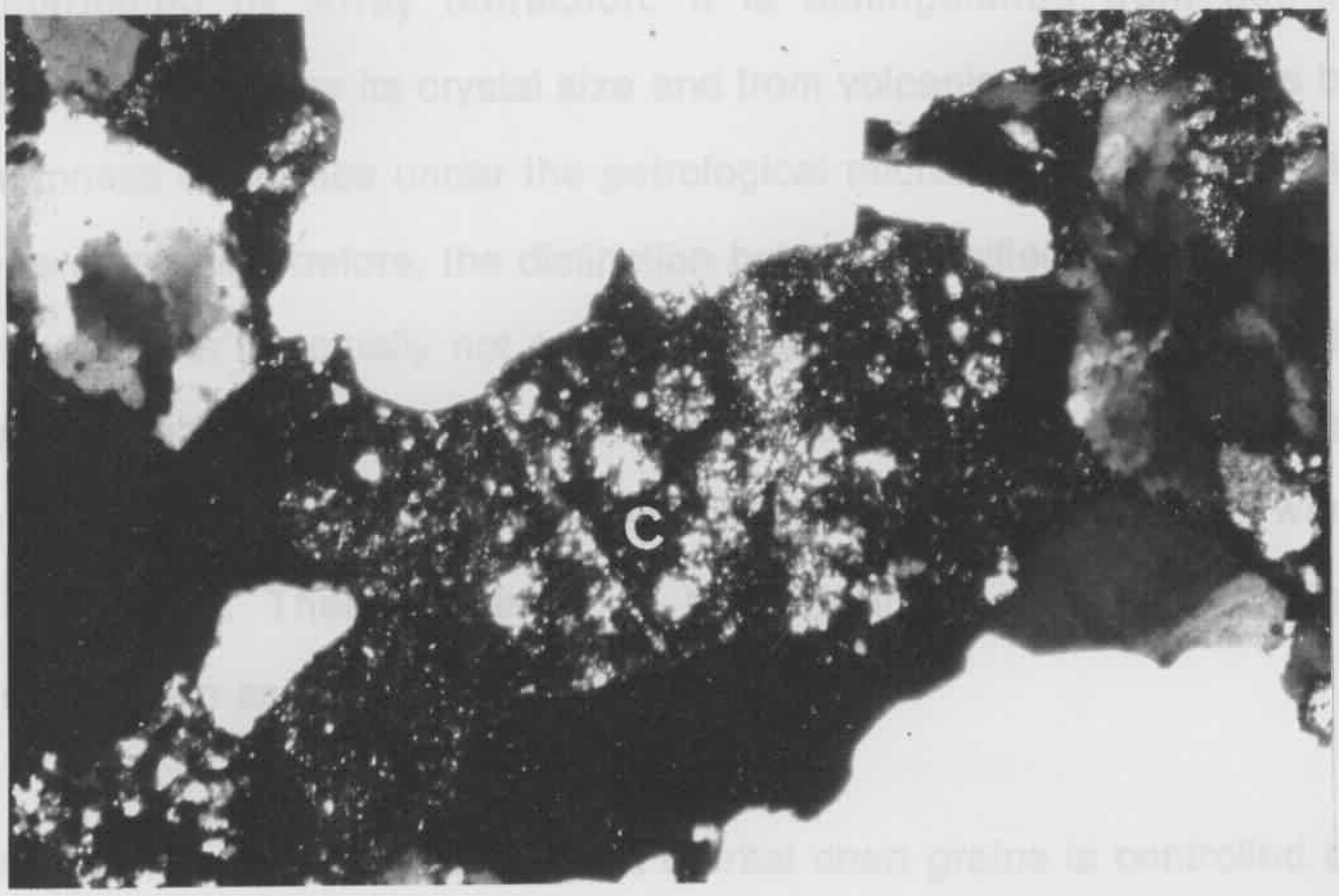
C

grains in size and tending to engulf the adjacent hard detrital grains as well as sedimentary lamination for shale fragments (Fig 5-17). However, they are very easily confused with argillized volcanic lithics. Thus it is very likely that the mudstone and shale fragments with a grain size similar to that of the surrounding detrital grains were counted as volcanic rock fragments. The sedimentary rock fragments generally account for less than 2.0 % of the total sandstone. In most of the thin sections, no sedimentary rock fragments were recognised.

(iii) Metamorphic Rock Fragments

Metamorphic rock fragments consist mainly of slate and schist fragments. They were recognised by the preferred orientation of elongate minerals in the fragment. In most of the samples no metamorphic rock fragments were seen. In the samples which do contain such fragments, the content is very small, generally less than 1.0 % of the total sandstone.

5.3.4 CHERT

Chert is made up of microcrystalline quartz (Midgley, 1951; Folk and Weaver, 1952), as determined by X-ray diffraction. It is distinguished from detrital polycrystalline quartz grains by its crystal size and from volcanic rock fragments by its relative cleanness of surface under the petrological microscope and its quartz composition. As mentioned before, the distinction between silicified volcanic lithics and detrital chert grains is actually not easy or possible in some thin sections. In this case, the uncertain detrital clast was counted as chert. In some chert grains, radiolarian remains, which occur as nearly perfect spheres filled with quartz, were recognised (Fig 5-19). Their presence is the strongest evidence for the identification of the grain as detrital chert.

In the southern Sydney Basin, the content of detrital chert grains is controlled by the stratigraphic horizon from which the sample was selected. Point count data

show that the chert content decreases upwards towards the top of the Narrabeen Group. The samples taken from the upper Narrabeen Group mostly have chert contents less than 1.0 %. By contrast, the lower Narrabeen Group is relatively rich in chert with contents of more than 2.0 %. The highest chert content was recorded in sample J501.2 in which detrital chert grains account for 17.0 % of the total sandstone (see Appendix III).

In the northern Sydney Basin, the detrital chert content does not vary with the stratigraphic horizon in a systematic way. In these sandstones, the majority of them have chert contents of 2.0 % to 4.0 %.

The detrital chert abundance generally increases with the increase of the detrital volcanic lithics. Sandstones rich in detrital volcanic lithics from the Wombarra and Scarborough Operational Units have the most abundant detrital chert grains. This relationship between the detrital volcanic lithics and detrital chert is expected as radiolarian cherts are abundant in the New England Fold Belt and rare in the Lachlan Fold Belt.

5.3.5 MICA

Mica includes muscovite and biotite with muscovite being more abundant. Due to mechanical compaction, elongated muscovite plates are usually deformed around the adjacent hard detrital grain (Fig 5-3). Approximately half of the samples do not contain mica. In the other half, its content ranges from 0.2 % to 1.2 % of the total sandstone.

5.3.6 HEAVY MINERALS

The heavy minerals tend to have a grain size smaller than the average grain size of the sample containing them. They include leucoxene, tourmaline and zircon (Fig 5-20). The percentages of heavy minerals are extremely low. In the majority of

Fig 5-20 Detrital zircon grain (centre of photograph). Top - plane polarised light, bottom - crossed nicols. From Oil Longley 1 at drilling depth 596.6 m (sample l596.6). Scale bar is 0.125 mm.

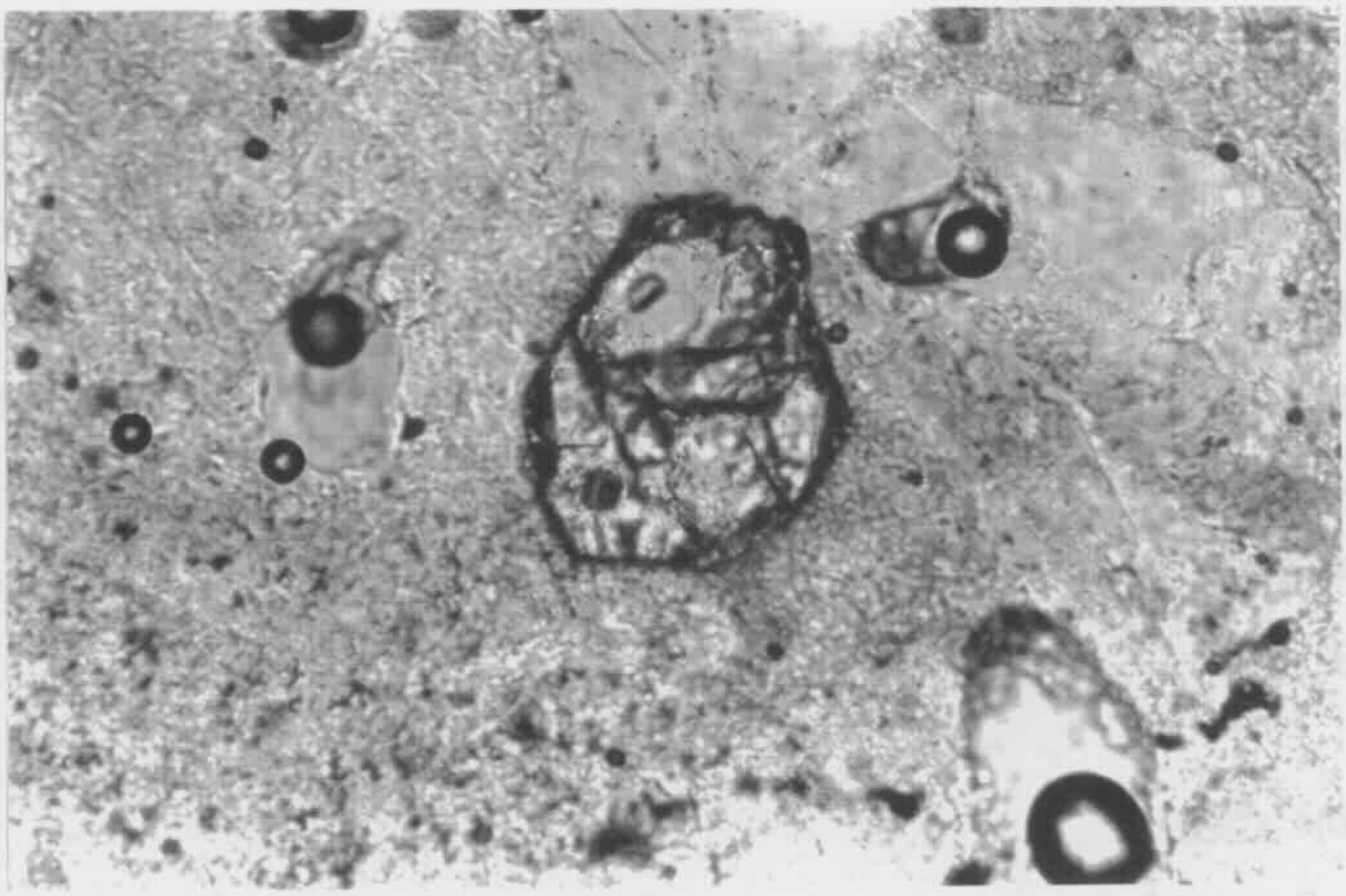

samples, no heavy minerals were identified. In the samples with heavy minerals, the content is generally 0.2 % to 0.4 %. The highest content of heavy minerals is 0.8 % in sample Y566.1.

5.3.7 OXIDES

Iron oxides are absent from most of the samples. In other samples, they are 0.2 % to 0.4 % of the total sandstone with the highest content of 1.2 % being recorded in samples Z512.4 and A295.6. They are determined by the brownish colour, irregular shape, opaqueness and aphanitic texture. Most of them are detrital grains. Diagenetic iron oxides have been recognised and they occur as coatings on detrital grains (Fig 5-21) and replacement of detrital grains (Fig 5-22). However, no attempt was made to separately count the two kinds of iron oxides since they account for a very minor proportion of the total sandstone.

5.3.8 CARBONATE

Carbonate occurs in two types of texture: microcrystalline and macrocrystalline with the latter as the dominate one. The former usually occurs as irregular patches filling inter-grain pore spaces. The latter generally shows two clear groups of cleavage and has a clean surface under plane polarised light. It is present as monocrystalline crystals (Figs 5-2 & 5-5) or mosaic crystals (Fig 5-23). The macrocrystalline carbonate crystals not only fill inter-grain pore spaces (Figs 5-5 & 5-23) but also partly or completely replace / corrode detrital grains (Figs 5-8 & 5-11) as well as coat detrital grains (Fig 5-24). Those coating detrital grains are much less common than those filling inter-grain pore spaces and those replacing / corroding detrital grains.

The majority of the sandstones contain carbonate cement. The highest content of carbonate (carbonate cements and replacement carbonate) was recorded as 56.0 % of the total sandstone in sample J650.3.

Fig 5-21 Diagenetic iron oxides (arrows), which coat detrital quartz (Q) and chert grains (CH), and carbonate cement (C). Top - plane polarised light, bottom - crossed nicols. From Coal Cliff 13 at drilling depth of 101.6 m (sample C101.6). Scale bar is 0.25 mm.

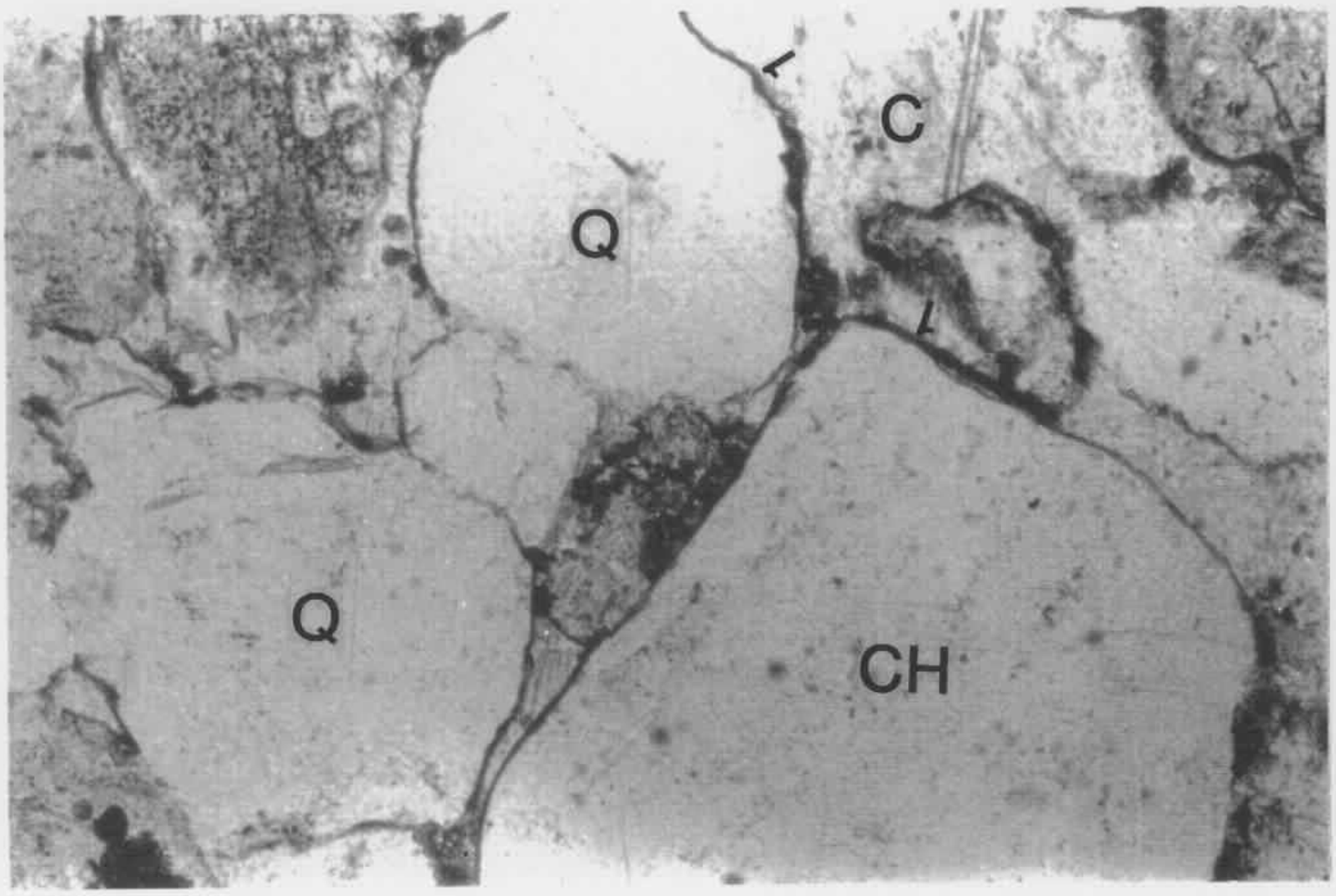
Q
C
Q
CH

Fig 5-22 Diagenetic iron oxides (O) replacing the volcanic rock fragment, chlorite (marked by arrow) coating detrital grains, and quartz cements (mega-quartz marked by Q) postdating chlorite. The rhombohedral crystals with an offwhite interference colour are probably siderites. The iron oxides might be formed by oxidation of the siderites. Top - plane polarised light, bottom - crossed nicols. From Coal Cliff 13 at drilling depth of 81.1 m (sample C081.1). Scale bar is 0.125 mm.

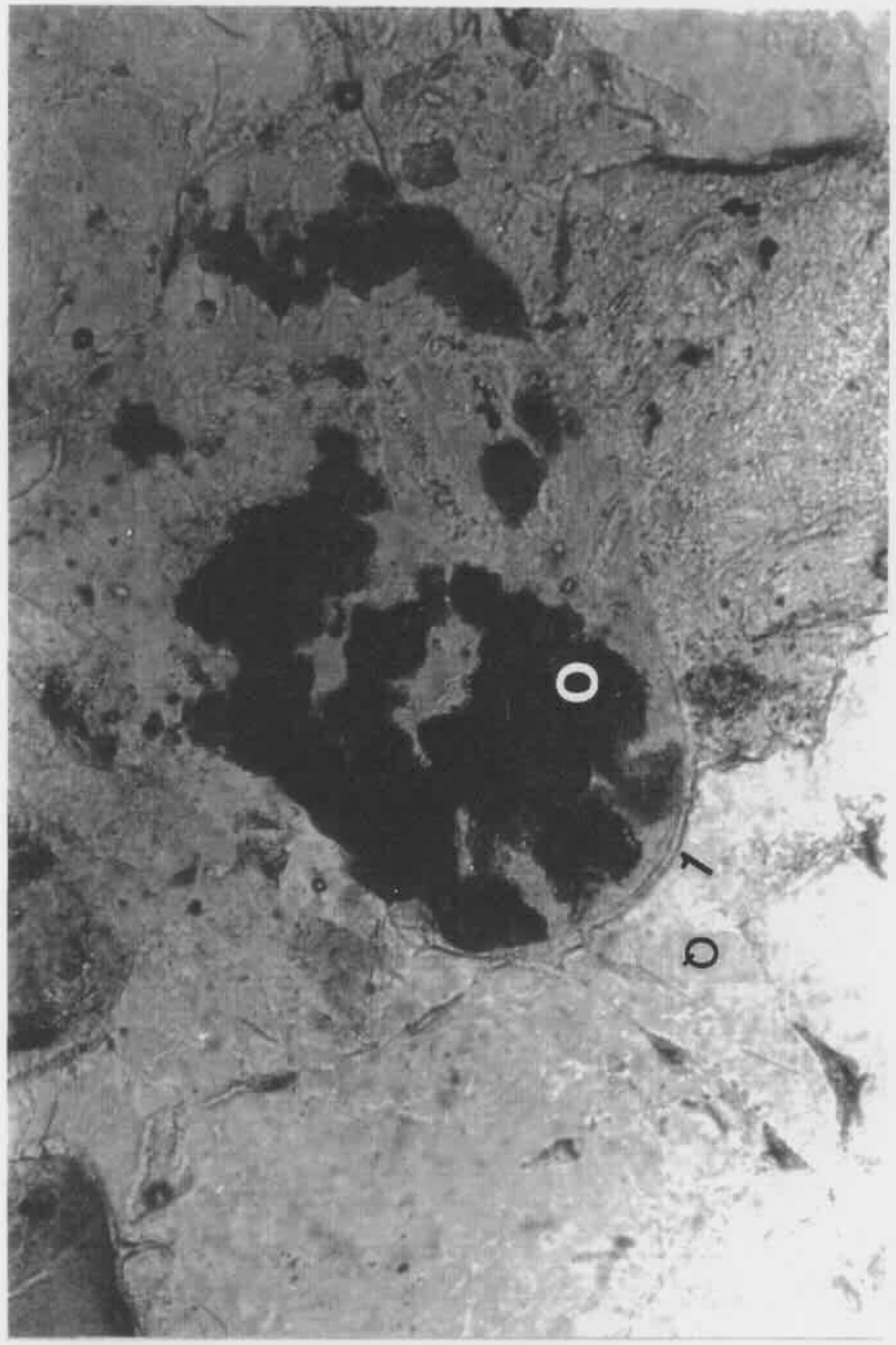
Q 1

Fig 5-23 Detrital quartz (Q) and volcanic rock fragment (V) floating within mosaic carbonate cements (C). Note: some of them are partly replaced by the carbonate. Top - plane polarised light, bottom - crossed nicols. From Cape Banks 1 at drilling depth of 650.3 m (sample J650.3). Scale bar is 0.625 mm.


Q
V

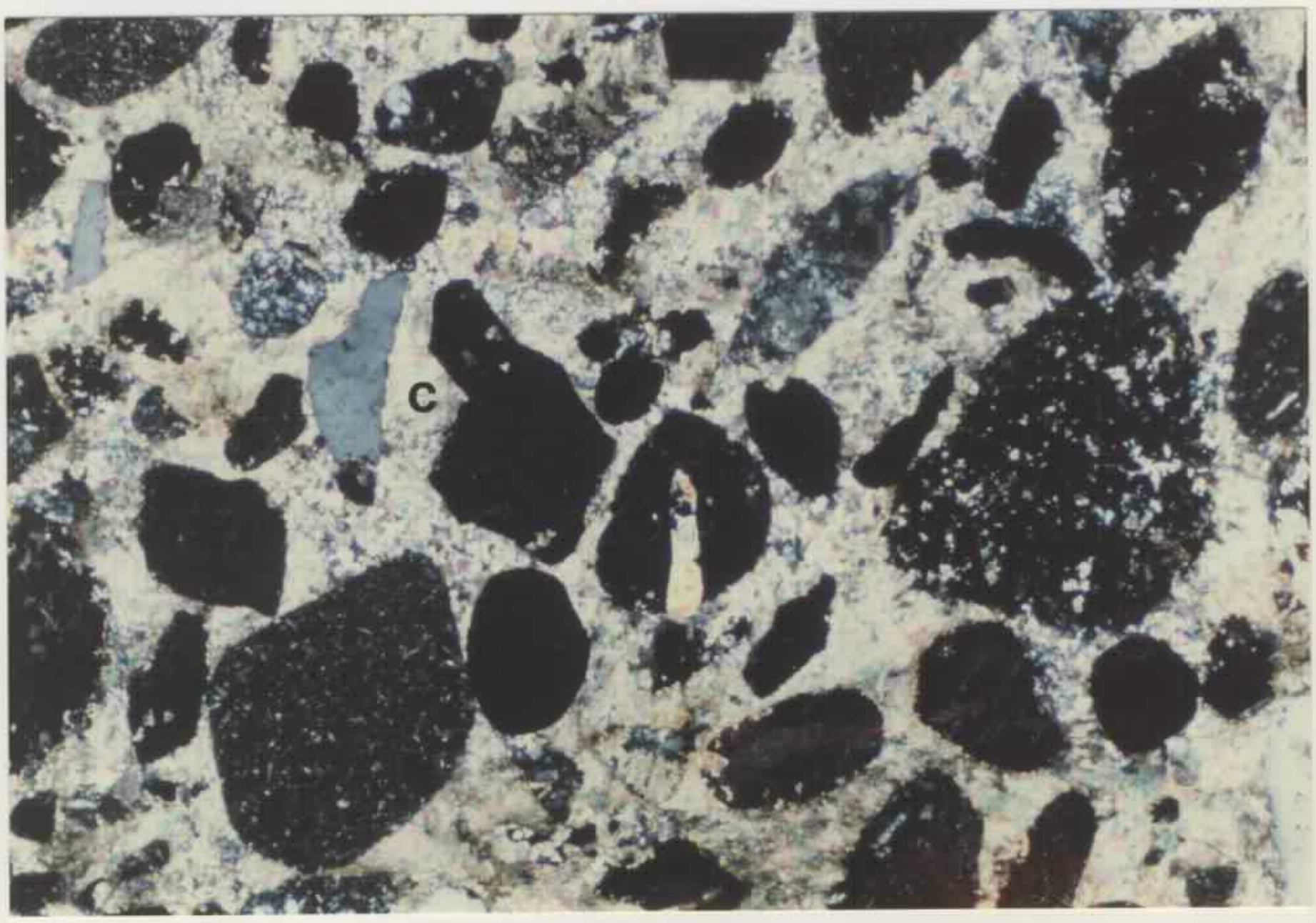
C

Fig 5-24 Carbonate crystals coating detrital quartz grains. Top - plane polarised light, bottom - crossed nicols. From Weromba 2 at drilling depth of 300.8 m (sample W300.8). Scale bar is 0.25 mm.

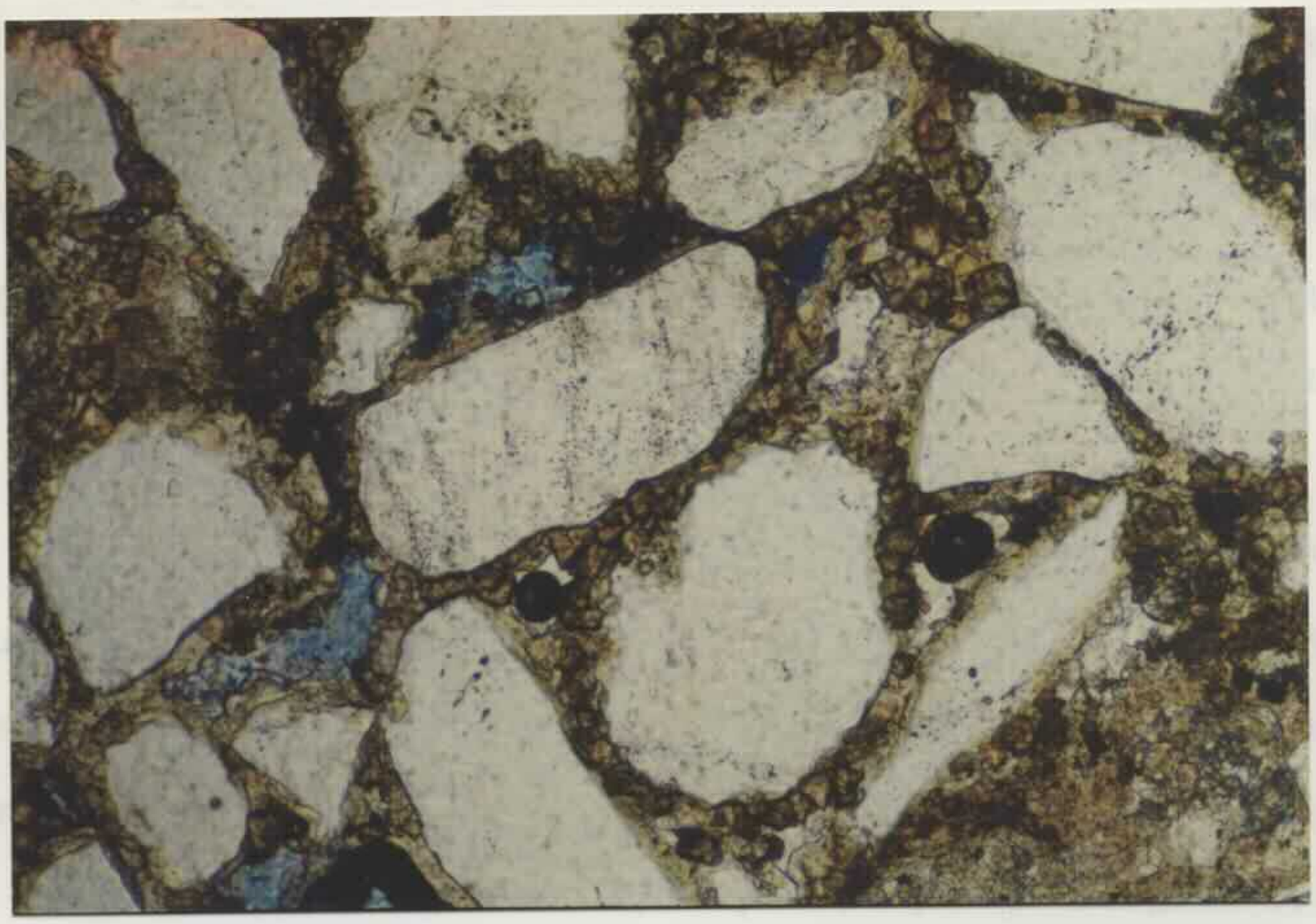

In some thin sections, dissolved carbonate cements were recognised. The dissolution has created secondary pore spaces. In the point counting no attempt was made to restore the components replaced by carbonates (mainly feldspars and volcanic rock fragments). Thus the contents of feldspars and rock fragments should be higher than their percentages indicate.

The carbonate cements include calcite, ferroan calcite, dolomite, ankerite, and siderite (determined by SEM / EDX analyses and further confirmed by microprobe and XRD studies). However, the differentiation of them is not easy under the petrological microscope. A more comprehensive discussion of carbonates found in the Narrabeen Group sandstones will be made in the next chapter.

5.3.9 CLAY MATRIX

The definition of clay matrix used here follows that of Morris et al. (1979). It generally refers to all particles which are too fine to be identified with the petrological microscope. Thus it includes all clay minerals, which may be detrital or diagenetic, clay and silt - sized mica, quartz, feldspar and the products created by breakdown of fine grained rock fragments. In some thin sections, authigenic chlorite coating detrital grains (Fig 5-25) and kaolin flakes filling inter-grain pore spaces (Fig 5-26) can be identified positively under the petrologic microscope.

The clay matrix commonly occurs as patches filling inter-grain pore spaces. The most common matrix observed in the thin sections consists of detrital clay minerals and silt-sized quartz grains (Fig 5-27). Most of the sandstones studied have a content of clay matrix more than 10.0 % of the total sandstone. The highest clay matrix of 32.0 % is recorded in sample M420.8. Sample J650.3 does not have clay matrix.

Fig 5-25 Earlier formed chlorite (arrow), which coats detrital polycrystalline quartz grain (Q), plagioclase (P), and volcanic rock fragments (V), and later formed carbonate cement (C). Top - plane polarised light, bottom - crossed nicols. From Liverpool 91 at drilling depth of 579.2 m (sample L579.2). Scale bar is 0.125 mm.


P
Q
C
V
V

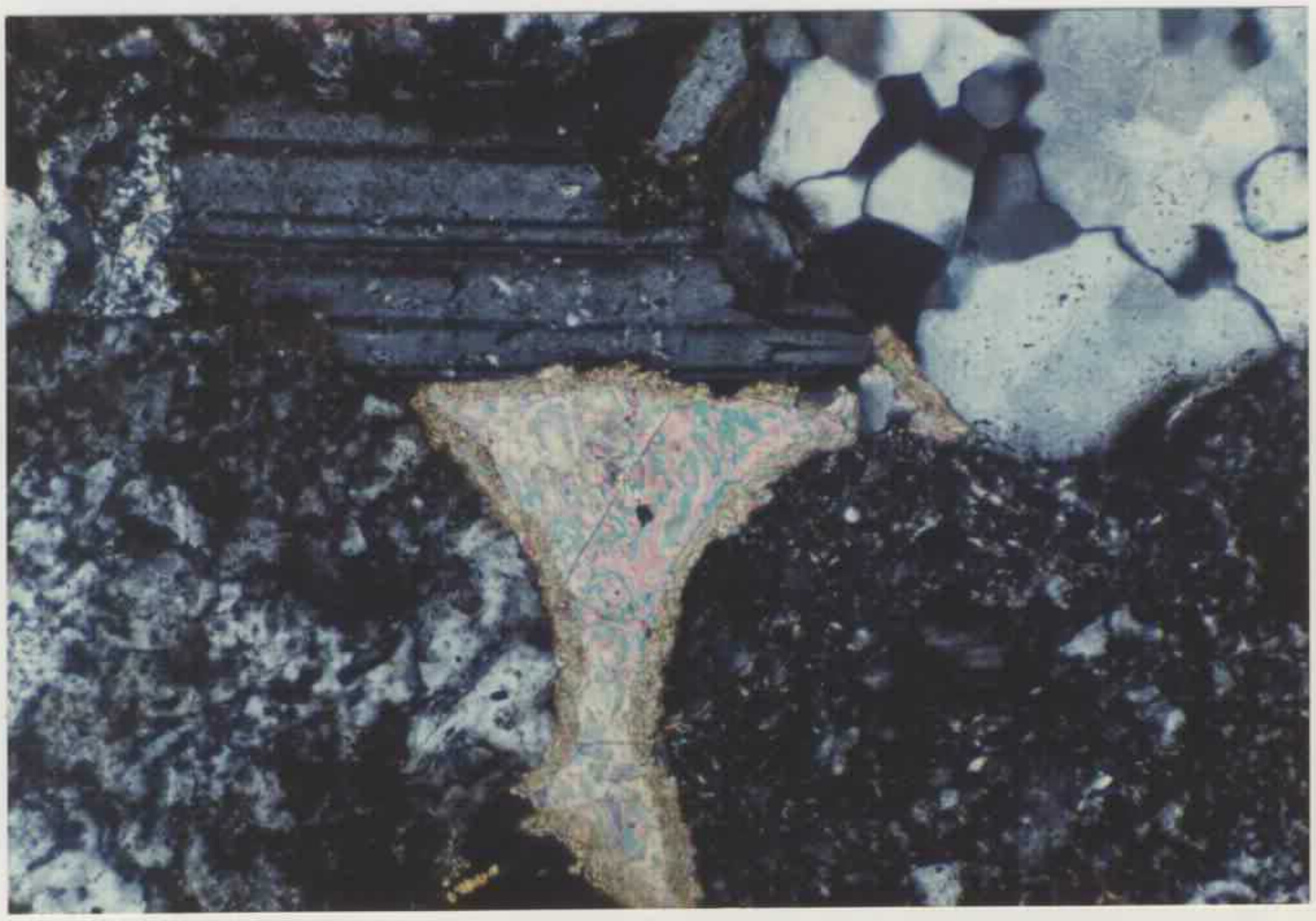

Fig 5-26 Pore-filling authigenic kaolin flakes, plane polarised light. From South Colah 1 at drilling depth of 296.5 m (sample O296.5). Scale bar is 0.0625 mm.

Fig 5-27 Clay matrix filling inter-grain pore spaces. O marks quartz overgrowths. Crossed nicols. From Cobbitty 3 at drilling depth of 508.2 m. Scale bar is 0.125 mm.

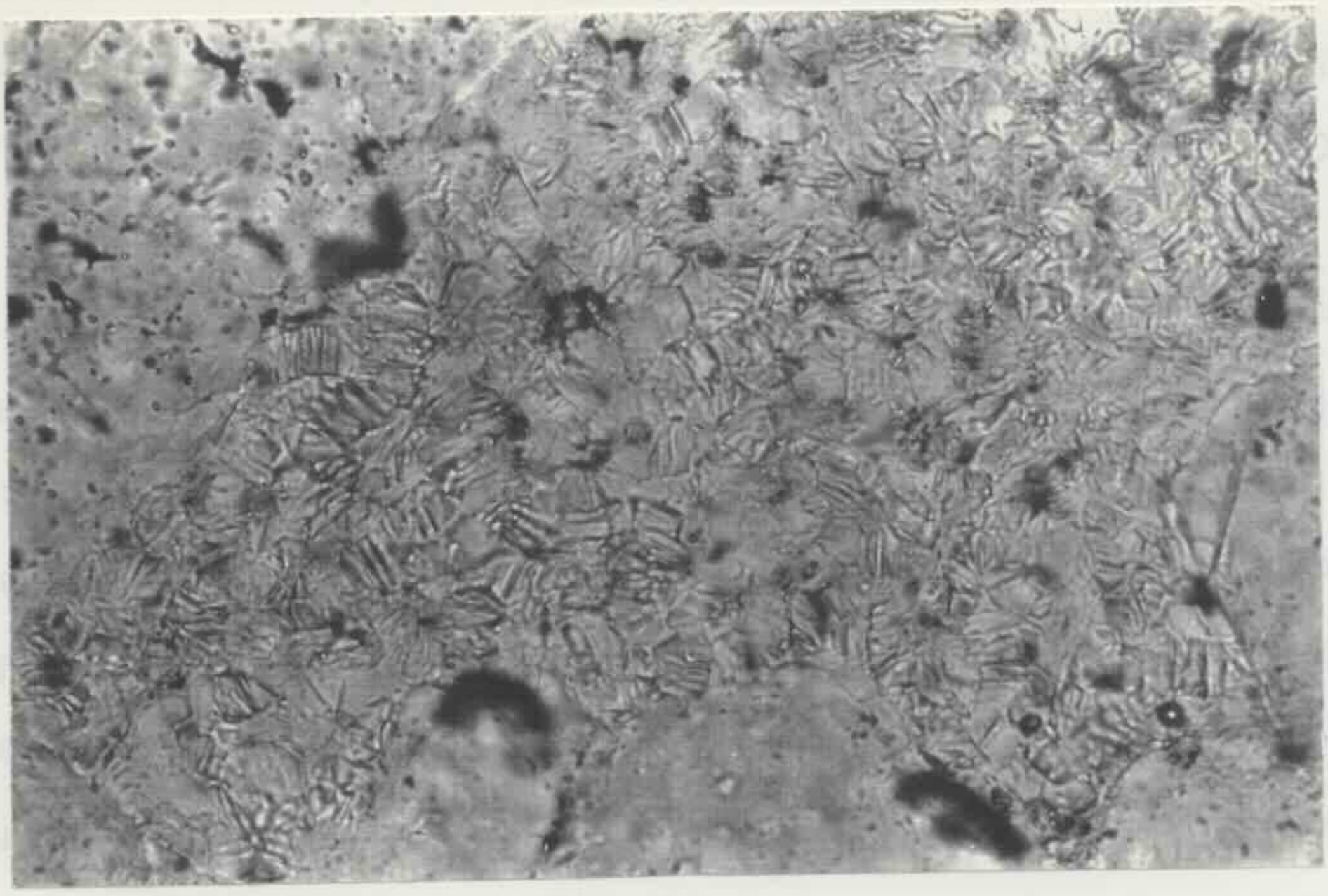

The point count data show that the amount of clay matrix is generally related to the grain size. It was found that the amount of clay matrix generally has an inverse relationship with the grain size. The coarse grained sandstones tend to have less clay matrix than the fine grained sandstones. In addition, the amount of clay matrix generally increases with the increase of volcanic rock fragments, but this general relationship becomes less clear in Boreholes D, E, and F in the northeast part of the Basin (Fig 5-4). The clay matrix and carbonate cement are also inversely related. The higher the carbonate cement, the lower the clay matrix.

5.3.10 POROSITY

Like mineral components, pore spaces were also evaluated in the modal analyses. Since all thin sections were impregnated with a blue dye, the pore spaces were identified by the blue colour under plane polarised light. Porosity includes that of both primary and secondary origin. Visual primary porosity varies from 1 to 17 % of the total sandstone.

The criteria used to recognise secondary porosity are those proposed by Schmidt and McDonald (1979b). In the sandstones studied, secondary porosity is mainly created by dissolution. The types of secondary porosity include oversized, mould, intra-grain, and intra-cement. The secondary porosity obtained from the modal analyses ranges from 0 to 11 % of the total sandstone. In three samples (X282.0, X436.6 and Z399.0) it is more than 10 % of the total sandstone, but in most of the samples it is less than 2.0 %. The high secondary porosity in these three samples was very likely an artifact of thin section preparation.

The porosity of sandstones was also measured in the laboratory (will be discussed in Chapter 8). By comparing the porosity values from the point counts with those from measurements in the laboratory, it was found that the counted porosity tends to be less than that measured. This may be due to microporosity in the sandstones,

which is not observable under the petrological microscope.

5.4 TEXTURE OF SANDSTONES

As indicated by point count data, the Narrabeen Group sandstones consist principally of detrital quartz grains with a range of 5 - 80 % of the total sandstone, lithic fragments (including chert) with a range of 0 - 75 % and to a less extent feldspar grains with a range of 0 - 15 %. The detrital quartz and lithic fragments generally have an equant to elongated shape (Fig 5-25) whereas the detrital feldspar grains are usually plate shaped (Figs 5-13 & 5-14).

The detrital fragments range in roundness from angular to well rounded with the majority of them being subangular to subrounded. The well rounded quartz grains probably represent second cycle sediments and were derived from earlier deposited sandstones. The rarely rounded angular quartz clasts (Fig 5-9) were derived from volcanic sources. The sandstones of the Narrabeen Group range in sorting (refer to sand fraction only) from very poorly to well sorted. Coarser sandstones tend to be poorly to very poorly sorted (Figs 5-7 & 5-18) whereas finer sandstones tend to be moderately to well sorted (Fig 5-13).

The detrital grain contacts are linear (Fig 5-6), which results from mechanical deformation following burial of sediments. In some sandstones, suture contacts among detrital quartz grains (Fig 5-28) were observed. In the sandstones containing a substantial amount of carbonate cement, however, the carbonate prevented detrital grains from deformation and so the detrital grains are either in point contact (Fig 5-24) or float within the carbonate cement (Fig 5-23).

5.5 CLASSIFICATION OF SANDSTONES

The classification of sandstones is a controversial subject. A large number of papers on this subject have been published (e.g. Klein, 1963; Okada, 1971). A

Fig 5-28 Sutured contact between detrital quartz grains (arrow). Crossed nicols. From Cobbitty 3 at drilling depth of 530.7 m (sample W221.1). Scale bar is 0.125 mm.

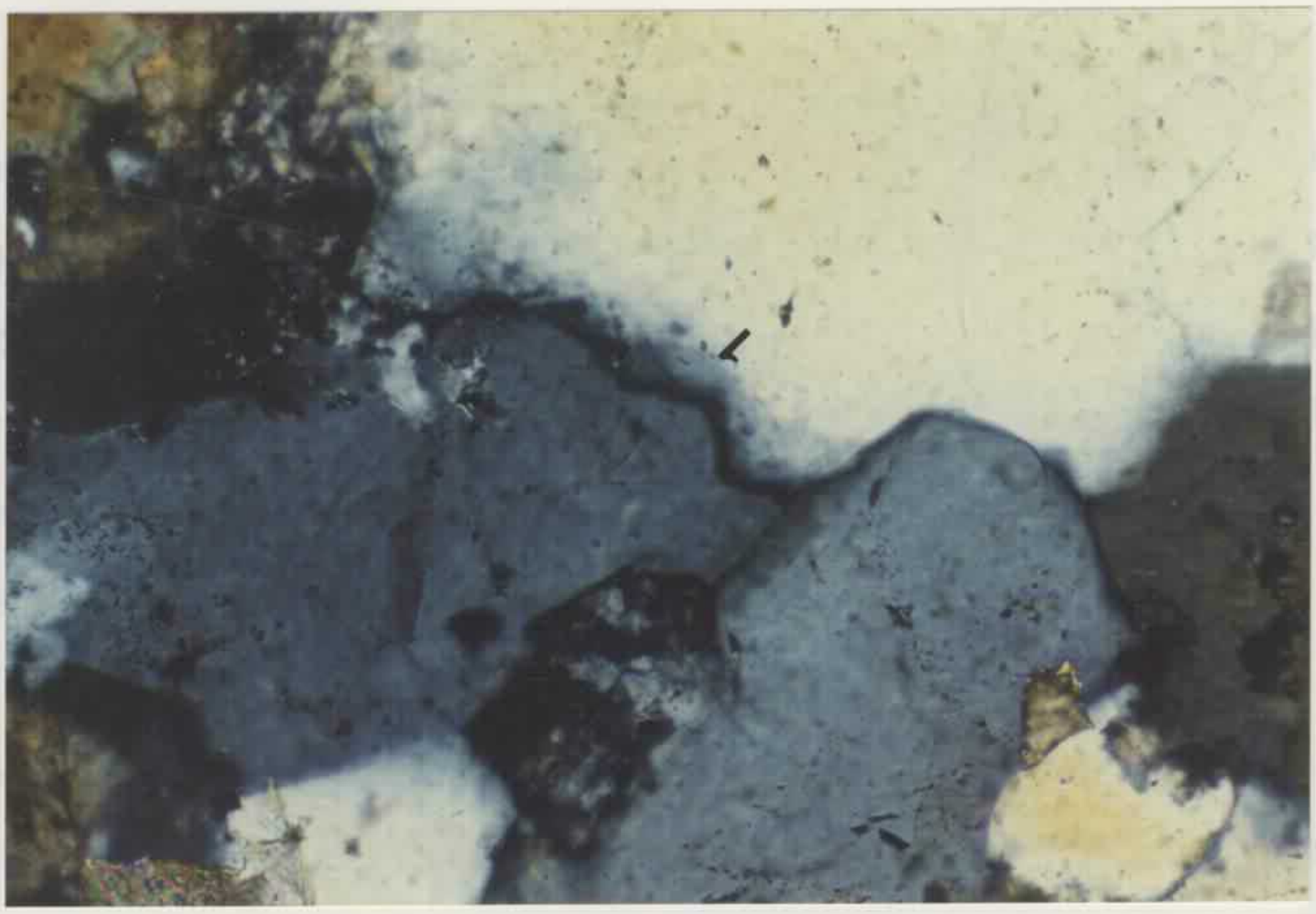

summary of sandstone classification was given more recently by Pettijohn et al. (1987).

The sandstone classification (Fig 5-29, Table 5-1) used in this thesis is modified from the one proposed by Folk (1968). The contents of the three poles follow those by Folk except that granite and gneiss fragments are excluded from the feldspar pole and they are included in the pole for the lithics. In addition, a 50 % quartz line is added to the Folk's classification to emphasise the sandstones with more than 50 % but less than 75 % detrital quartz grains.

The stable poles of Hayes (1979) are incorporated into the classification. As indicated by Hayes, the quartz pole (monocrystalline and polycrystalline quartz) represents the particles which are both chemically and physically stable. The feldspar pole (all kinds of feldspars) consists of the particles which are physically stable but chemically unstable. The lithic pole (all kinds of lithic fragments plus chert) represents the particles which are both chemically and physically unstable. The chemically and physically stable chert is included in the lithic pole since the detrital chert grains are considered to be derived from the same source (New England Fold Belt) as fine grained volcanic rock fragments. More importantly, chert grains are not always easily distinguished from fine grained volcanic rock fragments in some samples. Thus the inclusion of chert grains in the lithic pole is more meaningful.

As mentioned before, all components (detrital grains, oxides, heavy minerals, carbonate cements, clay matrix, and pore spaces) of the sandstone were counted. Since only detrital framework grains are required for sandstone classification, the percentage of each type of detrital clasts was recalculated (Table 5-1). The recalculated values for the five detrital clasts (monocrystalline, polycrystalline quartz, feldspar, lithics and chert) are listed in Appendix IV. These values were

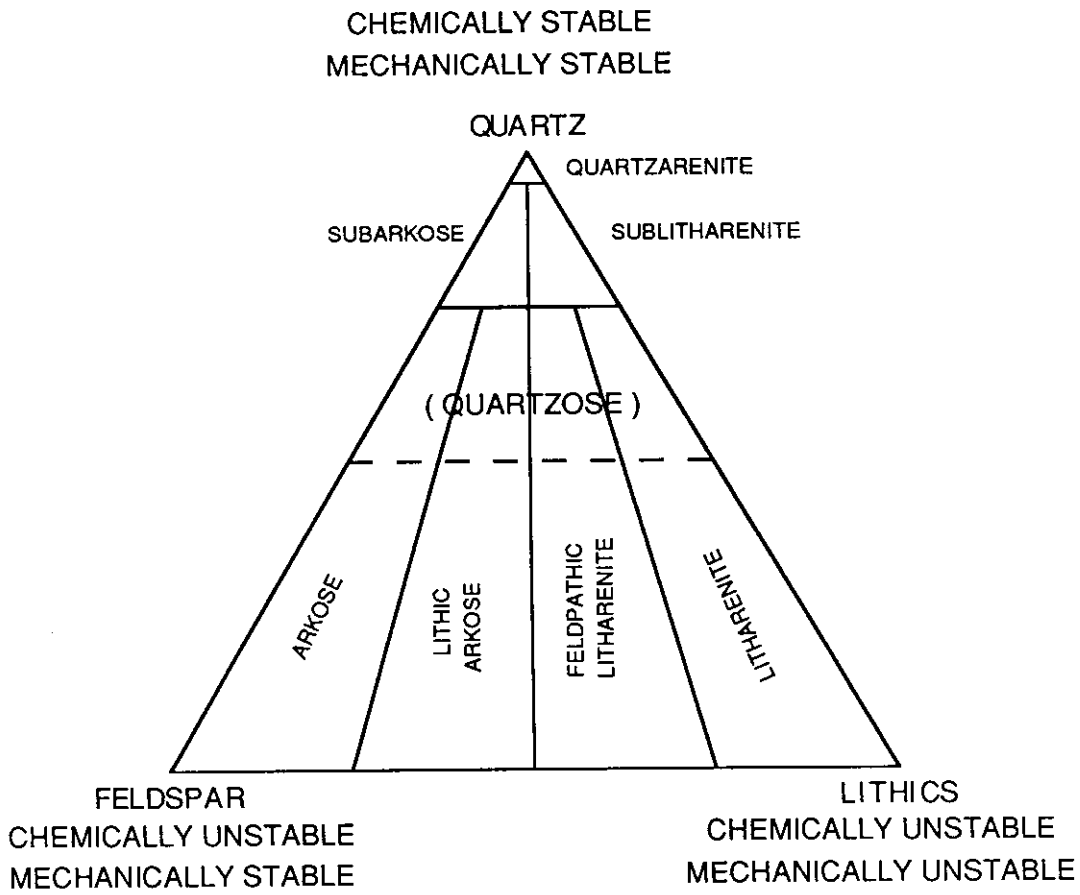

Fig 5-29 Sandstone classification.

Table 5-1 Sandstone classification

Quartz (Q) = monocrystalline quartz (QM) + polycrystalline quartz (QP)

Feldspar (F) = potassium feldspar (KF) + plagioclase (PL)

Lithics (L) = igneous rock fragments (IR) + metamorphic rock fragments (MR)
+ sedimentary rock fragments (SR) + chert (CH)

$Q\% = Q / (Q + F + L) \times 100\%$

$QM\% = QM / (Q + F + L) \times 100\%$

$QP\% = QP / (Q + F + L) \times 100\%$

$F\% = F / (Q + F + L) \times 100\%$

$L\% = L / (Q + F + L) \times 100\%$

$CH\% = CH / (Q + F + L) \times 100\%$

used to plot the position of each sample in the triangular plot of sandstone classification.

5.6 DETRITAL COMPOSITION OF NARRABEEN GROUP SANDSTONES

To discuss the detrital composition of the sandstones in the Narrabeen Group, the Sydney Basin is divided into four parts based on the similarity of detrital compositions of the sandstones in each part: southern region, northern region, west margin and east coast zone (Fig 5-4). The southern basin refers to the part south of the boundary between the northern and southern regions (including the southern region, southern west margin and southern east coast zone). The northern basin refers to the part north of the boundary (including the northern region, northern west margin and northern east coast zone). Boreholes A, N, O, P, X, Y, and Z are located in the southern region; Boreholes D, E, F, G, H, I, S, U, and V in the northern region (Borehole K is also included in this region); Boreholes Q, T, and W in the west margin (Borehole R is also included in this margin); and Boreholes B, C, J, L and M in the east coast zone.

5.6.1 WOMBARRA (WO) OPERATIONAL UNIT

In both the southern and northern regions, there is a dominance of litharenites over quartzose litharenites with one occurrence of sublitharenite in the northern region. Quartzose litharenites, litharenites and sublitharenites comprise the sandstones in the west margin. The sandstones consist largely of litharenites in the east coast zone. (Fig 5-30)

5.6.2 SCARBOROUGH (SC) OPERATIONAL UNIT

In the southern region, litharenites, quartzose litharenites and sublitharenites comprise the sandstones. To the north, the sandstones consist of litharenites, quartzose litharenites, and quartzose feldspathic litharenites. In the west margin, sublitharenites and quartzose litharenites comprise the sandstones. In the east

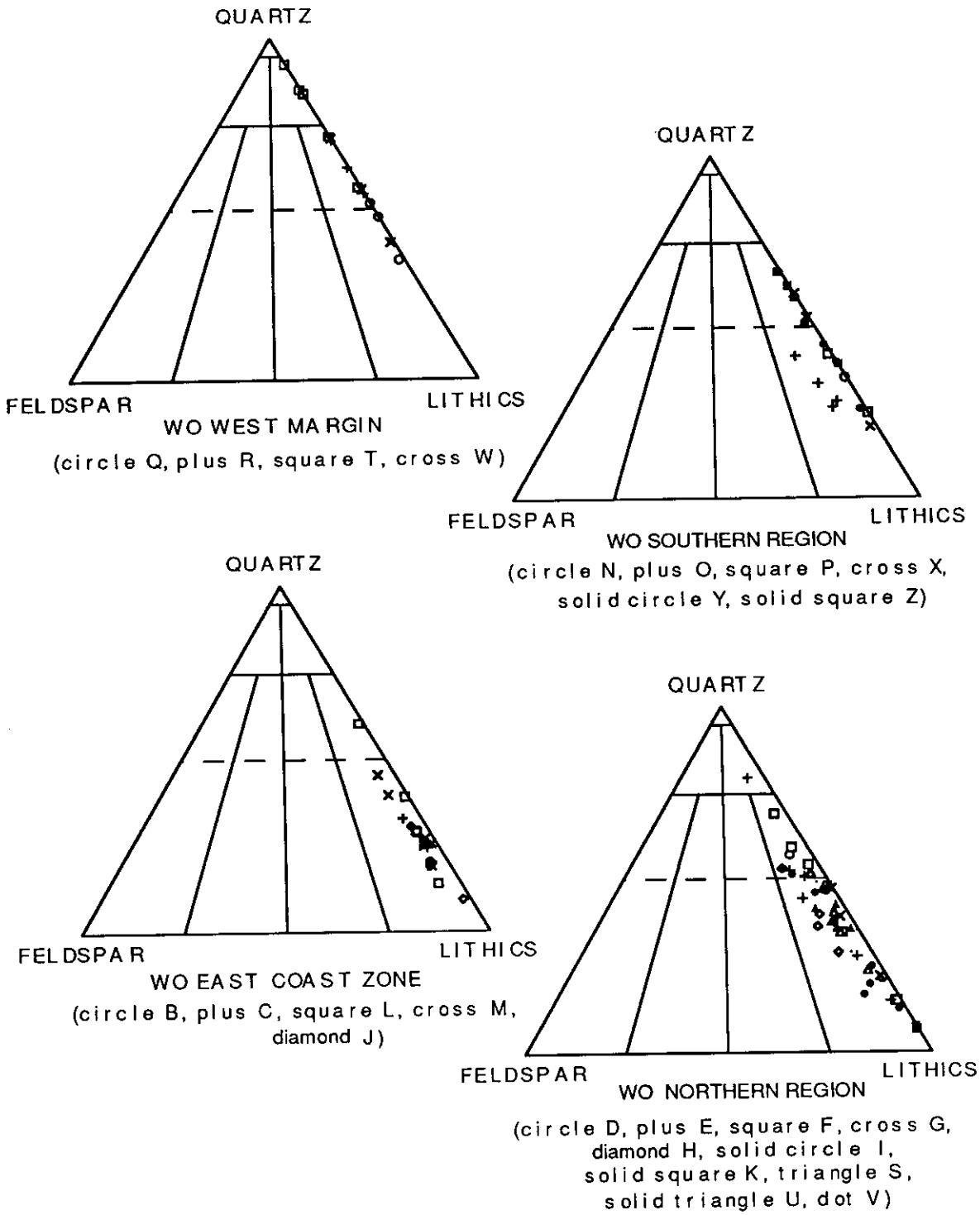

Fig 5-30 Compositions of sandstones in the Wombarra Operational Unit.

coast zone, there is an overwhelming dominance of litharenites over quartzose litharenites with one occurrence of sublitharenite and two occurrences of feldspathic litharenites. (Fig 5-31)

5.6.3 LOWER BULGO (LB) OPERATIONAL UNIT

In the southern region, the sandstones consist of sublitharenites and quartzose litharenites. A large number of litharenites and a lesser number of quartzose litharenites plus one sublitharenite comprise the sandstones in the northern region. Sublitharenites dominate sandstones in the west margin. To the east, the sandstones consist of quartzose litharenites and litharenites plus one sublitharenite and one quartzose feldspathic litharenite. (Fig 5-32)

5.6.4 UPPER BULGO (UB) OPERATIONAL UNIT

The sandstones in the southern region are characterised by a dominance of quartzose litharenites over sublitharenites. To the north, the sandstones consist largely of quartzose litharenites with one sublitharenite and two litharenites. There is a dominance of sublitharenites over quartzarenites and litharenites in the west margin. To the east, the sandstones consist of a larger number of quartzose litharenites and a lesser number of litharenites as well as one sublitharenite. (Fig 5-33)

5.6.5 BALD HILL (BH) OPERATIONAL UNIT

The sandstones consist of quartzarenites and sublitharenites in both the west margin and the southern region. However, in the southern region sublitharenites overwhelm quartzarenites. Quartzose litharenite dominates sandstones in the northern region. Only one sample is available in Borehole M in the east coast zone and is a quartzose litharenite. (Fig 5-34)

5.7 MAIN FACTORS CONTROLLING COMPOSITION OF SANDSTONES

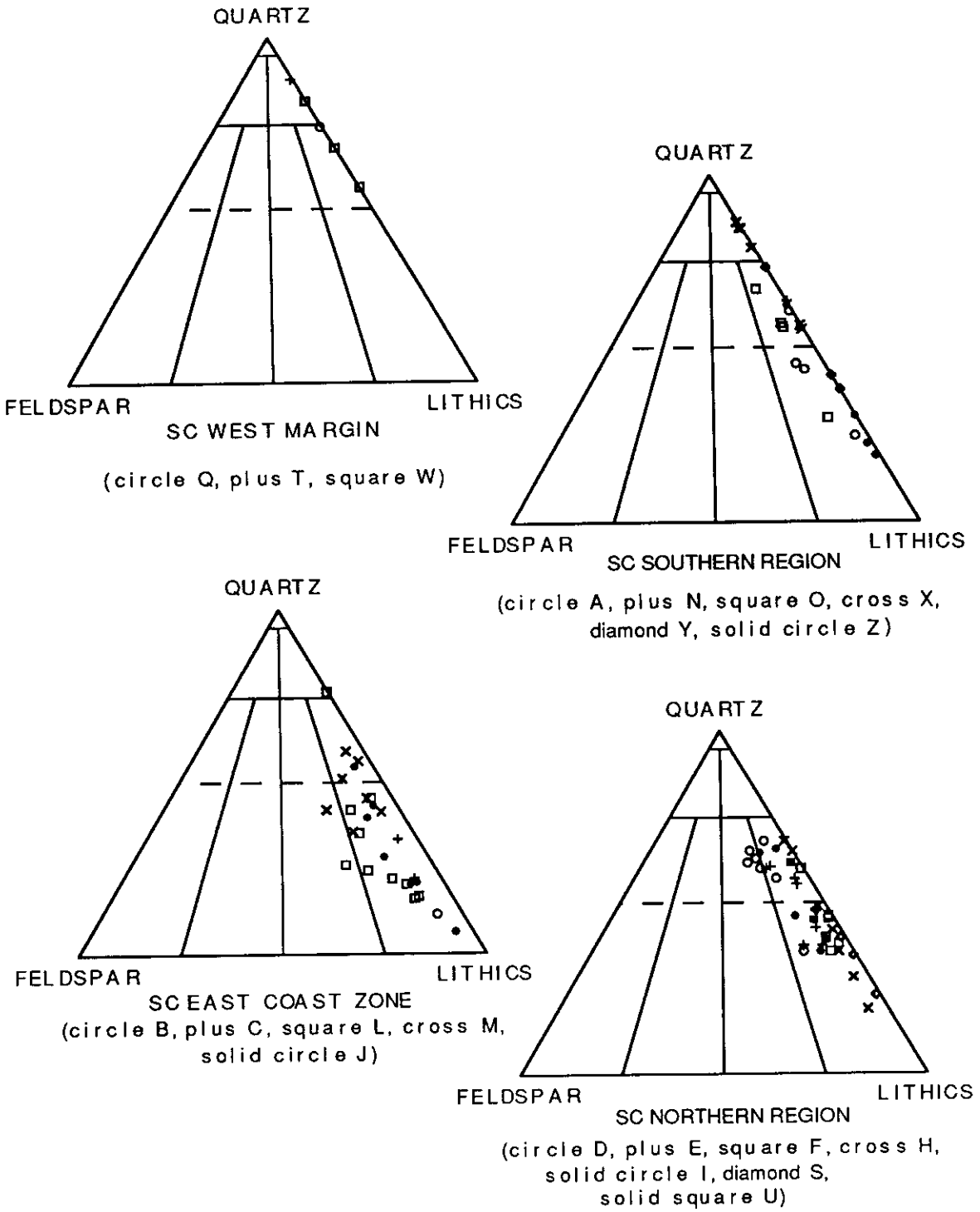

Fig 5-31 Compositions of sandstones in the Scarborough Operational Unit.

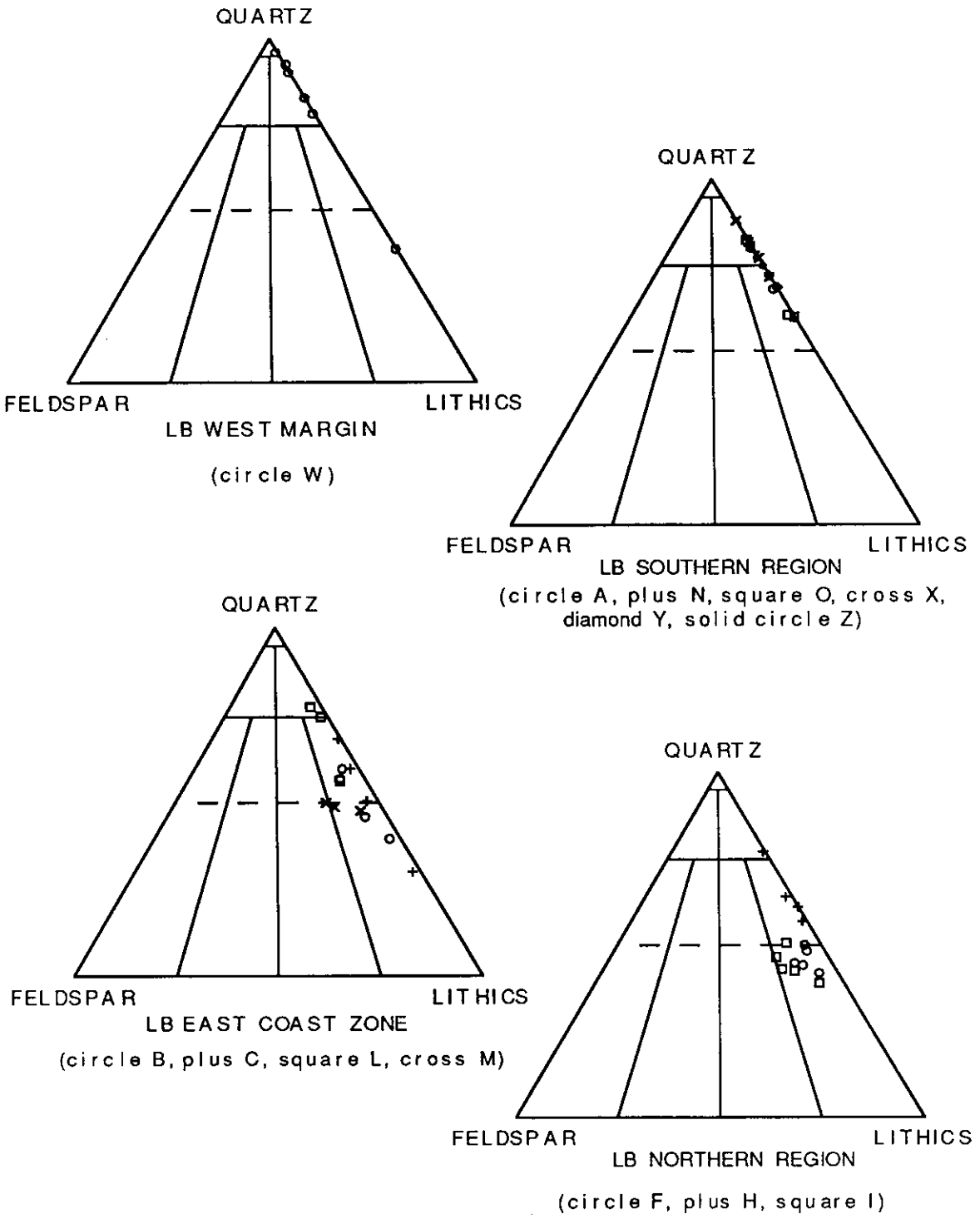

Fig 5-32 Compositions of sandstones in the Lower Bulgo Operational Unit.

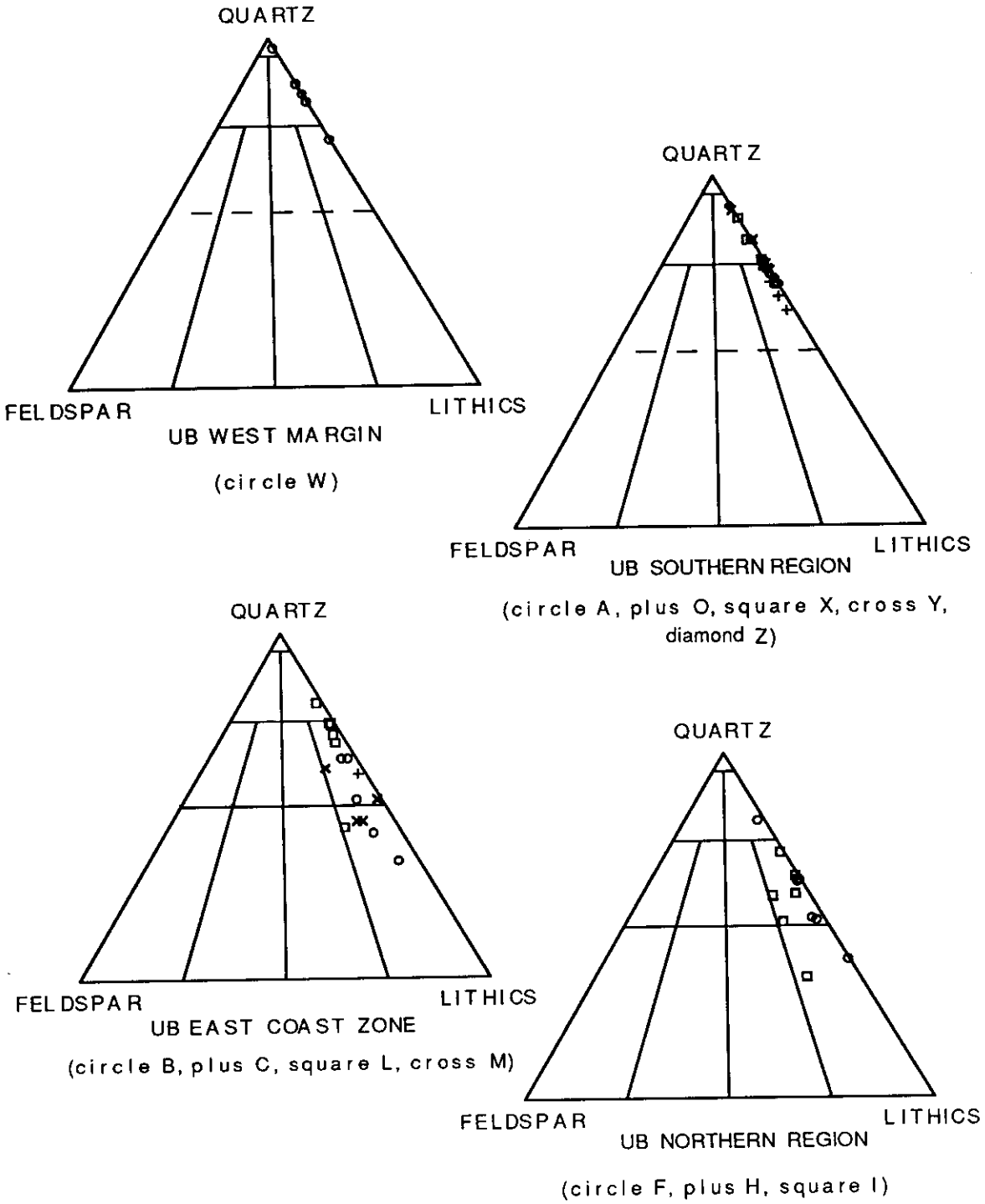

Fig 5-33 Compositions of sandstones in the Upper Bulgo Operational Unit.

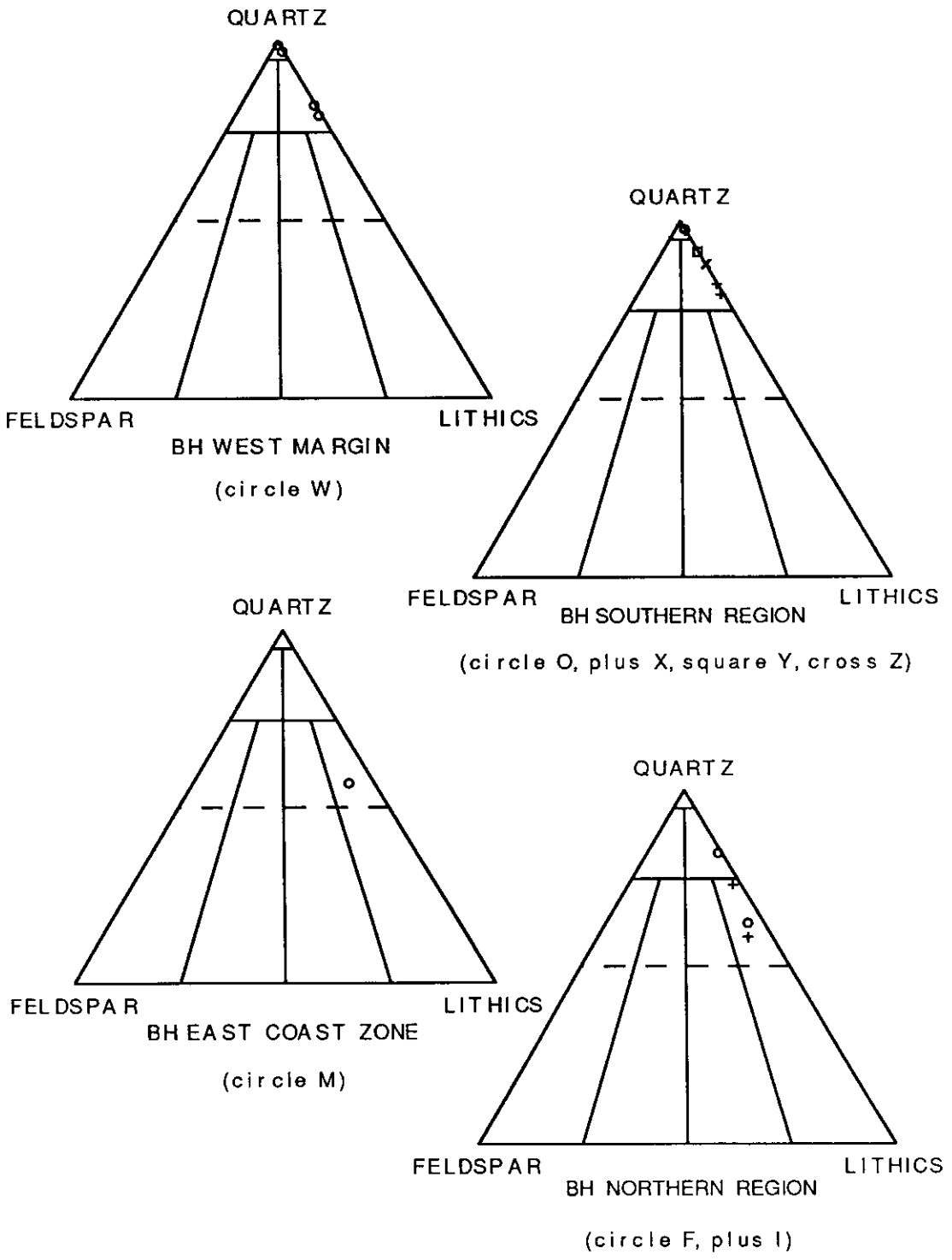

Fig 5-34 Compositions of sandstones in the Bald Hill Operational Unit.

Sandstone compositions are affected by a number of factors. Grain size, transportation, depositional environment, diagenesis and provenance are among the main factors (Suttner, 1974).

5.7.1 INFLUENCE OF GRAIN SIZE ON SANDSTONE COMPOSITION

The dependence of sandstone composition on grain size has been demonstrated by a number of workers (e.g. Blatt, 1967; Basu, 1976; Mack and Suttner, 1977). The sandstones used for this petrological study vary from very fine to very coarse. Such a wide range of sandstones supplies the opportunity to study the relationships between the grain size and the detrital composition in the Narrabeen Group sandstones.

Taking the drilling depth as the Y axis, and the recalculated percentage of individual detrital clasts (Appendix IV) and the average grain size measured under petrological microscope as double X axes, six diagrams (Figs 5-35 to 5-40) were drawn for selected boreholes from different locations in the basin. From comparison of grain size with the percentage of individual detrital clasts (polycrystalline quartz, monocrystalline quartz, and lithics including chert), general conclusions with regard to the influence of grain size on sandstone composition can be made.

In the west margin, the western portion of the southern region and the southwestern portion of the northern region of the basin, which are close to the western Lachlan Fold Belt quartzose source, the detrital polycrystalline quartz abundance has a clear relationship with the grain size (Fig 5-35). The coarser the sandstones, the more abundant are the detrital polycrystalline quartz grains. This is easily interpreted by the fact that polycrystalline quartz grains contain three or more monocrystalline quartz crystals (by definition) so that they are unlikely to be present in fine grained sandstones in large amounts. To the northeast portion of the

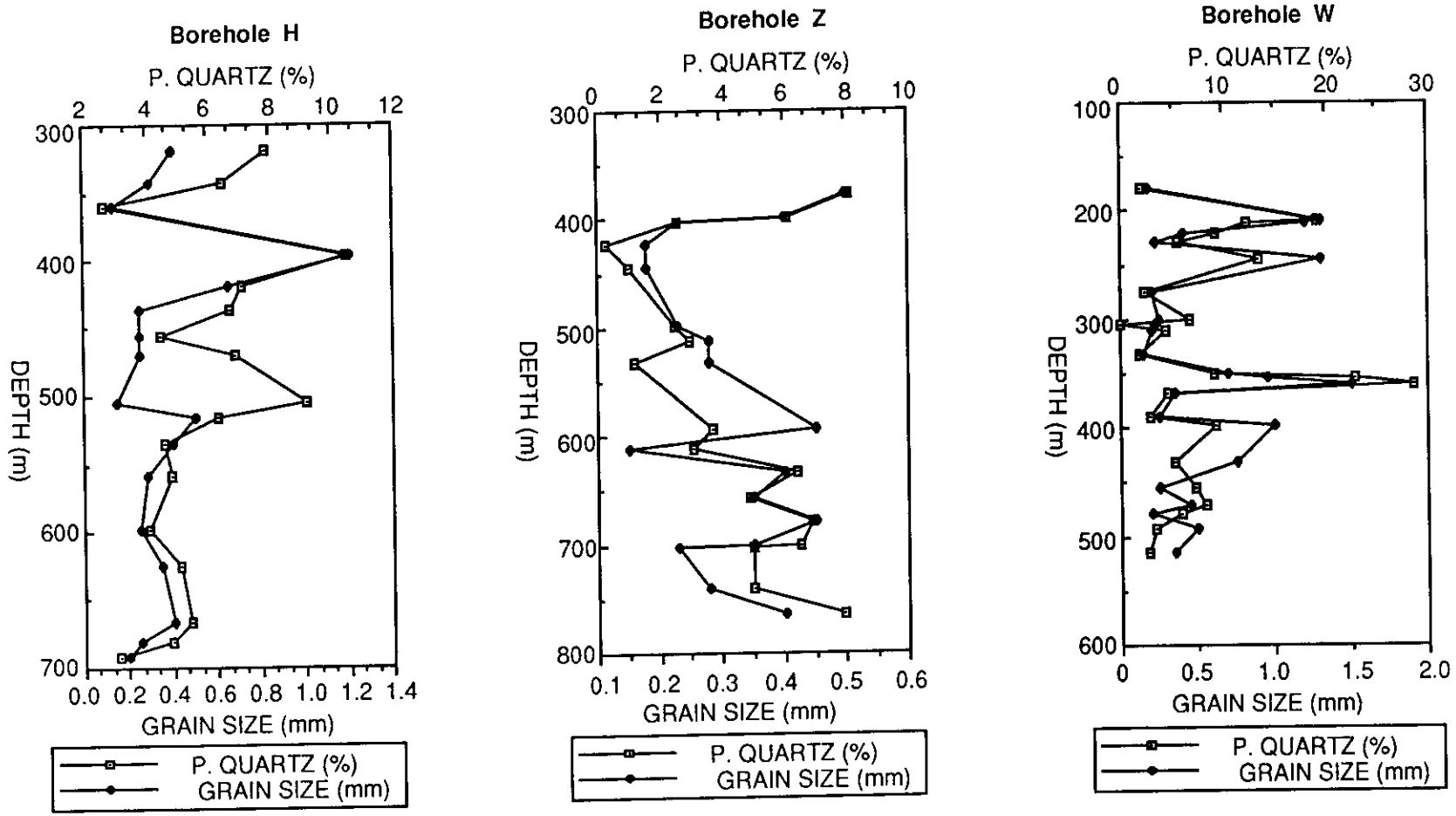

Fig 5-35 The variation of detrital polycrystalline quartz grains with the average grain size and drilling depth for Borehole H in the southwestern portion of the northern region, Borehole Z in the western portion of the southern region, and Borehole W in the west margin of the Sydney Basin.

northern region and the east coast zone, which is close to the northeastern New England Fold Belt lithic as well as quartzose source and the eastern offshore volcanic source (which will be discussed later), this relationship is not as evident (Fig 5-36). This may be attributed to the influence of the detrital lithic sources. The influence of grain size on composition is overshadowed by that of provenance.

Both the detrital monocrystalline quartz grains and the detrital lithics do not have a clear relationship with the grain size, as indicated in Figs 5-37 to 5-40. The contents of detrital monocrystalline quartz grains and lithics in the total detrital framework grains are generally independent of grain size of sandstones.

In conclusion, grain size has a minor influence on the detrital compositions of the Narrabeen Group sandstones by controlling the content of the minor component - detrital polycrystalline quartz grains in sandstones in the west margin, the western portion of the southern region and the northeastern portion of the northern region of the basin.

5.7.2 INFLUENCE OF TRANSPORTATION, DEPOSITIONAL ENVIRONMENT AND DIAGENESIS ON SANDSTONE COMPOSITION

The sediments of the Narrabeen Group were deposited in fluvial / lacustrine depositional systems (refer to Chapter 4). The transportation and the depositional environment should not be significantly different from one individual sandstone facies to another. Thus it is considered that these two factors do not control the detrital composition of the Narrabeen Group sandstones to any great extent.

It has been known for a long time that sands undergo a variety of textural and mineralogical changes during burial and subsidence in a sedimentary basin, during structural deformation of burial sequences, and during outcrop weathering (McBride, 1985). Some of these post-depositional processes can severely change

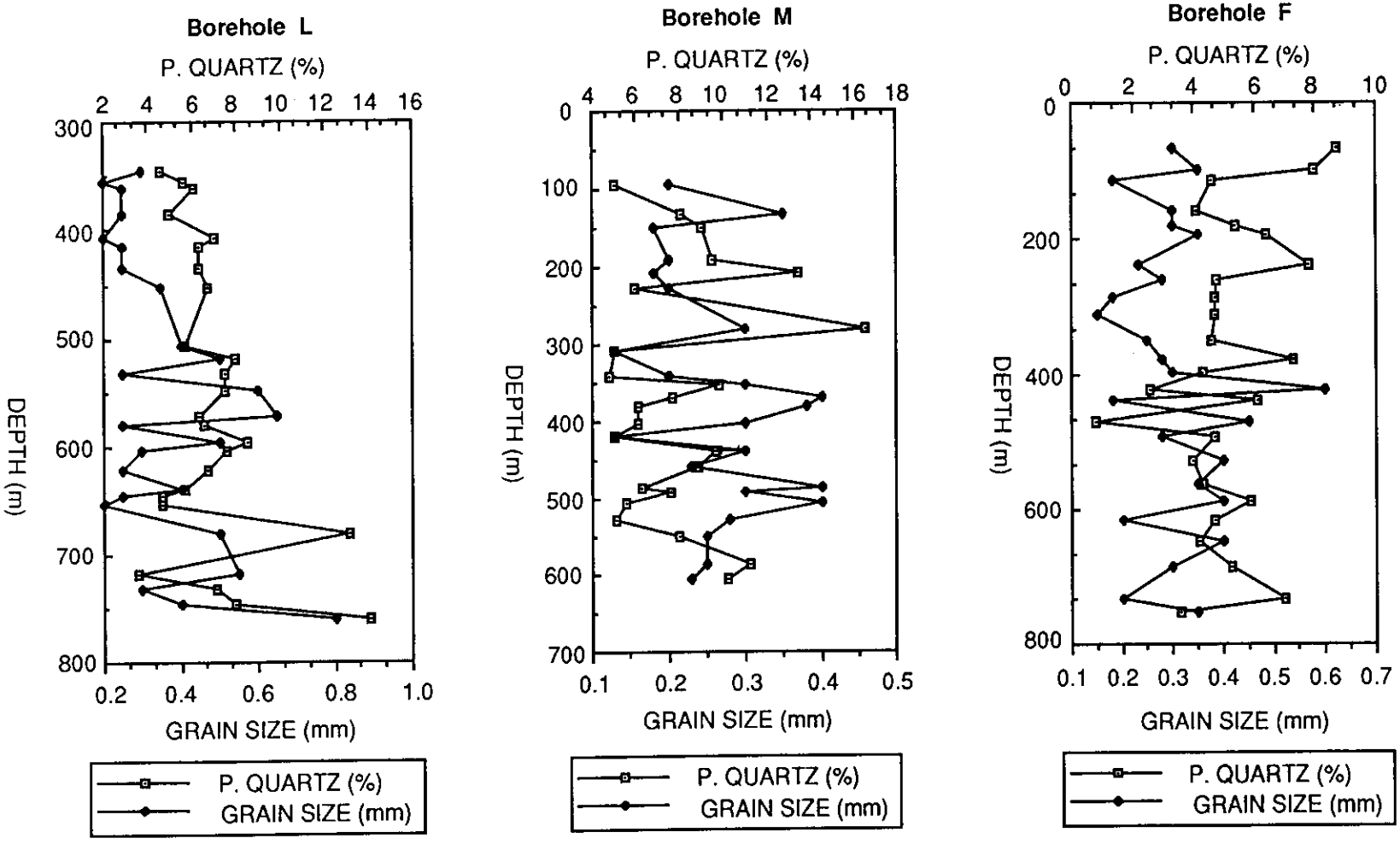

Fig 5-36 The variation of the detrital polycrystalline quartz grains with the average grain size and drilling depth for Boreholes L and M in the east coast zone and Borehole F in the northeastern portion of the northern region of the Sydney Basin.

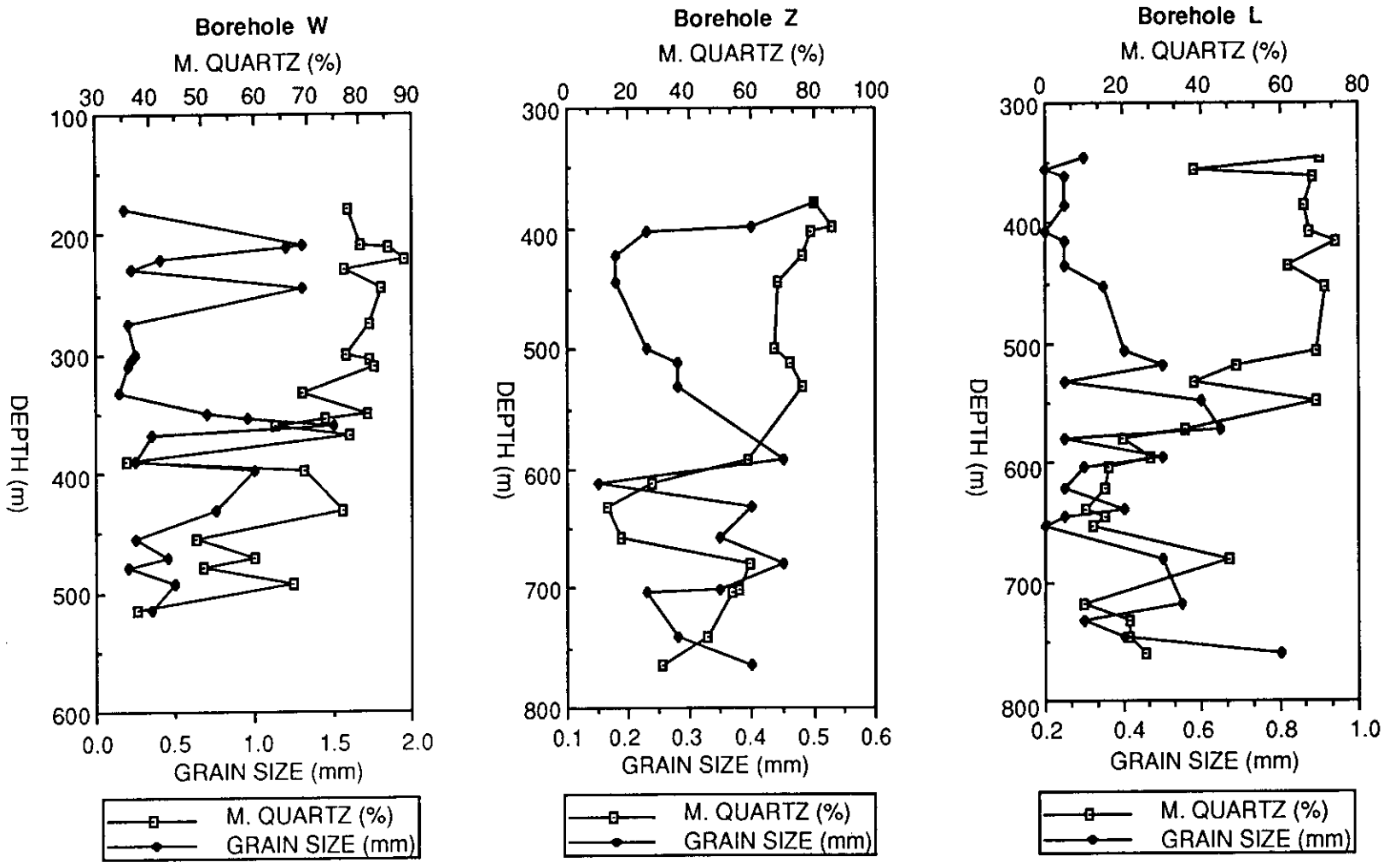

Fig 5-37 The variation of the detrital monocrystalline quartz grains with the average grain size and drilling depth for Boreholes W, Z, and L.

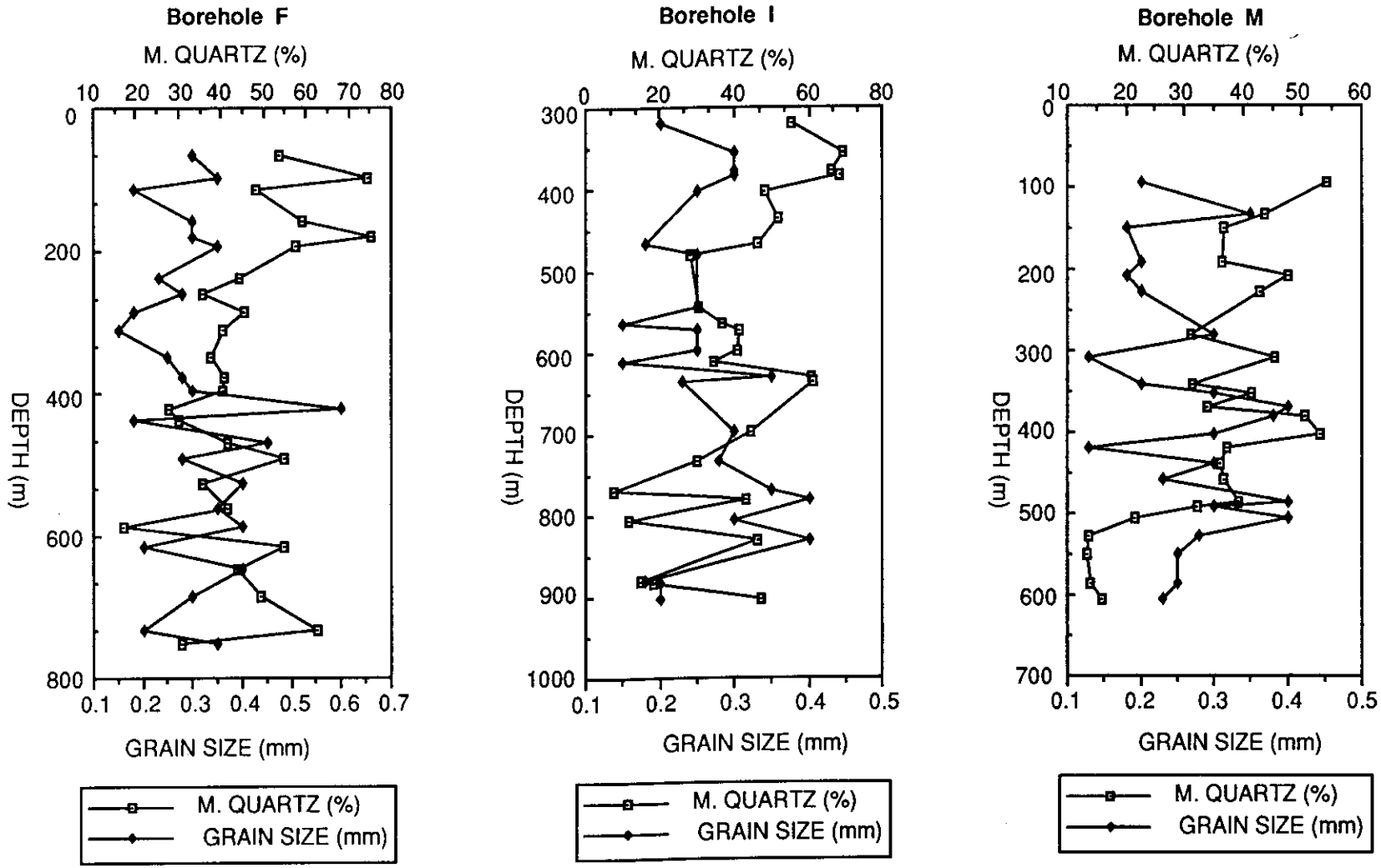

Fig 5-38 The variation of the detrital monocrystalline quartz grains with the average grain size and drilling depth for Boreholes F, I, and M.

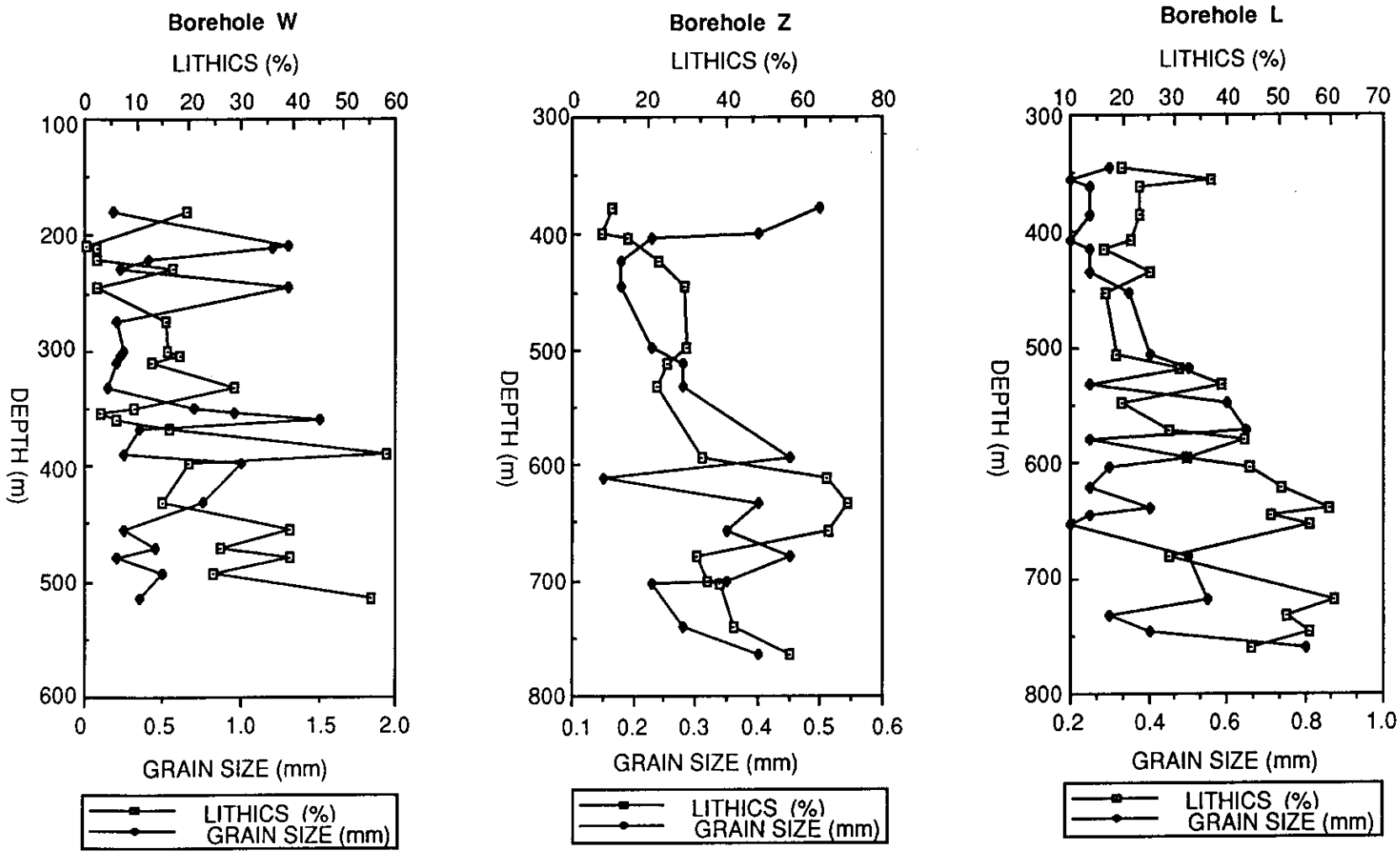

Fig 5-39 The variation of the detrital lithics with the average grain size and drilling depth for Boreholes W, Z, and L.

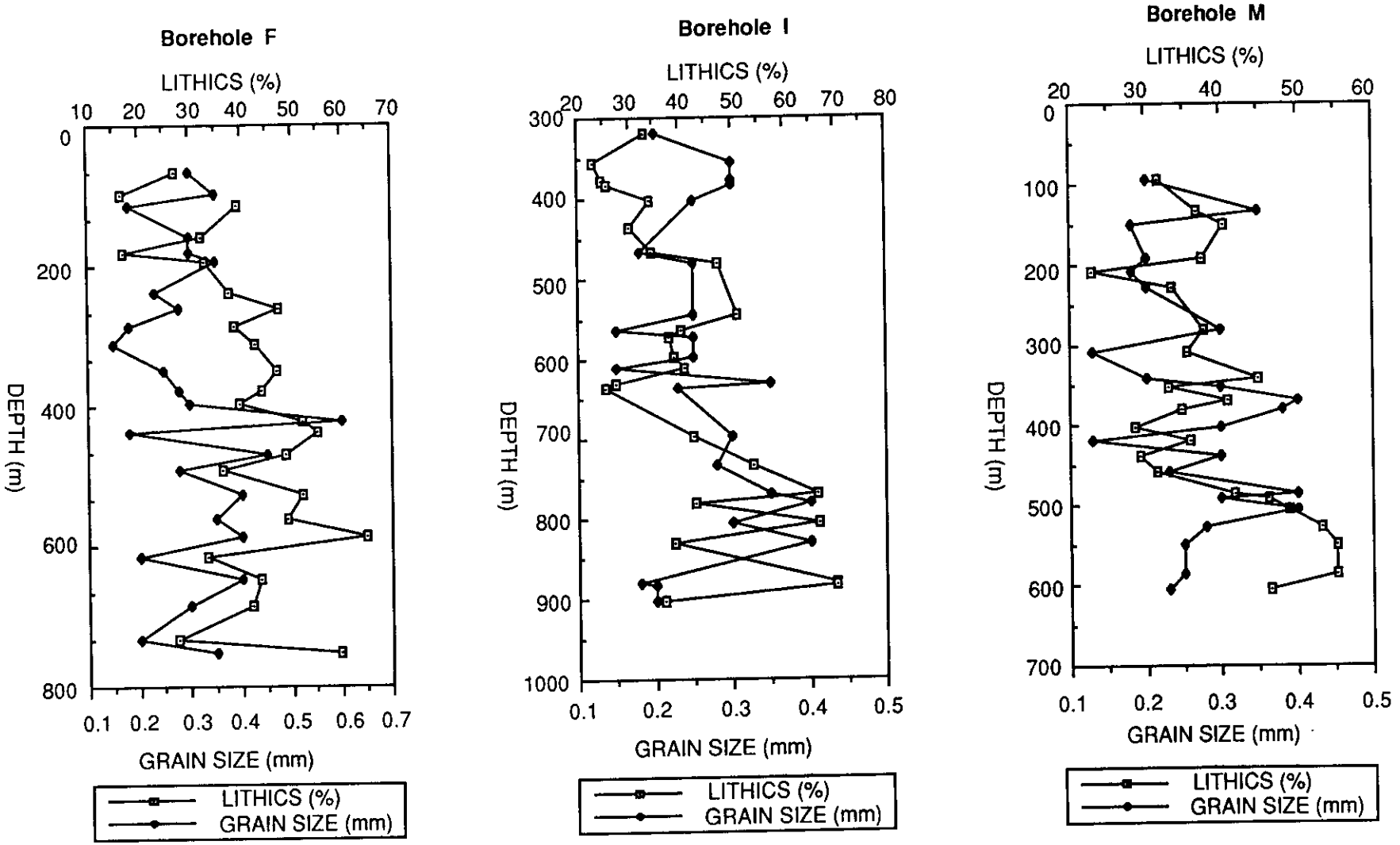

Fig 5-40 The variation of the detrital lithics with the average grain size and drilling depth for Boreholes F, I, and M.

the original composition of the sands. Therefore these changes should be considered when any attempt is made to deduce the provenance of an ancient sandstone.

In the case of the Narrabeen Group sandstones, the diagenetic changes affecting the original composition of the sandstones mainly include carbonate replacement of feldspar and volcanic lithics and dissolution / alteration of feldspar and volcanic lithics (will be discussed in the next Chapter). As a result of these diagenetic changes, the contents of the detrital feldspar grains and lithics from point counting would be lower than their original contents in the sandstone. However, in the majority of sandstones studied the replacement carbonates account for less than 2.0 % of the total sandstone (refer to Appendix III). In a very few samples they exceed 5.0 % of the total sandstone. The dissolution porosity is less than 2 % of the total sandstone in most of the sandstones. Complete alteration of detrital volcanic lithics and feldspar to authigenic minerals took place in an even smaller scale in the sandstones. Thus it is considered that these diagenetic changes recognised in the Narrabeen Group sandstones did not alter the original composition of the sandstones to a significant extent.

One final point should be noted. The counting of quartz overgrowths in the sandstones from Boreholes W to Z into "monocrystalline or polycrystalline quartz" leads to higher contents of detrital quartz clasts than their real contents in these sandstones. As mentioned before, however, visual estimates under the petrological microscope indicate that quartz overgrowths in most of the sandstones from Boreholes W to Z are not higher than 2 % of the total sandstone. In addition, point counting data show that quartz overgrowths account for less than 2 % of the total sandstone in the majority of sandstones from Boreholes A to V. Based on their low content, the inconsistent treatment of quartz overgrowths during point counting is considered not to significantly change the detrital composition variations of the

sandstones.

Since grain size, transportation, depositional environment, and diagenesis do not affect the detrital composition of the Narrabeen Group sandstones significantly, the composition of the sandstones is thought to be controlled mainly by their provenance. Accordingly from the variation of the sandstone compositions, the provenances for the Narrabeen Group sandstones can be deduced.

5.8 PROVENANCE OF NARRABEEN GROUP SANDSTONES

It has been known that the detrital composition of the Narrabeen Group sandstones changes both vertically throughout the group and regionally across the basin. Petrological studies carried out as part of this thesis have established certain systematic changes and these changes have been presented in some detail.

Based on the results of sandstone modal analyses, a composition profile has been compiled for each of the 26 boreholes studied. The regional variation of detrital composition is discussed for four stratigraphic intervals using the average percentage values of the detrital clasts of the sandstones. From the variations of the detrital composition of sandstones and the palaeocurrent data obtained by previous researchers, conclusions have been drawn regarding provenance and mineral dispersal. Changes in provenance with time are deduced from the variation of detrital composition.

5.8.1 VERTICAL VARIATION OF DETRITAL COMPOSITIONS OF SANDSTONES

The petrological data for this thesis have been taken entirely from fully cored boreholes of which some have penetrated the whole Narrabeen Group. These type of data are very suitable as a record of petrological change of a fixed point in the basin throughout the period of the Narrabeen Group sedimentation.

The petrological data are presented in tabular form in Appendixes III and IV, with the stratigraphic position, and depth of each sample against compositional data. The compositional change of sandstones can be more clearly shown by using graphic plots of the compositional data against the stratigraphic position of the sample.

The detrital composition variations of sandstones in a vertical sense are shown by the changes of detrital quartz (monocrystalline and polycrystalline quartz), detrital feldspar, and detrital lithics (including detrital chert), i.e. the three poles defined in the sandstone classification versus the drilling depth (stratigraphic horizon), as presented in Figs 5-41 to 5-47. The percentage of each of the three major detrital components is from Appendix IV.

From Figs 5-41 to 5-47, it is clear that the percentage of detrital quartz grains generally increases and that of detrital lithics decreases as the sequence is ascended, especially in the boreholes in the southern Sydney basin, corresponding to the development of more quartz rich sandstones. However, these changes do not proceed at a uniform rate. Depending upon the borehole location, one to three distinctive boundaries, across which the detrital composition has a sudden and significant change and / or one abnormally lithic - rich interval can be recognised in different boreholes. The boundaries are taken at the middle point of the drilling depths between the samples whose detrital composition differs significantly from each other (see Fig 5-41). The lowermost boundary is defined as DB3, the middle boundary as DB2 and the uppermost boundary as DB1 with DB2 being the most obvious. The sudden changes of detrital compositions across certain horizons have been noted by Ward (1971a, b). He proposed three steps to describe these sudden changes, which are similar to the three distinctive boundaries presented here.

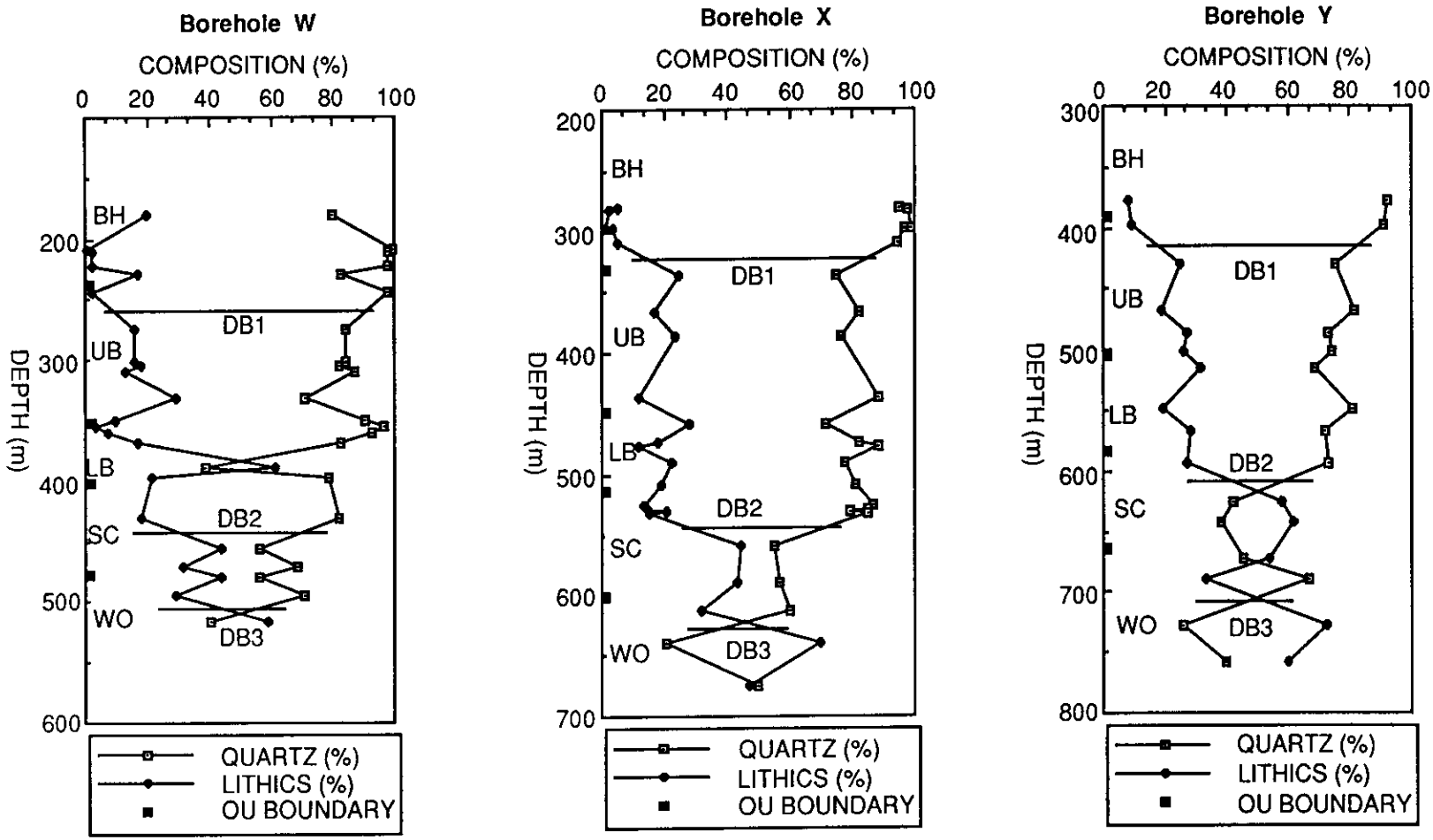

Fig 5-41 The vertical variation of the detrital clasts of the sandstones in Boreholes W, X, and Y. Most of the sandstones from the three boreholes do not contain feldspar so that no feldspar variation profile is shown in this diagram (DB = distinctive boundary, OU = operational unit).

The lowermost distinctive boundary DB3 occurs over a large area across the basin. It is recognised in Boreholes O, X, Y, and Z (Figs 5-41 to 5-43) in the southern region, in Boreholes T and W (Figs 5-41 & 5-43) in the west margin, in Borehole H (Fig 5-44) in the northern region, and in Borehole M (Fig 5-44) in the east coast zone. In other boreholes D, E, F, I, S, and U in the northern region, no DB3 can be recognised due to the complicated variation of the detrital composition (Figs 5-44 to 5-46). In Boreholes B, C, J, and L in the southern east coast zone, the abundance of detrital lithics in the lower Narrabeen Group results in the lack of DB3 in these boreholes (Figs 5-42 & 5-47).

The detrital lithics are more abundant than the detrital quartz clasts below DB3. DB3 marks a major source change from lithic to quartzose or a mixture of the two. The position of DB3 in the stratigraphic horizon is not consistent from one borehole to another throughout the whole basin, suggesting the source change did not take place uniformly in the whole basin. In the west margin, it occurs within the lower part of the WO unit in Boreholes T and W (Figs 5-41 & 5-43). In Boreholes X, Y and Z in the southern region, DB3 is within the middle part of the WO unit (Figs 5-41 & 5-42). In Borehole O near the boundary between the southern and northern regions of the basin (Fig 5-4), DB3 is within the top part of the WO unit (Fig 5-43). In Borehole M in the east coast zone, DB3 is recognised near the top of the WO unit (Fig 5-44). In the northern region it is located in the upper part of the SC unit in Borehole H (Fig 5-44). The position change of DB3 is characterised by the trend towards the younger stratigraphic horizon from the southwest to the northeast, suggesting that the major source change from the lithic to the quartzose or the mixture of the two happened earlier in the west margin and the western portion of the southern region and later in the east coast zone and the northeastern portion of the northern region.

The middle distinctive boundary (DB2) is recognised only in the boreholes in the

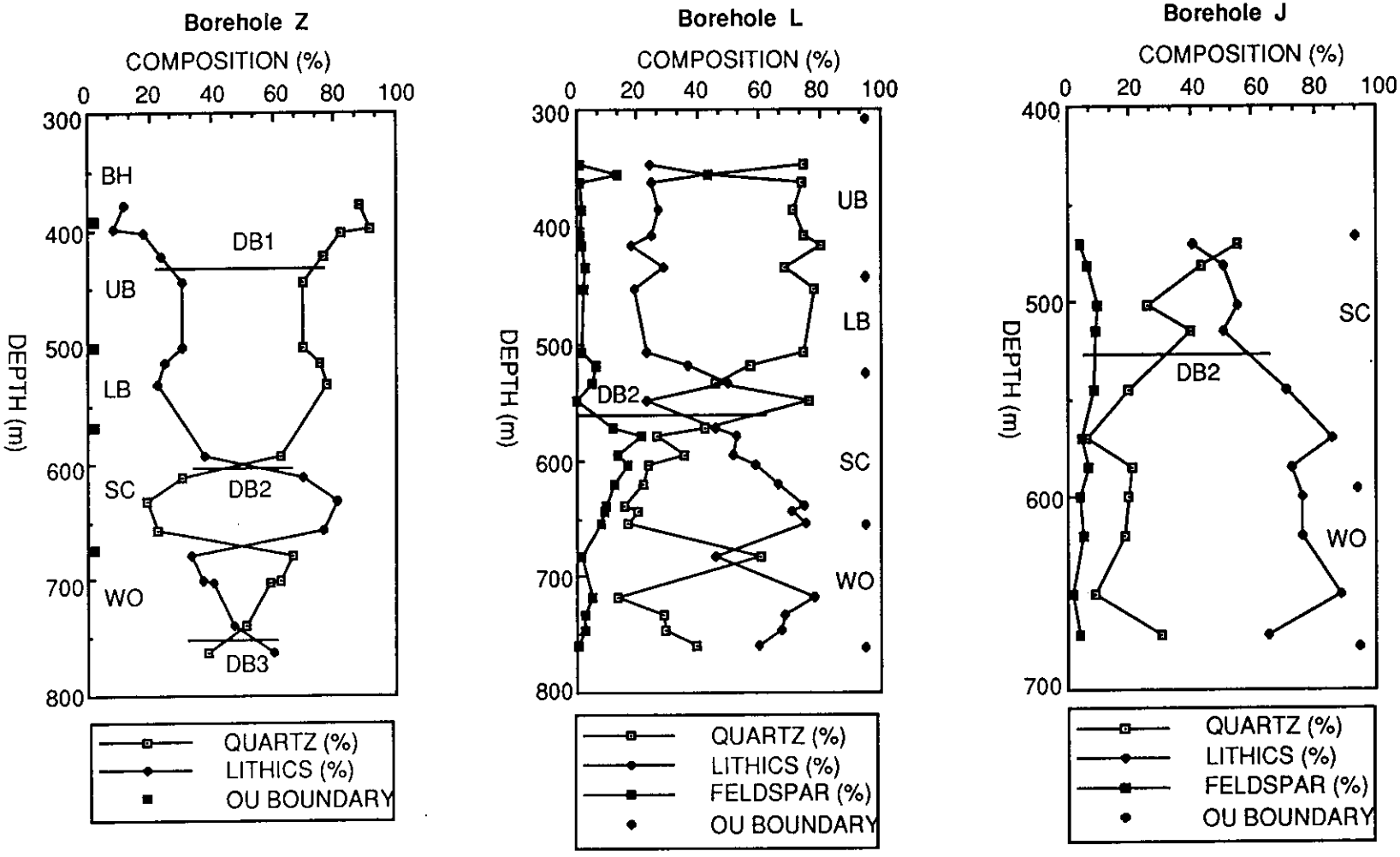

Fig 5-42 The vertical variation of the detrital clasts of the sandstones in Boreholes Z (Most of the sandstones from it do not contain feldspar so that no fledspar variation profile is shown for this borehole), L, and J.

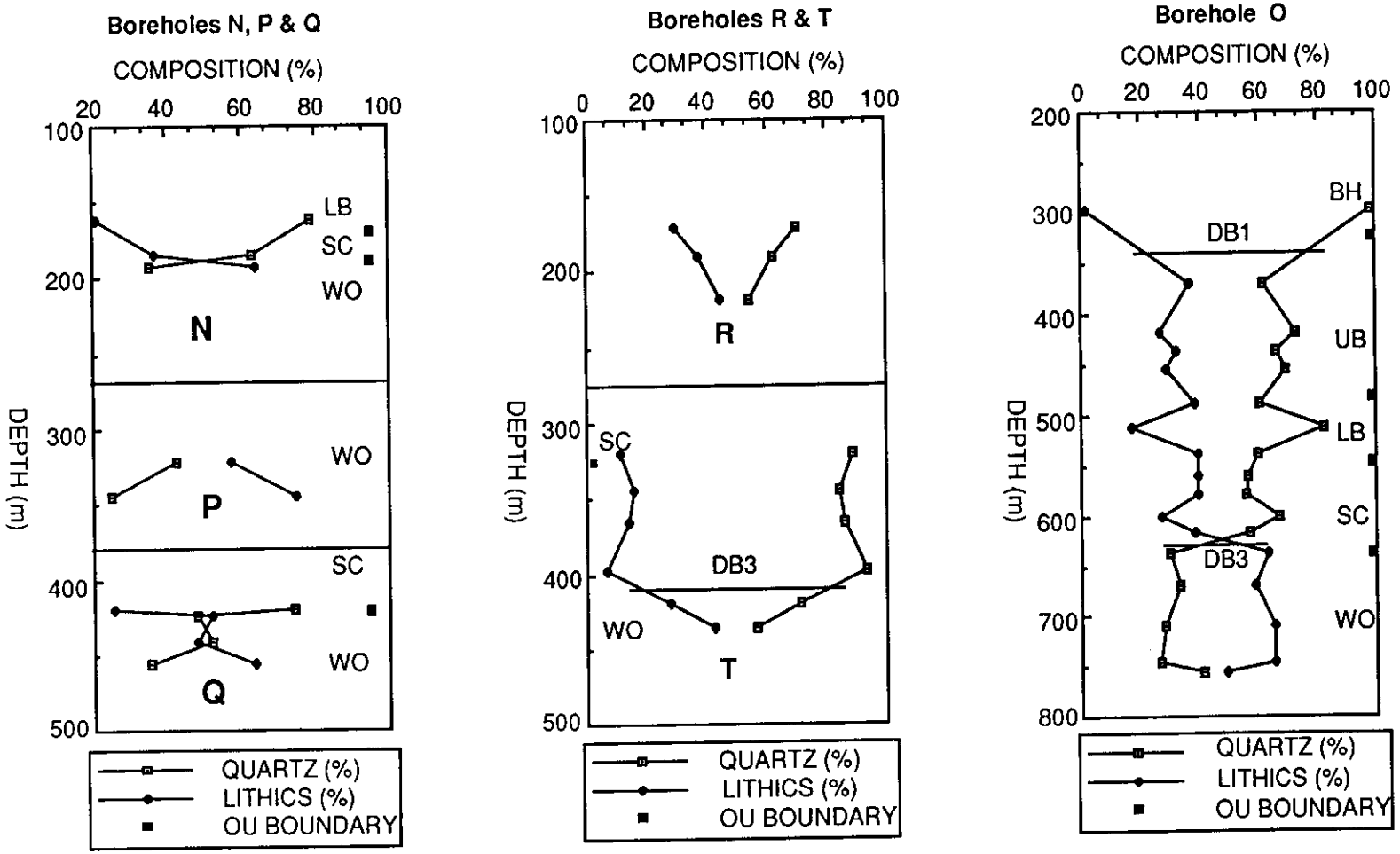

Fig 5-43 The vertical variation of the detrital clasts of the sandstones in Boreholes N, P, Q (compiled in one); R, T (compiled in one); and O. Most of the sandstones from these boreholes do not contain feldspar so that no feldspar variation profile is shown in this diagram.

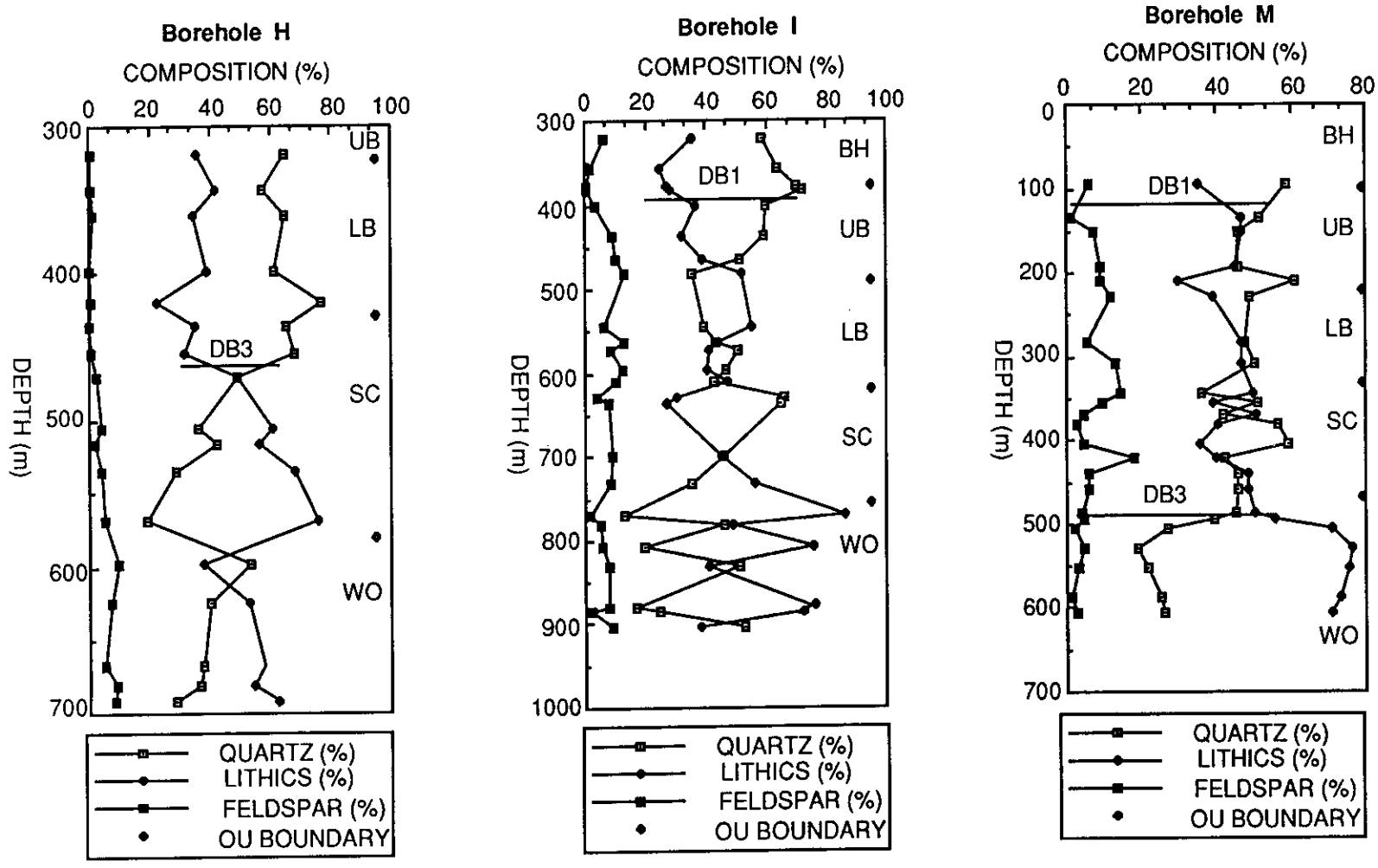

Fig 5-44 The vertical variation of the detrital clasts of the sandstones in Boreholes H, I, and M.

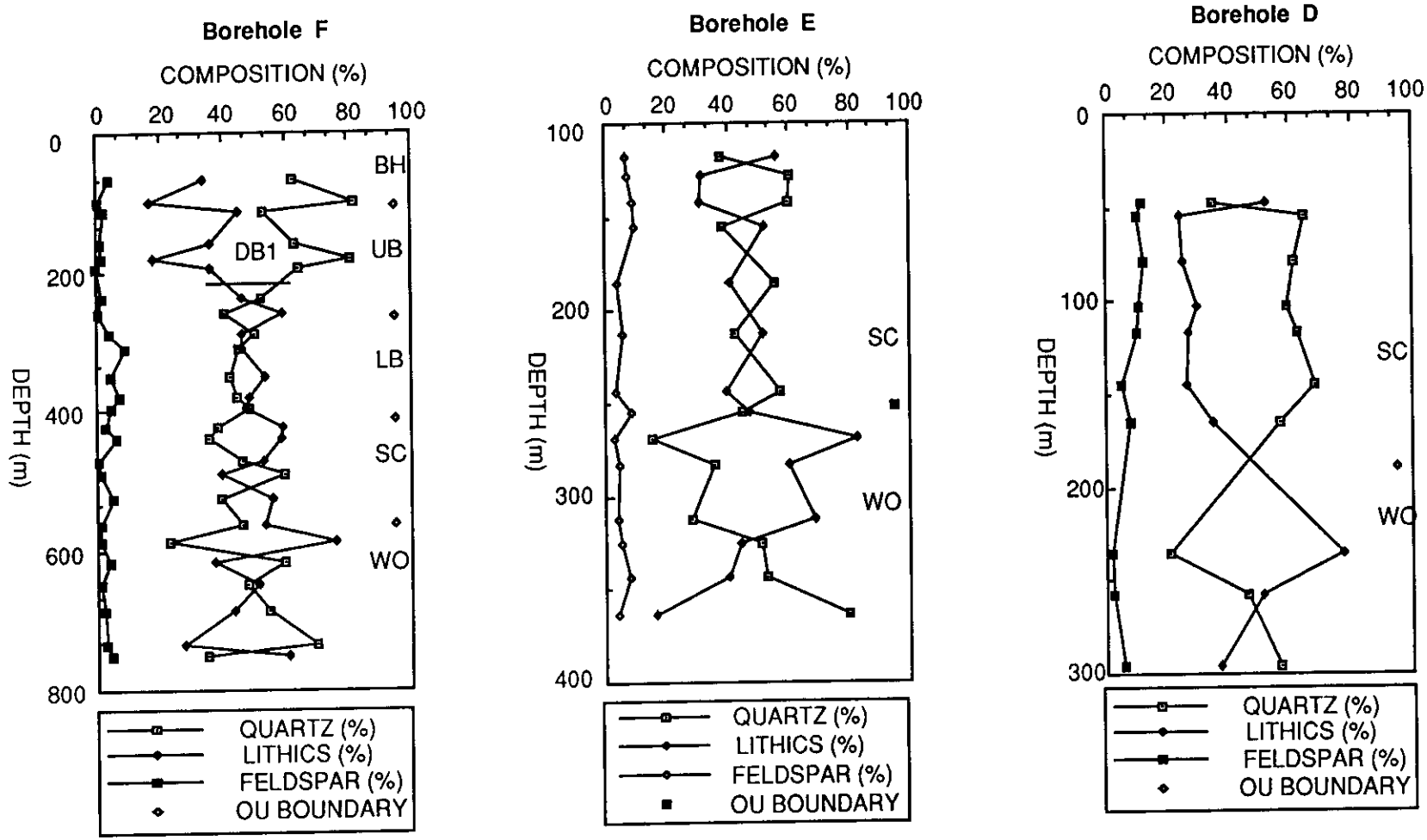

Fig 5-45 The vertical variation of the detrital clasts of the sandstones in Boreholes F, E, and D.

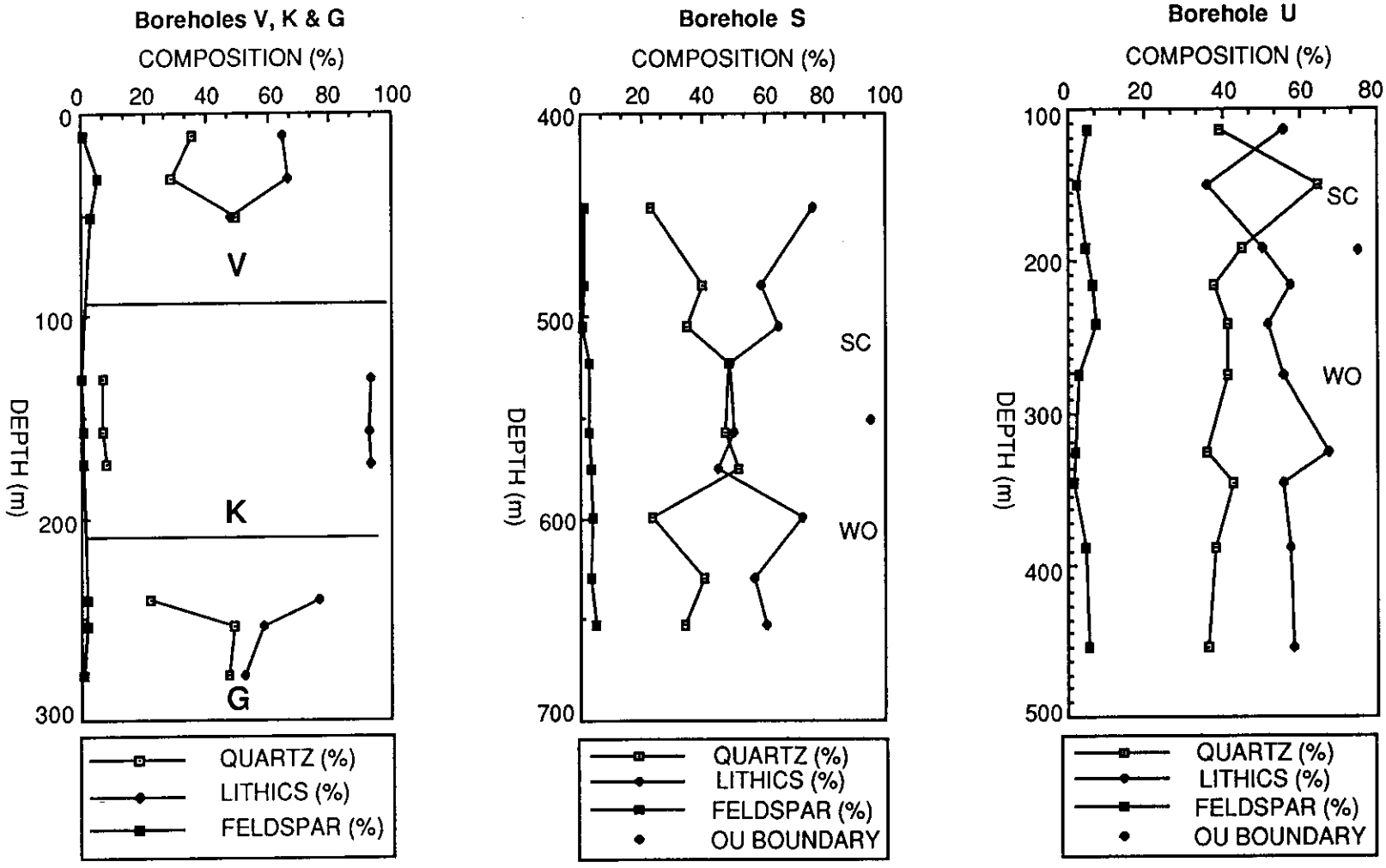

Fig 5-46 The vertical variation of the detrital clasts of the sandstones in Boreholes K, V, G (compiled in one); S; and U.

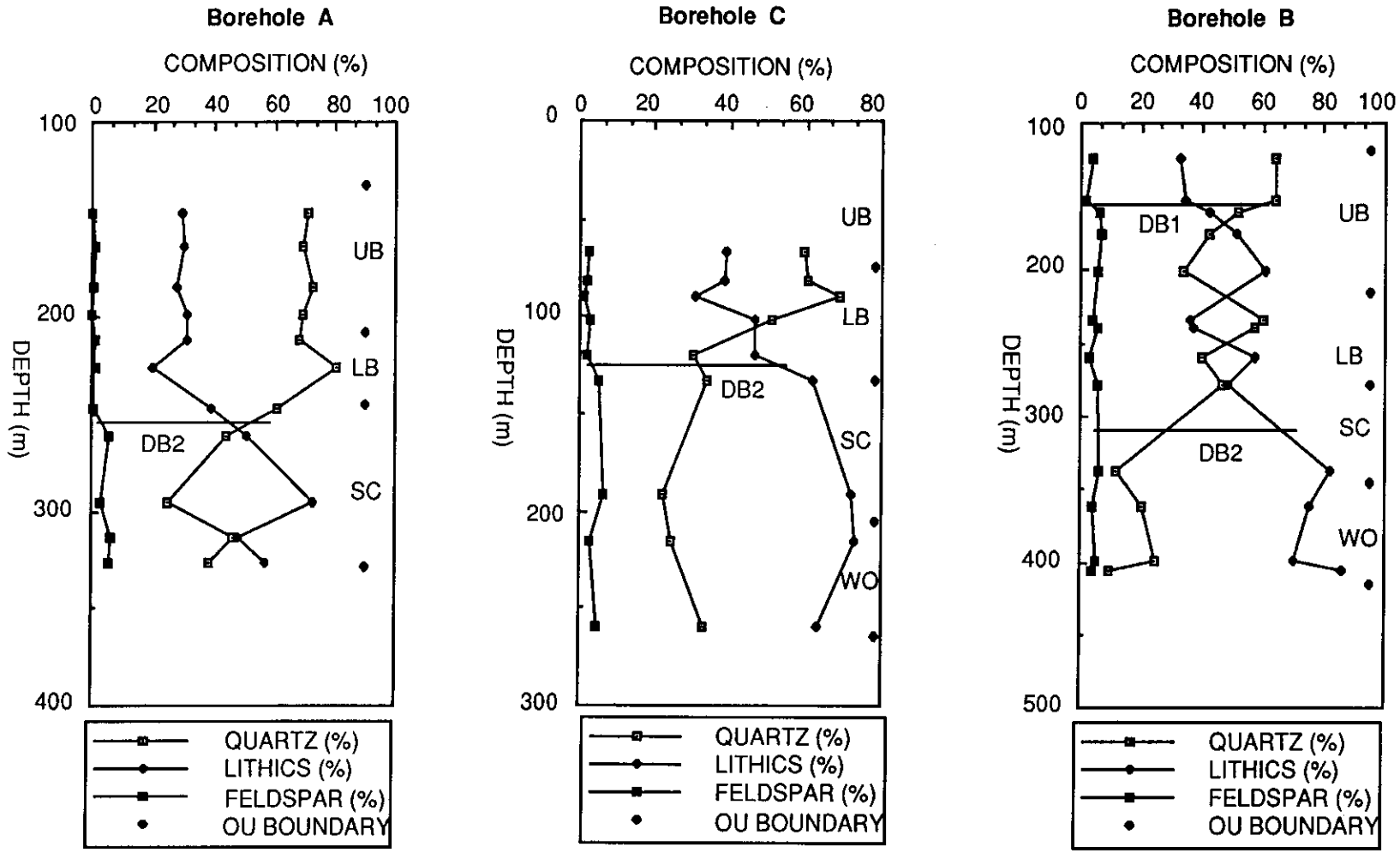

Fig 5-47 The vertical variation of the detrital clasts of the sandstones in Boreholes A, C, and B.

southern basin (Borehole O is an exception). Its position in the stratigraphic horizon is generally consistent in these boreholes. It occurs within the SC unit in Boreholes W to Z, L, J, A, and B (Figs 5-41, 5-42 & 5-47). However, in Borehole C it is within the bottom part of the LB unit (Fig 5-47). In the boreholes in the northern basin and Borehole O, no DB2 can be recognised (Figs 5-43 to 5-46).

DB2 marks the top boundary of a lithic - rich interval (defined here as an abnormally lithic - rich interval) whose bottom boundary generally occurs at that between the SC and WO units. In the abnormally lithic - rich interval the lithics overwhelm the quartz clasts or they are significantly more abundant than those in the underlying and overlying intervals. The interval broadly correlates with the lower part of the SC unit (Figs 5-41, 5-42 & 5-47). In Borehole C, however, it seems to correlate with the whole SC unit since DB2 occurs near the boundary between the LB and SC units in this borehole (Fig 5-47). The lithic rich interval is shown most clearly in the boreholes in the east coast zone (such as in Borehole J) and becomes less clear westwards. In Borehole W it is hardly seen. Due to absence of DB2 in the boreholes in the northern basin and in Borehole O, no abnormally lithic - rich interval is present in these boreholes.

The uppermost distinctive boundary DB1 is recognised in Boreholes W to Z, O, F, I and M where the sampling of sandstones from the Bald Hill Operational Unit is available. In Boreholes W to Z and O in the west margin and the southern region, it is most clearly shown (Figs 5-41 to 5-43). It is also tentatively seen in Borehole B in the southern east coast zone (Fig 5-47).

The position of DB1 in the stratigraphic horizon is generally consistent throughout the whole basin and it occurs near the boundary between the BH and UB units (In Borehole F, it is within the lower part of the UB unit, Fig 5-45) but within the UB unit (In Borehole X it is within the bottom part of the BH unit, Fig 5-41). Across DB1

upwards, the quartz percentage is much higher than the lithic percentage in the sandstone in the boreholes W to Z and O in the west margin and the southern region (Figs 5-41 to 5-43) and it is higher than the lithic percentage in the sandstones in Boreholes F, I, M and B in the northern region and the east coast zone (Figs 5-44, 5-45 & 5-47). The further increase of detrital quartz clasts across DB1 upwards suggests that the quartz source became more important after DB1.

In Boreholes N, P, Q, R, K, V, and G (Figs 5-43 & 5-46) where only limited core samples from the bottom part of the Narrabeen Group are available, no distinctive boundary and / or abnormally lithic - rich interval can be recognised.

Even though the three distinctive boundaries proposed in this petrology study are similar to the three steps designed by Ward (1971b), there are two differences. (1) The position of DB3 (equivalent of "step A" of Ward) is not consistently in the stratigraphic horizon across the basin. Thus it cannot be used as a time - stratigraphic correlation marker as proposed by Ward. (2) The presence of DB2 is considered to be related to the eastern volcanic source (discussed later). It is recognised only in the boreholes in the southern basin. The speculation that "the step B" (equivalent of DB2) persists to the North Coast made by Ward is not supported by this study.

In summary, the sandstones change their detrital composition in the northern Sydney Basin in a much more complicated way than in the southern Sydney Basin. In the southern basin, the percentage of detrital lithics decreases and that of detrital quartz clasts increases upwards if the abnormally lithic - rich interval is excluded from the whole sequence but this change does not proceed at a uniform rate, as indicated by the occurrence of one to three distinctive boundaries. The sandstones between DB1 and DB2 are of much same composition. By contrast, the general trend of the detrital composition variation found in the southern basin is not clearly

shown in the boreholes in the northern Sydney Basin. In this part of the basin, the detrital composition varies greatly in a random way towards the top of the Narrabeen Group and the sandstones between DB1 and DB3 or the bottom of the Narrabeen Group are of a considerably variable composition.

5.8.2 REGIONAL VARIATION OF DETRITAL COMPOSITIONS OF SANDSTONES AND DEDUCTION OF DETRITAL SOURCES

The detrital composition of sandstones in a given unit at one place differs from that of sandstones in the same unit at another place of the basin. The variation in detrital components for a given unit across the basin has been contoured, as shown in Figs 5-48 to 5-53. The value used for each borehole is an average for the interval of strata in question calculated from Appendix IV (recalculated point counting data). The regional variation of detrital composition is discussed for four stratigraphic intervals: Wombarra Operational Unit, Scarbourough Operational Unit, Lower and Upper Bulgo Operational Units (excluding the top part of the UB unit, i.e. the part between DB1 and the top of the UB unit) as a single interval, and the top part of the UB unit and BH unit as a single interval.

(i) Wombarra Operational Unit

The detrital composition variation in this unit is characterised by a clear west to east change and a less obvious south to north change. Along the western margin of the basin, the sandstones generally contain a high content of detrital quartz clasts with the highest being recorded as 93.0 % in sample T397.6 and the average quartz percentage of sandstones in Borehole T in the unit is 78.2 %. In Borehole B in the east coast zone of the basin, the detrital quartz averages only 18.2 %.

The west to east variation is clearly shown in the southern Sydney Basin from Borehole W in the west margin to Borehole J in the east coast zone. The percentage of detrital lithics increases eastwards with an average of 44.0 % in

Borehole W, through 54.9 % in Borehole Y, 63.9 % in Borehole L, to 76.6 % in Borehole J (Fig 5-48). As a result of the variation of detrital lithics, the average percentage of detrital quartz clasts decreases towards the east.

This west - east detrital composition variation is also shown by the boreholes in the northern Sydney Basin even though not as clearly as in the southern Sydney Basin. From 37.3 % in Borehole R in the west margin, the average percentage of the lithics increases to 56.9 % in Borehole S and 57.7 % in Borehole U in the northern region (Fig 5-48).

From south to north, the average percentage of the lithics in the sandstones of the unit does not change much until to the northernmost borehole K, which is located in the adjacent Gunnedah Basin. In this borehole the average content of the detrital lithics in the sandstones of the WO unit is recorded as 92.9 % of the total detrital clasts (Fig 5-48), which is much higher than the average of 59.6 % in the nearby borehole V.

In the west margin and the southern region of the basin, the sandstones (except those at the basal part) do not contain detrital feldspar grains. As a result, the average percentage of detrital feldspar grains is less than 1.0 % of the total detrital clasts in the boreholes (except Borehole O) in this part of the basin. To the east coast zone and the northern region of the basin, detrital feldspar grains become much more abundant. The average percentage of detrital feldspar grains ranges from 2.6 % in Borehole V to 7.8 % in Borehole H (0.4 % in Borehole K is an exception). However the variation of detrital feldspar grains throughout the basin is not as regular as that of the major components - detrital quartz clasts and detrital lithics.

The characteristics of the detrital composition variations (Figs 5-48 & 5-49) can be

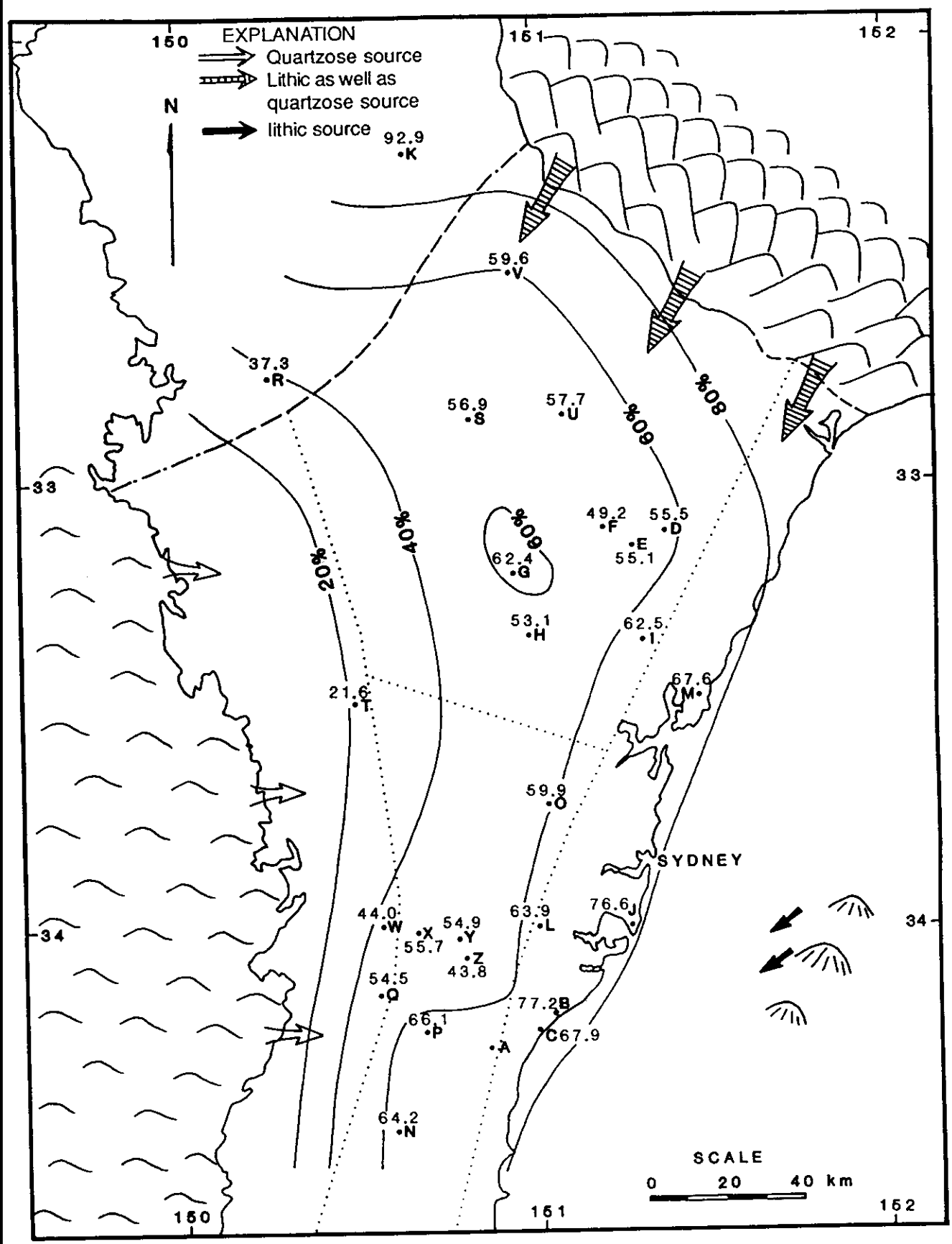

Fig 5-48 Regional variation of the average percentage of detrital lithics of sandstones in the Wombarra Operational Unit and the deduced detrital sources.

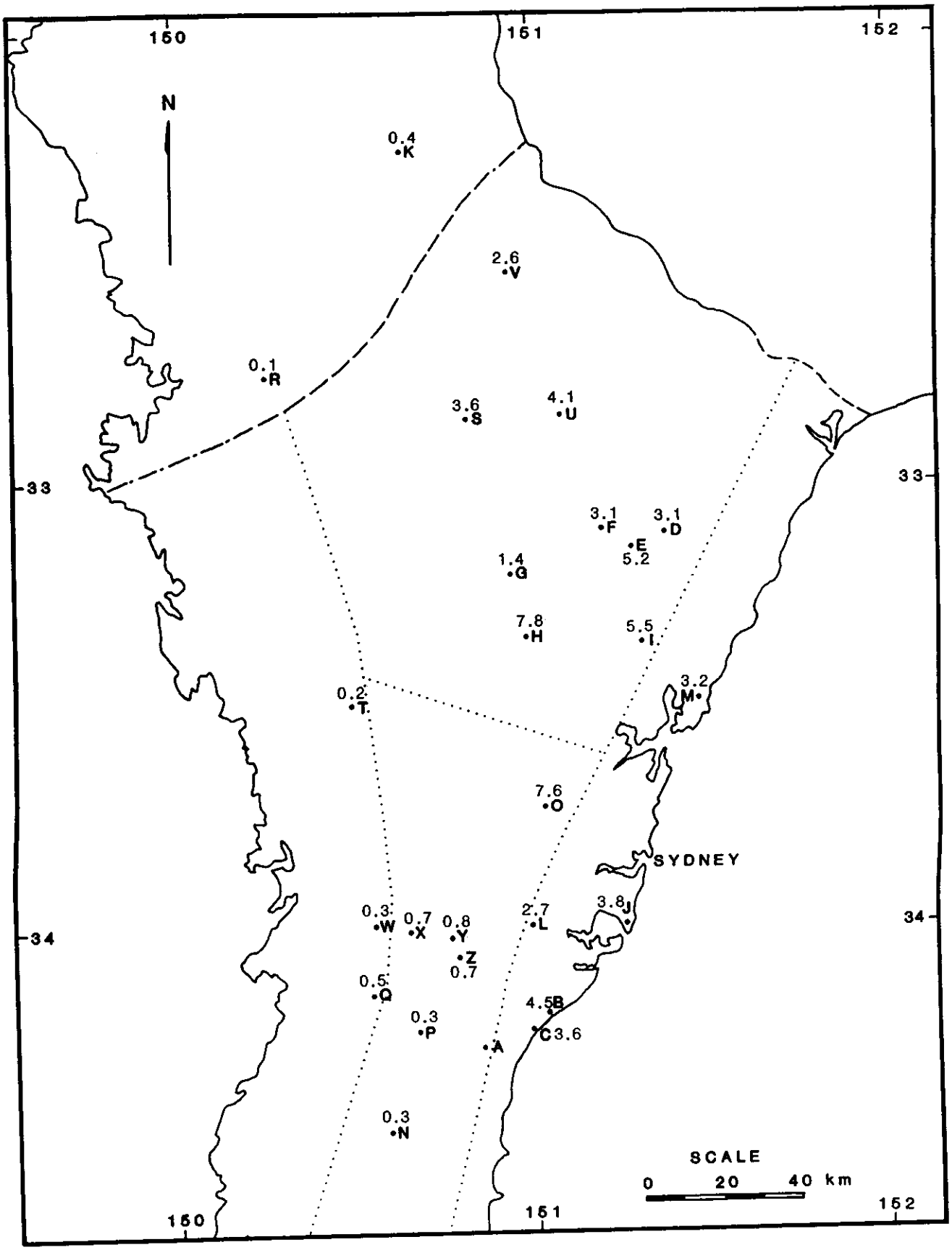

Fig 5-49 Regional variation of the average percentage of detrital feldspar of sandstones in the Wombarra Operational Unit.

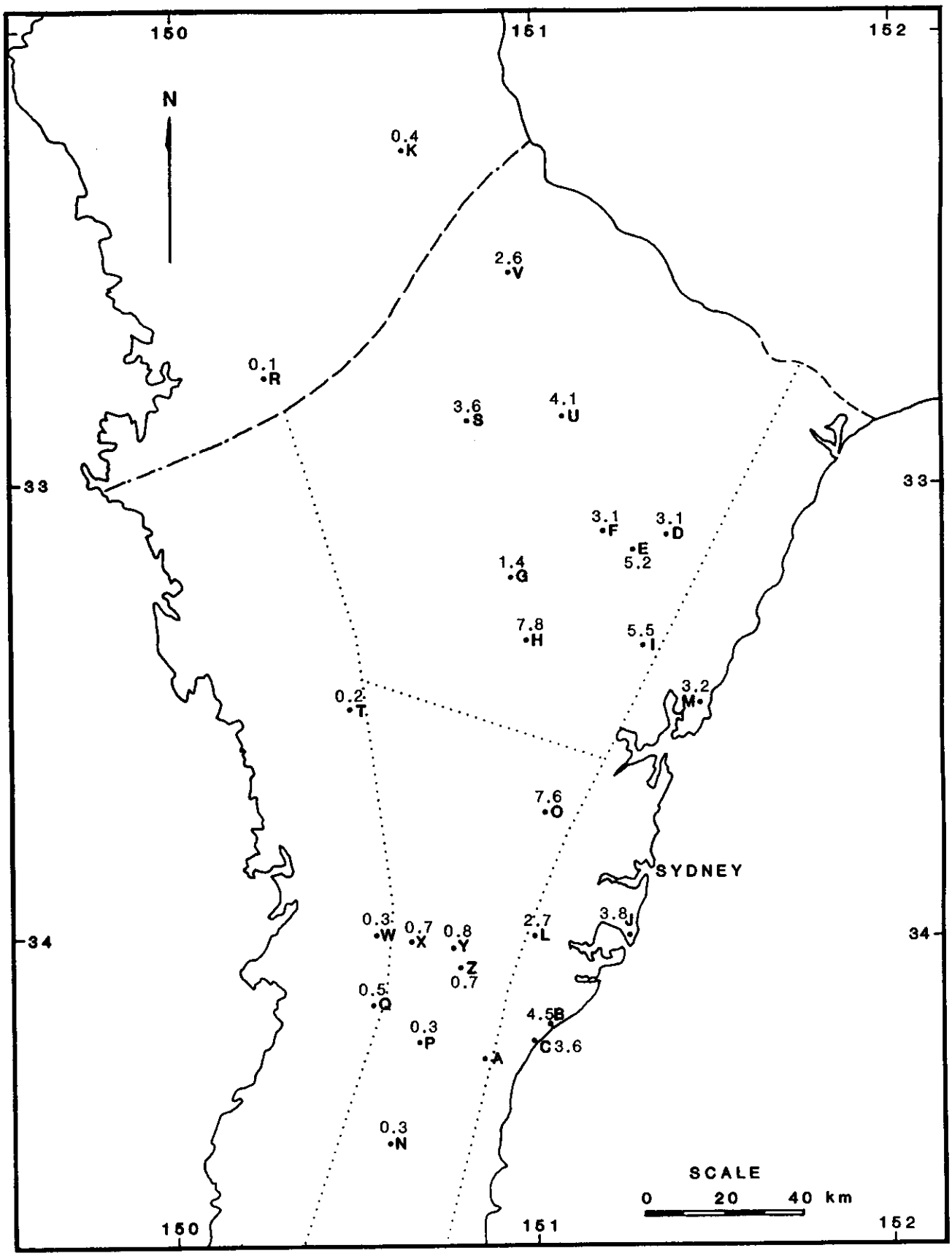

Fig 5-49 Regional variation of the average percentage of detrital feldspar of sandstones in the Wombarra Operational Unit.

used to deduce the detrital sources for the sediments in the Narrabeen Group. During the deposition of the WO unit, there probably existed three detrital sources: the northeastern New England Fold Belt supplying mainly detrital volcanic lithics and volcanic derived quartz clasts as well as detrital feldspathic clasts, the western Lachlan Fold Belt mainly supplying detrital quartz clasts, and an eastern volcanic source which principally supplied detrital volcanic lithics and feldspathic clasts during its active period. The former two were major sources and the last one minor.

During early WO time, the New England Fold Belt acted as the principal detrital source over the whole Sydney Basin. Until the time corresponding to DB3, then the Lachlan Fold Belt replaced the New England Fold Belt to supply significant quantities of detritus to the west margin and western portion of the southern region of the basin. This is reflected by the upwards increase of the detrital quartz (sudden increase across DB3) in the sandstones in this part of the basin. The upwards increase also suggests that the Lachlan Fold Belt source became more and more important as sedimentation proceeded.

In the northern region of the basin, the detrital clasts were largely derived from the New England Fold Belt as well as Lachlan Fold Belt. To the northeast margin of the basin, the detrital clasts were principally supplied by the New England Fold Belt, which is supported by a very high average percentage of detrital lithics in the northernmost borehole K. The relative amount of the detrital components, which the depositional site received from each source, was principally controlled by the location of the depositional site in the fluvial depositional system and its relative distance from the source at the time of deposition. In the northern east coast zone, the volcanic lithics were largely derived from the New England Fold Belt.

In the southern east coast zone, the sandstones contain abundant detrital volcanic lithics (Fig 5-48), suggesting the presence of a nearby volcanic source. It was

probably located to the east of present day coast line of Cape Banks 1 borehole (Borehole J) (probably east of the present continental shelf, i.e. now part of Lord Howe Rise). The volcanic lithics from this source were transported to the basin southwesterly and southerly and deposited in the southern east coast zone and the southernmost portion of the basin. This is supported by the palaeocurrent data (Diessel et al., 1967; Ward, 1972). In the Illawarra region in the south coast, a mean palaeocurrent trend of 220° is recorded at the basal portion of the Narrabeen Group (Diessel et al, 1967), and Ward (1972) gave a mean palaeocurrent trend of 178° in the overlying Coal Cliff Sandstone (equivalent of WO unit, refer to Fig 4-3).

In Borehole J and L nearer to the proposed volcanic source, the sandstones in the middle part of the WO unit are more volcanic lithics rich than those in the upper and lower parts of the WO unit (Fig 5-42). This probably suggests that this volcanic source was active only during the middle period of WO time. The detrital lithics from this eastern volcanic source seem to be intermediate volcanic rock fragments, which are different from the acidic volcanic rock fragments derived from the New England Fold Belt. This difference was also documented by Ward (1971a, b).

Galloway and Hamilton (1988) proposed a volcanic source terrane termed the "Cape Banks Volcanic Apron" to explain the occurrence of a small amount of volcanic lithics in the coastal exposures (correlating with the Scarborough Operational Unit) south of Sydney. Ward (1972) indicated a volcanic source (the Gerringong Volcanics) to explain the volcanic lithics in the "volcanic facies" of the Bulgo Sandstone (correlating with the Upper Bulgo Operational Unit, refer to Fig 4-3). The volcanic source suggested here started to supply detrital volcanic lithics to the basin in WO time, which was earlier than Galloway and Hamilton proposed and much earlier than Ward's.

(ii) Scarborough Operational Unit

In the southern Sydney Basin, the SC unit generally consists of two parts: the abnormally lithic - rich interval and the interval overlying DB2. Due to the presence of this abnormally lithic - rich interval, the sandstones in this unit change greatly in their detrital composition with time. For example, the detrital lithics range from 23.3 % to 66.0 % of the total detrital clasts in Borehole L, 37.5 % to 76.3 % in Borehole Z and 26.8 % to 61.9 % in Borehole Y (refer to Appendix IV). Thus the sandstones in this unit have a wide range of detrital composition from litharenite, through quartzose litharenite, to sublitharenite (Fig 5-31).

Regionally there is an eastward increase of the average detrital lithics in the abnormally lithic - rich interval in the southern Sydney Basin (Fig 5-50). The average percentage of detrital lithics changes from 37.7 % in Borehole W in the west margin, through 43.8 % in Borehole X, 60.0 % in Borehole Y, 75.5 % in Borehole Z, to 82.0 % in Borehole B in the east coast zone. As a result of this change the average percentage of detrital quartz clasts greatly decreases towards the east. This clear variation of detrital composition obviously indicates that an eastern volcanic source existed (Fig 5-50).

In the northern Sydney Basin, the abundance of detrital lithics in sandstones does not vary as greatly as in the southern Sydney Basin in a single borehole. Regionally the detrital lithics generally increase northwards, which is reflected by the compositional change from quartzose litharenites, quartzose feldspathic litharenite and litharenites in Boreholes D, E, and F to dominant litharenites in Boreholes U and S (Fig 5-31).

Like in the underlying WO unit, in this unit the detrital feldspar clasts generally *increase from the west margin to the east coast zone, and from the southern region* to the northern region (Fig 5-51).

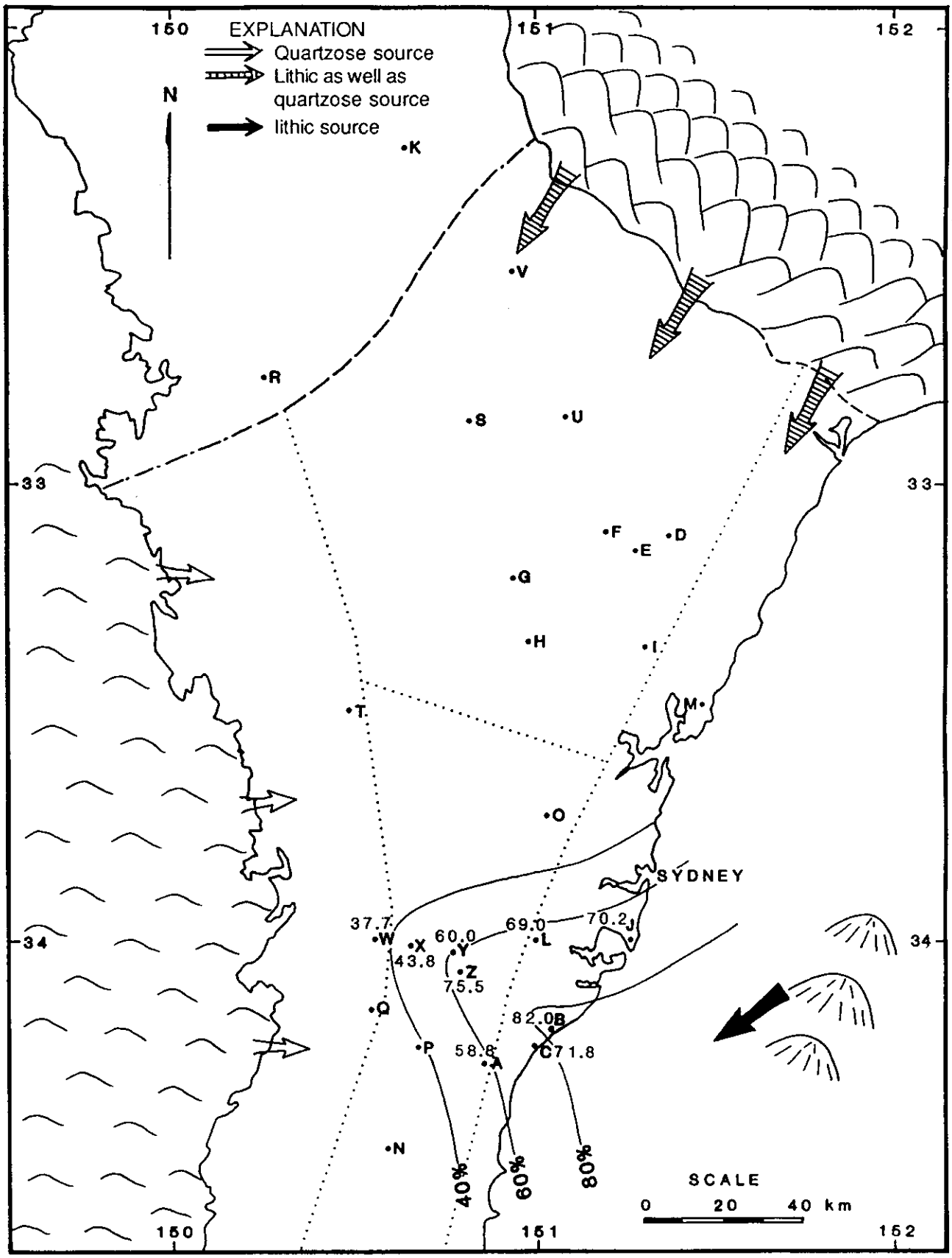

Fig 5-50 Regional variation of the average percentage of detrital lithics of sandstones in the abnormally lithic - rich interval in the southern Sydney Basin and the deduced detrital sources.

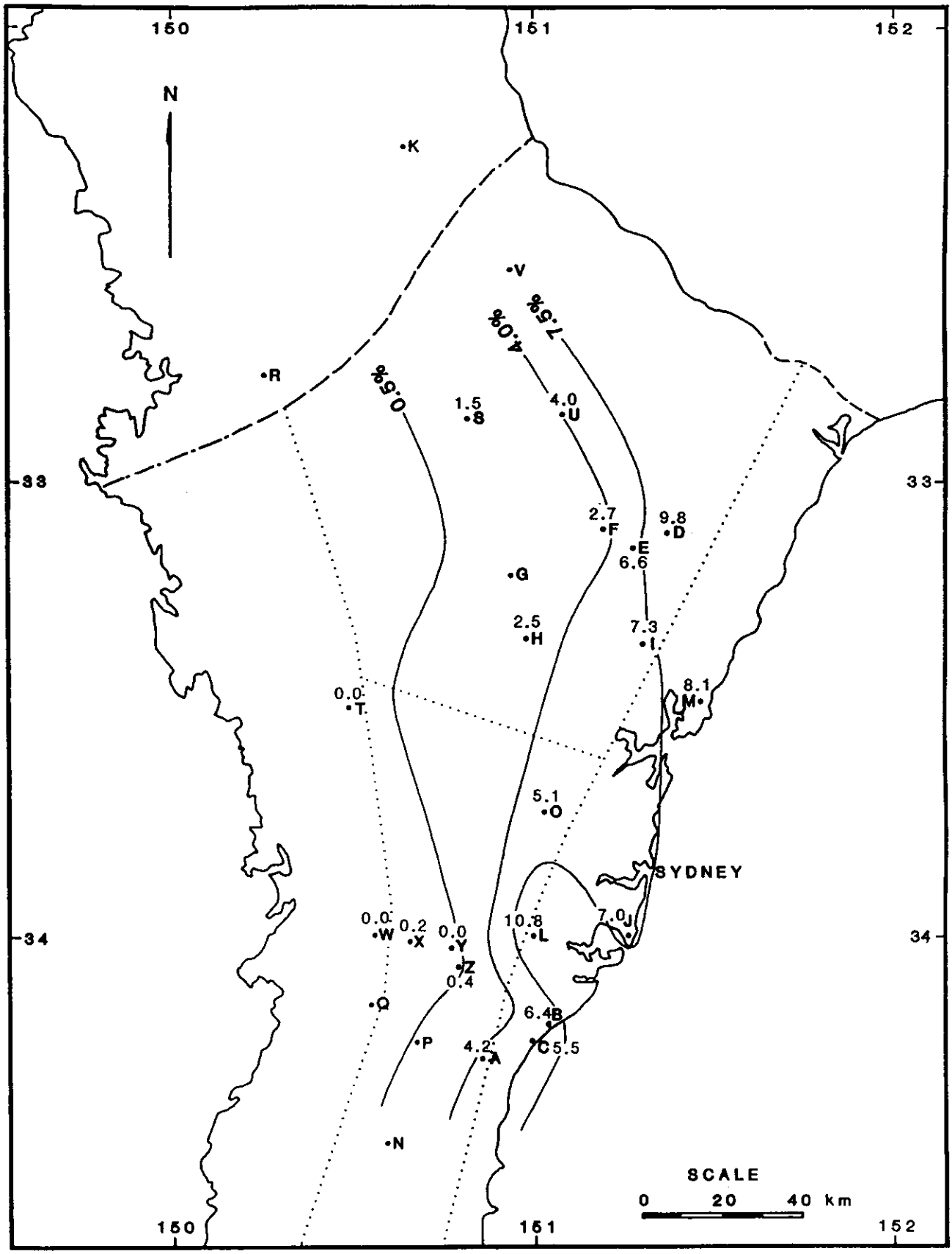

Fig 5-51 Regional variation of the average percentage of detrital feldspar in the Scarborough Operational Unit.

In the southern Sydney Basin, during the deposition of the lower part of the SC unit, the eastern volcanic source active in middle WO time, became very active. It probably supplied a substantial amount of volcanic lithic clasts to the southern Sydney Basin, especially the southern east coast zone, as implied by the more abundant volcanic lithics in the sandstones from the lower SC unit than in the sandstones from the WO unit in Boreholes X to Z, L, J, B and C (Figs 5-41, 5-42 & 5-47). As a result, the abnormally lithic - rich interval correlating with the lower part of the SC unit was deposited. The sediments from this source were dispersed to the basin by southerly to southwesterly currents, as suggested by the mean palaeocurrent trend of 224° in the topmost Scarborough Sandstone and 206° in the basal Bulgo Sandstone (the two stratigraphic horizons broadly correlate with the middle Scarborough Operational Unit, refer to Fig 4-3) in the south coast (Ward, 1972). As the distance from this source increased, its influence diminished (Fig 5-50).

During the deposition of the upper SC unit, the offshore volcanic source ceased to supply large amounts of detrital volcanic clasts, as implied by the sudden upwards decrease of the detrital lithics across DB2. Thus the detrital clasts were largely derived from the Lachlan Fold Belt in the west margin and western portion of the southern region and resulted in the deposition of sublitharenites and quartzose litharenites of the upper SC unit. To the east coast zone where the sandstones consist of roughly equal amount of detrital lithics and detrital quartz clasts, the Lachlan Fold Belt became less important and the eastern volcanic source probably continued to supply some detrital lithics.

In the northern Sydney Basin, the detrital clasts were mainly derived from the New England Fold Belt and the Lachlan Fold Belt even during early period of SC time when the eastern volcanic source was very active.

(iii) Lower and Upper Bulgo Operational Units (excluding top part of UB unit)

DB1, which is found in all the boreholes where the sandstones from the whole Narrabeen Group are available as well as in Borehole B, occurs near the boundary between the BH / UB units with Borehole F as an exception (Fig 5-45) and it is within the UB unit with Borehole X as an exception (Fig 5-41). In the sequence between DB1 and the LB/SC boundary, the sandstones change little in each of the individual boreholes except Boreholes B, M, F and I , which are located in the east coast zone and the northeastern portion of the northern region and are relatively far away from the Lachlan Fold Belt. Thus the LB and UB units (excluding the part between DB1 and the top of the UB unit) are discussed together here as a single sedimentary sequence.

In this sequence detrital composition changes regularly in the regional direction. Towards the northeast, the abundance of detrital quartz clasts decreases and that of detrital lithics increases. The average percentage of detrital quartz clasts in the sandstones of this sequence decreases from 75.1 % of the total detrital clasts in Borehole Y, through 67.6 % in Borehole O, to 47.5 % in Borehole I and 46.0 % in Borehole F (Fig 5-52). The abundance of detrital feldspathic clasts generally increases northeastwards.

In the west margin and the southern region of the basin, the sandstones in this sequence consist largely of quartzose litharenites and sublitharenites, indicating they were mainly derived from a quartzose source. The Lachlan Fold Belt is considered to be the principal source in this part of the basin (Fig 5-52).

In Boreholes F, I and M in the northern basin, which are far away from the Lachlan Fold Belt, the sequence between DB1 and the LB/SC boundary consists of quartz - rich intervals and lithic - rich intervals (Figs 5-44 & 5-45). This suggests that the sediments in this part of the basin were not supplied by a single principal source.

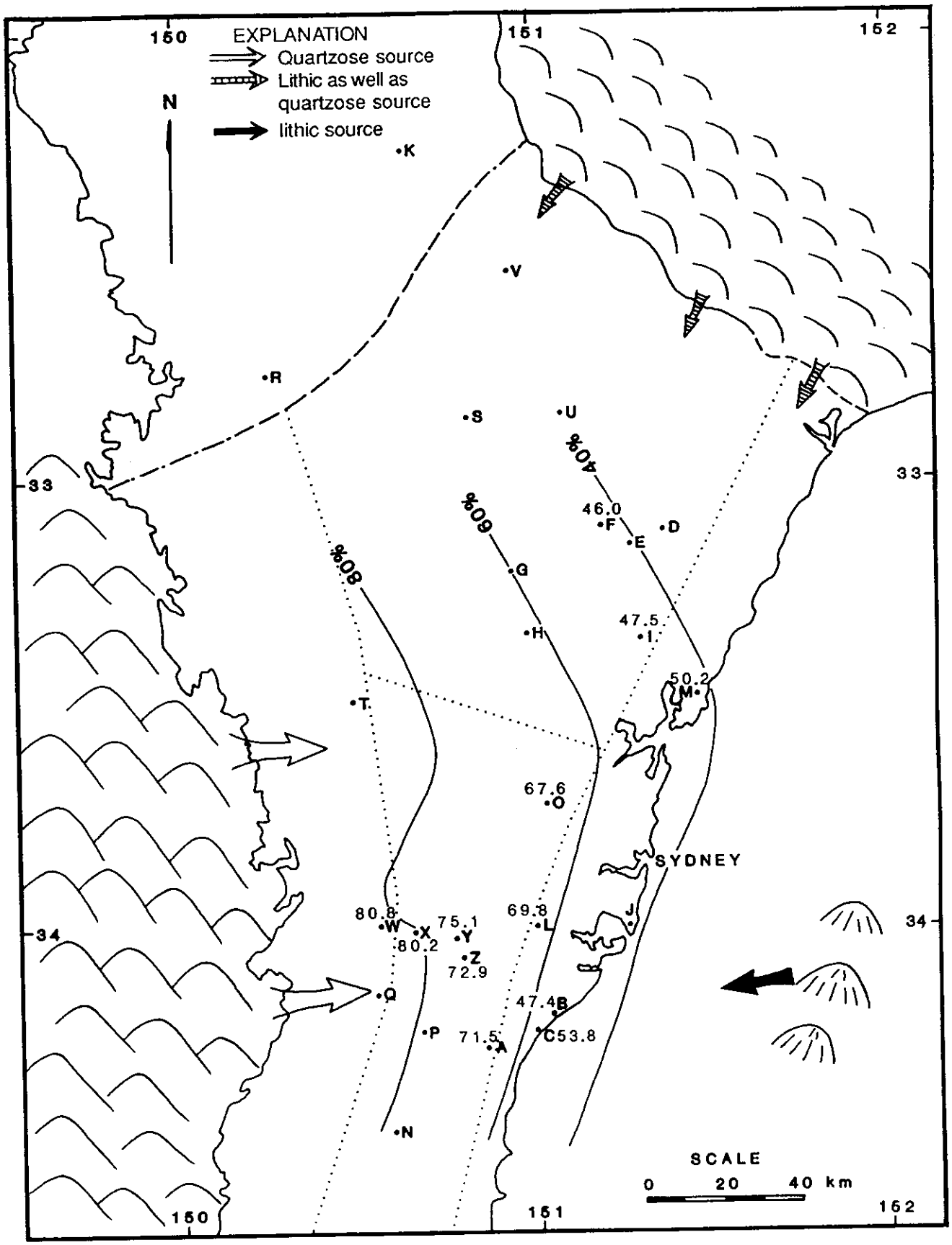

Fig 5-52 Regional variation of the average percentage of detrital quartz grains in the Lower and Upper Bulgo Operational Unit (excluding the top part of the BH unit) and the deduced detrital sources.

Both the Lachlan Fold Belt and the New England Fold Belt contributed detrital clasts to it without one dominating the other over a long period of time.

In Boreholes B and C in the southern east coast zone, the vertical variations of the detrital composition of sandstones (Fig 5-47) imply that the eastern volcanic source was active from time to time with the early and middle periods of UB time being more active. This is suggested by the abundance of detrital volcanic lithics in the sandstones in the lower and middle parts of the UB unit. This source supplied large amounts of detrital volcanic lithics to the southern east cost zone of the basin and led to the low average percentage of detrital quartz in this sequence in Boreholes B and C (Fig 5-52). The influence of the volcanic source was restricted to this zone, as indicated by the lack of the significantly lithic - rich interval in Boreholes A and L within the LB and UB units, which are only further away from this eastern volcanic source than Boreholes B and C. The detrital volcanic lithics were supplied to the basin westerly from this source, as indicated by the palaeocurrent data. At Garie south, a mean palaeocurrent trend of 261° was measured by Ward (1972) in the middle facies ("volcanic facies") of the Bulgo Sandstone, which correlates with the Upper Bulgo Operational Unit (refer to Fig 4-3).

(iv) Bald Hill (BH) Operational Unit and Top Part of UB Unit

Detrital quartz is much more abundant than detrital lithics in the BH unit and the top part of the UB unit, which are considered here as a single sedimentary sequence. For this sequence, the average percentage of detrital quartz clasts decreases northeastwards from 98.1 % in Borehole O and 96.5 % in Borehole X, to 68.3 % in Borehole I and 67.4 % in Borehole F (Fig 5-53) so that the average percentage of detrital lithics generally increases to the northeast. Detrital feldspar is generally absent in the sandstones of this sequence in the southern Sydney Basin but increases away from the Lachlan Fold Belt source towards the northeast. In Boreholes M, I and F, the average percentage of detrital feldspar grains from this

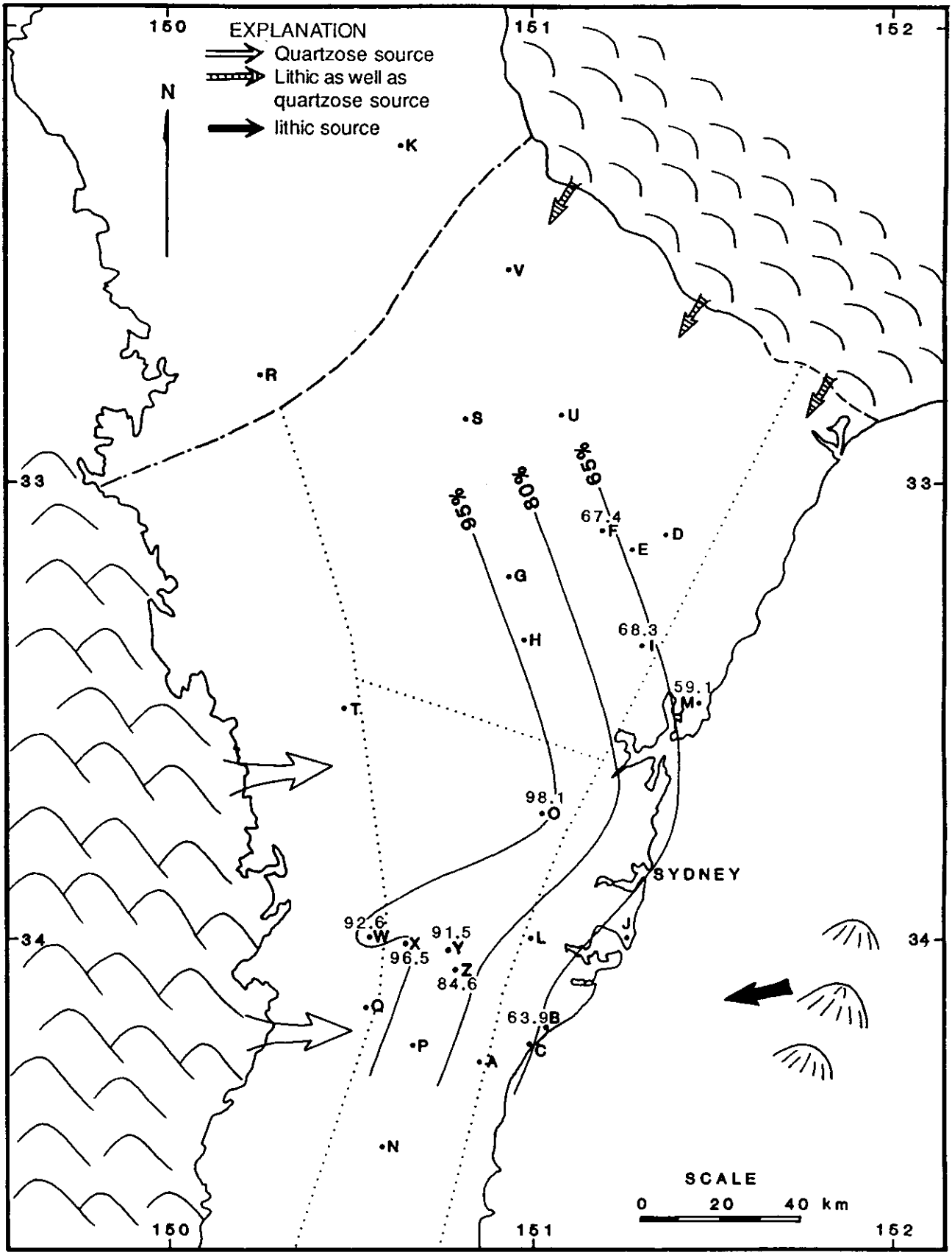

Fig 5-53 Regional variation of the average percentage of detrital quartz grains in the Bald Hill Operational Unit and top part of the UB unit and the deduced detrital sources.

sequence was recorded as 5.9 %, 2.2 % and 1.6 % of the total detrital clasts respectively.

The characteristics of detrital composition variation indicates that the Lachlan Fold Belt was the principal source during the deposition of this sequence (Fig 5-53). The New England Fold Belt supplied minor amounts of lithic detritus only to the northeastern portion of the northern region of the basin, but the New England Fold Belt source is considered to be more important near the northeast margin of the basin. As mentioned in the last chapter, the eastern volcanic source also contributed sediments, mainly clay sized detritus, to the basin during deposition of BH unit and led to the deposition of the characteristic chocolate claystones in this unit (Ward, 1972).

In summary, three detrital sources - Lachlan Fold Belt, New England Fold Belt, and eastern volcanic source, existed during the deposition of the Narrabeen Group with the former two being more important than the latter. The New England Fold Belt was the major detrital source for the whole Sydney Basin during early WO time. As sedimentation proceeded, its influence decreased and the Lachlan Fold Belt played a more and more important role in supplying detritus to the basin. It finally replaced the New England Fold Belt as the major source. However, this replacement did not take place at the same time throughout the whole basin. It happened in the early period of WO time in the west margin as DB3 is within the lower part of the WO unit in Boreholes T and W, in the middle period of WO time in the western portion of the southern region of the basin as DB3 is within the middle part of the WO unit in Boreholes X to Z, at the end of WO time in the central part of the basin (near the boundary between the southern and northern regions) as DB3 is situated near the boundary of the SC and WO units in Boreholes M and O, in the late period of SC time in the southwestern portion of the northern region of the basin as DB3 is within the upper part of the SC unit in Borehole H. Further

northeastwards, in the northeastern portion of the northern region, this replacement occurred even later until to the UB time (DB1 marks the major source change and is within the UB unit in Boreholes F and I). The third source, the eastern volcanic source, supplied detritus to the southern east coast zone and the eastern portion of the southern region of the basin from time to time starting from middle WO time during deposition of the Narrabeen Group. However, sandstone petrology data indicate that the source seems to be very active only during two periods: the early SC time and the early and middle UB time, which is supported by the presence of the abnormally lithic - rich interval generally correlating with the lower part of the SC unit in the southern basin and the relatively abundance of detrital lithics in the lower and middle parts of the UB units in the boreholes near the source.

The major source shift from the New England Fold Belt to the Lachlan Fold Belt can be explained by the tectonic development of the Sydney Basin as a foreland basin. Following a mid-Permian period of diastrophism (Leitch, 1974), the Sydney Basin took its final structural shape as a result of subsidence of the foreland. This subsidence was coeval with the uplift of the northeast New England Fold Belt accompanied by active magmatism (Jones et al., 1984). The newly uplifted Fold Belt supplied large quantities of detritus through southwest flowing flows to the basin deposited as the Permian Coal Measures and the lower part of the Narrabeen Group. Without regeneration through uplift and volcanism, however, the New England Fold Belt was reduced in height and extent and so reduced in capacity to supply large amounts of detritus to the whole basin due to continued erosion and settling. Meanwhile, continued westward migration of lithospheric loading caused by thrusting in the New England Fold Belt resulted in the development of a peripheral bulge (refer to Quinlan and Beaumont, 1984) on the eastern edge of the Lachlan Fold Belt. The uplift on the peripheral bulge continued so that the Lachlan Fold Belt increased its capacity to supply detritus to the basin and finally replaced the New England Fold Belt as the major source for the basin.

The gradual uplift of the Lachlan Fold Belt and the gradual lowering of the New England Fold Belt were responsible for the gradual process of the source shift from the New England Fold Belt to the Lachlan Fold Belt.

Prior to the deposition of the Narrabeen Group, the Sydney Basin experienced a cold climate during Late Carboniferous and Permian time (Crowell and Frakes, 1971a, b; 1975). The cold climate conditions and the high relief of the New England Fold Belt as a result of its uplift during mid-Permian diastrophism resulted in an immature stage of weathering of the parent rocks in the Fold Belt. Thus the detritus derived from it were mainly detrital lithic clasts and volcanic derived quartz clasts as well as detrital feldspar grains.

The detrital clasts from the Lachlan Fold Belt were largely detrital quartz grains, which resulted from a mature intensive weathering of the parent rocks in the Fold Belt so that unstable materials such as detrital lithics and feldspar grains were removed and only stable detrital quartz clasts were left. Under the cold climate conditions, the mature weathering was achieved by a low relief of the Fold Belt so that the weathering was prolonged. Such prolonged weathering of the granites, quartzites and sandstones / conglomerates in the Fold Belt produced the quartz-dominant detritus.

CHAPTER SIX

DIAGENESIS OF THE NARRABEEN GROUP SANDSTONES

6.1 INTRODUCTION

The diagenesis of sandstones has received more and more attention in the last twenty or so years. The ever-increasing interest in the topic can probably be attributed to two main reasons. One is that diagenesis controls porosity and permeability of sandstones so that it plays an important role in the potential of sandstones as hydrocarbon reservoir rocks. The other reason is that diagenesis is also important from a purely academic point of view since it deals with the processes taking place from the moment of sediment deposition up to the moment of sediments entering the metamorphic or weathering regime.

The diagenesis of the Narrabeen Group sandstones has not been systematically studied. This is probably mainly due to the unsuccessful exploration for hydrocarbons in the basin. The current study aims at discussing the potential of the Narrabeen Group sandstones as hydrocarbon reservoirs. It is hoped that this study may supply some guidance for future hydrocarbon exploration or even exploitation in the Sydney Basin.

6.2 ANALYTICAL PROCEDURES

Scanning electron microscope (SEM) / energy dispersive X-ray (EDX) analyses of 167 sandstones from 25 boreholes, X-ray diffraction (XRD) studies of 63 samples from 14 boreholes and microprobe analyses of carbonates in 20 samples from 10 boreholes (see Appendix I), together with petrology data of the sandstones form the basis for discussion of diagenesis of the Narrabeen Group sandstones. Following petrological microscope examinations of the 417 samples collected from the geological logging, 167 sandstones were selected for SEM / EDX studies. The sandstone was first cut into small chips of about 4-8 mm across with a pair of pliers to get fresh surfaces. The small chips were then mounted on aluminium stubs by

means of double adhesive tape and coated with a thin platinum or gold layer of about 200 Å. After the coating, carbon dag was put around the coated chips in order to increase conductivity (reducing sample charging). They were analysed using a PHILLIPS 505 scanning electron microscope equipped with energy dispersive X-ray (EDX) analyser.

Authigenic minerals were identified using the criteria proposed by Wilson and Pittman (1977) and reference to the book - SEM Petrology Atlas by Welton (1984). A summary of authigenic minerals identified by the SEM / EDX is presented in Appendix V. In the summary, no authigenic quartz and albite are listed. The former was found in all the samples studied under SEM / EDX and the latter in the majority of the samples containing detrital feldspar grains.

To confirm the identification of clay minerals recognised by petrological microscope and SEM / EDX studies, 63 samples were selected for further XRD analyses from the 167 samples studied under SEM / EDX. The XRD analyses were carried out on a separated fine fraction of sandstone samples which enabled detection and identification of clay minerals even when they are present in small amounts. During XRD analyses, the orientated fine fraction was first analysed in air-dried conditions and then further analysed following treatment of the sample with ethylene glycol in order to identify any swelling clays present. The samples were analysed using a Phillips IL powder diffractometer fitted with a graphite monochromator, which is located in The Department of Geology and Geophysics, The University of Sydney.

The XRD analyses are qualititative. However, based on relative intensity of the strongest peaks for different minerals, the relative abundance of clay minerals in the same sample is classified into three grades: major amount, minor amount, and trace amount. The results of the XRD analyses are listed in Table 6-1.

Table 6-1 Results of XRD studies

Sample no.	OU	Kaolin	Illite	Illite/smectite	Chlorite
WEST MARGIN					
W180.1	BH	X	M	T	
W274.6	UB	X	M	M	
W388.8	LB	X	M	M	
W430.8	SC	X	T	T	
W455.6	SC	X	M	M	
W493.9	WO	X		M	
SOUTHERN REGION					
X278.0	BH	X			
X309.3	BH	X	M	T	
X413.3	UB	T	X	X	
X473.1	LB		X	X	
X528.7	SC	X		M	
X588.5	SC	M		X	
X612.9	WO	X		M	
X675.5	WO	M		X	
Y377.5	BH	X	M	T	
Y429.0	UB	X	T	T	
Y486.5	UB	X	T	T	
Y549.1	LB		X	X	
Y593.9	SC	X	T	M	
Y642.2	SC			X	
Y690.1	WO	T	X	M	
Y757.9	WO	X	T	T	
Z422.6	UB	X	M	M	
Z499.0	UB	X	T	M	
Z531.9	LB	X	T	T	
Z593.0	SC	X	T	M	
Z632.7	SC			X	
Z679.4	WO		X	X	
Z703.3	WO	X	T	T	
Z763.8	WO	X	T	T	
A146.5	UB	X	M	M	
A260.8	SC	M		X	T
A352.0	WO	M	T	X	
O296.5	BH	X	T		
O668.5	WO	X	M		
O755.9	WO	X	T	M	

Sample no.	OU	Kaolin	Illite	Illite/smectite	Chlorite
EAST COAST ZONE					
B151.7	UB	X	T	M	
B406.2	WO	X		M	M
C081.1	LB	X	T		X
C101.6	LB	X	T		X
C132.6	SC	M		T	X
J481.6	SC	X			X
J599.9	WO	X	T	M	X
J672.3	WO	X	T		X
L406.8	UB	X	M	M	
L469.6	LB	T	M	X	
L579.2	SC	X	T	T	X
L595.2	SC		M		X
L717.8	WO	M		X	
M094.1	BH	X	M		T
M209.9	UB	X	T		X
M341.8	SC	X		T	X
M492.2	WO	X			X
M605.3	WO	X	T	T	X
NORTHERN REGION					
G553.8	WO			X	
H419.7	LB	X		M	
H470.1	SC	M		X	
H568.7	SC			X	
I 320.1	BH	X	T	T	
I 465.6	UB	X	T	T	
I 596.6	LB	X			M
I 781.5	WO	X		M	M
I 879.9	WO	X	T	T	X

NOTE:

OU = operational unit, BH = Bald Hill, UB = Upper Bulgo, LB = Lower Bulgo

SC = Scarborough, WO = Wombarra,

X = major amount, M = minor amount, T = trace amount.

Highly polished thin sections were prepared for microprobe analyses of carbonates in the 20 sandstone samples selected from those which underwent both point counting and SEM / EDX examinations (see Appendix I). The microprobe analyses were made on a Etec-Siemens Autoprobe using the wavelength dispersive system, which is located in The Electron Microscope Unit, The University of Sydney. They were carried out under the setting of 15 kv acceleration potential and 20 nÅ sample current with a beam scan of 10x10 μm. Detection limits at 15 kv and 20 nÅ are as follows: Mg 0.06%, Ca 0.03%, Fe 0.06%, Mn 0.08%, and Sr 0.05%. The standards are MgO for Mg, apatite for Ca, haematite for Fe, rhodonite for Mn, and $SrTiO_3$ for Sr. Only Mg, Ca, Fe, and Mn (Sr included in some samples) concentrations were analysed.

In each of the 20 samples, a few carbonate cements and / or replacements were selected for analyses. One to five analyses were carried out on the same cement or replacement. The analyses results are reported in both oxide percentage and molar percentage. They are presented in Appendix VI. It should be noticed that the 20 samples do not contain all types of carbonates (calcite, Fe calcite, siderite, dolomite, and ankerite) suitable for microprobe analyse. Actually, only one type of carbonate (calcite or siderite or ankerite) or two types of carbonate (calcite and ankerite or siderite and ankerite or siderite and dolomite) could be analysed by microprobe in the same sample. Of the 20 samples, calcite was analysed in four samples, siderite in 11 samples, ankerite in 13 samples and dolomite in one sample (Appendix VI).

6.3 DIAGENETIC (AUTHIGENIC) MINERALS IN THE NARRABEEN GROUP SANDSTONES

6.3.1 GENERAL STATEMENT

SEM / EDX analyses, together with petrological microscope examinations of the sampled sandstones, showed that there are three principal groups of diagenetic minerals in the Narrabeen Group sandstones: carbonates, clay minerals and

quartz cements (Appendix V). Carbonates consist of calcite, dolomite, ankerite, and siderite, of which siderite is the most common. The authigenic clay minerals include kaolin (kaolinite and dickite), illite, chlorite and mixed-layer illite / smectite with kaolin being the most common. Micro-quartz, mega-quartz and quartz overgrowths comprise quartz cements with quartz overgrowth being the most abundant. In addition, authigenic albite was commonly found in sandstones containing detrital plagioclase. A minor amount of haematite, pyrite, apatite, anatase, and analcime were also found.

Before describing each of the individual authigenic minerals, a few terms are defined: CLAY or CARBONATE COATING: Authigenic clay or carbonate coats the entire surface of framework grains except points of grain to grain contact and the authigenic minerals show a preferred orientation normal or parallel to the detrital grain surface; CLAY or CARBONATE PORE FILLING means that clay or carbonate plugs interstitial pores as individual flakes, or aggregates of flakes or crystals and the authigenic minerals do not show any apparent alignment relative to the detrital grain surfaces (Wilson and Pittman, 1977). The definitions of anhedral, subhedral and euhedral of crystals follow those defined by Friedman (1965).

6.3.2 CARBONATES

CALCITE ($CaCO_3$): Depending on whether a substantial amount of ferrous iron is present or not, calcite is divided into two types: Non-ferroan calcite and ferroan calcite. The calcite occurs in three forms in terms of crystal size: very small equant anhedral to subhedral crystals with a size of 2-6 μm, small polyhegonal euhedral crystals with a size of 10-20 microns, and large (> 20 μm) anhedral to euhedral crystals. The former two forms coat detrital grain surfaces (Figs 6-1 & 6-2). They were only found in two (W300.8 and W310.4) of the samples studied under SEM / EDX. The latter form fills inter-grain pore spaces (Figs 6-3 & 6-4). The calcite cement was usually found in the sandstones of the lower Narrabeen Group in the east coast zone and the northern region of the basin (in Boreholes B, C, J, M and I).

Fig 6-1 (top left) Grain coating very small equant anhedral to subhedral non-ferroan calcite crystals (C), together with euhedral rhombohedral siderite crystals (S) and prismatic quartz crystals (Q). From Weromba 2 at drilling depth of 310.4 m (sample W310.4).

Fig 6-2 (top right) Grain coating non-ferroan calcite crystals (C) coarsening towards the pore centre. Note euhedrality increasing with crystal size from subhedral to euhedral. From Weromba 2 at drilling depth of 300.8 m (sample W300.8).

Fig 6-3 (upper left) Pore filling subhedral to euhedral non-ferroan calcite cement (C). From Liverpool 91 at drilling depth of 595.2 m (sample L595.2).

Fig 6-4 (upper right) Pore filling anhedral to subhedral non-ferroan calcite cement (C). From Cape Banks 1 at drilling depth of 641.2 m (sample J641.2).

Fig 6-6 (lower left) Slightly dissolved pore-filling ferroan calcite crystals (Fe C) engulfed by quartz overgrowths. White dot is the point where EDX analysis was made. Refer to Fig 6-7a for the EDX spectrum. From Cobbitty 3 at drilling depth of 528.7 m (sample X528.7).

Fig 6-8 (lower right) Large pore filling anhedral dolomite cement (D). The cross point of the two white lines is the point where EDX analysis was made. Refer to Fig 6-7b for the EDX spectrum. From Oil Longley 1 at drilling depth of 465.5 m (sample I465.5).

Fig 6-9 (bottom left) Pore-filling euhedral dolomite cement (D). From St Albans 1 at drilling depth of 681.2 m (sample H681.2).

Fig 6-10 (bottom right) Grain coating euhedral rhombohedral siderite crystals enclosed by a large pore-filling euhedral ankerite crystal. Q marks quartz overgrowths. See Fig 6-11 on page 181 for enlargement. From Cobbitty 3 at drilling depth of 531.9 m (sample X531.9).

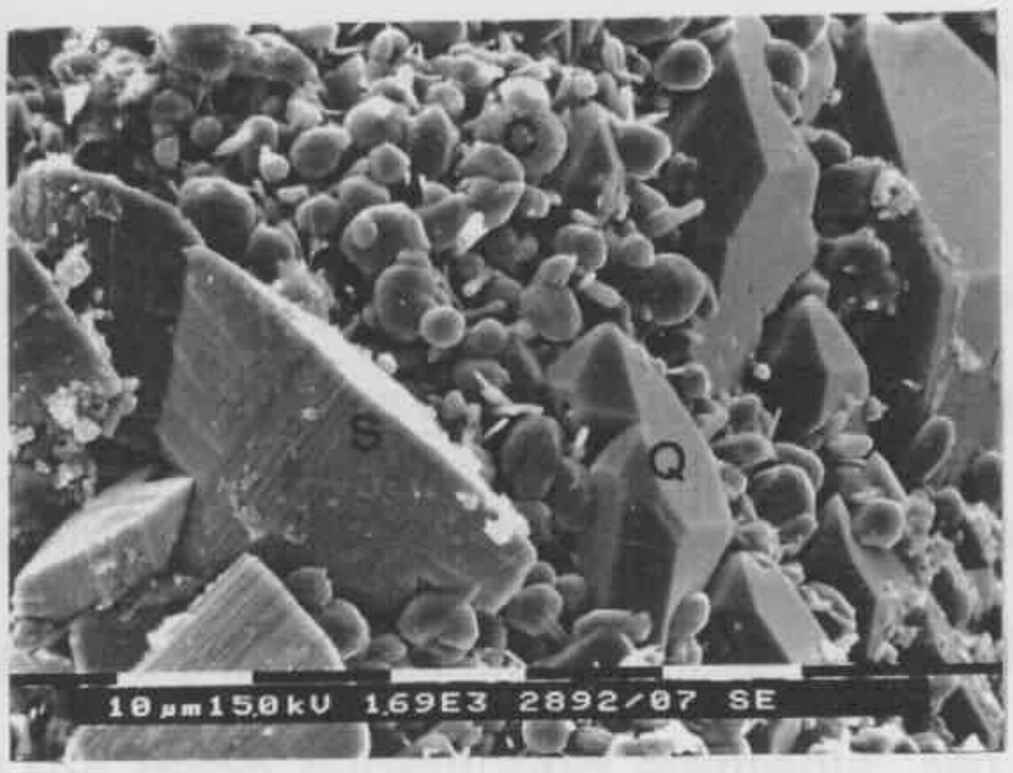
S
Q
10 µm 15.0 kV 1.69E3 2892/07 SE

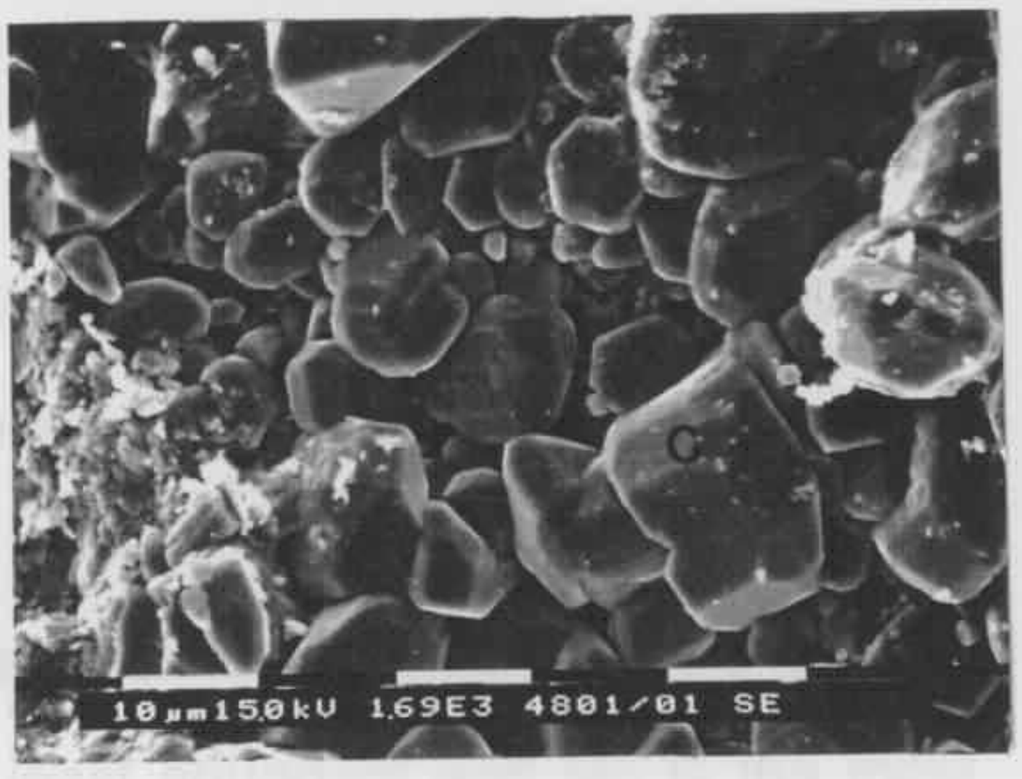
C
10 µm 15.0 kV 1.69E3 4801/01 SE


C
0.1 mm 15.0 kV 1.94E2 2702/01 SE

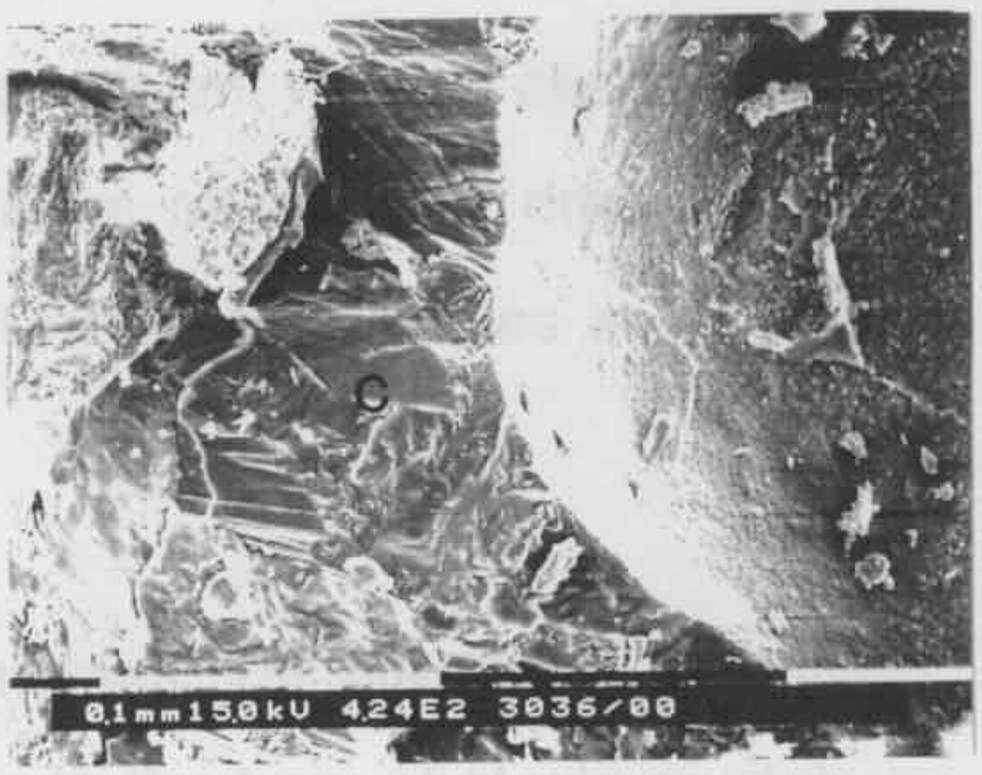
C
0.1 mm 15.0 kV 4.24E2 3036/00


Fe C
0.1 mm 15.1 kV 8.45E2 4513/01 SE


D
0.1 mm 15.0 kV 6.00E2 3723/00 SE

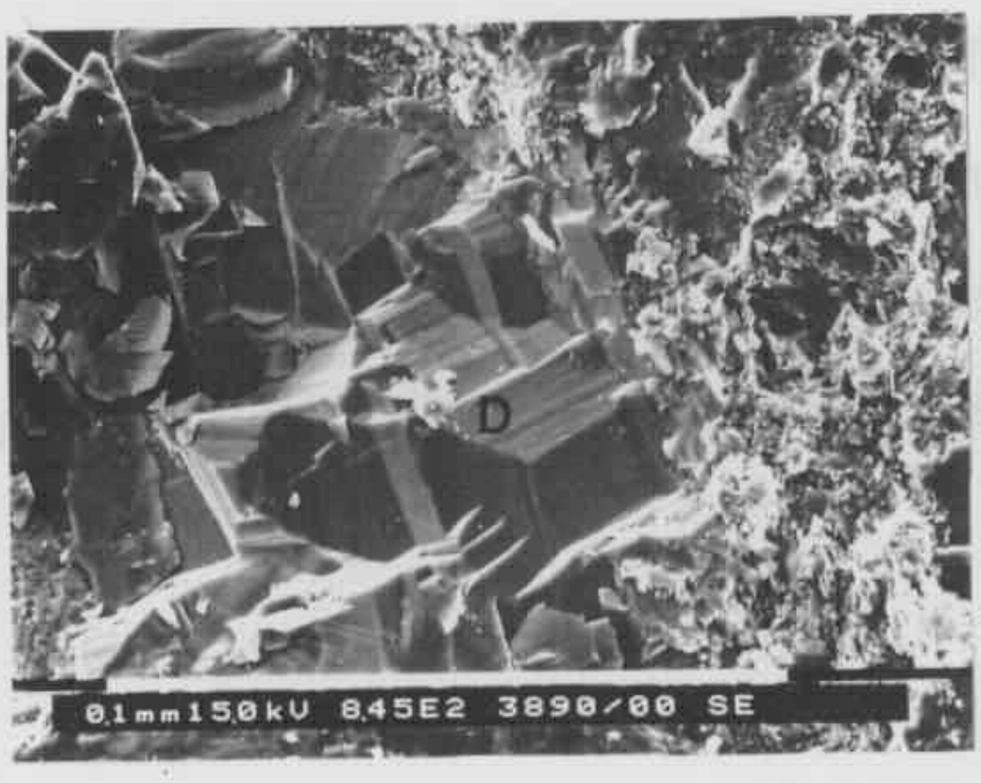
D
0.1 mm 15.0 kV 8.45E2 3890/00 SE


Q
0.1 mm 15.0 kV 2.12E2 3660/01 SE

Generally it dose not coexist with other kinds of carbonates (Appendix V).

Of the 20 samples selected for microprobe analyse, four samples (B394.1, L579.2, J514.8 and J599.9) from three boreholes contain suitable calcite for microprobe analyses. The results show overall similarity of calcite compositions in the four samples with 3 to 9 mole % Mg + Fe + Mn substitution for Ca (refer to Appendix VI). Of the three substituting elements, Mg is the least abundant and Mn is the most abundant (Fig 6-5). The relatively high Mn concentration (2 to 6 mole %) in these calcites of meteoric origin (see next chapter) is consistent with the observations of the association of Mn with calcite in pore waters of meteoric origin in other geological settings (Meyers,1974; Mount and Cohen, 1984; Boles et al., 1985; Boles, 1987).

Ferroan calcite is identified from SEM / EDX analyses. It is present as pore-filling large (> 20 μm) subhedral to euhedral crystals in the form of single crystals or mosaic crystals (Figs 6-6 & 6-7a). It was found in a number of volcanic lithic rich sandstones in the lower Narrabeen Group but was not as common as pore filling large calcite. Ferroan calcite crystals were generally found to coexist with siderite crystals (Appendix V). In the 20 samples selected for microprobe analyses, no suitable ferroan calcite was found for the analyses.

DOLOMITE [$CaMg(CO_3)_2$]: It is identified by EDX analyses. Dolomite fills inter-grain pore spaces as anhedral (Figs 6-8 & 6-7b) to euhedral crystals (Fig 6-9). The replacement of a detrital grain by a single dolomite crystal was also seen under the SEM / EDX analyses. Dolomite was found only in three of the samples studied (H681.2, I465.6 and W455.6) under the SEM (Appendix V). Microprobe analyses was carried out for the dolomite in sample W455.6. The analysis results indicate that it has 6.33 mole % Fe substitution for Mg with Ca:Mg ≈ 1:1 (Appendix VI).

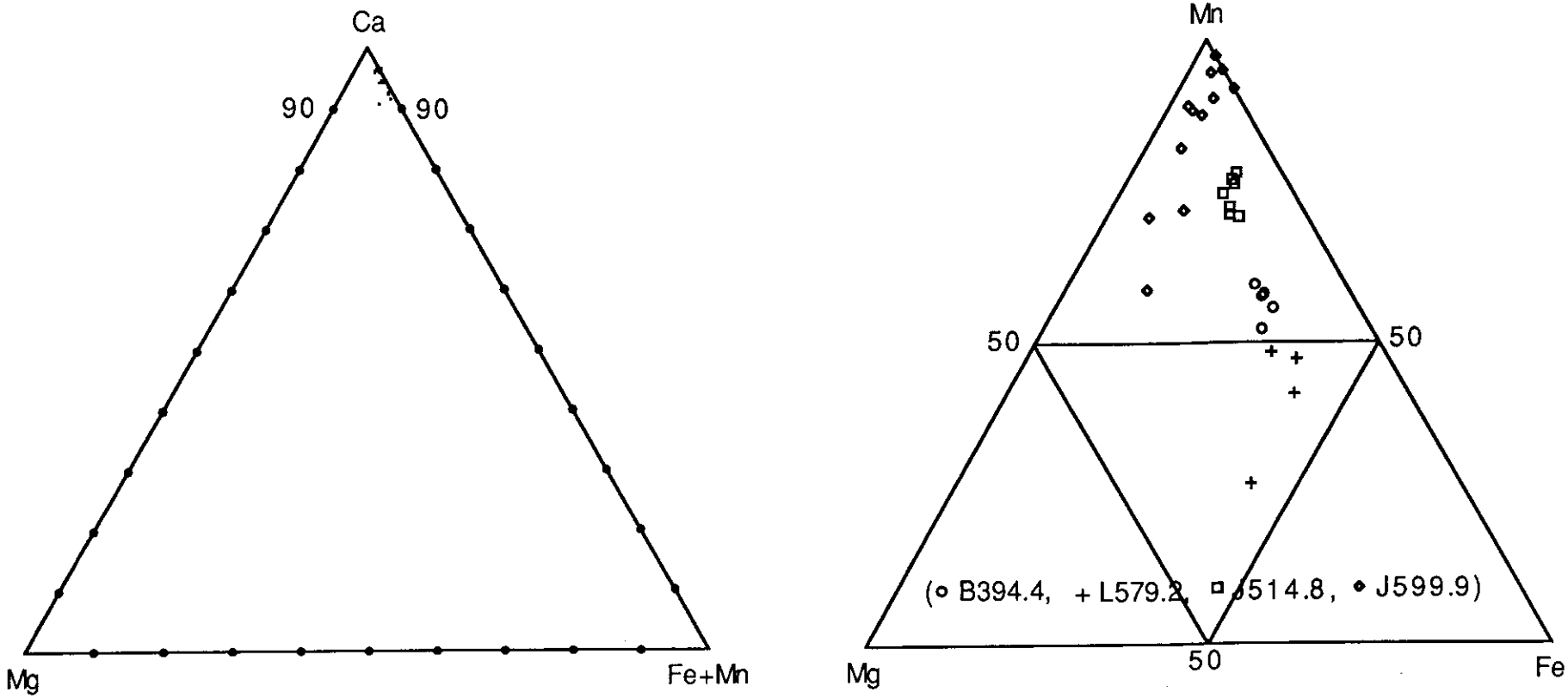

Fig 6-5 Calcite compositions (mole %) from the Narrabeen Group sandstones. Data from microprobe analyses of 4 samples from three boreholes.

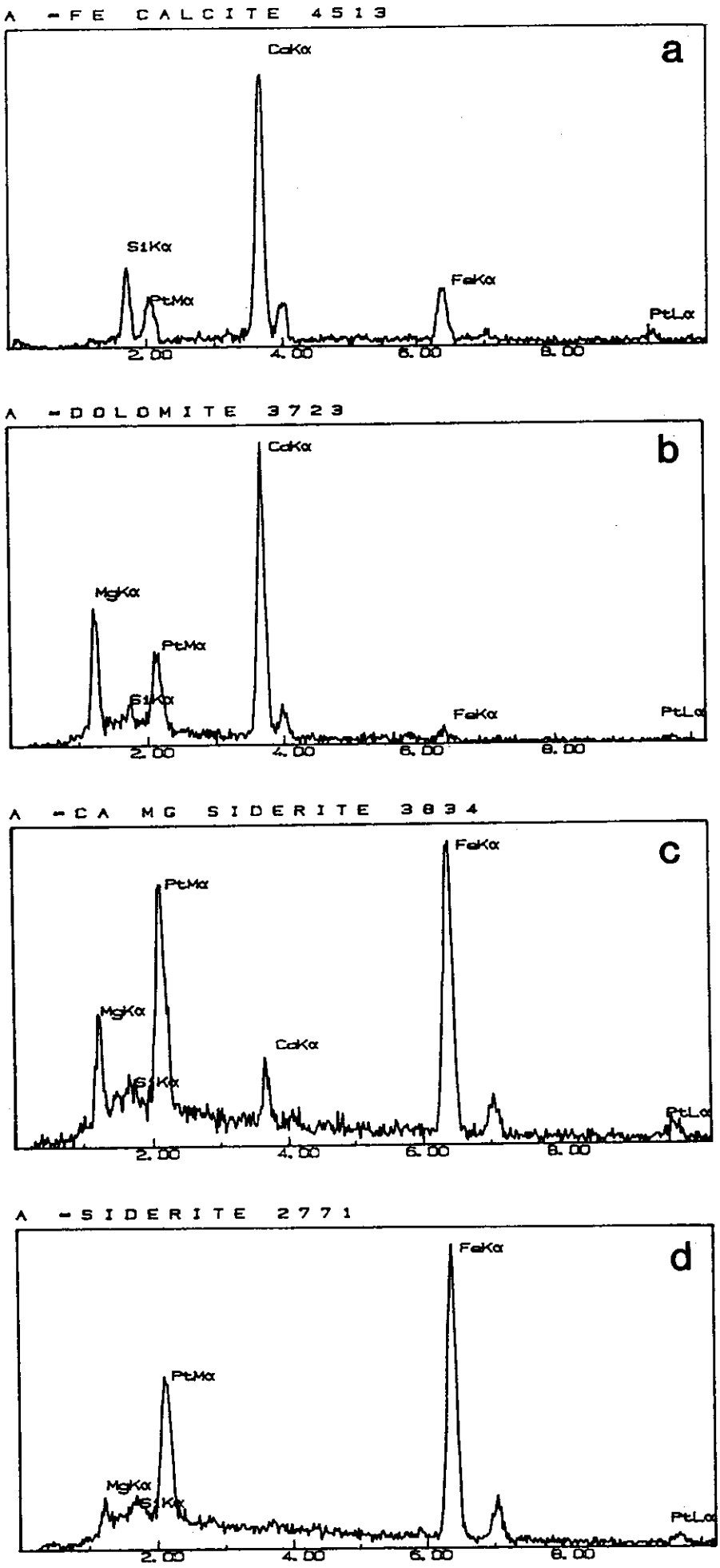

Fig 6-7 EDX spectrum.

ANKERITE [$Ca(Mg,Fe^{+2},Mn)(CO_3)_2$]: It is used here for material with Mg:Fe < 4:1, i.e. the mineral is termed ferroan dolomite if it has up to 20 % of the Mg positions filled by Fe^{2+} or Mn, and ankerite if it is richer than this in ferrous ion and manganese (Deer et al., 1966). Ankerite was identified by EDX analyses and confirmed by microprobe study. Ankerite is present as pore filling cements in the form of single (Figs 6-10 & 6-11) or mosaic (Fig 6-12) crystals with a crystal size larger than 20 μm. Pore filling ankerite cement can be very large in crystal size (200 or more microns) and it is able to enclose a detrital grain (Figs 6-13 & 6-14). The replacement of detrital volcanic lithics and feldspar grains by single ankerite crystals was also found. Ankerite crystals can be anhedral, subhedral, or euhedral. They are generally restricted to the lower Narrabeen Group and tend to coexist with pore filling siderite cements (Appendix V).

Of the 20 samples selected for microprobe analyses, 13 samples from 9 boreholes contain suitable ankerite for the analyses. The analysis results indicate that ankerite has a 9 to 23 mole % Fe substitution for Mg with Ca : (Mg+Fe) > 1:1 (Appendix VI). Throughout the whole Narrabeen Group sandstones across the entire basin, the Ca concentration in the ankerites varies in the range of 50 % to 59 % with few exceptions (Fig 6-15). The Mn concentration in the ankerites is quite low. It is generally less than 2 mole %. Zoned ankerite cements were found, as suggested by the Mg/Fe concentration variation across the same cement (e.g. sample Y566.1). From the microprobe analyses, no characteristic composition variation of ankerites could be established either vertically throughout the Narrabeen Group or regionally in the same stratigraphic horizon across the Sydney Basin.

SIDERITE ($FeCO_3$): It is the most common carbonate cement in the sandstones and was found in most of the samples studied under SEM / EDX (Appendix V). The siderite can be divided into two types in terms of crystal size: small uniform

Fig 6-11 (top left) Enlargement of Fig 6-10. S marks siderite and A ankerite.

Fig 6-12 (top right) Subhedral to euhedral ankerite crystals (A) enclosed by quartz overgrowths (Q). From Cobbitty 3 at drilling depth of 490.9 m (sample X490.9).

Fig 6-13 (upper left) A very large subhedral to euhedral ankerite cement (a) enclosing an altered detrital volcanic clast (V). From South Colah 1 at drilling depth of 755.9 m (sample O755.9).

Fig 6-14 (upper right) Enlargement of Fig 6-13. A marks ankerite.

Fig 6-16 (lower left) Euhedral rhombohedral siderite crystals coating a detrital grain (see Fig 6-17 for enlargement). From Weromba 2 at drilling depth of 310.4 m (sample W310.4).

Fig 6-17 (lower right) Enlargement of Fig 6-16. S marks siderite and Q quartz overgrowths.

Fig 6-18 (bottom left) Mosaic pore-filling euhedral siderite crystals (S) and prismatic quartz (mega-quartz) crystals (Q). From Campbelltown 5 at drilling depth of 468.5 m (sample Y468.5).

Fig 6-19 (bottom right) Mosaic euhedral siderite crystals (S) enclosed by quartz overgrowths (Q). From Weromba 2 at drilling depth of 274.6 m (sample W274.6).

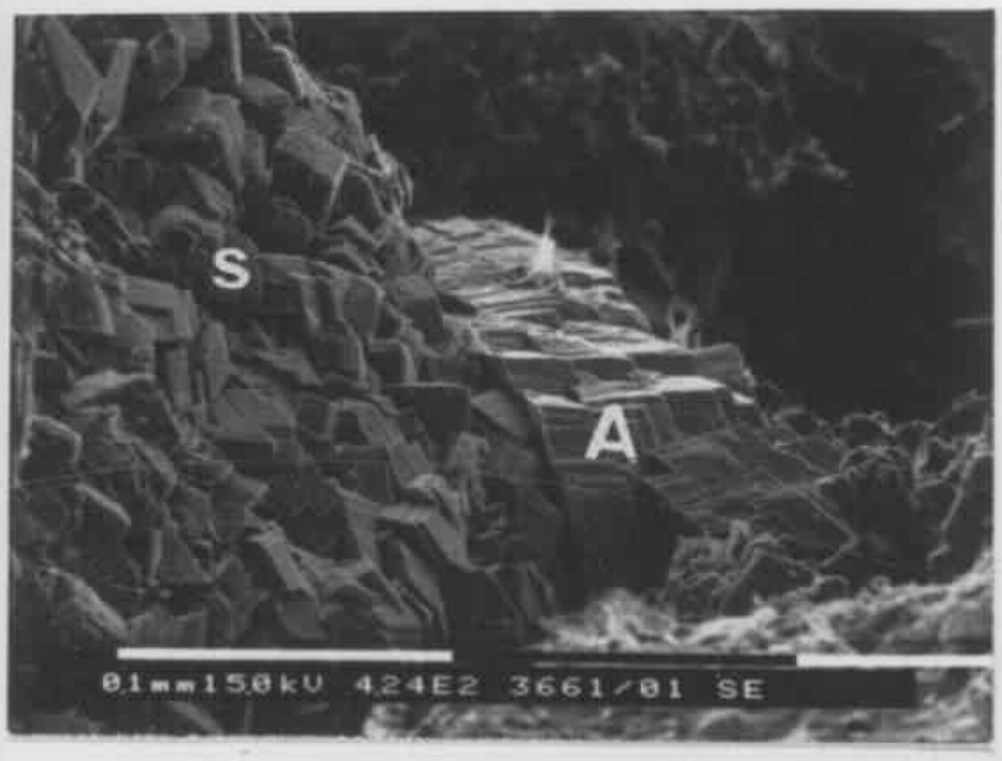
S
A
01mm150kV 424E2 3661/01 SE

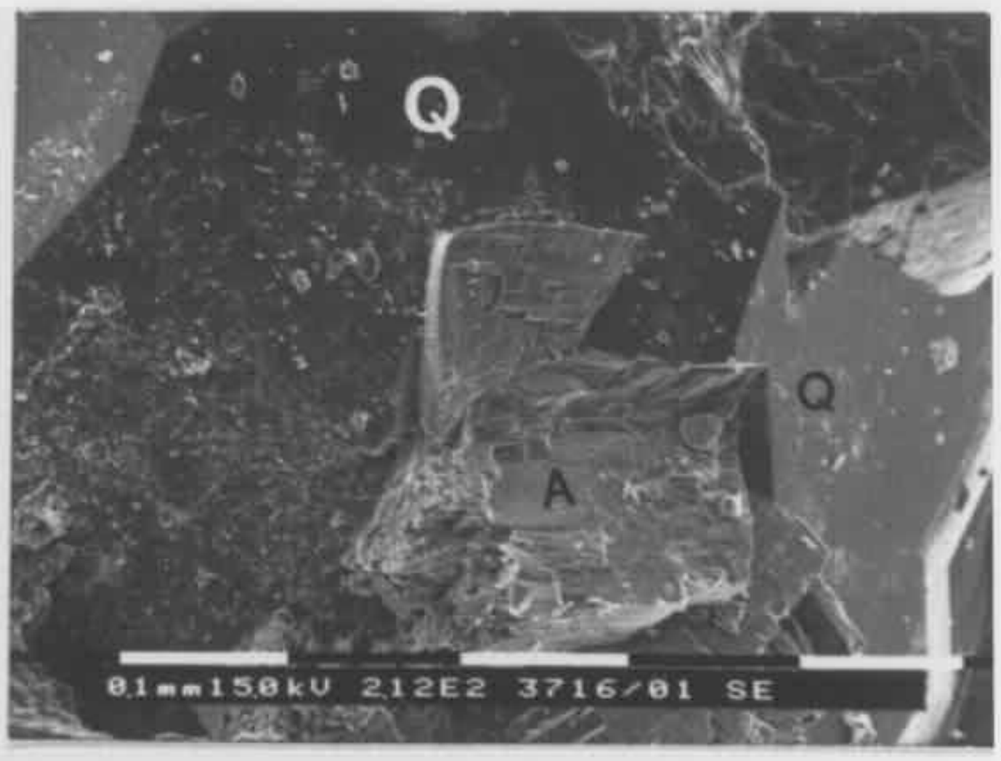
Q
A
Q
01mm150kV 212E2 3716/01 SE

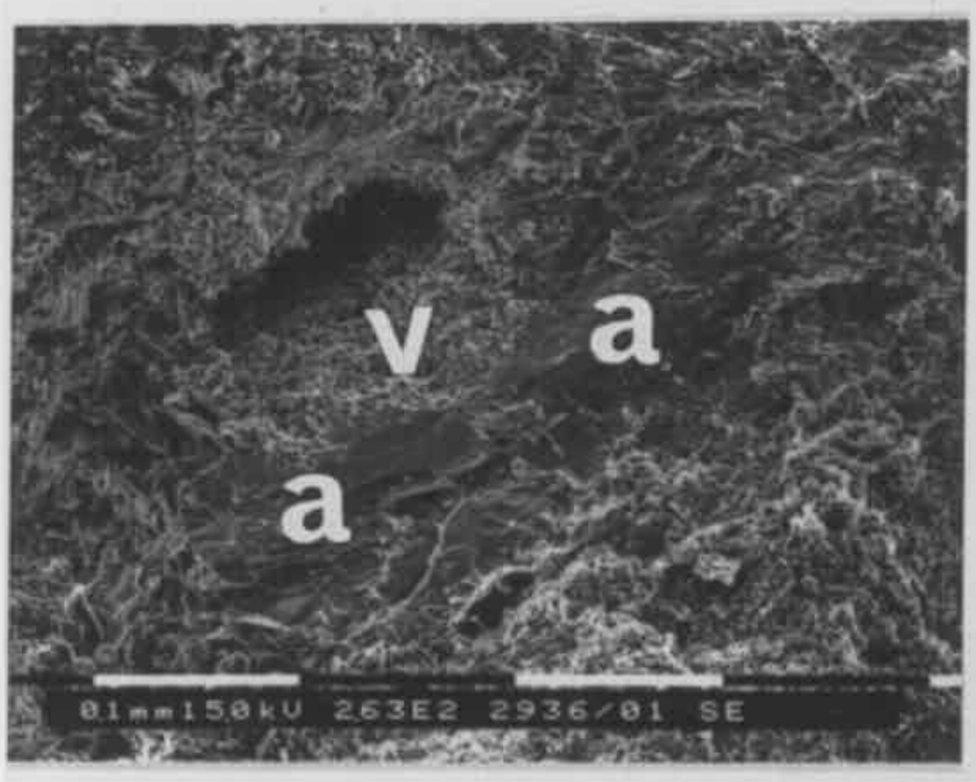
v
a
a
01mm150kV 263E2 2936/01 SE

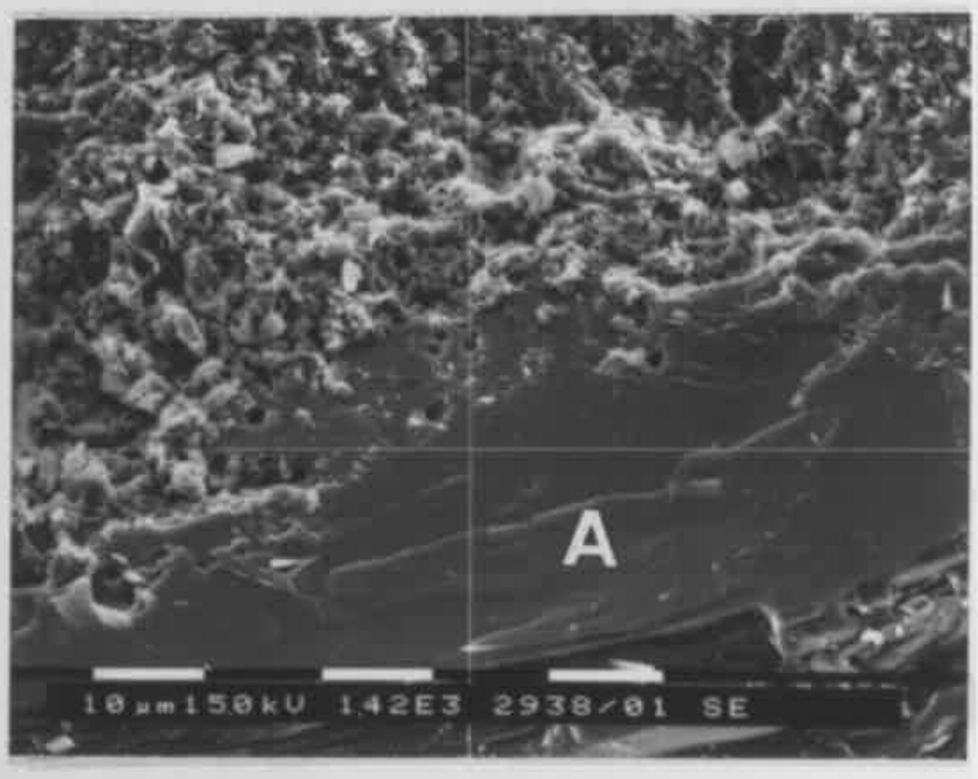
A
10µm150kV 142E3 2938/01 SE

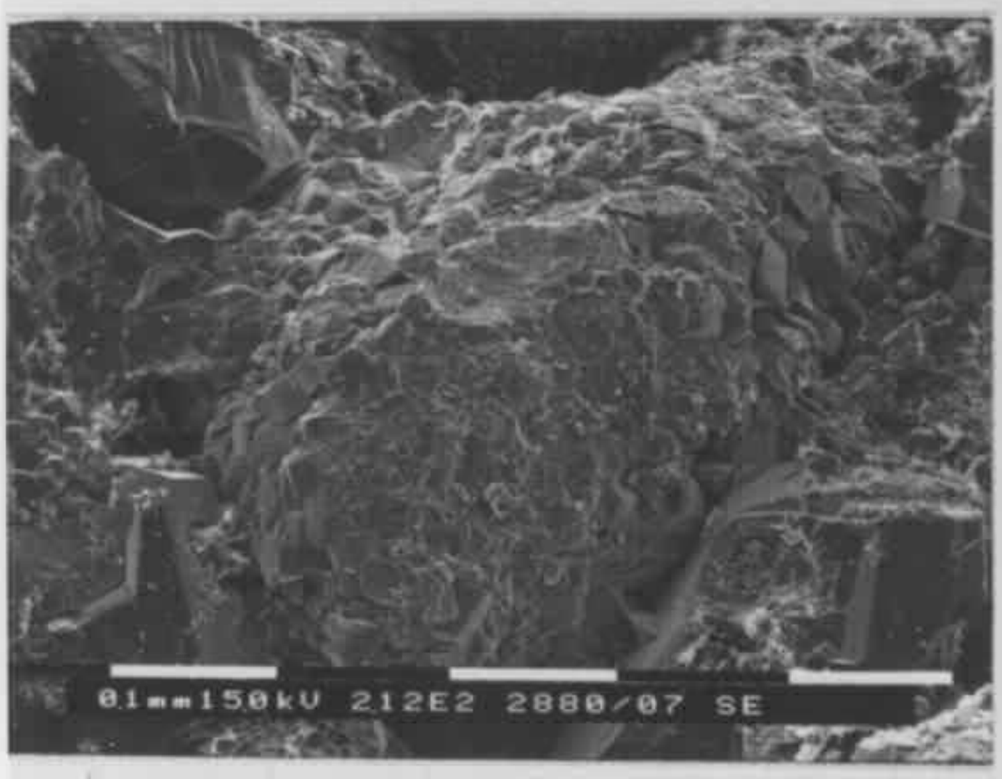
01mm150kV 212E2 2880/07 SE

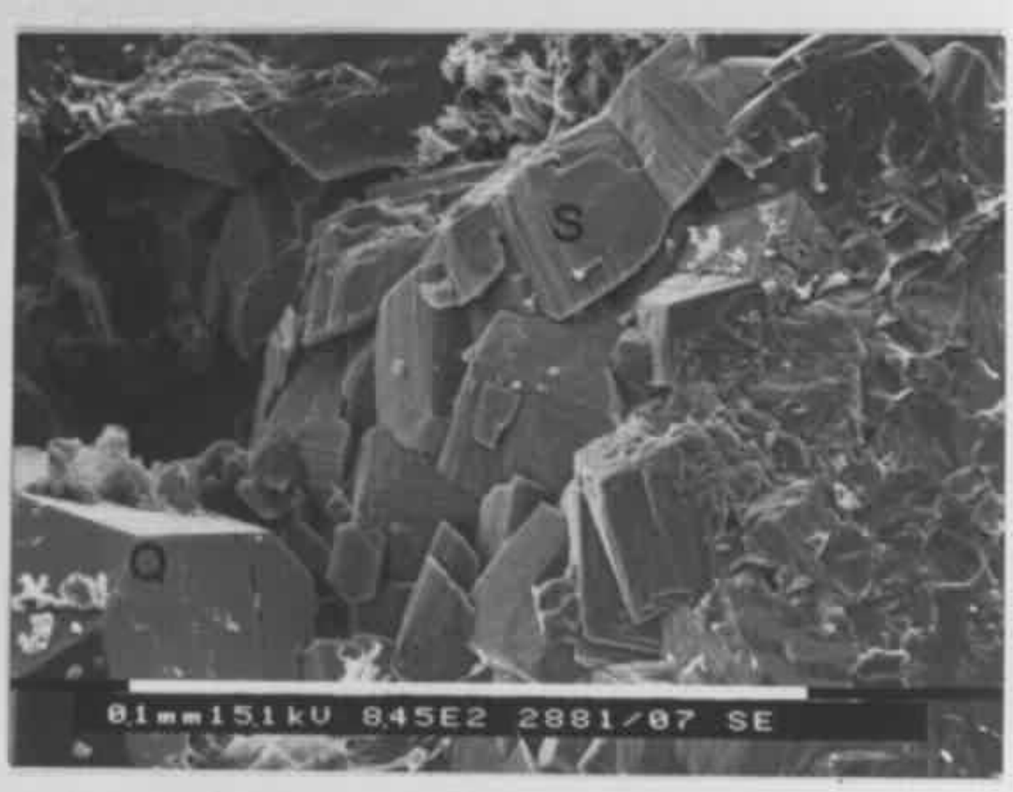
S
Q
01mm151kV 845E2 2881/07 SE

S
Q
01mm150kV 424E2 5268/01 SE

Q
S
Q
S
01mm150kV 424E2 4720/01 SE

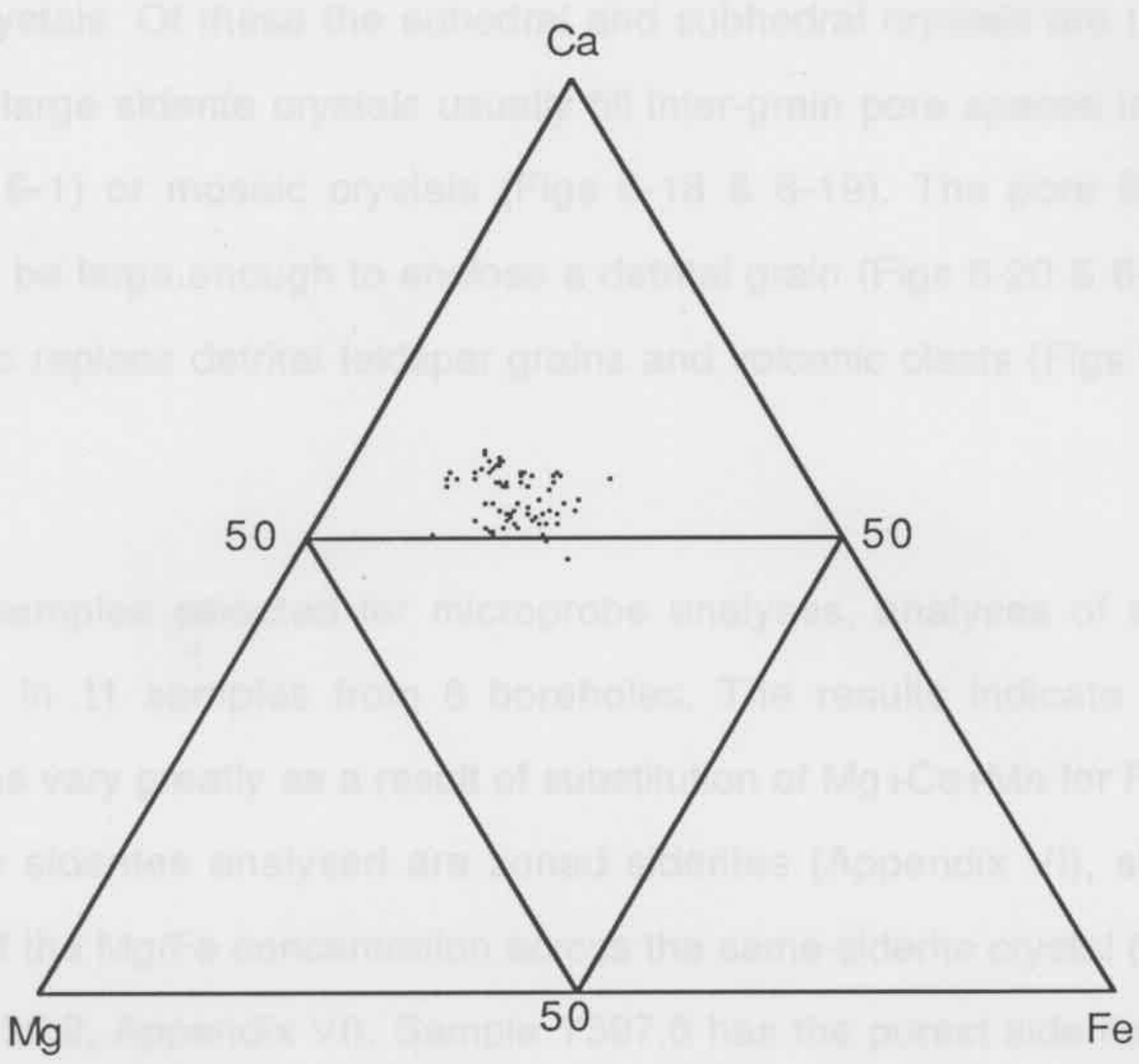

Fig 6-15 Ankerite compositions (mole %) from the Narrabeen Group sandstones. Data from microprobe analyses of 13 samples from 9 boreholes.

rhombohedral crystals with a size of 10-20 μm and larger crystals with a size of much greater than 20 μm. The former coat detrital grain surfaces (Figs 6-10, 6-11, 6-16 & 6-17), but this morphology is not common. It was found only in three samples (W300.8, W310.4 and X531.9). In contrast, the large siderite crystals are very common. They range from euhedral rhombohedrons, subhedral crystals to anhedral crystals. Of these the euhedral and subhedral crystals are the dominant forms. The large siderite crystals usually fill inter-grain pore spaces in the form of single (Fig 6-1) or mosaic crystals (Figs 6-18 & 6-19). The pore filling siderite cement can be large enough to enclose a detrital grain (Figs 6-20 & 6-7c). Siderite crystals also replace detrital feldspar grains and volcanic clasts (Figs 6-21, 6-22 & 6-7d).

Of the 20 samples selected for microprobe analyses, analyses of siderite were carried out in 11 samples from 8 boreholes. The results indicate that siderite compositions vary greatly as a result of substitution of Mg+Ca+Mn for Fe (Fig 6-23). Most of the siderites analysed are zoned siderites (Appendix VI), shown by the variations of the Mg/Fe concentration across the same siderite crystal (e.g. samples Y566.1, O435.2, Appendix VI). Sample Y397.6 has the purest siderite with $FeCO_3$ up to 95 mole % whereas the siderite in sample W455.6 has 36 to 44 mole % Mg substitution for Fe (Fig 6-23). The appreciable Mg substitution for Fe in the non-marine (meteoric water) siderites (see next chapter) is similar to that observed in both marine siderites (Matsumoto and Iijima,1981, Boles, 1987) and non-marine siderites (Eadington et al., 1989) in other geological settings. The microprobe analyses do not show any characteristic variation of siderite compositions vertically in the same borehole or regionally in the same stratigraphic horizon across the basin.

6.3.3 CLAY MINERALS

KAOLIN [$Al_4(Si_4O_{10})(OH)_8$]: As a broad term used here, it includes both kaolinite and dickite. It is the most common clay mineral in the samples (Table 6-1 and

Fig 6-20 (top left) Large anhedral to subhedral Ca Mg siderite cement (S) enclosing a detrital grain. The cross point of the two white lines is the point where EDX analysis was made. Refer to Fig 6-7c for the EDX spectrum. From St Albans 1 at drilling depth of 568.7 m (sample H568.7).

Fig 6-21 (top right) Euhedral siderite crystals replacing a detrital grain (volcanic clast). From Liverpool 91 at drilling depth of 285.2 (sample L285.2).

Fig 6-22 (upper left) Enlargement of Fig 6-21. S marks siderite. The cross point of the two white lines is the point where EDX analysis was made. Refer to Fig 6-7d for the EDX spectrum.

Fig 6-24 (upper right) Stacked kaolin blocks (K) on the surface of a detrital grain. From Oil Longley 1 at drilling depth of 437.4 m (sample I437.4).

Fig 6-25 (lower left) Individual kaolin flakes on a detrital grain surface. From Weromba 2 at drilling depth of 359.4 m (sample W359.4).

Fig 6-26 (lower right) Individual kaolin flakes on the surface of well developed quartz overgrowths (Q). S marks an euhedral siderite crystal. From Weromba 2 at drilling depth of 274.6 m (sample W274.6).

Fig 6-27 (bottom left) Stacked kaolin flakes filling inter-grain pore spaces together with diagenetic illite. From Campbelltown 5 at drilling depth of 468.5 m (sample Y468.5).

Fig 6-28 (bottom right) Stacked kaolin flakes (K) filling dissolution pore spaces of a subhedral ankerite crystal (A). From Campbelltown 5 at drilling depth of 566.1 m (sample Y566.1).

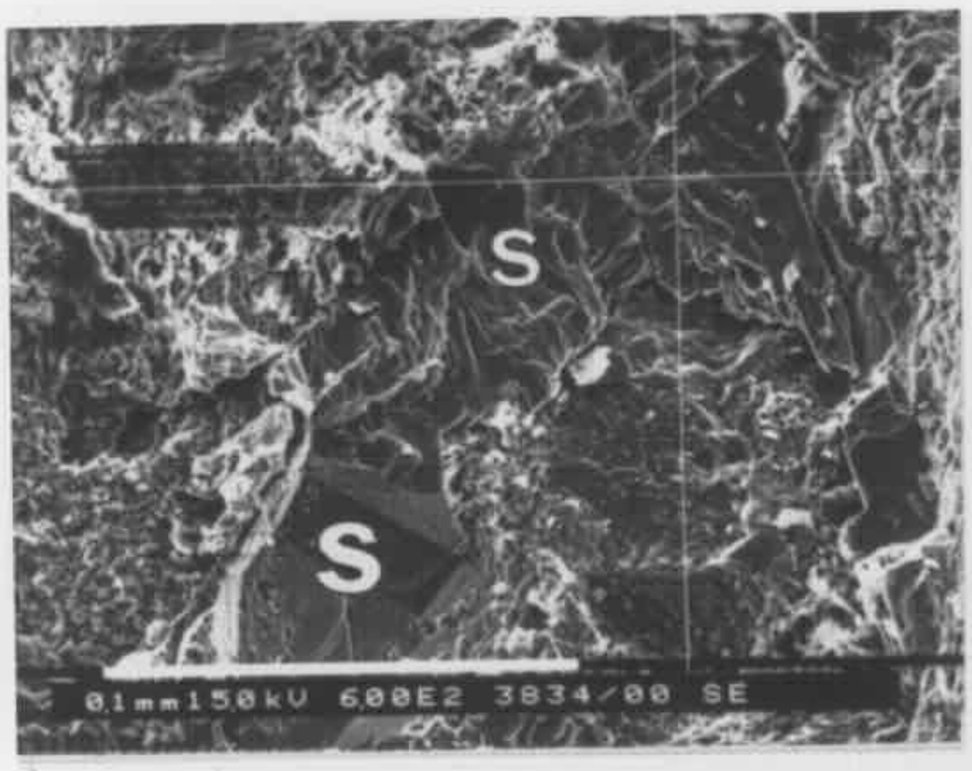
S
S
0.1mm 15.0kU 6.00E2 3834/00 SE


0.1mm 15.0kU 3.26E2 2772/01 SE

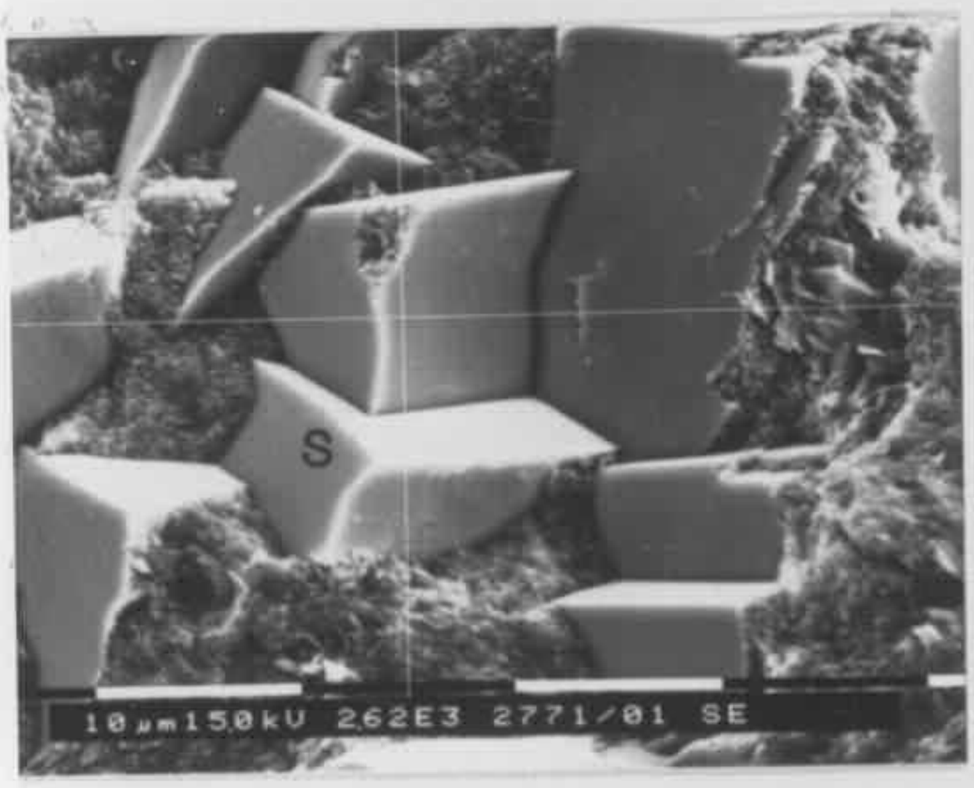
S
10µm 15.0kU 2.62E3 2771/01 SE


K
10µm 15.0kU 5.00E3 3706/00 SE


0.1mm 15.0kU 8.45E2 2855/07 SE


Q
S
0.1mm 15.0kU 4.24E2 4723/01 SE

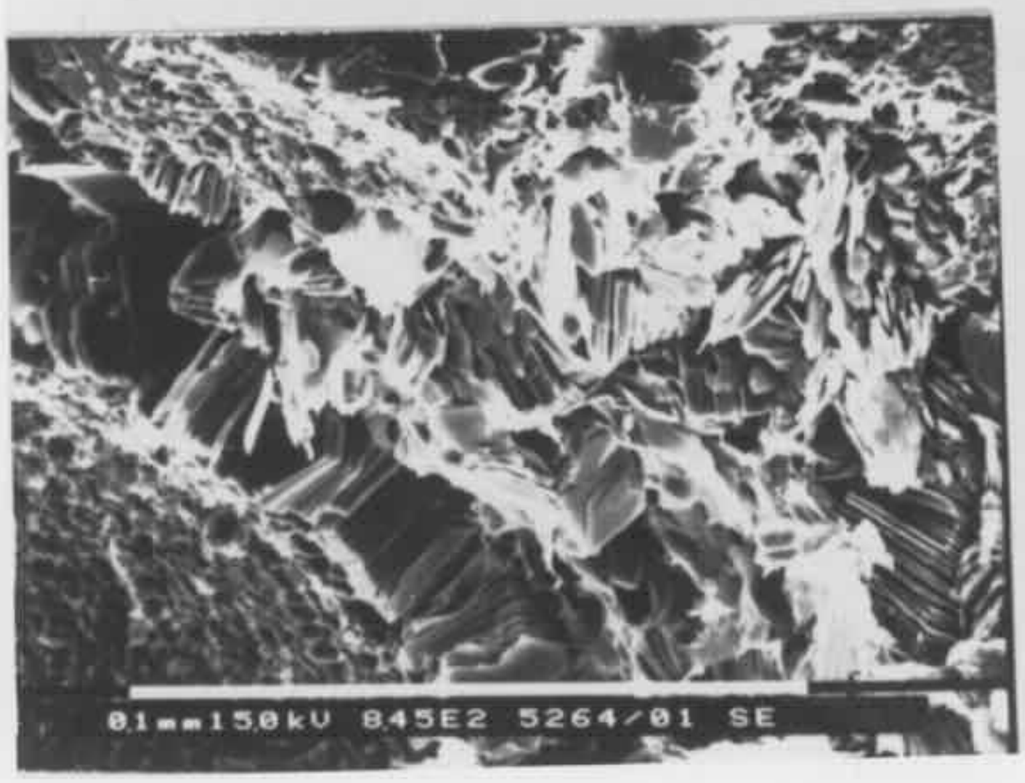
0.1mm 15.0kU 8.45E2 5264/01 SE


A
0.1mm 15.0kU 8.45E2 5017/01 SE

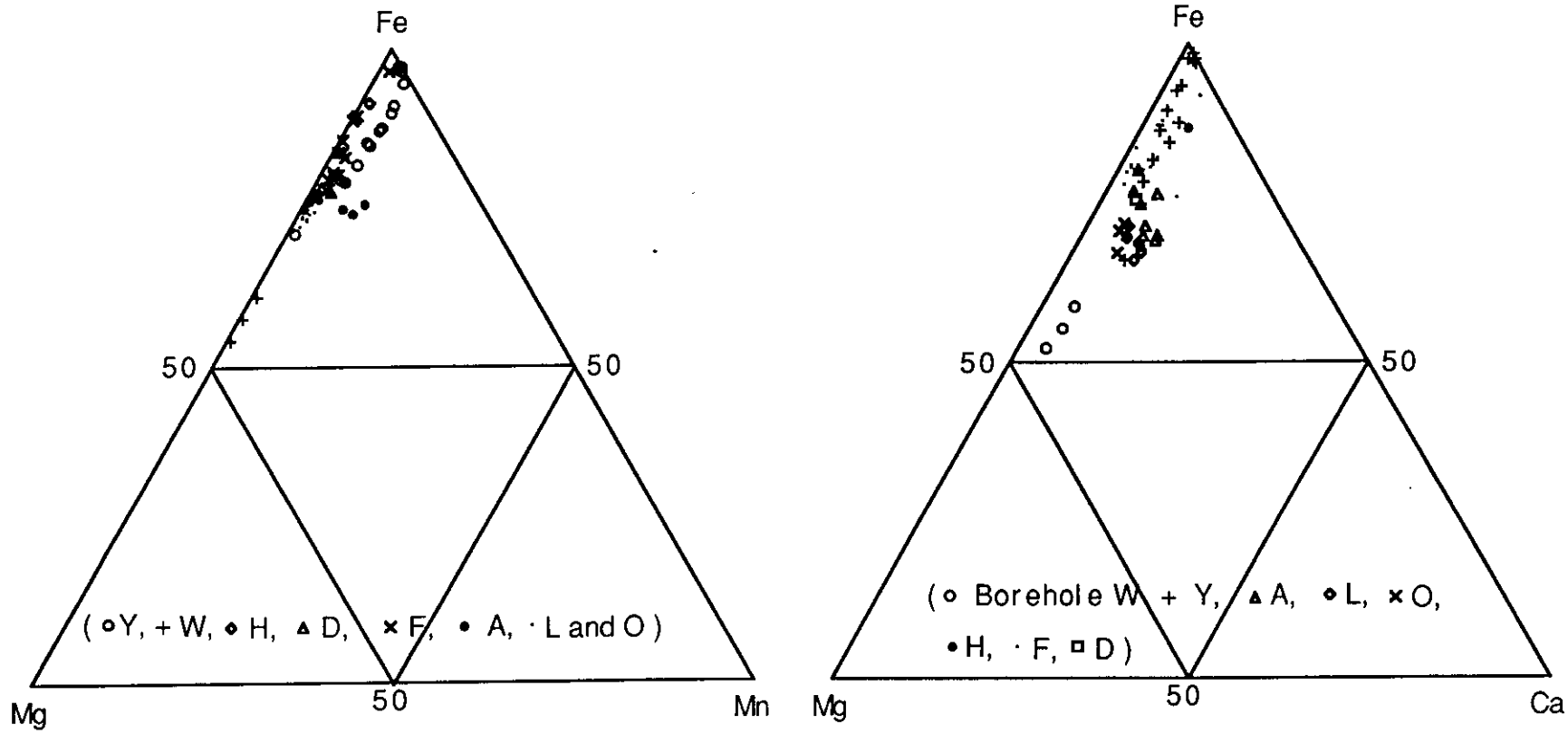

Fig 6-23 Siderite compositions (mole %) from the Narrabeen Group sandstones. Data from microprobe analyses of 11 samples from 8 boreholes.

Appendix V). On the XRD trace, it was identified by its typical peaks at 7.15, 3.58 and 2.38 Å.

The authigenic kaolin occurs in two forms in terms of morphology: blocky and flaky with the latter being the overwhelmingly dominant form. An individual blocky kaolin crystal is 2-3 μm across with a thickness of 1-2 μm (Fig 6-24). The blocky kaolin is likely to be kaolinite.

An individual flaky kaolin crystal is about 5-15 μm across with a thickness of much less than 1 μm. The majority of flaky kaolin crystals are 5-10 μm across. The larger flaky kaolin is likely to be dickite. It occurs either as individual pseudo-hexagonal flakes or as face to face stacks of pseudo-hexagonal flakes (stacked kaolin flakes) with the latter being more common. The individual kaolin flakes are generally present on the surfaces of both detrital grains (Fig 6-25) and authigenic minerals (carbonates and quartz overgrowths) (Fig 6-26). The stacked kaolin flakes fill inter-grain pore spaces (Fig 6-27) and secondary pore spaces (Fig 6-28), form a mass with the outline of an altered detrital grain (Figs 6-29 to 6-32), are present on quartz overgrowths and carbonate crystals (Fig 6-33), and are enclosed by quartz overgrowths (Fig 6-34). Some stacked kaolin flakes have ragged edges (Fig 6-35). Other stacked kaolin flakes show illitisation at their edges (Figs 6-36 & 6-37).

ILLITE [$K_{1-1.5}Al_4(Si_{7-6.5}Al_{1-1.5}O_{20})(OH)_4$]: It is a less commonly found diagenetic mineral in these samples (Table 6-1 and Appendix V). SEM / EDX studies show that authigenic illite is present within altered detrital grains (Figs 6-38 & 6-39). It also occurs on carbonate crystals and prismatic quartz crystals (Fig 6-40), bridges inter-grain pore spaces (Figs 6-41 & 6-42), fills secondary pore spaces and is present on quartz overgrowths (Figs 6-43 & 6-44). The illite was identified by its fibrous morphology and EDX analyses, which yield the major elements of Si, Al, and K. The identification was further confirmed by XRD study.

Fig 6-29 (top left) A detrital grain altered to stacked kaolin flakes (see next figure for enlargement) and prismatic quartz crystals (see Fig 6-63 on page 194 for enlargement). From Campbelltown 2 at drilling depth of 593.0 m (sample Z593.0).

Fig 6-30 (top right) Stacked kaolin flakes. Enlargement of Fig 6-29.

Fig 6-31 (upper left) A detrital grain altered to stacked kaolin flakes. From Campbelltown 2 at drilling depth of 422.6 m (sample Z422.6).

Fig 6-32 (upper right) Enlargement of Fig 6-31. The bar is 10 μm.

Fig 6-33 (lower left) Stacked kaolin flakes (K) on quartz overgrowths (q) and dissolved siderite cement (S). From Cobbitty 3 at drilling depth of 297.7 m (sample X297.7).

Fig 6-34 (lower right) Stacked kaolin flakes (K) enclosed by quartz overgrowths (Q). From Campbelltown 5 at drilling depth of 377.5 m (sample Y377.5).

Fig 6-35 (bottom left) Stacked kaolin flakes with ragged edges. From South Colah 1 at drilling depth of 435.2 m (sample O435.2).

Fig 6-36 (bottom right) Staked kaolin flakes which are illitised at edges. From Oil Longley 1 at drilling depth of 320.1 m (sample I320.1).

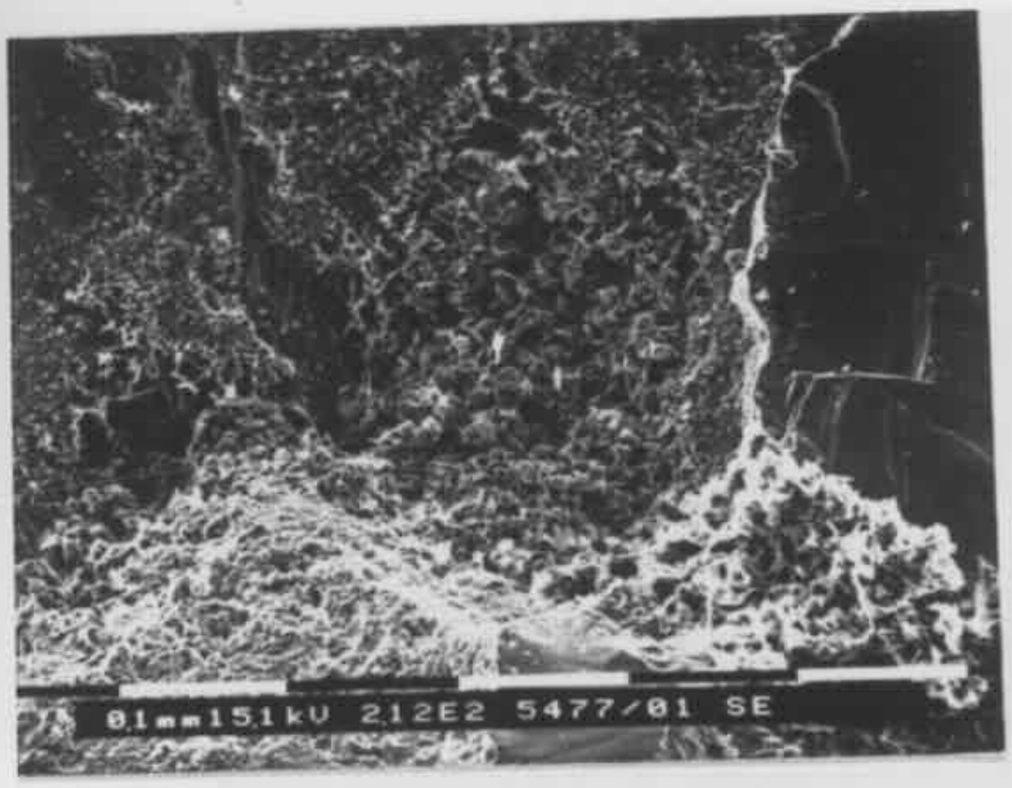
0.1mm 15.1kV 2.12E2 5477/01 SE


10µm 15.0kV 1.69E3 5475/01 SE


01mm 14.9kV 424E2 5516/01 SE


FWD: 25.0mm


q
k
S
0.1mm 15.0kV 8.45E2 3735/01 SE


Q
K
10µm 15.0kV 1.69E3 5319/01 SE


10µm 15.0kV 2.40E3 2797/01 SE


10µm 15.0kV 3.38E3 3689/00 SE

Fig 6-37 (top left) Staked kaolin flakes which are illitised at edges. From Campbelltown 2 at drilling depth of 593.0 m (sample Z593.0).

Fig 6-38 (top right) Authigenic illite (see Fig 6-39 for enlargement) within an altered detrital grain (centre of photograph). From Campbelltown 2 at drilling depth of 422.6 m (sample Z422.6).

Fig 6-39 (upper left) Enlargement of Fig 6-38. I marks illite.

Fig 6-40 (upper right) Authigenic illite (I) on prismatic quartz (mega-quartz) crystals (q) and ferroan calcite crystal (C). From Campbelltown 2 at drilling depth of 593.0 m (sample Z593.0).

Fig 6-41 (lower left) Illite lining inter-grain pore spaces. From Wollongong 45 at drilling depth of 260.8 m (sample A260.8).

Fig 6-42 (lower right) Enlargement of Fig 6-41. I marks illite.

Fig 6-43 (bottom left) Authigenic illite (see Fig 6-44 for enlargement) on quartz overgrowths which enclose dissolved siderite crystals. From Liverpool 91 at drilling depth of 469.6 m (sample L469.6).

Fig 6-44 (bottom right) Enlargement of Fig 6-43. I marks illite, Q quartz overgrowths and S siderite.


10 µm 15.1 kV 3.38E3 5470/01 SE


0.1 mm 14.9 kV 1.06E2 5520/01 SE


I
10 µm 15.0 kV 1.69E3 5521/01 SE

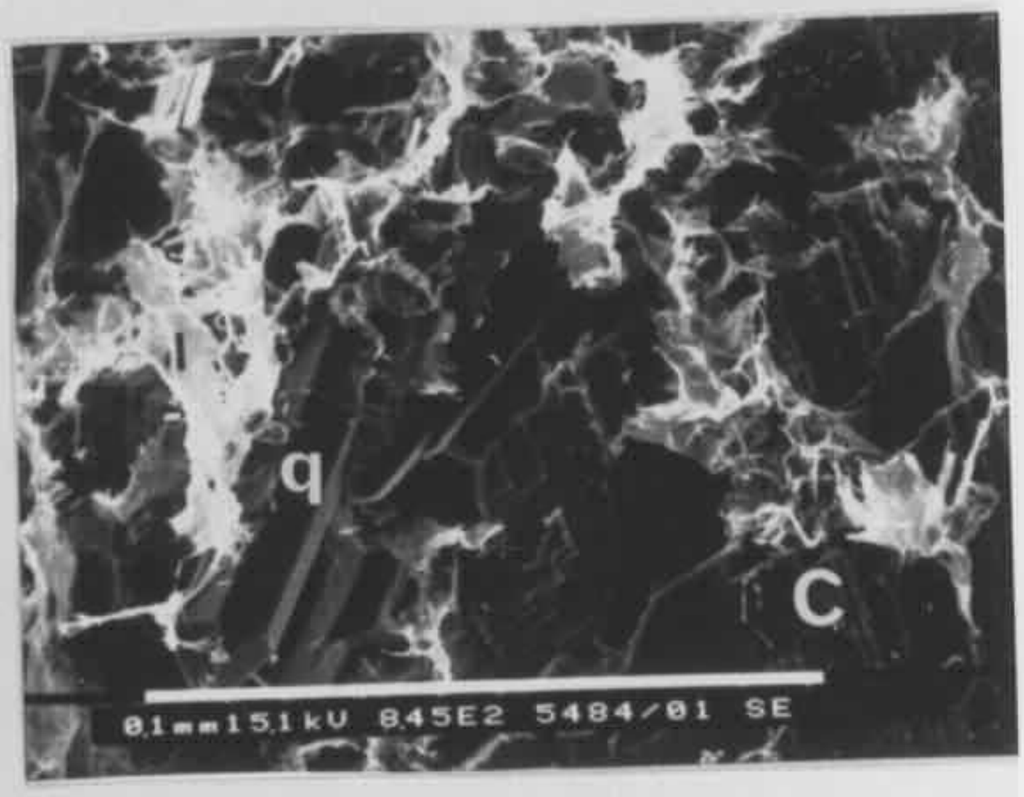
I
q
C
0.1 mm 15.1 kV 8.45E2 5484/01 SE

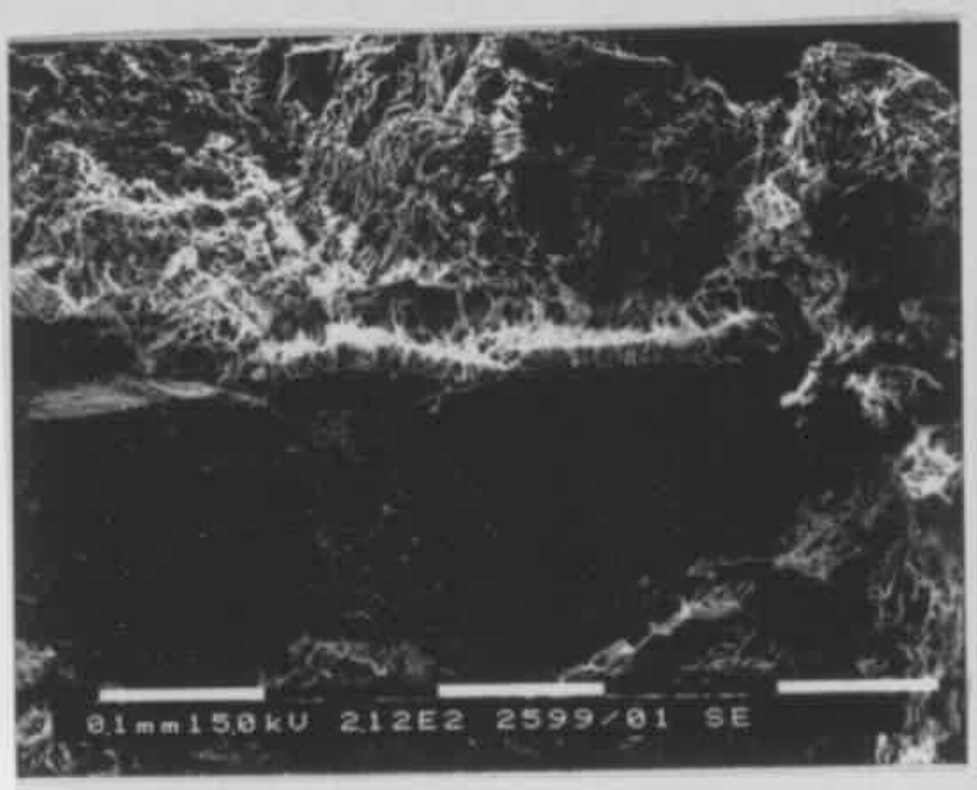
0.1 mm 15.0 kV 2.12E2 2599/01 SE

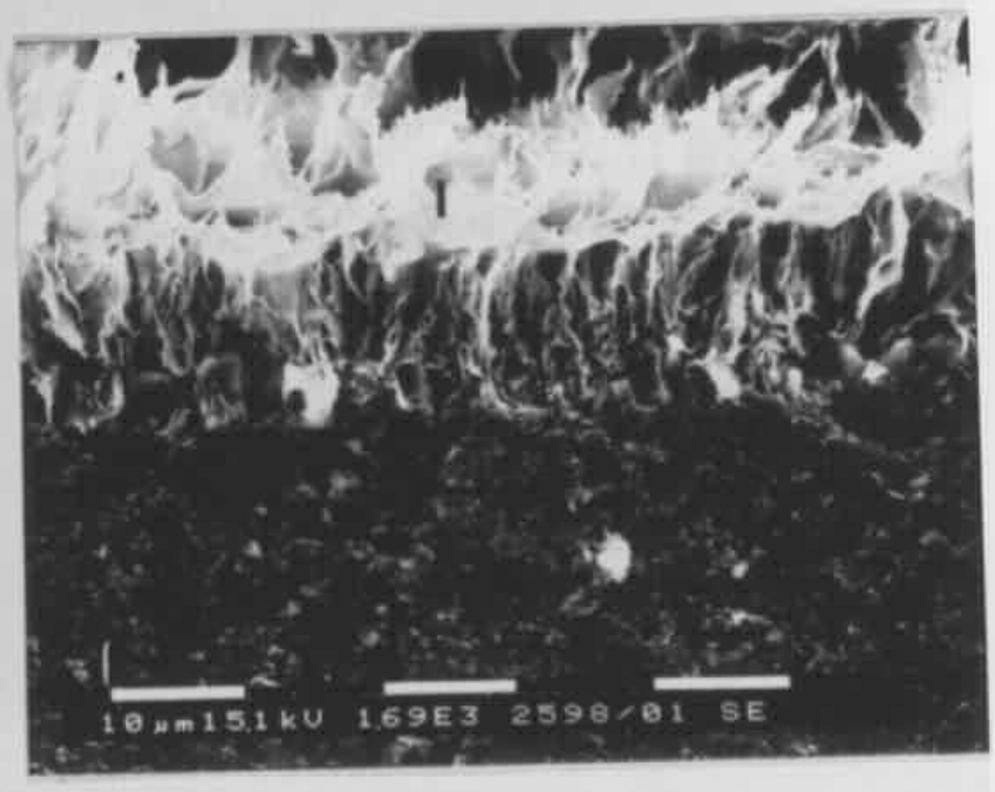
I
10 µm 15.1 kV 1.69E3 2598/01 SE


0.1 mm 15.0 kV 4.42E2 2682/01 SE

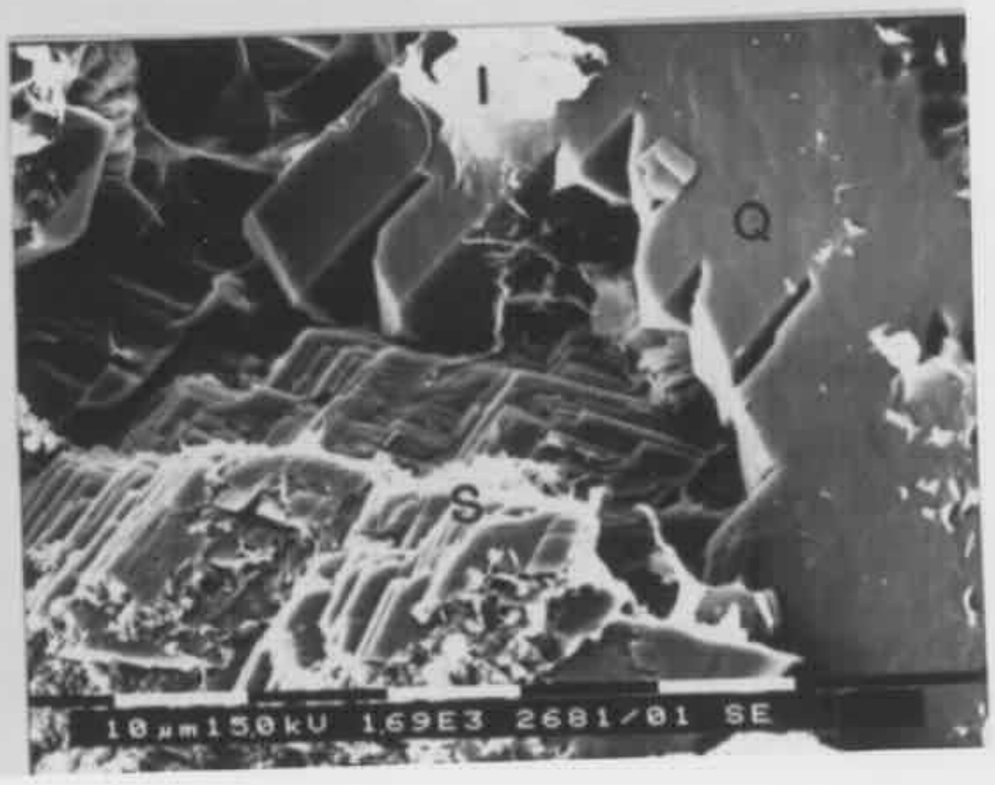
I
Q
S
10 µm 15.0 kV 1.69E3 2681/01 SE

MIXED-LAYER ILLITE / SMECTITE: It was identified by the morphology - well developed lath-like projections with short fibrous edges from the substrate under the SEM (Wilson and Pittman, 1977). In some cases, the identification was substantiated by the EDX analyses yielding a minor amount of Fe in addition to the major elements of Si, Al and K. Mixed-layer illite / smectite coats detrital grain surfaces (Figs 6-45 to 6-48, 6-49a, 6-50, 6-51 & 6-49b). The coating layer, which is clearly seen under the SEM, is usually so thin that it is not easily identified with the petrological microscope. For some of the illite / smectite crystals, the EDX analyses show that they have the composition similar to that of illite. The elements Fe, Ca and Mg, which smectite generally contains, were not detected. This can probably be attributed to a very low proportion of smectite in the mixed-layer illite / smectite, which is indicated by the XRD analyses. The mixed-layer illite / smectite has a basal spacing varying from 10.40 to 11.20 Å. The variation of basal spacing is caused by different proportions of illite and smectite in different samples. Referring to Table 1 of Weaver (1956), it is known that smectite accounts for 20 to 40 % of the mixed-layer illite / smectite identified in these samples.

CHLORITE $\{(Mg,Al,Fe)_{12}[(Si,Al)_8O_{20})](OH)_{16}\}$: It was identified by its morphology and EDX analyses. The identification was further confirmed by XRD study. It was generally found in the lower Narrabeen Group sandstones from the east coast zone and the northern region of the basin (Table 6-1 and Appendix V). Chlorite coats detrital grains (Figs 6-52 to 6-55 & 6-49c) and fills inter-grain pore spaces (Figs 6-56 to 6-59 & 6-49d) with the former being more common. Grain coating chlorites are usually smaller (an individual crystal is 2 to 3 μm across, much less than 1 μm thick), subhedral to euhedral, pseudohexagonal crystals. These individual crystals are oriented on edges and are perpendicular to the detrital grain surfaces. The pore filling chlorites are larger (an individual crystal is 5-8 μm across and much less than 1 μm thick), euhedral, pseudohexagonal crystals. The pore filling chlorite is seen in some samples to form rosettes (Fig 6-60). All the EDX analyses of authigenic chlorites indicate major peaks of Si, Al, Mg, and Fe. The

Fig 6-45 (top left) Grain coating mixed-layer illite / smectite enclosed by mega-quartz crystals (q). From Oil Longley 1 at drilling depth of 378.5 m (sample l378.5).

Fig 6-46 (top right) Enlargement of Fig 6-45. The cross point of the two white lines is the point where EDX analysis was made. Refer to Fig 6-49a for the EDX spectrum. I / S marks illite / smectite.

Fig 6-47 (upper left) Grain coating mixed-layer illite / smectite together with early kaolins (generation I). From Cobbitty 3 at drilling depth of 612.9 m (sample X612.9).

Fig 6-48 (upper right) Enlargement of Fig 6-47. K marks kaolin and I / S illite / smectite.

Fig 6-50 (lower left) Mixed-layer illite / smectite coating an altered detrital volcanic rock fragment and illite lining inter-grain pore spaces. From Wollongong 45 at drilling depth of 295.6 m (sample A295.6).

Fig 6-51 (lower right) Enlargement of Fig 6-50. I marks illite and I/S mixed-layer illite / smectite. The cross point of the two white lines is the point where EDX analysis was made. Refer to Fig 6-49b for the EDX spectrum.

Fig 6-52 (bottom left) Grain coating chlorite enclosed by micro-quartz crystals. From Oil Longley 1 at drilling depth of 629.3 m (sample l629.3).

Fig 6-53 (bottom right) Enlargement of Fig 6-52. Q marks micro-quartz crystal.

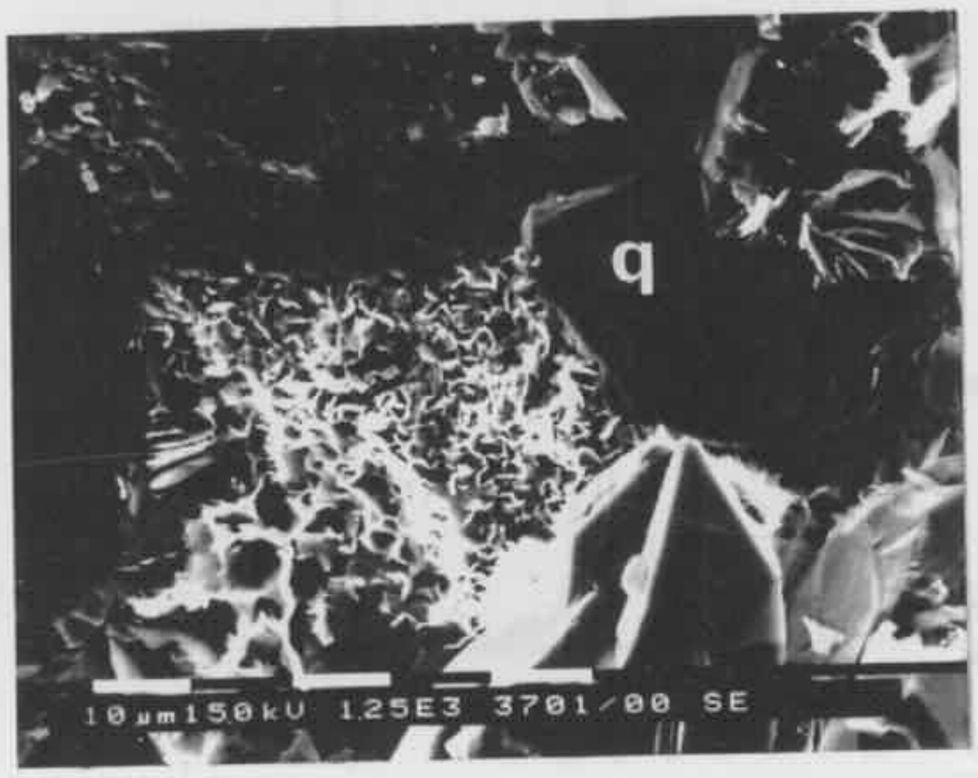
q
10µm15.0kV 1.25E3 3701/00 SE

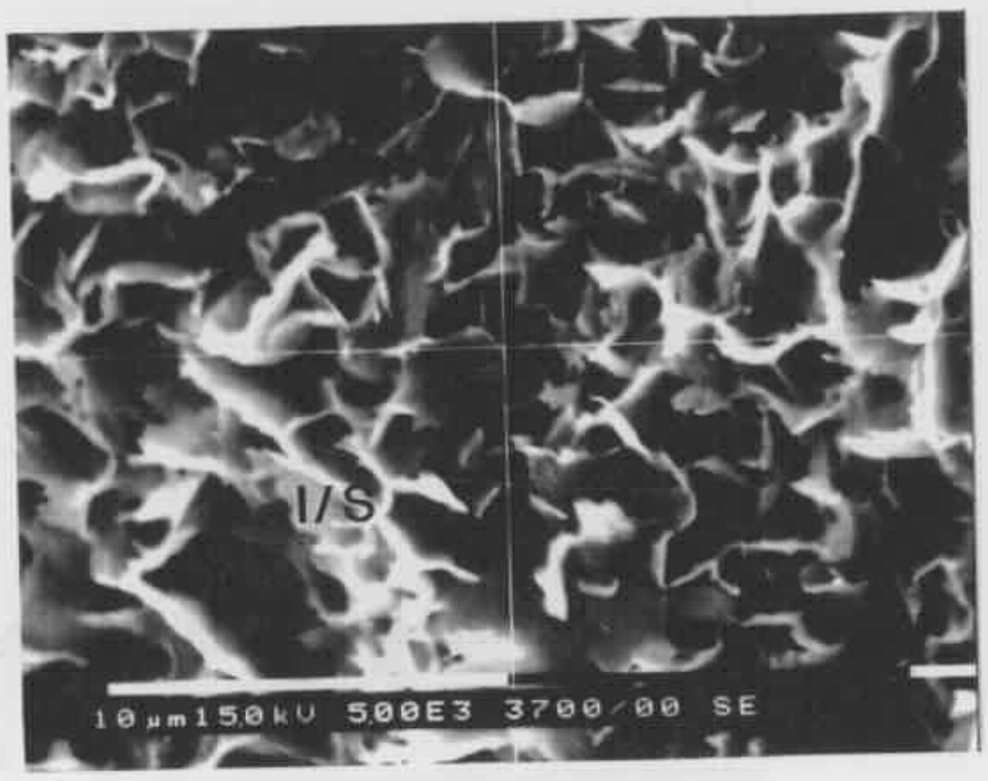
I/S
10µm15.0kV 5.00E3 3700/00 SE

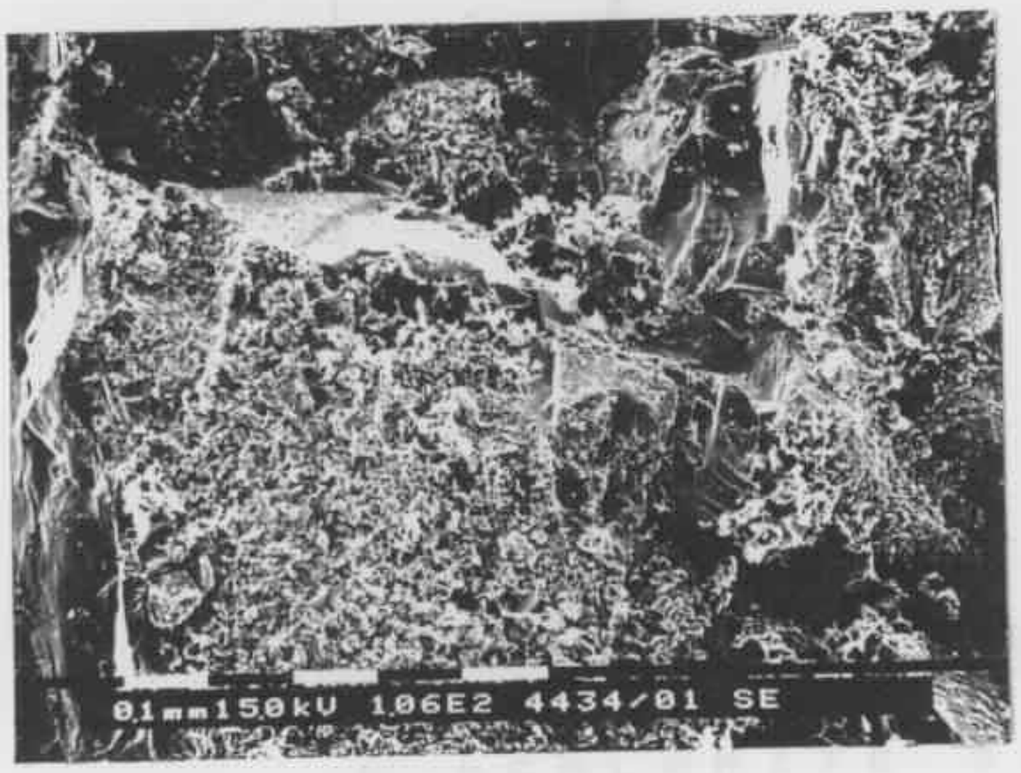
0.1mm15.0kV 1.06E2 4434/01 SE


10µm15.0kV 1.69E3 4439/01 SE

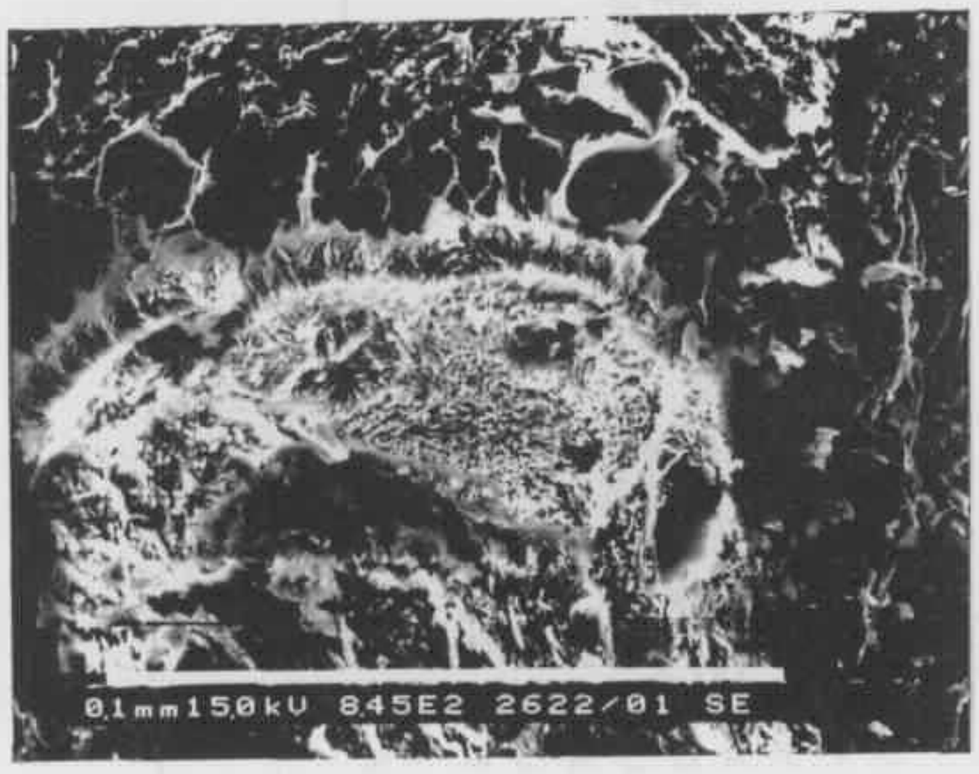
0.1mm15.0kV 8.45E2 2622/01 SE

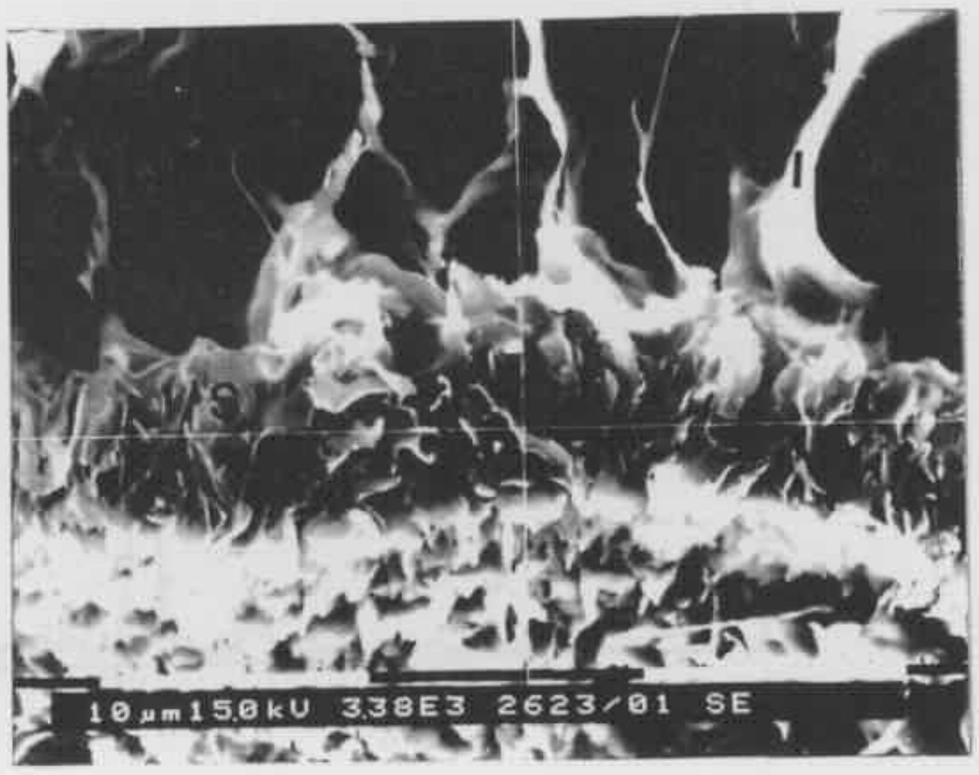
10µm15.0kV 3.38E3 2623/01 SE

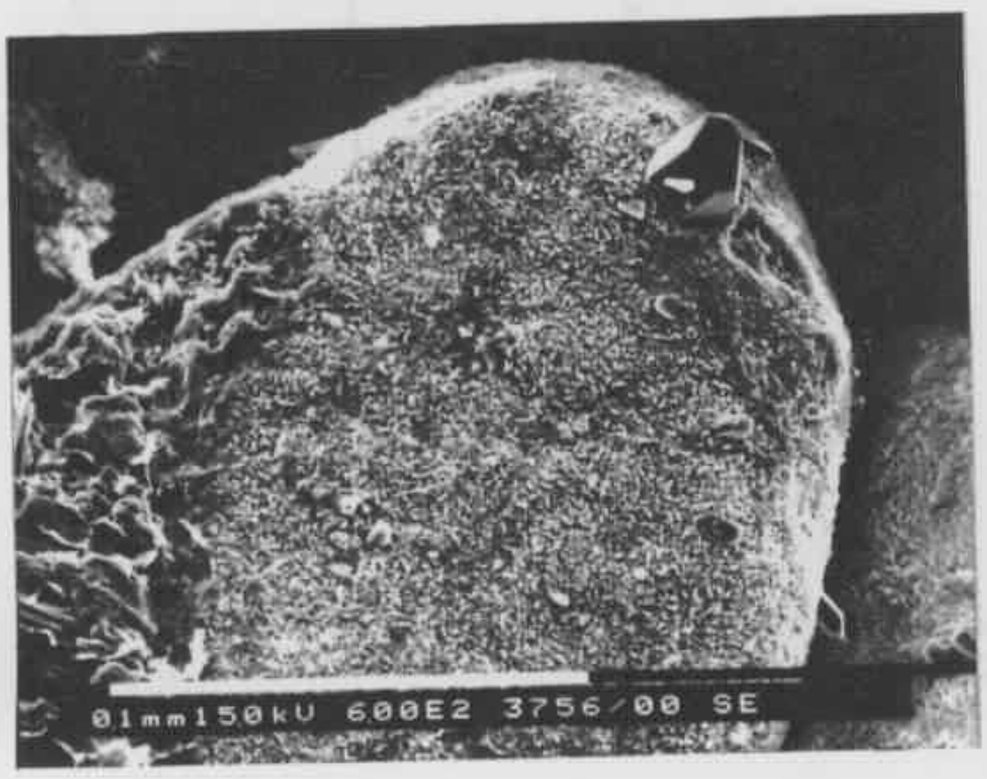
0.1mm15.0kV 6.00E2 3756/00 SE


10µm15.0kV 5.00E3 3757/00 SE

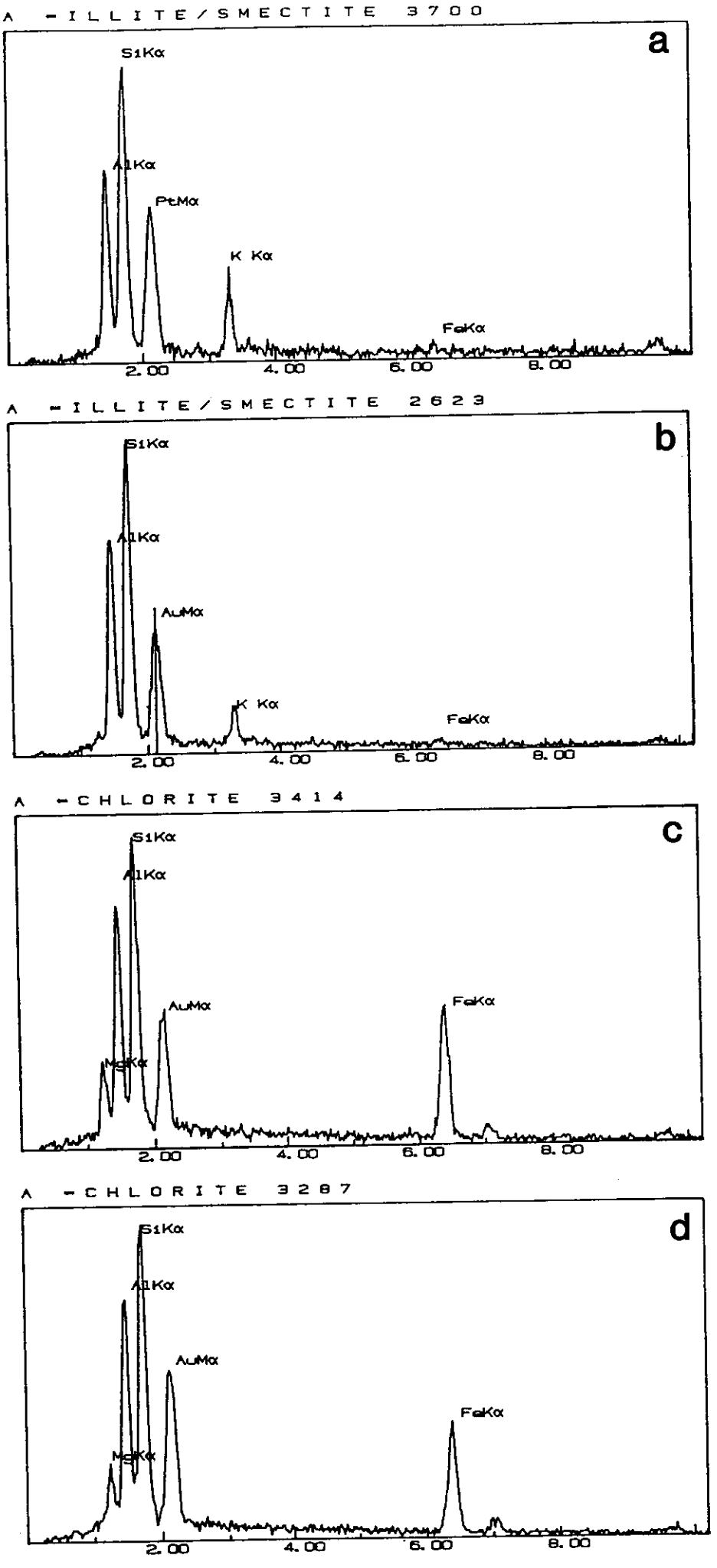

Fig 6-49 EDX spectrum.

Fig 6-54 (top left) Grain coating chlorite. From Strevens Cape Three Points at drilling depth of 369.0 m (sample M369.0).

Fig 6-55 (top right) Enlargement of Fig 6-54. The cross point of the two white lines is the point where EDX analysis was made. Refer to Fig 6-49c for the EDX spectrum. C marks chlorite.

Fig 6-56 (upper left) Pore-filling chlorite. Note due to charging some of the chlorite flakes are distorted. From Liverpool 91 at drilling depth of 579.2 m (sample L579.2). See Fig 5-25 on page 117 for grain coating chlorite in this sample.

Fig 6-57 (upper right) Enlargement of Fig 6-56. C marks chlorite.

Fig 6-58 (lower left) Pore-filling chlorite. Q marks quartz overgrowths. From Coal Cliff 13 at drilling depth of 81.1 m (sample C081.1).

Fig 6-59 (lower right) Enlargement of Fig 6-58. The cross point of the two white lines is the point where EDX analysis was made. Refer to Fig 6-49d for the EDX spectrum. C marks chlorite.

Fig 6-60 (bottom left) Pore-filling chlorite (C) in the form of rosettes enclosed by authigenic albite crystals (a). From Strevens Cape Three Points at drilling depth of 492.2 m (sample M492.2).

Fig 6-61 (bottom right) Very small polyhegonal micro-quartz crystals enclosed by coalescing polyhegonal mega-quartz crystals (Q). From Campbelltown 5 at drilling depth of 377.5 m (sample Y377.5).

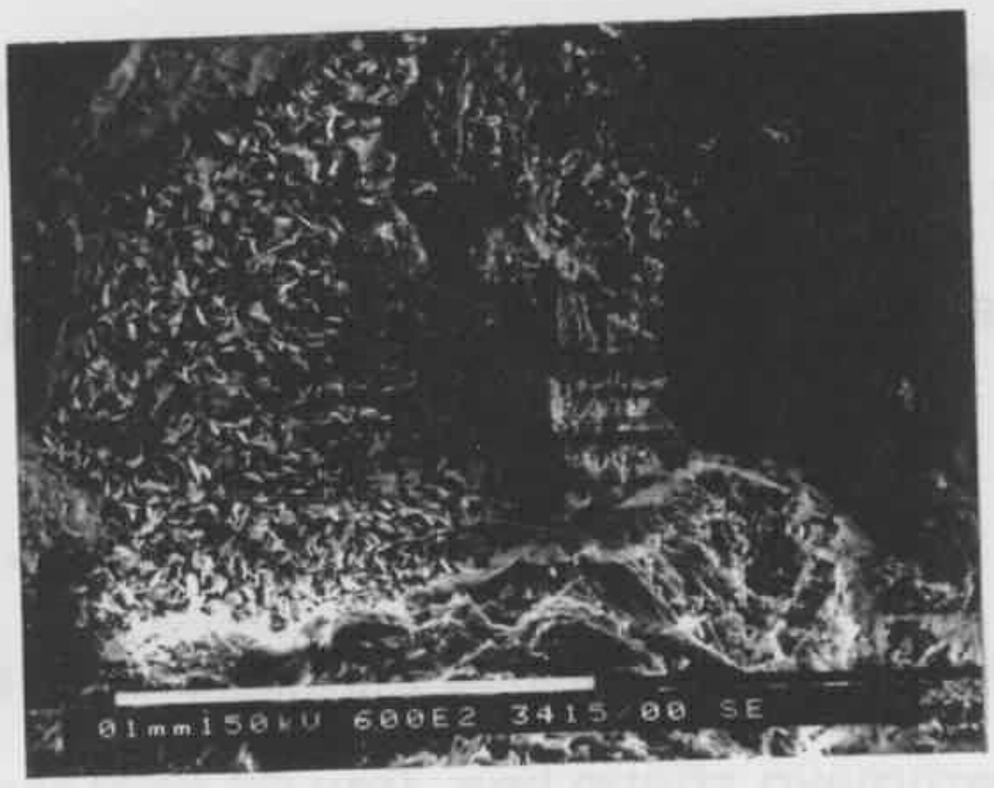
01mm150kU 600E2 3415/00 SE


C
10µm150kU 500E3 3414/00 SE


C
01mm150kU 549E2 2693/01 SE


C
10µm150kU 338E3 2692/01 SE


01mm150kU 845E2 3288/00 SE


10µm150kU 338E3 3287/00 SE


C
a
10µm150kU 338E3 3421/00 SE

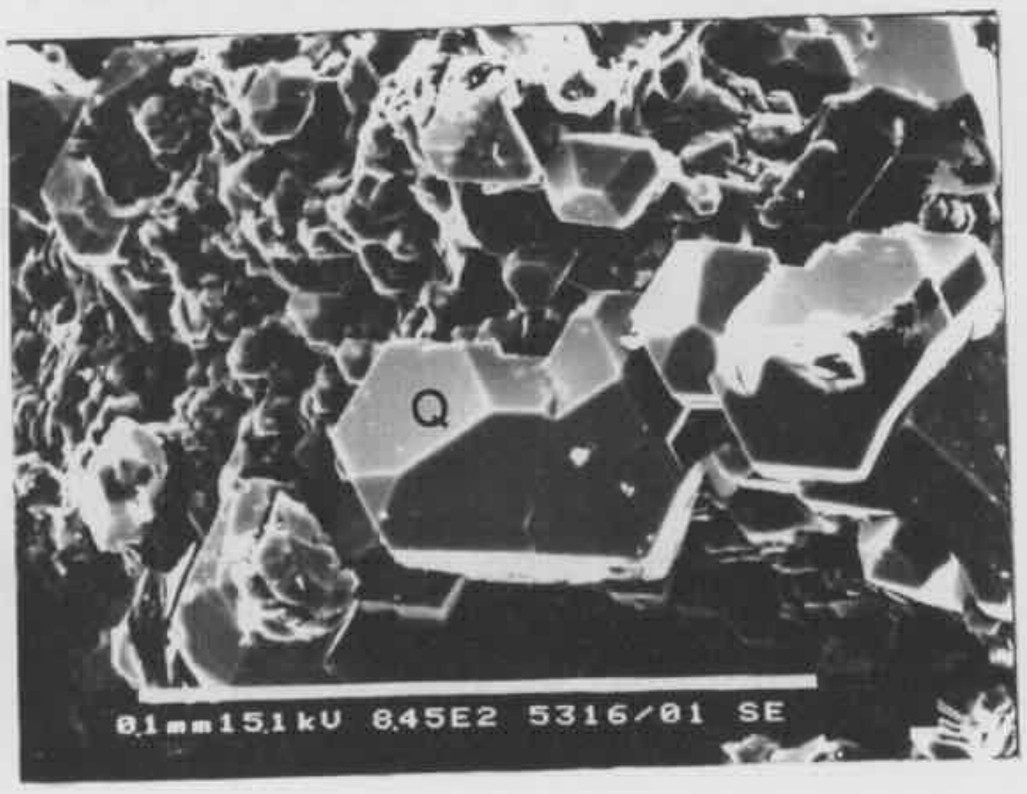
Q
01mm151kU 845E2 5316/01 SE

chlorite is very iron rich (Figs 6-49c & 6-49d). Under the petrological microscope, the chlorite coating was seen as a very thin greenish to reddish layer. The reddish colour is considered to be created by the oxidation of Fe in the chlorite.

6.3.4 QUARTZ (SiO_2) CEMENT

The quartz cement consists of three types: micro-quartz, mega-quartz (crystal size larger than 20 μm), and quartz overgrowths. The micro-quartz occurs either as very small equant polyhedral crystals with a size of less than 10 μm or as prismatic crystals whose length is generally less than 20 μm. It grows on detrital quartz grains (Figs 6-61 & 6-62). Micro-quartz crystals can coalesce to form a larger single polyhedral crystal (Fig 6-61). Mega-quartz occurs in the form of prismatic crystals. It fills inter-grain pore spaces (Fig 6-63), or occurs within altered detrital grains (Fig 6-64). In the three thin sections with abundant quartz cement (samples B234.7, C132.6, and J470.1) described in the last chapter, the quartz cement is mega-quartz in the form of mosaic inter-locking crystals. Quartz overgrowths (Figs 6-33, 6-34 & 6-62) are the most commonly found quartz cement. They were found in all the samples studied under SEM / EDX.

6.3.5 OTHER AUTHIGENIC MINERALS

ALBITE ($NaAlSi_3O_8$): Authigenic albite was identified by its euhedral crystals and EDX analyses, which yield the major elements of Si, Al and Na. It was found to be present in four forms: (1) filling inter-grain pore spaces (Figs 6-65 & 6-66), (2) occurring within altered detrital grains (Figs 6-67, 6-68 & 6-69a), (3) replacing original plagioclase grains (albitisation) (Figs 6-70 & 6-71), and (4) growing from the detrital plagioclase (plagioclase overgrowths) (Fig 6-72). Authigenic albite was identified in the majority of samples containing detrital plagioclase grains.

HAEMATITE (Fe_2O_3): It was identified by SEM / EDX analyses and found only in two samples (C081.1 and C101.6) from Borehole C in the south east coast zone (Appendix V). It occurs in the form of coatings on detrital grains and as replacement

Fig 6-62 (top left) Very small prismatic micro-quartz crystals enveloped by well developed quartz overgrowths (Q). From Oil Longley at drilling depth of 543.4 m (sample l543.4).

Fig 6-63 (top right) Prismatic quartz (mega-quartz) crystals (q) filling inter-grain pore spaces. From Campbelltown 2 at drilling depth of 656.8 m (sample Z656.8).

Fig 6-64 (upper left) Prismatic quartz crystals (q) within an altered detrital grain on which authigenic illite (I) occurs. Enlargement of Fig 6-29. From Campbelltown 2 at drilling depth of 593.0 m (sample Z593.0).

Fig 6-65 (upper right) Pore-filling authigenic albite crystals. From Liverpool 91 at drilling depth of 496.6 m (sample L496.6).

Fig 6-66 (lower left) Enlargement of Fig 6-65. A marks albite.

Fig 6-67 (lower right) Authigenic albite crystals within an altered detrital plagioclase grain. From Liverpool 91 at drilling depth of 469.6 m (sample L469.6).

Fig 6-68 (bottom left) Enlargement of Fig 6-67. The cross point of the two white lines is the point where EDX analysis was made. Refer to Fig 6-69a for the EDX spectrum. A marks albite.

Fig 6-70 (bottom right) Albitised plagioclase (see Fig 6-71 on page 197 for enlargement). From Liverpool 91 at drilling depth of 638.9 m (sample L638.9).

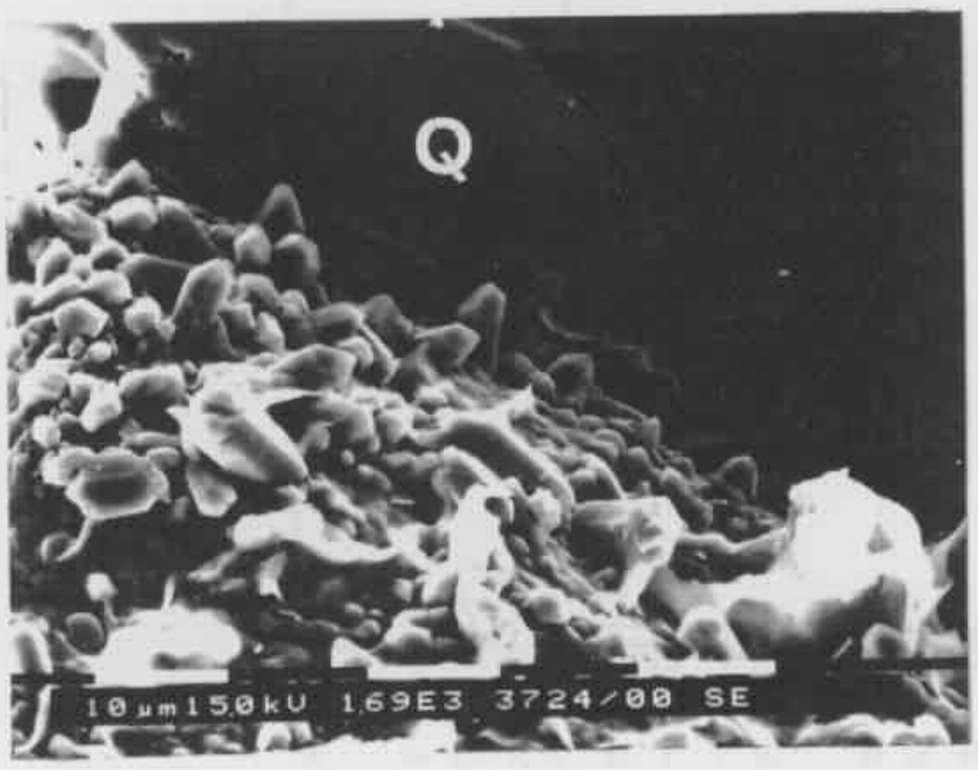
Q
10 µm 15.0 kV 1.69E3 3724/00 SE


q
0.1 mm 15.0 kV 4.24E2 5447/01 SE


I
q
10 µm 15.0 kV 1.69E3 5476/01 SE

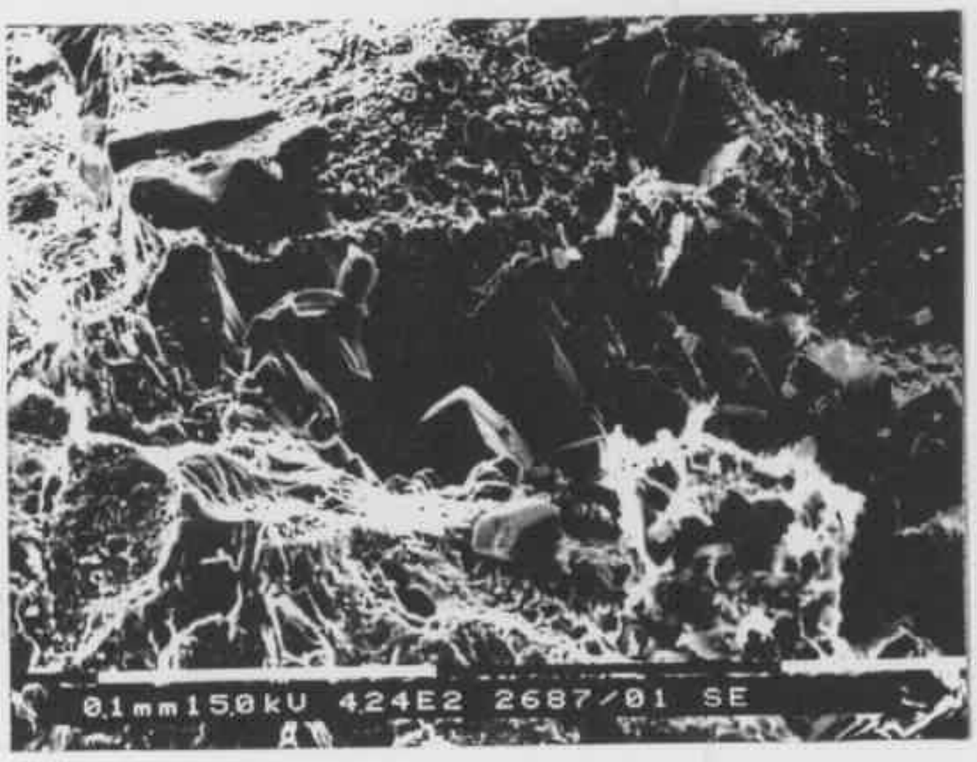
0.1 mm 15.0 kV 4.24E2 2687/01 SE

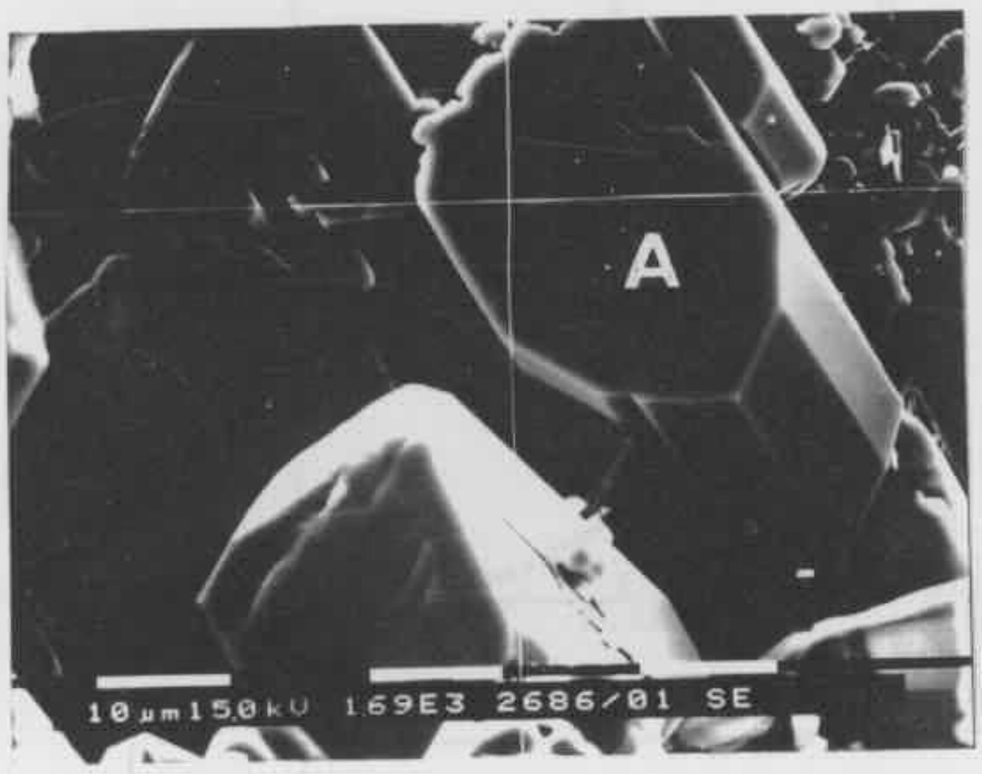
A
10 µm 15.0 kV 1.69E3 2686/01 SE

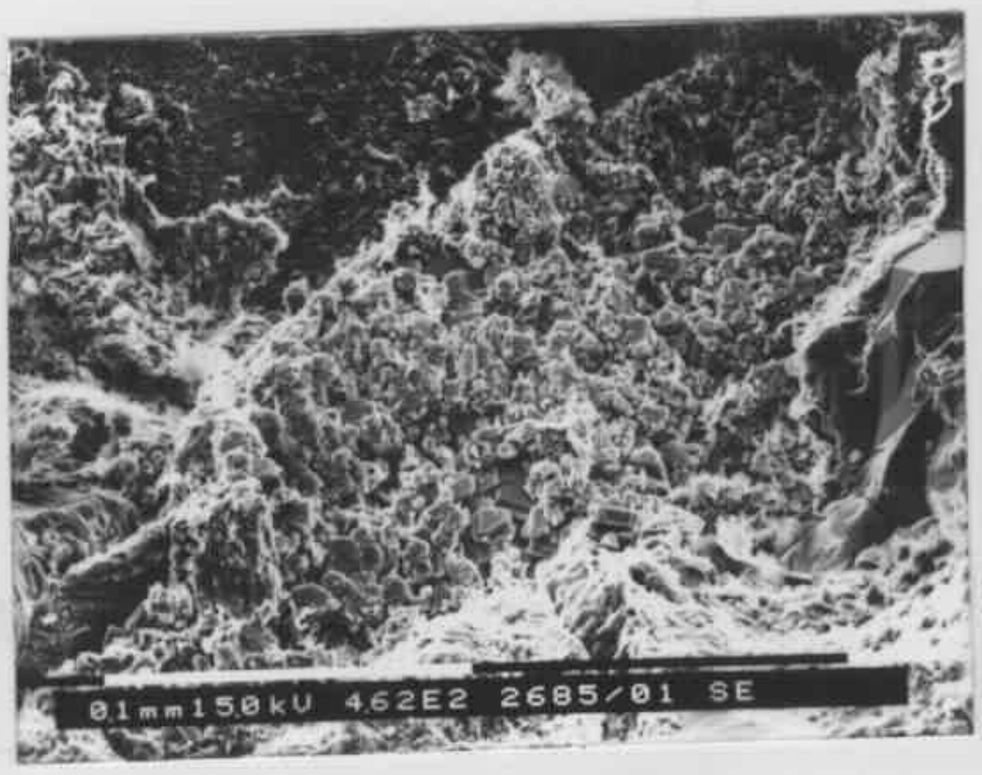
0.1 mm 15.0 kV 4.62E2 2685/01 SE

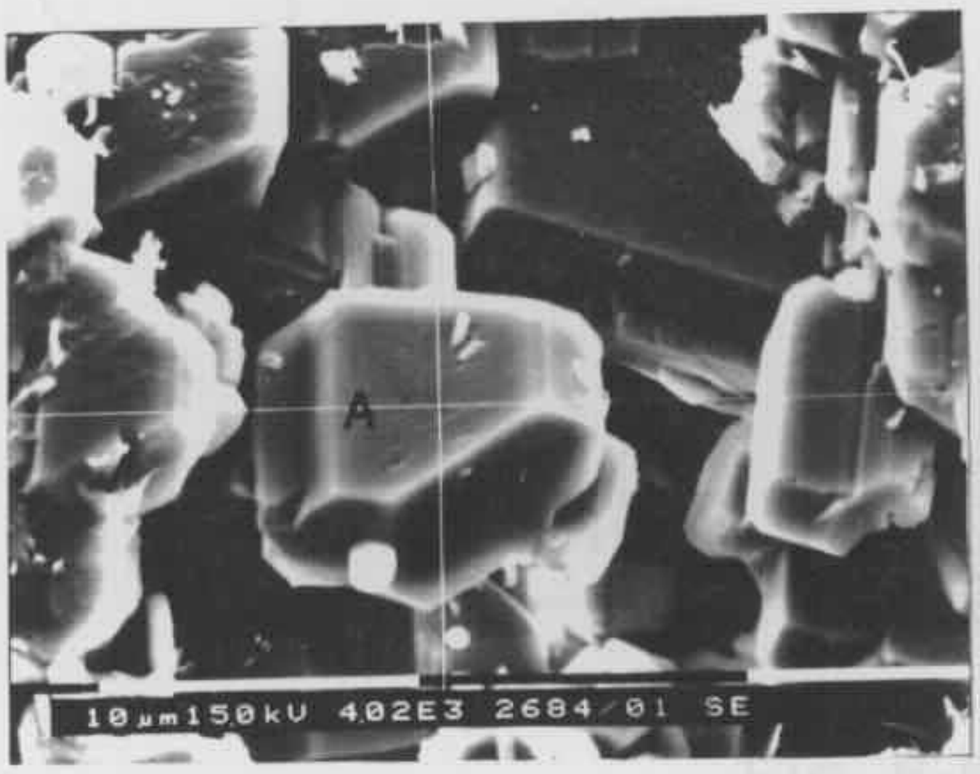
A
10 µm 15.0 kV 4.02E3 2684/01 SE


0.1 mm 15.0 kV 6.25E2 3293/00 SE

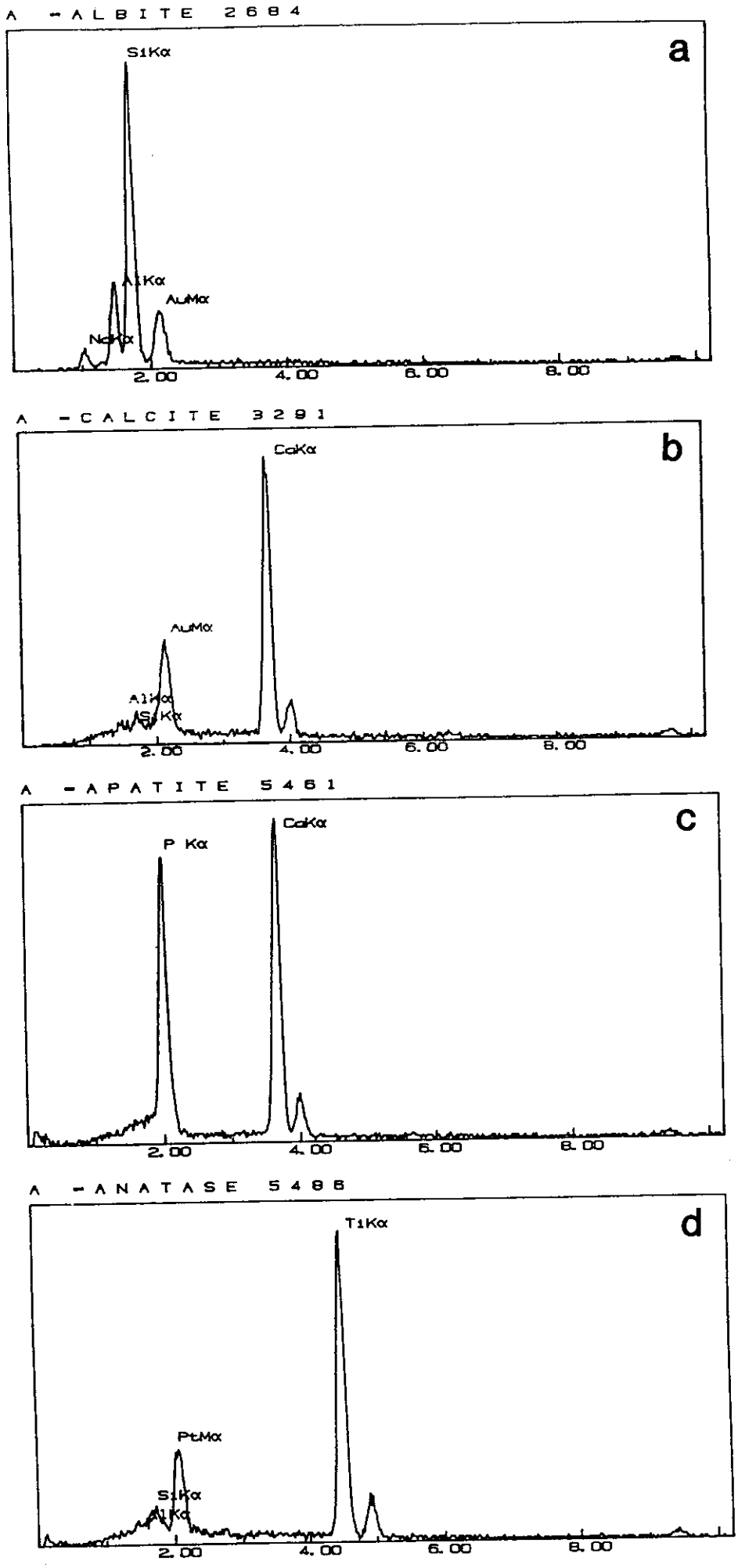

Fig 6-69 EDX spectrum.

of detrital lithics. It was among the earliest diagenetic products.

PYRITE (FeS_2): Authigenic pyrite was identified in a few samples studied (Appendix V). It is present in the form of framboids (Figs 6-73 & 6-74), which are spheres consisting of closely packed tiny (1-2 μm across) crystallites. The EDX analyses yield the major elements of Fe and S, which confirms the identification.

APATITE [$Ca_5(PO_4)_3(OH,F,Cl)$]: Authigenic apatite (Figs 6-75 & 6-76 & 6-69c) was identified in one of the samples (Z611.3) by the crystal morphology and EDX analyses yielding the major elements of P and Ca.

ANATASE (TiO_2): An authigenic crystal of TiO_2, tentatively identified by SEM / EDX analyses as anatase - the low temperature polymorph of TiO_2 (Figs 6-77, 6-78 & 6-69d), was found in one sample (Z531.9). It is up to 0.1 mm across. Its exact timing of formation is not clear but it is considered to be the early product of diagenesis as a result of alteration of Ti-bearing minerals such as sphene and ilmenite.

ANALCIME [$Na(AlSi_2O_6)\cdot H_2O$]: Authigenic analcime (Figs 6-79 & 6-80) was tentatively identified in one of the samples (Z703.3). The identification was based on the cubo-octahedral morphology of the crystals and EDX analyses yielding the major elements of Si, Al and Na.

DAWSONITE [$NaAlCO_3(OH)_2$]: Dawsonite is not a well known mineral. It was found as patches of fibrous crystals (Figs 6-81 & 6-82) in a few samples mainly from the boreholes in northern region of the basin (Appendix V). EDX analyses yield major elements of Na and Al.

6.4 PARAGENETIC SEQUENCE OF AUTHIGENIC MINERALS

By carefully studying the textural relationships among the authigenic minerals

Fig 6-71 (top left) Calcite (C) produced as the by-product of albitization of plagioclase. A marks albitised plagioclase. Enlargement of Fig 6-70. The cross point of the two white lines is the point where EDX analysis was made. Refer to Fig 6-69b for the EDX spectrum.

Fig 6-72 (top right) Plagioclase overgrowths (O). From Oil Longley 1 at drilling depth of 596.6 m (sample I596.6).

Fig 6-73 (upper left) Authigenic pyrite in framboidal form. From Cobbitty 3 at drilling depth of 476.2 m (sample X476.2).

Fig 6-74 (upper right) Enlargement of Fig 6-73.

Fig 6-75 (lower left) Authigenic apatite. From Campbelltown 2 at drilling depth of 611.3 m (sample Z611.3).

Fig 6-76 (lower right) Enlargement of Fig 6-75. White dot is the point where EDX analysis was made. Refer to Fig 6-69c for the EDX spectrum.

Fig 6-77 (bottom left) Authigenic anatase. From Campbelltown 2 at drilling depth of 531.9 m (sample Z531.9).

Fig 6-78 (bottom right) Enlargement of Fig 6-77. Black dot is the point where EDX analysis was made. Refer to Fig 6-69d for the EDX spectrum.


A
C
C
C
10µm15.0kV 3.54E3 3291/00 SE

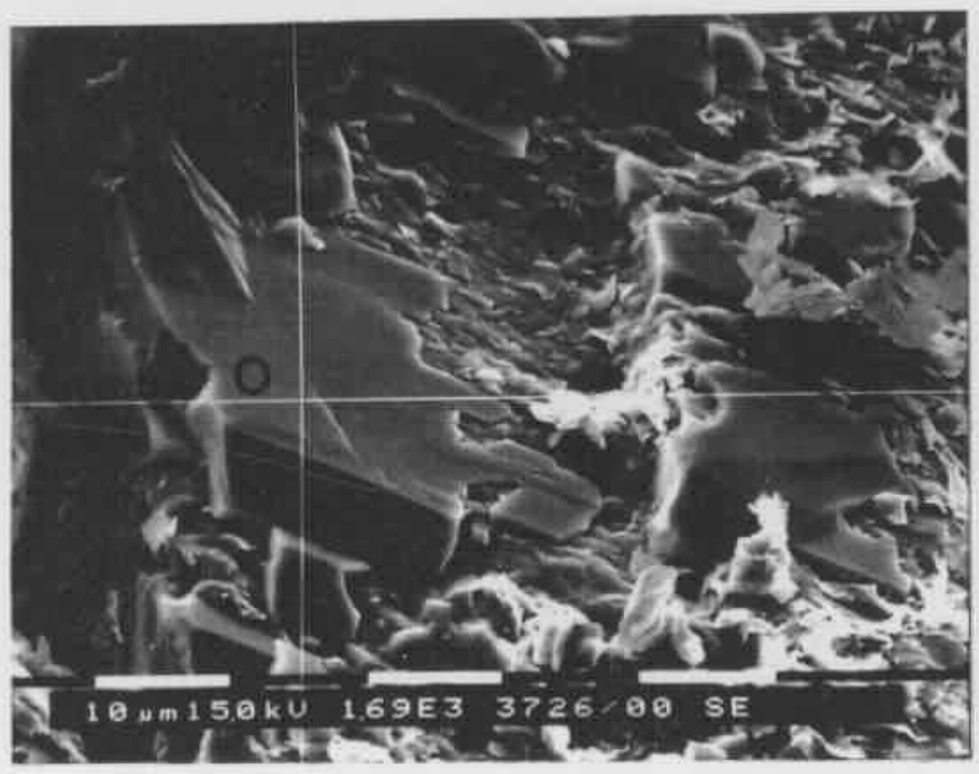
O
10µm15.0kV 1.69E3 3726/00 SE

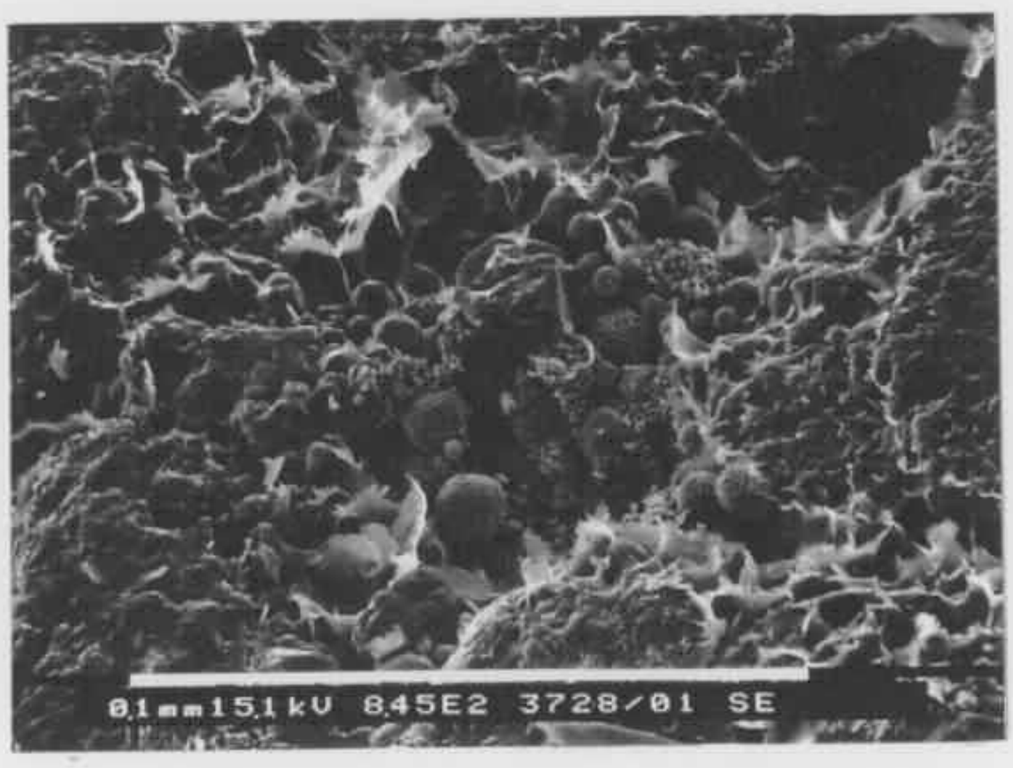
0.1mm15.1kV 8.45E2 3728/01 SE


10µm15.0kV 3.38E3 3729/01 SE


0.1mm15.0kV 8.45E2 5462/01 SE

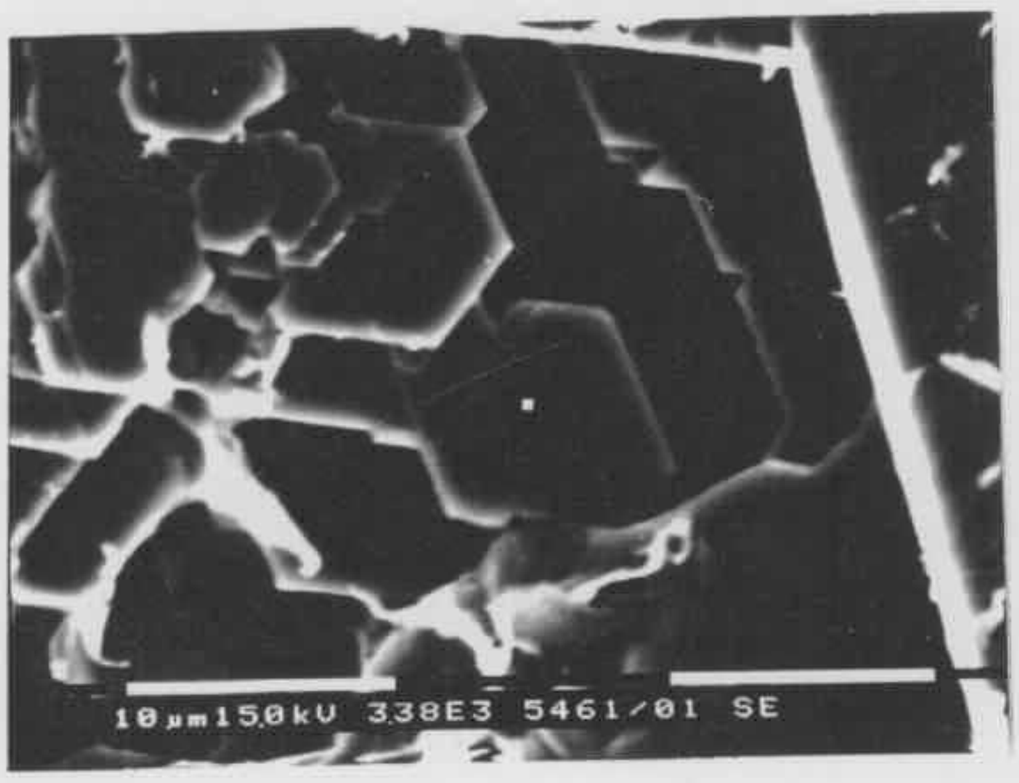
10µm15.0kV 3.38E3 5461/01 SE

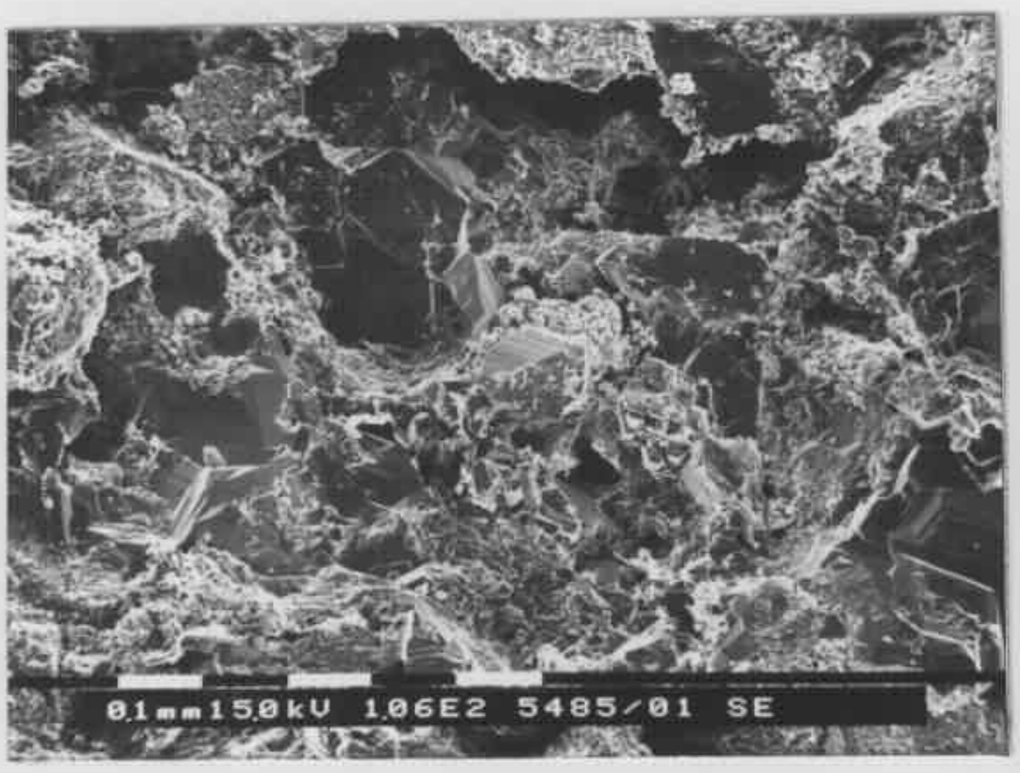
0.1mm15.0kV 1.06E2 5485/01 SE

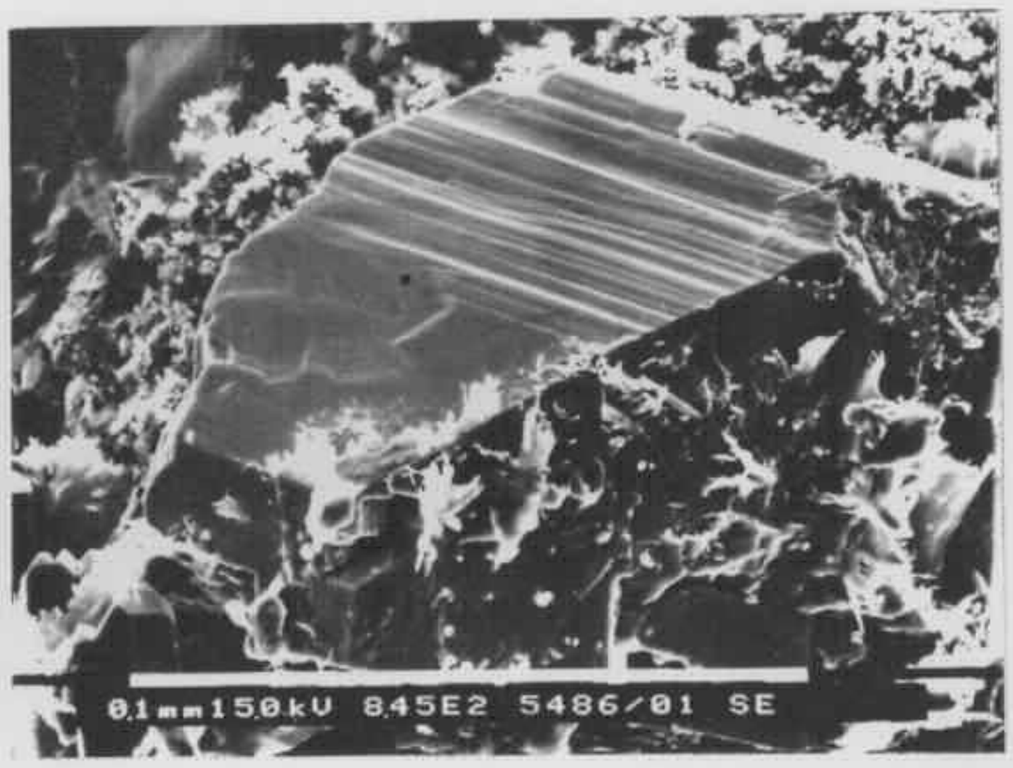
0.1mm15.0kV 8.45E2 5486/01 SE

Fig 6-79 (top left) Authigenic analcime (see Fig 6-80 for enlargement) resulting from alteration of a detrital grain. From Campbelltown 2 at drilling depth of 703.3 m (sample Z703.3).

Fig 6-80 (top right) Enlargement of Fig 6-79. I marks illite and a analcime.

Fig 6-81 (upper left) Authigenic dawsonite lining inter-grain pore spaces. From Murrays Run 1 at drilling depth of 751.7 m (sample F751.7).

Fig 6-82 (upper right) Enlargement of Fig 6-81 and d marks dawsonite.

Fig 6-84 (lower left) Euhedral siderite crystals enclosing subhedral to euhedral calcite crystals. From Weromba 2 at drilling depth of 300.8 m (sample W300.8).

Fig 6-85 (lower right) Enlargement of Fig 6-84. S marks siderite and C calcite.

Fig 6-86 (bottom left) Euhedral siderite crystals (S) enclosing euhedral calcite crystals (C). From Weromba 2 at drilling depth of 300.8 m (sample W300.8).

Fig 6-87 (bottom right) Pore-filling calcite (C) with a rim of iron-bearing clay (chlorite ?). The cross point of the two white lines is the point where EDX analysis was made. Refer to Fig 6-89b for the EDX spectrum. From Liverpool 91 at drilling depth of 579.2 m (sample L579.2).

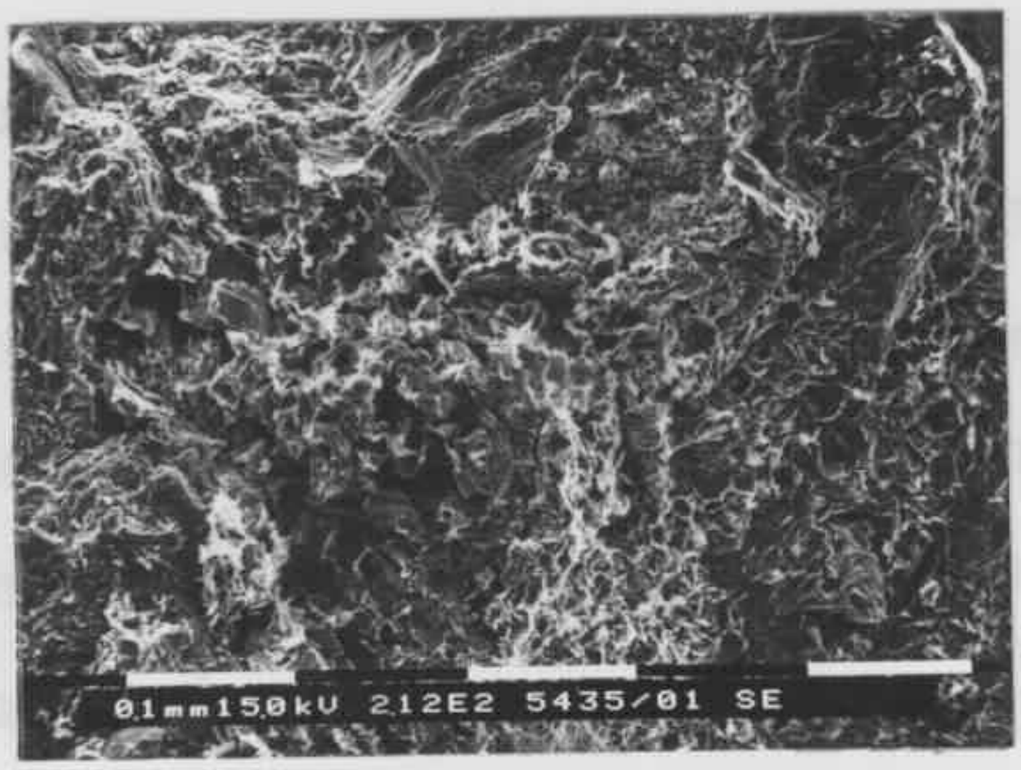
0.1mm15.0kV 2.12E2 5435/01 SE

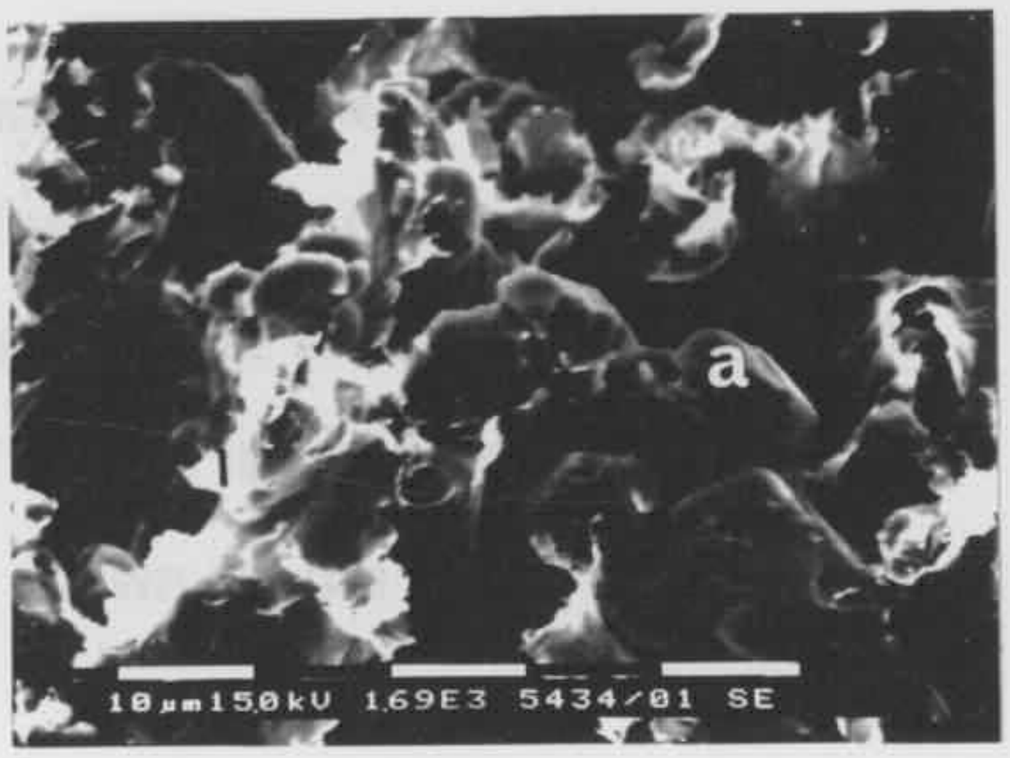
a
10µm15.0kV 1.69E3 5434/01 SE


10µm15.0kV 1.25E3 4587/00 SE

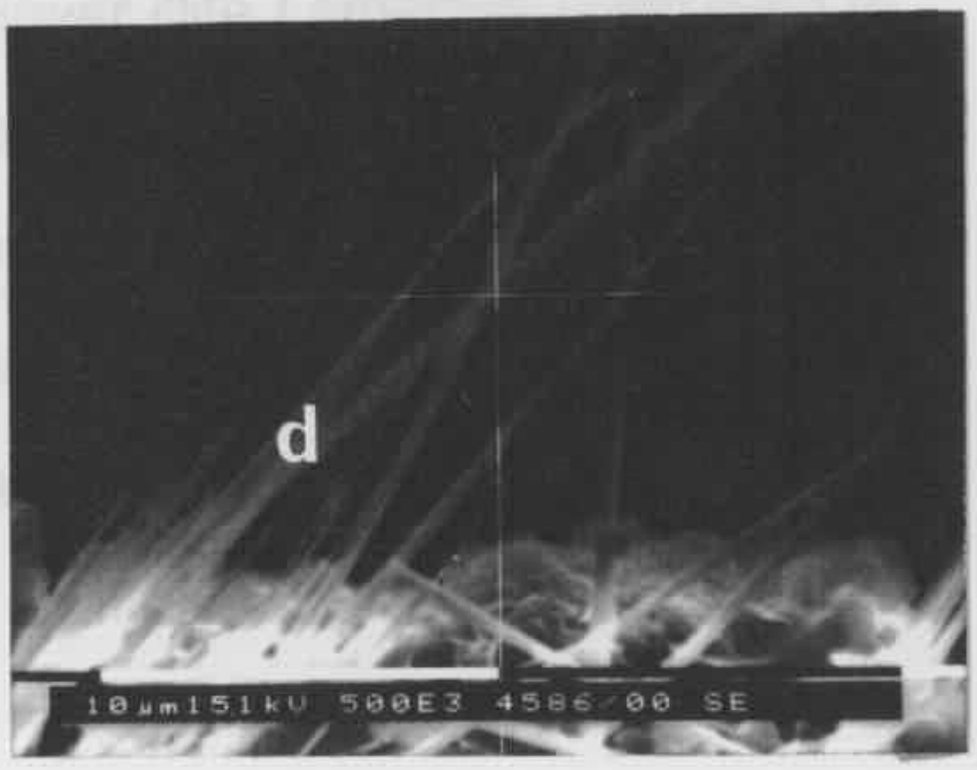
d
10µm15.0kV 500E3 4586/00 SE


0.1mm15.0kV 8.45E2 3903/01 SE

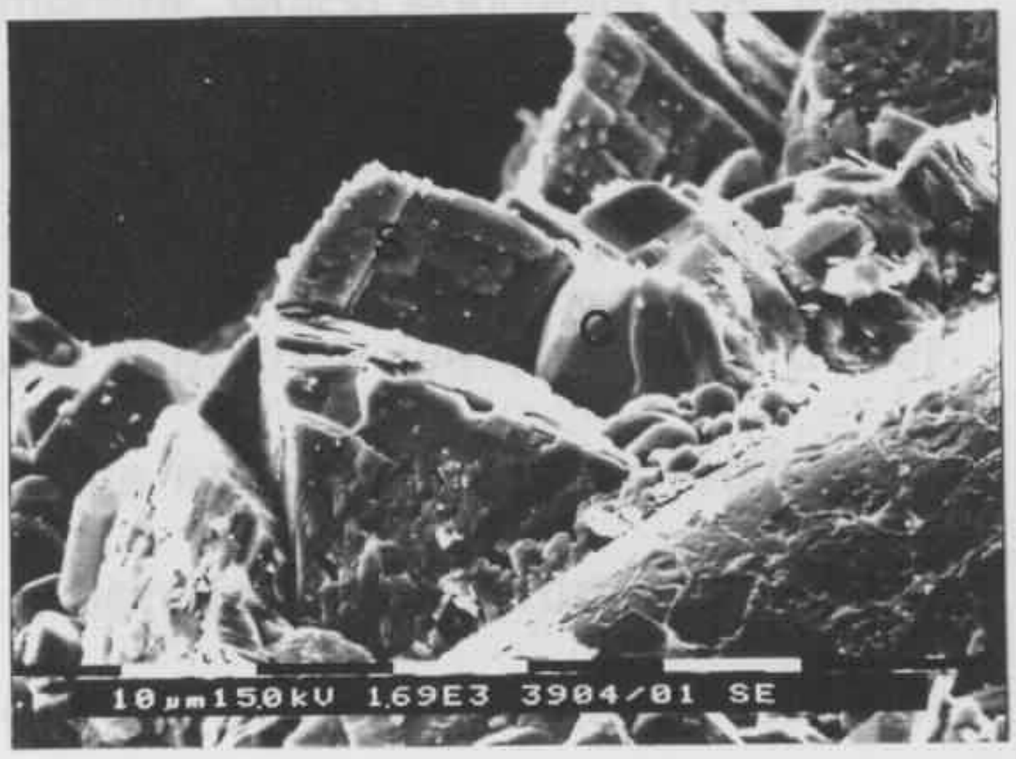
10µm15.0kV 1.69E3 3904/01 SE

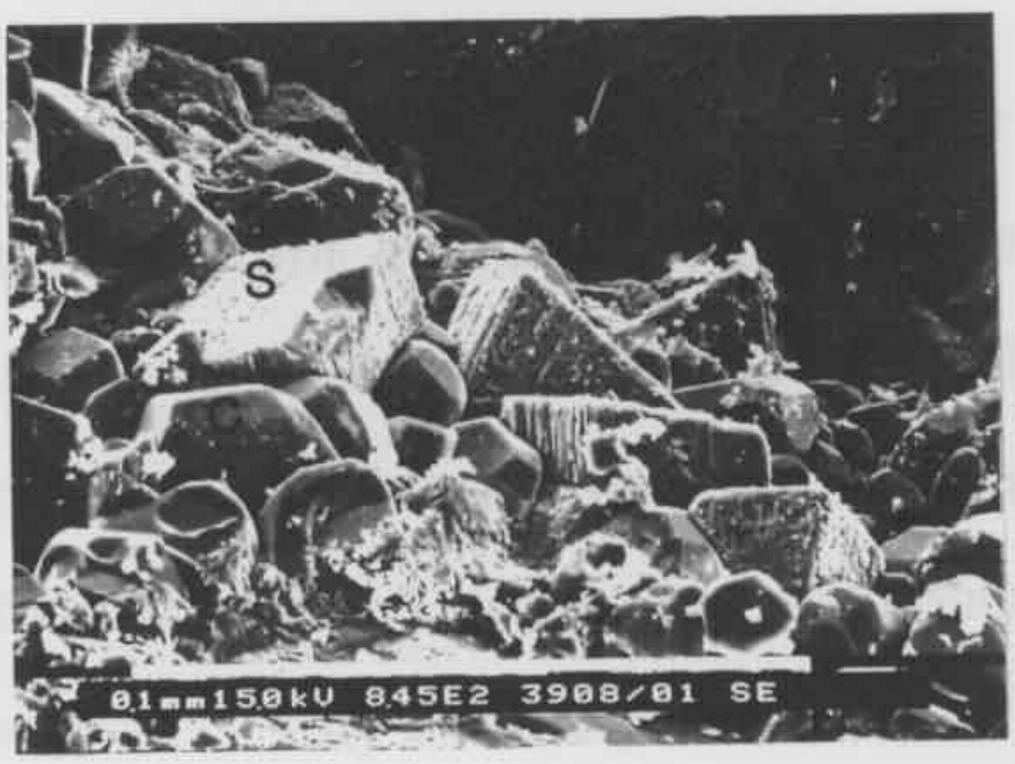
S
0.1mm15.0kV 8.45E2 3908/01 SE

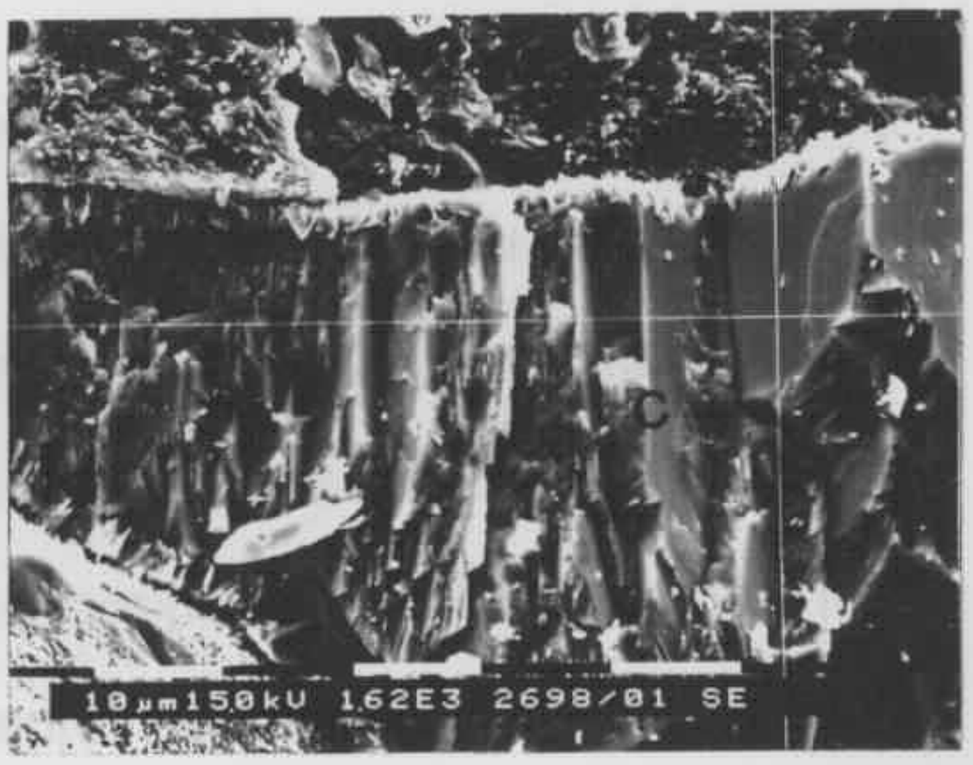
C
10µm15.0kV 1.62E3 2698/01 SE

under the SEM / EDX and petrological microscope, a paragenetic sequence is established and summarised in Fig 6-83. The criteria used to deduce the paragenetic sequence are mainly texture characteristics. It should be mentioned that the paragenetic sequence is a compound one. It is unlikely that one single sample contains all the authigenic minerals shown in the entire paragenetic sequence.

Grain coating haematite and grain coating mixed-layer illite / smectite (Figs 6-45 to 6-48) and chlorite (Figs 6-52 to 6-55) are among the earliest products of diagenesis of the sandstones in the Narrabeen Group. The evidence for this interpretation is that they are the closest to the detrital grains and are enclosed by other diagenetic minerals (Figs 6-45 & 6-52). Haematite, as very thin coatings on some detrital grains, could even be formed in the detrital source areas.

Some stacked kaolin flakes (Figs 6-47 & 6-48), i.e. first generation of kaolin, coexist with the early grain coating mixed-layer illite / smectite, which suggests that these kaolin flakes are also among the earliest products of diagenesis. But the grain coating illite / smectite and early kaolin are not found together with the early grain coating chlorite. This mutual exclusion suggests that they were formed under different physico-chemical conditions. Illite / smectite and kaolin were precipitated from oxygenated and mildly acidic pore waters whereas chlorite from anoxic and neutral to mildly alkaline pore waters. This will be discussed further in later sections.

Carbonate cementation is the next major diagenetic event. In different parts of the basin, different carbonates and different habits of the same carbonate were precipitated. In a few quartz-rich sandstones from west margin and the western portion of the southern region of the basin, carbonates were precipitated as non-ferroan calcite and siderite crystals coating detrital grains. The calcite was the first precipitated. Very small equant anhedral to subhedral calcite crystals are enclosed

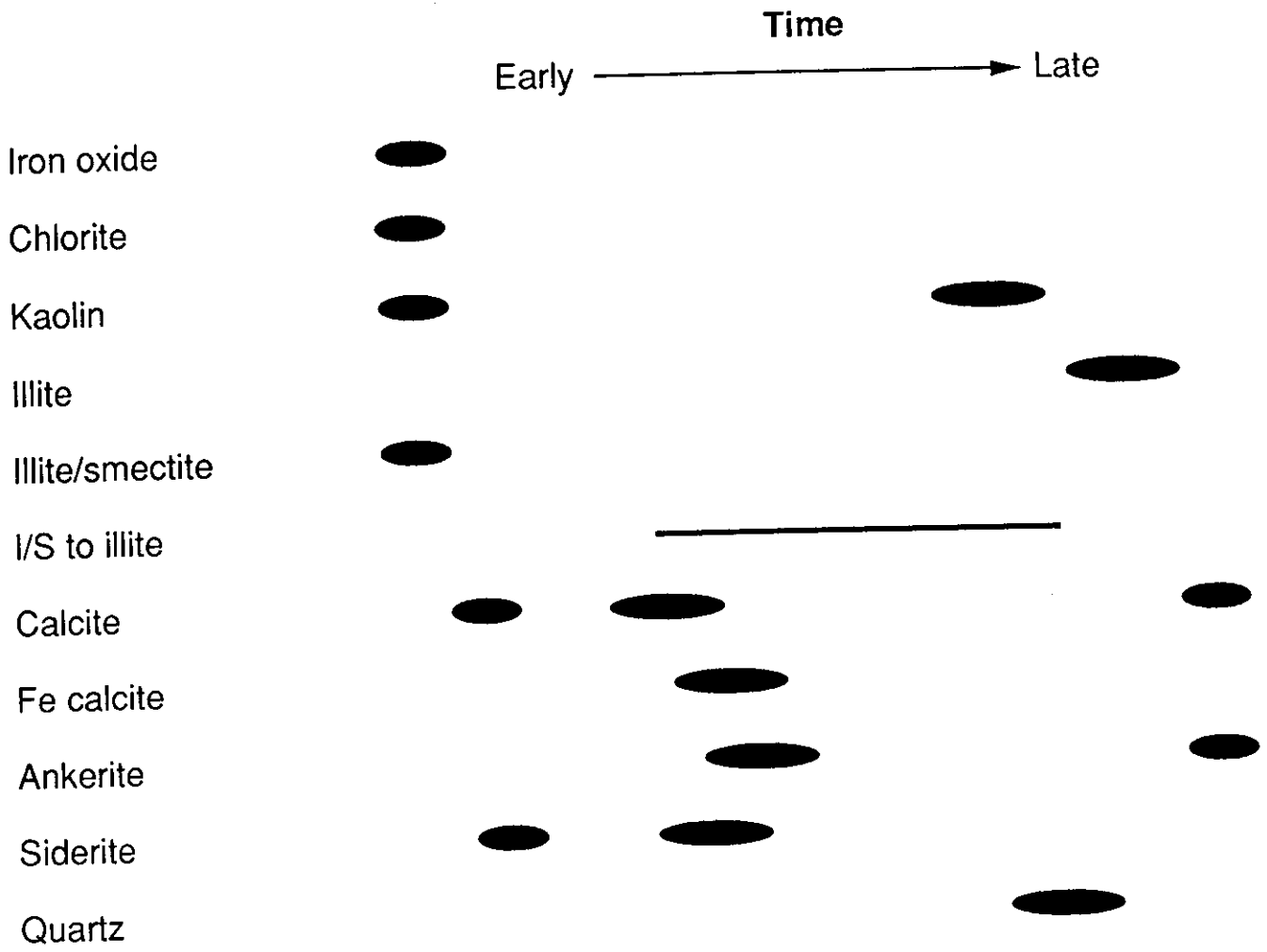

Fig 6-83 Generalised paragenetic sequence of the diagenetic minerals in the Narrabeen Group sandstones.

by small equant subhedral to euhedral calcite crystals (Fig 6-2). The small size and poor crystal morphology of the non-ferroan calcite crystals suggests that they were rapidly precipitated from a supersaturated pore water (cf. Folk, 1974). The coarsening of calcite crystals toward the pore centre (Fig 6-2) may be a distinctive characteristic of early cementation in a freshwater (meteoric water) phreatic environment (Loucks, 1977). Following the calcite cementation, siderite cementation took place. This is supported by the textural relationship: non-ferroan calcite crystals are enclosed by uniform rhombohedral siderite crystals (Figs 6-84 to 86).

In some lithic-rich sandstones from the east coast zone and the northern region of the basin, calcite cements and replacements are abundant. Calcite, including cement and replacement, accounts for more than 10 % of the total sandstone (point count data). Calcite cement generally fills inter-grain pore spaces as anhedral to euhedral crystals and they enclose coating chlorite (?) if present (Figs 6-87, 6-88, 6-89a & 6-89b). The large crystal size of the pore filling calcite cement (Figs 6-3 & 6-4) and the "floating" appearance of detrital framework grains within the calcite cement are considered to be evidence for the early formation of calcite in these sandstones.

In the majority of sandstones containing two or more different kinds of carbonates, the clear textural relationships showing the formation sequence were not always found. This limited the determination of the paragenetic sequence among these carbonates. However, some clear texture relationships have been found in a few sandstones. In one of the sandstones studied (sample X531.9), uniform, rhombohedral siderite crystals are enclosed by a large euhedral ankerite crystal (Figs 6-10 & 6-11). This textural relationship was taken as evidence for the late formation of ankerite. In another sample I437.4, the euhedral Ca, Mg-rich siderite is enclosed by the anhedral Fe calcite (Figs 6-90, 6-89c & 6-89d), which suggests that the Fe calcite is later.

Fig 6-88 (top left) Enlargement of Fig 6-87. The cross point of the two white lines is the point where EDX analysis was made. Refer to Fig 6-89a for the EDX spectrum. Ch marks possible chlorite.

Fig 6-90 (top right) Euhedral Ca Mg siderite (S) enclosed by anhedral Fe calcite (Fe C). The cross point of the two white lines and the black dot are the points where EDX analyses were made. Refer to Figs 6-89c and 6-89d for the EDX spectrum. From Oil Longley 1 at drilling depth of 437.4 m (sample l437.4).

Fig 6-91 (upper left) Secondary mould pore space (P). From Weromba 2 at drilling depth of 300.8 m (sample W300.8).

Fig 6-92 (upper right) Dissolved detrital potassium feldspar grain. From Oil Longley 1 at drilling depth of 320.1 m (sample l320.1).

Fig 6-93 (lower left) Dissolved detrital plagioclase grain. From Murrays Run 1 at drilling depth of 113.9 m (sample F113.9).

Fig 6-94 (lower right) Post quartz overgrowth calcite. From Oil Longley at drilling depth of 781.5 m (sample l781.5).

Fig 6-95 (bottom left) Enlargement of Fig 6-94. The cross point of the two white lines is the point where EDX analysis was made. Refer to Fig 6-96a for the EDX spectrum. Q marks quartz overgrowth and C calcite.

Fig 6-97 (bottom right) Post quartz overgrowth (Q) ankerite (A). The cross point of the two white lines is the point where EDX analysis was made. Refer to Fig 6-96b. From Coal Cliff 17 at drilling depth of 151.7 m (sample B151.7).


Ch
10 µm 15.0 kV 6.50E3 2697/01 SE


S
Fe
0.1 mm 15.0 kV 8.45E2 3709/00 SE

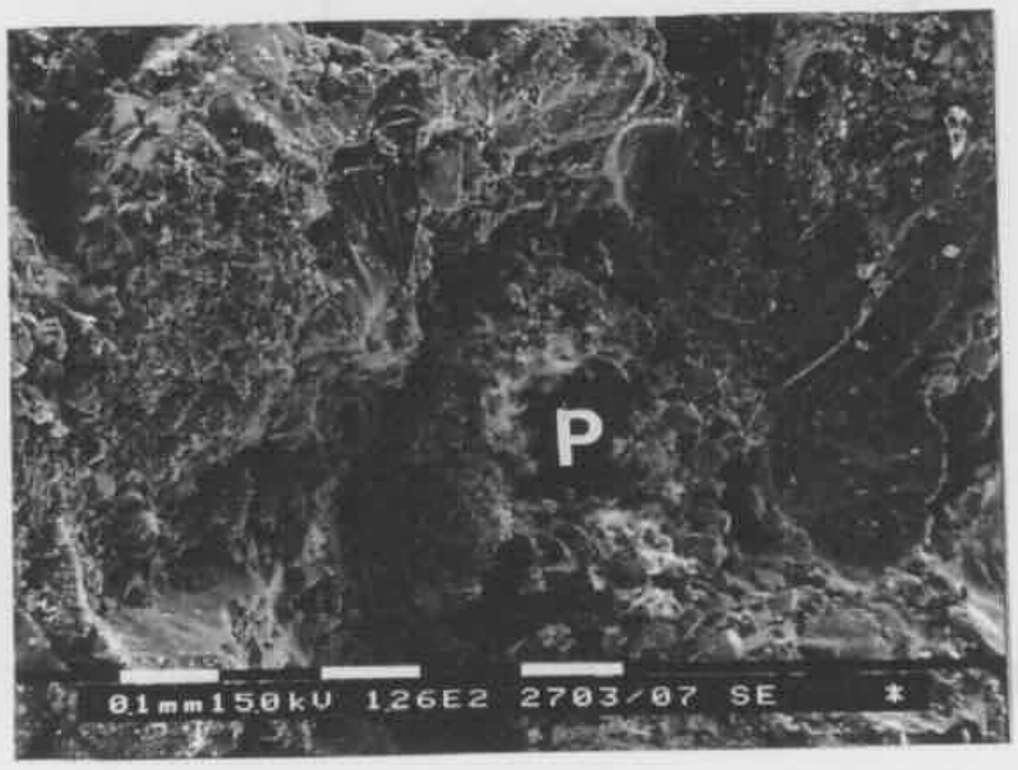
P
0.1 mm 15.0 kV 1.26E2 2703/07 SE


0.1 mm 15.0 kV 8.45E2 3688/00 SE

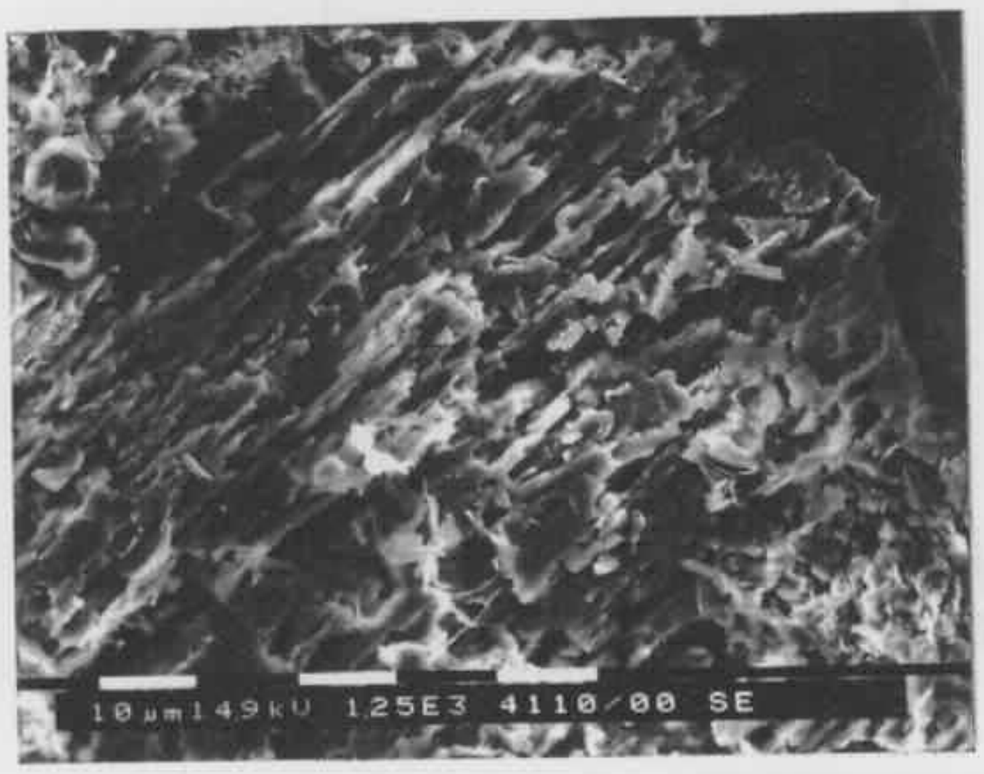
10 µm 14.9 kV 1.25E3 4110/00 SE

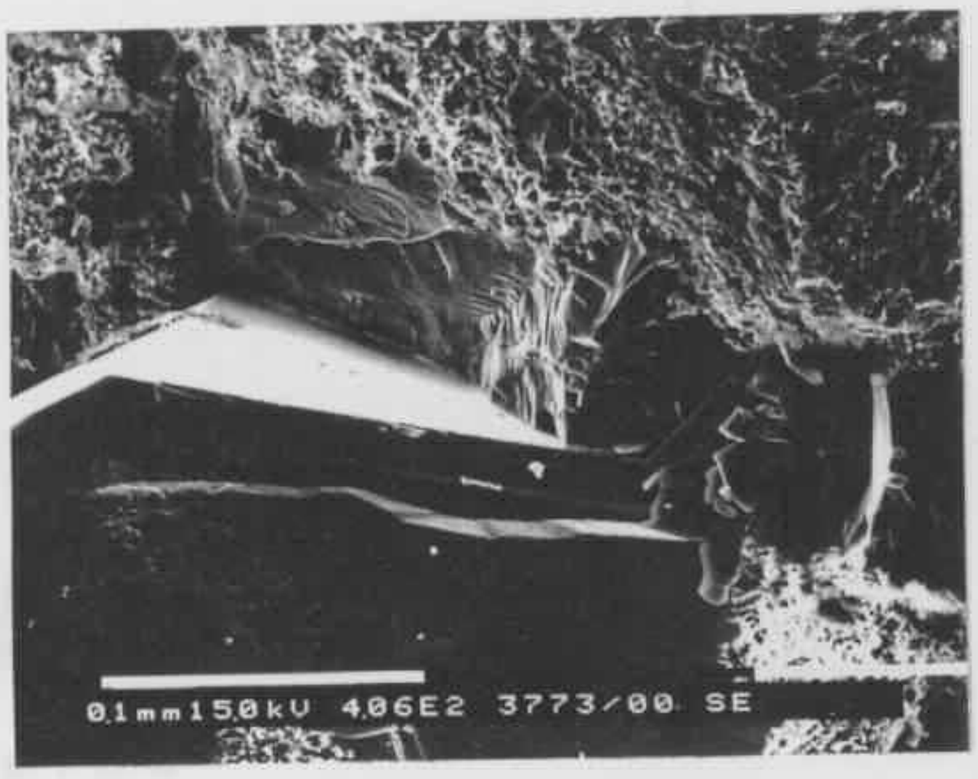
0.1 mm 15.0 kV 4.06E2 3773/00 SE

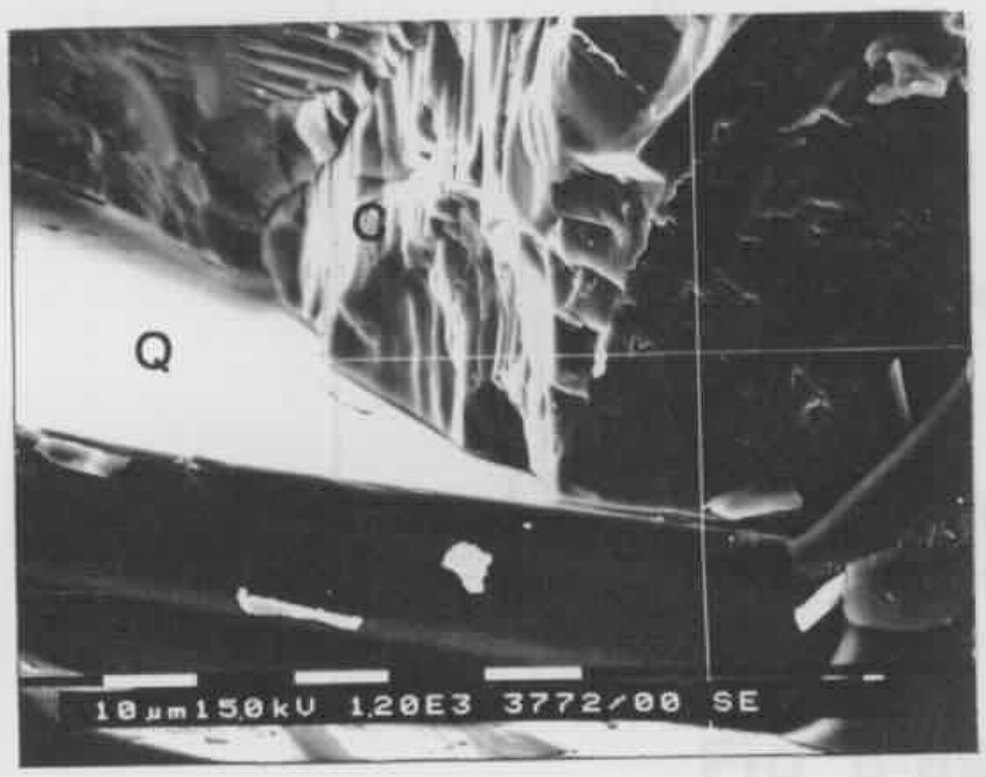
Q
Q
10 µm 15.0 kV 1.20E3 3772/00 SE

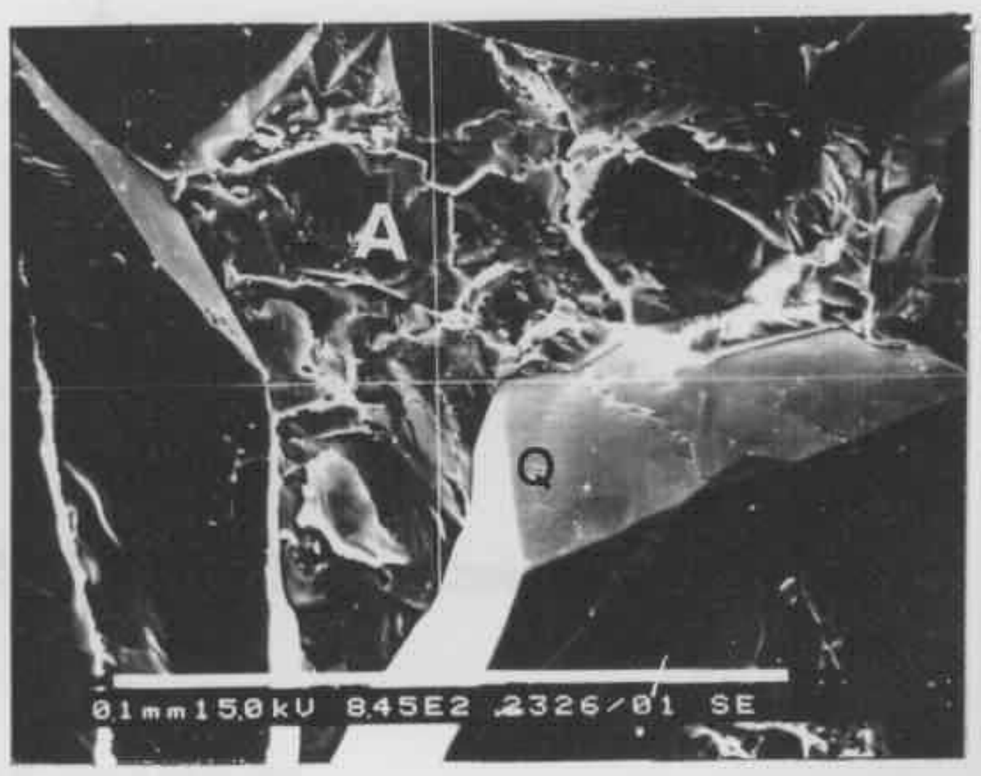
A
Q
0.1 mm 15.0 kV 8.45E2 2326/01 SE

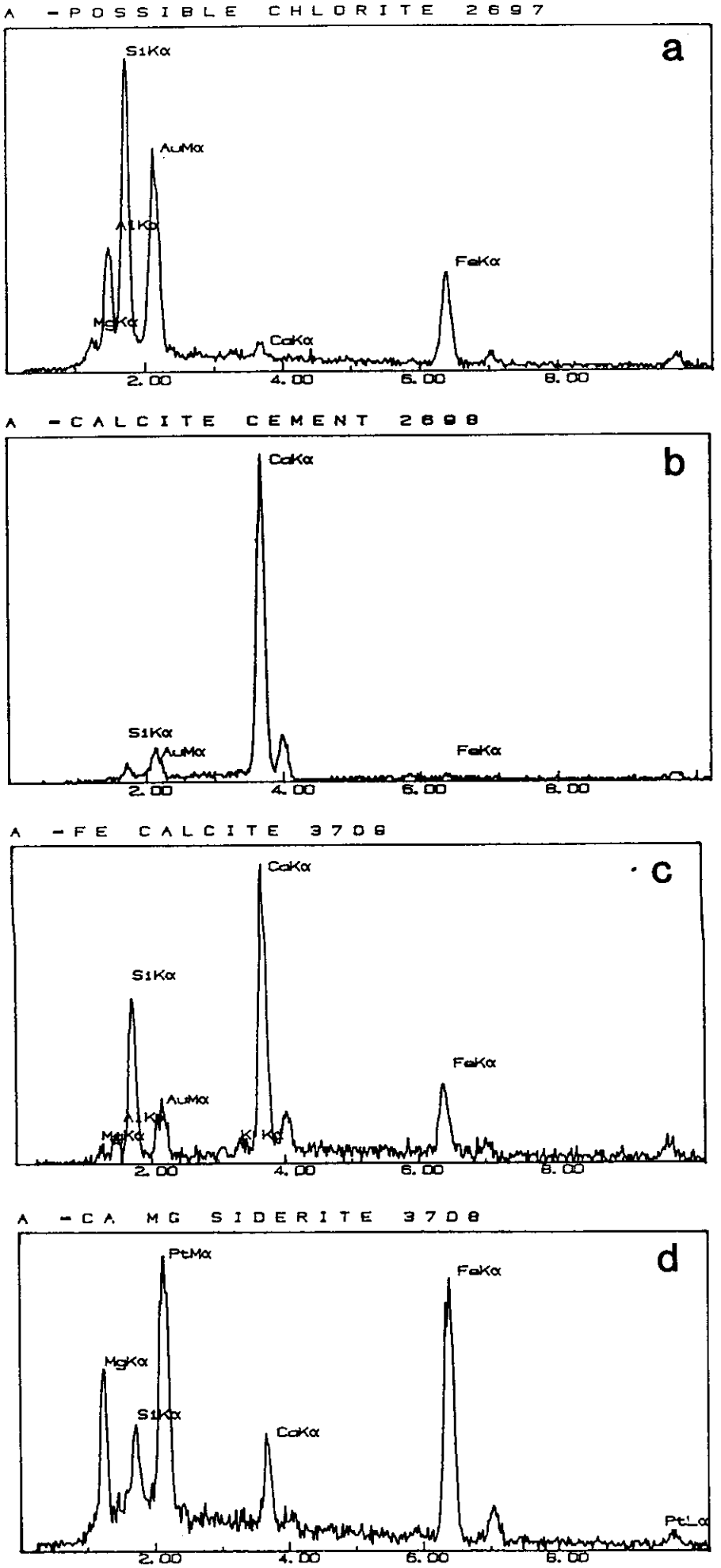

Fig 6-89 EDX spectrum.

In summary, among these diagenetic carbonates, grain coating non-ferroan calcite was the earliest formed carbonate, which was followed by grain coating siderite, pore-filling calcite, pore-filling siderite, and finally pore-filling ferroan calcite and ankerite (Fig 6-83). Because of the rare occurrence of dolomite, no clear textural relationship with other kinds of carbonates has been found.

The major carbonate cementation episode was followed by dissolution processes and the extensive alteration of unstable detrital grains. The textural evidence includes the following: 1) the secondary mould pore space (Fig 6-91), 2) the presence of dissolved siderite (Fig 6-33), ferroan calcite (Fig 6-6), and ankerite (Fig 6-28) as well as dissolved detrital potassium feldspar (Fig 6-92) and plagioclase (Fig 6-93) grains, and 3) the alteration of unstable detrital particles into kaolin / quartz (Figs 6-29 & 6-31) or illite / quartz (Fig 6-38).

During the major dissolution / alteration processes, a relatively large amount of kaolin (second generation) as well as a minor amount of pore lining and bridging illite formed. Evidence for this is the presence of kaolin and illite on carbonate crystals (Figs 6-33 & 6-40) and filling of secondary pore spaces by kaolin (Fig 6-28) and illite (Fig 6-91). Prismatic quartz (mega-quartz) crystals (Figs 6-29 & 6-64), which occur with stacked kaolin flakes within altered detrital grains, were also formed during the alteration process. SEM / EDX studies show that illite / prismatic quartz crystals or kaolin / prismatic quartz crystals take the original outline of altered detrital grains (Figs 6-29 & 6-38). This feature is taken as evidence which supports the conclusion that the alteration happened after the major carbonate cementation. Otherwise the altered, easily compacted detrital grains would show obvious compaction features.

Precipitation of kaolin continued until, and in some sandstones probably after, precipitation of quartz overgrowths, which is the next major diagenetic event. The

textural evidence for this interpretation is the intergrowth of kaolin with quartz overgrowths and the existence of kaolin on the smooth surface of well developed quartz overgrowths (Figs 6-26 & 6-33). The textural evidence for the late formation of quartz overgrowths includes: 1) quartz overgrowths enclose the stacked kaolin flakes (Fig 6-34), 2) they engulf euhedral carbonate crystals (Figs 6-6, 6-12 & 6-19), and 3) the detrital quartz grains coated by carbonate crystals rarely have quartz overgrowths. In addition, the high average homogenisation temperature of 95-120°C of aqueous fluid inclusions within quartz overgrowths is another evidence for late formation of quartz overgrowths, which will be discussed in the next chapter.

Authigenic illite formed after quartz overgrowths. It occurs on the well-developed surfaces of quartz overgrowths (Figs 6-43 & 6-44) and bridges inter-grain pore spaces with a filamentous morphology.

Following quartz overgrowths, carbonate cementation again took place. The carbonate occurs as pore filling non-ferroan calcite (Figs 6-94, 6-95 & 6-96a) or ankerite (Figs 6-97, 6-98, 6-96b & 6-96c). They fill inter-grain pore spaces which were not fully occupied by quartz overgrowths. They are the last diagenetic phase in the Narrabeen Group sandstones.

Authigenic albite and albitisation of plagioclase are considered to be related to the major dissolution / alteration processes. The timing relative to other diagenetic minerals is still to be determined. Dawsonite is another late diagenetic mineral. Its exact position in the generalised paragenetic sequence is not known

Finally there are other authigenic minerals to be considered: pyrite, apatite, anatase, and analcime. Since no clear textural relationships relating them with other authigenic minerals have been found, their position in the diagenetic

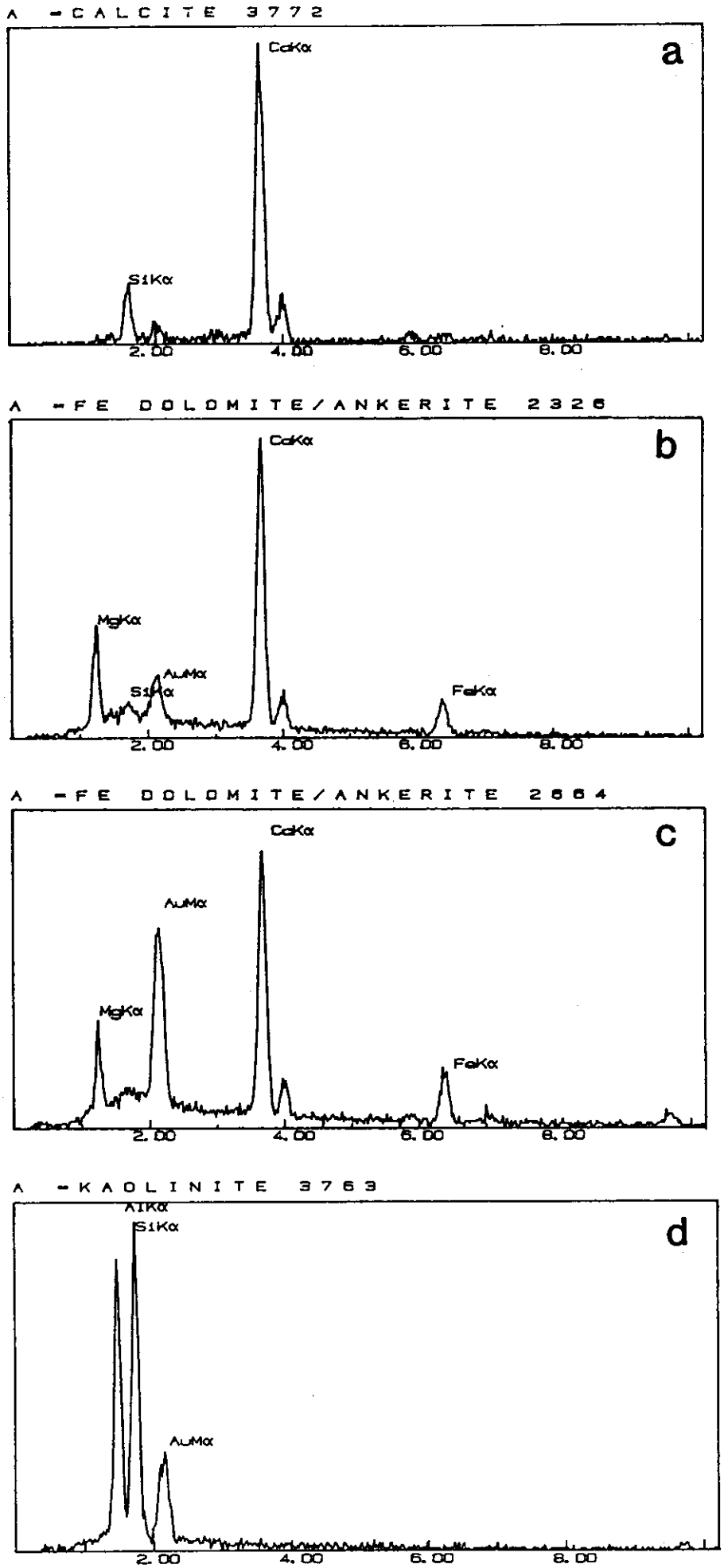

Fig 6-96 EDX spectrum.

sequence is uncertain. The authigenic pyrite is an early product of diagenesis and formed in the bacterial sulphate reduction zone. The formation of analcime is probably related to the alteration of volcanic rock fragments. It may be formed during the extensive alteration of unstable detrital grains and the formation postdated the major carbonate cementation.

6.5 DISCUSSION OF DIAGENESIS OF THE NARRABEEN GROUP SANDSTONES

The diagenesis of sandstones of the Narrabeen Group can be divided into two broad stages: early and late diagenesis. The former ended with the major carbonate cementation. The latter began with the major dissolution / alteration. The early diagenesis includes two phases. Phase I refers to the early minor dissolution / alteration of unstable detrital particles (volcanic rock fragments, feldspar and mica), which resulted in the formation of grain coating mixed-layer illite / smectite, early kaolin (generation I) and chlorite. Phase II is characterised by the major carbonate cementation. The late diagenesis consists of three phases: III, IV and V. Phase III refers to the major dissolution / alteration of unstable detrital particles, which led to the formation of a large (relative to generation I) amount of kaolin (generation II) as well as prismatic quartz (mega-quartz) crystals and a minor amount of illite (relative to post quartz overgrowth filamentous illite). Phase IV is represented by the development of quartz overgrowths and the formation of post-quartz overgrowth filamentous illite. The formation of a minor amount of post quartz overgrowth pore filling calcite and ankerite comprise the last phase of diagenesis.

The five phases of diagenesis are not found in all the samples studied. In the sandstones cemented by abundant carbonate (Figs 6-3, 6-4, 6-8, 6-13 & 6-14) in the lower Narrabeen Group from the east coast zone and the northern region of the basin, only the early diagenesis can be recognised. Other sandstones generally experienced the early stage of diagenesis and the phases III and IV of the late stage of diagenesis. The last diagenetic phase (phase V) is found only in two

sandstones (samples B151.7 and L422.3) in the east coast zone and one sandstone (sample I781.5) in the northern region of the basin.

6.5.1 EARLY STAGE OF DIAGENESIS

(i) Phase I: Formation of Early Clays

Diagenesis begins at the moment of deposition of sediments. Immediately after sediment deposition, pore water will react with the deposited sediment if they are not in equilibrium. These reactions will lead to the dissolution / alteration of unstable detrital grains and precipitation of authigenic minerals. If the pore water migrates, a large amount of authigenic minerals may be formed.

The initial diagenetic modifications of sediments are promoted by bacterial processes. Curtis (1978) suggested that aerobic bacterial bicarbonate production decreases pH (increase the activity of hydrogen ion) and facilitates the dissolution of amorphous and relatively unstable detrital alluminosilicate minerals. The diagenesis of the Narrabeen Group sandstones began with the early minor dissolution / alteration of the unstable detrital minerals, which are composed mainly of volcanic rock fragments and a minor amount of feldspar and mica fragments. They released various cations to pore water. Depending on the availability of cations and physico-chemical conditions of pore waters, different clay minerals formed.

Under oxygenated and mildly acidic conditions, kaolin and mixed-layer illite / smectite were precipitated from oversaturated pore water in sandstones. However, during the early diagenesis only a minor amount of kaolin was formed, which was probably attributed to the lack of Al^{3+} in pore waters. The early grain coating illite / smectite was probably formed by mechanical infiltration of colloidal clay-rich waters through the vadose zone (Galloway, 1974; Burns and Ethridge, 1979). In addition to direct precipitation from pore waters, kaolin and mixed-layer illite /

smectite could also be formed as a result of early alterations of the unstable detrital grains. Their presence at the edges of altered detrital grains supports such an interpretation.

Under anoxic and mildly alkaline conditions, chlorite formed. Chlorite fills inter-grain pore spaces and coat detrital grains. Chlorite coatings are present on various detrital grains including detrital quartz, feldspar and rock fragments (including chert) (see Fig 5-25). This indicates that mineralogy of the coated detrital framework grains apparently does not control the distribution of chlorite coatings. Similar grain coating chlorites have been reported as early diagenetic features in numerous studies in different geological settings. Dutton and Land (1985), Kantorowicz (1985), Dutta and Sutner (1986), Longstaffe (1986), Longstaffe and Ayalon (1987), Ayalon and Longstaffe (1988) and Girard et al. (1989) are among the most recent studies.

The pore filling chlorite differs from the coating chlorite only in the crystal size and euhedrality. The two different forms of chlorites were probably formed at roughly the same time. They generally do not occur together in the same sample, which probably implies that authigenic chlorites had taken different forms in different sandstones due to different physico-chemical conditions. Grain coating chlorites were rapidly precipitated from a supersaturated pore water. In contrast, pore filling chlorites were precipitated from a dilute pore water at a slower rate so that they are larger and more euhedral than coating chlorites.

Chlorite coatings and pore fillings appear to form by direct precipitation from pore waters. But for some chlorites which are associated with altered detrital grains (detrital volcanic rock fragments and feldspar) (Fig 6-99), they are most likely to be created by alteration of these grains. Ions necessary for the formation of chlorite come from alteration of unstable volcanic rock fragments (Land and Dutton, 1978; Davies et al., 1979). Alteration of ferromagnesium alumino-silicates is facilitated

Fig 6-98 (top left) Post quartz overgrowth (Q) ankerite (A). The cross point of the two white lines is the point where EDX analysis was made. Refer to Fig 6-96c for the EDX spectrum. From Liverpool 91 at drilling depth of 422.3 m (sample L422.3).

Fig 6-99 (top right) Authigenic chlorite at the margin of an altered detrital feldspar grain. From Jilliby CK 1 at drilling depth of 128.0 m (sample D128.0).

Fig 6-101 (upper left) Kaolinization of mica. The cross point of the two white lines is the point where EDX analysis was made. Refer to Fig 6-96d for the EDX spectrum. K marks kaolin. From Oil Longley 1 at drilling depth of 629.3 m (sample I629.3).

Fig 6-102 (upper right) Stacked kaolin flakes (K) resulting from extensive dissolution / alteration of a detrital volcanic clast. From Jilliby CK 1 at drilling depth of 102.5 m (sample D102.5).

Fig 6-103 (lower left) Prismatic quartz crystals coalescing to form submature quartz overgrowths (Q). From Cobbitty 3 at drilling depth of 612.9 m (sample X612.9).

Fig 6-104 (lower right) Enlargement of Fig 6-103.

Fig 6-105 (bottom left) Prismatic quartz crystals coalescing and enveloping to form quartz overgrowths (Q). From Oil Longley 1 at drilling depth of 543.4 m (sample I543.4).

Fig 6-106 (bottom right) Well developed quartz overgrowths enveloping micro-quartz crystals, which are in turn enveloped by later quartz overgrowths. From St Albans 1 at drilling depth of 419.7 m (sample H419.7).


Q
01mm15.0kV 7.10E2 2664/01 SE


10µm15.0kV 2.50E3 4022/00 SE

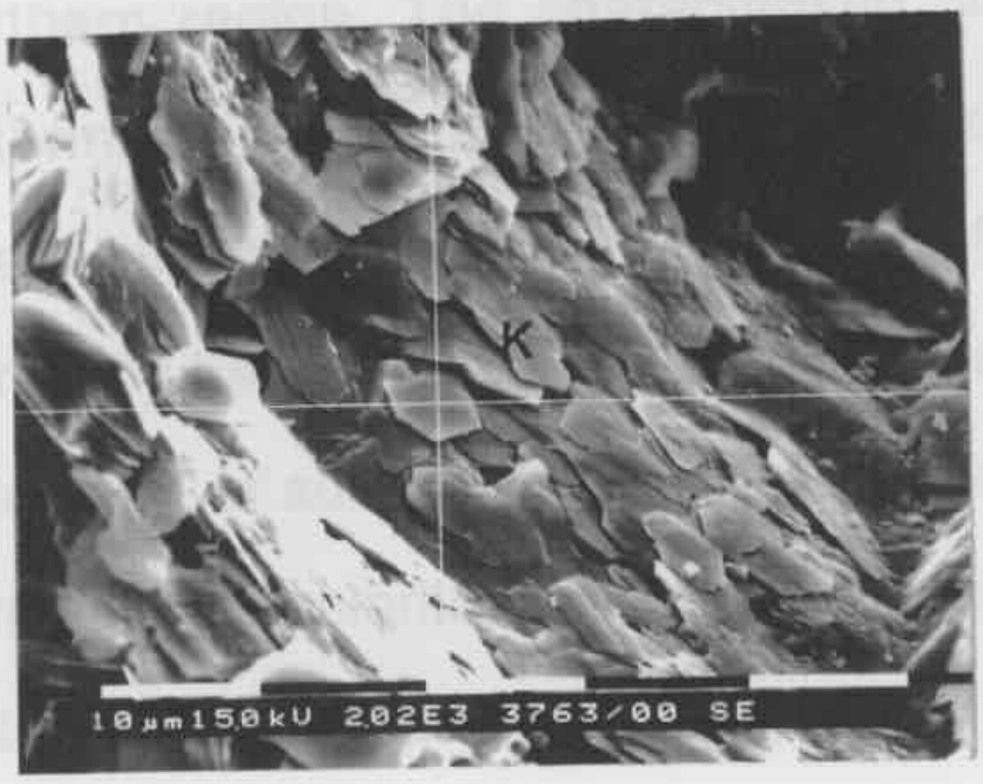
K
10µm15.0kV 2.02E3 3763/00 SE

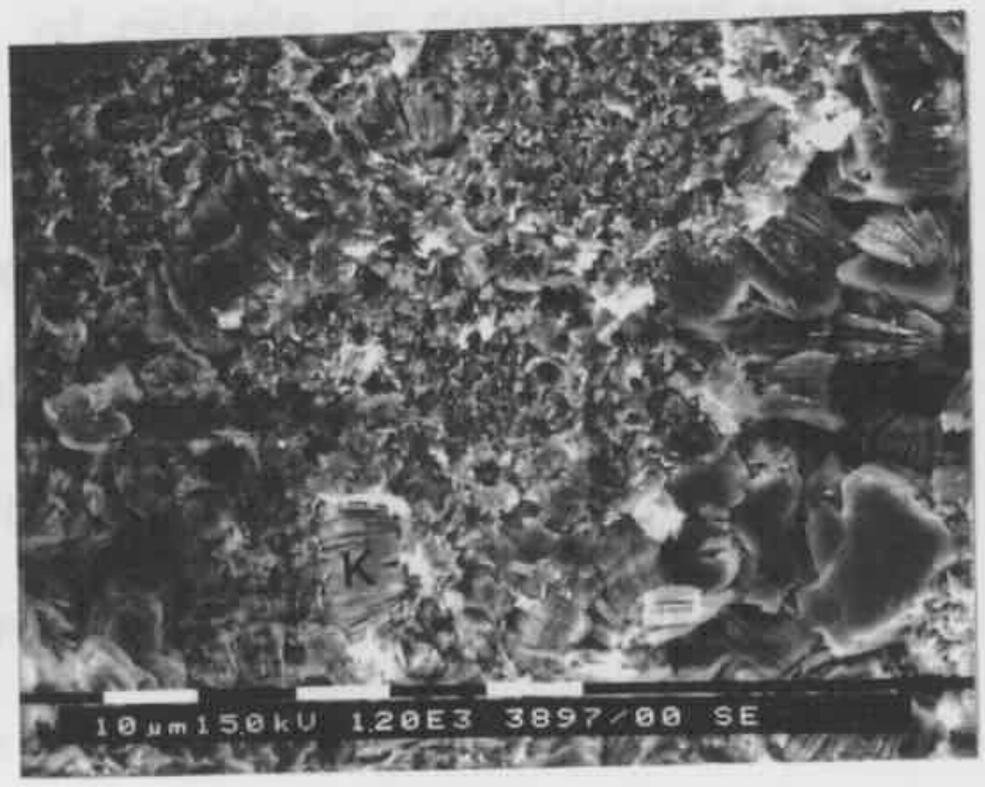
K
10µm15.0kV 1.20E3 3897/00 SE


Q
01mm15.0kV 8.45E2 4380/01 SE

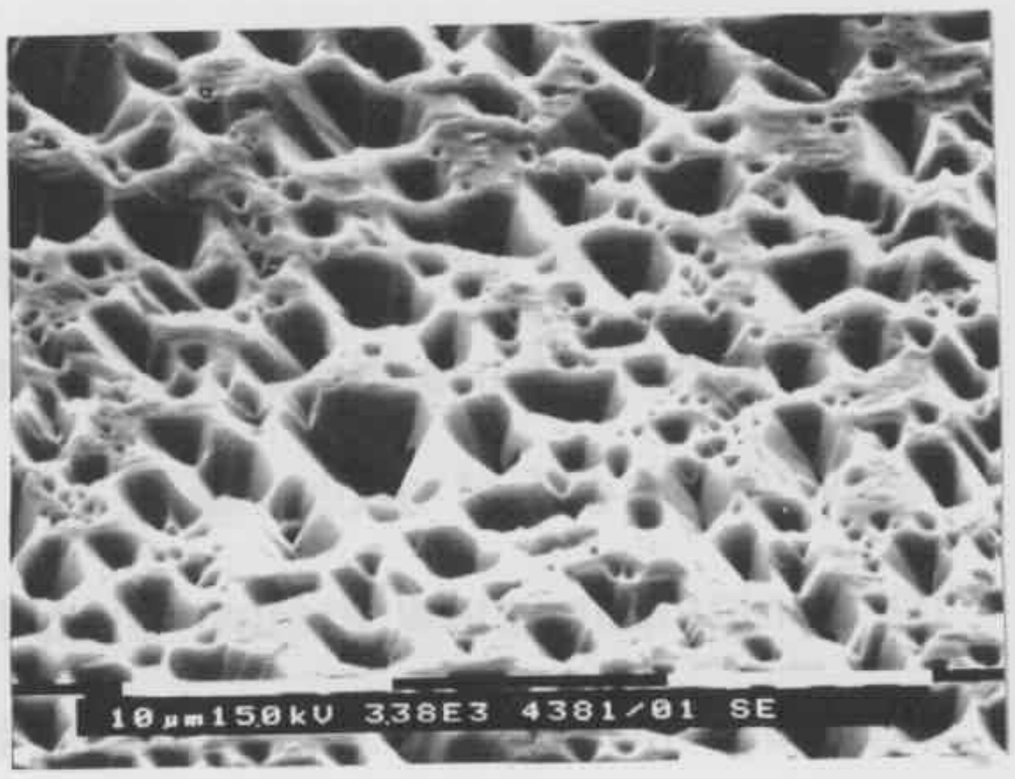
10µm15.0kV 3.38E3 4381/01 SE

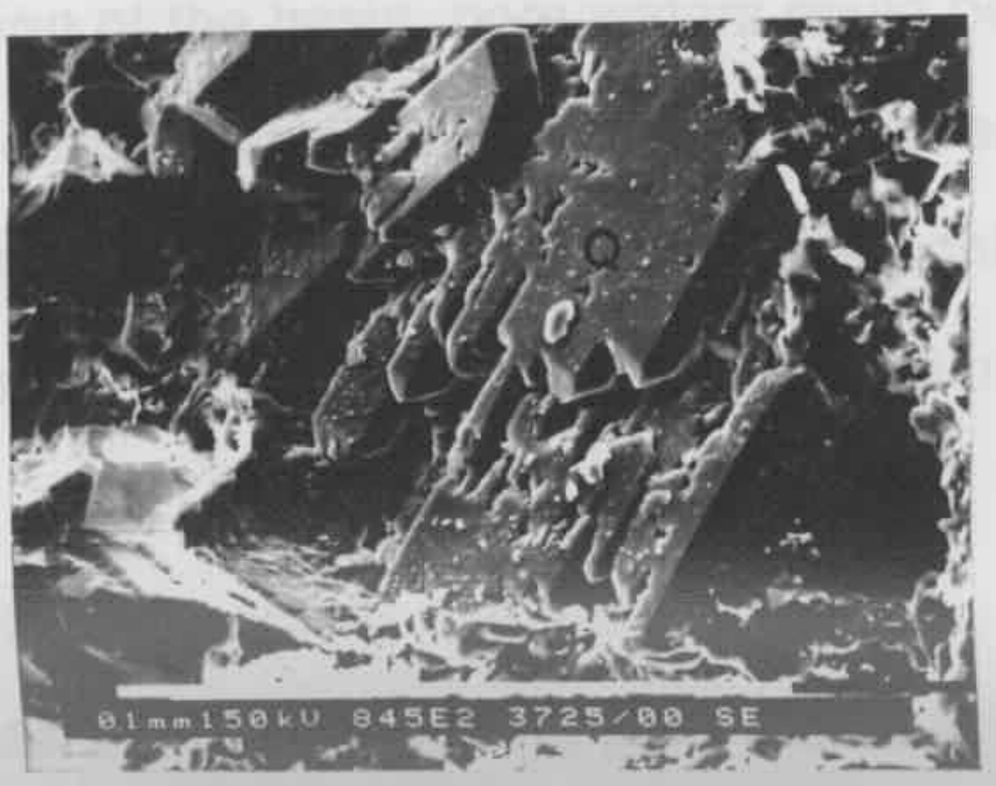
Q
01mm15.0kV 8.45E2 3725/00 SE


01mm15.0kV 6.00E2 3828/00 SE

under reducing, alkaline conditions (Imam and Shaw, 1985). The adjacent shales may also have been the ion source for chlorite, as suggested by Moncure et al. (1984) in the Frio Formation sandstones.

In the Narrabeen Group sandstones, authigenic chlorite was not found together with early kaolin and mixed-layer illite / smectite. It is present in sandstones rich in volcanic rock fragments in the east coast zone and the northeastern portion of the northern region. The characteristic distribution of chlorite is considered to be determined by two factors: detrital composition of sandstones and physico-chemical conditions of pore waters. Sandstones containing authigenic chlorite generally have a significant amount of detrital volcanic rock fragments (Fig 6-100). Alteration of such rock fragments could have provided the necessary ions for the formation of chlorite. A strong relationship between the occurrence of authigenic chlorite and volcanic rock fragments has been demonstrated in many previous studies (e.g. Carrigy and Mellon, 1964; Brenchley, 1969; Surdam and Boles, 1979; Smosna, 1988).

During the initial diagenesis of Narrabeen Group sediments, fresh water recharge was probably from the southwest. In the west margin, southern region and the southwestern portion of the northern region of the basin close to the fresh water recharge, oxygenated and acidic conditions of pore waters were maintained so that kaolin and mixed-layer illite / smectite could have formed. Away from the fresh water recharge in the east coast zone and the northeastern portion of the northern region of the basin, pore waters could become alkaline and anoxic due to bacterial processes which progressively removed all oxygen and raised pH. As a result, chlorite had formed. A similar reasoning was used by Kantorowicz (1985) to explain the mutually exclusive distribution of kaolinite and chlorite.

After the earliest diagenetic minerals, the physico-chemical conditions of pore waters changed and the pore waters in the sandstones in the whole basin became

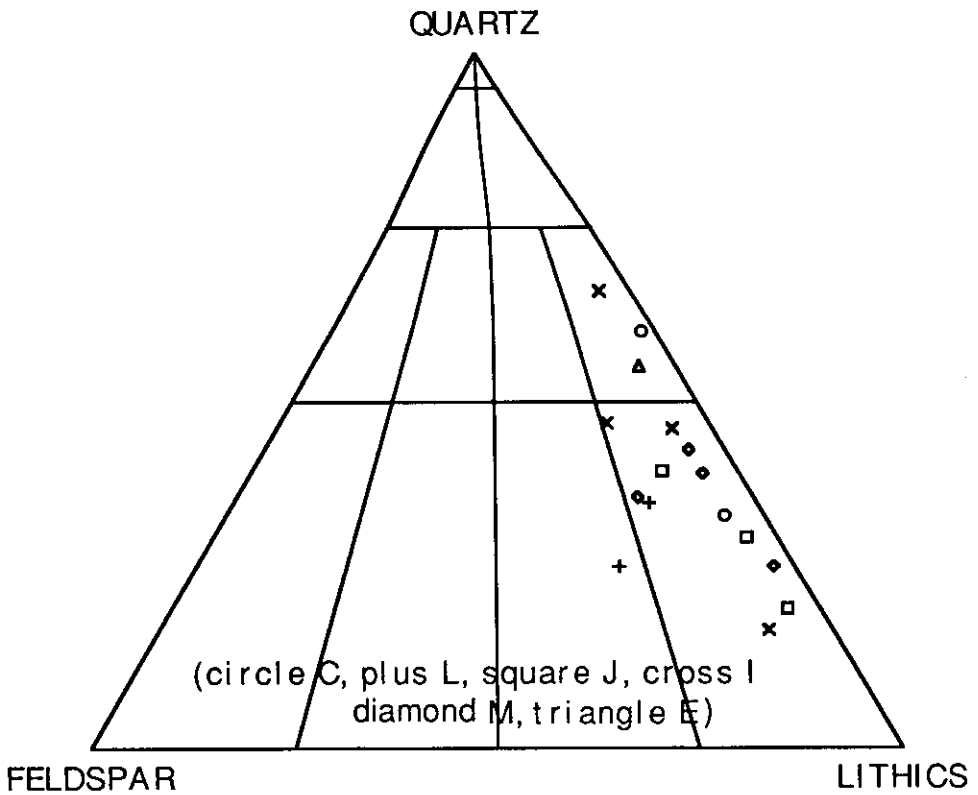

Fig 6-100 Compositions of 16 sandstones containing authigenic chlorites from 6 boreholes.

alkaline. In such conditions carbonates were able to precipitate.

(ii) Phase II Carbonate Cementation

Formation of calcite

Non-ferroan calcite was the first carbonate precipitated from pore waters. Its formation is considered to be determined by the relative abundance of Fe^{2+} and Ca^{2+} in pore waters of sandstones (Berner, 1971; Matsumoto and Iijima, 1981; Kaiser, 1984; Curtis et al., 1986). Calcite was formed in the environment where Fe^{2+} was almost absent.

For calcite and siderite, Berner (1971) established the following reaction:

$$FeCO_3 + Ca^{2+}{}_{aq} = CaCO_3 + Fe^{2+}{}_{aq} \quad (1)$$

siderite calcite

$$K = 0.05 = aFe^{2+}/aCa^{2+}$$

He indicated that calcite was not stable in the pore water where the concentration of Fe^{2+} was greater than 5 percent of that of Ca^{2+}.

Kaiser (1984) proposed the following reaction regarding calcite and ferroan calcite.

$$CaCO_3 + 0.05\ Fe^{2+} = Ca_{.95}Fe_{.05}CO_3 + 0.05Ca^{2+} \quad (2)$$

calcite ferroan calcite

He concluded that the virtual absence of Fe^{2+} was required to form non-ferroan calcite.

In the Narrabeen Group sandstones, the virtual absence of Fe^{2+} in pore waters for the formation of calcite was achieved probably in two ways, which are shown by

the calcite in the sandstones from the west margin of the basin and in the sandstones from the east coast zone and the northern region of the basin.

In samples W300.8 and W310.4 from the west margin, calcite coats detrital grains as very small (2-6 μm) equant anhedral to subhedral crystals and small (10-20 μm) equant euhedral crystals. The calcite crystals predate coexisting siderite crystals. As indicated before they were formed in a fresh water phreatic zone where calcite must have been precipitated in an oxidising environment in order to satisfy the condition for the virtual absence of Fe^{2+}.

In the sandstones from the east coast zone and the northern region of the basin, calcite is present as pore filling cements. It generally does not coexist with other carbonates. In these sandstones chlorite is generally present as the earliest formed authigenic mineral (Figs 6-87, 6-88, 6-89a & 6-89b). Its formation must have greatly reduced the Fe^{2+} concentration in pore waters so that non-ferroan calcite could be precipitated from the pore waters in which Fe^{2+} was virtually absent. The precipitation took place in a reducing environment following chlorite formation.

Ferroan calcite generally coexists with siderite. It followed the formation of siderite. This implies that Fe^{2+} in the pore waters was probably reduced to a large extent after the precipitation of siderite. Thus ferroan calcite could be precipitated directly from the pore waters.

Formation of siderite

The geochemical requirements for the formation of siderite crystals have been investigated by many researchers (e.g. James, 1966; Curtis, 1967; Curtis and Spears, 1968; Berner, 1971, 1980). From their investigations the following general conclusions may be made: 1) Siderite formation requires negative Eh (reducing environment), low sulphide ion concentration, low calcium ion activity, high ferrous

ion activity and the presence of carbon dioxide (HCO_3^-); and 2) It is generally formed in a fresh water (low salinity) environment.

As discussed in Chapter 4, the sediments of the Narrabeen Group were deposited in a fluvial / lacustrine environment. With deposition the sediments were buried and were no longer affected by the surface bacterial activity and environment. Due to the depletion of dissolved oxygen in pore waters with organic decay, a reducing environment evolved and the Fe ions in the pore water existed in the ferrous form. After the pore water became over saturated with $FeCO_3$, siderite crystals were precipitated from the pore water.

Formation of dolomite and ankerite

Dolomite and ankerite are present in the sandstones in the form of pore filling cements and rare replacement of detrital grains. They do not show any texture of replacing calcite or Fe calcite. Thus it is considered that they were precipitated directly from pore waters and not the product of dolomitisation of calcite and Fe calcite. The precipitation probably proceeded according to the following reaction:

$$Ca^{2+} + (Mg,Fe)^{2+} + 2CO_3^{2-} \rightarrow Ca(Mg,Fe)(CO_3)_2 \quad (3)$$

The requirements for the reaction to proceed are high enough carbonate alkalinity (Lippman, 1973), sufficient supply of suitable cations plus sufficient time (Irwin, 1980) and lack of sulphate.

Siderite is the most commonly found carbonate in the Narrabeen Group and occurs in the majority of samples studied under SEM / EDX. Another Fe^{2+} bearing carbonate - ankerite is also commonly found in the lower Narrabeen Group sandstones. The extensive presence of siderite and ankerite, together with the existence of ferroan calcite, rare pyrite and iron rich chlorite strongly suggests that

Fe^{2+} was present in relatively high concentration in pore waters during the diagenesis of the Narrabeen Group sandstones. The extensive presence of Fe^{2+} during carbonate cementation limited the formation of non-ferroan calcite.

Fe^{2+} used in the formation of Fe-bearing carbonates seems to be largely derived from redox reactions in adjacent shales / mudstones. Iron oxides and hydroxides produced by weathering in the detrital source areas may be absorbed on detrital clay particles and have been transported to the basin. In reducing conditions, they can be reduced to ferrous iron according to the following reactions:

$$6(CH_2O) + 3SO_4^{2-} + 2\,FeOOH \rightarrow FeS + FeS_2 + 6HCO_3^- + 4H_2O \text{ (Irwin, 1980)} \quad (4)$$

or

$$2Fe_2O_3 + CH_2O + 3H_2O \rightarrow HCO_3^- + 4Fe^{2+} + 7OH^- \text{ (Curtis et al., 1986)} \quad (5)$$

Reaction (4) occurs during sulphate reduction. The authigenic pyrite found in a few sandstones probably formed according to this reaction. The rare occurrence of authigenic pyrite in the Narrabeen Group sandstones is related to the lack of a SO_4^{2-} source. The low dissolved sulphate in circulating meteoric pore waters limited the formation of pyrite and sulphate reduction was not a significant process during burial diagenesis of the Narrabeen Group.

Iron may be also released directly from organic matter since it complexes with humic acids (Picard and Felbeck, 1976), and is present in iron porphyrins of "life pigment" (Irwin, 1980). Alteration of volcanic rock fragments was another source for the Fe^{2+} used in the formation of iron-bearing carbonates.

Microprobe analyses of the carbonates indicate calcites, siderites and ankerites all have a small amount of $MnCO_3$. Mn in the carbonates is considered to be largely derived from reduction of Mn^{4+} oxides (produced in detrital source areas and

transported to the basin) in the adjacent shales / mudstones in a similar manner to reduction of Fe^{3+} oxides [refer to reaction (5)]. The reaction can be expressed as such:

$$2MnO_2 + CH_2O + H_2O \rightarrow HCO_3^- + 2Mn^{2+} + OH^- \text{ (Curtis, e al., 1986) (6)}$$

Reductions of Fe_2O_3 [reaction (5)] and MnO_2 [reaction (6)] raise activity of Mn and Fe and reduce acidity of pore waters. As a result, carbonates can be precipitated from oversaturated pore waters (Curtis, 1983a; Coleman, 1985). Depending on availability of other cations (Ca^{2+} and Mg^{2+}), ferroan calcite, or ankerite or siderite would form.

Due to greater free energy release from reduction of MnO_2 than that of Fe_2O_3, Mn^{4+} should be preferentially reduced to Mn^{2+}. The transitional zone between oxidising and reducing conditions will tend to have the maximum concentration of Mn^{2+} (Froelich et al., 1979). Carbonates formed in this zone will be richer in Mn^{2+} than those formed in deeper burial. This was documented by Curtis et al. (1986) and is also considered to be the case for the burial diagenesis of the Narrabeen Group sandstones, as supported by the microprobe analyses of the carbonates. In the Narrabeen Group, pore filling calcites formed early at a shallower depth, which was probably close to the transitional zone. During the precipitation of calcites, Mn^{2+} existed in a relatively high concentration in pore waters. Thus the early formed calcites would be relatively rich in Mn, which is supported by the microprobe data. The analysed calcites have 2-6 mole % of $MnCO_3$. Ankerite was formed later at a deeper burial. At such a burial depth, pore waters in the sediments would probably have a very low concentration of Mn^{2+}. The precipitated ankerite would be expected to be relatively poor in Mn, which is supported by the microprobe analyses. They indicate that $MnCO_3$ in the ankerites is less than 2 mole % and in the majority of them $MnCO_3$ is less than 1 mole %. Most of the pore filling

siderites analysed by microprobe have a lower $MnCO_3$ than the calcites, suggesting they formed at a deeper burial. The siderites in samples A146.5 and Y566.1 have a $MnCO_3$ content of 4-8 mole %. The high $MnCO_3$ content in these siderites probably resulted from local abundance of Mn^{2+} in pore waters during their precipitation.

The presence of dolomite, ankerite and Ca Mg siderite in the sandstones indicates that Mg^{2+} did occur in pore waters during the formation of carbonates. Mg^{2+} is considered to be supplied by exchange reactions involving clay minerals and organic matter (Mg is a constituent of chlorophyll). Obviously alteration of volcanic rock fragments was another source for Mg^{2+}.

The Ca^{2+} used for the formation of Ca-bearing carbonates is considered to be produced by the initial hydration of volcaniclastic sediments according to the following reaction:

$$Ca^{2+}\text{-silicate} + H_20 \rightarrow H^+ \text{- silicate} + Ca^{2+} \quad \text{(Surdam and Boles, 1979)} \quad (7)$$

The dissolution / alteration (including albitisation) of detrital plagioclase grains probably also supplied a minor amount of Ca^{2+} to the pore waters.

The Ca^{2+} from hydration as well as alteration probably did not travel far from where it was produced. This is supported by the close relationship between the occurrence of Ca-bearing carbonates and the abundant detrital volcanic lithics in the sandstones. Calcium-bearing carbonates - calcite, ferroan calcite, dolomite, and ankerite are generally restricted to the sandstones rich in volcanic rock clasts from the lower Narrabeen Group (Appendix V). The pore filling Ca-bearing carbonate in a large amount is particularly limited and found only in some sandstone samples from the east coast zone and the northern region of the basin

where abundant detrital volcanic clasts are recorded in the sandstones (Table 6-2). The conclusion from the characteristic distribution of Ca-bearing carbonate is that abundant volcanic lithics favour the formation of Ca-bearing carbonates.

6.5.2 LATE STAGE OF DIAGENESIS

(i) Phase III: Major Dissolution / Alteration of Unstable Detrital Grains

The dissolution / alteration processes require acidic conditions or the presence of carbon dioxide. It is known that the major sources for CO_2 are meteoric water and the maturation of organic matter. As will be discussed in the next chapter, diagenesis of the Narrabeen Group sandstones entered into a closed regime after the major carbonate cementation. In a closed system, meteoric waters with dissolved atmospheric CO_2 were unlikely to enter pore spaces of the sediments in large amounts. Thus the acidic conditions responsible for phase III of the diagenesis are most likely to be achieved by the maturation of organic matter. The dissolution porosity present throughout the Narrabeen Group was largely created by the CO_2 from this source.

The acidic conditions also facilitated the further alteration of the unstable detrital particles (volcanic rock fragments, feldspar and mica), which accompanied or immediately followed the dissolution process. The textural evidence for this is that the stacked kaolin flakes fill the dissolved pore spaces within the carbonate cements and occur on the surfaces of them. It is common that kaolin is the first precipitate to reduce dissolution pore spaces in sandstones (Curtis, 1983b).

Kaolins are generally dispersed uniformly throughout most of the pore spaces in the same sandstone. Such a distribution implies that the authigenic kaolin was precipitated from migrating oversaturated pore waters. Kaolin could also form from alteration of unstable detrital grains. Some sandstones contain sand sized masses, which consists of stacked kaolin flakes and / or prismatic quartz crystals and keeps the rough outline of original detrital grains (Figs 6-29 to 6-32). These masses are

Table 6-2 Distribution of abundant carbonate in sandstones.

Sample no.	OU	Location	Carbonate*	Rock fragment**
L595.2	SC	ECZ	36.2	51.3
J650.3	WO	ECZ	56.0	88.8
J672.3	WO	ECZ	32.0	65.7
M094.1	BH	ECZ	30.2	35.0
I 465.6	UB	NR	36.0	38.5
H681.2	WO	NR	30.0	54.3
F525.8	SC	NR	30.6	55.7
F734.9	WO	NR	30.4	27.7
U388.2	WO	NR	44.2	57.4
O668.5	WO	SR	30.2	58.9

* percentage (cement and replacement) in the total sandstone from Appendix III - point counts.

** percentage in the total detrital grains from Appendix IV.

ECZ = east coast zone, NR = northern region, SR = southern region

considered to be the result of complete alteration of original detrital grains. The association of authigenic kaolins with partly altered detrital muscovite (Figs 6-101 & 6-96d), K-feldspars and volcanic clasts (Fig 6-102) indicates that alteration of muscovite, feldspar and volcanic rock fragments could all have created authigenic kaolin.

The SEM / EDX studies show that authigenic kaolin tends to be more common and abundant in quartz-rich sandstones than in lithic-rich sandstones. The lesser abundance of kaolins in lithic-rich sandstones is considered to be related to porosity modification. In lithic-rich sandstones, inter-grain pore spaces are greatly reduced by pore filling carbonates and mechanical compaction during early diagenesis. After early diagenesis, large quantities of pore waters are unlikely to have passed through low porosity and low permeability lithic-rich sandstones to either deposit abundant pore filling kaolins or cause extensive alteration of unstable detrital grains to kaolins.

(ii) Phase IV: Development of Quartz Overgrowths and Precipitation of Post Quartz Overgrowth Illite

The way that quartz overgrowths develop has been discussed by a number of workers e.g. Ernst and Blatt (1964), Waugh (1970) and Pittman (1972). Pittman proposed two ways for the formation of quartz overgrowths: (1) overlap and / or emergence of the initial very small quartz crystals and (2) envelopment of earlier multiple overgrowths by an outer shell.

In the Narrabeen Group sandstones, the former way for the development of quartz overgrowths is clearly and convincingly established by the current study. In this process quartz overgrowths are developed in three stages: initial, submature and mature stages. The micro-quartz crystals growing on detrital quartz grains (Figs 6-61 & 6-62) are considered to be the product of the initial stage. They are present as projections from the substrate - detrital quartz grains. If physico-chemical

conditions, space, time and silica sources are all favourable for the further development of quartz overgrowths, the formation of quartz overgrowths enters into the submature stage. The closely spaced initial prismatic micro-quartz crystals with the same crystallographic orientation emerge and coalesce to form larger planar surfaces during this stage (Figs 6-103 to 6-105). But the surfaces are not fully developed so that "V" shaped impressions can be seen on them (Figs 6-104 & 6-105). If the formation of quartz overgrowths continues, it enters to the final mature stage during which the smooth surfaces are developed and overgrowth can continue as a single crystal (Figs 6-26, 6-62 & 6-94). The formation of quartz overgrowths by the outer shell envelopment is also shown by the study, as indicated by Figs 6-105 & 6-106. The late well developed quartz overgrowths enclose the early quartz crystals (coalesced micro-quartz crystals?).

For the well developed quartz overgrowths found in the samples studied, it is impossible to determine in which of the two ways or a combination of them quartz overgrowths formed since the well developed smooth surfaces mask the characteristics of early stages.

Both petrological microscope and SEM / EDX studies indicate that quartz overgrowths generally occur in a trace to minor amount throughout the whole Narrabeen Group. However, they are more abundant in the upper Narrabeen Group, which is richer in detrital quartz, than in the lower Narrabeen Group. In the sandstones rich in volcanic rock fragments, quartz overgrowths tend to be restricted to the detrital quartz grains which are adjacent to other detrital quartz grains. Isolated detrital quartz grains surrounded by detrital lithic clasts rarely have quartz overgrowths.

The distribution of quartz overgrowths suggests that the source for the silica is related to the detrital quartz grains. Thus pressure solution may be the major source for the silica for the overgrowths. This interpretation is supported by the

existence of sutured contacts between adjacent quartz grains (see Fig 5-28) and the dimples recognised on the detrital quartz grain surfaces under SEM.

Another possible source is the alteration of unstable detrital clasts, which happens prior to the formation of quartz overgrowths and releases silica to the pore water. Illitisation of smectite is another well cited source for silica.

$$\text{smectite} + K^+ + Al^{3+} \rightarrow \text{illite} + Si(OH)_4 + H^+ \quad (8)$$

This reaction requires a temperature of about 60-100°C to proceed (Hower et al., 1976). H^+ released from this reaction may be used to dissolve feldspars, carbonates and volcanic rock fragments to supply more silica.

After quartz overgrowths, illite was precipitated from pore waters. Filamentous illite identified in the sandstones was largely formed during this phase of diagenesis. Formation of illite requires a high concentration of K^+ (Garrels and Christ, 1965). How the high concentration of K^+ was achieved is not clear. It was probably related to the cessation of illitisation of mixed-layer illite / smectite. Towards the end of quartz overgrowth formation, the illitisation had ceased (Fig 6-83). As a result, K^+ previously used in the illitisation could build up. When the pore waters became saturated with illite, it would crystallise.

(iii) Phase V: Formation of Post Quartz Overgrowth Carbonate

Only some sandstones in the east coast zone and northern region of the basin experienced the last phase of diagenesis during which minor amounts of calcite and ankerite crystallised. The ions used for the formation of the late diagenetic minerals are considered to be supplied by an internal source. They were derived from previous diagenetic reactions. Depending upon the availability of Ca^{2+}, Fe^{2+}, Mg^{2+}, and physico-chemical conditions of pore waters, calcite or ankerite

crystallised in pore waters in different sands. Late calcite was found in one sandstone (sample I781.5) from the northern region of the basin and late ankerite in two sandstones (samples B151.6 and L422.3) from the east coast zone.

(iv) Other Reactions Taking Place during the Late Stage of Diagenesis.

Albitisation of plagioclase and formation of zeolites are related to the alteration of unstable detrital grains in the Narrabeen Group. They formed late, but their exact timing relative to the other diagenetic minerals is not clear. Thus they can not be classified to the three phases of the late diagenesis.

Albitisation of plagioclase

Albitisation begins as an equal volume replacement reaction. The conversion of the anorthite component of oligoclase and andesine receives Na^+ ions from solution and releases Ca^{2+} to the solution (Merino, 1975; Boles, 1982).

$$0.8NaAlSi_3O_8.0.2CaAl_2Si_2O_8 + 0.203H_4SiO_4 + 0.201\ Na^+ + 0.796\ H^+ =$$

$$1.001\ NaAlSi_3O_8 + 0.2Ca^{+2} + 0.199Al^{3+} + 0.804H_2O \qquad (9)$$

The above reaction requires a substantial amount of silica and sodium to proceed. The conversion of smectite to illite in the adjacent shales / mudstones is the most likely source for a large quantity of sodium ions according to the following reaction (Helmold and ven de Kamp, 1984):

$$\text{smectite} + Al^{3+} + K^+ = \text{illite} + Si^{4+} + Na^+ + Ca^{+2} + Mg^{+2} + Fe^{+2+3} + H_2O \quad (10)$$

It is modified from reaction (8).

XRD studies indicate that the mixed-layer illite / smectite contains 20-40 percent

expendable smectite in fine fractions of the sandstones studied. The low percentage of expandable layer in the mixed-layer mineral is considered to have resulted from the conversion of smectite to illite. Despite lack of systematic study of the clay mineralogy of the adjacent shales / mudstones in the Narrabeen Group, a similar conversion is speculated to have taken place in the shales / mudstones. If the sodium ions were not taken up by forming other Na-bearing clay minerals and if it is assumed that the shales / mudstones were not a completely closed system with regard to sodium, they would move to adjacent sandstones.

In some feldspars, the albitisation also produced a minor amount of calcite as a by-product in some albitised detrital plagioclase grains (Figs 6-70 & 6-71). The calcite is included in the newly - formed albite. This finding is similar to the case documented by Boles (1982). As Boles speculated, calcite was formed by combining Ca^{2+} released during albitisation with carbonate ions from pore fluids. The precipitation of calcite as a by-product of the albitisation differs from the cases documented by Castaño and Sparks (1974) and Helmold and van de Kamp (1984) where laumonite precipitates concurrently with albitisation.

The difference is probably due to the variation in the activity of CO_2 relative to that of H_2O in the different geographic areas (Zen, 1961). Where aCO_2/aH_2O is high, calcite will be formed as a by-product of the albitisation according to the following reaction proposed by Helmold and van de Kamp (1984):

$$NaAlSi_3O_8{\cdot}CaAl_2Si_2O_8 + 4SiO_2 + 2Na^+ + CO_3^{2-} = 3NaAlSi_3O_8 + CaCO_3 \quad (11)$$

plagioclase albite calcite

Where aCO_2/aH_2O is low, on the other hand, the formation of laumonite will accompany albitisation according to either of the following two reactions (Boles and Coombs, 1977), depending upon the extent of albitisation of plagioclase:

$i_3O_8{\cdot}CaAl_2O_8 + 2SiO_2 + 4H_2O = NaAlSi_3O_8 + CaAl_2Si_4O_{12}{\cdot}4H_2O$ (12)

lagioclase albite laumonite

ironment where calcium-bearing plagioclase is partly albitised and partly
y laumonite.

or

$_3O_8{\cdot}CaAl_2Si_2O_8 + 3SiO_2 + 2H_2O + Na^+ = 2NaAlSi_3O_8 +$

plagioclase albite

$0.5CaAl_2Si_4O_{12}{\cdot}4H_2O + 0.5Ca^{+2}$ (13)

laumonite

onment in which complete albitisation has taken place.

e Narrabeen Group is concerned, albitisation is considered to be a late
vent. It probably took place during and following the major dissolution /
f unstable detrital grains (phase IV). During the albitisation reaction, a
rge quantity of CO_2 might be present as a result of organic maturation in
dstones. Thus albitisation proceeded in a chemical environment where
was high so that calcite was precipitated concurrently with albitisation
reaction (11). However, calcite formed in this way is very rare.

ation

common diagenetic minerals in volcaniclastic sandstones and form by
on of saline, alkaline aqueous solutions and unstable volcanic detritus
959; Hay, 1966; Surdam and Boles, 1979; Mathisen, 1984). Zeolites
by two major diagenetic reactions: volcanic glass to zeolite and
to zeolite (Surdam and Boles, 1979). Volcanic glass and plagioclase

are unstable and commonly dissolve in saline, alkaline solution. The dissolution produces silica and aluminium to the pore water from which the zeolites precipitate.

Although the volcanic rock fragments account for a principal part of the sandstones in the lower Narrabeen Group, zeolites are rarely found in these sandstones. Analcime is one exception and was tentatively identified in one sample (Figs 6-79 & 6-80) and whose formation is considered to be related to the major dissolution / alteration of unstable detrital grains during the late stage of diagenesis. There is no petrologic evidence for the presence of volcanic glass. Plagioclase constitutes a minor part of the sandstone in the lower Narrabeen Group and generally accounts for less than 5 percent of the total sandstone. Moreover, plagioclase tends to be albitised. The rare existence of zeolites can probably be explained by the absence of detrital volcanic glass and paucity of plagioclase, and the tendency of albitisation of plagioclase.

The unsuitable chemical environment is probably another factor limiting the formation of zeolites. As indicated by Hay (1966), the alteration of glass to smectite is an important factor in providing the chemical environment, particularly an alkaline pH and high activity of silica, suitable to the formation of zeolites. The absence of volcanic glass made it impossible for such a reaction (glass to smectite) to have taken place in the sandstones studied.

6.6 SUMMARY

There are three principal types of diagenetic minerals in the Narrabeen Group sandstones: carbonates, clay minerals, and quartz cements. Carbonates consist of calcite, dolomite, ankerite, and siderite with siderite being the most common. Clay minerals include kaolin, illite, mixed-layer illite / smectite, and chlorite with kaolin being the most common. Micro-quartz, mega-quartz and quartz overgrowths comprise quartz cements with quartz overgrowths being the most abundant.

Diagenesis of the Narrabeen Group sandstones began with the formation of rare grain coating haematite and early clays including kaolin, grain coating mixed-layer illite / smectite and chlorite. Following the formation of these early clays, major carbonate cementation took place. Among the diagenetic carbonates, calcite coating detrital grains was the first to crystallise and was succeeded by siderite coating detrital grains, pore filling calcite, pore filling siderite, and pore filing ferroan calcite and ankerite. After the major carbonate cementation, kaolin, quartz overgrowths and filamentous pore-bridging illite crystallised. The latest cements to form were calcite and ankerite

The formation of early authigenic clay minerals was mainly controlled by the physico-chemical features of the pore waters. The early mixed-layered illite / smectite coating detrital grains and early kaolin were precipitated in sands with oxygenated and mildly acidic pore waters whereas the chlorite crystallised in sands with anoxic and neutral to mildly alkaline pore waters. The formation of chlorites was also controlled by the detrital composition of sandstones, as suggested by the close association of the occurrence of authigenic chlorite with abundant volcanic rock fragments.

The type of carbonate formed during carbonate cementation was controlled by the relative concentration of Ca^{2+}, Fe^{2+}, Mg^{2+} and Mn^{2+} and physico-chemical conditions in pore waters. Non-ferroan calcite crystallised in pore waters where Fe^{2+} was virtually absent. The extensive presence of Fe^{2+} in pore waters during carbonate cementation determined the limited formation of non-ferroan calcite. Non-ferroan calcite coating detrital grains was found only in two samples from the west margin. Pore filling non-ferroan calcite is restricted to the volcanic lithic-rich sandstones in the east coast zone and northern region of the basin. In the presence of a high concentration of Fe^{2+}, Fe calcite, or dolomite, or ankerite, or

siderite crystallised depending on the concentrations of other cations and physico-chemical conditions.

The Fe^{2+} used in forming these carbonates was derived from reduction of Fe_2O_3, alteration of volcanic rock fragments and organic matter in that order of importance. The Ca^{2+} used in forming these carbonates was largely derived from the initial hydration of volcanic rock fragments. The produced Ca^{2+} was incorporated with HCO_3^- at or near where it was produced so that pore filling calcite, ferroan calcite and ankerite are restricted to the lower Narrabeen Group sandstones, which are generally rich in detrital volcanic lithics.

Kaolins were formed by direct precipitation from migrating pore waters and alteration of volcanic rock fragments, feldspar and mica. They are more common and abundant in the sandstones rich in quartz.

Quartz overgrowths developed in two ways and / or a combination of the two: overlap and / or emergence of the initial micro-quartz crystals and envelopment of earlier multiple overgrowths by an outer shell. They are more common and abundant in quartz-rich sandstones than in lithic-rich sandstones. The silica used for the overgrowths was largely derived from pressure solution.

Precipitation of post quartz overgrowth illite was related to the build up of K^+ in pore waters following quartz overgrowths. Cessation of illitisation of smectite was probably the contributing factor for the built up.

CHAPTER SEVEN

ISOTOPIC, FLUID INCLUSION AND CHEMICAL KINETIC MODELLING STUDIES OF PORE FLUID HISTORY IN THE NARRABEEN GROUP SANDSTONES, SOUTHERN SYDNEY BASIN

7.1 INTRODUCTION

An integrated approach was employed to investigate the aqueous and hydrocarbon fluid history during diagenesis of the Narrabeen Group sandstones in the southern Sydney Basin. Such an approach included petrological examination (as discussed in the last two chapters), and stable isotope and fluid inclusion techniques, which will be discussed in this chapter.

Nine sandstone samples were selected for this study. They are from eight boreholes in the southern Sydney Basin (Fig 7-1) and from within a stratigraphic interval from the upper part of the Scarborough Operational Unit to the lower part of the Upper Bulgo Operational Unit (Fig 7-2). Of these nine samples, four were subject to fluid inclusion investigations. Further sample descriptions are given in Table 7-1.

7.2 METHODOLOGY

7.2.1 STABLE ISOTOPE TECHNIQUE

(i) Mineral Separation

Using the techniques outlined by Jackson (1979), a <10 μm clay fraction was obtained from each of the nine samples and a pure quartz separate from six of them. The procedures for mineral separation are summarised in Fig 7-3.

Each (*ca*. 400 grams) of the sandstone samples was initially cleaned on exterior surfaces and disaggregated to a size less than 450 μm by breaking and disc milling. Then carbonates were separated from silicates (detrital framework grains and clay minerals) by repeated magnetic and heavy liquid treatments. The

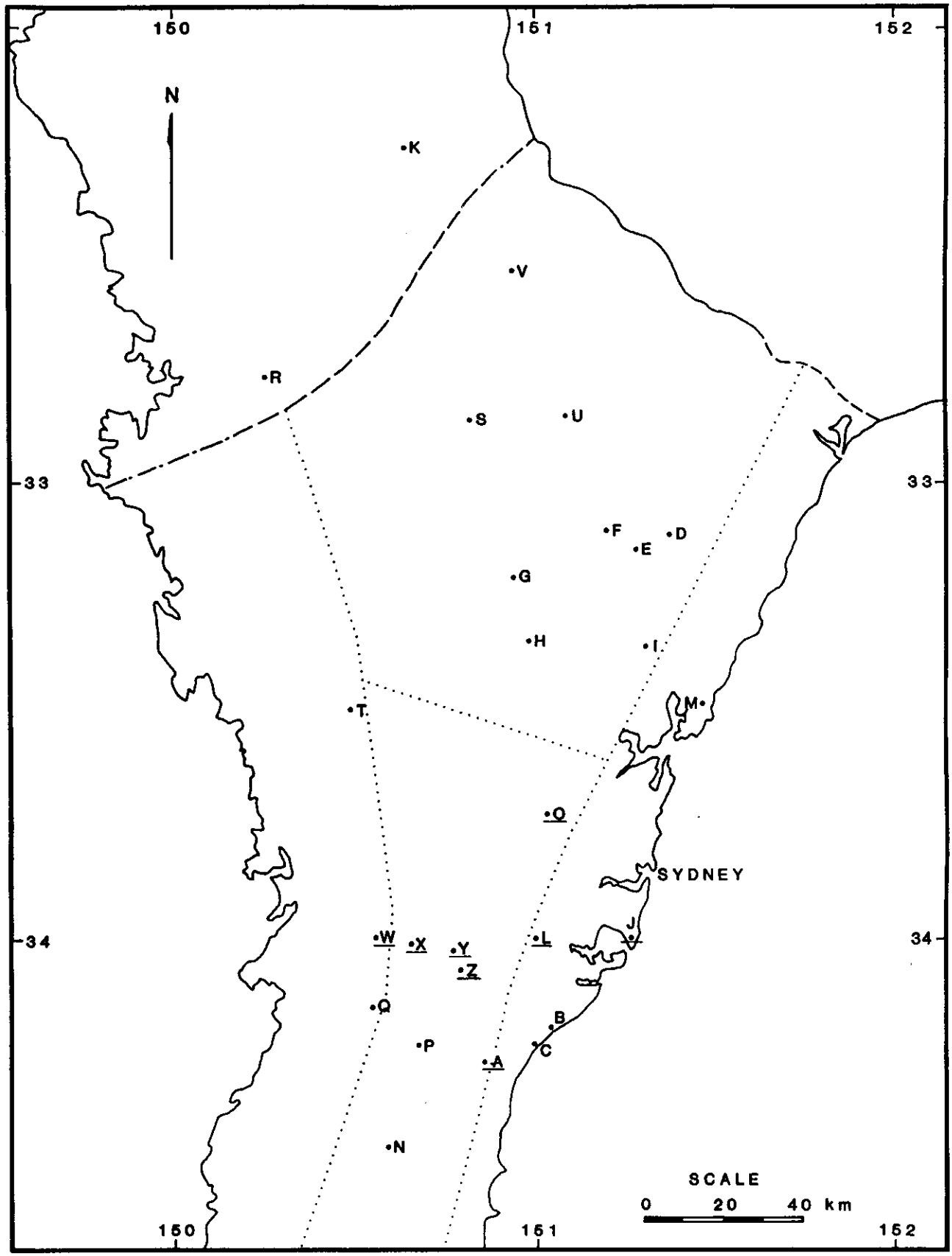

Fig 7-1 Locations of the boreholes (underlined) from which samples were selected for isotope and fluid inclusion investigations.

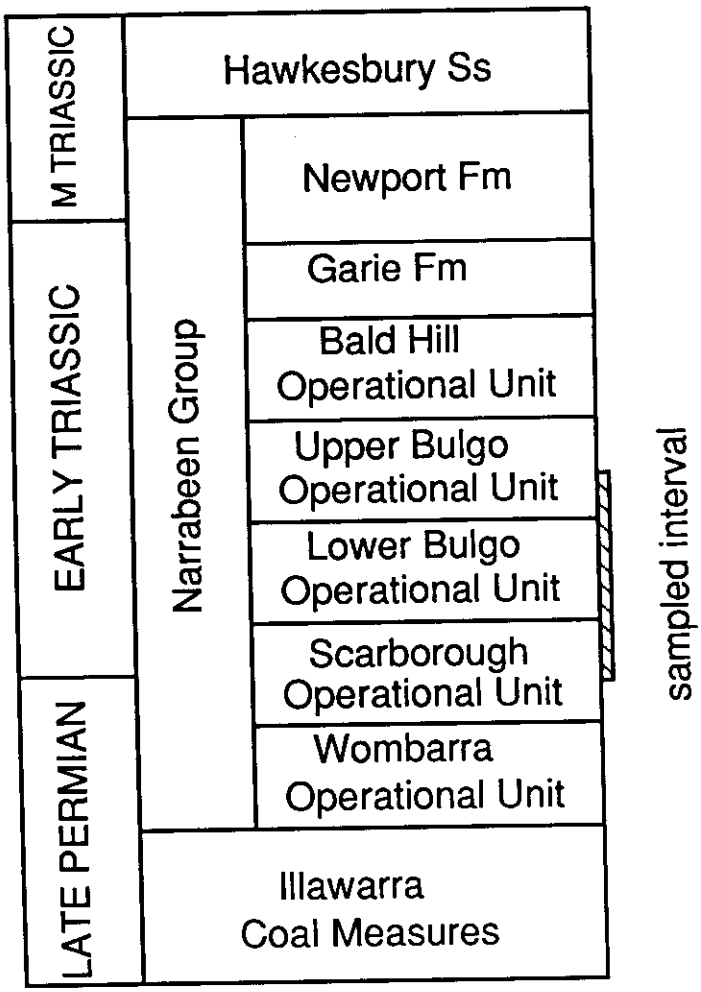

Fig 7-2 Generalized stratigraphic column.

Table 7-1 Locations and descriptions of samples.

Borehole	Depth (m)	Sample No.	Formation	Lithology
Liverpool 91	506.7	L506.7	Lower Bulgo	off-white, cross bedded, medium grained, moderately sorted quartzose litharenite
South Colah 1	488.2	O488.2	Lower Bulgo	off-white, cross bedded, medium grained, moderately sorted quartzose litharenite
South Colah 1	600.9	O600.9	Scarborough	off-white, cross bedded, coarse grained, moderately sorted quartzose litharenite
Campbelltown 2	512.4	Z512.4	Lower Bulgo	off-white, cross bedded, medium grained, well sorted quartzose litharenite
Cobbitty 3	531.9	X531.9	Scarborough	medium grey, massive, coarse grained, poorly sorted sublitharenite
Campbelltown 5	593.9	Y593.9	Scarborough	light grey, cross-bedded, medium grained, well sorted quartzose litharenite
Weromba 2	388.8	W388.8	Lower Bulgo	light grey, massive, medium grained, poorly sorted litharenite
Wollongong 45	146.5	A146.5	Upper Bulgo	off-white, cross-bedded, fine grained, well sorted quartzose litharenite
Cape Banks 3	514.8	J514.8	Scarborough	medium grey, cross-bedded, medium grained, well sorted litharenite

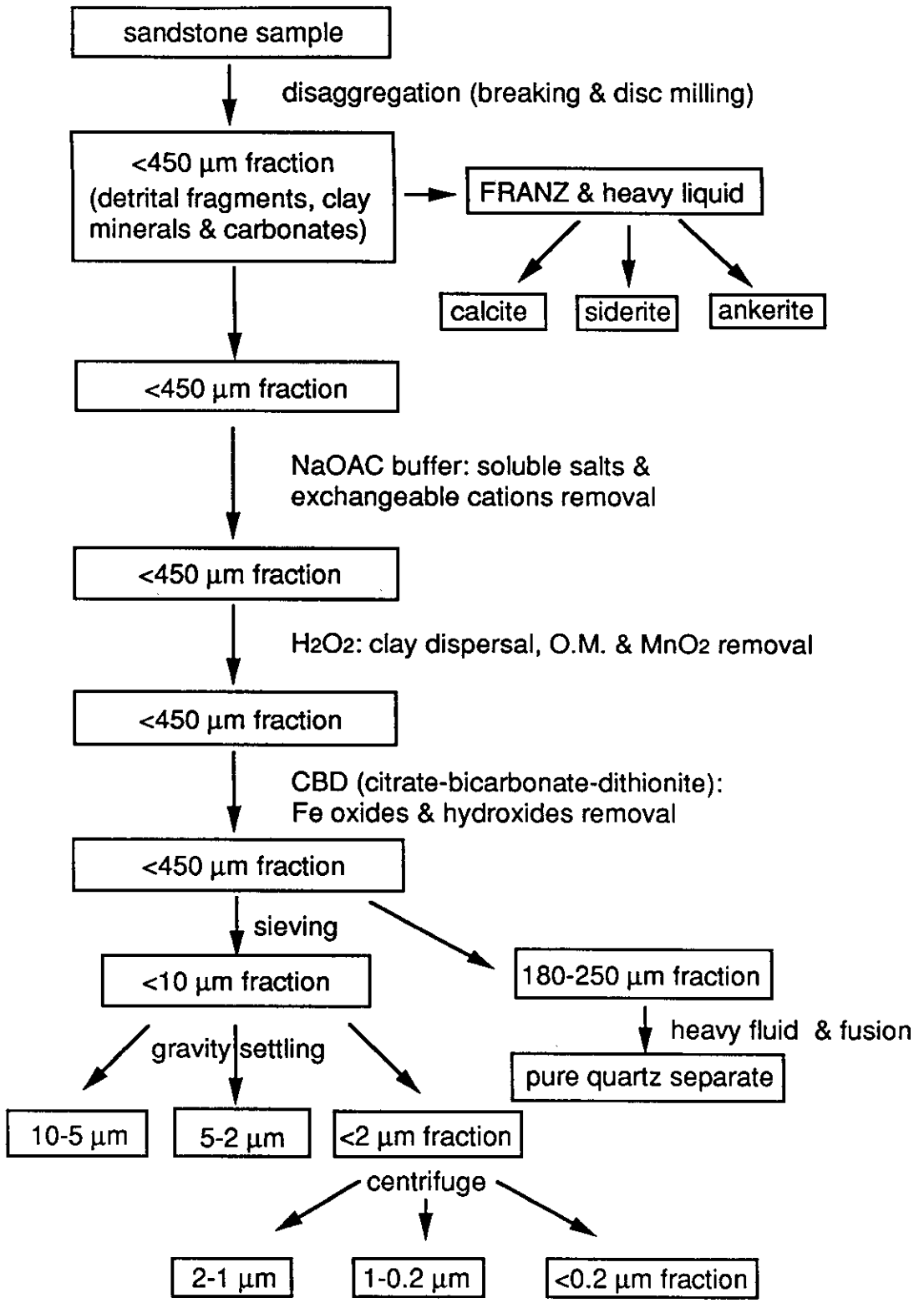

Fig 7-3 Flow chart showing stages involved in mineral separation of sandstones.

carbonate separates were used for measurements of oxygen and carbon isotopes. The silicate portions were then subject to further physico-chemical treatments to obtain pure quartz and clay separates. The chemical treatments can be simplified as three major steps: buffer washing, H_2O_2 oxidation and CBD (sodium citrate - bicarbonate - dithionite) treatment. The physical treatments refer to size separation by sieving, gravity settling and centrifugation.

Buffer washing

In order to prevent flocculation of clays and to give effective dispersion of them, the sample was washed by a slightly acidic NaOAc buffer (82 g of NaOAc and 27 ml of glacial HOAc acid in one litre of distilled water) with a pH of about 5. This was done by adding buffer to the sample contained in a beaker. The beaker was then left on a hot water bath at a temperature of about 60 °C and the sample stirred with a glass rod for about 30 minutes. The sample was then washed with the buffer three more times. The buffer washing removed soluble salts and exchangeable polyvalent cations and assisted the dissolution of Ca and Mg carbonates.

H_2O_2 oxidation

Following buffer washing, hydrogen peroxide (H_2O_2) was added to the beaker to give complete dispersion of clays and to remove organic matter and MnO_2. The amount and the concentration of H_2O_2 for this treatment depend on the abundance of organic matter in the sample. For the samples used in this study, 10 - 20 % H_2O_2 was used over a period of two or more days. After that, the beaker was placed on a hot water bath at a temperature of 60 - 70 °C to evaporate until the sample became a paste. During evaporation, the sample was constantly stirred. The sample was washed again with the buffer three more times and then left in 95% methanol overnight.

CBD treatment

This treatment aims at removing iron oxides and hydroxides from the sample. In the buffered neutral citrate - bicarbonate - dithionite (CBD) system, sodium dithionite ($Na_2S_2O_4$) is employed for reduction, sodium bicarbonate (pH 7.3) as a buffer, and sodium citrate as a chelating or complexing agent for ferrous and ferric iron ions.

A mixture of 0.3 M sodium citrate and 1 M sodium bicarbonate in a ratio of 8:1 was added to the sample. Then the beaker was placed on a hot plate and temperature was strictly kept at 75-80 °C. About 2 gm of dithionite powder was added to the sample and another 1 gm after 5 minutes. After leaving the beaker on the hot plate for 15-20 minutes during which the sample was constantly stirred by an automatic stirrer, the sample was then treated with acetone to promote flocculation.

Following the CBD treatment, the sample was washed with 1 M NaCl several times until the smell of dithionite and the yellowish colour of the supernatant disappeared. Then ethanol was added to the beaker to wash the sample. Finally the sample was left in 0.1 M sodium hexametaphosphate (calgon) and was ready for size separation

Size Separation

Microscopic examination of size fractions of the silicate separates indicated that detrital quartz grains with a size of 250-180 μm have the greatest proportion of quartz overgrowths and least amount of composite grains. Thus the 250-180 μm silicate separates were used to obtain pure quartz separates.

The 250-180 μm fraction was obtained by wet sieving. It was washed with distilled water a few times and the supernatant containing finer particles from each washing was transferred back to the <180 μm fraction. Then the 250-180 μm fraction was washed with water several more times. The supernatant from each washing in which flaky minerals such as micas were suspended was decanted.

Next 30% HCl acid was added to the beaker containing the 250-180 μm fraction and the beaker was left on a hot water bath at a temperature of 60-70 °C to speed up the reaction between the acid and the unstable minerals such as carbonates left from previous NaOAc buffer washing. The acid treatment may be repeated a few times until no reaction between HCl and unstable minerals in the coarse fraction could be observed. Afterwards the 250-180 μm fraction was washed with water, then acetone and finally dried. The dry coarse fraction was treated by heavy liquid separation technique and / or fusion with $NaHSO_4$ to obtain >95 % pure quartz. Purity of quartz separates was determined by examination of grain mounts under binocular microscope and SEM. Pure quartz separates were obtained for six of the nine samples.

The <180 μm fraction was separated into 180-125 μm, 125-45 μm, 45-20 μm, 20-10 μm, 10-5 μm, 5-2 μm and less than 2 μm fractions by gravity settling (here the grain size is equivalent sphere diameter). The <2 μm fraction was further separated into 2-1 μm, 1-0.2 μm and <0.2 μm fractions by a high speed centrifuge.

(ii) Analytical Procedures

For isotopic analyses of carbonates, approximately 15 mg materials were used. CO_2 was released from calcite by reaction overnight with 100 % phosphoric acid at 25 °C and CO_2 was released from siderite and ankerite by reacting with phosphoric acid for 3 hours at 100 °C. The carbon dioxide was separated from water vapour by using a refrigerated acetone (saturated with dry ice) trap in which CO_2 does not freeze and H_2O does. To calculate the oxygen isotope results for carbonates, the employed oxygen fractionation factors (α) between the $\delta^{18}O$ of the carbonate and that of the H_3PO_4 - extracted CO_2 are 1.01025 for calcite at 25 °C (Rosenbaum and Sheppard, 1986, modified from Sharma and Clayton, 1965), 1.00881 at 100 °C for siderite and 1.00901 at 100 °C for ankerite (Rosenbaum and

Sheppard, 1986) (α and δ will be defined in later paragraphs).

To analyse the oxygen isotope of quartz overgrowths, the 250-180 pure quartz separates were used following the method of Lee and Savin (1985). Each of the six quartz separates was soaked in 50% HF acid for 5 minutes. The HF acid preferentially attacks the weakly bounded boundaries between the overgrowths and the detrital core (Figs 7-4 & 7-5). After neutralisation of the HF acid, the quartz separates were treated with ultra-high frequency sonic vibration in distilled water, leading to overgrowth detachment and concentration towards finer size fractions. Four resultant size fractions (250-180, 180-125, 125-75, and 75-20 μm), together with the 250-180 μm fraction without HF treatments, were used for oxygen isotope analyses.

For isotopic analyses of clay minerals, the finer clay fractions (10-5, 5-2, 2-1, 1-0.2, and <0.2 μm) were used. They were first examined by X-ray diffraction (XRD). Only the fraction, of which one single clay mineral accounts for more than 90% , was used.

For each analysis of oxygen isotope ratio of clays and quartz, 10 - 15 mg materials were used. Oxygen was released from clay and quartz by reaction overnight with bromine pentafluoride (BrF_5) at 550 °C (Clayton and Mayeda, 1963) and then converted to CO_2 by reacting with a hot graphite rod. Clays were preheated in the reaction vessels for two hours at a temperature of about 200 °C to remove absorption water.

For deuterium determination, a minimum amount of 100 mg sample is required. Following overnight degassing at 120 °C, the clays were melted under vacuum at 1100 °C . The released water was reduced to hydrogen by reacting with uranium (Bigeleisen et al., 1952).

Fig 7-4 A typical detrital quartz grain with quartz overgrowths. From Campbelltown 2 at drilling depth of 512.4 m (sample Z512.4).

Fig 7-5 A detrital quartz grain with quartz overgrowths treated with HF acid. HF acid preferentially attacks the weekly bounded boundaries between the detrital cores and overgrowths. After treatment of ultra-sonic vibration, quartz overgrowths will detach from the detrital cores and concentrate into progressively finer sized fractions. From Liverpool 91 at drilling depth of 506.7 m (sample L506.7).

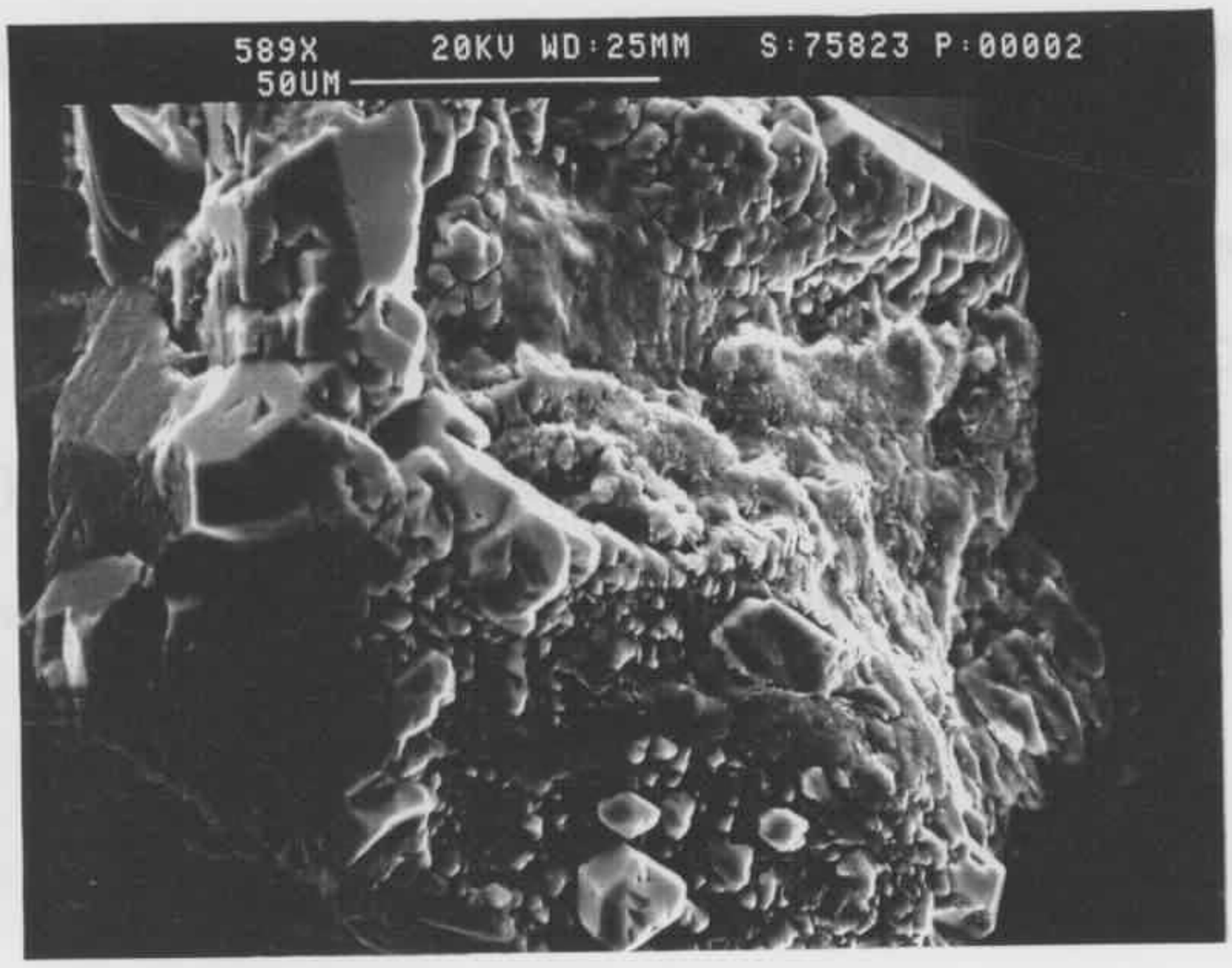
589X
50UM
20KV WD:25MM
S:75823 P:00002

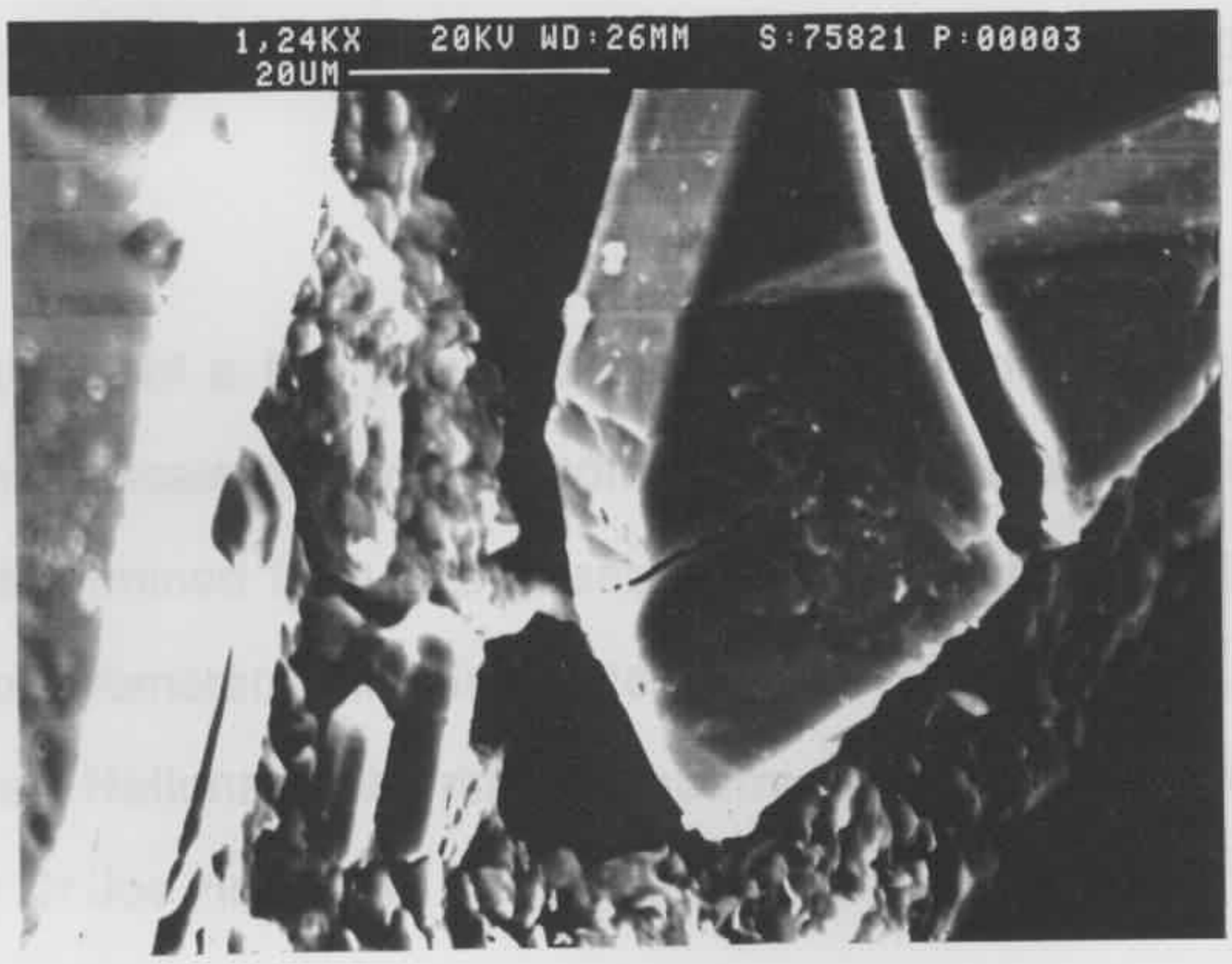
1,24KX
20UM
20KV WD:26MM
S:75821 P:00003

Oxygen and carbon isotope ratios were measured with reference to carbon dioxide from a calcite standard and hydrogen isotope ratios were measured with reference to hydrogen from a water standard in a Micromass 602 D mass spectrometer, which is located in The Division of CSIRO Exploration Geoscience at North Ryde, New South Wales. The raw data were corrected using the methods of Craig (1957) and Deines (1970). Isotope ratios are reported in the usual delta per mil (δ ‰) notation as parts per 10^3 deviation from a standard ratio. The δ value is defined as

$$\delta \text{‰} = (R_{sample} - R_{standard}) / R_{standard} \times 1000$$

where R is the isotope ratio. For oxygen and deuterium the internationally accepted standard is the Standard Mean Ocean Water (SMOW) and for carbon it is the Belemnitella americana from the Cretaceous PeeDee Formation (PDB), South Carolina. The oxygen and hydrogen isotope data are reported with respect to SMOW and the carbon isotope data with respect to PDB. Precision of $\delta^{13}C$ and $\delta^{18}O$ for carbonate is +/- 0.1 ‰, that of $\delta^{18}O$ for silicates +/-0.25 ‰, and that of δD for clays +/- 2 ‰.

Potassium abundances of a few illite separates selected for age determination were determined in duplicate by flame photometry. Argon isotope composition and abundance were determined from gas released by fusion under vacuum with a noble gas mass spectrometer, which is located in The Research School of Earth Sciences, Australian National University, Canberra, ACT. These K-Ar analyses were conducted by Dr Joe Hamilton.

7.2.2 FLUID INCLUSION TECHNIQUE

Most sandstone diagenesis involves overgrowths on original minerals (e.g. quartz

overgrowths) or growth of new minerals. The new growth of diagenetic minerals may trap fluids as inclusions, which can provide data not only on the composition, pressure and density of the fluids present during diagenesis, but particularly temperature at which the host mineral crystallised. The use of fluid inclusions for deciphering the trapping temperature of fluid inclusions (formation temperature of host mineral) is made possible by differential shrinkage of the host mineral and the inclusion fluid on cooling from the temperature of trapping to that of observation (Roedder, 1984). The fluid shrinks far more than the host mineral and the difference shows up as a bubble in the fluid at room temperature. If this process is reversed and the sample is heated up until the bubble disappears (i.e. the fluid inclusion homogenises), the bubble disappearance temperature (homogenisation temperature of fluid inclusions) can be obtained.

A wafer about 50 μm thick and polished on both sides was prepared for investigation of fluid inclusions by petrological microscope. The bubble disappearance temperatures (homogenisation temperatures) and ice melting point temperatures were measured on pieces cut from the wafer with a Chaix Mecca heating - freezing chamber mounted on a petrological microscope. The measurements were made by observing the phase changes within the fluid inclusion while the sample was being heated or cooled.

To determine homogenisation temperatures, the sample was heated faster (5 °C / min) at first and then the heating rate was slowed down (1 °C / min) when homogenisation was considered to be imminent. Homogenisation temperature was taken as the mean value of the highest temperature at which the gas bubble within the inclusion was observed and the lowest temperature at which the bubble was not observed. When homogenisation was considered to have taken place, the temperature was lowered a few degrees. If the gas bubble reappeared, this meant that homogenisation had not taken place yet as first thought. If the gas bubble did

not reappear until the temperature was lowered more than 10 °C, this meant that homogenisation had finally taken place.

For measurements of ice melting point temperatures, the sample was cooled down to approximately -50 °C to -60 °C so that the fluid inclusions were frozen. Then the sample was heated up at a higher rate (3 °C / min) at beginning and then at a lower rate (0.25 °C / min) when the gas bubble within the inclusion was considered to start to move imminently. The heating continued until the gas bubble within the fluid inclusion started to move. The ice melting point temperature was taken as the mean value of the highest temperature at which the gas bubble within the inclusion was immobile and the lowest temperature at which the bubble started to move. The ice melting point temperature was used to determine salinity of aqueous salt solutions in the sediments.

Homogenisation temperatures were estimated to be accurate to +/-2 °C with a precision of +/-1 °C. Ice melting point temperatures were accurate to +/-0.5 °C with a precision of +/-0.25 °C.

The homogenisation temperature is the minimum entrapment temperature of the fluid inclusion and the end point for an isochore, which is the temperature - pressure relationship at constant density. The isochore for an aqueous salt solution is predictable if the salt content of the solution, which can be calculated from the depression of the ice melting point, and the homogenisation temperature are known. The isochore for hydrocarbon inclusions can not be predicted based on measurements of ice melting points. To predict the isochore requires detailed compositional data of the hydrocarbon inclusions. If the pressure, at which the aqueous fluid inclusions were trapped, is independently known, the entrapment temperatures of the inclusions can be deduced and vice versa.

Using ultra-violet and violet illumination and short wavelength barrier filters, hydrocarbon fluid inclusions were identified by their fluorescence (Burruss, 1981). The fluorescence originates in a trace amount of compounds with conjugated bonds, i.e. condensed aromatic hydrocarbons. The 3, 4, and 5 condensed aromatic hydrocarbons fluorescence with blue, green, and red light respectively. As oil matures, the intensity of blue fluorescence increases.

A lengthy discussion of categories of fluid inclusions was made by Roedder (1984). In this thesis, only primary and secondary inclusions were discussed even though other categories of fluid inclusions (Roedder, 1984) were recognised. Primary inclusions are defined as those formed during crystallisation of the host crystal and they should be aligned parallel to crystal growth faces. Secondary inclusions are defined as those formed after crystallisation of the host crystal and are formed during the healing of fractures.

Fluid inclusions at the boundary of the detrital quartz core and quartz overgrowths and within the quartz overgrowths were formed during precipitation of the overgrowths and thus they are primary inclusions. Fluid inclusions in curved and linear arrays, which cut both the detrital quartz core and the quartz overgrowths, are regarded as decorating healed fractures and were formed after precipitation of the quartz overgrowths. Thus they are secondary inclusions.

7.3 STABLE ISOTOPE INVESTIGATION

7.3.1 ISOTOPE GEOCHEMISTRY

Stable isotopes (O, C and H) are widely used as valuable tracers of low temperature water - rock interactions. $\delta^{18}O$ and δD of the formation fluid provide a diagnostic signature of both the source (e.g. seawater or meteoric water) and of important physical and chemical processes by which the formation fluid was modified during its evolution. $\delta^{18}O$ and δD of diagenetic minerals characterise the

features of the formation fluid with which they were equilibrated during sedimentary diagenesis. In addition, under certain conditions, the precipitation temperature or temperature range of diagenetic minerals can be calculated from their oxygen isotope ratios.

Different types of waters have different $\delta^{18}O$ and δD compositions. By definition ocean water has $\delta^{18}O = \delta D = 0$. However, meteoric waters are ^{18}O and D depleted with regard to ocean water due to fractionation during evaporation and precipitation. The exact values of $\delta^{18}O$ and δD in meteoric water vary to a large extent depending upon altitude, latitude and distance from ocean (Dansgaard, 1964; Yurtsever and Gat, 1981). Craig (1961) first defined the relationship of isotopic compositions of meteoric water as $\delta D = 8\ \delta^{18}O + 10$. With burial, formation waters show overall trends to increasing $\delta^{18}O$ due to exchange with ^{18}O-enriched framework silicates (Craig, 1966; Hitchon and Friedman, 1969; Land, 1980).

$\delta^{13}C$ can be diagnostic of carbon source for diagenetic carbonates, which means that the carbon in carbonates is from ocean water or degrading organic matter. The carbon from the latter source is depth related (Irwin et al, 1977). Soon after sediments are buried, bacterial oxidation and bacterial sulphate reduction produce CO_2 with $\delta^{13}C$ similar to that of the parent organic matter, i.e. -25 ‰. Once the available sulphate is exhausted, bacterial fermentation takes place producing CO_2 with $\delta^{13}C$ of about +15 ‰, certainly positive. As the burial of sediments continues, thermally - induced decarboxylation (abiotic reaction) at greater depth operates, predominantly producing CO_2 with $\delta^{13}C$ of around -20 ‰.

The stable isotope equilibrium fractionation factor for two phases, A and B, is defined as: $\alpha_{A\text{-}B} = R_A/R_B$ where R = $^{18}O/^{16}O$, $^{13}C/^{12}C$, D/H, et al. The oxygen isotope

fractionation factors for mineral pairs or mineral-water pairs α_{A-B} can be determined experimentally. They are temperature dependent. The temperature dependence of α forms the basis of oxygen - isotope geochemistry. The quantity called permil fractionation, $10^3 \ln \alpha_{A-B}$ (O'Neil, 1979), can be estimated by the following equation:

$$\Delta_{A-B} = 10^3 \ln \alpha_{A-B} \approx (\alpha-1)10^3 \approx \delta_A - \delta_B$$

If the permil fractionation is larger than 10, which is usually the case for minerals formed at low temperatures, the above approximation becomes inaccurate and it is better to determine Δ_{A-B} precisely (Longstaffe, 1983).

Equilibrium fractionation of oxygen isotopes between pore water and oxygen bearing diagenetic mineral is assumed for the diagenetic cement formation. The temperature dependence is expressed in the form of $10^3 \ln\alpha = AT^{-2} + B$ where A and B are constants, T is temperature in ^oK, and α is the fractionation factor equal to $(10^3 + \delta^{18}O_{mineral}) / (10^3 + \delta^{18}O_{water})$. The interdependency of temperature and $\delta^{18}O$ of pore water means that if one is known or can be assumed the other can be calculated according to the known equations for different diagenetic minerals, which are presented in Table 7-2.

7.3.2 RESULTS OF STABLE ISOTOPE DETERMINATIONS

(i) Carbonates

A total of 11 carbonates from eight sandstone samples, which consist of 8 siderites, 2 ankerites and 1 calcite, were analysed and the results are presented in Table 7-3. All but one (a grain coating siderite) are pore filling carbonates predating quartz overgrowths.

Table 7-2 Temperature dependent fractionation equations.

Oxygen isotopes

$10^3 \ln\alpha_{calcite - H_2O} = 2.78\ (10^6)T^{-2} - 2.89$ (Friedman and O'Neil, 1977)

$10^3 \ln\alpha_{siderite - H_2O} = 3.13\ (10^6)T^{-2} - 3.50$ (Carothers et al., 1988)

$10^3 \ln\alpha_{ankerite - H_2O} = 2.78\ (10^6)T^{-2} + 0.32$ (Dutton and Land, 1985)

$10^3 \ln\alpha_{kaolin - H_2O} = 2.5\ (10^6)T^{-2} - 2.87$ (Land and Dutton, 1978)

$10^3 \ln\alpha_{quartz - H_2O} = 3.38\ (10^6)T^{-2} - 2.90$ (Friedman and O'Neil, 1977)

$10^3 \ln\alpha_{illite - H_2O} = -2.87 + 1.83X + 0.0614X^2 - 0.00115X^3$ (Lee, 1984, cited in Lee et al, 1989), where $X = 10^6T^{-2}$

Hydrogen isotopes

$10^3 \ln\alpha\ D_{kaolin - H_2O} = -4.53\ (10^6)T^{-2} + 19.36$ (Lambert and Epstein, 1980)

$10^3 \ln\alpha\ D_{illite - H_2O} = -19.6\ (10^3)/T + 25$ (Yeh, 1980)

Table 7-3 Stable isotope data for carbonates.

Sample no.	Mineralogy	Phase	$\partial^{18}O$ ‰ (SMOW)	$\partial^{13}C$‰ (PDB)
L506.7	siderite	II	8.30	-6.09
O488.2	siderite	II	9.25	-4.37
O488.2	ankerite	II	9.33	-4.71
O600.9	siderite	II	9.06	-4.91
Z512.4	siderite	II	9.86	-6.32
X531.9	siderite	I	14.57	-6.12
X531.9	ankerite	II	13.28	-5.60
			13.25	-5.22
Y593.9	siderite	II	7.75	-4.36
W388.8	siderite	II	14.71	-4.71
A146.5	siderite	II	10.79	-8.22
J514.8	calcite	II	5.78	-7.96
			6.54	-8.13

I = earlier grain coating carbonate
II = later pore filling carbonate

Table 7-4 Stable isotope data for kaolin-rich clays (SMOW).

	$\partial^{18}O$ ‰				∂D ‰	
Sample no.	I	II	III	IV	V	VI
L506.7		10.65				
O488.2			9.49		-112.0	
			9.31			
O600.9				7.03		-117.6
				6.62		
Z512.4			8.39	6.61	-127.9	
			8.06			
W388.8		6.36		7.47		-120.9
				7.34		
A146.5				7.48		-122.6
				7.48		
J514.8	12.10					
	13.05					

I = 0.2-1 μm e.s.d. (equivalent sphere diameter) II = 1-2 μm,
III = 2-5 μm, IV = 5-10 μm, V = 2-5 μm, VI = 5-10 μm.

The $\delta^{13}C$ values have a small range from -4.36 ‰ to -8.22 ‰. In contrast, the $\delta^{18}O$ values fall in a much greater range from 6.16 ‰ to 14.71 ‰. The $\delta^{13}C$ values and $\delta^{18}O$ values of the carbonates do not show any relationship, as illustrated in Fig 7-6.

Calcite: One calcite separate was obtained from sample J514.8. The 0.76 ‰ difference of the two analyses (5.78 ‰ and 6.54 ‰) for this sample is well outside of experimental errors, which is probably caused by heterogeneity of the calcite. Nevertheless, reproducibility of $\delta^{13}C$ is quite good. Of the carbonates, the calcite has the lowest $\delta^{18}O$ value.

Siderite: The $\delta^{18}O$ and $\delta^{13}C$ values of the seven pore filling siderite samples range from 7.75 ‰ to 14.71 ‰ and -4.36 ‰ to -8.22 ‰ respectively with 6 $\delta^{18}O$ values falling in a more restricted range from 7.75 ‰ to 10.79 ‰. The other siderite sample has a $\delta^{18}O$ value of 14.71 ‰, which is nearly identical with the $\delta^{18}O$ value of 14.57 ‰ of the grain coating siderite.

Ankerite: Two pore filling ankerite samples from X531.9 and O488.2 yielded a quite different $\delta^{18}O$ values of 13.27 ‰ and 9.33 ‰ and a similar $\delta^{13}C$ values of -5.41 ‰ and -4.71 ‰. Reproducibility of $\delta^{18}O$ for sample X531.9 is very good and the $\delta^{13}C$ values are in a reasonable agreement even though their difference (0.38 ‰) is larger than the experiment errors (0.2 ‰).

(ii) Clay Minerals

Pure clay minerals were obtained from all the nine sandstone samples subject to isotope studies. They consist of 9 kaolins from 7 of the nine samples and 16 illites from 8 of them. Chlorite is present in sample J514.8, but none of the size fractions

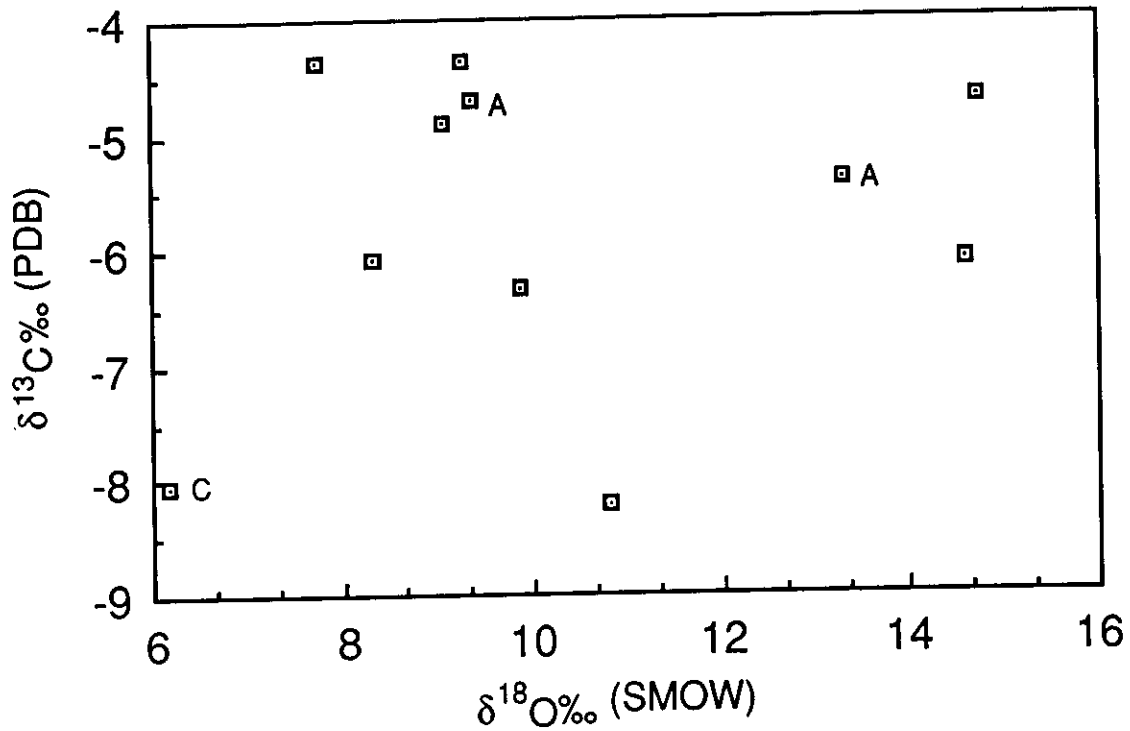

Fig 7-6 Cross plot of $\delta^{13}C$ vs. $\delta^{18}O$ of carbonates. A = ankerite, C = calcite, unmarked points = siderite.

of this sample was sufficiently chlorite - rich (more than 90 %) to merit analyses.

Kaolin: The $\delta^{18}O$ values of 9 kaolin samples (purity >90%) are illustrated in Table 7-4. It seems that there exists a general relationship between the $\delta^{18}O$ value and the size of kaolins. The $\delta^{18}O$ value increases with the decrease of fraction size with the 2-1 μm size fraction of sample W388.8 as an exception. The 10-5 μm kaolin fractions have very similar $\delta^{18}O$ values ranging from 6.61 ‰ to 7.48 ‰. By contrast, the fine sized kaolin fractions have much larger $\delta^{18}O$ values with the $\delta^{18}O$ of 2-1 μm fraction of sample L506.7 and the $\delta^{18}O$ of 1-0.2 μm fraction of sample J514.8 being 10.65 ‰ and 12.65 ‰ respectively. Reproducibility of $\delta^{18}O$ for the kaolins is very good and is generally within the experimental errors. The poor reproducibility for sample J514.8 is probably caused by sample heterogeneity.

Of the nine kaolin samples which were subject to oxygen isotope analyses, only 5 of them had enough material for hydrogen isotope analyses. The analyses results are listed in Table 7-4. The δD values range from -127.9 ‰ to -112.0 ‰.

Illite: A total of 16 illite samples were analysed for oxygen isotope and the results are presented in Table 7-5. The $\delta^{18}O$ values of the illites vary from 5.12 ‰ to 8.12 ‰. The duplicates of illite analyses show very good agreement. In addition, the $\delta^{18}O$ values of illite separates are generally independent of the size of the separates. Different sized fractions have similar $\delta^{18}O$ values for the same sample.

Twelve of the 16 illite fractions were subject to hydrogen isotope analyses. The results are listed in Table 7-5. The δD values fall in a range from -127.7 ‰ to -99.4 ‰ with 11 of them varying in a more narrow range from -127.7 ‰ to -109.4 ‰. They do not have any relationship with the size of the illite fraction.

Table 7-5 Stable isotope for illite-rich clays (SMOW).

	∂^{18}O ‰			∂D ‰	
Sample no.	I	II	III	IV	V
L506.7	7.49	7.78			-114.5
O488.2	6.63	6.42		-112.5	-112.9
		6.21			
O600.9	5.92	6.12			-109.4
	5.95	5.93			
Z512.4	5.48	5.32	5.92	-116.3	-116.8
	5.91		5.89		
X531.9	8.12	7.30			-116.1
		7.10			
Y593.9	5.24	5.81		-127.7	-119.8
	5.01	5.73			
		5.78			
W388.8	5.14			-117.0	
	5.09				
A146.5	5.95	6.12		-122.4	-99.4
	5.80	5.93			

I = <0.2 μm, II = 0.2-1 μm, III = 1-2 μm, IV = <0.2 μm, V = 0.2-1μm

Table 7-7 Potassium - argon illite ages.

Sample no.	Size fraction (μm)	K wt. %	Age 10^6 years
L506.7	<0.2	5.75	90.5 +/- 0.9
		5.76	
Z512.4	<0.2	6.66	123.1 +/- 1.4
		6.64	
X531.9	<0.2	6.35	121.5 +/- 1.3
		6.28	
	0.2-1	6.00	126.2 +/- 1.3
		5.85	
W388.8	<0.2	5.99	146.2 +/- 1.6
		5.94	

(iii) Quartz overgrowths:

Pure quartz separates were obtained for 6 of the nine samples subject to isotope studies. The values of the various sized fractions of the six samples are listed in Table 7-6. Reproducibility for coarse fractions (>125 μm) is generally poor, which is attributed to heterogeneity in these fractions of overgrowth abundance relative to detrital quartz abundance. By contrast, reproducibility is generally good for finer sized fractions (<125 μm) with most of the duplicates being well within the experimental errors.

As described in the methodology section, the treatment of quartz separates with HF and following ultrasonic vibration is expected to detach overgrowths from detrital cores and lead to concentration of overgrowths into progressively finer sized fractions (Lee and Savin, 1985). However, this is not confirmed by the analyses results of four of the six samples (L506.7, O600.9, Z512.4 and X531.9). For the four samples, there is no significant variation in the $\delta^{18}O$ values between the coarse sized and the fine sized fractions. Thus it is assumed that the HF attack and the following ultrasonic vibration treatment for the four samples did not work efficiently to detach overgrowths from detrital cores. For the other two samples (Y593.9 and A146.5), there is a significant difference (>1 ‰) in the $\delta^{18}O$ values between the coarse sized and the fine sized fractions. $\delta^{18}O$ values of the fractions increase progressively with decreasing particle size (Fig 7-7), suggesting finer sized fractions contain higher concentration of quartz overgrowths. The highest value of 13.13 ‰ obtained for sample Y539.9 defines a lower limit for the $\delta^{18}O$ value of the quartz overgrowths. The two smallest size fractions for sample A146.5 have very similar $\delta^{18}O$ values (13.48 ‰ and 13.85 ‰). The slight increase in $\delta^{18}O$ from 13.48 ‰ to 13.85 ‰ with decreasing particle size suggests a two component system (detrital quartz core and diagenetic quartz overgrowth) in which the $\delta^{18}O$ of the

Table 7-6 Oxygen isotope data for quartz separates (SMOW).

Sample no.	∂^{18}O ‰ I	II	III	IV	V
L506.7	12.95	12.48	12.35	12.20	12.55
	13.44	11.84	12.59		
O600.9	9.90	10.21		10.48	10.28
	10.50	10.64	10.69	10.42	10.17
Z512.4	11.65	12.32	12.56	11.57	11.91
	12.35	12.35	13.47	12.00	11.84
X531.9	11.29	10.59	11.52	10.59	
	10.68			10.22	
Y593.9	11.65	12.11	12.28	13.13	12.67
	10.95	11.91	12.59		12.70
A146.5	12.16	12.58	12.58	13.46	13.49
	11.56	11.77	12.63	13.49	14.21

I = 250-180 μm fraction prior to HF treatment etc.

II = 250-180 μm fraction after HF/ultrasonic treatment and sieving

III = 180 - 125 μm fraction after HF/ultrasonic treatment and sieving

IV = 125-75 μm fraction after HF/ultrasonic treatment and sieving

V = 75-20 μm fraction after HF/ultrasonic treatment and sieving

Table 7-8 Petrographic data on liquid hydrocarbon inclusions in quartz overgrowths.

sample no.	presence of fluorescing clays	presence of liquid hydrocarbon inclusions in overgrowths	in fractures	colour of fluorescence
L506.7	yes	yes	no	light blue
O600.9	yes	yes		light yellow-cream
			yes	blue
Z512.4	yes	no	yes	yellow-orange and blue
X531.9	yes	yes		yellow-blue
			yes	blue and yellow-orange

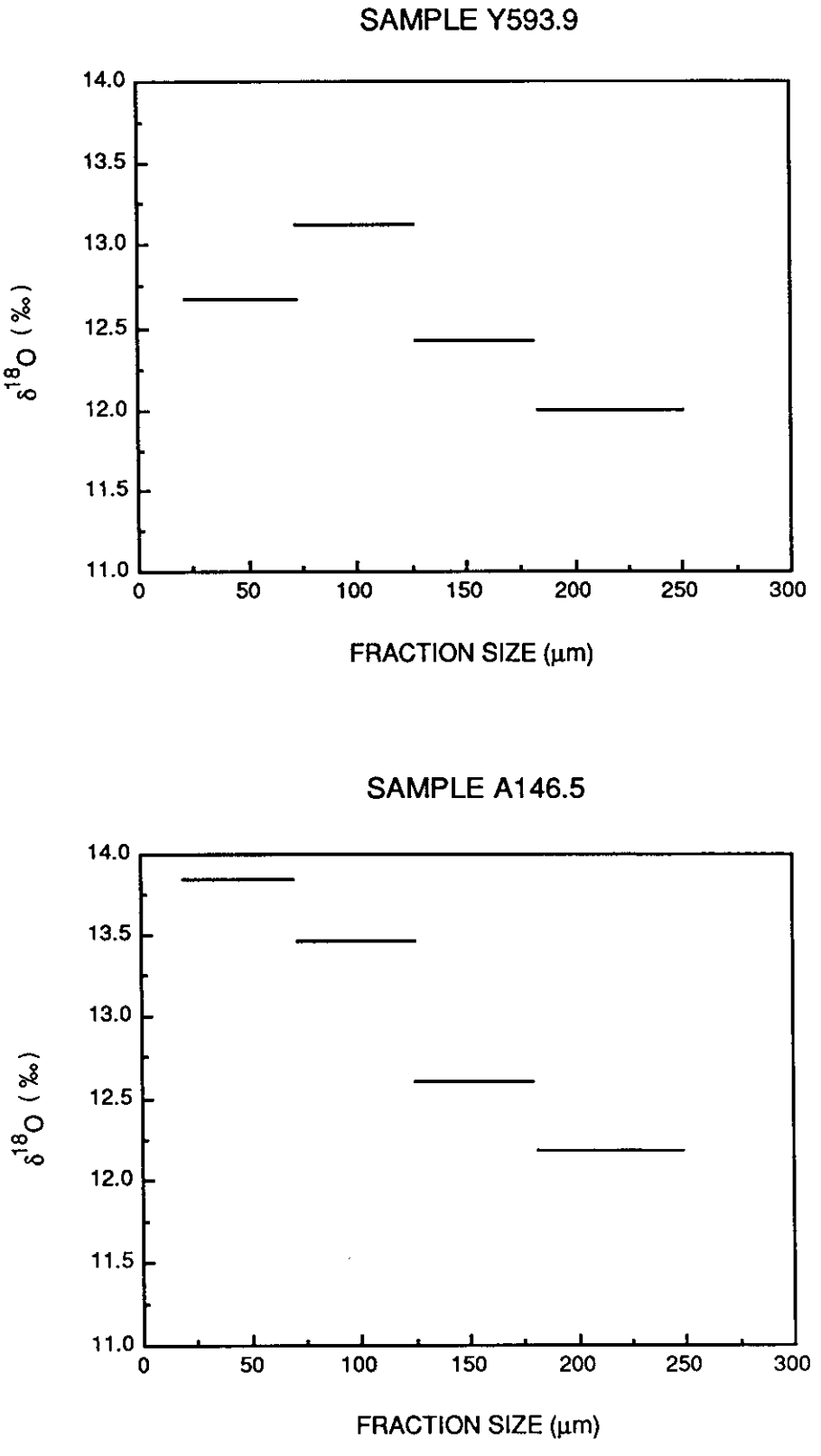

Fig 7-7 $\delta^{18}O$ vs. fraction size of quartz separates after HF treatment.

diagenetic quartz overgrowth is slightly greater than 13.85 ‰ (cf. Lee and Savin, 1985). The conclusion from these analyses is that the $\delta^{18}O$ values of quartz overgrowths are estimated to lie between 13 ‰ and 14 ‰.

7.3.3 POTASSIUM - ARGON ILLITE AGES

The K-Ar age dating was carried out for high purity <0.2 μm size fractions from four samples and a coarser 1-0.2 μm fraction from one of the four samples. The results are presented in Table 7-7. The illite ages range from 146.2 Ma for sample W388.8 from Weromba 2 in the west margin of the basin, to about 123 Ma for samples X531.9 and Z512.4 from Cobbitty 3 and Campbelltown 5 in the southern region of the basin, and finally to 90.5 Ma for sample L506.7 from Liverpool 91 in the east coast zone of the basin. The age of the coarser fraction for sample X531.9 was determined to be 126.2 Ma which is about 5 Ma older than the age of the finer fraction of the same sample.

7.4 FLUID INCLUSION INVESTIGATION

7.4.1 PETROGRAPHY OF AQUEOUS AND HYDROCARBON FLUID INCLUSIONS

In all the four samples investigated, aqueous fluid inclusions were recognised. They occur at the boundary between detrital quartz cores and quartz overgrowths and actually within overgrowths. Their relationships with the quartz overgrowths suggest they were formed during quartz cementation. Despite the common occurrence of carbonate cements in the four samples, only one aqueous fluid inclusion suitable for measurement of homogenisation temperature was found in a carbonate host.

The aqueous fluid inclusions are normally 4-10 μm in diameter and have rounded, elongated or irregular shapes. At room temperature, they consist of a colourless liquid and a gas bubble. Figs 7-8 and 7-9 show an example of the aqueous fluid inclusions within the quartz overgrowths and at the boundary between the detrital

Fig 7-8 (top left) Aqueous fluid inclusions within a quartz overgrowths observed with plain polarised light. From South Colah 1 at drilling depth of 600.9 m (sample O600.9). Scale bar is 10 μm.

Fig 7-9 (top right) Aqueous fluid inclusions between detrital core and overgrowths observed with plain polarised light. From Liverpool 91 at drilling depth of 506.7 m (sample L506.7). Scale bar is 20 μm.

Fig 7-10 (upper left) Liquid fluid inclusion fluorescing light blue within quartz overgrowths. Outline of detrital quartz grain is marked by a line of clays with pale cream fluorescence. The fluorescence was excited by violet light illumination. From South Colah 1 at drilling depth of 600.9 m (sample O600.9). Scale bar is 10 μm.

Fig 7-11 (upper right) Same detrital quartz grain and subject as in Fig 7-10 but observed with plane polarised light. The outline of the detrital grain is marked by a curved trail of inclusions in the bottom right of the photograph. Scale bar is 10 μm.

Fig 7-12 (lower left) Fluorescing film of liquid oil trapped between siderite crystals and quartz overgrowths. The oil has a yellow green fluorescence and the siderite has brown fluorescence. The fluorescence was excited by ultraviolet light illumination. From Cobbitty 3 at drilling depth of 531.9 m (sample X531.9). Scale bar is 50 μm.

Fig 7-13 (lower right) Same detrital quartz grain and subject as in Fig 7-12 but observed with plane polarised light. Rhombohedral siderite crystals are enclosed by quartz overgrowths. Scale bar is 50 μm.

Fig 7-14 (bottom left) Yellow-green fluorescing liquid oil inclusions with a conchoidal distribution decorating a healed fracture that formed across a detrital quartz grain. The fluorescence was excited by ultraviolet light illumination. From Cobbitty 3 at drilling depth of 531.9 m (sample X531.9). Scale bar is 20 μm.

Fig 7-15 (bottom right) Same detrital quartz grain and subject as in Fig 7-14 but observed with plane polarised light. Scale bar is 20 μm.

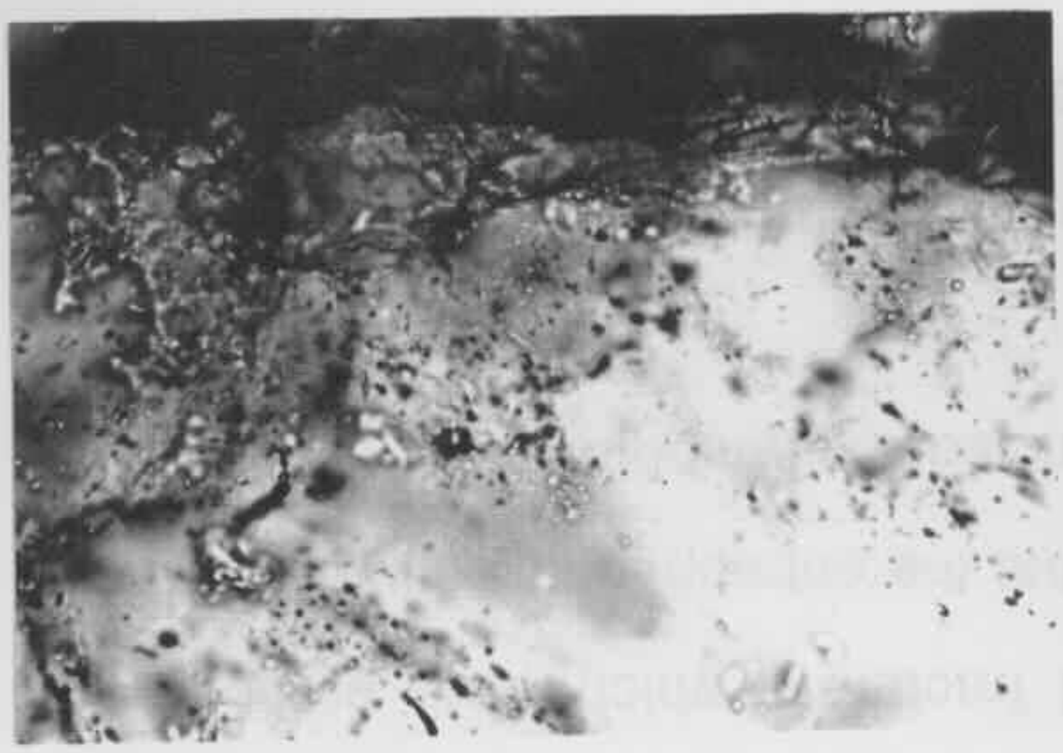

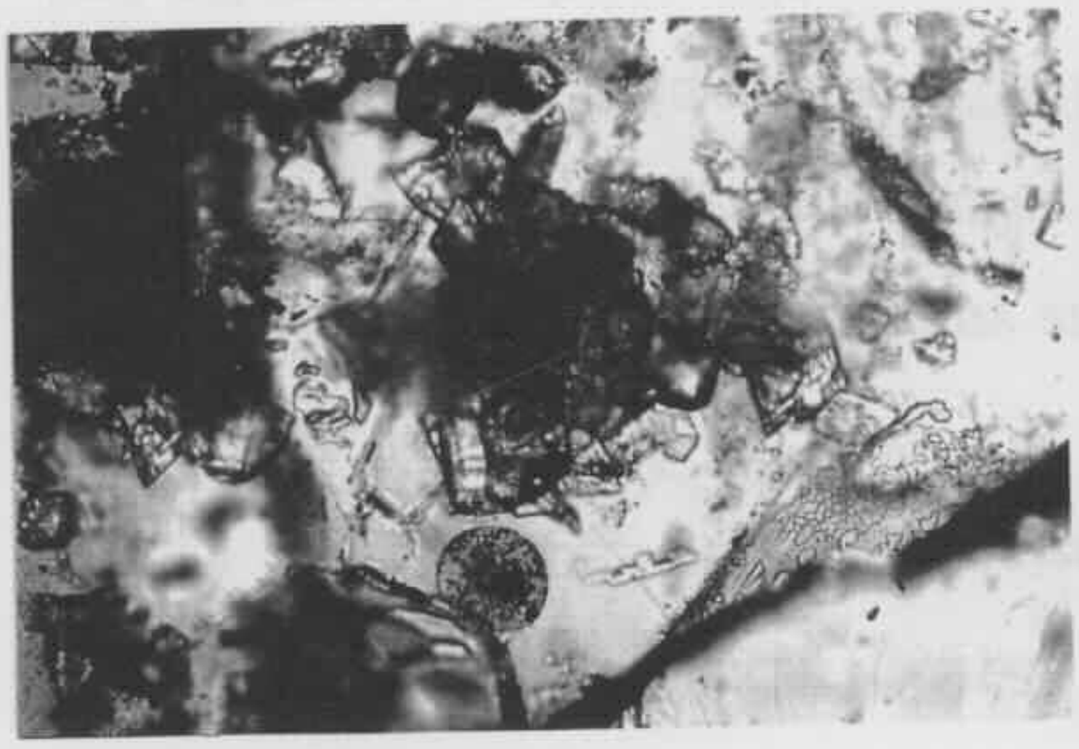

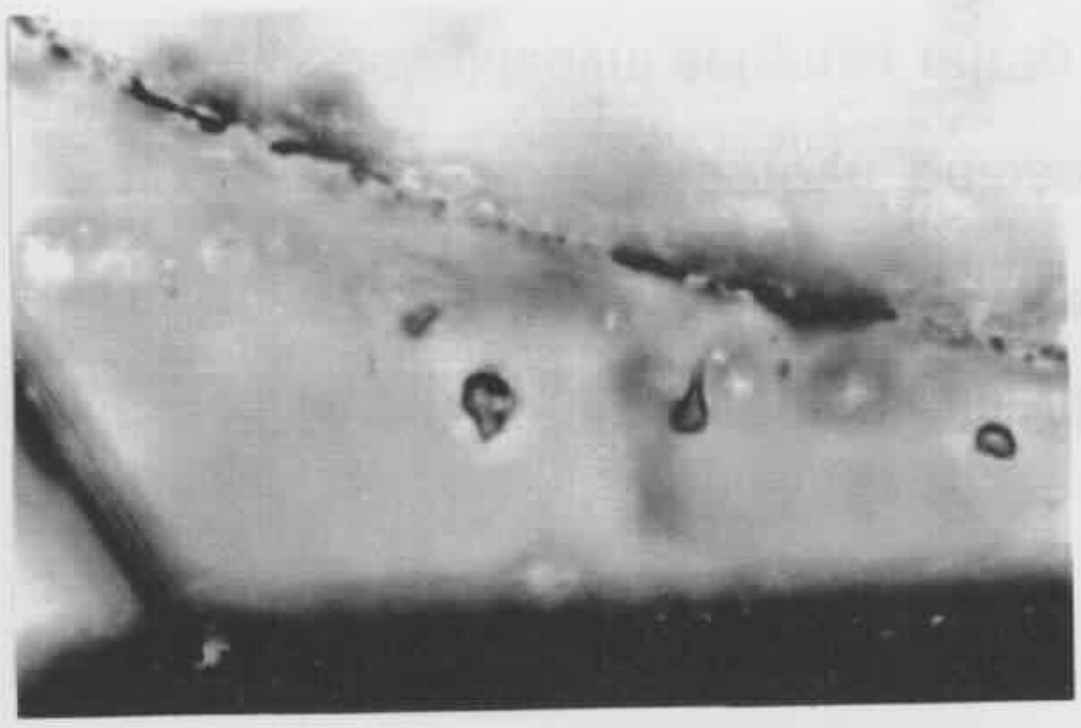

quartz core and overgrowths.

Hydrocarbon fluid inclusions are recognised by their fluorescence. They tend to be larger than the aqueous fluid inclusions. At room temperature they contain a colourless liquid and a gas bubble. Fluorescing hydrocarbon inclusions were observed within quartz overgrowths in three of the samples investigated - X531.9, L506.7 and O600.9 (Table 7-8). Their relationship with quartz overgrowths suggests that they were formed during precipitation of quartz overgrowths. Figs 7-10 and 7-11 illustrate an example of the fluorescing hydrocarbon inclusions within the quartz overgrowths in sample O600.9 from South Colah 1. In sample X531.9 from Cobbitty 3, fluorescing liquid hydrocarbons were found to coat diagenetic rhombohedral siderite crystals which are in turn enclosed by quartz overgrowths (Figs 7-12 & 7-13).

Fluorescing hydrocarbon inclusions were also found in healed fractures that cut through both detrital quartz cores and quartz overgrowths. The inclusions occur in three of the samples - O600.9, X531.9 and Z512.4 (Table 7-8). Figs 7-14 & 7-15 show an example of liquid hydrocarbon inclusions in healed fractures.

The fluorescing colour of liquid hydrocarbons varies from yellow orange, which is characteristic of low maturity oil, to bluish white, which is characteristic of high maturity oil and condensate (McLimans, 1987). In sample O600.9 from South Colah 1, liquid hydrocarbon inclusions, which occur within quartz overgrowths and thus were formed during precipitation of quartz overgrowths, fluoresce light yellow-cream whereas those occurring in healed fractures, which were presumably formed later, fluoresce blue. This suggests that the entrapped liquid hydrocarbons were increasing in maturity with time due to increasing temperature.

Liquid hydrocarbon inclusions with blue fluorescence occur within quartz overgrowths in sample L506.7 from Liverpool 91 and those with yellow-blue occur

in sample X531.9 from Cobbitty 3. Liquid hydrocarbon inclusions with blue and yellow-orange fluorescence were observed to decorate healed fractures in sample Z512.4 from Campbelltown 2 and sample X531.9 from Cobbitty 3. The variability of fluorescence colour of the liquid hydrocarbon inclusions suggests different times of entrapment of liquid hydrocarbons and precipitation of quartz overgrowths relative to hydrocarbon maturation at different locations of the study area.

7.4.2 RESULTS OF FLUID INCLUSION TEMPERATURE MEASUREMENTS

Homogenisation temperatures were measured for 38 different aqueous fluid inclusions from the four samples. The results are presented in Table 7-9. No measurement was made for hydrocarbon inclusions since they were rarely seen in the four samples and more importantly the isochores for hydrocarbon inclusions are much more difficult to predict than those for aqueous fluid inclusions. The distribution of homogenisation temperatures of aqueous inclusions for the four samples is illustrated in Fig 7-16. The mean homogenisation temperatures range from 95 °C in sample O600.9 from the Scarborough Operational Unit in South Colah 1 borehole to 120 °C in sample Z512.4 from the Lower Bulgo Operational Unit in Campbelltown 2 borehole. The standard deviations fall in the range from 7.6 °C to 15.8 °C (Table 7-9).

Ice melting point temperatures were measured for 21 different aqueous fluid inclusions. The results are presented in Table 7-10. Positive melting points are attributed to decomposition of clathrate compounds of carbon dioxide ($CO_2 5.75H_2O$) or methane. Clathrate compounds decompose between -14 °C and +9 °C depending on salinity and gas pressure (Collins, 1979; Hanor, 1980). The distribution of the non-positive melting points for the four samples are illustrated in Fig 7-17. The means of ice melting point temperatures range from -0.5 °C to -0.93 °C.

Table 7-9 Homogenisation temperatures of aqueous fluid inclusions in quartz overgrowths.

Sample no.	Th (°C)	Mean	Standard Deviation
L506.7	101.0		
	123.0		
	105.0		
	98.5	113	13.4
	126.5		
	117.0		
	122.0		
O600.9	94.0		
	105.0		
	80.0		
	87.0		
	120.0		
	92.5		
	101.0		
	96.0	95	15.8
	86.0		
	90.0		
	111.0		
	122.0		
	87.0		
	83.0		
	76.0		
Z512.4	131.0		
	131.5		
	118.0		
	120.0		
	115.0	120	9.8
	134.5		
	109.0		
	100.0		
	79.5*		
X531.9	90.0		
	109.0		
	105.0		
	101.5	105	7.6
	115.5		
	103.0		
	111.0		

Th = homogenisation temperature * This inclusion is within carbonate.

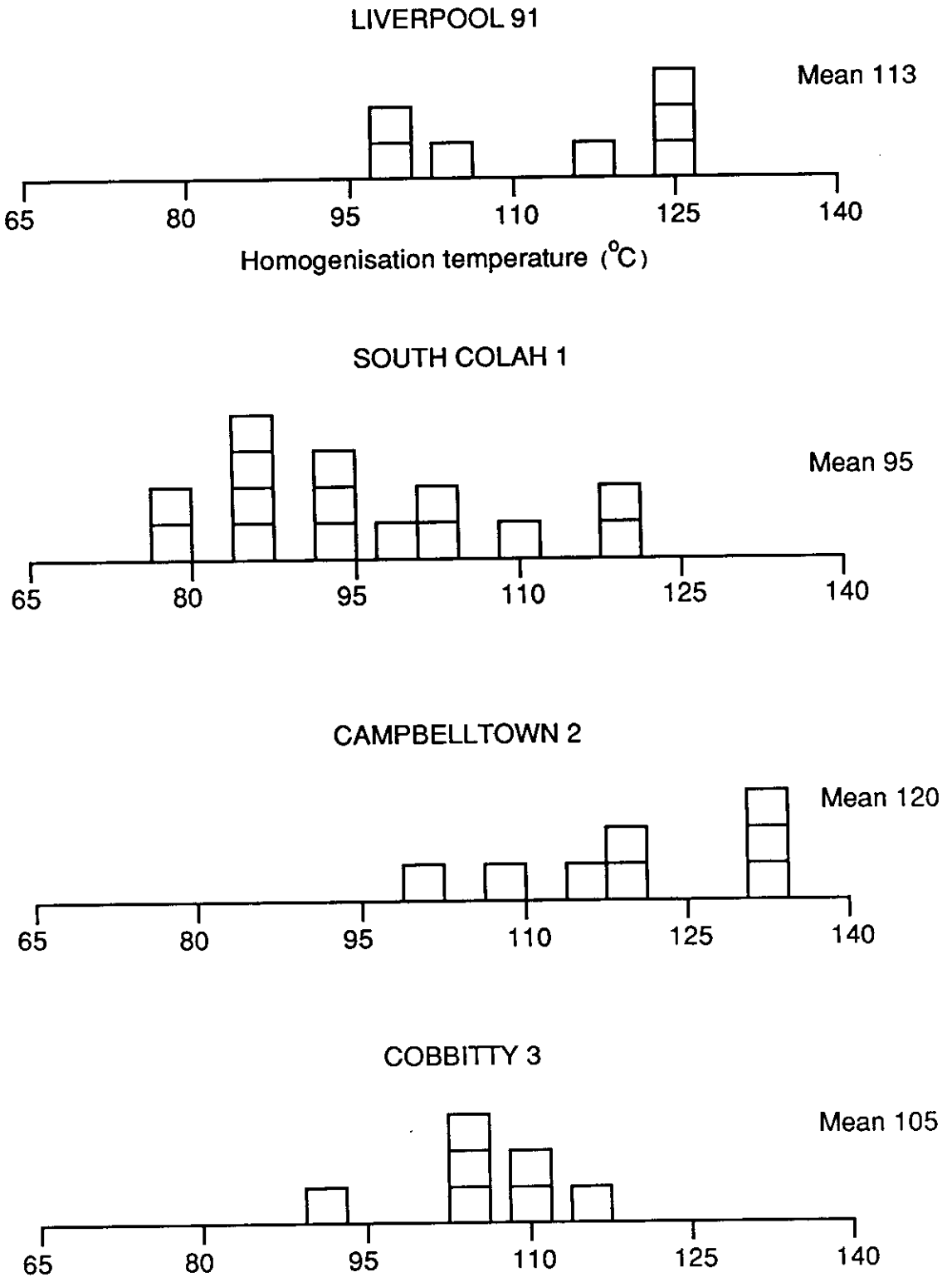

Fig 7-16 Histograms of homogenisation temperatures for aqueous fluid inclusions in quartz overgrowths.

Table 7-10 Melting points and salinities of aqueous fluid inclusions in quartz overgrowths.

sample no.	* Tm (°C)	** Mean	salinity (wt % NaCl equivalent)
L506.7	-0.5		
	-0.55		
	-0.7	-0.77	1.34
	-1.3		
	-0.8		
O600.9	-0.5		
	-0.9		
	-1.25	-0.93	1.61
	-1.45		
	-0.75		
	-0.7		
	+0.2***		
	+0.35***		
	+0.35***		
	+1.2***		
Z512.4	-0.5	-0.5	0.87
	-0.5		
X531.9	-0.5		
	-0.65	-0.73	1.27
	-1.1		
	-0.65		

* Tm = ice melting point temperature

** It is the mean of non-positive melting points.

*** Positive melting points are attributed to decomposition of clathrate compounds of carbon dioxide (CO_2 $5.75H_2O$) or methane. Clathrate compounds decompose between -14 and +9°C.

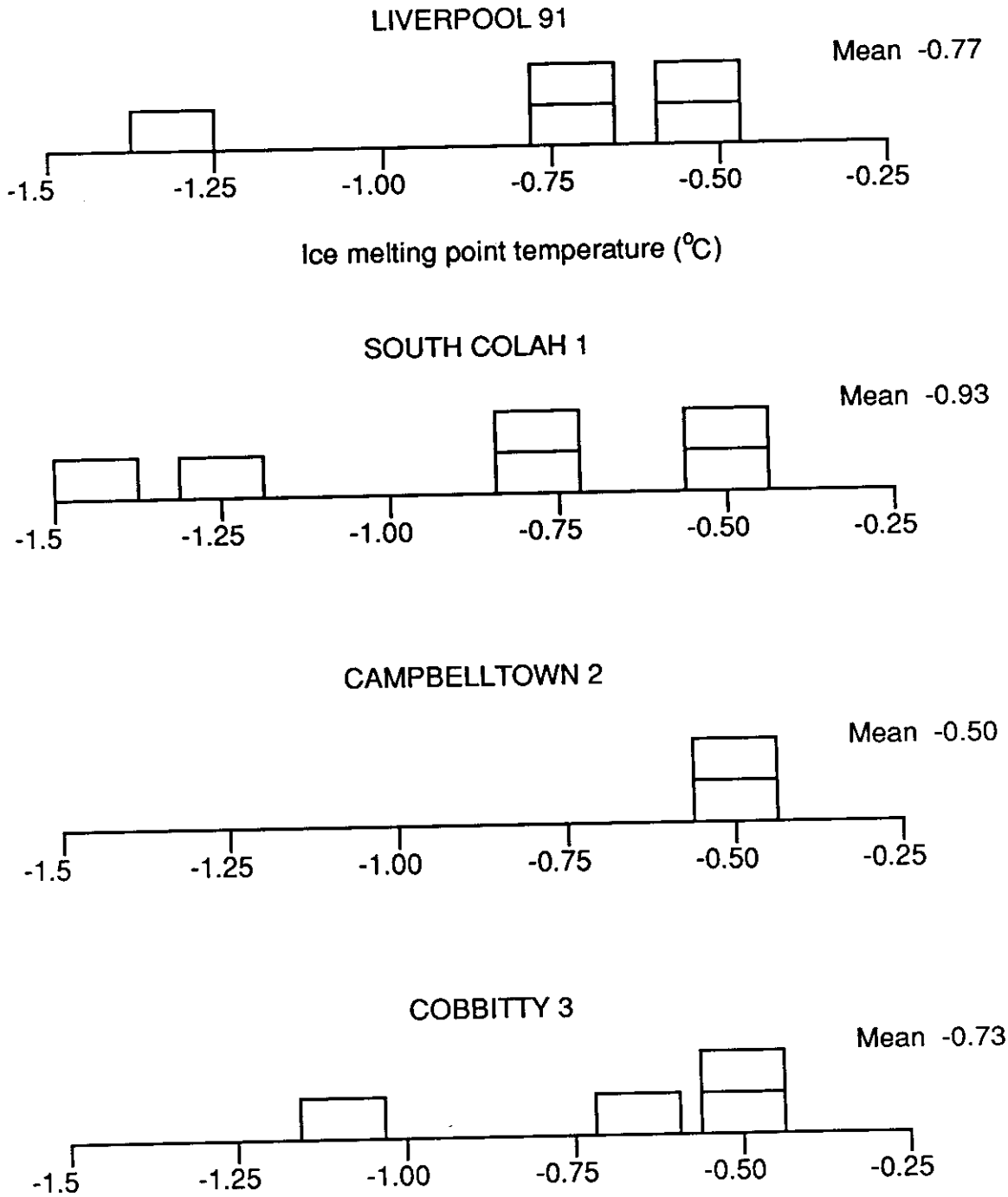

Fig 7-17 Histograms of ice melting temperatures for aqueous fluid inclusions in quartz overgrowths.

Ice melting point temperatures can be used to obtain the concentration of dissolved solids in the pore waters to constrain the slope of the isochore as well as to identify differences in the character of the pore waters. The approximate salt contents were calculated from the depression of ice melting points according to the following formula.

$$\text{Salt content} = 1.77Ø - 4.238 .10^{-2} Ø^2 + 5.278 .10^{-4} .Ø^3$$

where Ø is the depression of freezing point for a NaCl solution (Potter et al., 1977). Salt contents corresponding to the mean ice melting points of -0.5 °C to -0.93 °C were calculated to be 0.87 to 1.61 wt.% (NaCl equivalent).

7.5 INTERPRETATION AND APPLICATION OF FLUID INCLUSION DATA

7.5.1. INTRODUCTION

The interpretation of fluid inclusion data is based largely on a comparison of the behaviour of the studied inclusion with that expected of a similar inclusion containing a simplified composition, for which pressure - volume - temperature - composition (P - V -T - X) data are already known through laboratory experiments (Roedder, 1984). Even though T - V plots are useful, isochores (lines of constant volume and hence constant density) on P - T plots are most commonly used for the interpretation of fluid inclusion data. Fluid inclusion isochores for pure water and aqueous salt solutions with known content of salt (wt. % NaCl equivalent) are well established by laboratory experiments. If the salt content of the fluid inclusion is known from the depression of the ice melting point of the inclusion, the fluid inclusion isochore can be predicted. As listed in Table 7-10, the mean salinities range from 0.87 to 1.61 wt. % (NaCl equivalent). The low salinities imply that isochores for pure waters (Roedder and Bodnar, 1980) can be used in the interpretation of the fluid inclusion temperature data.

In this thesis, fluid inclusion data are applied to determine the formation (precipitation) temperature of quartz overgrowths, which will be used in reconstruction of chemical evolution of pore waters, and to deduce thermal history, which will be used to theoretically calculate timing and amount of oil generation. In this application, a number of assumptions and approximations are involved. They will be stated latter in the appropriate paragraphs. All the involved theoretical calculations and modelling were carried out in a personal computer using the programme of Dr Peter Eadington (CSIRO, North Ryde). The stratigraphic data inputs are listed in Table 7-11. Depth and lithology of the formations are from geological logging of the four boreholes. Ages of the formations tops were derived from correlation (see Fig 4-3) of the operational units with the composite stratigraphic column of the Sydney Basin (Retallack, 1980). The absolute ages are from the 1989 Global Stratigraphic Chart (Supplement to Episodes 12 (2), June, 1989). The current heat flow value, shown below the borehole name in Figs 7-18 & 7-19, at a given borehole location was derived from the data of Sass et al. (1976). Vitrinite reflectance (R_v) was estimated by extrapolation from profiles measured by Diessel (1975) and from the results measured by Middleton (1983).

7.5.2. DETERMINATION OF PRECIPITATION TEMPERATURE OF QUARTZ OVERGROWTHS AND DEDUCTION OF THERMAL HISTORY

Hydrostatic pressure is assumed during the burial diagenesis of the Narrabeen Group. Thus the pressure scale can be transformed to the depth scale and fluid inclusion isochores illustrated on the depth (pressure) - temperature plots. The temperature profile, which shows the relationship between temperature and burial depth, is used as a guide to determine the precipitation temperature of quartz overgrowths.

The temperature at a given depth (temperature profile) is calculated using the method of Falvey and Middleton (1981) and Falvey (1982).

Table 7-11 Lithology, formation tops, and age of formations.

Formation name	Lithology	Type of stratigraphy	Drilling depth (m) at formation tops	Age (Ma) at formation tops
		Liverpool 91		
unconformity	sandstone	unconformity	0	0
Triassic	sandstone	sedimentation	0	205
Bald Hill	shale	sedimentation	270	241
Upper Bulgo	sandstone	sedimentation	308	243
Lower Bulgo	sandstone	sedimentation	442	245
Scarborough	sandstone	sedimentation	525	247
Wombarra	shale	sedimentation	657	252
Illawarra	coal measures	sedimentation	762	256
Base of section			919	258
		South Colah 1		
unconformity	sandstone	unconformity	0	0
Triassic	sandstone	sedimentation	0	205
Bald Hill	sandstone	sedimentation	289	241
Upper Bulgo	sandstone	sedimentation	323	243
Lower Bulgo	sandstone	sedimentation	482	245
Scarborough	sandstone	sedimentation	546	247
Wombarra	shale	sedimentation	638	252
Illawarra	coal measures	sedimentation	756	256
Base of section			936	258
		Campbelltown 2		
unconformity	sandstone	unconformity	0	0
Triassic	sandstone	sedimentation	0	205
Bald Hill	shale	sedimentation	349	241
Upper Bulgo	sandstone	sedimentation	391	243
Lower Bulgo	sandstone	sedimentation	500	245
Scarborough	sandstone	sedimentation	569	247
Wombarra	shale	sedimentation	674	252
Illawarra	coal measures	sedimentation	776	256
Base of section			836	258
		Cobbitty 3		
unconformity	sandstone	unconformity	0	0
Triassic	sandstone	sedimentation	0	205
Bald Hill	shale	sedimentation	276	241
Upper Bulgo	sandstone	sedimentation	332	243
Lower Bulgo	sandstone	sedimentation	449	245
Scarborough	sandstone	sedimentation	514	247
Wombarra	shale	sedimentation	602	252
Illawarra	coal measures	sedimentation	692	256
Base of section			770	258

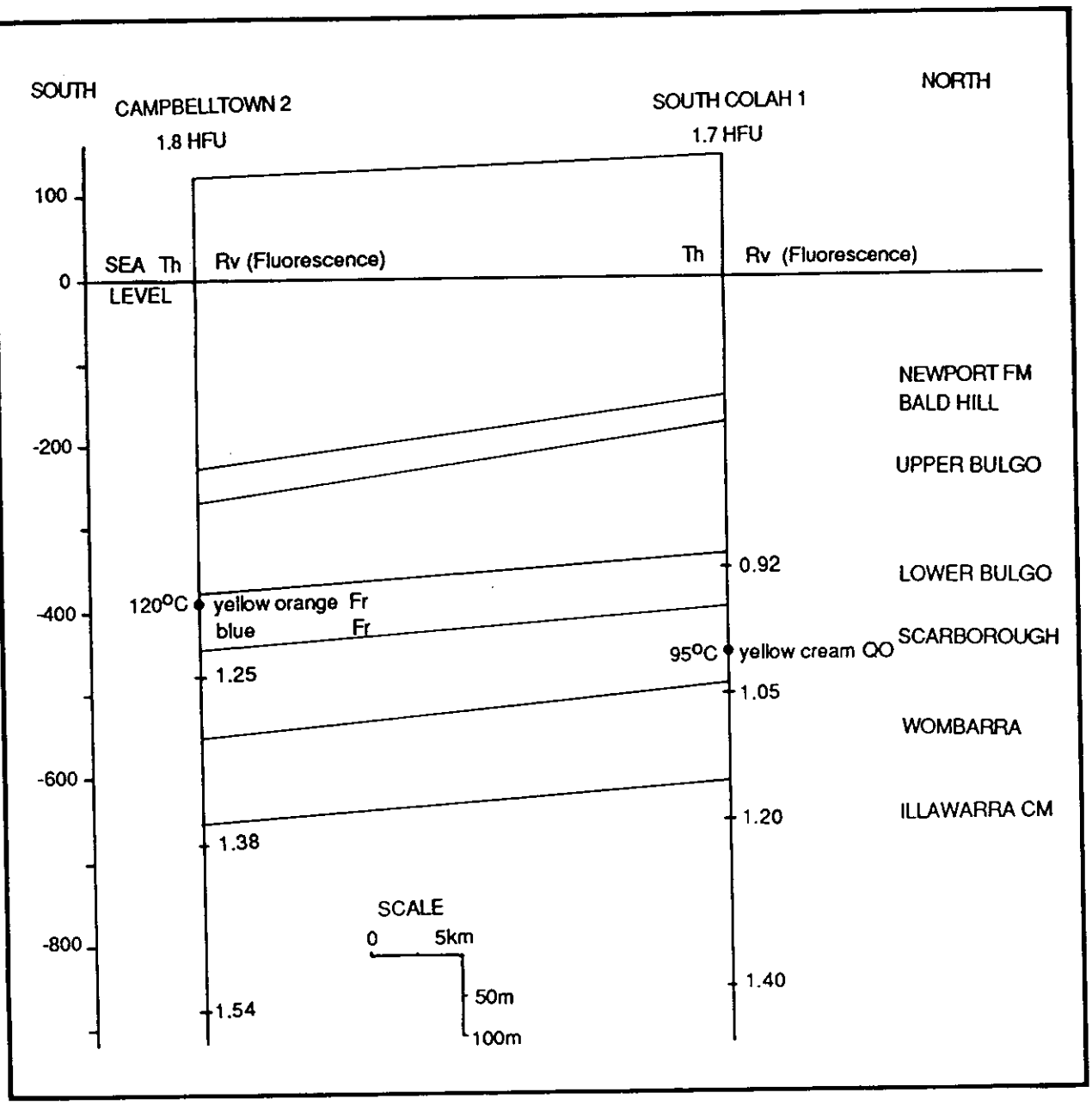

Fig 7- 18 North-south cross section through the southern Sydney Basin, showing the distribution of liquid hydrocarbon inclusions (LHI), homogenisation temperatures (T_h) of aqueous fluid inclusions and vitrinite reflectances (R_v) estimated by extrapolation from profiles measured by Diessel (1975). Fr = fracture. QO = quartz overgrowths. Fluorescence refers to that of LHI.

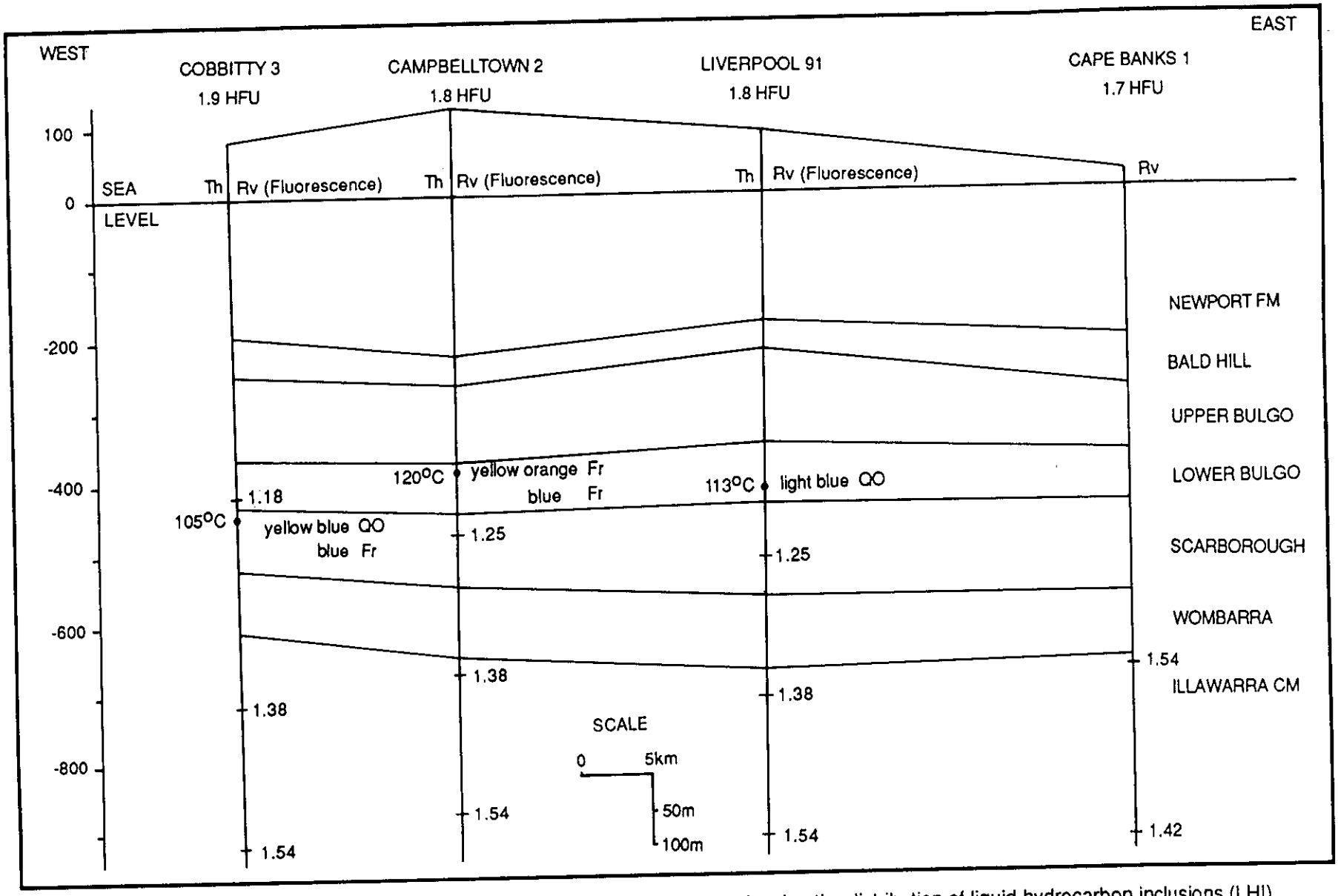

Fig 7-19 East-west cross section through the southern Sydney Basin, showing the distribution of liquid hydrocarbon inclusions (LHI), homogenisation temperatures (Th) of aqueous fluid inclusions and vitrinite reflectances (Rv) estimated by extrapolation from profiles measured by Diessel (1975). Rv in CAPE BANKS 1 is from the results measured by Middleton (1983). Fr = fracture. QO = quartz overgrowths. Fluorescence refers to that of LHI.

$$T = \int_0^h [Q / K_{(h)}]\, d_h \quad (I) \qquad K_{(h)} = K_D - (K_D - K_U) \exp(-\beta h) \quad (II)$$

Where T = temperature at a given depth h (°C), Q = heat flow (HFU, 10^{-6} cal cm^{-2} sec^{-1}), $K_{(h)}$ = depth and lithology related thermal conductivity (cal cm^{-1} sec^{-1} $°C^{-1}$), K_D = maximum thermal conductivity at zero porosity and deep basin temperature, K_U = minimum thermal conductivity at surface porosity and temperature, ß = constant for a given section (cm^{-1}), and h = burial depth (cm). The inter-dependency of temperature and heat flow means that if one is known, the other can be calculated using equation (I). The values of K_D, K_U and ß used in the calculation are listed in the following table (Table 7-12).

LITHOLOGY	K_U (cal cm^{-1} sec^{-1} $°C^{-1}$)	K_D (cal cm^{-1} sec^{-1} $°C^{-1}$)	ß (cm^{-1})
shale*	2.3×10^{-3}	5.0×10^{-3}	6.0×10^{-6}
sandstone *	4.5×10^{-3}	9.0×10^{-3}	3.0×10^{-6}
coal measures #	3.0×10^{-3}	6.0×10^{-3}	4.5×10^{-6}

* From Falvey (1982)

\# Assigned by the current author (P.J. Eadington, personal communication) to best fit the temperature profile of interbedded sand / shale.

The upper right diagram in Fig 7-20 illustrates the current temperature profile and the fluid inclusion isochore. The temperature profile was calculated according to equation (I) using a heat flow value of 1.9 HFU, a surface temperature of 20 °C, and lithological data of this borehole (Cobbitty 3). The isochore shown here is for pure water (Roedder and Bodnar, 1980). It shows the relationship between temperature and burial depth (pressure) at the precipitation of quartz overgrowths and illustrates possible temperature and pressure combinations for the trapping of

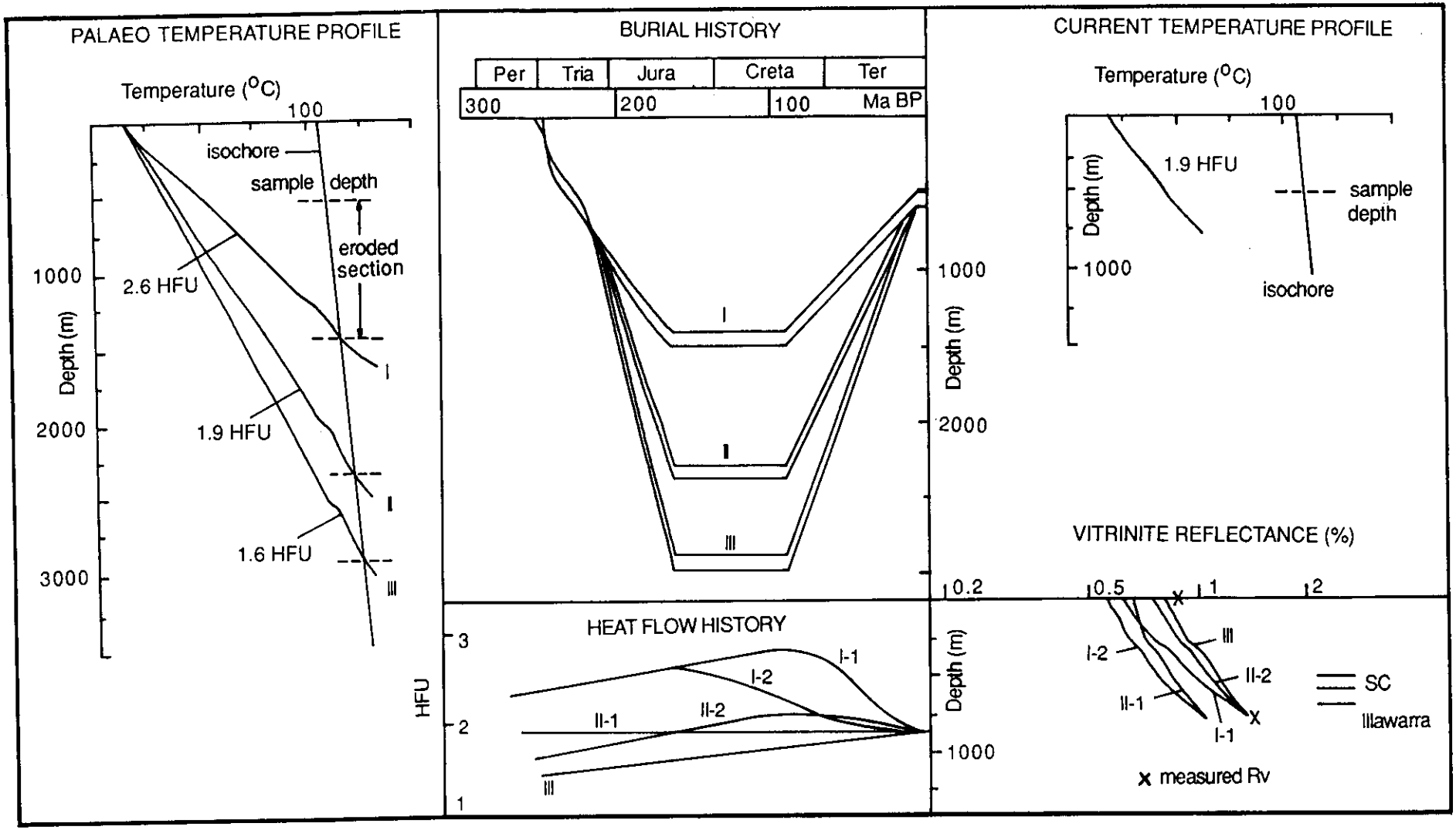

Fig 7-20 Current and palaeo temperature profiles, burial history (top and bottom of the Scarborough Operational Unit) and heat flow history models, and calculated vitrinite reflectance depth profiles for Cobbitty 3. Lines marked with the same symbol (I, II, III, I-1, I-2, II-1 and II-2) in different diagrams correspond to one another. Measured vitrinite reflectances (R_v) are estimated by extrapolation from profiles measured by Diessel (1975).

fluid inclusions. The end temperature of the isochore is the mean homogenisation temperature of 105 °C for sample X531.9 from Cobbitty 3. At the current sample depth of 531.9 m, the formation temperature is ~ 45 °C (obtained from the current temperature profile), which is 60 °C lower than the mean homogenisation temperature. The higher homogenisation temperature is considered to result from either higher paleo heat flow than the current value of 1.9 HFU at this borehole location or greater depth of burial or a combination of the two.

If the fluid inclusions were trapped at the current sample depth, the precipitation temperature of quartz overgrowths would be ~ 110 °C (obtained from the isochore). To reach this temperature at a burial depth of 531.9 m, a heat flow of 7 HFU was required, which was calculated according to equation (I). Considering that the mean heat flow in the Red Sea, a newly formed active spreading centre, is only 3.53 +/- 0.96 HFU with the maximum of 4.71 +/-2.00 HFU (Erickson et al., 1975), it is unlikely that a heat flow of 7 HFU existed in the geological past in the southern Sydney Basin. The conclusion is that the higher homogenisation temperature at least partly resulted from greater depth of burial and the overburden was latter eroded away.

Using the simplest case, the eroded sediments were modelled as deposition from the Late Triassic to Mid-Jurassic with erosion from the Late Cretaceous. Overall, the burial history of the Sydney Basin was modelled here by subsidence through Permian to Mid-Jurassic, stable conditions from Mid-Jurassic to 90 Ma ago, followed by rapid uplift and erosion to 10 Ma BP, and then stable conditions. This model is similar to that used by Middleton and Schmidt (1982). In this model, the time at which the basin was buried to the maximum depth was artificially assigned to a time from within a range of 180 to 152 Ma BP, which are the boundaries of Middle Jurassic (1989 Global Stratigraphic Chart, Supplements to Episodes 12 (2), June, 1989). In reconstruction of burial curves, compaction of sediments was

corrected using the method of Dykstra (1987). Using the stratigraphic data of the Cobbitty 3 borehole (Table 7-11) and assigning that the basin at this borehole location was buried to the maximum depth at a time of 165 Ma BP, the burial curves for the top and bottom of the Scarborough Operational Unit, from which sample X531.9 was selected, were reconstructed with different amounts of eroded sediments, as shown in the upper middle diagram in Fig 7-20.

Quartz (overgrowth) is a late diagenetic product, as indicated in the last chapter. Its crystallisation lasted a certain period of time during basin subsidence. The cessation time of quartz overgrowth is assumed to be the time when the basin was buried to the maximum depth. Thus the time at which quartz overgrowth ceased can be known from the burial history of the basin. This time is taken as the time when the inclusions were trapped within quartz overgrowths even though strictly speaking it was slightly younger than the latter since a period was required so that quartz overgrowth could develop further and was able to trap (enclose) the inclusions. Since the time at which the basin at a given borehole location was buried to the maximum depth was artificially assigned to a time from within a range of 180 to 152 Ma BP, as mentioned before, the formation time of fluid inclusions was artificially set too and can vary from 180 to 152 Ma BP. However, no matter what a particular time from the range of 180 to 152 Ma BP was set for the formation time of fluid inclusions, this age would be older than that of finest illite separates (146.2 to 90.5 Ma, Table 7-7) which constrains the earliest time at which the illite formation ceased. This is consistent with the observed paragenetic sequence in which quartz overgrowth formed earlier than illite.

The burial history diagram in Fig 7-20 illustrates three cases with different amounts of eroded sediments. They will be discussed one by one with one of them being chosen as the favoured model on the basis of optimising the fit between fluid inclusion constraints and maturity constraints using computed maturity as a mean for comparison. Vitrinite reflectance is used here as the maturity measure. It was

calculated {$\%R_o$ = 12exp[-3.3(H/C)] - O/C)} using the kinetic scheme and reaction rate constraints of Burnham and Sweeney (1989) for the chemical reactions (cracking to CO_2, H_2O, CH_4 and CH_n) which accompany increased reflectance in vitrinite (Saxby et al., 1986). The detailed procedures involved in this calculation were explained by Burnham and Sweeney (1989). The kinetic calculation was carried out along a temperature - burial depth path with decompaction and with temperature computed from equation (I).

Case I: An eroded section of 900 m was restored. After this restoration, the reconstructed burial history curves for the top and bottom of the SC unit are those marked with I, as shown in the upper middle diagram in Fig 7-20. The sample (X531.9) at the current depth of 531.9 m would be buried to ~ 1430 (900 + 531.9) m at 165 Ma BP when the fluid inclusions were trapped. This burial led to the formation temperature of the fluid inclusions being ~ 113 °C (obtained from the isochore, refer to the left diagram in Fig 7-20). To get this temperature at a burial depth of 1430 m, the heat flow at 165 Ma BP should be 2.6 HFU, which was calculated from equation (I) if the surface temperature was 15 °C and K_U, K_D and ß of coal measures were used for the eroded sediments. The lithologies of eroded sediments are unknown. It is expected that they are an interbedded sandstone / shale sequence. As shown in Table 7-12, K_U, K_D and ß of coal measures lie between those of sandstones and those of shales. Thus it is probably appropriate that K_U, K_D and ß of coal measures were used for the eroded sediments. The paleo temperature profile corresponding to a heat flow value of 2.6 HFU is the one marked with I, as shown in the left diagram in Fig 7-20.

The above calculation resulted in a heat flow of 2.6 HFU at 165 Ma BP. Obviously there are a countless number of heat flow variations from 2.6 HFU at 165 Ma BP to 1.9 HFU at the present time, but the variation can be constrained by the measured vitrinite reflectance data (Diessel, 1975). Two possible variation models I-1 and I-2

are shown in the lower middle diagram in Fig 7-20. In model I-1, heat flow increased to the maximum of 2.8 HFU at ~ 90 Ma BP and then decreased to the current value of 1.9 HFU. In model I-2, heat flow reached to the maximum of 2.6 HFU at 165 Ma BP and then declined to the current value. Using burial history model I and heat flow history model I-1 or I-2, the vitrinite reflectance (R_v) depth profiles (I-1 and I-2) were theoretically calculated, as illustrated in the lower right diagram in Fig 7-20. R_v profile I-2 neither matches the measured R_v at the surface nor the R_v at the top of the Illawarra Coal Measures. Thus heat flow history model I-2 is discarded. R_v profile I-1 fits the measured R_v at the top of the coal measures but it does not fit the R_v at the surface. Thus heat flow history model I-1 is also discarded. Other heat flow history models were tried (not shown in the lower middle diagram in Fig 7-20). The results were that the calculated R_v depth profiles could not well fit both the measured R_v at the surface and the R_v at the top of the coal measures. The conclusion from Case I modelling is that the amount of eroded sediments should be increased to approximate the surface maturity measurements.

Case II. An eroded section of 1800 m was restored. After this restoration, the burial history curves for the top and bottom of the SC unit were reconstructed and marked with II, as shown in the burial history diagram (Fig 7-20). When the fluid inclusions were trapped, the sample was buried to ~ 2330 (1800 + 531.9) m, leading to the formation temperature of fluid inclusions of ~ 121 °C. Using the same approach as described in Case I, the calculated heat flow was 1.9 HFU at 165 Ma BP. The corresponding paleo temperature profile is the one marked with II and illustrated in the paleo temperature profile diagram in Fig 7-20. Similar to Case I, two possible heat flow variation models II-1 and II-2 are shown in the heat flow history diagram (Fig 7-20). In model II-1, heat flow did not change with time. In model II-2, heat flow was modelled as reaching to the maximum of 2.1 HFU at ~ 90 Ma BP and then declining to the current value of 1.9 HFU. Using burial history model II and heat

flow history model II-1 or II-2, the calculated R_v depth profile is II-1 or II-2, as illustrated in the vitrinite reflectance diagram (Fig 7-20). R_v profile II-1 does not match either the measured R_v at the surface or the R_v at the top of the Illawarra Coal Measures and so heat flow history model II-1 is discarded. In contrast, R_v profile II-2 fits the maturity measurements reasonably well.

Case III: The eroded section is further increased to 2400 m. After the restoration of the 2400 m overburden, the reconstructed burial history curves for the top and bottom of the SC unit are the ones marked with III in the burial history diagram (Fig 7-20). The fluid inclusions were trapped at a burial depth of ~ 2930 (2400 + 531.9) m and a temperature of ~ 125 °C. At 165 Ma BP, the heat flow was calculated to be 1.60 HFU and the corresponding paleo temperature profile is the one marked with III. One possible heat flow variation model (marked with III) is shown in the heat flow history diagram (Fig 7-20). It was modelled as increasing linearly from 1.60 HFU at 165 Ma BP to the current value of 1.9 HFU. Using this heat flow history model and burial history model III, the calculated R_v depth profile is the one marked with III. This profile matches the measured R_v values very well.

Sea floor spreading in the Tasman Sea commenced at 76 Ma BP (Shaw, 1978). Prior to it, a regime of high heat flow is expected to occur (Falvey, 1974). This regime must have had an influence on the heat flow in the adjacent Sydney Basin. Therefore, it is most likely that the maximum heat flow occurred in the southern Sydney Basin prior to the Tasman Sea spreading. On this geological ground, heat flow history model III is discarded even though the calculated R_v depth profile (III) fits the measured R_v very well. Heat flow history model II indicates a thermal event at ~ 90 Ma BP and corresponding calculated R_v depth profile II fits the maturity measurements reasonably well. Thus it is taken as the deduced heat flow history model. The amount of eroded sediments is ~ 1800 m thick and the precipitation temperature of quartz overgrowths ~ 121 °C at the Cobbitty 3 borehole.

It should be noted that the particular time (formation time of fluid inclusions) at which the basin was modelled to be buried to the maximum depth bears no significant influence on the deduced heat flow history. If this time was changed from 165 Ma BP to another one within the range of 180 to 152 Ma BP, a much the same heat flow history, a much the same amount of eroded sediments and a much the same precipitation temperature of quartz overgrowths would be obtained by modelling.

Using this approach, the amount of eroded sediments, the precipitation temperature of quartz overgrowths and heat flow history at the other three boreholes have been obtained. The computed current temperature profile and paleo temperature profile are shown in Figs 7-21 & 7-22. The current temperature profile starts at a surface temperature of 20 °C and the paleo temperature profile at 15 °C. The time (formation time of fluid inclusions) beside it was artificially set in individual boreholes. It is 170 Ma BP at Campbelltown 2 (Fig 7-21), 168 Ma BP at South Colah 1, and 165 Ma BP at Liverpool 91 (Fig 7-22). The heat flow value at this time is computed and shown in the diagrams (Figs 7-21 & 7-22)

The burial history curves for the top and bottom of the stratigraphic unit, from which the sample was selected, are shown in Figs 7-23 and 7-24. The deduced heat flow history, together with the speculated variation of surface temperature with time, at individual boreholes are illustrated in Fig 7-25 and the theoretical calculated vitrinite reflectance depth profiles in Fig 7-26.

The modelling results are that the amount of eroded sediments and the precipitation temperature of quartz overgrowths are ~ 2200 m and ~ 135 °C at Campbelltown 2, ~ 1950 m and ~ 126 °C at Liverpool 91, ~ 1800 m and ~ 121 °C at Cobbitty 3, and ~ 1600 m and ~ 110 °C at South Colah 1. The larger amount of eroded sediments at Campbelltown 2 suggests there was an apparent depocenter

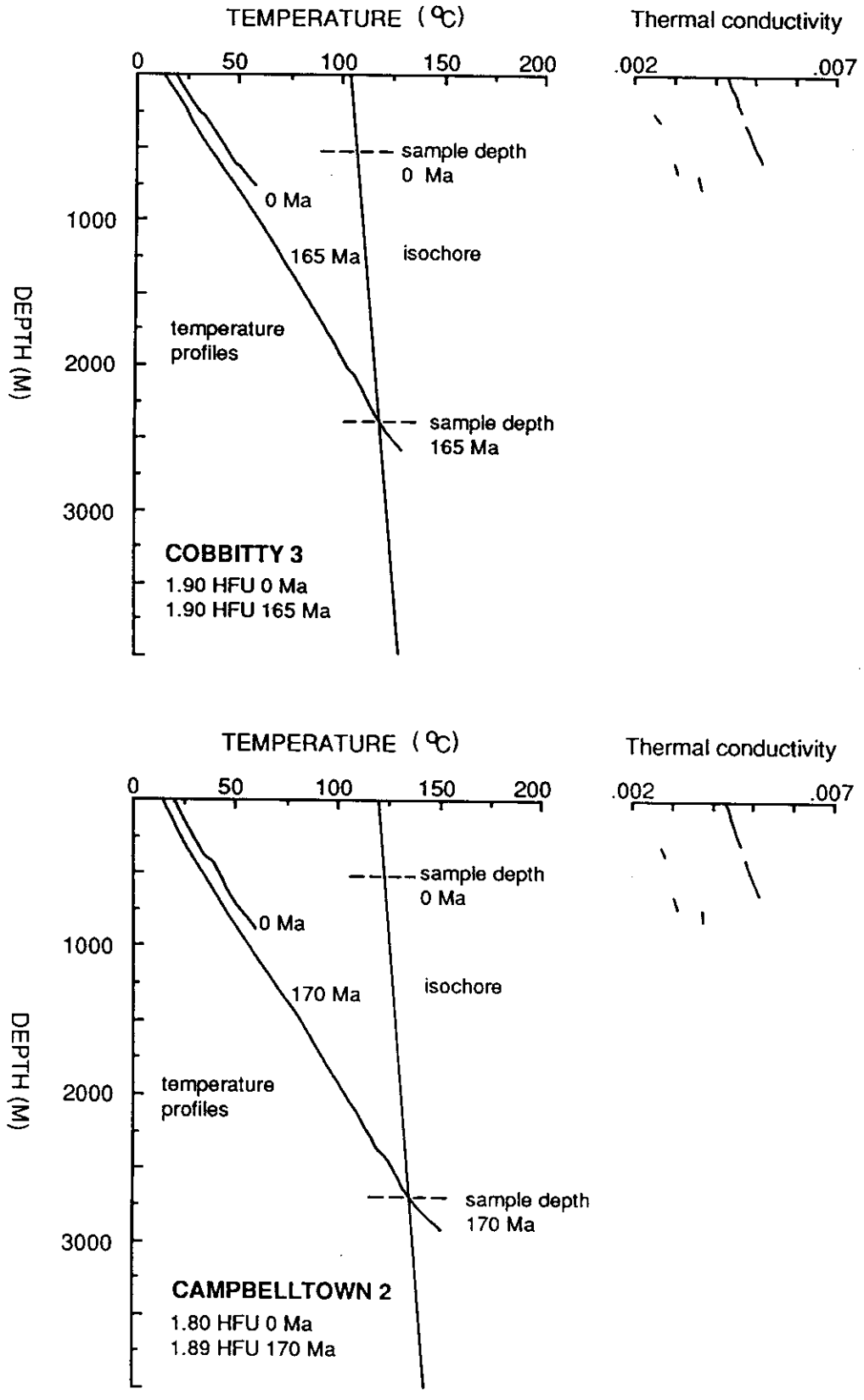

Fig 7-21 Pressure - temperature - depth relations during quartz cementation from aqueous fluid inclusions in quartz overgrowths in the Cobbitty 3 and Campbelltown 2 boreholes.

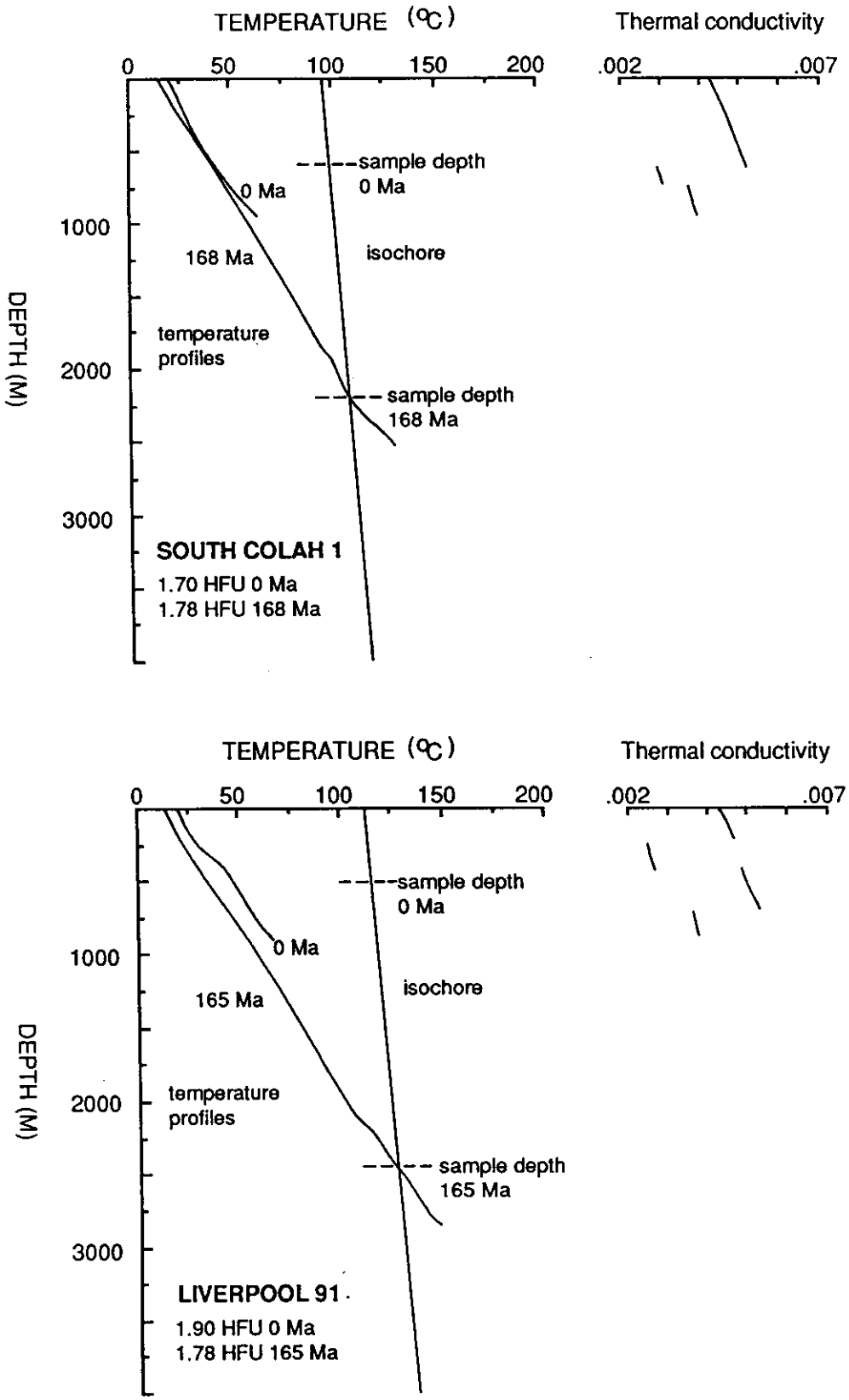

Fig 7-22 Pressure - temperature - depth relations during quartz cementation from aqueous fluid inclusions in quartz overgrowths in the South Colah 1 and Liverpool 91 boreholes.

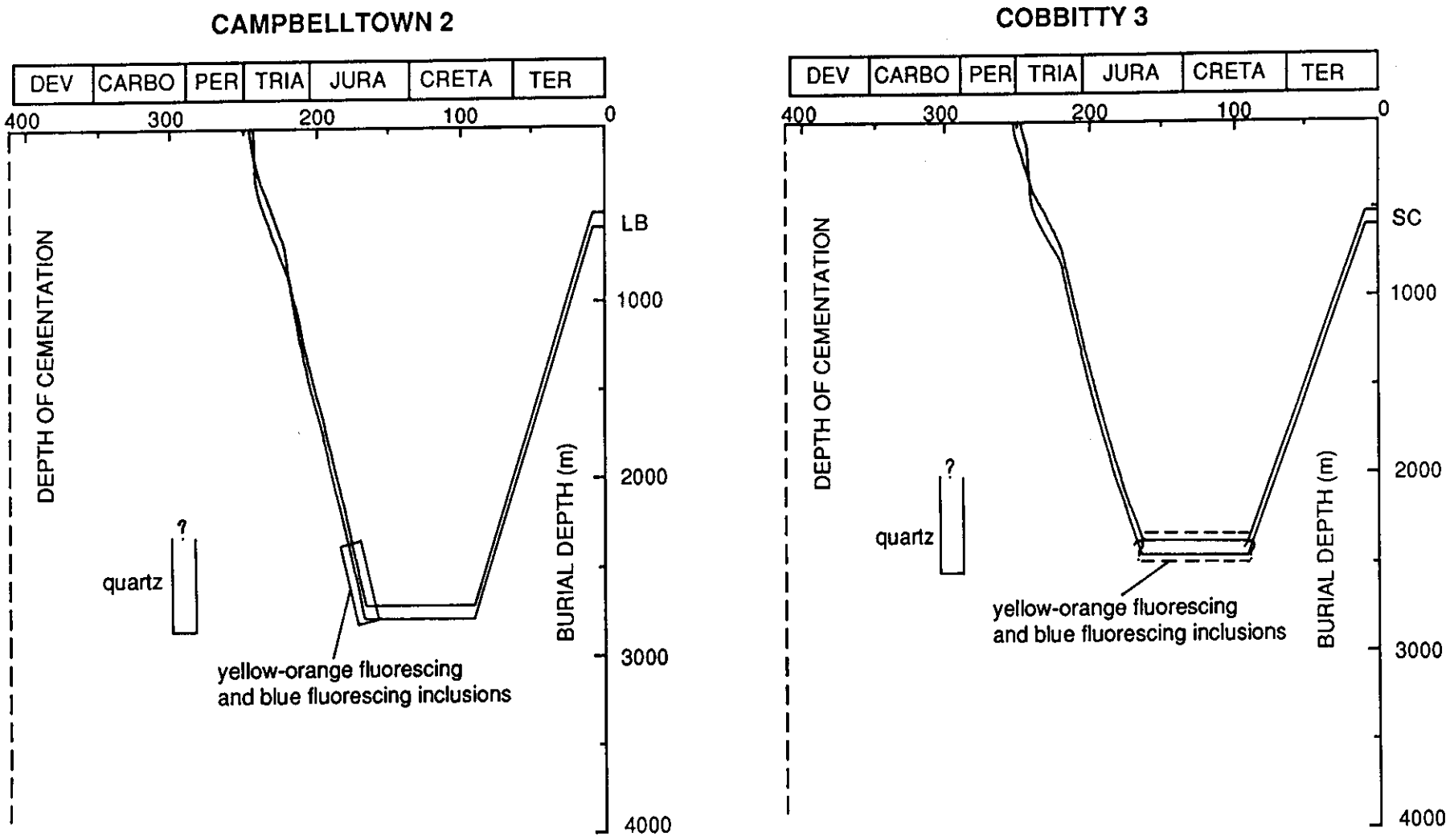

Fig 7-23 Oil migration in reationship to burial history and depth of diagenesis for the Campbelltown 2 and Cobbitty 3 boreholes. LB = Lower Bulgo Operational Unit, SC = Scarborough Operational Unit.

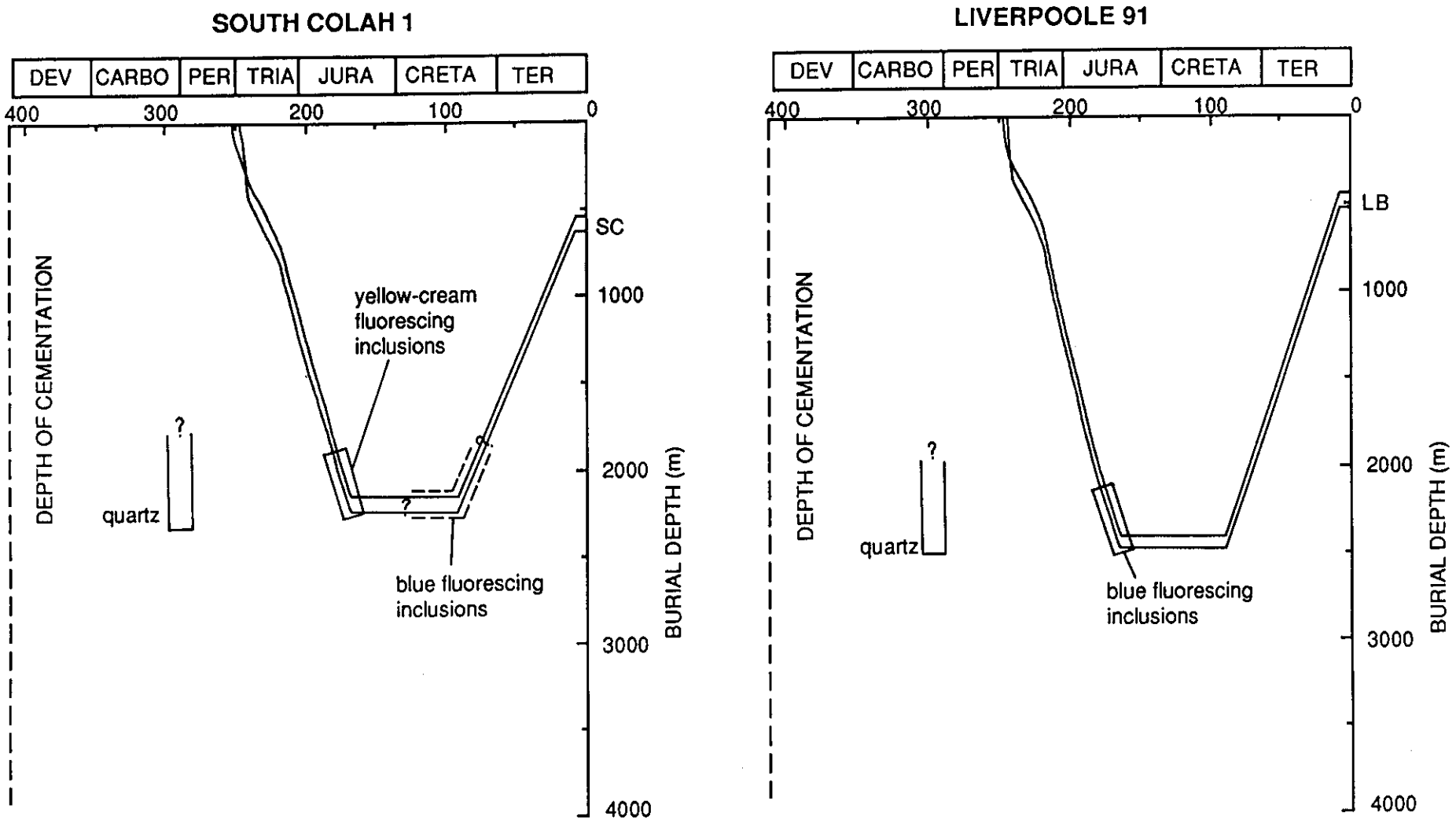

Fig 7-24 Oil migration in relation to burial history and depth of diagenesis for the South Colah 1 and Liverpool 91 boreholes. SC = Scarborough Operational Unit, LB = Lower Bulgo Operational Unit.

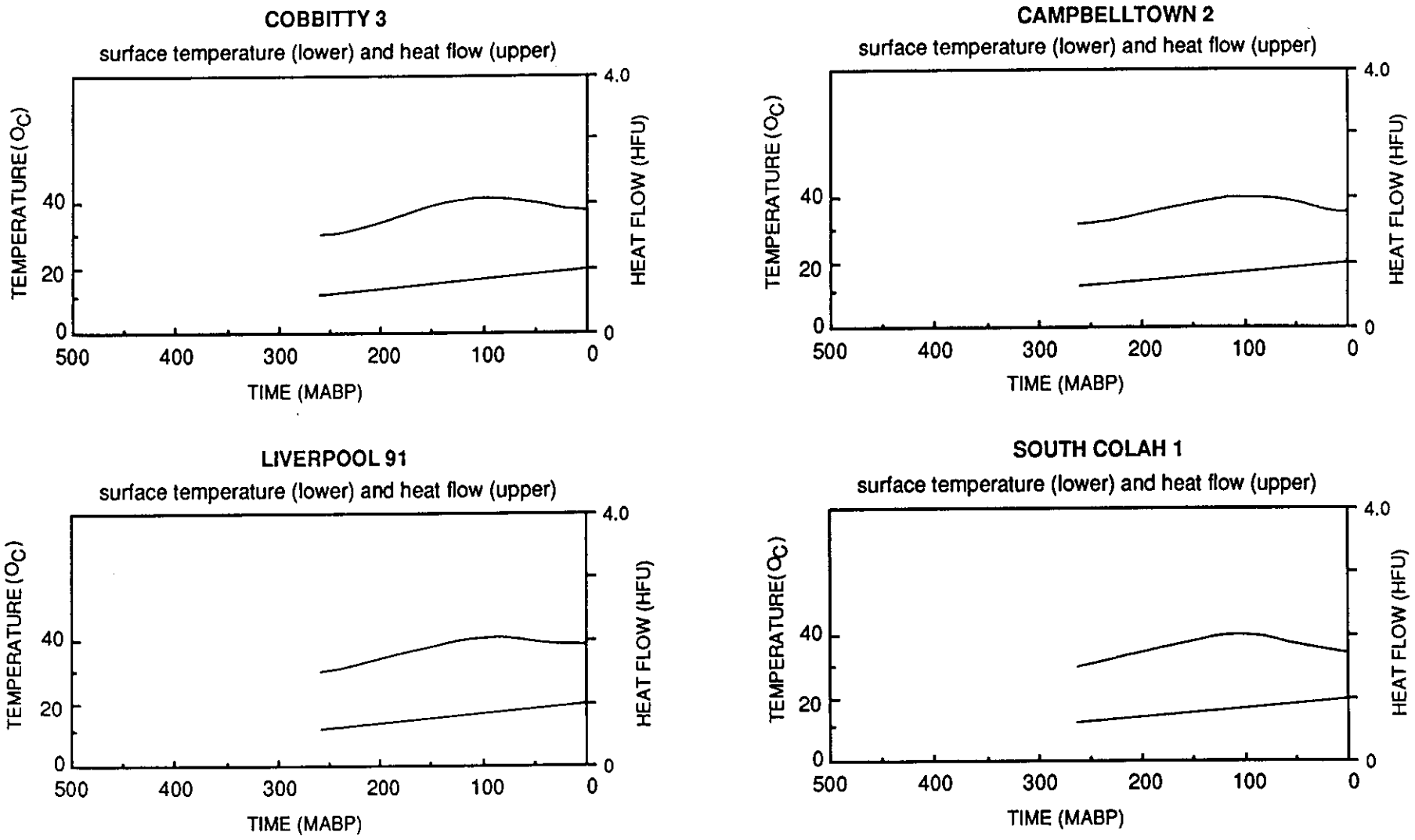

Fig 7-25 Variation of heat flow and surface temperature from the Permian to present day for the Cobbitty 3, Campbelltown 2, Liverpool 91 and South Colah 1 boreholes.

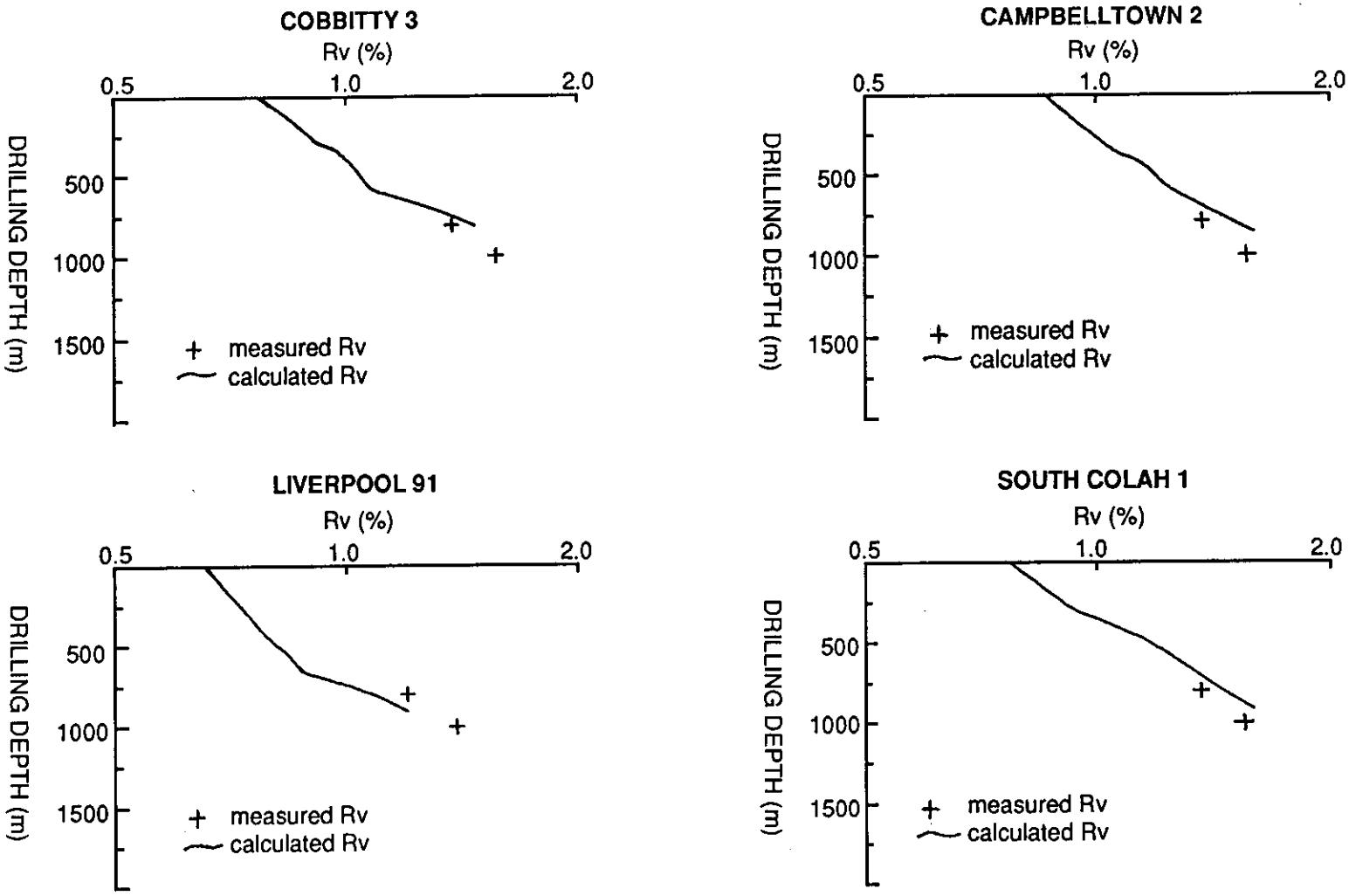

Fig 7-26 Measured and calculated vitrinite reflectance for the Cobbitty 3, Campbelltown 2, Liverpool 91 and South Colah 1 boreholes. Measured vitrinite reflectance was estimated by extrapolation from profiles measured by Diessel (1975).

near this borehole in middle-Jurassic. In the Sydney Basin, such a large amount of eroded section has been a matter of contention in regard to where the eroded sediments have been deposited (Branagan, 1983). Middleton and Hunt (1989) attempted to resolve this problem. They suggested that opening of the Tasman Sea in the Late Cretaceous would have created a change in oceanic circulation. As a result, the eroded sediments would have been redistributed after initial deposition in offshore eastern Australia during the Late Cretaceous and Paleocene. However, there is no concrete evidence to support this suggestion.

The proposed heat flow history which best fit the fluid inclusion and vitrinite reflectance data is one with a maximum heat flow of 2.1 HFU at ~ 90 Ma BP relative to the current heat flow of 1.7 to 1.9 HFU in the study area. The suggested maximum heat flow and its timing are consistent with several independent lines of evidence for high paleotemperatures in the Sydney Basin. These include 1) magnetic overprinting in several igneous intrusions in the Sydney Basin occurring from 100 to 70 Ma BP (Schmidt and Embleton, 1981); 2) fission track analyses of basement apatites from the Sydney Basin and its southern margin indicating a widespread thermal event at 110 - 80 Ma BP (Moore et al., 1986); and 3) high coal ranks in the Sydney Basin (Facer et al., 1980; Middleton and Schmidt, 1982; Middleton, 1983). The mid-Cretaceous timing of high heat flow was probably related to the late Cretaceous Tasman Sea spreading.

7.5.3 TIMING AND AMOUNT OIL GENERATION

Using the thermal and burial histories obtained from evaluation of fluid inclusion and vitrinite reflectance data, hydrocarbon generation was calculated. The progress of oil generation was modelled by evaluation of the sum:

$$X = \Sigma X_{i,0} \{1-\exp [-A \int(-E_i/RT)d_t]\}$$

over i reaction groups with activation energies (E) between 40 and 80 Kcal/mole,

using an interval of 2 kcal/mole (Ungerer and Pelet, 1987). X is the amount of oil generated, X_0 the initial oil generating potential (wt./wt.), A the frequency factor, R the universal gas constant, T absolute temperature (°K), and t time (secs). The subscript i refers to groups of reacting entities with similar activation energies. Variables with i subscript vary with the type of organic matter. For type I and type II organic matter the reaction rate constants of Ungerer and Pelet (1987) were used and for type III organic matter the reaction rate constants of Burnham and Sweeney (1989) were used. Rate constants for thermal cracking of liquids to gas were added by the current author under the advice of Dr Peter Eadington.

The method has been validated by successfully modelling long term experiments (over 6 years) for the generation of hydrocarbons from Australian source rocks (Eadington et al., 1989). In the experiments Loy Yang brown coal in the Gippsland Basin was selected as type III organic matter and Glen Davis oil shale in the Sydney Basin as type I organic matter (Saxby et al., 1986).

The composition of organic matter used in the calculation is 95% type III and 5% type II. This is typical of the Sydney Basin coals (Hunt, 1989). The diagrams showing the progress of oil generating reactions in the Illawarra Coal Measures are illustrated in Fig 7-27. They indicate wt./wt. conversion of organic matter to water, carbon dioxide, methane and oil on a fractional basis. As shown in these diagrams, about 10 wt.% of the organic matter was converted to methane and oil with most of the oil contributed by type II macerals and about 35 wt.% to water and carbon dioxide. Approximately 55 wt.% of the organic matter was left as a residuum. Oil was generated between about 190 and 170 Ma BP and methane between about 170 and 140 Ma BP. As indicated above, cessation of quartz overgrowths was assumed to take place from 170 to 165 Ma BP. This suggests that overlap of oil migration and precipitation of quartz overgrowths occurred. This is consistent with the petrological observations of fluorescing liquid hydrocarbons in

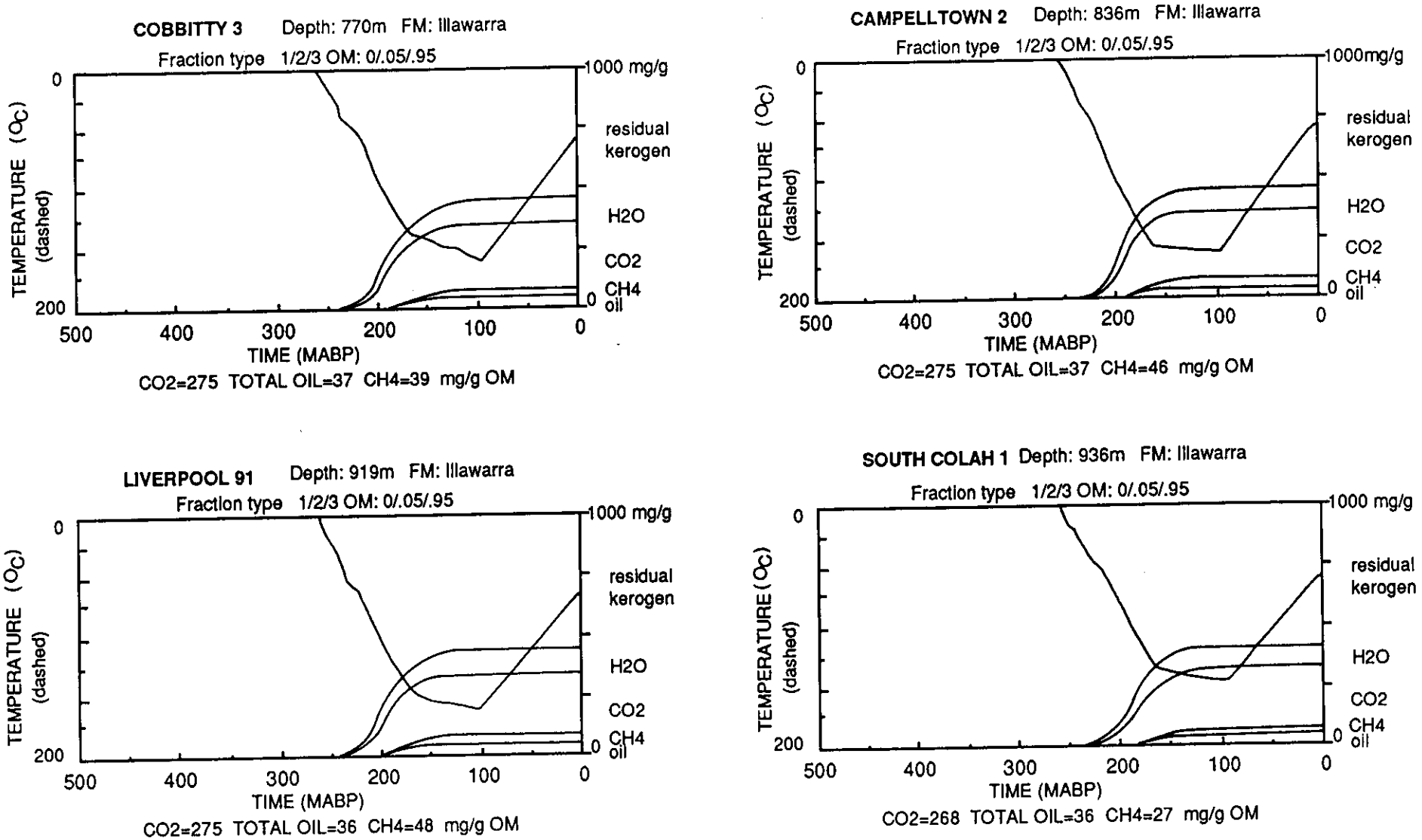

Fig 7-27 Timing of generation of CO2, CH4 and oil from sedimentary organic matter using a chemical kinetic model in the Cobbitty 3, Campbelltown 2, Liverpool 91 and South Colah 1 boreholes.

quartz overgrowths of the sandstones in the Scarborough and Lower Bulgo Operational Units.

To evaluate oil migration, the volume of oil generated in the source rocks is required to be calculated. This is illustrated as a depth profile for the Campbelltown 2 borehole (Fig 7-28). The volume of oil generated was computed by multiplying the extent of oil generation (left hand profiles) by the wt.% of organic matter and the proportion of type II and III organic matter (middle profiles) and converting the units to conventional barrels/hectare - metre, i.e. bbls/10^4m^3 (right hand profile).

An average total organic content (TOC) of 0.5 wt.% was assigned for the Wombarra Operational Unit, which is dominated by dark grey to black shales in the Campbelltown 2 borehole. The average TOC of the underlying Illawarra Coal Measures was calculated by treating the coal measures as an entity. Using thickness of coal (36 m) and coal measures (214 m) in the type section (Wilson, 1969), an ash content of 20% for coals, a specific gravity of 1.25 for ash-free coal and a specific gravity of 2.35 for the clastic sediments, TOC was computed to be 10 wt.%. The threshold for oil migration depends upon the porosity and permeability properties of particular source rocks. The threshold is about 120 bbls/hectare-m for shales and mudstones, which was obtained by Eadington et al. (1989) from an evaluation of oil migration in the Gulf Coast Tertiary Section of the USA (Hinch, 1980). But it not known for coals. It is expected to be higher for coals if there is adsorption of oil onto the coal maceral surfaces and into microporosity.

As shown in Fig 7-28, the generated oil in the Wombarra Operational Unit shales is about 50 bbls/10^4m^3 if the total organic content (TOC) of 0.5 wt.% is assigned for the shales. This value does not reach the threshold (120 bbls/10^4m^3) of oil migration for shales and mudstones. To produce oil at the expulsion threshold, the TOC is required to be at least 1.5 wt.%. Thus, the information on the TOC and

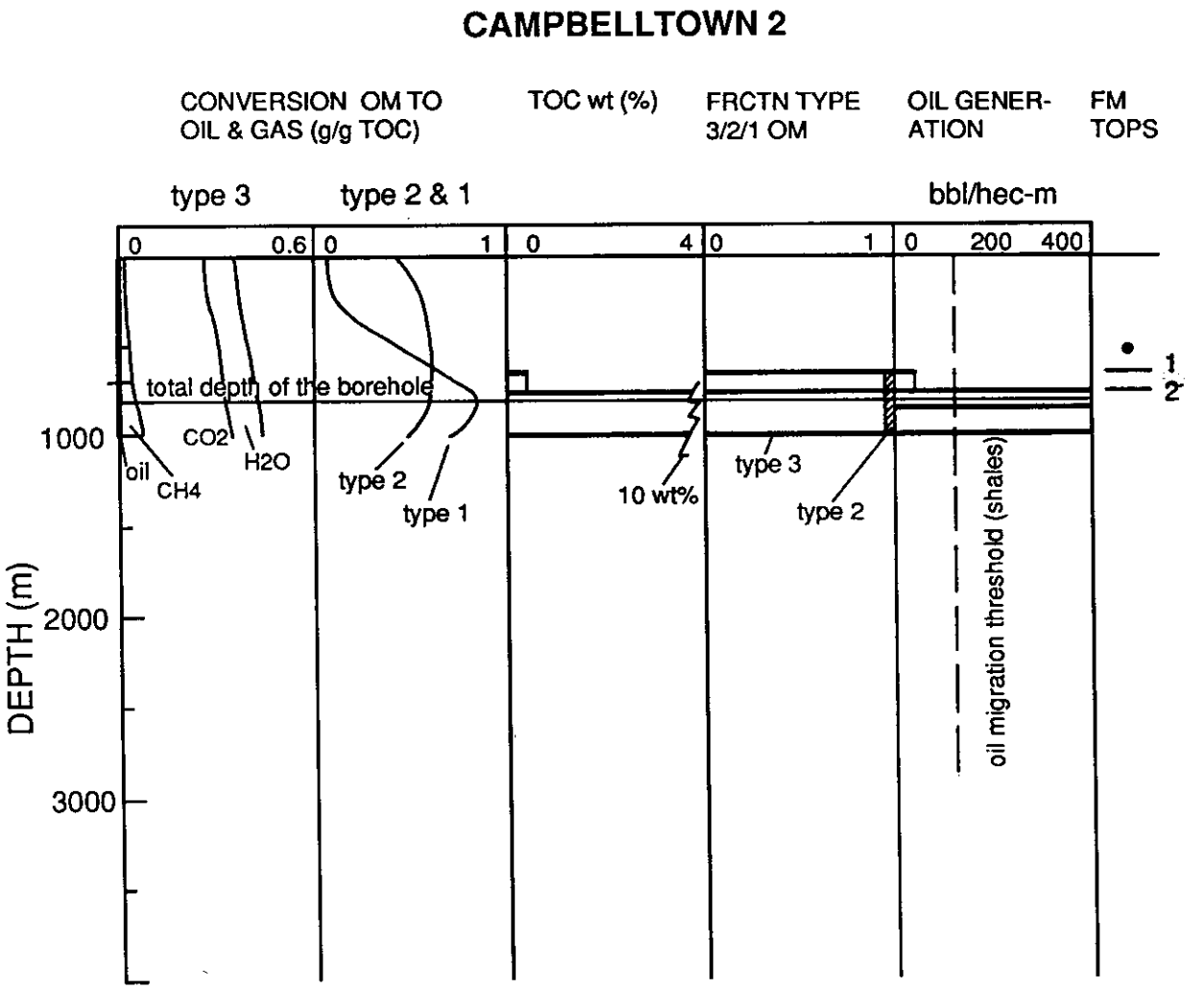

• fluorescing hydrocarbon inclusions in quartz overgrowths
1 top of Wombarra Operational Unit; 2 top of Illawarra Coal Measures

Fig 7-28 Depth profile of oil generation of hydrocarbons, carbon dioxide and methane from organic matter in Campbelltown 2.

maceral composition of shales could be important in predicting oil generation and migration in clastic rocks from theoretical calculations.

The Illawarra Coal Measures have produced significant amounts of oil (about 400 bbls/10^4m^3) but the oil has been converted to gas below the level of the Wombarra Operational Unit (Fig 7-28). Oil accumulated in the WO unit and overlying units is above the oil deadline and thus should not be thermally degraded to gas. As indicated above, the calculation of oil generation in the coal measures was carried out by treating the coal measures as a single unit and taking its average total organic matter (wt.%). Oil generated in individual coal seams should be much higher than the average value for the coal measures. The expulsion threshold of oil migration for coals is not known. Even if it is two or three times higher than the threshold for organic rich shales, however, the liquid hydrocarbons generated in the coal measures should be able to reach the threshold so that they must have been expelled from the coal measures and migrated to reservoirs rocks.

Methane generated from the Illawarra Coal Measures after oil migration would displace oil in reservoirs rocks. The displacement was probably a contributing factor for the sparse oil shows recorded in the Sydney Basin. The sandstones selected for this fluid inclusion investigation have high porosity and permeability and thus they may provide a more complete record of oil migration than the low permeability sandstones elsewhere in the basin due to focussing of fluid flow. Extrapolation of the data presented here to evaluate oil migration, accumulation and dispersal in other parts of the basin requires careful consideration for the effects of permeability difference on oil migration.

7.6 INTERPRETATION OF STABLE ISOTOPE DATA

7.6.1 PORE WATER EVOLUTION

Based on combined data from stable isotope and fluid inclusion analyses, and the

observed petrologic relationships of the diagenetic minerals, an evolution of pore water chemistry can be proposed with respect to temperature and time, as shown in Fig 7-29. Temperature estimates were derived from the fractionation of oxygen isotopes between the pore water and the precipitating oxygen - bearing diagenetic mineral and the $\delta^{18}O$ values of the mineral according to the temperature dependent equations, which are given in Table 7-2. The formation temperature of quartz overgrowths were obtained from the homogenisation temperature of aqueous fluid inclusions within the overgrowths. The relative timing of the diagenetic minerals (paragenetic sequence), which has already been discussed in detail in the last chapter, was established by petrological microscope observations and SEM/EDX analyses.

To reconstruct the evolution, the original $\delta^{18}O$ and δD compositions of depositional waters are considered first. As mentioned previously, the $\delta^{18}O$ and δD compositions of meteoric surface waters are strongly correlated with latitude, altitude and distance from the coastline and they reflect the mean annual air temperature (Dansgaard, 1964; Yurtsever and Gat, 1981). Based on the knowledge of the past position of the Sydney Basin with respect to the south pole and the coastline, and the fluvial / lacustrine origin of the Narrabeen Group, the $\delta^{18}O$ and δD of the initial pore waters within the Narrabeen Group sediments can be estimated at the beginning of the diagenesis of the Narrabeen Group sandstones. It is known that southeast Australia lay south of about 65°S from latest Permian to latest Cretaceous (Embleton, 1984). Using the present day range of meteoric water composition at this sort of latitude and the relationship $\delta D = 8\ \delta^{18}O + 10$ (Craig, 1961) for meteoric waters, the initial pore waters of the Narrabeen Group sediments are estimated to have had approximate values of -15 ‰ for $\delta^{18}O$ and -110 ‰ for δD at the beginning of their diagenesis (early Triassic).

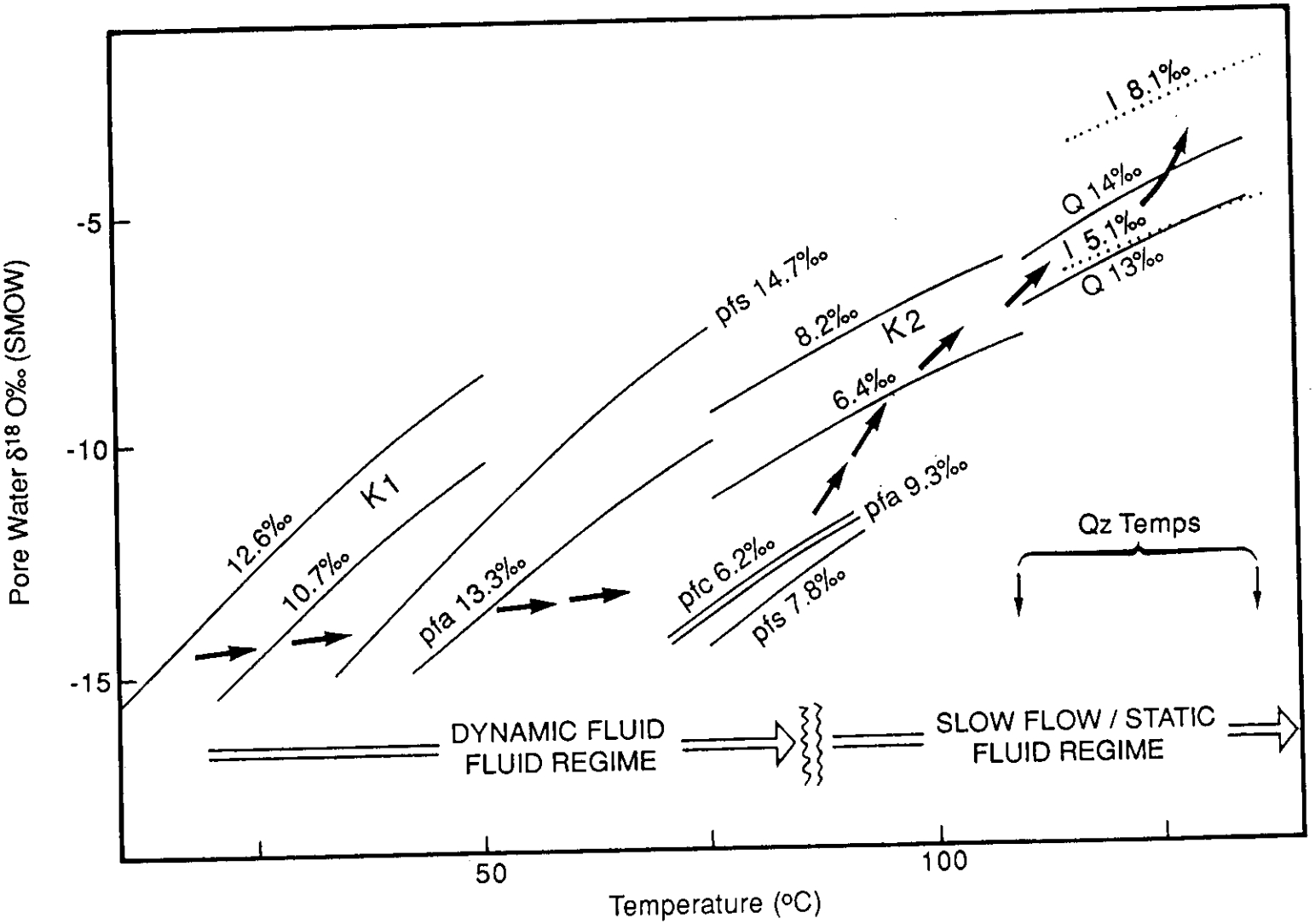

Fig 7-29 Evolution of pore water δ^{18} O composition with temperature and time, calculated from the measured δ^{18}O of diagenetic minerals. K = kaolin. I = illite. Q = quartz. pfs = pore filling siderite. pfa = pore filling ankerite. pfc = pore filling calcite. Qz Temps = precipitation temperatures of quartz overgrowths from fluid inclusion temperatures.

Bird and Chivas (1988) calculated isotopic composition of early Permian (Sakmarian - Artinskian) meteoric water in the adjacent Gunnedah Basin from measurements of kaolinite samples selected from both in situ kaolinitic weathering profiles and eroded and redeposited products of this weathering. They gave a composition of $\delta^{18}O$ of $\leq$ -17 ‰ and δD ‰ of $\leq$ -125 ‰. In the early Permian, the Gunnedah - Sydney basin was positioned nearer the south pole than the Sydney Basin in the early Triassic so that a further ^{18}O - depleted meteoric water would be expected. Eadington et al. (1989) suggested a $\delta^{18}O$ composition of -13 ‰ for the Early Jurassic depositional waters in the Eromanga Basin, which lay further away from the south pole than the Sydney Basin. Thus it would be expected that the deposition waters had a more ^{18}O - enriched isotopic composition than in the Sydney Basin.

Of the kaolin fractions, the finest size fraction has the most - enriched ^{18}O. The $\delta^{18}O$ values are 12.58 ‰ and 10.65 ‰ for the 1-0.2 μm fraction of sample J514.8 and the 2-1 μm fraction of sample L506.7 respectively (Table 7-4). As one of the earliest diagenetic products, they provide the earliest record of the pore waters in the Narrabeen Group sediments. If it is assumed that they were precipitated from pore waters with $\delta^{18}O$ of -15 ‰, it is calculated that the formation temperature for the two kaolins would be 11 °C and 29 °C respectively from the kaolin fractionation equations of Land and Dutton (1978). The temperatures are in good agreement with those prevailing during the earliest stage of sandstone diagenesis. It should be noted that early grain coating chlorites were observed with petrological examinations in sample J514.8. Since kaolin and chlorite can not be cogenetic, it is unlikely that both were of early origin. Thus some components of the 1-0.2 μm kaolin fraction of this sample are possibly detrital in origin.

The grain coating siderite for sample X531.9 has a $\delta^{18}O$ value of 14.57 ‰ (Table 7-

3). From this value and the siderite fractionation equation of Carothers et al. (1988), the calculated formation temperature is 40 °C if crystallisation was from the same pore waters as the earliest kaolins.

The $\delta^{18}O$ values of pore filling siderites for samples W388.8 and A146.5 are 14.71 ‰ and 10.79 (Table 7-3) ‰ respectively and formation temperatures are calculated to be 34 °C and 54 °C respectively if the $\delta^{18}O$ value of the pore waters was hardly modified. These particular pore filling siderites probably represent prolonged siderite cementation as a result of lack of competing cementation from any other type of carbonates. Using this approach, the other ^{18}O-depleted pore filling carbonates (pore filling calcite, ankerite and siderite) were calculated to be precipitated at higher temperatures of *ca* 70 °C to 85 °C from the pore waters whose $\delta^{18}O$ value increased slightly from the original pore waters of -15 ‰ to about -12 ‰ during the carbonate cementation (Fig 7-29).

The little modification of pore waters' $\delta^{18}O$ value is typical of diagenesis proceeding in a dynamic fluid flow regime in which meteoric water was replenished through the aquifer (porous sandstone bodies) by a topographic head. The meteoric water flushing diluted or even eliminated the effect of the oxygen isotope fractionation between the pore waters and the ^{18}O enriched detrital silicate clasts on the isotopic composition of the bulk pore waters. As a result, oxygen isotope composition of pore waters was hardly changed.

As mentioned in the last chapter, the rare occurrence of pyrite and common occurrence of siderite suggest that bacterial sulphate reduction had not been a significant process during the burial of the Narrabeen Group. Thus it could not be a major source for carbon in the carbonates. Fe^{2+} and Mn^{2+} used in the formation of carbonates are suggested to be largely derived from reduction of Fe^{3+} and Mn^{4+}

oxides in the adjacent shales / mudstones. The reduction resulted in the oxidation of organic matter (Irwin, 1980; Curtis et al., 1986). It produced HCO_3^- and raised pH so favouring precipitation of carbonate. Thus oxidation of organic matter should be one of the sources for the carbon in the pore filling carbonates. Carbon derived from this source is ^{13}C depleted (Irwin et al., 1977; Curtis et al., 1986) (probably similar to $\delta^{13}C$ value of parental organic matter, i.e -25 ‰).

Oxygen isotope data of the carbonates suggest they formed at a temperature of *ca* 30 to 85 °C (Fig 7-29), generally in the bacterial fermentation zone (less than 1.5 km). In this temperature range, bacterial fermentation is likely to be the predominant HCO_3^- providing reaction. Carbon derived from this source has $\delta^{13}C$ of *ca* +15 ‰ (Irwin et al., 1977; Curtis et al., 1986). A combination of the carbon derived from oxidation of organic matter (^{13}C-depleted) and the carbon derived from bacterial fermentation (^{13}C-enriched) sources could create the measured $\delta^{13}C$ values of -4 ‰ to -8 ‰. However, there is another possible carbon source. It is very likely that flushing meteoric waters bearing dissolved CO_2 from the atmosphere also provided HCO_3^- for carbonate precipitation. The carbonate $\delta^{13}C$ signals of -4 ‰ to -8 ‰ could all be derived from this source, depending on CO_2, HCO_3^-, carbonate equilibria, pH, and temperature. The conclusion is that the carbon in the pore filling carbonates was derived from oxidation of organic matter, bacterial fermentation, and atmosphere.

Petrological examinations indicate that the abundant pore filling kaolins were later than carbonate cementation but pre-/syn-quartz overgrowths. The $\delta^{18}O$ values of the pore filling kaolins range from 6.36 ‰ to 8.22 ‰. The relative timing and the $\delta^{18}O$ data suggest that the oxygen isotope composition of the pore waters must have begun to be enriched more rapidly, as illustrated in Fig 7-29. The $\delta^{18}O$ value

of the pore waters increased from -12 ‰ up to as high as -6 ‰. Accompanying the ^{18}O enrichment process, the burial temperature increased from 80-85 °C to as high as 110-135 °C, which were the formation temperature of quartz overgrowths obtained from the fluid inclusion investigation. This is typical of diagenesis under conditions of a slow flow / static fluid regime. With the low ratio of pore waters to sediments, which is considered to have been achieved at this stage of burial, the exchange of pore waters with ^{18}O enriched framework silicates would result in the increase of the $\delta^{18}O$ value of the pore waters.

The formation temperature of quartz overgrowths lie between 110 °C and 135 °C, which was obtained from the fluid inclusion investigation. Using the temperature data and the estimate of quartz overgrowths $\delta^{18}O$ values of 13 ‰ to 14 ‰, the $\delta^{18}O$ values of pore waters during precipitation of quartz overgrowths were calculated to be between -7 ‰ and -3.5 ‰ from the quartz fractionation equation of Friedman and O'Neil (1977). They overlap with the $\delta^{18}O$ values of pore waters during precipitation of pore filling kaolins (second generation). This implies that quartz overgrowths and pore filling kaolins were coprecipitated from the pore waters. This is substantiated by the inter-growth of quartz overgrowths and kaolins observed under the SEM.

The pore water compositions after quartz overgrowths can be reconstructed from the oxygen isotope data for the post quartz overgrowth illite. If it is assumed that the illites crystallised at the much same temperatures as quartz overgrowths, the calculated $\delta^{18}O$ values of the pore waters would be in the range of -6 ‰ to -3 ‰ from the illite fractionation equation of Lee (1984, cited in Lee et al., 1989). Thus the $\delta^{18}O$ value of the pore waters continued to increase, as shown in Fig 7-29.

As discussed above, oxygen isotope data suggest that the pore filling kaolins

crystallised at temperatures of between 80 °C and 135 °C and illites formed at approximate temperatures of between 110 °C and 135 °C or higher. Using these temperature data and the measured δD values of kaolins and illites, the δD values of pore waters during precipitation of kaolins (second generation) and illites were calculated to be -100 ‰ to -120 ‰ according to hydrogen fractionation equations of kaolin and illite given by Lambert and Epstein (1980) and Yeh (1980) (Table 7-2). They are very similar to the estimated δD value of -110 ‰ of original depositional pore waters. This implies that the δD value of the pore waters was virtually unmodified throughout the diagenetic history from the earliest kaolins to the post quartz overgrowth illites. The little δD modification of the pore waters can be explained by the fact that the hydrogen content of pore waters was so high relative to that of the sediments with which the pore waters reacted that isotope fractionation accompanying precipitation of small amounts of hydrogen - bearing kaolins and illites must have had little effect on the bulk δD composition of the pore waters.

7.6.2 POTASSIUM - ARGON ILLITE AGES

K-Ar age dating has been used in previous studies to determine the age of diagenetic illites in sandstones (Lee et al., 1985, 1989; Hamilton et al., 1987; Liewig et al., 1987; Girard et al., 1989). Hamilton et al. (1989) discussed the principles of interpreting K-Ar age data. Illite is one of only a few diagenetic minerals in sandstones which contain sufficient long - lived radioisotope (^{40}K) to allow radiometric age determination of their formation time. K-Ar dating of illite can provide information on the duration of illite formation, the age of fluid flow events in sedimentary basins and the timing and the nature of hydrocarbon accumulations in sandstone reservoirs.

The nature of authigenic, fibrous illite growth determines that filaments are often

coarser at the point of growth origin than at ends of fibres. Thus coarser illite separates tend to have a greater proportion of earlier-formed illite than finer illite separates. The finest-sized illite should be derived from the latest-formed illite. Thus its age should provide a record of the timing of the cessation of illite formation. The K-Ar age data indicate that the two size separates for sample X531.9 do in fact have an age difference of approximate 5 Ma between the coarser, older illite and the finer, younger illite. This implies that the minimum duration of illitisation is about 5 Ma. Cessation of illite formation may be affected in a variety of different ways. These include displacement of aqueous pore fluids by migrating hydrocarbons and other changes in chemical and / or physical environment such as diminished supply of nutrient elements (e.g. potassium) or temperature decrease.

K-Ar ages for the finest illite separate constrain the earliest time at which illite formation ceased. The present day lack of accumulated hydrocarbons in the analysed sandstones limit the interpretation of the illite age data in the context of the timing of hydrocarbon migration. However, the age decrease from 146 Ma in the west to 90.5 Ma in the east suggests that illitisation proceeded for longer and by referring to the obtained burial history and thermal history models from the fluid inclusion investigation, to higher burial temperatures in the eastern part of the study area. The youngest illite age (90.5 Ma) is coincident with the time at which the proposed heat flow reached to its peak of ~ 2.1 HFU.

7.7 SUMMARY

Fluid inclusion investigation indicates that the mean homogenisation temperatures of aqueous fluid inclusions in quartz overgrowths are 45 °C to 60 °C higher than the current formation temperatures at the sample depths of 500-600 m. The high fluid inclusion temperature, together with vitrinite reflectance data, imply that a section with a thickness of *ca* 1600 to 2200 m was eroded away. The proposed

heat flow varied with time and reached a peak of 2.1 HFU relative to the current values of 1.7-1.9 HFU at approximately 90 Ma BP.

Chemical kinetic modelling suggests that significant volumes of oil (an average of about 400 bbls/10^4m^3) were generated in, and expelled from, the Illawarra Coal Measures. Oil migrated through the sandstones of the Scarborough and Lower Bulgo Operational Units during and probably after precipitation of quartz overgrowths, as demonstrated by the presence of fluorescing liquid hydrocarbon inclusions in quartz overgrowths and fractures. Oil migration probably occurred at a time of 190 Ma to 170 Ma years ago (Early and Middle Jurassic). There may have been oil columns at that time.

The data from stable isotope analyses suggest that the diagenesis of the Narrabeen Group sandstones proceeded in two different fluid flow regimes - early dynamic fluid flow regime and late slow flow / static fluid regime. The former was characterised by a slight increase of the $\delta^{18}O$ of pore waters from the estimated initial value of -15 ‰, typical of Triassic meteoric waters, to -12 ‰ with the temperature increasing from ~ 10 ° to 80-85 °C. In the early dynamic fluid flow regime, early clay and pore filling carbonates were precipitated from the pore waters. The late slow flow / static fluid regime was characterised by rapid ^{18}O-enrichment of pore water $\delta^{18}O$. The $\delta^{18}O$ of pore waters increased greatly from -12 ‰ to -3 ‰ with the temperature increasing from 85 °C to 110-135 °C. In the late diagenetic regime, kaolin (generation II), quartz and illite crystallised.

CHAPTER EIGHT
POTENTIAL OF THE NARRABEEN GROUP SANDSTONES AS RESERVOIR ROCKS

8.1 INTRODUCTION

Porosity and permeability were measured in the laboratory for selected Narrabeen Group sandstones. In this chapter, the author will emphasis factors controlling porosity and permeability, briefly describe the distribution of porosity and permeability throughout the group and discuss the potential of sandstones as reservoir rocks.

Porosity is the ratio of pore space to the total rock volume and it is usually expressed as a percentage. It includes two types: effective and absolute porosity. The former is the percentage of interconnected pore space in the total rock volume. The latter is the percentage of total pore space in the total rock volume. The porosity can be primary, secondary or a combination of the two. Primary porosity is that which the rock possesses at the end of its depositional phase. Secondary porosity is additional void space due to post depositional processes.

Permeability is the property of a medium of allowing fluids to pass through it without change in the structure of the medium or displacement of its parts. Permeability determined for a homogeneous fluid is called absolute permeability (K). It is independent of the nature of the fluid. When two or more immiscible fluids (e.g. gas, oil and water) are present in the formation, there is an effective permeability for each fluid in the presence of the others (K_g, K_o, and K_w). The effective permeabilities depend not only upon the rock itself, but also upon the relative amounts of the different fluids present in the pores. Since the mutual interferences are retardative and not enhancing, the sum of K_g, K_o and K_w is less than $K_{absolute}$. The relative permeabilities are the ratios of the effective permeabilities to the absolute permeability. Thus, for a gas - oil - water system, the

relative permeability for gas is equal to K_g / K, that for oil is equal to K_o / K and that for water is equal to K_w / K.

The quality of reservoir rocks is usually evaluated by their porosity and permeability. In terms of the absolute values of porosity and permeability, reservoir rocks can be classified into several different grades. The criteria used for the classification follow those proposed by North (1985). They are shown in the following table (Table 8-1).

Table 8-1 Grades of reservoir rocks

Porosity (%)	Qualitative evaluation	Permeability (md)	Qualitative evaluation
0 - 5	negligible	< 1.0 - 15	poor to fair
5 - 10	poor	15 - 50	moderate
10 - 15	fair	50 - 250	good
15 - 20	good	250 - 1000	very good
20 +	very good	> 1000	excellent

(after North 1986, p.115 & p.124)

8.2 METHODOLOGY

Of the 417 sandstone samples taken from the 26 fully cored boreholes, 175 samples from 21 boreholes were selected for porosity and permeability measurements with most of them from the boreholes in the west margin and the southern region of the basin (Appendix I). The measurements were carried out in The Petrophysics Laboratory, The Department of Geology and Geophysics, The University of Sydney. Sandstone samples were first drilled parallel to bedding with a Triefus diamond bit to obtain cylindrical plugs and then plugs were cut at both ends. The plugs are 25 mm in diameter and 15 to 40 mm in length.

Sample plugs were oven dried at a temperature of less than 60 °C over at least one day and weighed to obtain the pore water free mass - dry weight. Unless they

were put in equipment for measurement, the dry plugs were kept in desiccators. Intrinsic permeability and grain volume of a sample plug were measured in an air permeameter and a helium porosimeter, which were supplied by Core Services Australia Inc. Sample plugs were evacuated in vacuum for at least 24 hours and saturated with Sydney tap water under vacuum and soaking for several days. The wet sample plugs were weighed to obtain wet weight and also weighed by being completely submerged in water to obtain the core volume according to Archimedes' principle.

$$\text{core volume} = \text{wet weight} - \text{submerged weight}$$

To measure permeability the plug was clamped in a rubber sleeve by a circumferential air pressure of 100 psi (690 kPa). Air was forced to pass through the plug with a pressure of 5-20 psi (34.5-138 kPa) depending on the permeability of the sample. The time taken for 10 cm^3 air to pass through the plug was recorded by timing a marked bubble in a 10 cm^3 column connected to the plug holder. Permeability was calculated from the Darcy equation:

$$K_{air} = (36.6 \times P_b \times Q_A \times L)/[(P_i - P_b) \times A]$$

P_b = atmospheric pressure in atmospheres read from a barometer in the laboratory,

$P_i = [P_b(\text{inches}) + 2.04529\ P_1(\text{psi})]/29.92$ in atmospheres in which

P_1 = preset upstream pressure (5-20 psi)

Q_A = air flow rate in cm^3/sec, L = length of sample in cm,

A = cross sectional area of sample in cm^2.

To measure porosity the plug was put into a stainless steel chamber and a known volume of helium (V_1) was injected to the chamber by the porosimeter at a pressure of 100 psi (P_1). Then the switch was turned to the sample side so that helium could

enter pore spaces in the sample. The pressure would decrease gradually and stabilise at a certain value (P_2). According to Boyle's Law, the volume of helium in the sample chamber (V_2) could be calculated: $V_2 = (P_1V_1)/P_2$. Grain volume (V_g) of the sample could be known: V_g = volume of the sample chamber (V_c) measured - V_2. Finally helium porosity of the sample ($\emptyset$) could be calculated:

$$\emptyset_h = \text{(sample volume - grain volume) / sample volume}$$

The calculated porosity values are considered to be accurate to +/- 1%.

The porosity of a sample could also be calculated using the wet techniques, which were designed in the Petrophysics Laboratory. The formula for this calculation is

$$\emptyset_w = \text{(wet weight - dry weight) / volume of core.}$$

$\emptyset_w$ was used as a check to $\emptyset_h$ obtained from the helium technique. They are generally in good agreement.

It should be noted that porosities and permeabilites were determined at room temperature and pressure. The porosities are helium injection values (effective porosities). The permeabilities are horizontal permeabilities and they are intrinsic values (absolute permeabilities) to which no Klinbenverg corrections have been applied. The results of porosity and permeability measurements are presented in Table 8-2, together with the position of samples in the stratigraphic column and average grain size. For 15 of the 175 sandstone samples subject to porosity and permeability measurements, which were selected from Boreholes W and X and marked with * in Table 8-2, porosity and permeability data were from Galloway and Hamilton (1988).

8.3 FACTORS CONTROLLING RESERVOIR QUALITY

Table 8-2 Results of porosity and permeability measurements.

SN	OU	GS	PO	PER	SN	OU	GS	PO	PER
BOREHOLE A									
A146.5	UB	0.20	9.23	0.25	A211.4	LB	0.35	11.54	0.81
A163.1	UB	0.25	13.56	1.17	A247.1	SC	1.80	12.25	3.03
A184.3	UB	0.20	14.18	1.19	A313.5	SC	0.40	10.21	0.33
BOREHOLE B									
B151.7	UB	0.25	7.33	0.14	B234.7	LB	0.25	7.17	
B211.4	UB	0.25	7.61		B406.2	WO	0.40	6.62	
BOREHOLE C									
C038.4	UB	0.20	12.81	1.02	C089.4	LB	1.00	11.18	1.34
C081.1	LB	0.25	8.44		C132.6	SC	0.25	5.35	
BOREHOLE D									
D053.9	SC	0.28	17.16	7.76	D236.0	WO	0.35	10.47	0.61
D064.9	SC	0.25	11.89	5.40	D257.5	WO	0.30	14.67	2.36
D102.5	SC	0.28	16.90	2.08	D295.9	WO	0.20	13.12	1.27
D164.9	SC	0.35	12.87	1.45					
BOREHOLE E									
E118.5	SC	0.25	11.13	0.80	E243.6	SC	0.40	15.25	4.76
E128.0	SC	0.30	20.71	51.26	E344.1	WO	0.35	15.95	1.85
E212.3	SC	0.45	12.83	1.01	E363.6	WO	0.30		13.53
E224.5	SC	0.30	13.82	1.10					
BOREHOLE F									
F219.2	UB	0.18	12.40	0.63	F563.0	SC	0.35	8.67	0.87
F255.6	UB	0.20	15.20	0.86	F573.8	WO	0.40	10.41	1.23
F470.4	SC	0.45	14.53	4.63	F751.7	WO	0.35	8.89	0.28
F484.2	SC	0.45	13.41	0.98					
BOREHOLE G									
G553.8	WO	0.30	12.89	0.68					
BOREHOLE H									
H319.0	UB	0.40	16.07	178.31	H516.2	SC	0.50	12.72	0.87
H378.2	LB	0.20	14.01	1.00	H535.1	SC	0.40	11.45	0.41
H419.7	LB	0.65	15.01	99.67	H597.9	WO	0.25	12.81	0.63
H454.9	SC	0.25	15.07	5.62	H625.4	WO	0.35	10.27	
BOREHOLE I									
I327.7	BH	0.25	11.01	0.23	I543.4	LB	0.25	15.63	3.64
I378.5	UB	0.30	17.24	1.29	I629.3	SC	0.35	12.71	7.12
I382.9	UB	0.30	14.20	1.23	I769.6	WO	0.35		8.73
I437.4	UB	0.20	10.66	0.15					
BOREHOLE J									
J451.4	SC	0.25	12.82		J641.2	WO	0.25	5.49	
J514.8	SC	0.35	6.79						
BOREHOLE K									
K30.7	WO	1.50	11.95		K73.4	WO	0.35	7.70	

SN	OU	GS	PO	PER	SN	OU	GS	PO	PER
BOREHOLE L									
L346.2	UB	0.30	9.03	0.39	L547.6	SC	0.60	8.43	1.36
L406.8	UB	0.20	11.46	0.37	L579.2	SC	0.25	9.13	0.39
L422.3	UB	0.20	5.67		L717.8	WO	0.55	3.13	
L487.8	LB	0.25	5.56	0.24	L759.9	WO	0.80	2.69	0.31
L532.9	SC	0.25	7.46						
BOREHOLE M									
M228.0	LB	0.20	9.86		M486.6	WO	0.40	11.65	1.20
M402.9	SC	0.30	12.92	1.31	M528.5	WO	0.28	7.53	0.69
BOREHOLE O									
O296.5	BH	0.33	13.54	16.99	O488.2	LB	0.25	11.33	0.36
O394.2	UB	0.25	13.47	0.79	O512.5	LB	0.30	14.80	1.39
O417.4	UB	0.25	13.65	0.77	O578.4	SC	0.30	8.99	0.38
O435.2	UB	0.20	14.80	0.48	O617.7	SC	0.20	10.35	0.32
O452.9	UB	0.30	11.34	0.38	O709.5	WO	0.23	9.16	
O469.2	UB	0.25	13.15	0.59	O745.8	WO	0.20	7.29	
BOREHOLE S									
S446.6	SC	0.30	13.57	0.28	S575.1	WO	0.25	12.79	0.73
S504.4	SC	0.35	15.54	0.82	S598.9	WO	0.35	11.33	0.39
S522.8	SC	0.30	15.89	0.99	S652.8	WO	0.30	9.26	0.40
S557.0	WO	0.25	12.16	0.56					
BOREHOLE T									
T320.5	SC	0.25	18.09	137.56	T397.6	WO	1.00	12.01	12.34
T365.4	WO	0.35	23.13	169.94	T419.0	WO	0.25	16.50	2.67
BOREHOLE U									
U191.5	SC	0.25	10.77	0.77	U326.0	WO	0.25	11.03	
BOREHOLE W									
W176.4	BH	0.18	9.28	0.90	W354.9*	LB	0.95	25.23	1283.00
W180.1	BH	0.18	12.98	3.15	W359.4*	LB	1.50	14.92	174.70
W182.6	BH	0.15	8.95	0.76	W368.0	LB	0.35	17.04	103.74
W209.8*	BH	1.30	15.63	58.02	W388.8	LB	0.25	4.93	0.37
W210.3*	BH	1.20	16.43	3226.30	W396.8*	LB	1.00	14.63	80.99
W229.8	BH	0.30	8.09	0.57	W401.6	SC	0.08	6.07	0.31
W243.9	UB	1.30	13.56	335.90	W430.8	SC	0.75	15.12	121.24
W274.6	UB	0.20	15.93	25.92	W455.6	SC	0.25	11.84	0.66
W300.8*	UB	0.25	17.45	178.90	W470.1	SC	0.45	13.80	2.63
W304.9	UB	0.23	13.75	8.98	W479.8	WO	0.20	7.77	0.53
W310.4*	UB	0.20	18.26	104.12	W493.9	WO	0.50	13.77	7.90
W349.9	UB	0.70	12.12	19.25	W515.6	WO	0.35	11.00	2.23

SN	OU	GS	PO	PER	SN	OU	GS	PO	PER
BOREHOLE X									
X281.3*	BH	0.35	7.94	0.80	X476.2*	LB	1.15	9.30	4.43
X282.0	BH	0.45	9.06	3.82	X489.0	LB	0.90		20.63
X296.6*	BH	0.65	14.29	801.90	X508.2*	LB	0.45	18.04	25.27
X297.7*	BH	0.30	13.36	84.81	X525.8*	SC	1.50	9.00	0.49
X309.3	BH	0.75	12.60	110.00	X528.7	SC	0.45	12.17	42.62
X336.1	UB	0.18	10.83	0.99	X530.7*	SC	0.40	13.38	9.44
X357.4	UB	0.05	1.87	0.29	X531.9*	SC	0.50	15.10	316.90
X365.6	UB	0.25	9.49	1.09	X559.4	SC	0.25	11.03	0.50
X386.8	UB	0.25	12.76	1.00	X588.5	SC	0.35	12.02	0.88
X413.3	UB	0.15	11.41	1.11	X612.9	WO	0.40	11.35	1.10
X436.6	UB	0.45	12.05	5.74	X640.0	WO	0.25	7.79	0.39
X458.9	LB	0.35	12.68	2.01	X675.5	WO	0.30	7.88	0.31
X473.1	LB	0.45	13.31	5.33					
BOREHOLE Y									
Y377.5	BH	0.45	14.09	34.67	Y566.1	LB	0.15	7.40	1.18
Y397.6	UB	0.23	11.19	2.70	Y593.9	SC	0.28	10.92	1.32
Y429.0	UB	0.23	13.54	5.33	Y624.7	SC	0.35	9.11	0.98
Y468.5	UB	0.28	13.06	4.36	Y642.2	SC	0.35	9.17	0.70
Y486.5	UB	0.23	13.88	3.25	Y672.9	WO	0.38	9.63	0.75
Y501.8	UB	0.18	9.23	0.60	Y690.1	WO	0.90	10.41	35.06
Y515.3	LB	0.25	13.00	1.67	Y727.4	WO	0.50	5.73	0.56
Y549.1	LB	0.45	10.13	4.22	Y757.9	WO	0.25	5.47	0.37
BOREHOLE Z									
Z402.9	UB	0.23	12.57	1.81	Z632.7	SC	0.40	7.25	0.60
Z422.6	UB	0.18	13.81	1.24	Z656.8	SC	0.40	6.40	0.58
Z444.2	UB	0.18	11.83	0.66	Z679.4	WO	0.45	9.09	0.91
Z499.0	UB	0.23	11.84	1.34	Z700.2	WO	0.35	9.28	1.17
Z512.4	LB	0.28	13.40	1.89	Z703.3	WO	0.23	7.30	0.84
Z531.9	LB	0.28	12.20	1.58	Z740.4	WO	0.28	8.32	1.00
Z593.0	SC	0.45	8.32	0.81	Z762.5	WO	0.33	7.48	0.37
Z611.3	SC	0.15	5.02	0.66	Z763.8	WO	0.40	7.07	0.54

Note:

SN = sample number, OU = operational unit, GS = average grain size (mm),

PO = porosity (%), PER = permeability (md).

BH = Bald Hill Operational Unit, UB = Upper Bulgo, LB = Lower Bulgo, SC = Scarborough, WO = Wombarra.

* Porosity and permeability data derived from Galloway and Hamilton (1988).

A number of factors affect the reservoir quality of sandstones and include detrital composition, texture, and diagenesis. To facilitate discussion, the Sydney Basin was broadly divided into two parts: combining the southern region and west margin as one (south-west region) and combining the northern region and east coast zone as the other (north-east region). In Figs 8-1 to 8-6, two plots were drawn. One is for the south-west region and the other for the north-east region.

8.3.1 DETRITAL COMPOSITION OF SANDSTONES

The influence of detrital composition of sandstones on the quality of sandstone as reservoirs is illustrated by Fig 8-1. It is a cross plot of permeability vs. quartz percentage. The plot shows that permeability generally increases with the increase in detrital quartz even though for a given quartz percentage there exists a great deal of variability. The variability is a function of texture and diagenesis. Of the 19 sandstones with a permeability greater than 50 md (lower limit for good reservoirs), 6 have a quartz percentage above 95 % and only two have a quartz percentage less than 75 %. In contrast, sandstones in which detrital quartz accounts for less than 50 % of the total detrital grains rarely have a permeability greater than 15 md (Fig 8-1), which is the lower limit required for moderate reservoirs according to the criteria in Table 8-1. The conclusions from the plot are that (1) the detrital composition of sandstones has a direct control on the quality of sandstones as reservoirs, (2) quartz arenites and sublitharenites are likely to comprise high quality reservoirs although a high quartz percentage does not ensure that the sandstone must be a high quality reservoir. In the same operational unit, sandstones in the south-west region of the basin generally contain more detrital quartz than those in the north-east region of the basin so that they are generally better reservoirs than sandstones in the north-east region.

8.3.2 INFLUENCE OF POROSITY ON PERMEABILITY

The absolute value of porosity affects permeability of sandstones. This is demonstrated by a cross plot of measured porosity vs. permeability (Fig 8-2).

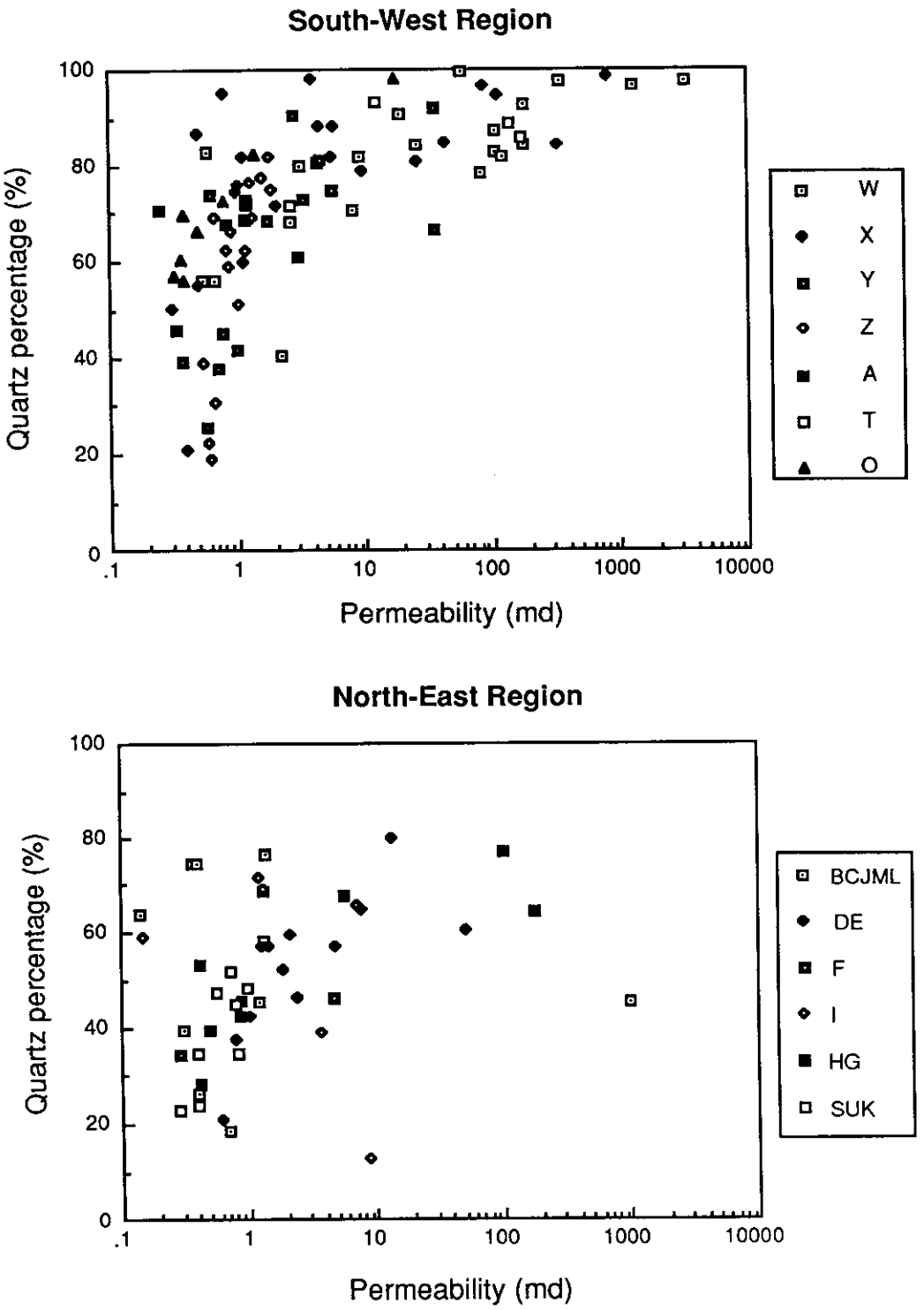

Fig 8-1 Cross plot of quartz percentage vs. permeability. Capital letters in the small rectangles are borehole keys. As shown in the diagram, a few boreholes may share the same symbol.

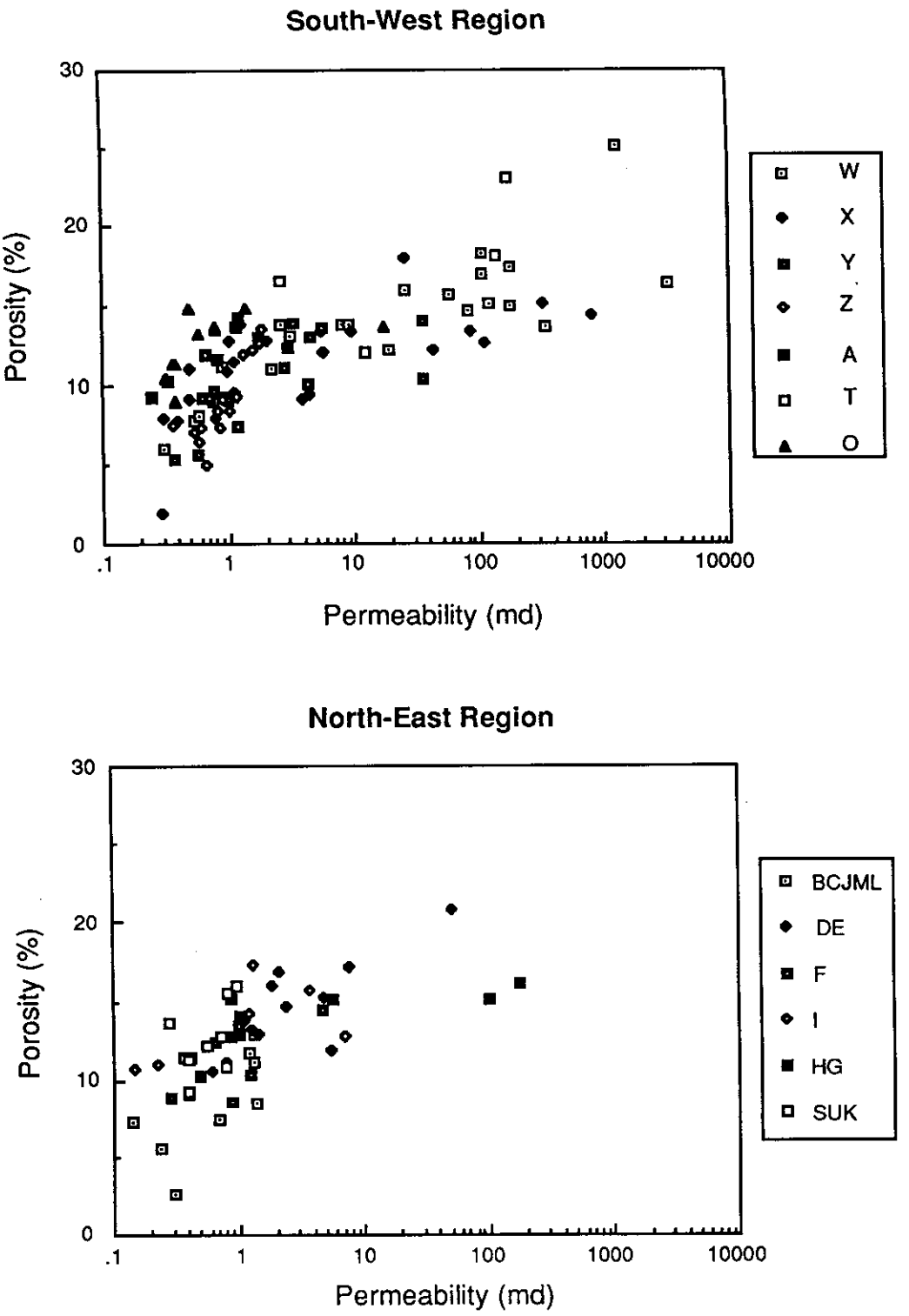

Fig 8-2 Cross plot of porosity vs. permeability. Capital letters in the small rectangles are borehole keys. As shown in the diagram, a few boreholes may share the same symbol.

Porosity and permeability keep a general positive relationship. Permeability increases with the increase in porosity. The relationship can be expressed by the familiar exponential function

$$\emptyset = a + b \log K$$

where $\emptyset$ = porosity, K = permeability, a, b = constants for a given sedimentary section. For the Narrabeen Group sandstones, 2 md seems to be a dividing point. The a, b values for the sandstones with permeability greater than 2 md are 10 and 2.5, and the a, b values for the sandstones with permeability less than 2 md are 11.5 and 8.5. For the relatively less permeable sandstones ($k < 2$ md), porosity affects permeability to a small extent. Permeability increases slightly with the increase in porosity. In contrast, porosity affects permeability to a large extent for the permeable sandstones ($k > 2$ md). Permeability increases greatly with increasing porosity.

Despite the general positive relationship, there is a great deal of variability. At a particular porosity value, the corresponding permeability can be in a wide range. This implies that permeability is not only affected by the absolute porosity value but also affected by the type of porosity (microporosity or macroporosity) and the size of the throat connecting pore spaces. For instance, a sandstone may have a high porosity but microporosity makes up a significant proportion of the porosity. In this type of sandstones, a high porosity is unlikely to be accompanied by a high permeability.

The measured porosity is generally greater than that derived from point counting. The difference in the two values can be taken as a rough measure of microporosity in the sandstone since microporosity is not observable under the petrological microscope. In quartz-rich sandstones, porosity consists largely of inter-grain pore spaces (macroporosity) whereas microporosity makes up a significant proportion of

the porosity in volcanic lithic-rich sandstones. The presence of diagenetic clays enhances microporosity in all kinds of sandstones.

As shown in Fig 8-2, for a given porosity value particularly if the value is greater than 10 %, the corresponding permeability tends to be lower for the sandstones in the north-east region than those in the south-west region. This is attributed to the type of porosity in different parts of the basin. In the northern region and the east coast zone, sandstones are generally rich in detrital lithics. In view of this composition and the presence of diagenetic illite and mixed-layer illite / smectite, pore spaces in these sandstones are expected to be mainly in the form of microporosity. The size of pore throats was greatly reduced by mechanical compaction and precipitation of diagenetic clay minerals. Thus a high porosity will not correspond to a high permeability.

8.3.3 GRAIN SIZE OF SANDSTONES

This influence is exhibited by cross plots of porosity and permeability vs. grain size. As shown in Fig 8-3, permeability has a general positive relationship with the average grain size. The larger the grain size the greater the permeability. Of the 19 sandstones with a permeability greater than 50 md, four are medium sandstones, nine coarse sandstones, four very coarse sandstones and only one is a fine sandstone with grain coating carbonates. Of the 21 sandstones with a permeability of 5-50 md, the majority are medium and coarse sandstones. For the sandstones with a similar grain size, however, the permeability can be remarkably different, which implies that the grain size is only one of the factors controlling porosity and permeability.

From the plots in Fig 8-4, it can be seen that the relationship between porosity and average grain size is not clear. For a given grain size, porosity can range from 5 to 20 %, which is caused by other depositional and diagenetic factors. However, sandstones with a grain size smaller than 0.25 mm rarely have porosities greater

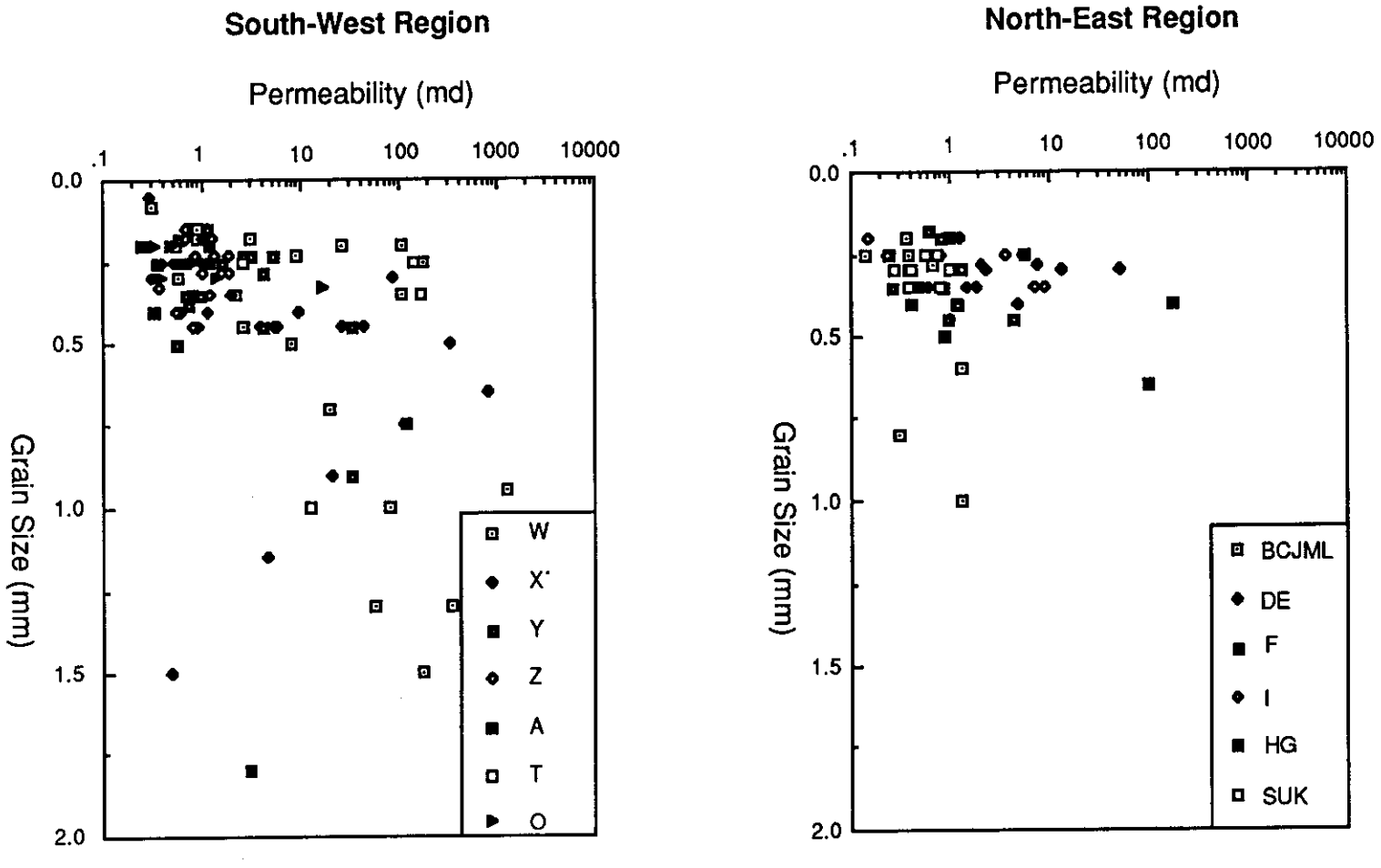

Fig 8-3 Cross plot of average grain size vs. permeability. Capital letters in the small rectangles are borehole keys. As shown in the diagram, a few boreholes may share the same symbol.

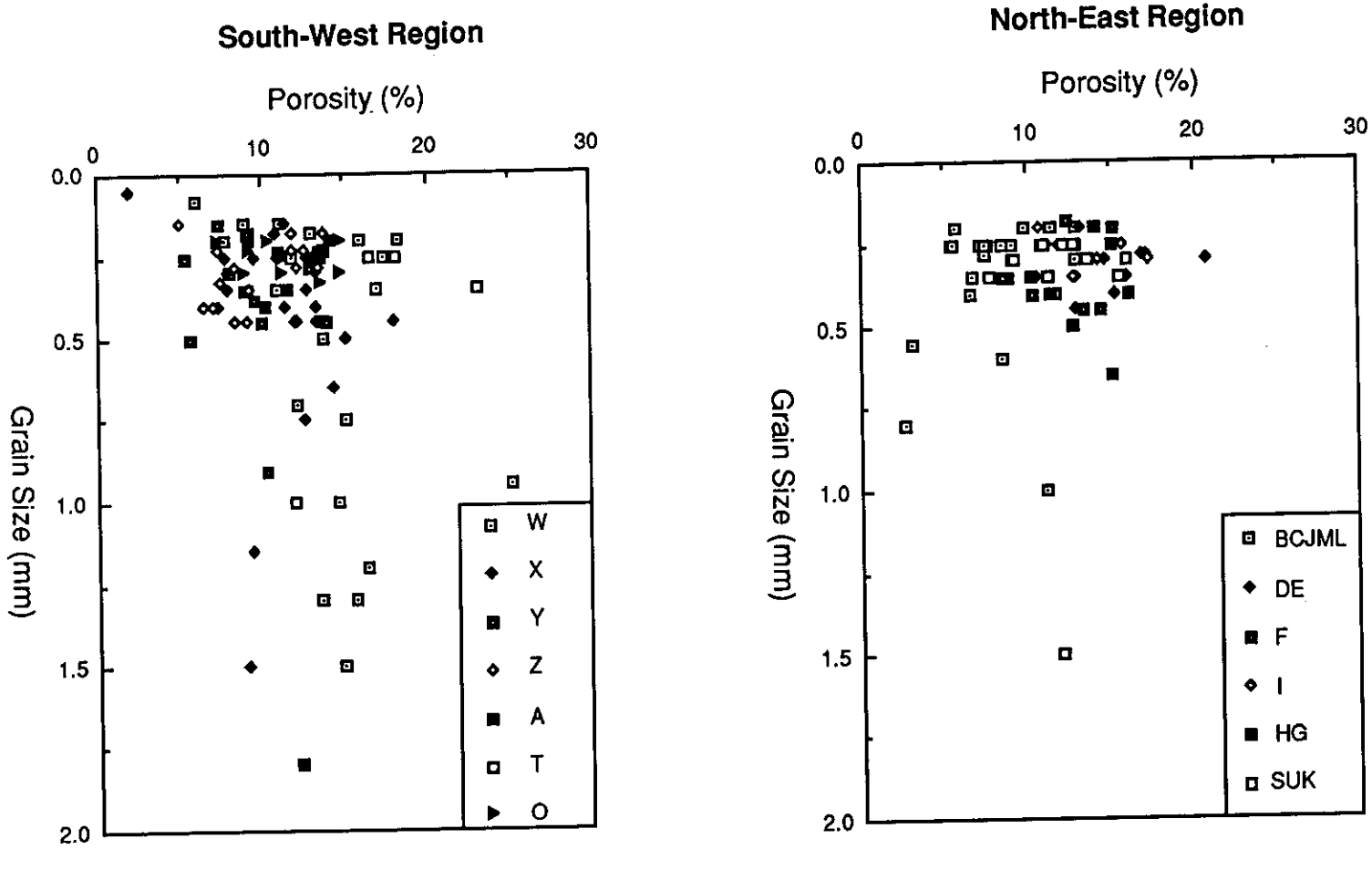

Fig 8-4 Cross plot of average grain size vs. porosity. Capital letters in the small rectangle are borehole keys. As shown in the diagram, a few boreholes may share the same symbol.

than 15 %, which is the minimum porosity value required for good reservoirs according to the criteria in Table 8-1. On the other hand, sandstones with a porosity greater than 15 % generally have a grain size larger than 0.25 mm.

The general conclusions from the two plots are that (1) sandstones should have a grain size greater than 0.25 mm to be high quality reservoirs even though sandstones with a grain size above 0.25 mm do not ensure higher porosities and permeabilities, and (2) very fine and fine grained sandstones are unlikely to be high quality reservoirs.

Grain sorting in sandstones obviously affects pore spaces. In poorly sorted sandstones, the fine particles fill the pore spaces among the coarse particles so that porosity is greatly reduced. Moderate to good sorting is another favourable factor for sandstones as high quality reservoirs, especially for fine and medium sandstones.

The amount of clay matrix (including diagenetic clays) also affects porosity and permeability. Clay matrix is destructive in view of porosity preservation. Porosity and particularly permeability generally decrease with the increase in clay matrix. In the Narrabeen Group sandstones, the association of abundant clay matrix (largely detrital) with very fine and fine sandstones is probably one of the factors which creates low porosity and permeability in very fine and fine sandstones. The increase of clay matrix with the increase in volcanic rock fragments is one of the factors responsible for low porosity and particularly permeability in lithic-rich sandstones so that in general quartz-rich sandstones in the south-west region tend to have higher porosity and permeability than lithic-rich sandstones in the north-east region of the basin.

8.3.4 BURIAL DEPTH

As discussed in the last chapter, the Narrabeen Group has been buried to much

greater depths than current drilling depths. The thickness of eroded sedimentary section varies across the basin. Sandstones at similar present day drill depth at different locations were probably buried to different depths. Thus the influence of burial depth on porosity and permeability is better discussed in the framework of comparing measured porosity and permeability values with drilling depth in the same borehole.

As shown in Figs 8-5 and 8-6, porosity and permeability generally decrease with the increase in drilling depth, particularly in the south-west region of the basin. Due to mechanical compaction, sandstones at the deeper burial depth are expected to have lower porosity and permeability than those at the shallower burial depth. However it should be noted that the detrital composition of sandstones changes from the bottom to top of the Narrabeen Group. The content of detrital quartz grains generally increases whereas that of lithic rock fragments generally decreases upwards towards the top of the Narrabeen Group, particularly in the south-west region. Therefore the decrease of porosity and permeability with the burial depth in the same borehole is probably more related with the variation of detrital composition of sandstones throughout the Narrabeen Group than the influence of burial depth, and the general decrease of porosity and permeability with the increase in drilling depth in the same borehole is more clearly shown in the south-west region than in the north-east region.

8.3.5 DIAGENESIS OF SANDSTONES

Porosity and permeability are also controlled by diagenetic processes. They include mechanical compaction, dissolution and cementation by quartz, carbonates and clay minerals.

(i) Mechanical Compaction

Linear contacts of detrital grains, suture contacts among detrital quartz grains, and deformed mica flakes around adjacent "hard" detrital grains are all indications that

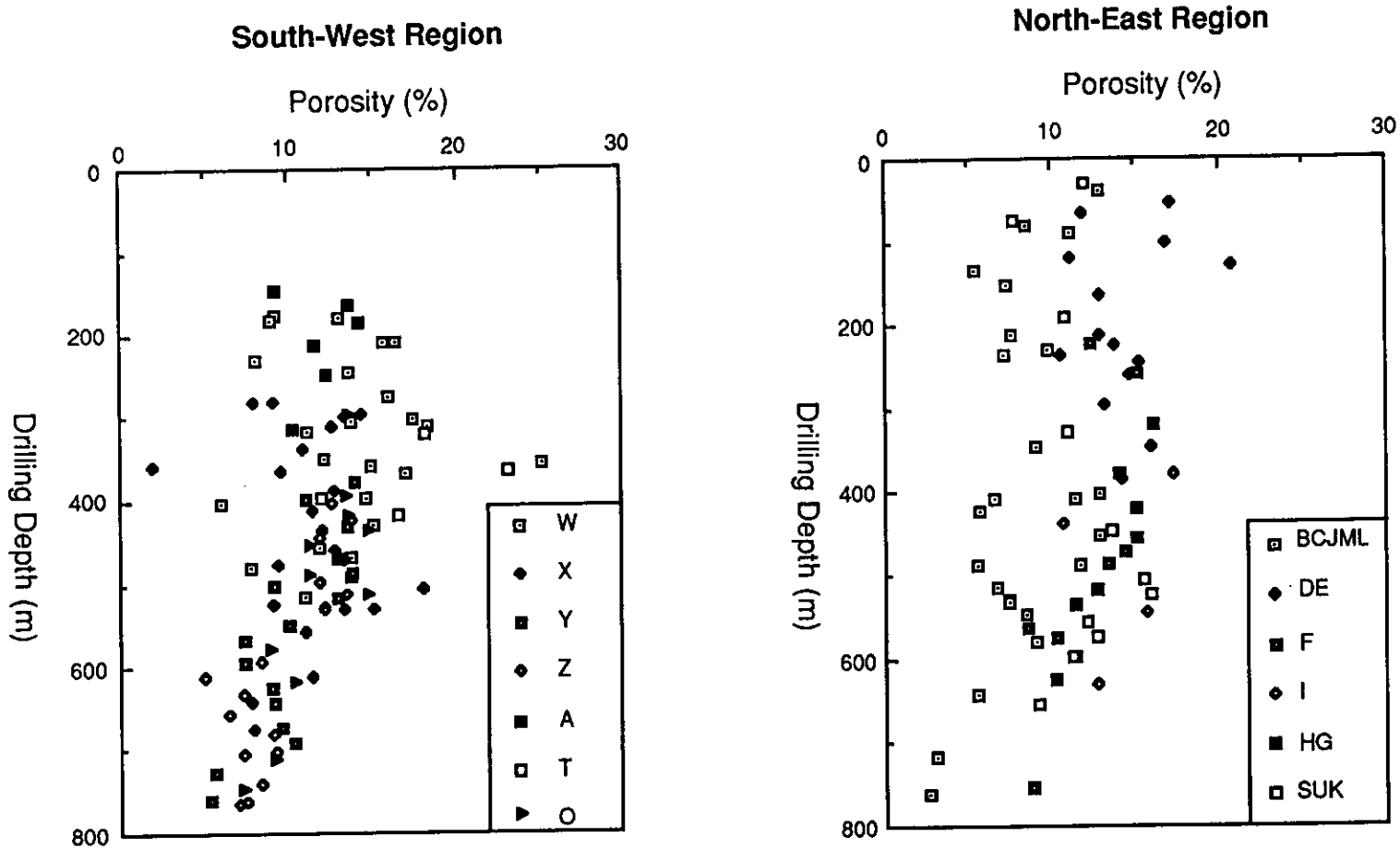

Fig 8-5 Cross plot of drilling depth vs. porosity. Capital letters in the small rectangle are borehole keys. As shown in the diagram, a few boreholes may share the same symbol.

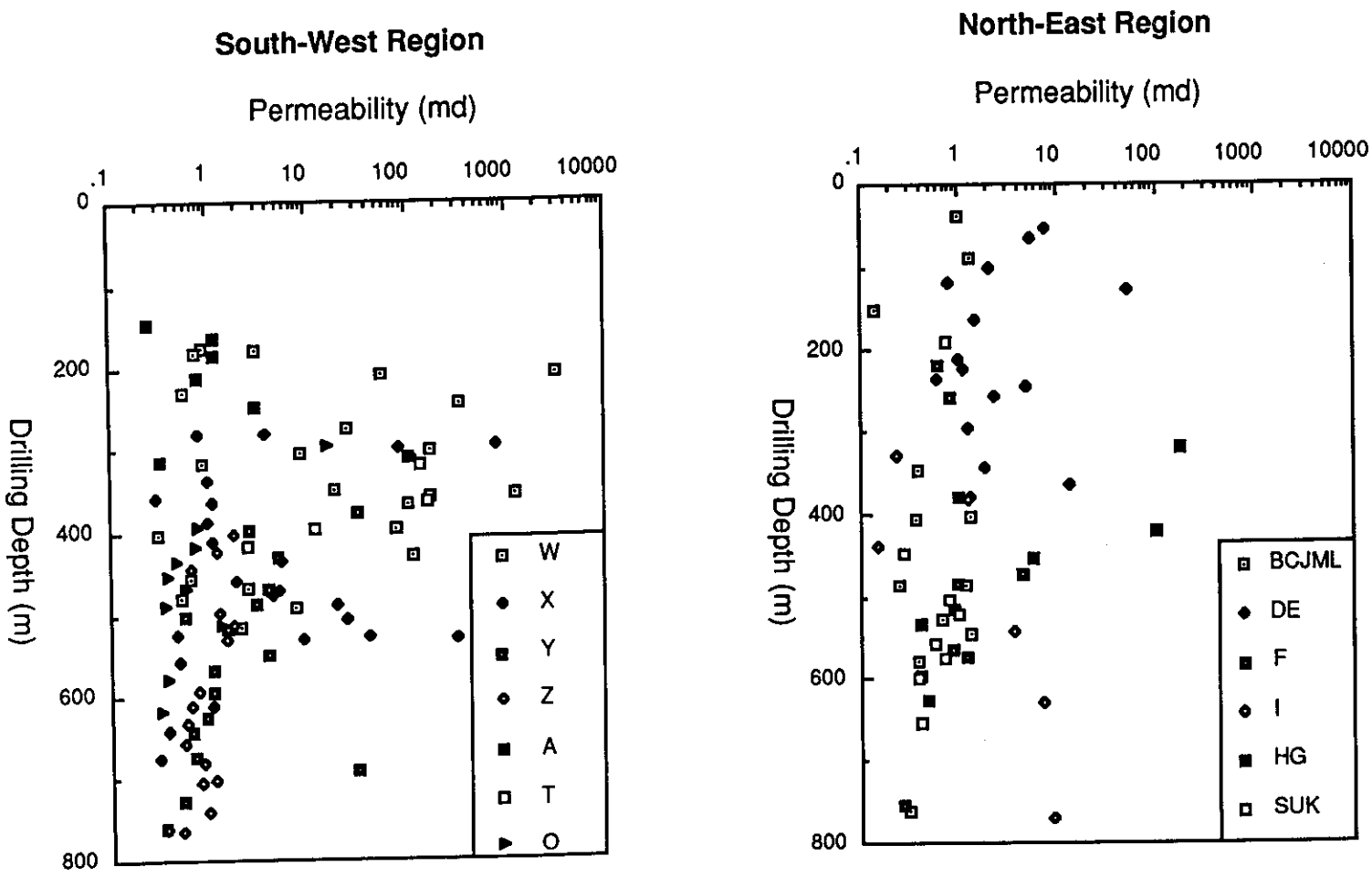

Fig 8-6 Cross plot of drilling depth vs. permeability. Capital letters within the small rectangles are borehole keys. As shown in the diagram, a few boreholes may share the same symbol.

mechanical compaction has taken place and it is an important mechanism reducing porosity and permeability. In sandstones rich in detrital quartz clasts (quartzarenite and sublitharenite), early cementation by clay minerals and siderite partly lithified sandstones. Such a lithification provided some resistance to mechanical compaction and so part of original inter-grain pore spaces are preserved. In sandstones rich in detrital lithics, the dissolution / alteration processes affecting detrital lithics and feldspar grains in the early stage of diagenesis made these unstable particles more ductile so that they facilitated further mechanical compaction. In these sandstones, inter-grain pore spaces (macroporosity) were largely lost due to mechanical compaction.

(ii) Cementation

In quartz-rich sandstones, quartz overgrowths and kaolins are the important cements reducing porosity and permeability. In some parts of the same sandstone, inter-grain primary pore spaces can be completely lost due to cementation by quartz (Fig 8-7). Quartz cementation is more destructive to porosity in fine sandstones than in medium and coarse sandstones. In the former, primary inter-grain pore spaces were small so that they were more likely to be mostly or completely occluded by quartz overgrowths. In the texturally mature medium and coarse sandstones, quartz overgrowths occur in the form of thin veneers. Primary inter-grain pore spaces could exist between quartz overgrowths.

Diagenetic kaolins reduce porosity but, more significantly they reduce permeability. Their presence changes pore spaces from macroporosity to microporosity. They reduce pore throats and may even block them. As a result, quartz-rich sandstones with abundant kaolins (e.g. samples from Borehole O) can have a high porosity but rarely have a corresponding high permeability.

In quartz-rich sandstones, siderite is normally the dominant type of carbonate cement. It generally occurs in single or mosaic crystals. Pore filling siderite cement

Fig 8-7 (top left) Quartz overgrowths reducing inter-grain pore spaces. From St Albans 1 at drilling depth of 419.7 m (sample H419.7). Measured porosity and permeability of this sample are 15.01 % and 99.67 md.

Fig 8-8 (top right) Porous sandstone with grain coating siderite. From Cobbitty 3 at drilling depth of 531.9 m (sample X531.9). Measured porosity and permeability of this sample are 15.10 % and 316.90 md.

Fig 8-9 (middle left) Porous sandstone with grain coating calcite and siderite. From Weromba 2 at drilling depth of 300.8 m (sample W300.8). Measured porosity and permeability of this sample are 17.45 % and 178.90 md.

Fig 8-10 (middle right) Post quartz overgrowth ankerite occluding inter-grain pore spaces. From Coal Cliff 17 at drilling depth of 151.7 m (sample B151.7). Measured porosity and permeability of this sample are 7.33 % and 0.14 md.

Fig 8-11 (bottom left) Calcite cement occluding inter-grain pore spaces. From Liverpool 91 at drilling depth of 595.2 m (sample L595.2). No measured porosity and permeability data for this sample.

Fig 8-12 (bottom right) Illite lining inter-grain pore spaces reducing porosity to a less extent but permeability to a large extent. From Cobbitty 3 at drilling depth of 476.2 (sample X476.8). Measured porosity and permeability of this sample are 9.30 % and 4.43 md.


01mm150kU 150E2 3827/00 SE


1mm150kU 530E1 3534/01 SE


0.1mm15.0kU 1.01E2 4796/01 SE


C
O
0.1mm15.0kU 2.12E2 2327/01 SE

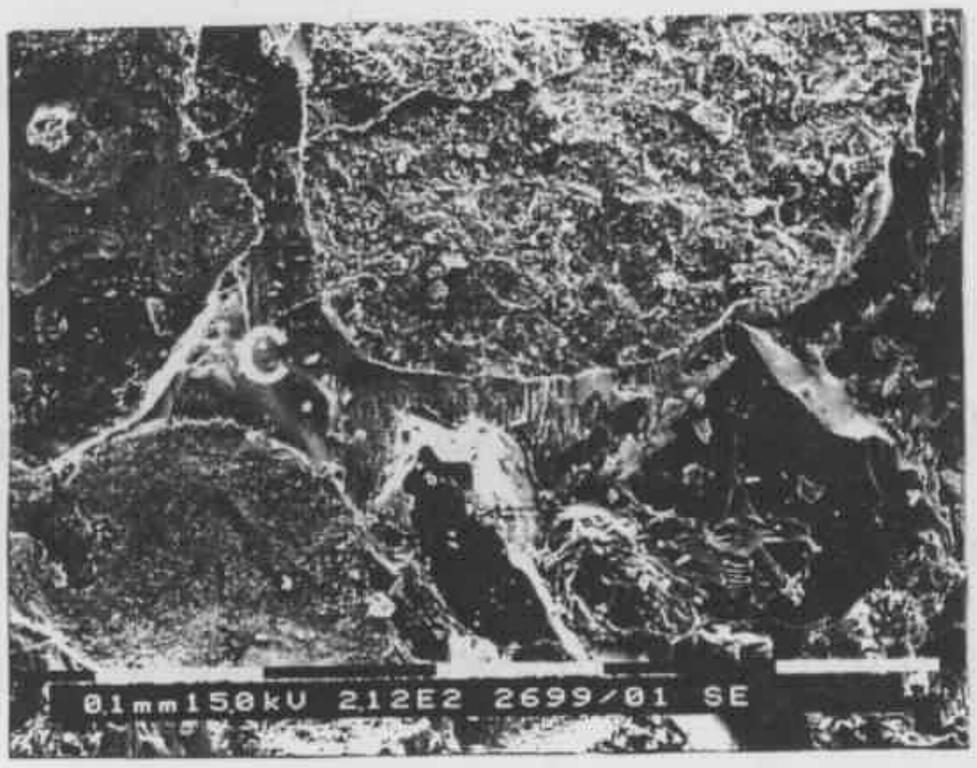
C
0.1mm15.0kU 2.12E2 2699/01 SE

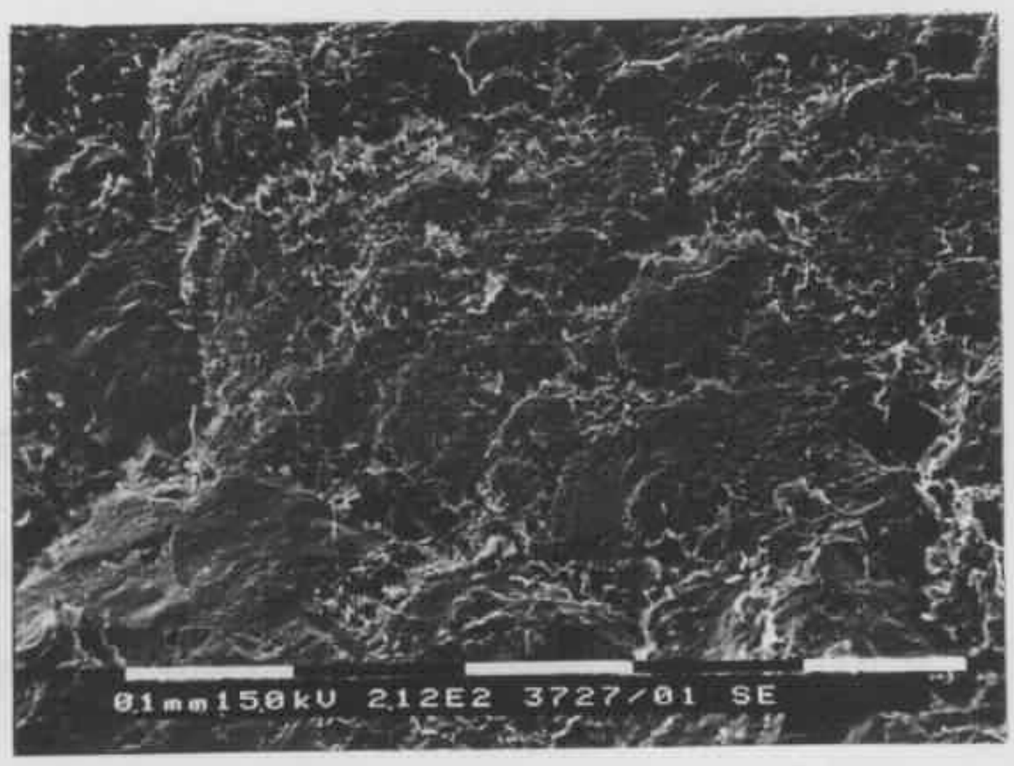
0.1mm15.0kU 2.12E2 3727/01 SE

in large amounts was found but very rare. Therefore, siderite cementation did not reduce porosity to any significant extent. In addition, grain coating siderites / calcites found in three quartz rich sandstones favour preservation of porosity since they prevent these sandstone from further diagenesis (quartz overgrowths and mechanical compaction) (Figs 8-8 & 8-9). The three sandstones containing grain coating carbonates have porosities and permeabilities of 17.45 % and 178.90 md for sample W300.8, 18.26 % and 104.12 md for sample W310.4, and 15.10 % and 316.90 md for sample X531.9. They are good and very good reservoirs. However, the factors controlling precipitation of grain coating carbonates are not clear so that the distribution of the sandstones containing grain coating carbonates remains enigmatic.

In some quartz-rich sandstones in the east coat zone and northern region, post quartz overgrowth calcite or ankerite was found both in thin sections and under SEM/EDX analyses. These late cements further reduce porosity (Fig 8-10). This is another factor why sandstones with a comparable detrital composition tend to have a lower porosity in the east coast zone and the northern region than in the west margin and the southern region.

In sandstones rich in detrital lithics, carbonate cementation can be a very important mechanism of porosity reduction. Pore filling calcite and / or ankerite cements occur in large amounts in some lithic-rich sandstones in the east coast zone and the northern region. In these sandstones, this sort of carbonate cementation can result in an almost complete loss of the primary inter-grain pore spaces (Fig 8-11).

Mixed-layer illite / smectite coats detrital grains and illite fills inter-grain pore spaces. They tend to extend out from the detrital grains at right angles (Fig 8-12). As a result, the thickness of the irreducible water layer associated with detrital grains is extended so that it reduces pore throats and even block them. Even though the presence of a small amount of mixed - layer illite / smectite and illite

does not reduce porosity much, it may result in a big reduction of permeability.

Grain coating chlorite is often cited as having inhibited subsequent cementation. The most often cited example of porosity preservation due to chlorite is the Cretaceous Tuscaloosa sandstone of the Gulf Coast (Thomson, 1979). However, grain coating chlorite does not favour porosity preservation in the Narrabeen Group sandstones simply due to the fact that it failed to prevent sandstones from further diagenesis. Quartz or carbonate cementation often succeeded precipitation of grain coating chlorite. Sandstones with grain coating chlorite tend to have a low porosity and permeability.

(iii) Dissolution

Dissolution processes increase porosity of sandstones and so enhance reservoir potential. Secondary porosity was mainly created by dissolution processes in the Narrabeen Group sandstones. It was studied both in thin sections and under SEM/ EDX analyses. The intra-grain, intra-cement and mould secondary porosities are isolated pore spaces. Increase of this sort of secondary porosity is not accompanied by an increase in permeability. Preserved oversized secondary porosity is more important with regard to reservoir potential. As mentioned in the petrology chapter, secondary porosity is present in most of the sandstones studied but in a trace amount (generally less than 2 % of the total sandstone). The ratio of secondary porosity to the total primary and secondary porosities is less than 1/5 for the majority of sandstones subjected to modal analyses. Thus the present preserved porosity is largely primary porosity. Secondary porosity is only locally important. Overall, dissolution is not an important factor in determining the reservoir potential of sandstones.

In summary, porosity and permeability of the Narrabeen Group sandstones are controlled by a combination of depositional and diagenetic factors. The former include detrital composition of sandstones and texture of sandstones (grain size,

sorting, and detrital clay matrix) and the latter mechanical compaction, cementation of diagenetic minerals and dissolution. Considering all these factors, high quality reservoirs should have the following three features: (1) a high percentage of detrital quartz clasts, (2) medium to coarse grain size (better if moderately to well sorted), (3) quartz overgrowth and siderite as the principal cements. These are similar to the conclusions of Hamilton and Galloway (1989). In addition, quartz-rich sandstones with grain coating siderite / calcite are high quality reservoirs.

8.4 RESERVOIR POTENTIAL OF THE NARRABEEN GROUP SANDSTONES

The measured porosities and permeabilities are described for each of the five operational units in the two parts: south-west region and north-east region. Based on the data from porosity and permeability measurements (Table 8-2), the reservoir potential of each operational unit is evaluated .

8.4.1 WOMBARRA OPERATIONAL UNIT

In the south-west region the measured porosity and permeability for this unit range from 5.47 to 13.77 % and from 0.37 to 169.94 md respectively. Most of the porosity values are less than 10 % and most of the permeability values are less than 10 md. For the sandstones from Boreholes O, Y and Z, the permeability is generally less than 2 md. For a few moderately to well sorted medium and coarse grained sandstones (such as samples T365.4 and Y690.1), the porosity reaches up to more than 10 % and the permeability is greater than 40 md. The sandstones from the west margin tend to have higher porosity and permeability than those from the southern region.

In the north-east region, the porosity varies from 2.69 to 15.95 % with the majority falling in the range of 7 to 12 %. The permeability varies from 0.28 to 13.53 md with the majority being less than 2 md. Sandstones from the east coast zone generally have smaller porosities and permeabilities than those from the northern region.

The measured porosity and permeability data indicate that the sandstones in this unit are generally poor reservoirs. In this unit, some moderately to well sorted, medium and coarse grained channel-fill sandstones may comprise fair to good reservoir rocks. However, this sort of sandstone is geographically restricted to the west margin and stratigraphically to the top part of the unit where sandstones are relatively rich in quartz.

8.4.2 SCARBOROUGH OPERATIONAL UNIT

In the south-west region, the measured porosity and permeability for this unit are in the range of 5.02 to 18.09 % and 0.31 to 137.56 md respectively. Most of the sandstones from this unit have a porosity of less than 10 % and a permeability of less than 2 md. This is particularly true for the sandstones from Boreholes A, O, Y and Z in the southern region. A few sandstones from Boreholes T, W and X are quite porous. They have porosities of more than 15 % and permeabilities of greater than 20 md. In sample T320.5, a porosity of 18.09 % and a permeability of 137.56 md were measured.

In the north-east region, the porosity and permeability fall in the range from 5.35 to 20.71 % and from 0.28 to 51.26 md. A few sandstones from Borehole E show good aspects as high quality reservoir rocks. Sample E128.0 has a porosity of 20.71 % and a permeability of 51.26 md.

Like the underlying Wombarra Operational Unit, the sandstones from the lower part of the unit have a very low potential as reservoir rocks. However, some sandstones from upper part of the unit in the west margin as well as in Boreholes X and E in the southern and northern regions comprise moderate to very good reservoirs.

8.4.3 LOWER BULGO OPERATIONAL UNIT

The sandstones within this unit have porosities ranging from 4.93 % to 25.23 % and permeabilities ranging from 0.37 to 1283.0 md. The majority of sandstones

from Borehole W have permeabilities of more than 80 md. In contrast, the sandstones from Boreholes A and O have permeabilities of less than 1.5 md.

In the north-east region, 8 sandstone samples from this unit were subject to porosity and permeability measurements. The porosity ranges from 5.56 to 15.63 % and the permeability from 0.24 to 99.67 md. If sample H419.7, which has a permeability of 99.67 md, is excluded from this group, the permeability will fall in a very small range and vary from 0.24 to 3.64 md.

The potential of sandstones in this unit as reservoirs is quite high, particularly for sandstones from the south-west region. The measured porosity and permeability indicate that some sandstones from Borehole W in the west margin are good to excellent reservoirs. A number of sandstones from Boreholes X and H are moderate to good reservoirs.

8.4.4 UPPER BULGO OPERATIONAL UNIT

In the south-east region, the data from the porosity and permeability measurements indicate porosity and permeability range from 9.23 % to 18.26 % and from 0.25 to 335.9 md respectively. Some sandstones from Borehole W have higher permeabilities of more than 100 md. The permeability in the majority of sandstones from other boreholes is less than 5 md.

In the north-east region, porosities fall in the range of 7.33 to 17.24 % and permeabilities in the range of 0.14 to 178.31 md with the majority being less than 15 md. One sandstone from Borehole H (sample H319.0) shows good aspects as a high quality reservoir as it has a porosity of 16.07% and a permeability of 178.31 md.

The sandstones in this unit could act as good to very good reservoirs, as demonstrated by some sandstones from Boreholes W and H. However, the

potential is not as high as that of the sandstones in the underlying Lower Bulgo Operational Unit. This is largely due to the smaller grain size of sandstones in this unit than those in the underlying LB unit.

8.4.5 BALD HILL OPERATIONAL UNIT

The data from porosity and permeability measurements indicate that porosities of the coarse and very coarse grained sandstones are greater than 13 % and permeabilities greater than 30 md. The permeability reaches up to 3226.3 md in one of the samples (sample W210.3). More significantly, in sandstones from Boreholes O and Y, porosities of more than 13 % and permeabilities of more than 15 md were measured.

Porosity and permeability were measured in only one sandstone (sample I327.7) in the north-east region. They are 11.01 % and 0.23 md, which does not show a high potential as a reservoir rock.

The measured porosity and permeability data demonstrate that this unit has the highest potential as reservoir rocks. Sandstones composing good to excellent reservoirs are not only from Borehole W in the west margin but also from Borehole X in the southern region. Some sandstones from Boreholes Y and O could act as moderate reservoirs.

8.5 DISTRIBUTION OF GOOD TO EXCELLENT RESERVOIRS

According to the criteria listed in Table 8-1, 19 of the 175 measured samples have permeabilities of greater than 50 md and so they are good to excellent reservoirs. Fig 8-13 shows the distribution of the 19 good to excellent reservoirs throughout the Narrabeen Group and across the basin. One of them is from the WO unit (169.94 md), four from the SC unit with an average of 156.70 md, five from the LB unit with an average of 348.42 md, four from the UB unit with an average of 199.31 md and five from the BH unit with an average of 856.21 md. Geographically, ten of

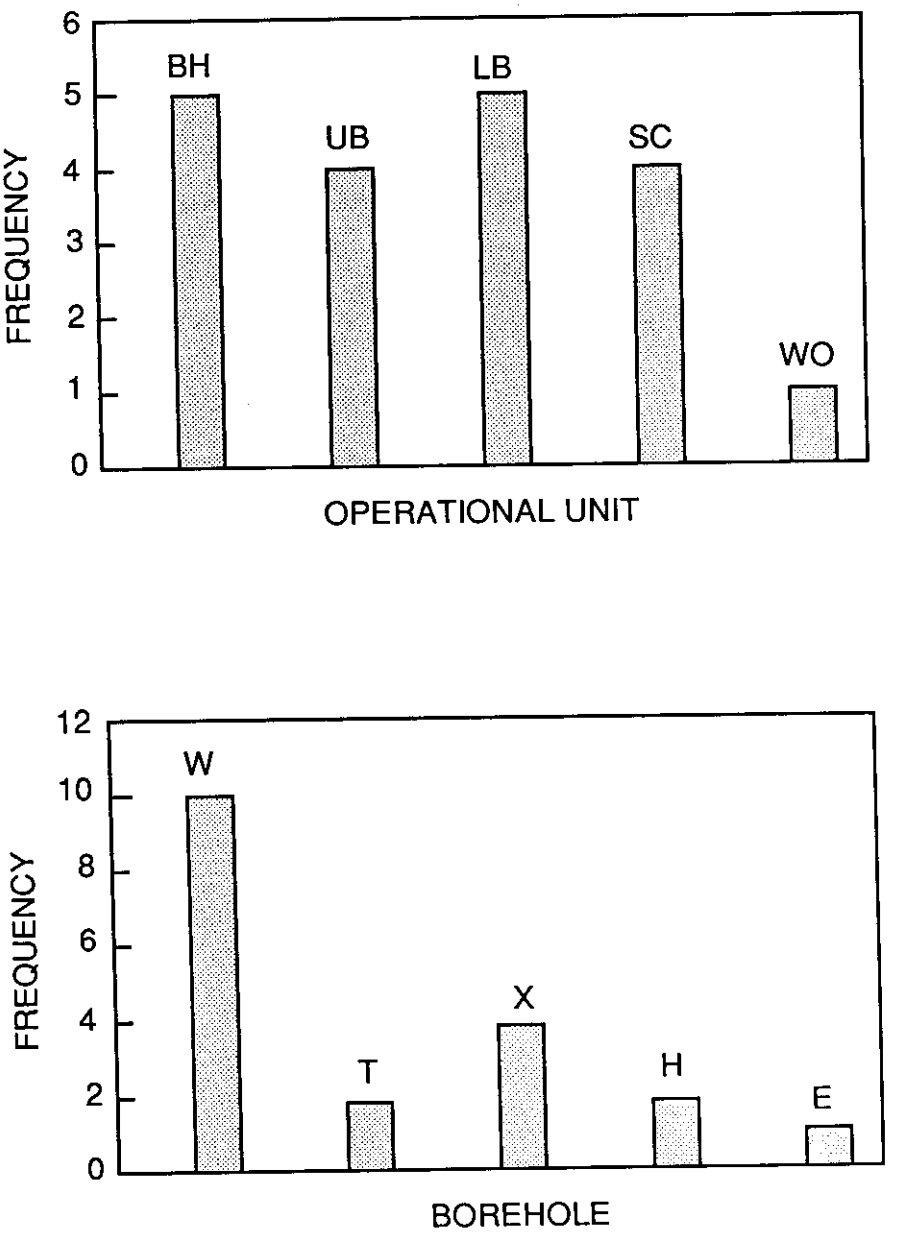

Fig 8-13 Distribution of high quality reservoirs throughout the Narrabeen Group and across the Sydney Basin.

them are from Borehole W, four from Borehole X, two from Boreholes T and H each, and one from Borehole E.

Based on the measured porosity and permeability data, the potential of the Narrabeen Group sandstones as hydrocarbon reservoirs can be summarised as: (1) In terms of stratigraphy, the BH has the highest potential, which is succeeded in order by the LB unit, UB unit, SC unit and WO unit; (2) Geographically, the west margin has the highest potential, which is succeeded in order by the southern region, northern region and the east coast zone. These conclusions are similar to those drawn by Hamilton and Galloway (1989).

CONCLUSIONS

1) Channel fill, inter-channel floodplain / lacustrine and channel margin are the three principal component facies recognised in the Narrabeen Group with the channel margin facies being of minor volumetric importance.

2) Conglomerate and sandstone are the lithological components of the channel fill deposits with sandstone being of much more volumetric importance. Sandstone commonly comprises the entire channel fill facies by itself although in some cases, together with channel lag conglomerate, makes up channel fill facies.

3) A single channel fill facies is normally 2 m thick. Channel fill facies can be stacked together to form amalgamated channel fill facies, which can be 15 m or more thick.

4) Inter-channel floodplain / lacustrine facies consists of shales / mudstones and very fine sandstones. Channel margin facies (natural levee and crevasse splay) are represented lithologically by silty shale, very fine and fine sandstones.

5) The sandstones in the Narrabeen Group consist largely of detrital quartz (5 - 80 % of the total sandstone) and lithics (0 - 75 %), which are inversely related to each other. Detrital feldspar is a minor component (0 - 15 %). In sandstones rich in quartz, detrital feldspar is rarely found.

6) The percentage of detrital quartz in the total detrital clasts generally increases upwards throughout the Narrabeen Group from 20 - 40 % at the basal part of the group to 80 - 95 % in the Bald Hill Operational Unit and that of detrital lithics decreases from 60 - 80 % to 20 - 40 %. These vertical variations are more clearly shown in the boreholes in the southern basin than in the northern basin.

7) The vertical variation of detrital composition does not proceed at a uniform rate. Depending upon the borehole location in the basin, one to three distinctive boundaries, across which detrital compositions of sandstones have a sudden and significant change, and / or one abnormally lithic - rich interval can be recognised. The lowermost boundary is defined as DB3, the middle one as DB2, and the uppermost one as DB1 with DB2 being the most obvious. Across DB2 upwards, a sudden 20 - 35 % increase in detrital quartz clasts and a sudden 20 - 35 % decrease in detrital lithics occur.

8) DB3 is recognised in boreholes in the west margin, the southern region, the southwestern portion of the northern region and the northern portion of the east coast zone of the basin. It marks the source change from lithic to quartzose or mixing source. Its position in the stratigraphic horizon varies from one borehole to another from within the lower part of the Wombarra Operational Unit to within the upper part of the Scarborough Operational Unit, suggesting the source change did not take place uniformly in the whole basin.

9) DB2 marks the top boundary of the abnormally lithic - rich interval, which generally correlates with the lower part of the Scarborough Operational Unit. Thus DB2 and the interval occur together in the same borehole. They are restricted to the boreholes in the southern basin. Their presence is related to the eastern volcanic source, which probably lay east of the present day coastline off Cape Banks 1 borehole (Borehole J).

10) DB1 is recognised in boreholes where the sampling of the Bald Hill Operational Unit sandstones is available. Across it upwards, the quartz percentage is further increased by 10 - 15 %. The further increase of detrital quartz clasts suggests that the quartzose source became more important after DB1. DB1 is generally consistent throughout the basin and located near the boundary between the Upper Bulgo and Bald Hill Operational Units.

11) Regionally, the average percentage of detrital quartz in sandstones in a given stratigraphic horizon decreases and that of detrital lithics increases eastwards and less obviously northwards.

12) During deposition of the Narrabeen Group, there existed three detrital sources: the Lachlan Fold Belt supplying detrital quartz clasts, the New England Fold Belt supplying detrital lithics as well as quartz clasts, and eastern volcanic source with the first two being more important quantitatively than the latter.

13) During early WO time (late Permian), the New England Fold Belt was the major source for the whole basin. As sedimentation proceeded, the Lachlan Fold Belt became more and more important and finally replaced the New England Fold Belt as the major detrital source. This was attributed to the reduction in height and extent in the New England Fold Belt caused by continued erosion and settling and the development of a peripheral bulge on the eastern edge of the Lachlan Fold Belt resulting from continued westward migration of lithospheric loading, which was caused by thrusting in the New England Fold Belt. The source replacement did not occur at the same time in the whole basin. It happened in early period of WO time in the west margin, in middle period of WO time in the western portion of the southern region, at the end of WO time in the central part of the basin (near the boundary between the southern and northern regions), in the late period of SC time in the southwestern portion of the northern region. In the northeastern portion of the northern region and northern portion of the east coast zone, it did not take place until the end of UB time.

14) The eastern volcanic source supplied volcanic lithics to the basin from middle WO time. The sandstone petrology data suggest that the volcanic source seemed to be very active only during two periods: early period of SC time and early and middle periods of UB time.

15) Detrital clasts are consolidated by clay matrix (both detrital and diagenetic) (0 - 32 % of the total sandstone) and carbonate cement (0 - 49 %). Quartz cement is not important since it accounts for less than 2 % of the total sandstone in the majority of sandstones studied. Clay matrix and carbonate cement are inversely related. The higher the clay matrix, the lower the carbonate cement.

16) There are three principal types of diagenetic minerals: carbonates, clay minerals, and quartz. In addition, authigenic albite was commonly found in sandstones containing detrital plagioclase. A minor amount of haematite, pyrite, apatite, anatase, analcime, and dawsonite were also found.

17) Carbonates consist of calcite (non-ferroan and ferroan), dolomite, ankerite, and siderite with siderite being the most common and dolomite the least common. Clay minerals include kaolin, illite, mixed - layer illite / smectite, and chlorite with kaolin being the most common. Micro-quartz, mega-quartz, and quartz overgrowths comprise quartz cement with quartz overgrowth being the most abundant.

18) Diagenesis began with the formation of rare grain coating haematite and early kaolin, grain coating mixed - layer illite / smectite and chlorite. It was succeeded by major carbonate cementation. Among the diagenetic carbonates, calcite coating detrital grains was the first to crystallise and was succeeded by siderite coating detrital grains, pore filling calcite, pore filling siderite, pore filling ferroan calcite and pore filling ankerite. After the major carbonate cementation, kaolin, quartz overgrowth and filamentous pore bridging illite crystallised. The last cements to form were a minor amount of pore filling calcite and ankerite.

19) Early kaolin (generation I) and grain coating mixed - layer illite / smectite can occur together, but they are exclusive with chlorite. This suggests that early kaolin and illite / smectite, and chlorite were formed in different physico-chemical

conditions. The kaolin and illite / smectite crystallised in sands with oxygenated and mildly acidic pore waters whereas chlorite formed in sands with anoxic and neutral to mildly alkaline pore waters. The formation of chlorites was also controlled by the detrital composition of sandstones, as suggested by the close association of the occurrence of chlorite with abundant volcanic rock fragments.

20) The type of carbonate formed during carbonate cementation was controlled by the relative concentration of Ca^{2+}, Fe^{2+}, Mg^{2+} and Mn^{2+} and physico-chemical conditions of pore waters. Non-ferroan calcite formed in pore waters where Fe^{2+} was virtually absent. Where Fe^{2+} was present in a higher concentration, other types of carbonates (Fe calcite, dolomite, ankerite or siderite) crystallised depending upon the concentration of other cations and physico-chemical conditions in pore waters.

21) Fe^{2+} used in forming carbonates was derived from reduction of Fe_2O_3 by organic matter in adjacent shales / mudstones, alteration of volcanic rock fragments during diagenesis and organic matter in that order of importance.

22) Ca^{2+} used in forming carbonate was largely derived from initial hydration of volcanic rock fragments. The produced Ca^{2+} was incorporated with HCO_3^- at or near where it was produced so that pore filling Ca bearing carbonates (calcite and ankerite) are restricted to the lower Narrabeen Group sandstones, which are generally rich in lithics.

23) Carbon in carbonates (or HCO_3^-) was derived from a combination of oxidation of organic matter by Fe^{3+} oxide (reduction of Fe_2O_3 by organic matter), bacterial fermentation in the adjacent shales / mudstones and meteoric water supply (CO_2 from atmosphere).

24) Kaolins (generation II) were formed by direct precipitation from migrating pore waters and alteration of volcanic rock fragments, feldspar, and mica. They are more common and abundant in sandstone rich in quartz than those rich in lithics.

25) Quartz overgrowths developed in two ways and / or a combination of them: overlap and / or emergence of initial mirco-quartz crystals and envelopment of these early multiple overgrowths by an outer shell. They are more common and abundant in quartz - rich sandstones than in lithic - rich sandstones. The silica used for the overgrowths was largely derived from pressure solution.

26) Precipitation of post quartz overgrowth illite was related to the build up of K^+ in pore waters. How a high concentration of K^+ was achieved is not clear. Cessation of illitisation of smectite was probably a main contributing factor for the build up.

27) Stable isotope data suggest that diagenesis proceeded in two different regimes: early dynamic fluid flow regime and late slow flow / static fluid regime, which correspond to early diagenesis and late diagenesis.

28) The early dynamic fluid flow regime was characterised by a slight increase of the calculated $\delta^{18}O$ of pore waters from the estimated initial value of -15 ‰, typical of Triassic meteoric waters, to -12 ‰ with temperature increasing from ~ 10 ° to 80 - 85 °C. Early kaolins (generation I) crystallised in pore waters with a $\delta^{18}O$ similar to that of original depositional waters (-15 ‰) at a temperature of ~ 10 ° to 30 °C. Pore filling carbonates were precipitated in pore waters with a $\delta^{18}O$ of -15 ‰ to -12 ‰ at a temperature of 35 ° to 80 -85 °C.

29) The late slow flow / static fluid regime was characterised by rapid ^{18}O-

enrichment of pore waters. The calculated $\delta^{18}O$ of pore waters enriched from -12 ‰ to -3 ‰ with the temperature increasing from 85 ° to 110 - 135 °C. Pore filling kaolins (generation II) crystallised in pore waters with a $\delta^{18}O$ of -12 ‰ to -6 ‰ at a temperature of 85 °to 110 -135 °C. Precipitation of quartz overgrowths occurred in pore waters with a $\delta^{18}O$ of -7 ‰ to -3.5 ‰ at a temperature of 110 - 135 °C and that of illite in pore waters with a $\delta^{18}O$ of -6 ‰ to -3 ‰ if it formed at similar temperatures as quartz overgrowths.

30) During the diagenetic history from the early kaolin (generation I) to the late post quartz overgrowth illite, δD of pore waters was hardly modified from the estimated original value of -110 ‰.

31) Means of measured homogenisation temperatures of aqueous fluid inclusions in quartz overgrowths range from 95 ° to 120 °C, which are 45 ° to 60 °C higher than the current formation temperatures at the sample depths of 500 - 600 m. The high fluid inclusion temperatures, together with vitrinite reflectance data, imply that a section with a thickness of *ca* 1600 to 2200 m was eroded away in the southern basin. The formation temperatures of quartz overgrowths were 110 - 135 °C. The proposed model for heat flow history describes the heat flow varied with time with its peak (2.1 HFU) being reached in late Cretaceous time (~ 90 Ma BP), which was coincident with the youngest dated illite age of 90.5 Ma.

32) Chemical kinetic modelling suggests that significant volumes of oil were generated (~ 400 bbls/$10^4 m^3$) in, and expelled from, the Illawarra Coal Measures. Oil migrated through the sandstones of Scarborough and Lower Bulgo Operational Units during and probably following precipitation of quartz overgrowths, as indicated by the presence of fluorescing liquid inclusions within quartz overgrowths and fractures. Oil migration probably occurred at a time of 190 to 170 Ma BP. There

may have been oil columns at that time.

33) To be high quality reservoirs (porosity > 15 % and permeability > 50 md), sandstones should have the three general features: (1) a high percentage of detrital quartz clasts, (2) medium to coarse grain size (better if moderately to well sorted), and (3) quartz overgrowths and siderite as the principal cements. Quartz - rich sandstones with grain coating siderite / calcite are high quality reservoirs with porosity ranging from 15.1 to 18.3 % and permeability from 104.1 to 316.9 md. They occur in the LB unit and the upper part of the SC unit in the west margin and the western portion of the southern region.

34) The potential of the Narrabeen Group sandstones as hydrocarbon reservoirs can be summarised as: (1) In terms of stratigraphy, the BH unit has the highest potential, which is succeeded in order by the LB, UB, SC, and WO units; (2) Geographically, the west margin has the highest potential, which succeeded in order by the southern region, northern region, and east coast zone.

REFERENCE

Almon, W.R. and Davies, D.K., 1979, Regional diagenetic trends in the Lower Cretaceous muddy sandstone, Powder River Basin: in Scholle, P.A. and Schluger, P.R. (eds.), Aspects of Diagenesis: Society of Economic Paleontologists and Mineralogists Special Publication No. 26, 379-400.

Almon, W.R., Fullerton, L.B. and Davies, D.K., 1976, Pore space reduction in Cretaceous sandstones through chemical precipitation of clay minerals: Journal of Sedimentary Petrology, 46, 89-96.

Ayalon, A. and Longstaffe, F.J., 1988, Oxygen isotope studies of diagenesis and pore water evolution in the western Canada sedimentary basin: Evidence from the Upper Cretaceous Basal Belly River Sandstone, Alberta: Journal of Sedimentary Petrology, 58, 489-505.

Balme, B.E. and Helby, R.J., 1973, Floral modifications at the Permian-Triassic boundary in Australia: in Logan, A. and Hills, L.V., The Permian and Triassic System and their mutual Boundary. Memoir of Canadian Society of Petroleum Geologists, 2, 433-444.

Basu, A., 1976, Petrology of Holocene fluvial sand derived from plutonic source rocks: Implications to paleoclimatic interpretation: Journal of Sedimentary Petrology, 46, 694-709.

Bembrick, C.S., 1980, Geology of the Blue Mountains, western Sydney Basin: in Herbert, C. and Helby, R.J. (eds.), A Guide to the Sydney Basin: Geological Survey of New South Wales Bulletin 26, 134 -161.

Bembrick, C.S., Herbert, C., Scheibner, E. and Stuntz, J., 1973, Structure subdivision of the New South Wales portion of the Sydney-Bowen Basin: Quarterly Notes of Geological Survey of New South Wales, 11, 1-13.

Bembrick, C.S., Herbert, C., Scheibner, E. and Stuntz, J., 1980, Structure subdivision of the Sydney Basin: in Herbert, C. and Helby, R.J. (eds.), A Guide to the Sydney Basin: Geological Survey of New South Wales Bulletin 26, 2-9.

Bembrick, C.S. and Lonergan, A.D., 1976, Sydney Basin: in Leslie, R.B., Evans, H.J. and Knight, C.L. (eds.), ECONOMIC GEOLOGY OF AUSTRALIA AND PAPUA NEW GUINEA. 3 PETROLEUM, 426-438.

Berner, R.A., 1971, PRINCIPALS OF CHEMICAL SEDIMENTOLOGY, McGraw-Hill, New York, 240 pp.

Berner, R.A., 1980, EARLY DIAGENESIS: A theoretical Approach. Princeton University Press, 241 pp.

Bigeleisen, J., Perlman, M.L. and Prosser, H.C., 1952, Conversion of hydrogenic materials to hydrogen for isotope analysis: Analytical Chemistry, 24, 1356-1357.

Bird, M.I. and Chivas, A.R., 1988, Stable isotope evidence for low temperature kaolinitic weathering and post-formational hydrogen-isotope exchange in Permian kaolinites: Chemical Geology, 72, 249-265.

Bjørlykke, K., 1983, Diagenetic reactions in sandstones: in Parker, A. and Sellwood, B.W. (eds.), SEDIMENT DIAGENESIS, NATO ASI series, D. Reidel Publishing Company, Dordrecht, Holland, 169-213.

Bjørlykke, K., 1984, Formation of secondary porosity: How important is it? in McDonald, D.A. and Surdam, R.C. (eds.), Clastic Diagenesis: American Association of Petroleum Geologists Memoir 37, 277-286.

Bjørlykke, K., Elverhøi, A. and Malm, A. O., 1979, Diagenesis in Mesozoic sandstones from Spitsbergen and the North Sea - a comparison: Geologisches Rundschau, 68, 1152-1171.

Blatt, H., 1967, Provenance determinations and recycling of sediments: Journal of Sedimentary Petrology, 37, 1031-1044.

Blatt, H., Middleton, G. and Murray, R., 1980, ORIGIN OF SEDIMENTARY ROCKS (2nd edn.), Prentice-Hall, Inc., Englewood Cliffs, New Jersey, USA, 782 pp.

Boles, J.R., 1982, Active albitization of plagioclase, Gulf Coast Tertiary: American Journal of Science, 282, 165-180.

Boles, J.R., 1984, Secondary porosity reactions in the Stevens Sandstone, San Joaquin Valley, California: in McDonald, D.A. and Surdam, R.C. (eds.), Clastic Diagenesis: American Association of Petroleum Geologists Memoir 37, 217-224.

Boles, J.R., 1987, Six million year diagenetic history, North Coles Levee, San Joaquin Basin, California: in Marshall, J. D. (ed.), Diagenesis of Sedimentary Sequence: Geological Society Special Publication No. 36, 191-200.

Boles, J.R. and Coombs, D.S., 1977, Zeolite facies alteration of sandstones in the Southland Syncline, New Zealand: American Journal of Science, 277, 982-1012.

Boles, J.R., Landis, C.A. and Dale, P., 1985, The Moeraki boulders - anatomy of some septarian concretions, Journal of Sedimentary Petrology, 55, 398-406.

Bowman, H.N., 1970, Paleonenvironment and revised nomenclature of the upper Shoalhaven Group and Illawarra Coal Measures in the Wollongong-Kiama area, New South Wales: Records of Geological Survey of New South Wales, 12, 163-182.

Bowman, H.N., 1980, Southern coalfield, upper Shoalhaven Group and Illawarra Coal Measures: in Herbert, C. and Helby, R.J. (eds.), A Guide to the Sydney Basin: Geological Survey of New South Wales Bulletin 26, 116-132.

Branagan, D.F., 1983, The Sydney Basin and its vanished sequence: Journal of

Geological Society of Australia, 30, 75-84.

Branagan, D.F. (ed.), Herbert, C. and Langford-Smith, T., 1976, AN OUTLINE OF THE GEOLOGY AND GEOMORPHOLOGY OF THE SYDNEY BASIN, Science Press for Department of Geology and Geophysics, University of Sydney, 60 pp.

Brenchley, P.J., 1969, Origin of matrix in Ordovician greywackes, Berwyn Hills, north Wales: Journal of Sedimentary Petrology, 39, 1297-1301.

Bryan, J.H., McElroy, C.T. and Rose, G., 1967, Explanatory Notes on the Sydney 1:250,000 Geological Sheet, 3rd edn., Geological Survey of New South Wales, Sydney, 46 pp.

Bunny, M.R. and Herbert, C., 1971, The Lower Triassic Newport Formation, Narrabeen Group, southern Sydney Basin: Records of Geological Survey of New South Wales, 13, 61-81.

Burly, S.D., 1984, Patterns of diagenesis in the Sherwood Sandstone Group (Triassic), United Kingdom: Clay Minerals, 19, 403-440.

Burnham, A.K. and Sweeney, J.J., 1989, A chemical kinetic model of vitrinite maturation and reflectance: Geochimica et Cosmochimica Acta, 53, 2649-2657.

Burns, L.K. and Ethridge, F.G., 1979, Petrology and diagenetic effects of lithic sandstones: Paleocene and Eocene Umpqua Formation, southwest Oregon: in Scholle, P.A. and Schluger, P.R. (eds.), Aspects of Diagenesis: Society of Economic Paleontologists and Mineralogists Special Publication No. 26, 307-317.

Burruss, R.C., 1981, Analysis of phase equilibria in C-O-H-S fluid inclusions: in Hollister, L.S. and Grawford, M.L. (eds.), Mineralogical Association of Canada, Short Course Handbook 6, Fluid Inclusions: Application to Petrology, 39-74.

Cant, D.J. and Walker, R.G., 1976, Development of a braided fluvial facies model for the Devonian Battery Point Sandstone, Quebec: Canadian Journal of Earth Sciences, 13, 102-119.

Carne, J.E., 1903, The Kerosene Shale Deposits of New South Wales: Memoir of Geological Survey of New South Wales 3, 333 pp.

Carothers, W.W., Adami, L.H. and Rosenbauer, R.J., 1988, Experimental oxygen isotope fractionation between siderite-water and phosphoric acid liberated CO_2-siderite: Geochimica et Cosmochimica Acta, 52, 2445-2450.

Carrigy, M.A. and Mellon, G.B., 1964, Authigenic clay mineral cements in Cretaceous and Tertiary sandstones of Alberta: Journal of Sedimentary Petrology, 34, 461-472.

Castaño, J.R. and Sparks, D.M., 1974, Interpretation of vitrinite reflectance

measurements in sedimentary rocks and determination of burial history using vitrinite reflectance and authigenic minerals, in Ducher, R.R., Hacquebard, P.A., Schopf, J.M. and Simon, J. A. (eds.), Carbonaceous materials as indicators of metamorphism: Geological Society of America Special Paper, 153, 31-52.

Chiarelli, A. and Duffaud, F., 1980, Pressure origin and distribution in Jurassic of Viking Basin (United Kingdom-Norway): American Association of Petroleum Geologists Bulletin, 64, 1245-1266.

Chilingarian, G.V., 1983, Compactional diagenesis: in Parker, A. and Sellwood, B.W. (eds.), SEDIMENT DIAGENESIS, NATO ASI series, D. Reidel Publishing Company, Dordrecht, Holland, 57-167.

Choquette, P.W. and Pray, L.C., 1970, Geological nomenclature and classification of porosity in sedimentary carbonates: American Association of Petroleum Geologists Bulletin, 54, 207 -250.

Clayton, R.N. and Mayeda, T.K., 1963, The use of bromine pentafluoride in the extraction of oxygen from oxides and silicates for isotopic analysis: Geochimica et Cosmochimica Acta, 27, 43-52.

Coleman, M.L., 1985, Geochemistry of diagenetic non-silicate minerals: kinetic consideration: Philosophical Transactions of Royal Society, London, A315, 39-56.

Collins, P.L.E., 1979, Gas hydrates in CO_2-bearing fluid inclusions and the use of freezing data for estimation of salinity: Economic Geology, 74, 1435-1444.

Conaghan, P.J., 1980, The Hawkesbury Sandstone: Cross stratification characteristics and depositional environment: in Herbert, C. and Helby, R.J. (eds.), A Guide to the Sydney Basin: Geological Survey of New South Wales Bulletin 26, 188-253.

Conaghan, P.J. and Jones, J.G., 1975, The Hawkesbury Sandstone and the Brahmaputra: a depositional model for continental sheet sandstones: Journal of Geological Society of Australia, 22, 275-283.

Conaghan, P.J., Jones, J.G. McDonnell, K.L and Royce, K., 1982, A dynamic fluvial model for the Sydney Basin: Journal of Geological Society of Australia, 29, 55-70.

Conolly, J.R., 1969, Models for Triassic deposition in the Sydney Basin: in Brown, D.A. (ed.), Geological Society of Australia Special Publications No. 2, 209-223.

Conolly, J.R. and Ferm, J.C., 1971, Permo-Triassic sedimentation patterns, Sydney Basin, Australia. American Association of Petroleum Geologists Bulletin, 55, 2018-2032.

Craig, H., 1957, Isotopic standards for carbon and oxygen and correction factors

for mass-spectrometric analysis of carbon dioxide: Geochimica et Cosmochimica Acta, 12, 133-149.

Craig, H., 1961, Isotopic variations in meteoric waters: Science, 133, 1702-1703.

Craig, H., 1966, Isotopic composition and origin of the Red Sea and Salton Sea geothermal brines: Science, 154, 1544-1548.

Crook, K.A.W., 1956, The stratigraphy and petrology of the Narrabeen Group in the Grose river district: Journal and Proceedings of the Royal Society of New South Wales, 90, 61-79.

Crossey, L.J., Frost, B.R. and Surdam, R.C., 1984, Secondary porosity in laumontite-bearing sandstones: in McDonald, D.A. and Surdam, R.C. (eds.), Clastic Diagenesis: American Association of Petroleum Geologists Memoir 37, 225-237.

Crowell, J.C. and Frakes, L.A., 1971a, Late Paleozoic glaciation. part IV. Australia: Geological Society of America Bulletin, 82, 2515-2540.

Crowell, J.C. and Frakes, L.A., 1971b, Late Paleozoic glaciation of Australia: Journal of Geological Society of Australia, 17, 115-155

Crowell, J.C. and Frakes, L.A., 1975, The late Paleozoic glaciation: in Campbell, K.S.W. (ed.), GONDWANA GEOLOGY, Australian National University Press, Canberra, Australia, 313-331.

Curtis, C.D., 1967, Diagenetic iron minerals in British Carboniferous sediments. Geochimica et Cosmochimica Acta, 31, 2109-2123.

Curtis, C.D., 1978, Possible links between sandstone diagenesis and depth related geochemical reactions occurring in enclosing mudstones: Journal of Geological Society, London, 135, 107-117.

Curtis, C.D, 1983a, Geochemistry of porosity enhancement and reduction in clastic sediments: in Brooks, J. (ed.), Petroleum Geochemistry and Exploration of Europe, Geological Special Publication No. 12, 113 -125.

Curtis, C.D., 1983b, Link between aluminium mobility and destruction of secondary porosity: American Association of Petroleum Geologists Bulletin, 67, 380-393.

Curtis, C.D., Coleman, M.L. and Love, L.G., 1986, Pore water evolution during sediment burial from isotopic and mineral chemistry of calcite, dolomite and siderite concretions: Geochimica et Cosmochimica Acta, 50, 2321-2334.

Curtis, C.D. and Spears, D.A., 1968, Formation of sedimentary iron minerals: Economic Geology, 63, 257-270.

Dansgaard, W., 1964, Stable isotopes in precipitation: Tellus, 16, 436-468.

Davies, D.K., Almon, W.R., Bonis, S.B. and Hunter, B.E., 1979, Deposition and

diagenesis of Tertiary-Holocene volcaniclastics, Guatemala: in Scholle, P.A. and Schluger, P.R. (eds.), Aspects of Diagenesis: Society of Economic Paleontologists and Mineralogists Special Publication No. 26, 281-306.

Deer, W.A., Howie, R.A. and Zussman, J., 1966, AN INTRODUCTION TO THE ROCK FORMING MINERALS, Richard Clay (The Chaucer Press) Ltd., Bungay, Suffolk, Great Britain, 528 pp.

Deffeyes, K.S., 1959, Zeolites in sedimentary rocks: Journal of Sedimentary Petrology, 29, 602-609.

Deines, P., 1970, Mass spectrometer correction factors for the determination of small isotopic variations of carbon and oxygen: International Journal of Mass Spectrometry and Ion Physics, 4, 283-295.

Dickins, J.M., 1968, Correlation of the Permian of the Hunter Valley, New South Wales and the Bowen Basin, Queensland: Bureau of Mineral Resources, Geology and Geophysics, Australia, Bulletin, 80, 27-44.

Dickinson, W.R., 1970, Interpreting detrital modes of graywacke and arkose: Journal of Sedimentary Petrology, 40, 695-707.

Dickinson, W.R., 1985, Interpreting provenance relations from detrital modes of sandstones: in Zuffa, G.G. (ed.) , PROVENANCE OF ARENITES, NATO ASI series, D. Reidel Publishing Company, Dordrecht, Holland, 333-361.

Dickinson, W.R., Ingersoll, R.V., Cowan, D.S., Helmold, K.P. and Suczek, C.A., 1982, Provenance of Franciscan graywackes in coastal California: Geological Society of America Bulletin, 93, 95-107.

Diessel, C.F.K., 1975, Coalification trends in the Sydney Basin, New South Wales: in Campbell, K.S.W. (ed.), GONDWANA GEOLOGY, Australian National University Press, Canberra, Australia, 295-309.

Diessel, C.F.K., 1980, Newcastle and Tomago Coal Measures: in Herbert, C. and Helby, R.J. (eds.), A Guide to the Sydney Basin: Geological Survey of New South Wales Bulletin 26, 100-114.

Diessel, C.F.K., Driver, R.C. and Moelle, K,H.R., 1967, Some geological investigations into a fossil river system in the roof strata of the Bulli Seam, Southern Coalfield, N.S.W., Proceedings of Australasian Institute of Mining and Metallurgy, 221, 19-37.

Dutta, P.K. and Sutner, L.J., 1986, Alluvial sandstone composition and paleoclimate, II. Authigenic mineralogy: Journal of Sedimentary Petrology, 56, 346-358.

Dutton, S.P. and Land, L.S., 1985, Meteoric burial diagenesis of Pennsylvanian arkosic sandstones, Southwestern Anadarko Basin, Texas: American Association of Petroleum Geologists Bulletin, 69, 22-38.

Dykstra, J., 1987, Compaction correction for burial history curves: application to Lopatin's Method for source rock maturation determination: Geobyte, 2, 16-24.

Eadington, P.J., Hamilton, P.J. and Green, P., 1989, Hydrocarbon fluid history in relation to diagenesis in the Hutton Sandstone, south-west Queensland: in O'Neil, B.J. (ed.), The Cooper and Eromanga Basins, Australia, Proceedings of The Cooper and Eromanga Basins Conference, Adelaide, 601-618.

Embleton, B.J.J., 1983, Continental palaeomagnetism: in Veevers, J.J. (ed.) PHANEROZOIC EARTH HISTORY OF AUSTRALIA, Clarendon Press, Oxford, U.K., 11-16.

Erickson, A.J., Von Herzen, R.P., Sclater, J.G., Girdler, R.W., Marshall, B.V. and Hyndman, R., 1975, Geothermal measurements in deep-sea drill holes: Journal of Geophysical Research, 80, 251-2528.

Ernst, W.G. and Blatt, H., 1964, Experimental study of quartz overgrowths and synthetic quartzites: Journal of Geology, 72, 461-469.

Facer, R.A., Cook, A.C. and Beck, A.E., 1980, Thermal properties and coal rank in rocks and coal seams of the southern Sydney Basin, New South Wales: a paleogeothermal explanation of coalification: International Journal of Coal Geology, 1, 1-17.

Fairbridge, R.W., 1967, Phases of diagenesis and authigenesis: in Larsen, G. and Chilingar, G.V. (eds.), Diagenesis in Sediments: Development in Sedimentology 8, 19-89.

Fairbridge, R.W., 1983, Syndiagenesis-anadiagenesis-epidiagenesis: phases in lithogenesis: in Larsen, G. and Chilingar, G.V. (eds.), Diagenesis in Sediments and Sedimentary Rock: Development in Sedimentology 25B, 17-113.

Falvey, D.A., 1974, The development of continental margins in plate tectonic theory: Journal of Australian Petroleum Exploration Association, 14, 95-106.

Falvey, D.A., 1982, Heat flow, temperature and maturation: in Van Hinte, J.E. and Falvey, D.A., SEDIMENTARY BASIN BURIAL AND THERMAL GEOHISTORY ANALYSES, a workshop manual to accompany course notes for an Earth Resources Foundation short course, The University of Sydney, Sydney, 1-24.

Falvey, D.A. and Middleton, M.F., 1981, Passive continental margins: evidence for a prebreakup deep crustal metamorphic subsidence mechanism: Oceanologica Acta, Geology of Continental Margins, Proceedings 26th International Geological Congress, symposium, Paris, 103-114.

Fisher, W.L. and McGowen, J.H., 1967, Depositional systems in the Wilcox Group (Eocene) of Texas and their relation to the occurrence of oil and gas: American Association of Petroleum Geologists Bulletin, 53, 30-54.

Folk, R.L., 1968, PETROLOGY OF SEDIMENTARY ROCK, University of Texas, Austin, U.S.A., 170 pp.

Folk, R.L., 1974, The natural history of crystalline calcium carbonate: effect of magnesium content and salinity: Journal of Sedimentary Petrology, 44, 40-53.

Folk, R.L. and Weaver, C.E., 1952, A study of the texture and composition of chert: American Journal of Science, 250, 498-510.

Frazier, D.E., 1974, Depositional episodes: their relationship to the Quaternary stratigraphic framework in the northwestern portion of the Gulf Basin: Geological Circular of Bureau of Economic Geology, University of Texas, Austin, Texas, 71-1, 28 pp.

Friedman, G.M., 1965, Terminology of crystallization textures and fabrics in sedimentary rocks: Journal of Sedimentary Petrology, 35, 643-655.

Friedman, I. and O'Neil, J.R., 1977, Compilation of stable isotope fractionation factors of geochemical interest, chapter KK: in Fleischer, M. (ed.), DATA OF GEOCHEMISTRY (6th edn.), U.S. Geological Survey Professional Paper, 440-KK, KK1-KK12.

Froelich, P.N., Klinkhammer, G.P., Bender, M.L., Luedtke, N.A., Heath, G.R., Cullen, D., Dauhphin, P., Hammond, D., Hartman, B. and Maynard, V., 1979, Early oxidation of organic matter in pelagic sediments of the eastern equatorial Atlantic: suboxic diagenesis: Geochimica et Cosmochimica Acta, 43, 1075-1090.

Fuchtbauer, H., 1983, Facies controls on sandstone diagenesis: in Parker, A. and Sellwood, B.W. (ed.): SEDIMENT DIAGENESIS, NATO ASI series, D. Reidel Publishing Company, Dordrecht, Holland, 269-288.

Galloway, M.C., 1967, The stratigraphy of the Putty-Upper Colo Area, Sydney Basin, N. S. W.: Journal and Proceedings of the Royal Society of New South Wales, 101, 23-36.

Galloway, W.E., 1974, Deposition and diagenetic alternation of sandstones in northeast Pacific arc-related basins: Implication for graywacke genesis: Geological Society of America Bulletin, 85, 379-390.

Galloway, W.E., 1979, Diagenetic control of reservoir quality in arc-derived sandstones: implications for petroleum exploration: in Scholle, P.A. and Schluger, P.R. (eds.), Aspects of Diagenesis: Society of Economic Paleontologists and Mineralogists Special Publication No. 26, 251-262.

Galloway, W.E. and Hamilton, D.S., 1988, Sydney Basin Reservoir Study: Report to AGL Sydney Ltd. (Sydney) (unpublished), 822 pp.

Garrels, R.M. and Christ, G.L., 1965, SOLUTION, MINERALS AND EQUILIBRIA, Harper and Row, New York, USA, 450 pp.

Gautier, D.L. (ed.), 1986, Roles of Organic Matter in Sediment Diagenesis: Society of Economic Paleontologists and Mineralogists Special Publication No. 38,

Tulsa, Oklahoma, U.S.A., 203 pp.

Girard, J.P., Savin, S.M., Aronson, J.L., 1989, Diagenesis of the lower Cretaceous arkoses of the Angola margin: petrologic, K/Ar dating and $^{18}O/^{16}O$ evidence: Journal of Sedimentary Petrology, 59, 519-538.

Goldbery, R., 1966, The geology of the upper Blue Mountains area: B.Sc (Hons.) Thesis, University of New South Wales (unpublished), 111 pp.

Goldbery, R., 1970, Stratigraphy and sedimentation of the Triassic units in the north-western Sydney Basin: M.Sc Thesis, University of New South Wales (unpublished), Volume 1 (text) - 116 pp; Volume 2 (measured sections) - 269 pp.

Goldbery, R. and Holland, W.N., 1973, Stratigraphy and sedimentation of redbed facies in Narrabeen Group of Sydney Basin, Australia: American Association of Petroleum Geologists Bulletin, 57, 1314-1334.

Gostin, V.A. and Herbert, C., 1973, Stratigraphy of the Upper Carboniferous and Lower Permian sequence, southern Sydney Basin: Journal of Geological Society of Australia, 20, 49-70.

Hamilton, D.S., 1991, Genetic stratigraphy of the Gunnedah Basin, NSW: Australian Journal of Earth Sciences, 38, 95-113.

Hamilton, D.S. and Galloway, W.E., 1989, New exploration techniques in the analysis of diagenetically complex reservoir sandstones, Sydney Basin, NSW: Journal of Australian Petroleum Exploration Association, 29, 235-257.

Hamilton, D.S., Galloway, W.E. and Reynolds, S.A., 1987, Depositional system of the Narrabeen Group: Proceedings of 21st Symposium on Advances in the study of the Sydney Basin, Department of Geology, University of Newcastle, N.S.W., 115-122.

Hamilton, P.J., Fallick, A.E., Macintyre, R.M. and Elliott, S., 1987, Isotopic tracing of the provenance and diagenesis of Lower Brent Group Sands, North Sea: in Brooks, J. and Glennie, K. (eds.), PETROLEUM GEOLOGY OF NORTH WEST EUROPE, Graham and Trotman, London, 939-949.

Hamilton, P.J., Kelley, S. and Fallick, A.E., 1989, K-Ar dating of illite in hydrocarbon reservoirs: Clay Minerals, 24, 215-231.

Hanlon, F.N., Osborne, G.D. and Raggatt, H.G., 1953, Narrabeen Group: its subdivisions and correlations between the South coast and Narrabeen-Wyong districts: Journal and Proceedings of the Royal Society of New South Wales, 87, 106-120.

Hanor, J.S., 1980, Dissolved methane in sedimentary brines: potential effect on the PVT properties of fluid inclusions: Economic Geology, 75, 603-609.

Hawkins, J.B., 1978, Relationship between diagenesis, porosity reduction, and oil

emplacement in late Carboniferous sandstone reservoirs, Bothamasall Oilfield, E Midlands: Journal of Geological Society, London, 135, 7-24.

Hay, R.L., 1966, Zeolites and zeolitic reactions in sedimentary rocks: Geological Society of America Special Paper 85, 130 pp.

Hayes, J.B., 1979, Sandstone diagenesis - the hole truth: in Scholle, P.A. and Schluger, P.R. (eds.), Aspects of Diagenesis; Society of Economic Paleontologists and Mineralogists Special Publication No. 26, 127-139.

Heald, M.T. and Larese, R.E., 1973, The significance of the solution of feldspar in porosity development: Journal of Sedimentary Petrology, 43, 458-460.

Helby, R.J., 1961, Contributions to the geology of the Lower Burragorang district: M.Sc (qual.) Thesis, University of Sydney (unpublished), 104 pp.

Helby, R.J. and Herbert, C., 1971, Relationship of the Clyde Coal Measures to the Pigeon House Creek Siltstone, southern Sydney Basin: Quarterly Notes of Geological Survey of New South Wales, 5, 1-6.

Helmold, K.P. and van de Kamp, P.C., 1984, Diagenetic mineralogy and controls on albitization and laumontite Formation in Paleogene Arkoses, Santa Ynez Mountains, California: in McDonald, D.A. and Surdam, R.C. (eds.), Clastic Diagenesis: American Association of Petroleum Geologists Memoir 37, 239-276.

Herbert, C., 1970, A synthesis of Narrabeen Group nomenclature, Sydney Basin: Quarterly Notes of Geological Survey of New South Wales, 1, 3-10.

Herbert, C., 1972, Paleodrainage patterns in the southern Sydney Basin: Records of Geological Survey of New South Wales, 14, 5-18.

Herbert, C., 1980a, Depositional development of the Sydney Basin: in Herbert, C. and Helby, R.J. (eds.), A Guide to the Sydney Basin: Geological Survey of New South Wales Bulletin 26, 10-52.

Herbert, C., 1980b, Southwestern Sydney Basin: in Herbert, C. and Helby, R.J. (eds.), A Guide to the Sydney Basin: Geological Survey of New South Wales Bulletin 26, 82-99.

Herbert, C., 1980c, Wianamatta Group and Mittagong Formation: in Herbert, C. and Helby, R.J. (eds.), A Guide to the Sydney Basin: Geological Survey of New South Wales Bulletin 26, 254-272.

Herbert, C. and Helby, R.J. (eds.), 1980, A Guide to the Sydney Basin, Geological Survey of New South Wales Bulletin 26, 603 pp.

Hinch, H.H., 1980, The nature of shales and the dynamics of hydrocarbon expulsion in the Gulf Coast Tertiary section: in Roberts, W.H., III and Cordell, R.J. (eds.), PROBLEMS OF PETROLEUM MIGRATION, Studies in Geology No. 10, The American Association of Petroleum Geologists, Tulsa, Oklahoma,

1-18.

Hitchon, B. and Friedman, I., 1969, Geochemistry and origin of formation waters in the western Canada sedimentary basin - I. Stable isotopes of hydrogen and oxygen: Geochimica et Cosmochimica Acta, 33, 1321-1349.

Hower, J., Eslinger, E.V., Hower, M.E. and Perry, E.A., 1976, Mechanism of burial metamorphism of argillaceous sediment: 1. mineralogical and chemical evidence: Geological Society of America Bulletin, 87, 725-737.

Hunt, J.W., 1989, Permian coals of eastern Australia: geological control of petrographic variation: International Journal of Coal Geology, 12, 589-634.

Imam, M.B. and Shaw, H.F., 1985, The diagenesis of Neogene clastic sediments from the Bengal Basin, Bangladesh: Journal of Sedimentary Petrology, 55, 665-671.

Ingersoll, R.V., 1978, Petrofacies and petrologic evolution of the Late Cretaceous fore-arc basin, northern and central California: Journal of Geology, 86, 335-352.

Ingersoll, R.V., Bullard, T.F, Ford, R.L., Grimm, J.P., Pickle, J.D. and Sares, S.W., 1984, The effect of grain size on detrital modes: A test of the Gazzi-Dickinson point-counting method: Journal of Sedimentary Petrology, 54, 103-116.

Irwin, H., 1980, Early diagenetic carbonate precipitation and pore fluid migration in the Kimmeridge Clay of Dorset, England: Sedimentology, 27, 577-591.

Irwin, H., Curtis, C.D. and Coleman, M.L., 1977, Isotopic evidence for source of diagenetic carbonates formed during burial of organic-rich sediments: Nature, 269, 209-213.

Jackson, M.L., 1979, SOIL CHEMICAL ANALYSIS-ADVANCED COURSE (2nd edn.), Madison, Wisconsin, 895 pp.

James, H.L., 1966, Chemistry of the iron-rich sedimentary rocks, chapter W: in Fleischer, M. (ed.), DATA OF GEOCHEMISTRY (6th edn.), U.S. Geological Survey Professional Paper 440-W, W1-W61.

Jett, G.A. and Heller, P.L., 1988, Tectonic significance of polymodal compositions in Melange sandstones, Western Melange Belt, North Cascade Range, Washington: Journal of Sedimentary Petrology, 58 , 52-61.

Jones , J.G., Conaghan, P.J., McDonnell, K.L., Flood, R.H and Shaw, S.E., 1984, Papuan Basin analogue and a foreland basin model for the Bowen-Sydney Basin: in Veevers, J.J. (ed.) PHANEROZOIC EARTH HISTORY OF AUSTRALIA, Clarendon Press, Oxford, U.K., 243-262.

Kaiser, W.R., 1984, Predicting reservoir quality and diagenetic history in the Frio Formation (Oligocene) of Texas: in McDonald, D.A. and Surdam, R.C. (eds.), Clastic Diagenesis: American Association of Petroleum Geologists Memoir 37,

195-215.

Kantorowicz, J.D., 1985, The petrology and diagenesis of Middle Jurassic clastic sediments, Ravenscar Group, Yorkshire: Sedimentology, 32, 833-853.

Klein, G. deV., 1963, Analysis and review of sandstone classifications in the North American Geological Literature, 1940-60: Geological Society of America Bulletin, 74, 555-576.

Lambert, S.J. and Epstein, S., 1980, Stable isotope investigations of an active geothermal system in Valles Caldera, Jemez Mountains, New Mexico, Journal of Volcanology and Geothermal Research, 8, 111-129.

Land, L.S., 1980, The isotopic and trace element geochemistry of dolomite: the state of the art: in Zenger, D.H., Dunham, J.B. and Ethington, R.L. (eds.), Concepts and Models of Dolomitization: Society of Economic Paleontologists and Mineralogists Special Publication No. 28, 87-110.

Land, L.S. and Dutton, S.P., 1978, Cementation of a Pennsylvanian deltaic sandstone: isotopic data: Journal of Sedimentary Petrology, 48, 1167-1176.

Larsen, G. and Chilingar, G.V. (eds.), 1967, Diagenesis in Sediments: Development in Sedimentology 8, Elsevier, Amsterdam, 551 pp.

Larsen, G. and Chilingar, G.V. (eds.), 1979a, Diagenesis in Sediments and Sedimentary Rocks: Development in Sedimentology, 25A, Elsevier, Amsterdam, 579 pp.

Larsen, G. and Chilingar, G.V. (eds.), 1979b, Introduction – diagenesis of sediments and sedimentary rocks: in Larsen, G. and Chilingar, G.V. (eds.), Diagenesis in Sediments and Sedimentary Rocks: Development in Sedimentology, 25A, 1-29.

Larsen, G. and Chilingar, G.V. (eds.), 1983, Diagenesis in Sediments and Sedimentary Rocks: Development in Sedimentology, 25B, Elsevier, Amsterdam, 572 pp.

Lee, M. and Savin, S.M., 1985, Isolation of diagenetic overgrowths on quartz sand grains for oxygen isotope analysis: Geochimica et Cosmochimica Acta, 49, 497-501.

Lee, M, Aronson, J.L. and Savin, S.M, 1985, K/Ar dating of time of gas emplacement in Rotliegendes sandstone, Netherlands: American Association of Petroleum Geologists Bulletin, 69, 1381-1385.

Lee, M, Aronson, J.L. and Savin, S.M, 1989, Timing and conditions of Permian Rotliegende sandstone diagenesis, southern North Sea: K/Ar and oxygen isotopic data: American Association of Petroleum Geologists Bulletin, 73, 195-215.

Leitch, E.C., 1974, The geological development of the southern part of the New

England Fold Belt: Journal of Geological Society of Australia, 21, 133-156.

Liewig, N., Clauser, N. and Sommer, F., 1987, Rb-Sr and K-Ar dating of clay diagenesis in a Jurassic sandstone oil reservoir, North Sea: American Association of Petroleum Geologists Bulletin, 71, 1467-1474.

Lindquist, S.J., 1977, Secondary porosity development and subsequent reduction, over-pressured Frio Formation sandstone (Oligocene), South Texas: Transactions of Gulf Coast Association of Geological Societies, 27, 99-107.

Lippman, F., 1973, SEDIMENTARY CARBONATE MINERALS, Springer-Verlag, Berlin, 228 pp.

Longstaffe, F.J., 1983, Diagenesis 4. Stable isotope studies of diagenesis in clastic rocks: Geoscience Canada, 10, 43-58.

Longstaffe, F.J., 1986, Oxygen isotope studies of diagenesis in the basal Belly River sandstone, Pembina I-pool, Alberta: Journal of Sedimentary Petrology, 56, 78-88.

Longstaffe, F.J. and Ayalon, A, 1987, Oxygen-isotope studies of clastic diagenesis in the Lower Cretaceous Viking Formation, Alberta: Implications for the role of meteoric water: in Marshall, J.D. (ed.), Diagenesis of Sedimentary Sequence: Geological Society Special Publication No. 36, 277-296.

Loucks, R.G., 1977, Porosity development and distribution in shoal-water carbonate complexes; subsurface Pearsall Formation (Lower Cretaceous), South Texas: Bureau of Economic Geology at the University of Texas, Austin, Report of Investigation, 89, 97-126.

Loucks, R.G., Dodge, M.M. and Galloway, W.E., 1984, Regional controls on diagenesis and reservoir quality in Lower Tertiary sandstones along the Texas Gulf Coast: in McDonald, D.A. and Surdam, R.C. (eds.), Clastic Diagenesis: American Association of Petroleum Geologists Memoir 37, 15-45.

Loughnan, F.C., 1962, Some tonstein-like rocks from New South Wales: Neues Juhrbuch Für Mineralogie, Abhandlungen, 99, 29-44.

Loughnan, F.C., 1963, A petrological study of a vertical section of the Narrabeen Group at Helensburgh, N.S.W., Journal of Geological Society of Australia,10, 177-192.

Loughnan, F.C., 1970, Flint clay in the coal-barren Triassic of the Sydney Basin, Australia: Journal of Sedimentary Petrology, 40, 822-828.

Loughnan, F.C., Ko Ko, M and Bayliss, P., 1964, The red beds of the Triassic Narrabeen Group: Journal of Geological Society of Australia, 11, 65-77.

Lovering, J.F., 1954, The stratigraphy of Wianamatta Group, Triassic System, Sydney Basin: Records of Australian Museum, 23, 169-210.

Lovering, J.F. and McElroy, C.T., 1969, Wianamatta Group: in Packham, G.H. (ed.), 1969, The Geology of New South Wales: Journal of Geological Society of Australia, 16, 417-423.

McBride, E.F., 1977, Secondary porosity - importance in sandstone reservoirs in Texas: Transactions of Gulf Coast Association of Geological Societies, 27, 121-122.

McBride, E.F., 1985, Diagenetic processes that affect provenance determinations in sandstone: in Zuffa, G.G. (ed.) , PROVENANCE OF ARENITES, NATO ASI series, D. Reidel Publishing Company, Dordrecht, Holland, 95-113.

McClung, G., 1980, Permian marine sedimentation in the northern Sydney Basin: in Herbert, C. and Helby, R.J. (eds.), A Guide to the Sydney Basin: Geological Survey of New South Wales Bulletin 26, 54-72.

McDonald, D.A. and Surdam, R.C. (eds.), 1984, Clastic Diagenesis, American Association of Petroleum Geologists Memoir 37, Tulsa, Oklahoma, U.S.A., 434 pp.

McDonnell, K.L., 1974, Depositional environment of Triassic Gosford Formation, Sydney Basin: Journal of Geological Society of Australia, 21, 107-132.

McDonnell, K.L., 1980, Notes on the depositional environment of the Terrigal Formation: in Herbert, C. and Helby, R.J. (eds.), A Guide to the Sydney Basin: Geological Survey of New South Wales Bulletin 26, 170-176.

McElroy, C.T., 1954, Petrology of sandstones of the southern coalfield: M.Sc Thesis, University of Sydney (unpublished), 88 pp.

McElroy, C.T. and Rose, G., 1962, Reconnaissance Geological Survey: Ulladulla 1-mile Military Sheet and Southern Part of Tianjara 1-mile Military Sheet: Geological Survey of New South Wales Bulletin, 17, 67 pp.

McKellar, M.G., 1969, Maitland Group: in Packham, G.H. (ed.), 1969, The Geology of New South Wales: Journal of Geological Society of Australia, 16, 329-334.

McKelvey, B.C., McClung, G.R. and Runnegar, B., 1971, Nowra-Muree sands - definition, internal morphology and age: Abstracts of 6th Symposium on Advances in the study of the Sydney Basin, Department of Geology, University of Newcastle, N.S.W., p.22.

McLimans, R.K., 1987, The application of fluid inclusions to migration of oil and diagenesis in petroleum reservoirs: Applied Geochemistry, 2, 585-603.

Mack, G.H. and Suttner, L.J., 1977, paleoclimate interpretation from a petrographic comparison of Holocene sands and the Fountain Formation (Pennsylvanian) in the Colorado Front Range: Journal of Sedimentary Petrology, 47, 89-100.

Marshall, J.D. (ed.), 1987, Diagenesis of Sedimentary Sequence: Geological Society Special Publication No. 36, Blackwell Scientific Publications, Oxford,

U.K., 360 pp.

Martin, K.R. and Baker, J.C., 1987, Petrography of Narrabeen Group sandstones: Report to AGL Sydney Ltd. (Sydney) (unpublished), 33 pp.

Mathisen, M.E., 1984, Diagenesis of Plio-Pleistocene nonmarine sandstones, Cagayan Basin, Philippines: Early development of secondary porosity in volcanic sandstones: in McDonald, D.A. and Surdam, R.C. (eds.), Clastic Diagenesis: American Association of Petroleum Geologists Memoir 37, 177-193.

Matsumoto, R. and Iijima, A., 1981, Origin and diagenetic evolution of Ca-Mg-Fe carbonates in some coalfield of Japan: Sedimentology, 28, 239-259.

Mayne, S.L., Nicholas, E., Bigg-Wither, A.L., Rasidi, J.S. and Raine, M.J., 1974, Geology of the Sydney Basin -- A Review: Bureau of Mineral Resources, Geology and Geophysics, Australia, Bulletin 149, 229 pp.

Menzies, I.A., 1974, Sydney - Bowen Basin: in Markham, N.L. and Basden, H. (eds.), THE MINERAL DEPOSITS OF NEW SOUTH WALES, Geological Survey, N.S.W., 453-503.

Merino, E., 1975, Diagenesis in Tertiary sandstones from Kettleman North Dome, California. I. diagenetic mineralogy: Journal of Sedimentary of Petrology, 45, 320-336.

Meyers, W.J., 1974, Carbonate cement stratigraphy of the Lake Valley Formation (Mississippian), Sacramento Mountains, New Mexico: Journal of Sedimentary Petrology, 44, 837-861.

Middleton, G.V., 1973, Johannes Walther's law of correlation of facies: Geological Society of America Bulletin, 84, 979-988.

Middleton, M.F., 1983, Coal rank trends in eastern Australia Permian coal basins, CSIRO, Institute of Energy and Earth Resources, Division of Fossil Fuels, Investigation Report 141, 28 pp.

Middleton, M.F. and Hunt, J.W., 1989, Influence of tectonic on Permian coal-rank patterns in Australia: International Journal of Coal Geology, 13, 391-411.

Middleton, M.F. and Schmidt, P.W., 1982, Paleothermometry of the Sydney Basin: Journal of Geophysical Research, 87, 5351-5359.

Midgley, H.G., 1951, Chalcedony and flint: Geological Magazine, 88, 179-184.

Moncure, G.K., Lahann, R.W. and Siebert, R.M., 1984, Origin of secondary porosity and cement distribution in a sandstone / shale sequence from the Frio Formation (Oligocene): in McDonald, D.A. and Surdam, R.C. (eds.), Clastic Diagenesis: American Association of Petroleum Geologists Memoir 37, 151-161.

Moore, G.F., 1979, Petrography of subductive zone sandstones from Nias Island, Indonesia: Journal of Sedimentary Petrology, 49, 71-84.

Moore, M.E., Gleadow, A.J.W. and Lovering, J.F., 1986, Thermal evolution of rifted continental margins: new evidence from fission tracks in basement apatites from southeastern Australia: Earth and Planetary Science Letters, 78, 255-270.

Morgan, J.T. and Gordon, D.T., 1970, Influence of pore geometry on water-oil relative permeability: Journal of Petroleum Technology, 22, 1199-1208.

Morris, R.C., Proctor, K.E. and Koch, M.R., 1979, Petrology and diagenesis of deep-water sandstones, Ouachita Mountains, Arkansas and Oklahoma, in Scholle, P.A. and Schluger, P.R. (eds.), Aspects of Diagenesis: Society of Economic Paleontologists and Mineralogists Special Publication No. 26, 263-279.

Mount J.F. and Cohen, A.S., 1984, Petrology and geochemistry of rhizoliths from Plio-Pleistocene fluvial and marginal lacustrine deposits, east Lake Turkana, Kenya: Journal of Sedimentary Petrology, 54, 263-275.

North, F.K., 1985, PETROLEUM GEOLOGY, Allen & Unwin, Boston, U.S.A., 607 pp.

Okada, H., 1971, Classification of sandstone: analysis and proposal: Journal of Geology, 79, 509-525.

O'Neil, J.R., 1979, Stable isotope geochemistry of rocks and minerals: in Jager, E. and Hunziker, J.C. (eds.), LECTURES IN ISOTOPE GEOLOGY, Springer-Verlag, Berlin, 235-263.

Osborne, G.D., 1949, The stratigraphy of the lower marine series of the Permian System in the Hunter River Valley, New South Wales: Proceedings of Linnean Society of N.S.W., 74, 203-223.

Packham, G.H. (ed.), 1969, The Geology of New South Wales: Journal of Geological Society of Australia, 16, 654 pp.

Parker, A. and Sellwood, B.W. (eds.), 1983, SEDIMENT DIAGENESIS, NATO ASI series, D. Reidel Publishing Company, Dordrecht, Holland, 427 pp.

Pettijohn, F.J., Potter, P.E. and Siever, R., 1987, SAND AND SANDSTONE, Springer-Verlag, Berlin, 553 pp.

Phipps, C.B, 1969, Post-burial siderisation of calcite in Eocene beds from the Maracaibo Basin, Venezuela: Geological Magazine, 106, 485-495.

Picard, G.L. and Felbeck, G.T., Jr., 1976, The complexation of iron by marine humic acid: Geochimica et Cosmochimica Acta, 40, 1347-1350.

Pittman, E.D., 1972, Diagenesis of quartz in sandstones as revealed by scanning electron microscopy: Journal of Sedimentary Petrology, 42, 507-519.

Potter, R.W., Clynne, M.A. and Brown, D.L., 1977, Freezing point depression of aqueous sodium chloride solutions: Economic Geology, 73, 284-285.

Quinlan, G.M. and Beaumont, C, 1984, Appalachian thrusting, lithospheric flexure, and the Paleozoic stratigraphy of the Eastern Interior of North America: Canadian Journal of Earth Sciences 21, 973-996.

Raggatt, H.G., 1938, Evolution of the Permo-Triassic Basin of east-central New South Wales: D. Sc Thesis, University of Sydney (unpublished), 149 pp.

Rattigan, J. H. and McKenzie, P.J., 1969, A. Hunter Valley: in Packham, G.H. (ed.), 1969, The Geology of New South Wales: Journal of Geological Society of Australia, 16, 426-434.

Reading, H.G., 1986, 2 Facies: in Reading, H.G. (ed.), SEDIMENTARY ENVIRONMENTS AND FACIES (2nd edn.), Blackwell Scientific Publications, Oxford, 4-19.

Reineck, H.-E. and Singh, I.B., 1980, DEPOSITIONAL SEDIMENTARY ENVIRONMENTS (2nd edn.), Springer-Verlag, Berlin, 551 pp.

Retallack, G., 1980, Late Carboniferous to Middle Triassic megafossil floras from the the Sydney Basin: in Herbert, C. and Helby, R.J. (eds.), A Guide to the Sydney Basin: Geological Survey of New South Wales Bulletin 26, 384-430.

Roedder, E., 1984, FLUID INCLUSIONS: Review in Mineralogy 12, Mineralogical Society of America, 644 pp.

Roedder, E. and Bodnar, R.J., 1980, Geological pressure determinations from fluid inclusion studies: Annual Review of Earth and Planetary Sciences 8, 263-301.

Rosenbaum, J. and Sheppard, S.M.F., 1986, An isotopic study of siderites, dolomites and ankerites at high temperatures: Geochimica et Cosmochimica Acta, 50, 1147-1150.

Runnegar, B.,1980, Marine Shoalhaven Group, southern Sydney Basin: in Herbert, C. and Helby, R.J. (eds.), A Guide to the Sydney Basin: Geological Survey of New South Wales Bulletin 26, 74-81.

Sass, J.H., Jaeger, J.C and Monroe, R.J., 1976, Heat flow and near surface radioactivity in the Australian continental crust: U.S. Department Interior, Geological Survey Open File Report, 76-250.

Saxby, J.D., Bennett, A.J.R., Corcoran, J.F., Lambert, D.E. and Riley, K.W., 1986, Petroleum generation: simulation over six years of hydrocarbon formation from torbanite and brown coal in a subsiding basin: Organic Geochemistry,9, 69-81.

Scheibner, E., 1976, Explanatory Notes on the Tectonic Map of New South Wales, scale 1:1,000,000, Geological Survey of N.S.W., 283 pp.

Schmidt, P.W. and Embleton, B.J.J., 1981, Magnetic overprinting in southeastern Australia and the thermal history of its rifted margin: Journal of Geophysical Research, 86, 3998-4008.

Schmidt, V. and McDonald, D.A., 1979a, The role of secondary porosity in the course of sandstone diagenesis: in Scholle, P.A. and Schluger, P.R. (eds.), Aspects of Diagenesis: Society of Economic Paleontologists and Mineralogists Special Publication No. 26, 175-207.

Schmidt, V. and McDonald, D.A., 1979b, Texture and recognition of secondary porosity in sandstones: in Scholle, P.A. and Schluger, P.R. (eds.), Aspects of Diagenesis: Society of Economic Paleontologists and Mineralogists Special Publication No. 26, 209-225.

Scholle, P.A. and Schluger, P.R. (eds.), 1979, Aspects of Diagenesis, Society of Economic Paleontologists and Mineralogists Special Publication No. 26, Tulsa, Oklahoma, U.S.A., 444 pp.

Sharma, T. and Clayton, R.N., 1965, Measurements of $^{18}O/^{16}O$ rations of total oxygen of carbonates: Geochimica et Cosmochimica Acta, 29, 1347-1353.

Shaw, R.D., Seafloor spreading in the Tasman Sea; a Lord Howe rise - eastern Australian reconstruction: Australian Society of Exploration Geophysicists, Bulletin, 9, 75-81.

Smosna, R., 1988, Low-temperature, low-pressure diagenesis of Cretaceous sandstones, Alaskan North Slope: Journal of Sedimentary Petrology, 58, 644-655.

Stonecipher, S.A., Winn, R.D., Jr. and Bishop, M.G., 1984, Diagenesis of the Frontier Formation, Moxa Arch: A function of sandstone geometry, texture and composition, and fluid flux: in McDonald, D.A. and Surdam, R.C. (eds.), Clastic Diagenesis: American Association of Petroleum Geologists Memoir, 37, 289-316.

Stuntz, J.,1969, The depositional and structural boundaries of the Sydney Basin: Abstracts of 4th Symposium on Advances in the study of the Sydney Basin, Department of Geology, University of Newcastle, N.S.W., 51-53.

Surdam, R.C. and Boles, J.R., 1979, Diagenesis of volcanic Sandstones: in Scholle, P.A. and Schluger, P.R. (eds.), Aspects of Diagenesis: Society of Economic Paleontologists and Mineralogists Special Publication No. 26, 227-242.

Surdam, R.C., Boese, S.W. and Crossey, L.J., 1984, The chemistry of secondary porosity: in McDonald, D.A. and Surdam, R.C. (eds.), Clastic Diagenesis: American Association of Petroleum Geologists Memoir 37, 127-149.

Suttner, L, J., 1974, Sedimentary petrographic provinces: an evaluation: in Ross, C.A. (ed.), Paleogeographic Provinces and Provinciality: Society of Economic

Paleontologists and Mineralogists Special Publication No. 21, 75-84.

Thomson, A., 1979, Preservation of porosity in the deep Woodbine / Tuscaloosa trend, Louisiana: Transactions of Gulf Coast Association of Geological Societies, 29, 396-403.

Ungerer, P. and Pelet, R., 1987, Extrapolation of the kinetics of oil and gas formation from laboratory experiments to sedimentary basins: Nature, 327, 52-54.

Vallance, T.G. and Branagan, D.F., 1968, New South Wales Geology - its origin and growth: in A Century of Scientific Progress, Sydney, Royal Society of New South Wales, 265-279.

Van Der Plas, L. and Tobi, A.C., 1965, A chart for judging the reliability of point counting results: American Journal of Science, 263, 87-90.

Visher, G.S., 1965, Fluvial process as interpreted from ancient and recent fluvial deposits: in Middleton, G.V. (ed.), Primary Sedimentary Structures and their Hydrodynamic Interpretation: Society of Economic Paleontologists and Mineralogists Special Publication No. 12, 116-132.

Voisey, A.H., 1959, Tectonic evolution of north-eastern New South Wales, Australia: Journal and Proceedings of the Royal Society of New South Wales, 92, 191-203.

Walker, R.W., 1984, General introduction: facies, facies sequences and facies models: in Walker, R.W. (ed.), FACIES MODELS (2nd edn.), Geoscience Canada Reprint Series, 1-9.

Walker, R.W. and Cant, D.J., 1984, Sandy fluvial systems: in Walker, R.W. (ed.), FACIES MODELS (2nd edn.), Geoscience Canada Reprint Series, 71-89.

Ward, C.R., 1971a, Mesozoic sedimentation and structure in the southern part of the Sydney Basin: Narrabeen Group: Ph.D Thesis, University of New South Wales (unpublished), 653 pp.

Ward, C.R., 1971b, Mineralogical change as marker horizons for stratigraphic correlation in the Narrabeen Group of the Sydney Basin, N.S.W: Journal and Proceedings of the Royal Society of New South Wales, 104, 77-88.

Ward, C.R., 1972, Sedimentation in the Narrabeen Group, Southern Sydney Basin, New South Wales: Journal of Geological Society of Australia, 19, 393-409.

Ward, C.R., Bradley, G.M., Skilbeck, C.G. and Stuchbury, R., 1986, A GUIDE TO CORED ROCKS IN THE SYDNEY BASIN, Earth Resources Foundation, University of Sydney, 150 pp.

Waugh, B. 1970, Formation of quartz overgrowths in the Penrith Sandstone (Lower Permian) of northwest England as revealed by scanning electron microscopy: Sedimentology, 14, 309-320.

Weaver, C.E., 1956, The distribution and identification of mixed-layer clays in sedimentary rocks: American Mineralogist, 41, 202-221.

Wellman, P., 1987, Eastern Highlands of Australia; their uplift and erosion: Bureau of Mineral Resources Journal of Australian Geology and Geophysics, 10, 277-286.

Welton, J.E., 1984, SEM PETROLOGY ATLAS, The American Association of Petroleum Geologists, Tulsa, Oklahoma, USA, 237 pp.

Wentworth, C.K., 1922, A scale of grade and class terms for clastic sediments: Journal of Geology, 30, 377-392.

Wilson, M.D. and Pittman, E.D., 1977, Authigenic clays in sandstones: recognition and influence on reservoir properties and paleoenvironmental analysis: Journal of Sedimentary Petrology, 47, 3-31.

Wilson, R.G., 1969, Illawarra Coal Measures: A southern coalfield: in Packham, G.H. (ed.), The Geology of New South Wales: Journal of Geological Society of Australia, 16, 370-379.

Yeh, H.W., 1980, D/H ratios and late-stage dehydration of shales during burial: Geochimica et Cosmochimica Acta, 44, 341-352.

Yurtsever, Y. and Gat, J.R., 1981, Atmospheric waters, In Gat, J.R. and Gonfiantini, R. (eds.), STABLE ISOTOPE HYDROLOGY: Deuterium and Oxygen - 18 in the Water Cycle, International Atomic Energy Agency, Vienna, 103-142.

Zen, E.A., 1961, The zeolite facies: an interpretation: American Journal of Science, 259, 401-409.

Zuffa, G.G., 1985, Optical analyses of arenites: influence of methodology on compositional results: in Zuffa, G.G. (ed.) , PROVENANCE OF ARENITES, NATO ASI series, D. Reidel Publishing Company, Dordrecht, Holland, 165-189.

		APPENDIX I - LIST OF SAMPLES USED IN VARIOUS STUDIES								
SN	OU	T/S	QE	S/E	XRD	PROB	ISO	F/I	PO	PER
Borehole A										
A146.5	UB	X	X	X	X	X	X		X	X
A163.1	UB	X	X						X	X
A184.3	UB	X	X						X	X
A198.3	UB	X	X							
A211.4	LB	X	X	X					X	X
A221.4	LB	X								
A225.8	SC	X	X							
A247.1	SC	X	X						X	X
A260.8	SC	X	X	X	X					
A295.6	SC	X	X	X						
A313.5	SC	X	X						X	X
A326.8	SC	X	X	X						
A352.0	WO	X		X	X					
Borehole B										
B124.0	UB	X	X							
B132.1	UB	X		X						
B151.7	UB	X	X	X	X	X			X	X
B161.0	UB	X	X							
B175.5	UB	X	X							
B200.1	LB	X	X							
B211.4	LB	X							X	
B234.7	LB	X	X	X					X	
B239.9	LB	X	X							
B259.2	LB	X	X	X						
B277.9	LB	X	X	X						
B338.0	SC	X	X							
B361.6	WO	X	X							
B394.4	WO	X	X	X		X				
B406.2	WO	X	X	X	X				X	
Borehole C										
C038.4	UB	X							X	X
C041.3	UB	X		X						
C066.0	UB	X	X							
C081.1	LB	X	X	X	X				X	
C089.4	LB	X	X						X	X
C101.6	LB	X	X	X	X					
C119.9	LB	X	X							
C132.6	SC	X	X	X	X				X	
C165.9	SC	X								
C191.5	SC	X	X							
C215.8	WO	X	X	X						
C228.7	WO	X								
C259.6	WO	X	X	X						
Borehole D										
D047.1	SC	X	X							
D053.9	SC	X	X	X					X	X

SN	OU	T/S	QE	S/E	XRD	PROB	ISO	F/I	PO	PER
D064.9	SC	X							X	X
D078.4	SC	X	X							
D102.5	SC	X	X	X					X	X
D117.2	SC	X	X							
D145.3	SC	X	X	X						
D164.9	SC	X	X	X		X			X	X
D194.5	WO	X								
D219.0	WO	X								
D236.0	WO	X	X	X					X	X
D257.5	WO	X	X						X	X
D295.9	WO	X	X	X					X	X
Borehole E										
E100.6	SC	X								
E118.5	SC	X	X						X	X
E128.0	SC	X	X	X					X	X
E137.8	SC	X								
E142.6	SC	X	X							
E155.3	SC	X	X							
E185.9	SC	X	X	X						
E212.3	SC	X	X						X	X
E224.5	SC	X							X	X
E243.6	SC	X	X						X	X
E254.9	WO	X	X							
E268.9	WO	X	X	X						
E282.8	WO	X	X							
E291.5	WO	X								
E312.5	WO	X	X	X						
E325.0	WO	X	X							
E344.1	WO	X	X						X	X
E357.7	WO	X		X						
E363.6	WO	X	X							X
Borehole F										
FO45.3	BH	X								
F066.5	BH	X	X	X						
F085.3	BH	X								
F099.4	BH	X	X							
F113.9	UB	X	X	X		X				
F144.1	UB	X								
F158.3	UB	X	X	X						
F176.1	UB	X								
F179.4	UB	X	X							
F194.0	UB	X	X							
F219.2	UB	X							X	X
F236.7	UB	X	X	X		X				
F255.6	UB	X							X	X
F259.3	UB	X	X							
F286.9	LB	X	X							
F301.6	LB	X								
F311.1	LB	X	X	X						

SN	OU	T/S	QE	S/E	XRD	PROB	ISO	F/I	PO	PER
F328.3	LB	X								
F349.3	LB	X	X							
F379.3	LB	X	X							
F396.5	LB	X	X							
F423.4	SC	X	X							
F428.8	SC	X								
F437.8	SC	X	X							
F454.2	SC	X								
F470.4	SC	X	X	X					X	X
F484.2	SC	X							X	X
F491.5	SC	X	X							
F497.1	SC	X								
F502.3	SC	X								
F525.8	SC	X	X	X						
F534.2	SC	X								
F563.0	SC	X	X						X	X
F573.8	WO	X							X	X
F586.2	WO	X	X							
F601.5	WO	X								
F616.7	WO	X	X							
F649.2	WO	X	X	X						
F687.3	WO	X	X							
F734.9	WO	X	X							
F751.7	WO	X	X	X		X			X	X
Borehole G										
G535.5	WO	X								
G540.4	WO	X	X							
G553.8	WO	X	X	X	X				X	X
G577.7	WO	X	X							
Borehole H										
H308.0	UB	X								
H319.0	UB	X	X						X	X
H325.0	LB	X								
H342.5	LB	X	X	X						
H360.6	LB	X	X							
H378.2	LB	X							X	X
H397.6	LB	X	X							
H419.7	LB	X	X	X	X				X	X
H436.1	SC	X	X							
H443.1	SC	X								
H454.9	SC	X	X						X	X
H470.0	SC	X	X	X	X					
H504.7	SC	X	X							
H516.2	SC	X	X						X	X
H535.1	SC	X	X						X	X
H553.7	SC	X								
H568.7	SC	X	X	X	X					
H597.9	WO	X	X						X	X
H625.4	WO	X	X						X	

SN	OU	T/S	QE	S/E	XRD	PROB	ISO	F/I	PO	PER
H632.7	WO	X		X						
H667.2	WO	X	X							
H681.2	WO	X	X	X		X				
H691.5	WO	X	X							
Borehole I										
I320.1	BH	X	X	X	X					
I327.7	BH	X							X	X
I356.0	BH	X	X							
I378.5	UB	X	X	X					X	X
I382.9	UB	X	X						X	X
I402.1	UB	X	X							
I420.9	UB	X								
I437.4	UB	X	X	X					X	X
I447.2	UB	X								
I465.6	UB	X	X	X	X					
I481.7	UB	X	X							
I485.1	UB	X								
I531.9	LB	X								
I543.4	LB	X	X	X					X	X
I564.1	LB	X	X							
I572.0	LB	X	X							
I596.6	LB	X	X	X	X					
I610.7	LB	X	X							
I629.3	SC	X	X	X					X	X
I635.9	SC	X	X							
I664.9	SC	X								
I687.6	SC	X								
I698.2	SC	X	X							
I701.2	SC	X								
I707.0	SC	X								
I708.7	SC	X								
I732.0	SC	X	X							
I749.0	SC	X								
I769.6	WO	X	X							X
I781.5	WO	X	X	X	X					
I806.9	WO	X	X							
I830.4	WO	X	X	X						
I873.5	WO	X								
I879.9	WO	X	X	X	X					
I884.4	WO	X	X							
I902.6	WO	X	X	X						
Borehole J										
J451.4	LB	X							X	
J470.1	SC	X	X							
J481.6	SC	X	X	X	X					
J501.2	SC	X	X							
J514.8	SC	X	X	X		X	X		X	
J545.2	SC	X	X							
J560.5	SC	X								

SN	OU	T/S	QE	S/E	XRD	PROB	ISO	F/I	PO	PER
J570.1	SC	X	X	X						
J582.0	SC	X								
J585.4	SC	X	X							
J599.9	WO	X	X	X	X	X				
J620.8	WO	X	X							
J641.2	WO	X		X					X	
J650.3	WO	X	X							
J672.3	WO	X	X	X	X					
Borehole K										
K030.7	WO	X	X	X					X	
K057.3	WO	X	X							
K073.4	WO	X	X	X					X	
Borehole L										
L285.2	BH	X		X						
L331.0	UB	X								
L338.9	UB	X								
L346.2	UB	X	X						X	X
L355.3	UB	X	X							
L361.8	UB	X	X							
L377.7	UB	X								
L386.0	UB	X	X							
L406.8	UB	X	X	X	X	X			X	X
L415.3	UB	X	X							
L422.3	UB	X		X					X	
L434.7	UB	X	X							
L452.1	LB	X	X							
L469.6	LB	X		X	X					
L487.8	LB	X							X	X
L506.7	LB	X	X	X			X	X		
L518.3	LB	X	X	X						
L532.9	SC	X	X						X	
L547.6	SC	X	X						X	X
L571.0	SC	X	X							
L579.2	SC	X	X	X	X	X			X	X
L595.2	SC	X	X	X	X					
L604.3	SC	X	X							
L621.0	SC	X	X							
L638.9	SC	X	X	X						
L644.7	SC	X	X							
L653.5	SC	X	X							
L681.8	WO	X	X							
L717.8	WO	X	X	X	X				X	
L732.1	WO	X	X	X						
L746.2	WO	X	X							
L759.9	WO	X	X						X	X
Borehole M										
M094.1	BH	X	X	X	X					
M116.7	UB	X								
M132.9	UB	X	X							

SN	OU	T/S	QE	S/E	XRD	PROB	ISO	F/I	PO	PER
M149.6	UB	X	X							
M192.6	UB	X	X							
M209.9	UB	X	X	X	X					
M228.0	LB	X	X						X	
M281.0	LB	X	X							
M308.7	LB	X	X							
M324.3	LB	X								
M341.8	SC	X	X	X	X					
M354.0	SC	X	X							
M369.0	SC	X	X	X						
M381.2	SC	X	X							
M394.3	SC	X								
M402.9	SC	X	X						X	X
M420.8	SC	X	X							
M428.1	SC	X								
M440.0	SC	X	X	X						
M458.8	SC	X	X							
M486.6	WO	X	X						X	X
M492.2	WO	X	X	X	X					
M506.0	WO	X	X							
M528.5	WO	X	X	X					X	X
M551.2	WO	X	X	X						
M586.4	WO	X	X							
M605.3	WO	X	X	X	X					
Borehole N										
N161.4	LB	X	X	X						
N171.9	SC	X								
N184.2	SC	X	X							
N193.1	WO	X	X	X						
Borehole O										
O296.5	BH	X	X	X	X				X	X
O300.3	BH	X								
O370.0	UB	X	X							
O394.2	UB	X							X	X
O417.4	UB	X	X						X	X
O435.2	UB	X	X	X		X			X	X
O452.9	UB	X	X						X	X
O469.2	UB	X							X	X
O488.2	LB	X	X	X			X		X	X
O512.5	LB	X	X						X	X
O538.9	LB	X	X							
O560.4	SC	X	X	X						
O578.4	SC	X	X						X	X
O600.9	SC	X	X	X			X	X		
O617.7	SC	X	X						X	X
O637.4	SC	X	X	X		X				
O668.5	WO	X	X	X	X					
O684.5	WO	X								
O709.5	WO	X	X						X	

SN	OU	T/S	QE	S/E	XRD	PROB	ISO	F/I	PO	PER
O745.8	WO	X	X	X					X	
O755.9	WO	X	X	X	X	X				
Borehole P										
P330.0	SC	X								
P354.6	SC	X								
P422.0	WO	X	X							
P444.7	WO	X	X							
Borehole Q										
Q419.9	SC	X	X							
Q423.0	WO	X	X							
Q435.0	WO	X								
Q438.3	WO	X								
Q440.7	WO	X	X	X						
Q455.2	WO	X	X							
Borehole R										
R071.2	WO	X	X							
R090.2	WO	X	X	X						
R118.2	WO	X	X							
Borehole S										
S446.6	SC	X	X						X	X
S484.1	SC	X	X	X						
S504.4	SC	X	X						X	X
S522.8	SC	X	X						X	X
S541.3	SC	X								
S557.0	WO	X	X						X	X
S575.1	WO	X	X						X	X
S598.9	WO	X	X	X					X	X
S611.1	WO	X								
S629.3	WO	X	X							
S639.6	WO	X								
S652.8	WO	X	X						X	X
Borehole T										
T320.5	SC	X	X	X					X	X
T344.4	WO	X	X							
T365.4	WO	X	X						X	X
T397.6	WO	X	X						X	X
T419.0	WO	X	X						X	X
T434.9	WO	X	X							
Borehole U										
U113.1	SC	X	X	X						
U123.6	SC	X								
U149.5	SC	X	X							
U191.5	SC	X	X						X	X
U196.5	WO	X								
U198.9	WO	X								
U215.5	WO	X	X	X						
U240.8	WO	X	X							
U274.6	WO	X	X							
U326.0	WO	X	X	X					X	

SN	OU	T/S	QE	S/E	XRD	PROB	ISO	F/I	PO	PER
U345.0	WO	X	X							
U373.0	WO	X								
U388.2	WO	X	X	X						
U429.3	WO	X								
U454.1	WO	X	X							
Borehole V										
V011.1	WO	X	X							
V031.8	WO	X	X							
V051.8	WO	X	X	X						
V062.5	WO	X								
Borehole W										
W176.4	BH	X							X	X
W180.1	BH	X	X	X	X				X	X
W182.6	BH	X		X					X	X
W209.8	BH	X	X						X	X
W210.3	BH	X	X						X	X
W222.1	BH	X	X							
W229.8	BH	X	X						X	X
W243.9	UB	X	X	X					X	X
W274.6	UB	X	X	X	X				X	X
W300.8	UB	X	X	X					X	X
W304.9	UB	X	X						X	X
W307.7	UB	X								
W310.4	UB	X	X	X					X	X
W331.7	UB	X	X							
W349.9	UB	X	X	X					X	X
W354.9	LB	X	X						X	X
W359.4	LB	X	X	X					X	X
W368.0	LB	X	X	X					X	X
W388.8	LB	X	X	X	X		X		X	X
W396.8	LB	X	X						X	X
W401.6	SC	X		X					X	X
W430.8	SC	X	X	X	X				X	X
W455.6	SC	X	X	X	X	X			X	X
W470.1	SC	X	X						X	X
W479.8	WO	X	X	X					X	X
W493.9	WO	X	X	X	X				X	X
W515.6	WO	X	X	X					X	X
Borehole X										
X278.0	BH	X		X	X					
X281.3	BH	X	X	X					X	X
X282.0	BH	X	X						X	X
X296.6	BH	X	X						X	X
X297.7	BH	X	X	X					X	X
X309.3	BH	X	X	X	X				X	X
X336.1	UB	X	X	X					X	X
X357.4	UB	X							X	X
X365.6	UB	X	X						X	X
X386.8	UB	X	X	X					X	X

SN	OU	T/S	QE	S/E	XRD	PROB	ISO	F/I	PO	PER
X396.8	UB	X								
X413.3	UB	X		X	X				X	X
X436.6	UB	X	X						X	X
X458.9	LB	X	X						X	X
X473.1	LB	X	X	X	X				X	X
X476.2	LB	X	X	X					X	X
X489.0	LB	X								X
X490.9	LB	X	X	X						
X508.2	SC	X	X	X					X	X
X525.8	SC	X	X	X					X	X
X528.7	SC	X	X	X	X				X	X
X530.7	SC	X	X						X	X
X531.9	SC	X	X	X			X	X	X	X
X559.4	SC	X	X						X	X
X588.5	SC	X	X	X	X				X	X
X612.9	WO	X	X	X	X				X	X
X640.0	WO	X	X	X					X	X
X675.5	WO	X	X	X	X				X	X
Borehole Y										
Y377.5	BH	X	X	X	X				X	X
Y397.6	UB	X	X	X		X			X	X
Y429.0	UB	X	X	X	X				X	X
Y468.5	UB	X	X	X					X	X
Y486.5	LB	X	X	X	X				X	X
Y501.8	LB	X	X						X	X
Y515.3	LB	X	X	X					X	X
Y549.1	LB	X	X	X	X				X	X
Y566.1	LB	X	X	X		X			X	X
Y593.9	SC	X	X	X	X		X		X	X
Y624.7	SC	X	X	X					X	X
Y642.2	SC	X	X	X	X				X	X
Y672.9	WO	X	X	X					X	X
Y690.1	WO	X	X	X	X				X	X
Y727.4	WO	X	X	X					X	X
Y757.9	WO	X	X	X	X	X			X	X
Borehole Z										
Z378.2	BH	X	X							
Z399.0	UB	X	X							
Z402.9	UB	X	X						X	X
Z422.6	UB	X	X	X	X				X	X
Z444.2	UB	X	X						X	X
Z499.0	UB	X	X	X	X				X	X
Z512.4	UB	X	X	X			X	X	X	X
Z531.9	LB	X	X	X	X				X	X
Z593.0	SC	X	X	X	X				X	X
Z611.3	SC	X	X	X					X	X
Z632.7	SC	X	X	X	X				X	X
Z656.8	SC	X	X	X					X	X
Z679.4	WO	X	X	X	X				X	X

SN	OU	T/S	QE	S/E	XRD	PROB	ISO	F/I	PO	PER
Z700.2	WO	X	X						X	X
Z703.3	WO	X	X	X	X				X	X
Z740.4	WO	X	X	X					X	X
Z762.5	WO	X							X	X
Z763.8	WO	X	X	X	X	X			X	X
NOTE:										
SN = sample number, OU = operational unit, T/S = thin section examination,										
QE = quantitative evaluation (point counting), S/E = SEM/EDX anaylyses,										
PROB = microprobe analyses, ISO = isotope analyses, F/I = fluid inclusion investigation,										
XRD = X-ray diffraction studies, PO = porosity measurement, PER = permeability measurement.										
BH = Bald Hill, UB = Upper Bulgo, LB = Lower Bulgo,										
SC = Scarborough, WO = Wombarra Operational Unit.										

APPENDIX II Grain - size scale for clastic sediments (after Wentworth, 1922).

	Name	Millimetre	Micrometer	Ø
Gravel	Boulder			
	Cobble	256.000		-8
	Pebble	64.000		-6
	Granule	4.000		-2
		2.000		-1
Sand	Very coarse sand	1.000		0
	Coarse sand	0.500	500	1
	Medium sand	0.250	250	2
	Fine sand	0.125	125	3
	Very fine sane	0.062	62	4
Mud	Coarse silt	0.031	31	5
Medium silt		0.016	16	6
	Fine silt	0.008	8	7
	Very fine silt	0.004	4	8
	Clay			

APPENDIX III - POINT COUNTING RESULTS

SN	OU	SO	GS	QM	QP	KF	PL	IR	MR	SR	CH	MI	OX	HM	CC	CR	QO	CL	VØ	SØ
Borehole A																				
A146.5	UB.	W.	0.20	48.4	3.4	0.0	0.0	19.6	0.0	0.8	1.0	0.2	0.0	0.4	6.2	0.8	0.8	12.4	4.8	1.2
A163.1	UB.	M.	0.25	53.0	1.8	1.0	0.0	17.8	0.0	0.2	5.6	0.0	0.2	0.0	5.8	0.2	0.0	9.0	5.0	0.4
A184.3	UB.	W.	0.20	51.8	3.6	0.4	0.0	18.2	0.0	0.0	2.8	0.0	0.2	0.0	2.4	0.0	0.0	13.6	6.6	0.4
A198.3	UB.	W.	0.25	49.2	4.6	0.0	0.0	19.0	0.0	1.2	3.8	0.2	0.0	0.6	5.4	0.6	0.0	11.4	3.6	0.4
A211.4	LB.	M.	0.35	46.4	4.4	0.8	0.0	18.6	0.0	0.4	4.2	0.0	0.0	0.2	3.8	0.8	0.0	12.6	6.2	1.6
A225.8	LB.	P.	0.25	57.0	5.8	0.2	0.0	14.6	0.0	0.0	0.6	0.6	0.0	0.0	2.6	0.6	0.0	11.0	5.6	1.4
A247.1	SC.	VP.	1.80	34.0	13.6	0.4	0.0	16.8	0.0	0.0	13.4	0.0	0.0	0.0	1.2	1.6	0.0	12.2	5.4	1.4
A260.8	SC.	M.	0.35	25.6	7.6	3.2	1.0	29.8	0.0	0.0	8.6	0.0	0.0	0.0	4.0	2.2	0.0	13.2	3.0	1.8
A295.6	SC.	M.	0.20	12.8	6.8	0.8	1.6	44.4	0.0	0.0	12.6	0.0	1.2	0.0	13.2	1.6	0.0	1.6	2.4	1.0
A313.5	SC.	P.	0.40	27.6	5.2	3.2	1.4	27.0	0.0	0.0	7.2	0.4	0.0	0.0	9.2	1.8	0.0	8.6	6.0	2.4
A326.8	SC.	VP.	0.20	20.2	5.2	3.4	0.2	32.2	0.0	0.0	5.4	0.4	0.2	0.0	8.6	1.4	0.0	18.2	3.8	0.8
Borehole B																				
B124.0	UB.	M.	0.15	40.0	5.2	2.6	0.0	18.4	0.0	0.0	4.6	0.8	0.2	0.4	6.0	0.8	0.0	13.4	7.4	0.2
B151.7	UB.	M.	0.25	42.0	5.0	1.4	0.0	19.0	0.0	0.0	6.0	0.2	0.2	0.0	10.8	1.2	0.0	6.0	4.0	4.2
B161.0	UB.	M.	0.20	30.6	4.6	3.8	0.4	21.2	0.0	0.0	7.4	0.0	0.6	0.0	3.6	0.8	0.0	14.8	9.6	2.6
B175.5	UB.	M.	0.25	27.2	3.6	4.8	0.2	29.6	0.4	0.0	7.4	0.2	0.2	0.2	2.2	2.4	0.0	16.8	4.6	0.2
B200.1	UB.	P.	0.20	21.4	4.8	3.8	0.4	38.0	0.4	0.0	8.6	0.6	0.4	0.2	0.0	2.0	0.0	14.6	4.2	0.6
B234.7	LB.	W.	0.25	39.6	3.2	2.4	0.2	21.8	0.2	0.0	3.6	0.8	0.0	0.0	9.2	1.4	3.2*	10.2	3.4	0.8
B239.9	LB.	M.	0.25	37.4	5.2	4.0	0.2	24.0	0.0	0.2	3.2	0.2	0.0	0.0	2.4	0.4	0.0	17.6	5.2	0.0
B259.2	LB.	P.	0.38	25.2	5.6	2.0	0.2	37.8	0.2	0.4	5.8	0.0	0.0	0.0	1.4	1.8	0.0	14.8	2.6	2.2
B277.9	LB.	P.	0.28	28.4	7.4	3.6	0.6	29.8	0.2	0.0	7.2	0.0	0.4	0.0	0.8	0.0	0.0	14.2	5.2	1.0
B338.0	SC.	P.	0.43	6.2	1.8	3.4	1.0	40.0	0.0	0.8	15.8	0.0	0.4	0.0	0.0	2.6	0.0	19.4	6.8	1.8
B361.6	WO.	W.	0.25	12.4	2.4	2.2	0.8	39.4	0.0	0.0	15.2	0.2	0.0	0.0	0.4	0.8	0.0	19.2	6.0	1.0
B394.4	WO.	W.	0.15	11.2	2.8	2.4	0.6	26.2	0.4	0.0	13.2	0.0	1.0	0.0	6.0	6.8	0.0	25.6	3.6	0.2
B406.2	WO.	W.	0.40	4.2	2.8	2.4	0.6	45.0	0.0	0.0	16.8	0.0	0.0	0.0	0.2	1.8	0.0	18.2	6.2	1.8
Borehole C																				
C066.0	UB.	P.	0.25	37.8	5.2	1.4	0.2	20.8	0.0	0.0	7.2	0.0	0.8	0.0	1.8	1.2	0.0	12.4	8.4	2.8
C081.1	LB.	M.	0.25	41.0	4.4	1.2	0.0	24.0	0.4	0.0	4.4	0.0	0.4	0.0	3.2	3.2	2.4	8.0	4.2	3.2

SN	OU	SO	GS	QM	QP	KF	PL	IR	MR	SR	CH	MI	OX	HM	CC	CR	QO	CL	VØ	SØ
C089.4	LB.	P.	1.00	46.4	6.8	0.6	0.0	17.2	0.0	1.0	5.6	0.0	0.0	0.0	0.2	1.6	0.0	14.8	3.8	2.0
C101.6	LB.	M.	0.35	28.2	5.8	1.8	0.0	24.8	0.0	0.4	5.8	0.0	0.0	0.0	14.4	5.2	0.0	10.2	1.0	2.4
C119.9	LB.	P.	0.25	13.2	8.8	1.0	0.4	39.6	0.8	0.8	8.6	0.4	0.0	0.0	0.0	0.4	0.0	22.8	2.4	0.8
C132.6	SC.	W.	0.25	16.2	7.2	2.4	1.0	34.0	0.8	0.0	8.2	0.0	0.0	0.0	0.6	0.0	8.8*	15.6	4.6	0.6
C191.5	SC.	M.	0.35	12.6	4.2	4.6	0.0	38.0	0.0	0.0	16.4	0.0	0.0	0.0	2.0	2.2	0.0	13.8	4.6	1.6
C215.8	WO.	W.	0.35	10.8	7.6	2.2	0.0	45.8	0.0	0.0	10.0	0.0	0.0	0.0	2.4	2.0	0.0	13.2	3.8	2.2
C259.6	WO.	M.	0.25	16.2	5.2	30.0	2.4	0.4	0.4	0.4	9.8	0.2	0.0	0.0	6.0	6.4	0.0	14.6	5.0	3.0
Borehole D																				
D047.1	SC.	M.	0.15	16.4	5.2	5.4	2.0	27.4	1.2	0.0	3.8	0.0	0.6	0.0	10.6	0.6	0.0	24.2	2.4	0.2
D053.9	SC.	M.	0.28	39.6	5.6	4.2	3.0	15.2	0.0	0.0	1.8	0.0	0.0	0.0	7.0	0.2	0.0	15.4	6.8	1.2
D078.4	SC.	M.	0.25	42.6	2.6	7.0	2.2	17.8	0.0	0.0	1.0	0.0	0.0	0.0	2.6	0.2	0.4	16.6	7.0	0.0
D102.5	SC.	W.	0.28	39.6	3.4	5.2	2.4	20.8	0.4	0.0	0.4	0.0	0.8	0.0	5.8	1.0	0.4	11.6	8.0	0.2
D117.2	SC.	VP.	0.30	39.6	1.8	4.6	2.0	13.8	0.2	0.2	3.6	0.0	0.2	0.0	4.2	0.6	0.4	17.4	10.2	1.2
D145.3	SC.	W.	0.50	39.2	3.6	1.8	1.4	15.8	0.0	0.0	0.8	0.0	0.0	0.0	17.0	3.6	0.2	8.2	7.2	1.2
D164.9	SC.	P.	0.35	33.8	4.0	3.2	2.0	22.2	0.0	0.0	1.0	0.0	0.4	0.0	7.8	2.8	0.4	13.8	8.0	0.6
D236.0	WO.	M.	0.35	11.6	4.6	1.0	0.2	49.2	1.0	0.0	9.2	0.0	0.6	0.0	4.2	0.4	0.0	12.8	5.2	0.0
D257.5	WO.	M.	0.30	30.4	5.8	1.4	0.4	36.2	1.4	0.0	2.8	0.0	0.2	0.0	1.8	0.6	0.0	12.6	6.2	0.2
D295.9	WO.	M.	0.20	37.4	3.0	3.0	0.8	25.4	0.0	0.0	1.0	0.0	0.0	0.0	7.6	1.0	0.2	15.8	4.8	0.0
Borehole E																				
E118.5	SC.	M.	0.25	23.4	5.0	3.6	1.4	38.2	0.2	0.0	3.6	0.2	0.2	0.0	5.2	0.2	0.0	14.4	3.6	0.8
E128.0	SC.	W.	0.30	44.6	5.4	4.2	2.0	25.6	0.0	0.0	0.6	0.0	0.2	0.0	1.6	0.0	1.2	8.4	6.0	0.2
E142.6	SC.	M.	0.23	41.2	3.4	4.0	2.6	21.8	0.4	0.0	0.8	0.0	0.0	0.0	2.8	0.2	0.6	14.6	7.4	0.2
E155.3	SC.	M.	0.20	23.0	4.0	5.2	1.6	32.8	0.8	0.0	3.2	0.4	0.0	0.0	1.2	0.0	0.0	22.8	4.6	0.4
E185.9	SC.	M.	0.40	38.4	4.0	1.6	1.6	24.4	0.0	0.0	6.8	0.0	0.0	0.0	3.6	0.6	0.6	10.8	7.2	0.4
E212.3	SC.	P.	0.45	28.8	4.8	3.4	1.2	35.2	0.4	0.6	4.6	0.0	0.2	0.0	1.0	1.0	0.0	16.0	2.4	0.4
E243.6	SC.	M.	0.40	40.2	3.8	1.0	1.6	28.6	0.0	0.0	2.0	0.0	0.2	0.0	5.8	1.4	0.4	9.6	4.4	1.0
E254.9	WO.	P.	0.50	30.2	2.6	3.8	2.4	32.8	0.2	0.0	1.4	0.0	0.2	0.0	3.6	0.8	0.2	15.8	5.2	0.8
E268.9	WO.	M.	0.35	5.6	4.8	1.4	0.4	44.4	1.4	0.0	10.8	0.0	0.0	0.0	11.0	1.0	0.0	12.8	5.6	0.8

SN	OU	SO	GS	QM	QP	KF	PL	IR	MR	SR	CH	MI	OX	HM	CC	CR	QO	CL	VØ	SØ
E282.8	WO.	M.	0.40	22.2	4.4	2.4	1.2	40.2	0.8	0.2	3.8	0.0	0.0	0.0	2.4	0.4	0.0	12.0	9.2	0.8
E312.5	WO.	M.	0.35	16.2	4.4	2.2	0.6	39.8	0.6	0.0	9.8	0.0	0.0	0.0	2.0	0.0	0.0	17.4	7.0	0.2
E325.0	WO.	P.	0.40	34.0	4.4	2.4	1.4	29.0	0.4	0.0	2.8	0.0	0.0	0.0	3.2	0.0	0.0	17.4	4.0	0.0
E344.1	WO.	P.	0.35	35.0	4.6	3.6	2.2	29.6	0.0	0.0	0.6	0.0	0.0	0.0	2.0	0.4	0.6	16.2	5.0	0.2
E363.6	WO.	P.	0.30	58.0	3.4	1.8	1.2	11.8	0.0	0.0	0.6	0.0	0.0	0.0	1.4	0.0	0.4	8.2	13.0	0.2
Borehole F																				
F066.5	BH.	M.	0.30	38.2	6.2	2.2	0.4	19.2	0.2	0.0	4.6	0.0	0.0	0.0	3.8	0.6	0.0	21.6	2.2	0.8
F099.4	BH.	VP.	0.35	52.0	5.6	0.6	0.0	11.2	0.4	0.0	0.2	0.0	0.0	0.2	5.0	0.0	0.0	19.0	4.4	1.4
F113.9	UB.	M.	0.18	31.4	3.0	1.4	0.2	25.4	0.4	0.0	3.6	0.0	0.4	0.0	12.8	1.8	0.0	15.6	3.2	0.8
F158.3	UB.	VP.	0.30	40.6	2.8	0.6	0.0	21.4	0.4	0.4	2.6	0.0	0.2	0.2	8.2	0.0	0.0	16.8	5.2	0.6
F179.4	UB.	W.	0.30	61.4	4.4	0.8	0.4	13.4	0.4	0.0	0.6	0.0	0.0	0.2	1.0	0.0	0.0	11.2	5.8	0.8
F194.0	UB.	W.	0.35	46.8	5.2	0.0	0.0	26.8	0.0	0.0	2.8	0.0	0.0	0.0	0.6	0.0	0.0	8.4	9.2	0.2
F236.7	UB.	M.	0.23	34.2	6.0	1.2	0.2	29.2	0.0	0.0	6.6	0.0	0.0	0.0	4.6	0.0	0.0	14.0	3.6	0.4
F259.3	UB.	M.	0.28	23.6	3.2	0.4	0.0	30.8	0.6	0.2	7.8	0.0	0.0	0.2	17.6	0.4	0.0	8.2	5.4	1.4
F286.9	LB.	M.	0.18	32.8	3.4	2.4	0.4	28.0	0.0	0.0	5.4	2.0	0.0	0.0	9.0	0.4	0.0	16.4	1.6	0.2
F311.1	LB.	M.	0.15	23.8	2.8	5.0	0.4	25.0	0.4	0.0	2.0	0.2	0.2	0.0	25.4	0.8	0.0	10.4	3.0	0.6
F349.3	LB.	M.	0.25	29.0	3.6	2.8	0.8	36.4	0.2	0.0	5.0	0.0	0.2	0.0	6.2	0.2	0.0	12.8	2.2	0.6
F379.3	LB.	M.	0.28	30.2	2.8	5.0	0.4	32.6	0.0	0.0	3.2	0.0	0.0	0.0	6.4	0.0	0.0	15.6	3.4	0.4
F396.5	LB.	M.	0.30	29.6	6.2	2.6	0.6	28.6	0.6	0.0	5.6	0.0	0.0	0.2	6.8	0.0	0.0	15.2	3.0	1.0
F423.4	SC.	M.	0.60	21.2	8.0	1.2	0.8	40.0	0.0	0.0	5.4	0.0	0.0	0.0	6.4	0.0	0.0	12.4	4.0	0.6
F437.8	SC.	M.	0.18	19.8	3.6	3.2	0.8	35.6	0.8	0.0	2.0	0.0	0.2	0.0	9.8	0.0	0.0	20.8	2.6	0.8
F470.4	SC.	M.	0.45	31.8	3.8	0.6	0.0	36.8	0.2	0.4	3.4	0.0	0.0	0.0	4.4	0.0	0.0	13.0	5.2	0.4
F491.5	SC.	P.	0.28	37.2	3.2	0.6	0.0	23.6	1.0	0.0	2.0	0.2	0.2	0.0	7.8	0.0	0.0	19.0	4.4	0.8
F525.8	SC.	P.	0.40	19.4	2.2	1.8	0.8	27.8	0.6	0.0	2.0	0.4	0.8	0.0	27.4	3.2	0.0	10.2	2.6	0.8
F563.0	SC.	M.	0.35	27.4	2.8	0.4	0.2	32.2	0.0	0.2	2.6	0.0	0.0	0.0	2.8	0.0	0.0	21.8	8.6	1.0
F586.2	WO.	P.	0.40	7.6	3.6	0.6	0.0	53.4	1.4	0.2	7.4	0.0	0.2	0.0	5.0	0.4	0.0	19.0	0.8	0.4
F616.7	WO.	P.	0.20	35.2	3.0	2.2	0.2	21.4	0.0	0.0	2.4	0.0	0.0	0.0	6.4	0.4	0.0	24.6	4.0	0.2
F649.2	WO.	M.	0.40	29.2	2.8	0.2	0.6	29.2	0.0	0.0	4.8	0.0	0.0	0.0	15.6	1.0	0.0	9.2	6.4	1.0
F687.3	WO.	P.	0.30	35.2	3.8	1.4	0.2	30.0	0.0	0.0	1.0	0.0	0.0	0.0	2.4	0.2	0.0	19.0	5.2	1.6

SN	OU	SO	GS	QM	QP	KF	PL	IR	MR	SR	CH	MI	OX	HM	CC	CR	QO	CL	VØ	SØ
F734.9	WO.	M.	0.20	35.6	4.0	1.2	0.4	15.6	0.0	0.0	0.2	0.0	0.0	0.0	26.8	3.6	0.0	7.4	4.2	1.0
F751.7	WO.	M.	0.35	20.8	2.4	1.8	1.2	39.8	0.2	0.0	1.0	0.0	0.0	0.0	17.2	2.0	0.0	9.8	2.8	1.0
Borehole G																				
G540.4	WO.	W.	0.28	12.0	5.0	1.0	0.4	50.8	1.2	0.0	7.8	0.0	0.0	0.0	4.2	0.4	0.4	10.4	6.0	0.4
G553.8	WO.	W.	0.30	23.0	5.6	0.8	0.6	37.0	0.6	0.0	4.8	0.0	0.0	0.0	6.6	0.4	0.2	13.6	6.2	0.6
G577.7	WO.	M.	0.45	28.4	6.6	0.2	0.2	32.4	1.2	0.0	5.0	0.0	0.0	0.0	5.4	0.2	0.0	15.0	4.8	0.6
Borehole H																				
H319.0	UB.	M.	0.40	44.4	6.2	0.0	0.2	21.6	0.0	0.0	6.0	0.0	0.0	0.0	2.4	0.2	1.4	9.0	8.0	0.6
H342.5	LB.	M.	0.30	36.0	4.6	0.6	0.0	27.0	0.0	0.0	2.6	0.2	0.0	0.0	7.2	0.4	1.2	13.2	5.8	1.2
H360.6	LB.	M.	0.13	40.8	1.8	0.8	0.0	21.4	0.0	0.0	1.4	0.2	0.0	0.0	5.8	0.2	0.2	23.4	2.6	1.4
H397.6	LB.	M.	1.20	38.6	8.0	0.0	0.0	25.4	0.0	0.0	4.4	0.0	0.0	0.0	5.6	0.2	0.2	8.2	9.4	0.0
H419.7	LB.	M.	0.65	53.2	5.4	0.4	0.0	14.0	0.0	0.4	2.6	0.0	0.0	0.0	3.2	0.4	2.2	7.8	10.0	0.4
H436.1	SC.	M.	0.25	41.8	4.8	0.0	0.0	22.2	0.0	0.0	2.8	0.0	0.0	0.0	5.2	0.2	0.8	16.2	5.4	0.6
H454.9	SC.	M.	0.25	47.8	3.4	0.6	0.0	21.0	0.0	0.2	2.4	0.0	0.0	0.0	3.0	0.0	0.6	14.8	6.0	0.2
H470.0	SC.	M.	0.25	27.0	4.4	1.2	0.2	27.2	0.0	0.0	4.2	0.2	0.0	0.0	7.6	0.0	0.4	19.8	6.8	1.0
H504.7	SC.	M.	0.15	16.2	5.6	1.8	0.6	31.4	0.2	0.0	5.4	0.2	0.0	0.0	8.2	1.0	0.0	27.2	2.0	0.2
H516.2	SC.	M.	0.50	25.4	4.4	0.2	1.0	35.2	0.4	0.0	3.8	0.0	0.0	0.0	4.6	1.0	0.0	14.6	8.4	1.0
H535.1	SC.	VP.	0.40	16.6	3.2	1.4	1.2	40.6	0.0	0.0	6.6	0.0	0.0	0.0	9.8	1.2	0.2	12.8	6.2	0.2
H568.7	SC.	M.	0.28	10.0	3.4	2.0	1.6	45.0	0.4	0.0	8.4	0.0	0.2	0.0	7.4	1.0	0.0	18.0	2.2	0.4
H597.9	WO.	W.	0.25	36.0	3.0	3.4	3.4	24.8	0.2	0.0	2.4	0.4	0.0	0.0	6.2	0.0	1.0	16.4	2.6	0.2
H625.4	WO.	P.	0.35	24.6	3.6	3.0	2.2	35.0	0.0	0.0	2.8	0.0	0.2	0.0	3.2	1.2	0.0	18.2	5.8	0.2
H667.2	WO.	P.	0.40	22.4	3.8	2.6	0.8	36.4	0.6	0.4	3.0	0.4	0.4	0.0	3.4	1.4	0.0	19.0	4.6	0.8
H681.2	WO.	W.	0.25	20.0	3.0	4.0	1.8	33.0	0.0	0.0	1.2	0.0	0.2	0.0	27.4	2.6	0.0	6.0	0.6	0.2
H691.5	WO.	P.	0.20	14.6	1.8	3.0	1.8	32.2	0.8	0.0	3.0	0.4	0.0	0.0	6.4	8.6	0.0	23.2	4.0	0.2
Borehole I																				
I320.1	BH.	W.	0.20	34.0	2.0	2.6	1.2	20.2	0.2	0.0	1.6	0.2	0.2	0.0	14.6	0.4	0.0	17.0	2.6	3.2
I356.0	BH.	W.	0.30	51.0	3.2	0.6	0.8	17.0	0.0	0.0	1.2	0.2	0.0	0.0	5.6	0.6	2.0	9.4	6.2	2.2
I378.5	UB.	W.	0.30	49.4	2.6	0.2	0.0	18.6	0.0	0.0	1.6	0.8	0.0	0.0	5.2	0.0	0.6	14.2	5.6	1.2
I382.9	UB.	M.	0.30	43.0	3.8	0.2	0.2	23.2	0.0	0.0	2.0	0.4	0.4	0.0	2.2	0.0	0.8	13.8	8.4	1.6

SN	OU	SO	GS	QM	QP	KF	PL	IR	MR	SR	CH	MI	OX	HM	CC	CR	QO	CL	VØ	SØ
I402.1	UB.	W.	0.25	37.0	8.8	1.6	1.2	26.4	0.0	0.0	2.2	0.2	0.0	0.0	5.2	0.8	0.0	9.6	5.8	1.2
I437.4	UB.	W.	0.20	32.0	4.6	4.6	1.0	18.8	0.0	0.0	1.2	0.0	0.4	0.0	22.2	1.2	0.0	7.4	4.0	2.6
I465.6	UB.	W.	0.18	27.4	2.8	4.6	1.4	19.8	0.4	0.0	2.4	0.0	0.6	0.0	32.6	3.4	0.0	3.4	0.8	0.4
I481.7	UB.	M.	0.25	20.4	5.0	5.6	3.8	34.2	0.0	0.0	3.2	0.2	0.0	0.0	3.4	0.0	0.0	12.4	10.4	1.4
I543.4	LB.	W.	0.25	21.4	6.2	3.2	1.0	35.8	0.2	0.0	2.6	0.0	0.0	0.0	2.6	1.0	0.0	13.2	9.4	3.4
I564.1	LB.	M.	0.15	23.2	3.8	5.8	2.2	25.2	0.0	0.0	2.4	0.0	0.6	0.0	8.6	0.4	0.0	17.6	8.8	1.4
I572.0	LB.	M.	0.25	29.6	6.6	4.6	1.4	27.0	0.0	0.0	2.2	0.0	0.0	0.0	6.4	1.0	1.0	9.2	9.6	1.4
I596.6	LB.	W.	0.25	30.0	4.2	4.8	4.4	28.4	0.0	0.0	1.2	0.0	0.0	0.0	1.8	0.2	0.0	16.0	8.0	1.0
I610.7	LB.	W.	0.15	24.0	5.8	5.2	1.8	28.6	0.0	0.0	4.4	0.2	0.2	0.0	9.4	1.4	0.0	11.0	6.6	1.4
I629.3	SC.	M.	0.35	45.6	3.8	1.0	1.8	20.6	0.0	0.0	2.2	0.0	0.0	0.0	3.4	0.2	0.8	8.8	9.2	2.6
I635.9	SC.	W.	0.23	42.0	2.6	3.8	1.8	17.4	0.2	0.0	1.2	0.4	0.2	0.0	2.4	0.0	2.0	13.8	10.0	1.8
I698.2	SC.	M.	0.30	35.2	1.6	4.8	2.4	34.0	0.0	0.0	1.6	0.0	0.0	0.0	0.2	0.2	0.8	7.2	9.8	2.2
I732.0	SC.	P.	0.28	23.0	4.0	4.6	1.6	41.0	0.0	0.0	1.8	0.0	0.0	0.0	0.4	0.4	0.2	13.0	8.8	1.2
I769.6	WO.	W.	0.35	6.0	4.0	0.6	0.6	52.0	0.4	0.0	15.2	0.0	0.0	0.0	1.6	0.2	0.0	9.4	8.2	1.8
I781.5	WO.	P.	0.40	31.4	2.2	2.8	0.8	31.4	0.0	0.0	4.4	0.0	0.0	0.0	4.8	0.4	1.0	11.8	7.2	1.8
I806.9	WO.	M.	0.30	8.6	5.6	3.0	1.0	49.0	0.2	0.0	6.0	0.2	0.0	0.0	0.4	0.2	0.0	18.6	6.8	0.4
I830.4	WO.	M.	0.40	34.0	3.8	2.4	3.4	28.2	0.0	0.4	1.6	0.0	0.0	0.0	2.4	0.4	0.6	13.8	7.2	1.8
I879.9	WO.	W.	0.18	9.8	1.4	4.0	1.2	45.8	0.4	0.0	3.2	0.2	0.0	0.0	13.0	2.0	0.0	13.8	4.0	1.2
I884.4	WO.	W.	0.20	14.6	5.0	1.4	0.2	55.4	0.0	0.0	2.4	0.0	0.0	0.0	0.8	0.0	0.0	13.4	5.4	1.4
I902.6	WO.	P.	0.20	29.8	3.8	3.6	2.0	23.4	0.0	0.0	0.8	0.0	0.0	0.0	12.0	0.6	0.2	19.0	4.6	0.2
Borehole J																				
J470.1	SC.	P.	0.40	34.6	9.8	2.8	0.6	25.6	0.4	0.4	6.4	0.2	0.0	0.0	0.0	0.4	8.8*	12.4	5.2	1.2
J481.6	SC.	M.	0.50	28.0	6.6	4.4	0.4	30.2	0.0	0.0	10.4	0.0	0.0	0.0	2.8	3.0	0.0	9.6	2.2	1.4
J501.2	SC.	M.	0.35	16.8	2.2	6.6	0.6	22.8	0.8	0.2	17.0	0.2	0.0	0.0	3.0	4.0	0.4	18.0	5.8	2.0
J514.8	SC.	W.	0.35	22.4	6.0	6.4	0.0	29.2	0.0	0.0	6.8	0.2	0.2	0.0	3.2	3.6	0.6	7.4	4.0	1.8
J545.2	SC.	M.	0.20	10.2	4.0	4.6	1.6	40.4	0.4	0.0	9.8	0.0	0.6	0.0	0.4	2.8	0.0	20.0	5.6	0.2
J570.1	SC.	M.	0.20	2.4	1.8	2.6	0.4	55.8	1.0	0.0	2.2	0.4	3.6	0.0	0.0	1.2	0.4	23.8	4.4	0.0
J585.4	SC.	M.	0.23	11.2	4.6	3.8	1.2	40.2	0.2	0.0	14.8	0.0	0.0	0.0	3.8	1.8	0.0	11.8	5.0	1.0
J599.9	WO.	M.	0.25	9.4	3.2	2.0	0.6	38.8	0.6	0.0	8.8	0.0	0.0	0.0	16.6	1.8	0.0	14.6	2.6	1.0

SN	OU	SO	GS	QM	QP	KF	PL	IR	MR	SR	CH	MI	OX	HM	CC	CR	QO	CL	VØ	SØ
J620.8	WO.	P.	0.23	10.0	3.6	2.4	1.4	41.2	0.0	0.0	13.8	0.0	0.0	0.0	0.0	0.0	0.0	24.0	3.2	0.0
J650.3	WO.	W.	0.25	3.4	0.6	0.8	0.0	35.8	0.0	0.0	2.2	0.0	0.0	0.0	49.4	6.6	1.0	0.0	0.0	1.2
J672.3	WO.	P.	0.15	13.0	1.4	1.6	0.2	25.2	0.0	0.0	5.8	0.0	0.0	0.0	16.2	15.8	0.0	18.2	2.2	0.4
Borehole K																				
K030.7	WO.	P.	1.50	3.4	2.2	0.0	0.0	64.0	0.4	6.4	4.8	0.0	0.0	0.0	4.8	0.6	0.0	9.4	4.0	0.0
K057.3	WO.	P.	1.40	3.4	1.6	0.2	0.4	56.2	2.2	1.0	10.8	0.0	0.0	0.0	6.2	0.4	0.0	8.6	8.2	0.8
K073.4	WO.	M.	0.35	3.6	1.4	0.2	0.0	56.2	0.6	0.4	3.2	0.0	0.0	0.0	24.4	1.6	0.0	6.0	2.4	0.0
Borehole L																				
L346.2	UB.	M.	0.30	57.4	3.8	0.0	0.8	16.0	0.2	0.0	3.8	0.0	0.0	0.0	4.2	0.4	0.0	8.2	4.0	1.2
L355.3	UB.	M.	0.20	24.6	3.6	2.6	6.0	23.8	0.0	0.0	3.8	0.0	0.6	0.0	11.0	0.8	0.0	17.2	4.6	1.4
L361.8	UB.	W.	0.25	53.8	4.8	0.0	0.8	18.2	0.0	0.0	1.4	0.0	0.2	0.0	5.6	0.6	0.0	10.2	3.4	1.0
L386.0	UB.	M.	0.25	47.8	3.6	0.2	1.0	16.8	0.0	0.0	2.8	0.2	0.0	0.0	10.4	1.0	0.0	13.0	2.2	1.0
L406.8	UB.	M.	0.20	46.6	4.8	0.0	0.6	14.8	0.0	0.0	2.2	0.2	0.8	0.0	7.4	1.0	0.0	17.4	4.0	0.2
L415.3	UB.	M.	0.25	58.8	5.0	0.0	1.2	13.0	0.0	0.0	1.4	0.0	0.2	0.2	4.4	0.2	1.2	11.8	2.0	0.6
L434.7	UB.	W.	0.25	47.4	4.8	0.0	2.2	18.6	0.6	0.0	2.6	0.0	0.0	0.0	4.0	0.2	0.0	13.6	4.6	1.4
L452.1	LB.	M.	0.35	57.6	5.4	1.8	0.2	13.4	0.0	0.0	2.2	0.0	0.0	0.0	4.2	0.0	3.8	6.0	3.8	1.6
L506.7	LB.	M.	0.40	51.0	4.2	1.2	0.2	13.6	0.2	0.0	3.4	0.0	0.0	0.0	3.4	0.6	1.2	12.8	6.8	1.4
L518.3	LB.	M.	0.50	39.0	6.4	4.2	0.8	24.6	0.0	0.2	4.8	0.0	0.0	0.0	5.4	1.6	2.2	5.8	3.6	1.4
L532.9	SC.	M.	0.25	27.4	5.4	2.6	1.0	27.8	0.2	0.0	7.6	0.4	0.0	0.0	8.0	1.0	0.0	13.6	4.2	0.8
L547.6	SC.	M.	0.60	59.0	6.4	0.2	0.0	16.2	0.4	0.2	3.0	0.0	0.0	0.0	2.6	0.0	0.8	5.8	4.6	0.8
L571.0	SC.	M	0.65	24.2	4.2	4.6	3.4	18.4	1.0	0.0	11.4	0.0	0.0	0.0	10.4	4.6	0.0	11.2	4.4	2.2
L579.2	SC.	W.	0.25	13.8	4.6	10.0	5.0	30.6	0.0	0.0	6.2	0.0	0.0	0.0	11.4	0.6	0.0	12.6	4.0	1.2
L595.2	SC.	P.	0.50	15.8	5.0	6.4	1.4	18.4	0.4	0.2	11.2	0.0	0.0	0.0	30.8	5.4	0.0	1.6	1.8	1.6
L604.3	SC.	M.	0.30	10.8	5.0	6.4	4.8	29.0	0.2	0.0	9.6	0.6	0.0	0.0	13.8	1.2	0.0	15.6	1.8	1.2
L621.0	SC.	M.	0.25	10.4	4.6	5.4	3.0	34.2	0.6	0.0	10.6	0.0	0.0	0.0	12.0	0.4	0.0	12.4	4.2	2.2
L638.9	SC.	M.	0.40	7.2	4.0	4.8	2.0	41.0	0.4	0.4	10.6	0.0	0.0	0.0	1.0	1.2	0.0	22.8	3.8	0.8
L644.7	SC.	M.	0.25	11.2	3.4	4.8	1.8	34.4	0.4	0.2	16.0	0.0	0.0	0.0	2.0	0.8	0.0	19.4	4.0	1.6
L653.5	SC.	W.	0.20	8.2	3.2	4.4	1.0	37.6	0.0	0.0	13.0	0.0	1.0	0.2	5.2	0.8	0.0	20.6	3.6	1.2
L681.8	WO.	P.	0.50	36.6	10.2	1.2	0.0	22.4	0.0	0.0	7.0	0.2	0.0	0.0	4.0	0.8	0.0	13.6	3.0	1.0

SN	OU	SO	GS	QM	QP	KF	PL	IR	MR	SR	CH	MI	OX	HM	CC	CR	QO	CL	VØ	SØ
L717.8	WO.	P.	0.55	6.6	2.4	3.0	0.4	35.4	0.0	4.6	11.8	0.0	0.0	0.0	14.8	3.2	0.0	12.2	4.4	1.2
L732.1	WO.	M.	0.30	15.2	5.0	1.8	0.4	36.0	0.0	0.0	11.8	0.0	0.0	0.2	5.4	2.4	0.0	17.4	2.6	1.8
L746.2	WO.	M.	0.40	13.4	5.0	1.6	0.2	34.0	0.8	0.0	7.2	0.6	0.0	0.0	13.4	4.2	0.0	13.8	3.8	2.0
L759.9	WO.	VP.	0.80	16.2	9.0	0.4	0.0	26.4	0.0	2.2	9.6	0.0	0.0	0.0	4.8	0.0	0.0	17.0	10.0	4.4
Borehole M																				
M094.1	BH.	M.	0.20	35.0	3.2	2.2	1.6	19.8	0.6	0.0	2.2	0.0	0.0	0.0	26.0	4.2	0.0	3.2	1.0	1.0
M132.9	UB.	M.	0.35	32.4	6.0	0.6	0.4	27.0	0.4	0.0	7.4	0.0	0.0	0.0	9.2	0.4	0.0	9.0	4.2	3.0
M149.6	UB.	M.	0.18	27.8	6.8	4.8	0.8	30.6	0.0	0.0	4.8	1.0	0.0	0.0	0.0	0.0	0.0	16.2	3.6	3.6
M192.6	UB.	M.	0.20	23.8	6.2	5.0	1.0	24.6	0.0	0.0	5.0	0.0	0.2	0.0	1.8	0.0	0.0	29.0	2.2	1.2
M209.9	UB.	W.	0.18	36.4	10.2	4.4	2.6	17.6	0.0	0.0	5.2	0.2	0.2	0.0	2.6	0.2	0.0	18.6	1.2	0.6
M228.0	LB.	M.	0.20	31.2	4.4	5.4	3.2	24.2	0.2	0.0	4.2	0.0	0.2	0.0	0.0	0.0	0.0	22.6	2.2	2.2
M281.0	LB.	W.	0.30	25.6	13.6	3.6	1.0	31.0	0.0	0.0	7.2	0.2	0.0	0.0	0.0	0.0	1.8	9.4	3.4	3.2
M308.7	LB.	M.	0.13	29.0	3.2	6.6	1.6	22.6	0.0	0.0	0.8	0.0	0.4	0.0	10.0	1.0	0.0	18.8	3.8	2.2
M341.8	SC.	M.	0.20	23.2	3.6	9.2	1.4	33.0	0.4	0.0	3.6	0.0	0.0	0.0	0.0	0.8	0.0	18.6	3.4	3.0
M354.0	SC.	M.	0.30	33.8	8.0	5.2	2.6	26.6	0.4	0.0	5.0	0.0	0.0	0.0	0.4	0.6	0.0	12.2	2.2	3.0
M369.0	SC.	M.	0.40	26.6	6.0	2.2	1.2	31.4	0.4	0.0	10.2	0.0	0.0	0.0	1.4	0.2	0.0	11.4	6.8	2.2
M381.2	SC.	P.	0.38	42.8	5.2	1.6	0.8	27.2	0.2	2.2	4.8	0.0	0.0	0.0	0.0	0.0	1.2	8.4	1.6	4.0
M402.9	SC.	M.	0.30	41.6	4.8	3.2	0.2	21.8	0.0	0.6	6.2	0.4	0.2	0.0	0.0	0.0	1.6	12.6	5.0	1.8
M420.8	SC.	M.	0.13	23.6	3.2	10.4	1.0	22.8	0.0	0.0	2.4	0.8	0.6	0.0	0.0	0.0	0.0	32.0	3.0	0.2
M440.0	SC.	M.	0.30	27.4	7.4	4.2	0.2	22.0	0.2	0.0	14.6	0.0	0.0	0.0	8.6	1.2	0.6	10.0	2.0	1.6
M458.8	SC.	P.	0.23	27.2	6.6	4.2	0.2	21.8	0.4	1.0	12.6	0.0	0.0	0.0	3.6	0.8	0.4	18.6	1.6	1.0
M486.6	WO.	M.	0.40	29.8	4.8	2.0	1.2	30.0	1.4	0.4	6.6	0.2	0.0	0.0	0.0	0.0	2.0	15.0	5.4	1.2
M492.2	WO.	M.	0.30	25.2	6.0	2.4	1.2	36.0	0.4	0.0	7.4	0.0	0.0	0.0	1.0	0.4	0.6	13.2	3.8	2.4
M506.0	WO.	M.	0.40	16.8	4.4	1.2	0.4	37.8	0.4	0.0	17.0	0.2	0.0	0.0	0.0	0.0	0.0	18.0	2.8	1.0
M528.5	WO.	M.	0.28	8.0	3.2	2.0	0.8	30.0	1.2	0.2	13.6	0.0	0.2	0.0	17.2	1.6	0.0	18.0	1.4	2.6
M551.2	WO.	M.	0.25	9.8	5.8	1.8	0.4	39.4	0.8	0.0	14.8	0.0	0.0	0.0	2.0	0.0	0.0	20.6	3.6	1.0
M586.4	WO.	W.	0.25	9.8	7.8	0.6	0.4	38.0	0.6	0.0	12.6	0.0	0.0	0.0	1.4	0.2	0.0	21.8	4.4	2.4
M605.3	WO.	W.	0.23	10.6	6.8	1.6	0.2	30.2	0.8	0.0	16.4	0.0	0.2	0.0	4.6	0.2	0.0	24.2	3.2	1.0
Borehole N																				

SN	OU	SO	GS	QM	QP	KF	PL	IR	MR	SR	CH	MI	OX	HM	CC	CR	QO	CL	VØ	SØ
N161.4	LB.	M.	0.25	51.6	3.0	0.0	0.0	13.2	0.0	0.0	1.4	0.0	0.0	0.0	4.0	0.0	0.0	17.6	9.2	0.0
N184.2	SC.	P.	0.28	45.0	4.6	0.0	0.0	24.6	0.0	0.0	4.2	0.0	0.0	0.0	0.2	0.0	0.0	14.4	6.6	0.4
N193.1	WO.	P.	0.23	19.2	6.4	0.2	0.0	34.2	0.0	0.0	12.2	0.0	0.0	0.0	3.8	0.0	0.0	18.2	5.8	0.0
Borehole O																				
O296.5	BH.	M.	0.33	68.4	4.4	0.0	0.0	1.4	0.0	0.0	0.0	0.2	0.0	0.0	1.8	0.4	1.2	15.6	5.4	1.2
O370.0	UB.	W.	0.23	38.2	7.4	1.2	0.0	19.2	0.0	0.0	8.0	0.2	0.4	0.0	4.4	0.6	2.0	14.4	3.6	0.4
O417.4	UB.	W.	0.25	52.6	3.4	0.6	0.0	15.2	0.0	0.0	5.2	0.2	0.0	0.2	3.4	0.4	0.0	13.4	4.0	1.4
O435.2	UB.	M.	0.20	39.0	6.2	1.0	0.0	15.2	0.0	0.0	7.0	0.2	0.0	0.0	8.8	0.6	0.2	17.0	4.2	0.6
O452.9	UB.	W.	0.30	49.4	4.4	1.2	0.0	18.4	0.0	0.0	3.8	0.0	0.0	0.0	3.6	0.0	2.2	12.0	4.4	0.6
O488.2	LB.	M.	0.25	37.2	6.4	0.8	0.0	21.2	0.0	0.0	6.4	0.0	0.0	0.0	7.4	0.2	0.4	16.0	3.2	0.8
O512.5	LB.	M.	0.30	58.8	5.2	0.2	0.0	10.8	0.0	0.0	2.6	0.0	0.0	0.0	1.6	0.0	2.2	10.2	8.0	0.4
O538.9	LB.	P.	0.30	38.8	3.6	0.2	0.0	17.2	0.2	0.0	10.8	0.0	0.0	0.0	5.2	0.2	0.6	14.8	7.2	1.2
O560.4	SC.	M.	0.25	32.8	6.6	2.8	0.2	20.0	0.0	0.0	7.6	0.0	0.0	0.0	3.4	0.0	2.0	15.8	8.0	0.8
O578.4	SC.	M.	0.30	34.0	6.2	2.6	0.6	20.4	0.2	0.0	7.6	0.0	0.0	0.0	4.8	0.0	1.8	17.2	4.2	0.4
O600.9	SC.	M.	0.50	40.0	5.8	3.0	0.8	13.2	0.0	0.0	5.4	0.0	0.0	0.0	6.4	0.0	4.2	12.6	7.4	1.2
O617.7	SC.	M.	0.20	31.2	4.6	2.0	0.6	17.0	0.0	0.0	7.2	0.0	0.4	0.0	4.2	0.0	1.4	18.0	13.4	0.0
O637.4	SC.	W.	0.25	13.6	5.4	3.2	1.2	30.6	0.0	0.0	9.4	0.0	0.0	0.0	20.6	2.8	0.8	11.2	1.2	0.0
O668.5	WO.	M.	0.20	10.8	8.4	4.0	0.4	26.4	0.4	0.0	7.0	0.0	0.0	0.0	25.4	4.8	0.0	9.8	2.4	0.2
O709.5	WO.	W.	0.23	15.0	5.2	4.0	0.2	36.0	0.0	0.2	10.6	0.0	0.0	0.0	9.2	0.8	0.0	15.2	2.8	0.8
O745.8	WO.	M.	0.20	11.0	6.8	3.0	2.0	27.6	1.2	0.0	14.8	0.0	0.0	0.0	6.0	0.4	0.0	22.6	2.0	2.6
O755.9	WO.	M.	0.25	20.8	6.0	4.8	1.2	25.6	0.4	0.0	5.8	0.0	0.0	0.0	6.4	0.2	0.0	25.4	2.4	1.0
Borehole P																				
P422.0	WO.	M.	0.25	26.6	4.2	0.4	0.0	37.8	0.4	0.0	3.4	0.0	0.0	0.2	3.8	0.0	0.0	12.2	11.0	0.0
P444.7	WO.	M.	0.25	14.4	2.0	0.0	0.0	47.4	0.0	0.0	1.8	0.0	0.4	0.2	14.0	0.0	0.0	12.6	7.2	0.0
Borehole Q																				
Q419.9	SC.	M.	0.55	53.4	5.4	0.2	0.0	16.8	0.0	0.0	3.4	0.0	0.0	0.2	1.0	0.0	0.0	7.2	12.4	0.0
Q423.0	WO.	P.	0.35	29.4	5.8	0.0	0.0	34.2	0.2	0.0	3.8	0.0	0.0	0.0	5.0	0.2	0.0	14.2	7.2	0.0
Q440.7	WO.	M.	0.40	31.4	4.0	0.2	0.0	29.6	0.4	0.0	2.6	0.0	0.0	0.0	13.8	0.2	0.0	10.8	7.0	0.0
Q455.2	WO.	M.	0.13	18.2	4.0	0.6	0.2	36.8	0.8	0.0	2.4	0.0	0.0	0.0	12.0	0.0	0.0	21.0	4.0	0.0

SN	OU	SO	GS	QM	QP	KF	PL	IR	MR	SR	CH	MI	OX	HM	CC	CR	QO	CL	VØ	SØ
Borehole R																				
R071.2	WO.	P.	0.25	50.0	2.6	0.0	0.0	21.8	0.0	0.0	0.2	0.0	0.0	0.0	0.0	0.0	0.0	18.2	6.6	0.6
R090.2	WO.	P.	0.28	42.8	5.8	0.0	0.0	26.0	0.0	0.0	3.0	0.0	0.0	0.0	0.6	0.0	0.0	13.0	8.4	0.4
R118.2	WO.	P.	0.25	36.0	5.4	0.2	0.0	30.4	0.0	0.0	3.8	0.0	0.0	0.0	0.0	0.0	0.0	17.6	6.0	0.6
Borehole S																				
S446.6	SC.	M.	0.30	11.6	4.0	0.6	0.2	42.8	0.8	0.4	7.2	0.0	0.0	0.0	6.6	0.2	0.0	19.0	5.4	1.2
S484.1	SC.	M.	0.35	24.0	4.4	0.4	0.4	36.4	1.0	0.0	4.6	0.0	0.2	0.0	6.8	0.8	0.0	18.4	2.6	0.0
S504.4	SC.	P.	0.35	19.4	7.0	0.2	0.4	43.0	0.6	0.0	5.6	0.0	0.0	0.0	6.0	0.4	0.0	15.2	1.8	0.4
S522.8	SC.	P.	0.30	31.0	4.4	1.2	1.0	33.0	0.6	0.0	2.4	0.0	0.0	0.0	3.6	0.2	0.0	17.2	4.0	1.4
S557.0	WO.	M.	0.28	29.6	3.0	1.4	0.4	32.2	0.0	0.0	2.4	0.0	0.2	0.0	7.8	0.2	0.0	20.0	2.2	0.6
S575.1	WO.	P.	0.25	31.0	3.4	2.0	0.2	26.2	0.0	0.0	3.6	0.0	0.0	0.0	8.0	0.8	0.2	21.6	2.8	0.2
S598.9	WO.	P.	0.35	13.6	3.4	1.8	0.8	47.6	0.6	0.0	3.4	0.0	0.0	0.0	8.8	0.0	0.0	15.8	4.2	0.0
S629.3	WO.	P.	0.40	24.6	2.8	1.0	1.2	37.0	0.2	0.0	1.2	0.0	0.2	0.0	4.8	0.0	0.4	21.4	5.0	0.2
S652.8	WO.	P.	0.30	20.8	5.0	2.6	1.2	42.2	0.2	0.0	3.0	0.2	0.4	0.0	1.4	0.0	0.0	21.2	1.6	0.2
Borehole T																				
T320.5	SC.	P.	0.25	64.4	3.6	0.0	0.0	8.4	0.0	0.0	0.4	0.0	0.0	0.0	0.0	0.0	0.4	12.0	10.4	0.4
T344.4	WO.	P.	0.35	63.0	3.8	0.0	0.0	11.2	0.0	0.0	1.2	0.0	0.0	0.0	0.4	0.0	0.0	10.2	9.8	0.4
T365.4	WO.	M.	0.35	65.4	3.0	0.0	0.0	10.6	0.0	0.0	0.8	0.0	0.0	0.0	0.8	0.0	0.0	9.2	9.8	0.4
T397.6	WO.	P.	1.00	63.4	8.6	0.0	0.0	4.8	0.2	0.0	0.4	0.0	0.0	0.0	2.6	0.4	0.0	9.0	10.6	0.0
T419.0	WO.	M.	0.25	46.2	5.8	0.2	0.0	17.4	0.0	0.0	3.2	0.0	0.0	0.0	2.4	0.0	0.0	13.8	10.8	0.2
T434.9	WO.	M.	0.23	34.8	5.2	0.6	0.0	26.8	0.2	0.0	3.2	0.0	0.0	0.0	12.0	0.0	0.0	13.8	3.4	0.0
Borehole U																				
U113.1	SC.	M.	0.25	24.8	3.4	2.4	1.2	37.8	0.0	0.0	2.2	0.2	0.0	0.0	5.2	0.2	0.0	19.0	3.4	0.2
U149.5	SC.	M.	0.13	37.6	3.0	1.4	0.2	22.0	0.0	0.0	1.8	0.2	0.4	0.0	4.8	0.0	0.0	25.4	3.2	0.0
U191.5	SC.	M.	0.25	31.6	1.0	2.0	1.4	34.2	0.0	0.0	2.0	0.0	0.4	0.0	2.2	0.2	0.0	20.8	4.0	0.2
U215.5	WO.	P.	0.30	25.2	4.6	2.6	2.2	44.0	0.0	0.0	1.4	0.0	0.0	0.0	3.4	0.2	0.0	14.2	1.8	0.4
U240.8	WO.	P.	0.25	25.2	3.4	3.4	1.4	35.0	0.0	0.0	0.4	0.0	0.0	0.0	0.6	0.0	0.2	26.0	4.2	0.2
U274.6	WO.	P.	0.35	22.8	2.8	1.0	0.8	33.4	0.2	0.0	1.0	0.0	0.2	0.2	19.0	3.6	0.0	10.2	4.2	0.6

SN	OU	SO	GS	QM	QP	KF	PL	IR	MR	SR	CH	MI	OX	HM	CC	CR	QO	CL	VØ	SØ
U326.0	WO.	P.	0.25	23.0	2.8	0.8	0.4	44.4	0.2	0.0	0.4	0.0	0.0	0.2	2.8	0.0	0.0	22.4	2.4	0.2
U345.0	WO.	P.	0.35	31.8	3.2	0.4	0.8	44.8	0.0	0.0	0.8	0.0	0.2	0.0	0.8	0.2	0.0	10.0	6.6	0.4
U388.2	WO.	M.	0.23	18.8	0.4	0.8	1.4	28.8	0.0	0.0	0.0	0.0	0.8	0.0	37.6	6.6	0.0	4.2	0.6	0.0
U454.1	WO.	P.	0.20	24.8	1.6	0.8	3.0	42.6	0.0	0.0	0.0	0.0	0.6	0.0	1.6	0.0	0.0	21.0	4.0	0.0
Borehole V																				
V011.1	WO.	M.	0.25	22.2	2.8	0.0	0.2	45.4	0.4	0.0	0.0	0.0	6.4	0.0	1.4	0.2	0.0	17.8	2.2	1.0
V031.8	WO.	P.	0.28	18.0	1.4	2.2	1.0	42.6	1.2	0.0	0.6	0.0	0.0	0.0	11.0	2.0	0.0	17.2	2.8	0.0
V051.8	WO.	M.	0.13	28.4	0.2	0.6	1.0	26.8	0.2	0.0	0.8	0.0	2.0	0.0	19.6	0.0	0.0	18.2	1.8	0.4

SN	OU	SO	GS	QM	QP	KF	PL	IR	MR	SR	CH	MI	OX	HM	CA	CL	VØ	SØ
Borehole W																		
W180.1	BH.	W.	0.18	58.4	1.6	0.4	0.0	14.4	0.0	0.4	0.0	1.2	0.2	0.0	5.0	16.6	1.8	0.0
W209.8	BH.	VP.	1.30	67.2	16.0	0.0	0.0	0.4	0.0	0.0	0.0	0.0	0.0	0.0	0.0	9.8	6.4	0.2
W210.3	BH.	M.	1.20	68.2	9.8	0.0	0.0	1.8	0.0	0.0	0.0	0.0	0.0	0.0	0.2	7.8	12.2	0.0
W222.1	BH.	VP.	0.40	72.2	7.6	0.0	0.0	1.8	0.0	0.0	0.0	0.0	0.0	0.0	0.0	9.6	8.8	0.0
W229.8	BH.	M.	0.23	58.8	4.2	0.2	0.0	12.0	0.0	1.0	0.0	0.6	0.6	0.0	1.6	19.2	1.8	0.0
W243.9	UB.	M.	1.30	58.8	9.4	0.0	0.0	1.4	0.0	0.2	0.0	0.0	5.4	0.0	0.0	13.0	11.4	0.4
W274.6	UB.	W.	0.20	55.2	1.6	0.0	0.0	9.0	0.0	1.4	0.2	0.4	0.0	0.0	5.2	19.0	7.8	0.2
W300.8	UB.	W.	0.25	45.4	4.0	0.0	0.0	9.2	0.0	0.0	0.0	0.0	0.4	0.0	22.4	4.0	10.2	4.4
W304.9	UB.	W.	0.23	58.6	0.0	0.0	0.0	13.0	0.0	0.0	0.0	0.0	0.0	0.6	0.8	22.4	3.2	1.4
W310.4	UB.	W.	0.20	63.4	3.4	0.0	0.0	9.8	0.0	0.0	0.0	0.0	0.6	0.0	1.6	15.0	5.4	0.8
W331.7	UB.	W.	0.15	51.4	1.4	0.0	0.0	20.4	0.0	1.0	0.2	0.4	0.0	0.0	3.4	18.8	2.0	1.0
W349.9	UB.	VP.	0.70	53.8	6.0	0.0	0.0	6.2	0.0	0.0	0.0	0.0	0.8	0.0	0.8	22.8	8.8	0.8
W354.9	LB.	M.	0.95	57.6	18.0	0.0	0.0	2.4	0.0	0.0	0.2	0.0	0.0	0.0	1.4	15.8	4.4	0.2
W359.4	LB.	VP.	1.50	48.8	21.8	0.0	0.0	4.6	0.0	0.0	1.0	0.0	0.0	0.0	2.8	15.2	4.0	1.8
W368.0	LB.	W.	0.35	55.8	3.2	0.2	0.0	11.6	0.0	0.0	0.4	0.2	0.0	0.0	1.6	18.8	8.0	0.2
W388.8	LB.	P.	0.25	22.2	1.8	0.2	0.0	36.4	0.0	0.0	1.8	0.0	0.8	0.0	6.6	25.4	4.8	0.0

SN	OU	SO	GS	QM	QP	KF	PL	IR	MR	SR	CH	MI	OX	HM	CA	CL	VØ	SØ
W396.8	LB.	VP.	1.00	52.8	7.0	0.0	0.0	15.2	0.0	0.0	1.0	0.0	0.0	0.0	0.6	15.6	4.4	3.4
W430.8	SC.	P.	0.75	59.2	4.0	0.0	0.0	11.6	0.0	0.0	2.4	0.0	0.0	0.0	0.8	13.2	8.6	0.2
W455.6	SC.	VP.	0.25	31.4	4.6	0.0	0.0	25.2	0.0	0.0	2.8	1.4	0.0	0.0	6.4	23.6	4.4	0.2
W470.1	SC.	P.	0.45	40.6	5.6	0.0	0.0	17.0	0.0	0.6	3.8	0.4	0.0	0.0	1.8	18.6	11.4	0.2
W479.8	WO.	M.	0.20	35.4	4.2	0.0	0.0	26.6	0.0	1.2	3.2	0.6	0.0	0.0	1.0	23.4	3.4	1.0
W493.9	WO.	M.	0.50	51.2	2.6	0.0	0.0	18.4	0.0	0.2	3.6	0.0	0.0	0.0	1.0	13.8	9.2	0.0
W515.6	WO.	W.	0.35	27.6	2.0	0.4	0.2	40.8	0.0	0.0	2.6	0.0	0.0	0.6	0.2	18.6	7.0	0.0
Borehole X																		
X281.3	BH.	P.	0.35	73.2	3.0	0.0	0.0	3.8	0.0	0.0	0.2	1.2	0.4	0.0	3.6	12.4	0.8	1.4
X282.0	BH.	M.	0.45	66.8	4.0	0.0	0.0	1.0	0.0	0.0	0.4	0.2	0.0	0.0	4.2	11.2	2.2	10.0
X296.6	BH.	VP.	0.65	68.2	10.0	0.0	0.0	0.8	0.0	0.0	0.2	0.4	0.0	0.2	1.8	6.4	9.8	2.2
X297.7	BH.	M.	0.30	73.2	7.2	0.0	0.0	3.0	0.0	0.0	0.0	0.2	0.0	0.0	1.0	10.0	5.2	0.2
X309.3	BH.	M.	0.75	63.0	5.8	0.2	0.0	3.8	0.0	0.0	0.0	0.0	0.0	0.0	4.2	17.4	2.0	3.6
X336.1	UB.	W.	0.18	54.2	2.8	0.6	0.0	17.0	0.0	0.0	1.8	0.0	0.0	0.0	2.8	11.0	6.2	3.4
X365.6	UB.	W.	0.25	63.2	1.2	0.4	0.2	12.8	0.0	0.4	0.2	0.2	0.0	0.0	4.2	11.8	4.0	1.4
X386.8	UB.	W.	0.25	57.6	1.8	0.2	0.0	18.2	0.0	0.0	0.0	0.4	0.0	0.0	4.0	12.8	4.2	0.8
X436.6	UB.	VP.	0.45	61.0	2.2	0.0	0.0	8.2	0.0	0.0	0.2	0.2	0.0	0.0	0.6	12.6	4.0	11.0
X458.9	LB.	VP.	0.35	52.0	2.4	0.2	0.0	20.8	0.0	0.0	0.6	0.6	0.6	0.0	3.0	16.8	3.0	0.0
X473.1	LB.	W.	0.45	62.8	2.8	0.0	0.0	11.2	0.0	0.2	3.0	0.0	0.0	0.2	1.4	10.0	8.0	0.4
X476.2	LB.	VP.	1.15	46.4	23.2	0.0	0.0	8.2	0.0	0.0	1.0	0.0	0.0	0.0	0.4	14.8	5.8	0.2
X490.9	LB.	P.	1.00	56.8	6.4	0.0	0.0	16.4	0.4	0.0	1.8	0.0	0.2	0.0	4.2	3.8	9.0	1.0
X508.2	LB.	M.	0.45	61.0	7.4	0.0	0.0	14.6	0.0	0.0	1.4	0.4	0.0	0.0	2.4	6.8	4.8	1.2
X525.8	SC.	VP.	1.50	60.0	7.8	0.0	0.0	9.6	0.0	0.0	0.8	0.0	0.0	0.0	3.0	12.6	4.6	1.6
X528.7	SC.	M.	0.45	66.6	2.2	0.2	0.0	10.8	0.0	0.0	1.0	0.6	0.0	0.0	2.4	10.4	5.0	0.8
X530.7	SC.	VP.	0.40	63.2	5.4	0.2	0.0	17.4	0.0	0.0	0.6	0.0	0.0	0.0	4.2	7.8	1.2	0.0
X531.9	SC.	P.	0.50	63.2	5.8	0.2	0.0	11.0	0.0	0.0	1.4	0.0	0.0	0.0	12.2	2.2	3.6	0.4
X559.4	SC.	W.	0.25	30.0	5.2	0.4	0.0	21.4	0.0	0.0	6.8	0.0	0.0	0.2	6.4	16.6	12.4	0.6

SN	OU	SO	GS	QM	QP	KF	PL	IR	MR	SR	CH	MI	OX	HM	CA	CL	VØ	SØ
X588.5	SC.	W.	0.35	36.6	3.4	0.0	0.0	26.0	0.0	0.0	4.6	0.0	0.2	0.0	4.2	13.8	11.0	0.2
X612.9	WO.	M.	0.40	34.4	4.4	0.0	0.0	20.8	0.0	0.0	5.2	0.8	0.0	0.0	9.2	15.4	9.8	0.0
X640.0	WO.	VP.	0.25	9.0	4.0	0.4	0.4	42.6	0.0	0.0	5.8	0.0	0.0	0.0	6.4	25.2	6.0	0.2
X675.5	WO.	W.	0.30	26.8	3.8	0.2	0.2	28.4	0.0	0.0	1.6	0.0	0.0	0.0	16.6	14.8	7.6	0.0
Borehole Y																		
Y377.5	BH.	M.	0.45	72.0	1.2	0.0	0.0	6.0	0.0	0.0	0.4	0.2	0.2	0.0	4.2	7.0	8.4	0.4
Y397.6	UB.	M.	0.23	68.6	1.4	0.0	0.0	7.0	0.0	0.0	0.0	0.2	0.2	0.2	4.6	10.8	3.2	3.8
Y429.0	UB.	W.	0.23	64.0	1.2	0.0	0.0	21.0	0.0	0.0	0.6	0.0	0.0	0.0	0.2	9.2	3.0	0.8
Y468.5	UB.	W.	0.28	66.8	2.8	0.0	0.0	15.4	0.0	0.0	0.2	0.0	0.0	0.2	1.6	6.6	4.4	2.0
Y486.5	LB.	W.	0.23	60.2	0.6	0.0	0.0	22.4	0.0	0.0	0.0	0.2	0.0	0.0	2.4	10.8	3.0	0.4
Y501.8	LB.	M.	0.18	54.2	1.8	0.0	0.0	19.2	0.0	0.0	0.4	0.4	0.4	0.6	4.4	17.2	1.4	0.0
Y515.3	LB.	W.	0.25	53.6	2.0	0.0	0.0	25.0	0.0	0.0	0.4	0.0	0.0	0.0	3.0	12.8	1.6	1.6
Y549.1	LB.	W.	0.45	61.4	2.8	0.0	0.0	14.6	0.0	0.0	0.6	0.0	0.0	0.0	3.0	10.6	6.6	0.4
Y566.1	LB.	W.	0.15	47.2	1.6	0.0	0.0	18.2	0.0	0.0	0.8	0.8	0.4	0.0	7.4	18.0	5.4	0.2
Y593.9	SC.	W.	0.28	55.2	2.2	0.0	0.0	20.0	0.0	0.0	1.0	0.2	0.2	0.0	2.2	13.0	4.4	1.6
Y624.7	SC.	M.	0.35	28.4	4.0	0.0	0.0	40.0	0.0	0.0	4.8	0.0	0.2	0.0	5.2	12.6	4.6	0.2
Y642.2	SC.	W.	0.35	22.4	4.4	0.0	0.0	38.8	0.0	0.0	4.8	0.0	0.0	0.0	12.0	11.2	6.4	0.0
Y672.9	WO.	M.	0.38	33.0	2.4	0.6	0.2	39.6	0.0	0.0	2.4	0.0	0.2	0.0	6.8	9.8	4.8	0.2
Y690.1	WO.	W.	0.90	44.8	9.8	0.0	0.0	24.2	0.0	0.0	3.2	0.0	0.0	0.0	1.4	5.6	11.0	0.0
Y727.4	WO.	W.	0.25	14.6	4.2	0.8	0.4	46.6	0.0	0.0	5.6	0.6	0.2	0.0	10.8	14.4	1.8	0.0
Y757.9	WO.	P.	0.25	25.6	3.4	0.2	0.0	42.2	0.0	0.0	1.6	0.0	0.0	0.0	8.6	13.6	4.4	0.4
Borehole Z																		
Z378.2	BH.	P.	0.50	61.6	6.2	0.0	0.0	7.6	0.4	0.0	1.0	0.2	0.0	0.0	15.8	2.2	2.6	2.4
Z399.0	UB.	P.	0.40	64.4	4.6	0.0	0.0	5.0	0.8	0.0	0.4	0.0	0.0	0.0	5.2	4.4	4.8	10.4
Z402.9	UB.	W.	0.23	61.2	2.0	0.0	0.0	11.2	0.0	0.0	2.8	0.0	0.0	0.2	4.8	7.0	5.8	5.0
Z422.6	UB.	W.	0.18	57.8	0.2	0.0	0.0	17.2	0.0	0.0	0.8	1.0	0.0	0.2	5.4	8.8	6.4	2.2
Z444.2	UB.	M.	0.18	53.8	0.8	0.0	0.0	23.0	0.0	0.0	1.0	0.2	0.8	0.0	4.8	9.4	4.8	1.4
Z499.0	UB.	W.	0.23	52.8	2.0	0.0	0.0	23.4	0.0	0.0	0.6	0.2	0.2	0.0	1.8	15.8	2.0	1.2

SN	OU	SO	GS	QM	QP	KF	PL	IR	MR	SR	CH	MI	OX	HM	CA	CL	VØ	SØ
Z512.4	LB.	W.	0.28	58.2	2.4	0.0	0.0	19.8	0.0	0.0	0.2	0.0	1.2	0.0	4.0	8.0	4.2	2.0
Z531.9	LB.	M.	0.28	61.4	1.0	0.0	0.0	17.8	0.0	0.0	0.2	0.4	0.0	0.2	3.6	10.2	2.4	2.8
Z593.0	SC.	M.	0.45	47.0	3.0	0.0	0.0	27.0	0.0	0.0	3.0	0.2	0.2	0.0	4.6	11.0	3.8	0.2
Z611.3	SC.	W.	0.15	19.6	2.2	0.0	0.0	47.0	0.0	0.0	2.6	1.0	0.4	0.0	13.4	12.6	0.8	0.0
Z632.7	SC.	M.	0.40	8.8	4.4	0.0	0.0	49.2	0.0	0.0	6.6	0.0	0.4	0.0	18.8	8.8	2.2	0.0
Z656.8	SC.	W.	0.35	13.6	3.8	0.6	0.4	51.4	0.0	0.0	7.8	0.0	0.4	0.0	9.4	11.8	0.8	0.0
Z679.4	WO.	M.	0.45	48.0	5.6	0.4	0.0	26.2	0.0	0.0	0.4	0.0	0.6	0.0	5.0	9.8	4.0	0.0
Z700.2	WO.	P.	0.35	42.8	5.0	0.2	0.2	26.8	0.0	0.0	1.8	0.0	0.0	0.0	2.6	3.2	17.4	0.0
Z703.3	WO.	M.	0.23	41.2	3.8	0.4	0.0	28.4	0.0	0.8	1.8	0.2	0.4	0.0	4.6	16.8	1.6	0.0
Z740.4	WO.	W.	0.28	31.2	3.4	0.8	0.4	28.2	0.2	0.0	3.6	0.0	0.2	0.0	10.8	10.4	9.0	1.8
Z763.8	WO.	M.	0.40	23.0	5.8	0.0	0.0	41.6	0.0	0.0	3.4	0.0	0.2	0.0	8.6	15.6	1.8	0.0

Note:

The abbreviations used in reporting the results are as follows:

SN = sample number, OU = operational unit, SO = estimated sorting, GS = average grain size (mm), QM = monocrystalline quartz, QP = polycrystalline quartz, KF = potassium feldspar, PL = plagioclase, IR = igneous rock fragments, MR = metamorphic rock fragments, SR = sedimentary rock fragments, CH = chert, MI = mica, OX = oxides, HM = heavy minerals, CC = carbonate cement, CR = carbonate replacement, CA = carbonate, QO = quartz overgrowths (* mega-quartz crystals, not overgrowths), CL = clay matrix, VØ = visual porosity, SØ = secondary porosity.

W. = well sorted, M. = moderately sorted, P. = poorly sorted, VP. = very poorly sorted, BH. = Bald Hill Operational Unit, UB. = Upper Bulgo, LB. = Lower Bulgo, SC. = Scarborough, and WO. = Wombarra.

APPENDIX IV - RECALCULATED PERCENTAGE FOR INDIVIDUAL DETRITAL CLASTS

SN	OU	SO	GS	QM	QP	FD	RF	CH	SN	OU	SO	GS	QM	QP	FD	RF	CH
Borehole A																	
A146.5	UB.	W.	0.20	66.1	4.6	0.0	27.9	1.4	A247.1	SC.	VP.	1.80	43.5	17.4	0.5	21.5	17.1
A163.1	UB.	M.	0.25	66.7	2.3	1.3	22.6	7.1	A260.8	SC.	M.	0.35	33.9	10.0	5.5	39.3	11.3
A184.3	UB.	W.	0.20	67.5	4.7	0.5	23.7	3.6	A295.6	SC.	M.	0.20	16.2	8.6	3.0	56.3	15.9
A198.3	UB.	W.	0.25	63.2	5.9	0.0	26.0	4.9	A313.5	SC.	P.	0.40	38.5	7.3	6.4	37.7	10.1
A211.4	LB.	M.	0.35	62.0	5.9	1.1	25.4	5.6	A326.8	SC.	VP.	0.20	30.3	7.8	5.4	48.4	8.1
A225.8	LB.	P.	0.25	72.8	7.4	0.3	18.7	0.8									
Borehole B																	
B124.0	UB.	M.	0.15	56.5	7.3	3.7	26.0	6.5	B259.2	LB.	P.	0.38	32.7	7.3	2.8	49.7	7.5
B151.7	UB.	M.	0.25	57.2	6.8	1.9	25.9	8.2	B277.9	LB.	P.	0.28	36.8	9.6	5.4	38.9	9.3
B161.0	UB.	M.	0.20	45.0	6.8	6.2	31.1	10.9	B338.0	SC.	P.	0.43	9.0	2.6	6.4	59.1	22.9
B175.5	UB.	M.	0.25	37.2	4.9	6.8	41.0	10.1	B361.6	WO	W.	0.25	17.1	3.3	4.1	54.5	21.0
B200.1	UB.	P.	0.20	27.6	6.2	5.4	49.7	11.1	B394.4	WO	W.	0.15	19.7	4.9	5.3	46.9	23.2
B234.7	LB.	W.	0.25	55.7	4.5	3.7	31.0	5.1	B406.2	WO	W.	0.40	5.8	3.9	4.2	62.7	23.4
B239.9	LB.	M.	0.25	50.4	7.0	5.7	32.6	4.3									
Borehole C																	
C066.0	UB.	P.	0.25	52.0	7.2	2.2	28.7	9.9	C132.6	SC.	W.	0.25	23.2	10.3	4.9	49.9	11.7
C081.1	LB.	M.	0.25	54.4	5.8	1.6	32.4	5.8	C191.5	SC.	M.	0.35	16.6	5.5	6.1	50.2	21.6
C089.4	LB.	P.	1.00	59.8	8.8	0.8	23.4	7.2	C215.8	WO	W.	0.35	14.2	9.9	2.9	59.9	13.1
C101.6	LB.	M.	0.35	42.2	8.7	2.7	37.7	8.7	C259.6	WO	M.	0.25	25.0	8.0	4.3	47.6	15.1
C119.9	LB.	P.	0.25	18.0	12.0	1.9	34.4	11.7									
Borehole D																	
D047.1	SC.	M.	0.15	26.6	8.5	12.1	46.6	6.2	D145.3	SC.	W.	0.50	62.6	5.8	5.1	25.2	1.3
D053.9	SC.	M.	0.28	57.0	8.1	10.4	21.9	2.6	D164.9	SC.	P.	0.35	51.1	6.0	7.9	33.5	1.5
D078.4	SC.	M.	0.25	58.1	3.6	12.6	24.3	1.4	D236.0	WO	M.	0.35	15.0	6.0	1.6	65.4	12.0
D102.5	SC.	W.	0.28	54.8	4.7	10.5	29.4	0.6	D257.5	WO	M.	0.30	38.7	7.4	2.3	48.0	3.6

SN	OU	SO	GS	QM	QP	FD	RF	CH	SN	OU	SO	GS	QM	QP	FD	RF	CH
D117.2	SC.	VP.	0.30	60.2	2.7	10.0	21.6	5.5	D295.9	WO	M.	0.20	53.0	4.2	5.4	36.0	1.4
Borehole E																	
E118.5	SC.	M.	0.25	31.1	6.6	6.6	50.9	4.8	E254.9	WO	P.	0.50	41.1	3.5	8.4	45.0	2.0
E128.0	SC.	W.	0.30	54.1	6.6	7.5	31.1	0.7	E268.9	WO	M.	0.35	8.1	7.0	2.6	66.6	15.7
E142.6	SC.	M.	0.23	55.5	4.6	8.9	29.9	1.1	E282.8	WO	M.	0.40	29.5	5.9	4.8	54.8	5.0
E155.3	SC.	M.	0.20	32.6	5.7	9.6	47.6	4.5	E312.5	WO	M.	0.35	22.0	6.0	3.8	54.9	13.3
E185.9	SC.	M.	0.40	50.0	5.2	4.2	31.8	8.8	E325.0	WO	P.	0.40	45.1	5.8	5.0	39.0	5.1
E212.3	SC.	P.	0.45	36.5	6.1	5.8	45.8	5.8	E344.1	WO	P.	0.35	46.2	6.1	7.7	39.2	0.8
E243.6	SC.	M.	0.40	52.1	4.9	3.4	37.0	2.6	E363.6	WO	P.	0.30	75.5	4.4	3.9	15.4	0.8
Borehole F																	
F066.5	BH.	M.	0.30	53.8	8.7	3.7	27.3	6.5	F423.4	SC.	M.	0.60	27.8	10.4	2.6	52.2	7.0
F099.4	BH.	VP.	0.35	74.3	8.0	0.8	16.6	0.3	F437.8	SC.	M.	0.18	30.1	5.5	6.1	55.3	3.0
F113.9	UB.	M.	0.18	48.1	4.6	2.4	39.4	5.5	F470.4	SC.	M.	0.45	41.3	4.9	0.8	48.6	4.4
F158.3	UB.	VP.	0.30	59.0	4.1	0.9	32.3	3.8	F491.5	SC.	P.	0.28	55.0	4.7	0.9	36.4	3.0
F179.4	UB.	W.	0.30	75.4	5.4	1.5	17.0	0.7	F525.8	SC.	P.	0.40	35.5	4.0	4.8	52.0	3.7
F194.0	UB.	W.	0.35	57.4	6.4	0.0	32.8	3.4	F563.0	SC.	M.	0.35	41.6	4.3	0.9	49.2	4.0
F236.7	UB.	M.	0.23	44.2	7.8	1.8	37.7	8.5	F586.2	WO.	P.	0.40	17.2	5.9	1.2	65.1	10.6
F259.3	UB.	M.	0.28	35.5	4.8	0.6	47.4	11.7	F616.7	WO	P.	0.20	54.7	4.7	3.7	33.2	3.7
F286.9	LB.	M.	0.18	45.3	4.7	3.9	38.7	7.4	F649.2	WO.	M.	0.40	43.7	4.2	1.2	43.7	7.2
F311.1	LB.	M.	0.15	40.1	4.7	9.1	42.8	3.3	F687.3	WO.	P.	0.30	49.2	5.3	2.2	41.9	1.4
F349.3	LB.	M.	0.25	37.4	4.6	4.6	47.0	6.4	F734.9	WO.	M.	0.20	62.5	7.0	2.8	27.4	0.3
F379.3	LB.	M.	0.28	40.7	3.8	7.3	43.9	4.3	F751.7	WO.	M.	0.35	31.0	3.6	4.5	59.4	1.5
F396.5	LB.	M.	0.30	40.1	8.4	4.3	39.6	7.6									
Borehole G																	
G540.4	WO.	W.	0.28	15.3	6.4	1.8	66.5	10	G577.7	WO	M.	0.45	38.4	8.9	0.5	45.4	6.8
G553.8	WO.	W.	0.30	31.9	7.7	1.9	51.9	6.6									

SN	OU	SO	GS	QM	QP	FD	RF	CH	SN	OU	SO	GS	QM	QP	FD	RF	CH
Borehole H																	
H319.0	UB.	M.	0.40	56.6	7.9	0.3	27.6	7.6	H516.2	SC.	M.	0.50	36.0	6.3	1.7	50.6	5.4
H342.5	LB.	M.	0.30	50.9	6.5	0.8	38.1	3.7	H535.1	SC.	VP.	0.40	23.9	4.6	3.7	58.3	9.5
H360.6	LB.	M.	0.13	61.7	2.7	1.2	32.3	2.1	H568.7	SC.	M.	0.28	14.1	4.8	5.1	64.1	11.9
H397.6	LB.	M.	1.20	50.5	10.5	0.0	33.2	5.8	H597.9	WO	W.	0.25	49.1	4.1	9.3	34.2	3.3
H419.7	LB.	M.	0.65	70.1	7.1	0.5	18.9	3.4	H625.4	WO	P.	0.35	34.6	5.1	7.3	49.1	3.9
H436.1	SC.	M.	0.25	58.4	6.7	0.0	31.0	3.9	H667.2	WO	P.	0.40	32.0	5.4	4.9	53.4	4.3
H454.9	SC.	M.	0.25	63.4	4.5	0.8	28.1	3.2	H681.2	WO	W.	0.25	31.7	4.8	9.2	52.4	1.9
H470.0	SC.	M.	0.25	42.0	6.9	2.2	42.4	6.5	H691.5	WO	P.	0.20	25.6	3.1	8.4	57.7	5.2
H504.7	SC.	M.	0.15	26.5	9.2	3.9	51.6	8.8									
Borehole I																	
I320.1	BH.	W.	0.20	55.1	3.2	6.1	33.0	2.6	I610.7	LB.	W.	0.15	34.4	8.3	10.0	41.0	6.3
I356.0	BH.	W.	0.30	69.2	4.3	1.9	23.0	1.6	I629.3	SC.	M.	0.35	60.8	5.1	3.7	27.5	2.9
I378.5	UB.	W.	0.30	65.9	3.5	0.3	24.8	2.1	I635.9	SC.	W.	0.23	61.1	3.7	8.1	25.4	1.7
I382.9	UB.	M.	0.30	68.2	3.6	0.3	25.7	2.2	I698.2	SC.	M.	0.30	44.3	2.0	9.0	42.7	2.0
I402.1	UB.	W.	0.25	47.9	11.4	3.6	34.2	2.5	I732.0	SC.	P.	0.28	30.3	5.3	8.2	53.9	2.3
I437.4	UB.	W.	0.20	51.5	7.4	9.0	30.2	1.9	I769.6	WO	W.	0.35	7.6	5.1	1.5	66.5	19.3
I465.6	UB.	W.	0.18	46.5	4.8	10.2	34.4	4.1	I781.5	WO	P.	0.40	43.0	3.0	5.0	43.0	6.0
I481.7	UB.	M.	0.25	28.3	6.9	13.0	47.4	4.4	I806.9	WO	M.	0.30	11.8	7.6	5.4	67.0	8.2
I543.4	LB.	W.	0.25	30.4	8.8	6.0	51.1	3.7	I830.4	WO	M.	0.40	46.1	5.1	7.9	38.8	2.1
I564.1	LB.	M.	0.15	37.0	6.1	12.8	40.3	3.8	I879.9	WO	W.	0.18	14.9	2.1	7.9	70.2	4.9
I572.0	LB.	M.	0.25	41.5	9.2	8.4	37.8	3.1	I884.4	WO	W.	0.20	18.5	6.3	2.0	70.2	3.0
I596.6	LB.	W.	0.25	41.1	5.8	12.6	38.9	1.6	I902.6	WO	P.	0.20	47.0	6.0	8.8	36.9	1.3
Borehole J																	
J470.1	SC.	P.	0.40	42.9	12.2	4.2	32.8	7.9	J585.4	SC.	M.	0.23	14.7	6.1	6.6	53.1	19.5
J481.6	SC.	M.	0.50	35.0	8.3	6.0	37.7	13	J599.9	WO	M.	0.25	14.9	5.0	4.1	62.1	13.9

SN	OU	SO	GS	QM	QP	FD	RF	CH	SN	OU	SO	GS	QM	QP	FD	RF	CH
J501.2	SC.	M.	0.35	22.8	3.0	9.8	32.3	23.1	J620.8	WO	M.	0.23	13.8	5.0	5.2	56.9	19.1
J514.8	SC.	M.	0.35	31.7	8.5	9.0	41.2	9.6	J650.3	WO.	P.	0.25	7.9	1.4	1.9	83.7	5.1
J545.2	SC.	W.	0.20	14.4	5.6	8.7	57.5	13.8	J672.3	WO	P.	0.15	27.5	3.0	3.8	53.4	12.3
J570.1	SC.	M.	0.20	3.7	2.7	4.5	82.8	3.3									
Borehole K																	
K030.7	WO.	P.	1.50	4.2	2.7	0.0	87.2	5.9	K073.4	WO	M.	0.35	5.5	2.2	0.3	88.1	4.9
K057.3	WO.	P.	1.40	4.5	2.1	0.8	78.4	14.2									
Borehole L																	
L346.2	UB.	M.	0.30	70.0	4.6	1.0	19.8	4.6	L579.2	SC.	W.	0.25	19.7	6.6	21.4	43.5	8.8
L355.3	UB.	M.	0.20	38.1	5.6	13.4	37.0	5.9	L595.2	SC.	P.	0.50	26.9	8.5	13.3	32.3	19.0
L361.8	UB.	W.	0.25	68.1	6.1	1.0	23.0	1.8	L604.3	SC.	M.	0.30	16.4	7.6	17.0	44.4	14.6
L386.0	UB.	M.	0.25	66.1	5.0	1.7	23.3	3.9	L621.0	SC.	M.	0.25	15.1	6.7	12.2	50.6	15.4
L406.8	UB.	M.	0.20	67.5	7.0	0.9	21.4	3.2	L638.9	SC.	M.	0.40	10.2	5.7	9.7	59.4	15.0
L415.3	UB.	M.	0.25	74.0	6.3	1.5	16.4	1.8	L644.7	SC.	M.	0.25	15.5	4.7	9.1	48.5	22.2
L434.7	UB.	W.	0.25	62.2	6.3	2.9	25.2	3.4	L653.5	SC.	W.	0.20	12.2	4.7	8.0	55.8	19.3
L452.1	LB.	M.	0.35	71.5	6.7	2.5	16.6	2.7	L681.8	WO.	P.	0.50	47.3	13.2	1.6	28.9	16.8
L506.7	LB.	M.	0.40	69.1	5.7	1.9	18.7	4.6	L717.8	WO.	P.	0.55	10.0	3.6	5.1	60.4	17.8
L518.3	LB.	M.	0.50	48.8	8.0	6.2	31.0	6	L732.1	WO.	M.	0.30	21.7	7.1	3.1	51.3	16.8
L532.9	SC.	M.	0.25	38.0	7.5	5.0	38.9	10.6	L746.2	WO	M.	0.40	21.6	8.0	2.9	55.9	11.6
L547.6	SC.	M.	0.60	69.0	7.5	0.2	19.8	3.5	L759.9	WO.	VP.	0.80	25.4	14.1	0.6	44.8	15.1
L571.0	SC.	P.	0.65	36.0	6.3	11.9	28.8	17									
Borehole M																	
M094.1	BH.	M.	0.20	54.1	5.0	5.9	31.6	3.4	M402.9	SC.	M.	0.30	53.1	6.1	4.3	28.6	7.9
M132.9	UB.	M.	0.35	43.7	8.1	1.3	36.9	10	M420.8	SC.	M.	0.13	37.2	5.0	18.0	36.0	3.8
M149.6	UB.	M.	0.18	36.8	9.0	7.4	40.5	6.3	M440.0	SC.	M.	0.30	36.1	9.7	5.8	29.2	19.2
M192.6	UB.	M.	0.20	36.3	9.5	9.1	37.5	7.6	M458.8	SC.	P.	0.23	36.8	8.9	5.9	31.4	17.0

SN	OU	SO	GS	QM	QP	FD	RF	CH	SN	OU	SO	GS	QM	QP	FD	RF	CH
M209.9	UB.	W.	0.18	47.6	13.4	9.2	23.0	6.8	M486.6	WO.	M.	0.40	39.1	6.3	4.2	41.7	8.7
M228.0	LB.	M.	0.20	42.9	6.0	11.8	33.5	5.8	M492.2	WO	M.	0.30	32.1	7.6	4.6	46.3	9.4
M281.0	LB.	W.	0.30	31.2	16.6	5.6	37.8	8.8	M506.0	WO.	M.	0.40	21.5	5.6	2.1	49.0	21.8
M308.7	LB.	M.	0.13	45.5	5.0	12.9	35.4	1.2	M528.5	WO.	M.	0.28	13.6	5.1	4.7	53.2	23.4
M341.8	SC.	M.	0.20	31.3	4.8	14.2	44.9	4.8	M551.2	WO	M.	0.25	13.5	8.0	3.0	55.2	20.3
M354.0	SC.	M.	0.30	41.4	9.8	9.6	33.1	6.1	M586.4	WO	W.	0.25	14.0	11.2	1.4	55.3	18.1
M369.0	SC.	M.	0.40	34.0	7.7	4.4	40.8	10.1	M605.3	WO	W.	0.23	16	10.2	2.7	46.5	24.6
M381.2	SC.	P.	0.38	50.5	6.1	2.8	34.9	5.7									
Borehole N																	
N161.4	LB.	M.	0.25	74.6	4.3	0.0	19.1	2	N193.1	WO	P.	0.23	26.6	8.9	0.3	47.3	16.9
N184.2	SC.	P.	0.28	57.4	5.9	0.0	31.4	5.3									
Borehole O																	
O296.5	BH.	M.	0.33	92.2	5.9	0.0	1.9	0	O578.4	SC.	M.	0.30	47.4	8.7	4.5	28.8	10.6
O370.0	UB.	W.	0.23	51.7	10.0	1.6	25.9	10.8	O600.9	SC.	M.	0.50	58.6	8.5	5.6	19.4	7.9
O417.4	UB.	W.	0.25	68.3	4.4	0.8	19.7	6.8	O617.7	SC.	M.	0.20	49.8	7.3	4.2	27.2	11.5
O435.2	UB.	M.	0.20	57.0	9.1	1.5	22.2	10.2	O637.4	SC.	W.	0.25	21.5	8.5	6.9	48.3	14.8
O452.9	UB.	W.	0.30	64.0	5.7	1.6	23.8	4.9	O668.5	WO.	M.	0.20	18.8	14.6	7.7	46.7	12.2
O488.2	LB.	M.	0.25	51.7	8.9	1.1	29.4	8.9	O709.5	WO	W.	0.23	21.1	7.3	5.9	50.8	14.9
O512.5	LB.	M.	0.30	75.8	6.7	0.3	13.9	3.3	O745.8	WO.	M.	0.20	16.6	10.2	7.5	43.4	22.3
O538.9	LB.	P.	0.30	54.8	5.1	0.3	24.6	15.2	O755.9	WO	M.	0.25	32.2	9.3	9.3	40.2	9.0
O560.4	SC.	M.	0.25	46.9	9.4	4.3	28.6	10.8									
Borehole P																	
P422.0	WO.	M.	0.25	36.5	5.8	0.5	52.5	4.7	P444.7	WO	M.	0.25	22.0	3.0	0.0	72.3	2.7
Borehole Q																	
Q419.9	SC.	M.	0.55	67.4	6.8	0.3	21.2	4.3	Q440.7	WO.	M.	0.40	46.0	5.9	0.3	44.0	3.8

SN	OU	SO	GS	QM	QP	FD	RF	CH	SN	OU	SO	GS	QM	QP	FD	RF	CH
Q423.0	WO.	P.	0.35	40.0	7.9	0.0	46.9	5.2	Q455.2	WO	M.	0.13	28.9	6.3	1.3	59.7	3.8
Borehole R																	
R071.2	WO.	P.	0.25	67.0	3.5	0.0	29.2	0.3	R118.2	WO	P.	0.25	47.5	7.1	0.3	40.1	5.0
R090.2	WO.	P.	0.28	55.1	7.5	0.0	33.5	3.9									
Borehole S																	
S446.6	SC.	M.	0.30	17.2	5.9	1.2	65.1	10.6	S575.1	WO	P.	0.25	46.7	5.1	3.3	39.5	5.4
S484.1	SC.	M.	0.35	33.7	6.2	1.1	52.5	6.5	S598.9	WO	P.	0.35	19.0	4.8	3.7	67.7	4.8
S504.4	SC.	P.	0.35	25.5	9.2	0.8	57.2	7.3	S629.3	WO	P.	0.40	36.2	4.1	3.2	54.7	1.8
S522.8	SC.	P.	0.30	42.1	6.0	3.0	45.6	3.3	S652.8	WO	P.	0.30	27.7	6.7	5.1	56.5	4.0
S557.0	WO.	M.	0.28	42.9	4.3	2.6	46.7	3.5									
Borehole T																	
T320.5	SC.	P.	0.25	83.9	4.7	0.0	10.9	0.5	T397.6	WO	P.	1.00	81.9	11.1	0.0	6.5	0.5
T344.4	WO.	P.	0.35	79.6	4.8	0.0	14.1	1.5	T419.0	WO.	M.	0.25	63.5	8.0	0.3	23.9	4.4
T365.4	WO.	M.	0.35	81.9	3.8	0.0	13.3	1	T434.9	WO.	M.	0.23	49.3	7.3	0.8	38.1	4.5
Borehole U																	
U113.1	SC.	M.	0.25	34.6	4.7	5.0	52.6	3.1	U274.6	WO	P.	0.35	36.8	4.5	2.9	54.2	1.6
U149.5	SC.	M.	0.13	60.0	4.6	2.4	33.3	2.7	U326.0	WO	P.	0.25	31.9	3.9	1.7	61.9	5.6
U191.5	SC.	M.	0.25	43.7	1.4	4.7	47.4	2.8	U345.0	WO	P.	0.35	38.8	3.9	1.5	54.8	1.0
U215.5	WO.	P.	0.30	31.9	5.8	6.1	55.7	1.8	U388.2	WO	M.	0.23	37.4	0.8	4.4	57.4	0.0
U240.8	WO.	P.	0.25	36.6	4.9	7.0	50.9	0.6	U454.1	WO	P.	0.20	34.1	2.2	5.2	58.5	0.0
Borehole V																	
V011.1	WO.	M.	0.25	31.3	3.9	0.3	64.5	0	V051.8	WO	M.	0.13	48.9	0.3	2.8	46.6	1.4
V031.8	WO.	P.	0.28	26.8	2.1	4.8	65.4	0.9									
Borehole W																	
W180.1	BH.	W.	0.18	77.7	2.1	0.5	19.7	0	W354.9	LB.	M.	0.95	73.6	23.0	0.0	3.1	0.3
W209.8	BH.	VP.	1.30	80.3	19.2	0.0	0.5	0	W359.4	LB.	VP.	1.50	64.1	28.6	0.0	6.0	1.3

SN	OU	SO	GS	QM	QP	FD	RF	CH	SN	OU	SO	GS	QM	QP	FD	RF	CH
W210.3	BH.	M.	1.20	85.5	12.3	0.0	2.2	0	W368.0	LB.	W.	0.35	78.3	4.5	0.3	16.3	0.6
W222.1	BH.	VP.	0.40	88.5	9.3	0.0	2.2	0	W388.8	LB.	P.	0.25	35.6	2.9	0.3	58.3	2.9
W229.8	BH.	M.	0.23	77.2	5.5	0.3	17.0	0	W396.8	LB.	VP.	1.00	69.5	9.2	0.0	20.0	1.3
W243.9	UB.	M.	1.30	84.2	13.5	0.0	2.3	0	W430.8	SC.	P.	0.75	76.7	5.2	0.0	15.0	3.1
W274.6	UB.	W.	0.20	81.9	2.4	0.0	15.4	0.3	W455.6	SC.	VP.	0.25	49.0	7.2	0.0	39.4	4.4
W300.8	UB.	W.	0.25	77.5	6.8	0.0	15.7	0	W470.1	SC.	P.	0.45	60.1	8.3	0.0	26.0	5.6
W304.9	UB.	W.	0.23	81.8	0.0	0.0	18.2	0	W479.8	WO	M.	0.20	50.2	5.9	0.0	39.4	4.5
W310.4	UB.	W.	0.20	82.8	4.4	0.0	12.8	0	W493.9	WO	M.	0.50	67.4	3.4	0.0	24.5	4.7
W331.7	UB.	W.	0.15	69.0	1.9	0.0	28.8	0.3	W515.6	WO	W.	0.35	37.6	2.7	0.8	55.4	3.5
W349.9	UB.	VP.	0.70	81.5	9.1	0.0	9.4	0									
Borehole X																	
X281.3	BH.	P.	0.35	91.3	3.7	0.0	4.7	0.3	X490.9	LB.	P.	1.00	69.5	7.8	0.0	20.5	2.2
X282.0	BH.	M.	0.45	92.5	5.5	0.0	1.4	0.6	X508.2	LB.	M.	0.45	72.3	8.8	0.0	17.3	1.6
X296.6	BH.	VP.	0.65	86.1	12.6	0.0	1.0	0.3	X525.8	SC.	VP.	1.50	76.7	10.0	0.0	12.3	1.0
X297.7	BH.	M.	0.30	87.8	8.6	0.0	3.6	0	X528.7	SC.	M.	0.45	82.4	2.7	0.3	13.4	1.2
X309.3	BH.	M.	0.75	86.5	8.0	0.3	5.2	0	X530.7	SC.	VP.	0.40	72.8	6.2	0.3	20.0	0.7
X336.1	UB.	W.	0.18	70.9	3.7	0.8	22.2	2.4	X531.9	SC.	P.	0.50	77.5	7.1	0.2	13.5	1.7
X365.6	UB.	W.	0.25	80.6	1.5	0.8	16.8	0.3	X559.4	SC.	W.	0.25	47.0	8.2	0.6	33.5	10.7
X386.8	UB.	W.	0.25	74.0	2.3	0.3	23.4	0	X588.5	SC.	W.	0.35	51.8	4.8	0.0	36.8	6.5
X436.6	UB.	VP.	0.45	85.1	3.1	0.0	11.5	0.3	X612.9	WO	M.	0.40	53.1	6.8	0.0	32.1	8.0
X458.9	LB.	VP.	0.35	68.3	3.2	0.3	27.4	0.8	X640.0	WO	VP.	0.25	14.5	6.4	1.3	68.5	9.3
X473.1	LB.	W.	0.45	78.5	3.5	0.0	14.2	3.8	X675.5	WO	W.	0.30	43.9	6.2	0.7	46.6	2.6
X476.2	LB.	VP.	1.15	58.9	29.4	0.0	10.4	1.3									
Borehole Y																	
Y377.5	BH.	M.	0.45	90.5	1.5	0.0	7.5	0.5	Y566.1	LB.	W.	0.15	69.6	2.4	0.0	26.8	1.2
Y397.6	UB.	M.	0.23	89.1	1.8	0.0	9.1	0	Y593.9	SC.	W.	0.28	70.4	2.8	0.0	25.5	1.3

SN	OU	SO	GS	QM	QP	FD	RF	CH	SN	OU	SO	GS	QM	QP	FD	RF	CH
Y429.0	UB.	W.	0.23	73.7	1.4	0.0	24.2	0.7	Y624.7	SC.	M.	0.35	36.8	5.2	0.0	51.8	6.2
Y468.5	UB.	W.	0.28	78.4	3.3	0.0	18.1	0.2	Y642.2	SC.	W.	0.35	31.8	6.3	0.0	55.1	6.8
Y486.5	LB.	W.	0.23	72.4	0.7	0.0	26.9	0	Y672.9	WO	M.	0.38	42.2	3.1	1.0	50.6	3.1
Y501.8	LB.	M.	0.18	71.7	2.4	0.0	25.4	0.5	Y690.1	WO	W.	0.90	54.6	12.0	0.0	29.5	3.9
Y515.3	LB.	W.	0.25	66.1	2.5	0.0	30.9	0.5	Y727.4	WO	W.	0.25	20.2	5.8	1.7	64.5	7.8
Y549.1	LB.	W.	0.45	77.3	3.5	0.0	18.4	0.8	Y757.9	WO	P.	0.25	35.0	4.7	0.3	57.8	2.2
Borehole Z																	
Z378.2	BH.	P.	0.50	80.2	8.1	0.0	10.4	1.3	Z611.3	SC.	W.	0.15	27.5	3.1	0.0	65.8	3.6
Z399.0	UB.	P.	0.40	85.7	6.1	0.0	7.7	0.5	Z632.7	SC.	M.	0.40	12.8	6.4	0.0	71.2	9.6
Z402.9	UB.	W.	0.23	79.3	2.6	0.0	14.5	3.6	Z656.8	SC.	W.	0.35	17.5	4.9	1.3	66.2	10.1
Z422.6	UB.	W.	0.18	76.1	0.3	0.0	22.6	1	Z679.4	WO.	M.	0.45	59.6	6.9	0.5	32.5	0.5
Z444.2	UB.	M.	0.18	68.4	1.0	0.0	29.3	1.3	Z700.2	WO.	P.	0.35	55.7	6.5	0.5	34.9	2.4
Z499.0	UB.	W.	0.23	67.0	2.5	0.0	29.7	0.8	Z703.3	WO.	M.	0.23	53.9	5.0	0.5	38.2	2.4
Z512.4	LB.	W.	0.28	72.2	3.0	0.0	24.6	0.2	Z740.4	WO.	W.	0.28	46.0	5.0	1.8	41.9	5.3
Z531.9	LB.	M.	0.28	76.4	1.2	0.0	22.1	0.3	Z763.8	WO.	M.	0.40	31.1	7.9	0.0	56.4	4.6
Z593.0	SC.	M.	0.45	58.8	3.7	0.0	33.8	3.7									

Note:

The abbreviations used in reporting the results are as follows.

SN = sample number, OU = operational unit, SO = estimated sorting, GS = average grain size (mm), QM = monocrystalline quartz, QP = polycrystalline quartz, FD = feldspar, RF = rock fragments, CH = chert.

W. = well sorted, M. = moderately sorted, P. = poorly sorted, VP. = very poorly sorted, BH = Bald Hill Operational Unit, UB = Upper Bulgo, LB = Lower Bulgo, SC = Scarborough, WO = Wombarra.

APPENDIX V - SEM SUMMARY

Diagenetic minerals identified in the Narrabeen Group sandstones

Sample no.	Type of diagenetic minerals								
	SID	ANKER	Fe CAL	CAL	KAO	ILL	ILL/SME	CHLO	OTHERS
WEST MARGIN									
T320.5					X				
W180.1	X				X				
W182.6	X				X				
W243.9					X	X			
W274.6	X				X	X			
W300.8	X			X	X	X			
W310.4	X			X	X				
W349.9	X				X		X		
W359.4	X				X				
W368.0	X					X			
W388.8	X				X				
W401.2	X						X		
W430.8	X				X				
W455.6	X				X				dolomite
W479.8					X				
W493.9	X				X	X			
W515.6					X				
SOUTHERN REGION									
X278.0	X				X				
X281.3	X				X				
X297.7	X				X				
X309.3	X				X				
X336.1	X				X	X			
X386.8	X	X				X	X		
X413.3	X				X				
X473.1	X	X			X				
X476.2					X				pyrite
X490.9	X	X							
X508.2	X	X					X		
X525.8			X						
X528.7	X	X	X		X				
X531.9	X	X			X				
X588.5	X	X				X			
X612.9	X				X		X		
X640.0	X					X			
X675.5	X	X			X				
Y377.5	X	X		X					
Y397.6	X				X				
Y429.0	X				X				
Y468.5	X				X	X	X		
Y486.5	X				X		X		
Y515.3	X	X			X				
Y549.1	X						X		
Y566.1	X	X	X		X				
Y593.9	X					X			
Y624.7	X	X							
Y642.2		X					X		
Y672.9	X	X	X			X			
Y690.1	X	X	X				X		
Y727.7	X								
Y757.9		X			X	X			

Sample no.	Type of diagenetic minerals								
	SID	ANKER	Fe CAL	CAL	KAO	ILL	ILL/SME	CHLO	OTHERS
SOUTHERN REGION									
Z422.6	X				X	X			
Z499.0	X								
Z512.4	X						X		
Z531.9	X				X				pyrite anatase
Z593.0	X		X		X	X			
Z611.3	X	X			X	X			apatite
Z632.7		X							
Z656.8	X								
Z679.4	X						X		
Z703.3	X					X			analcime
Z740.4	X	X			X	X			
Z763.8	X	X	X		X				
N161.4					X				
N193.1					X				
Q440.7	X	X				X			
A146.5	X				X	X	X		
A211.4	X				X				
A260.8	X						X		
A295.6	X		X				X		
A326.8	X								
A352.0		X							
O296.5	X				X				
O435.2	X				X				
O488.2	X	X				X			
O560.4	X				X				
O600.9	X	X			X	X			
O637.4	X	X							
O668.5		X			X				
O745.8	X				X				
O755.9	X		X		X		X		dawsonite
EAST COAST ZONE									
B132.1		X				X			
B151.7		X							
B234.7	X								
B259.2							X		
B277.9							X		
B394.4				X					
B406.2				X			X		
C041.3	X								
C081.1	X							X	haematite
C101.6				X					haematite
C132.6				X				X	
C215.8							X		
C259.6	X	X			X		X		
L285.2	X								
L406.8	X				X		X		
L422.3		X					X		
L469.6	X						X		
L506.7	X				X				
L518.3	X	X							

Sample no.	Type of diagenetic minerals								
	SID	ANKER	Fe CAL	CAL	KAO	ILL	ILL/SME	CHLO	OTHERS
EAST COAST ZONE									
L579.2	X			X				X	
L595.2				X				X	
L638.9				X					
L717.8				X					pyrite
L732.1	X								
J481.6				X	X		X		
J514.8				X				X	
J570.1							X		
J599.9				X				X	
J641.2				X					
J672.3				X			X	X	
M094.1				X					
M209.9						X			dawsonite
M341.8							X	X	
M369.0								X	
M440.0				X	X				
M492.2							X	X	
M528.5							X		
M551.2	X						X		
M605.3				X				X	
NORTHERN REGION									
I320.1	X				X	X			
I378.5	X							X	
I437.4	X	X	X		X				
I465.5									dolomite
I543.4	X								
I596.6				X	X		X	X	
I629.3							X	X	
I781.5				X	X			X	
I830.4				X	X	X		X	
I879.7				X		X			
I902.6	X			X		X			
G553.8	X	X							
H342.5	X	X				X			
H419.7	X	X							
H470.0	X				X	X	X		
H568.7	X			X			X		
H632.7	X								
H681.2		X							dolomite
D053.9	X				X				
D102.5	X								
D145.3				X	X				
D164.9	X	X			X				
D236.0	X						X		
D295.9	X	X					X		
E128.0	X							X	dawsonite
E185.9				X	X				
E268.9	X						X		
E312.5	X						X		
E357.7	X	X					X		

Sample no.	Type of diagenetic minerals								
	SID	ANKER	Fe CAL	CAL	KAO	ILL	ILL/SME	CHLO	OTHERS
NORTHERN REGION									
F066.5	X				X		X		
F113.9	X	X							
F158.3	X	X			X	X			
F236.7	X	X			X				
F311.1	X			X					
F470.4	X	X			X				
F525.8	X								
F649.2	X			X		X			
F751.7	X					X			dawsonite
U113.1	X				X	X			
U215.5					X			X	
U326.0	X				X				
U388.2	X	X		X	X				
S484.1		X	X						
S598.9	X				X				
K030.7	X								
K073.4	X								
V051.8					X				dawsonite
R090.2					X				

NOTE:
SID = siderite, ANKER = ankerite,
Fe CAL = Fe calcite, CAL = calcite, KAO = kaolinite, ILL = illite,
ILL/SME = mixed-layer illite / smectite, CHLO = chlorite.
Sample no. is named by borehole letter and drilling depth in metre.

APPENDIX VI - RESULTS OF MICROPROBE ANALYSES

SIDERITE												
	REPORTED IN OXIDES (%)						REPORTED IN MOLES (%)					
	MgO	CaO	FeO	MnO	SrO	TOTAL	Mg	Ca	Fe	Mn	Sr	TOTAL
W455.6												
SID 1	12.73	2.14	36.44	0.41	0.00	51.71	36.42	4.40	58.52	0.66	0.00	100.00
SID 2	16.71	2.11	35.53	0.29	0.00	54.64	43.59	3.97	52.01	0.43	0.00	100.00
	15.13	2.37	37.18	0.30	0.01	55.00	39.95	4.51	55.08	0.45	0.01	100.00
Y397.6												
SID 1	0.04	0.56	55.34	1.79	0.00	57.73	0.12	1.23	95.52	3.13	0.00	100.00
	0.31	0.55	54.23	2.41	0.00	57.51	0.95	1.22	93.61	4.22	0.00	100.00
	0.14	1.17	56.90	1.42	0.00	59.65	0.42	2.49	94.67	2.39	0.03	100.00
	0.10	0.96	56.04	1.27	0.00	58.38	0.31	2.09	95.41	2.19	0.00	100.00
SID 2	5.99	2.17	49.45	2.01	0.02	59.64	16.42	4.28	76.13	3.14	0.03	100.00
	3.37	2.26	49.21	2.23	0.00	57.07	9.94	4.79	81.52	3.75	0.00	100.00
SID 3	0.08	0.93	56.40	1.43	0.08	58.86	0.23	2.01	95.28	2.44	0.04	100.00
Y566.1												
SID 1	3.61	1.22	52.49	2.66	0.02	60.01	10.19	2.48	83.04	4.27	0.02	100.00
	2.73	0.96	52.20	2.75	0.00	58.64	7.96	2.01	85.46	4.57	0.00	100.00
	1.65	0.90	53.13	2.90	0.01	58.58	4.88	1.92	88.31	4.88	0.01	100.00
	1.35	1.01	52.63	2.75	0.00	57.74	4.07	2.20	89.03	4.70	0.00	100.00
SID 2	5.78	1.29	49.22	2.54	0.00	58.83	16.15	2.60	77.22	4.03	0.00	100.00
	4.67	1.86	49.13	2.49	0.03	58.18	13.34	3.82	78.76	4.04	0.04	100.00
	2.41	0.02	52.33	2.87	0.00	58.62	7.05	2.15	86.03	4.77	0.00	100.00
Y757.9												
SID 1	9.42	4.10	43.18	0.62	0.00	57.32	25.48	7.98	65.59	0.95	0.00	100.00
	6.48	2.75	45.22	0.72	0.00	55.17	18.92	5.77	74.11	1.20	0.00	100.00
A146.5*												
SID1	6.38	1.82	45.77	4.52		58.50	17.76	3.63	71.46	7.15		100.00
	6.52	2.75	45.12	3.36		57.75	18.24	5.54	70.87	5.35		100.00
	5.53	1.23	46.98	5.06		58.81	15.51	2.49	73.94	8.06		100.00
SID2	7.28	4.18	46.07	0.94		58.47	19.85	8.20	70.49	1.46		100.00
	5.49	3.45	46.98	2.32		58.24	15.41	6.97	73.92	3.70		100.00
	7.65	4.41	44.94	0.39		57.39	21.09	8.74	69.56	0.61		100.00
SID 3	6.95	5.20	44.39	0.27		56.80	19.43	10.45	69.69	0.43		100.00
	7.02	5.36	43.98	0.28		56.64	19.65	10.79	69.12	0.44		100.00
	7.87	4.46	43.25	0.34		55.92	22.15	9.01	68.29	0.55		100.00
L406.8*												
SID 1	8.63	4.47	41.00	0.63		54.72	24.51	9.12	65.35	1.02		100.00
	7.79	4.06	42.51	0.78		55.14	22.26	8.34	68.14	1.26		100.00
	8.09	4.72	42.51	0.46		55.78	22.71	9.54	67.02	0.73		100.00
SID2	7.79	2.90	44.51	1.09		56.29	21.97	5.87	70.41	1.75		100.00
	8.37	3.06	44.32	0.92		56.67	23.27	6.12	69.16	1.45		100.00
	8.52	3.13	44.06	1.05		56.76	23.60	6.24	68.51	1.65		100.00
O435.2*												
SID 1	7.91	2.37	43.96	0.43		54.67	22.91	4.93	71.45	0.71		100.00
	7.94	2.15	40.80	0.42		51.31	24.34	4.74	70.18	0.74		100.00
	8.66	2.93	39.52	0.35		51.46	26.13	6.36	66.91	0.60		100.00

SIDERITE												
	REPORTED IN OXIDES (%)						REPORTED IN MOLES (%)					
	MgO	CaO	FeO	MnO	SrO	TOTAL	Mg	Ca	Fe	Mn	Sr	TOTAL
H681.3*												
SID 1	2.01	2.85	47.96	0.69		53.52	6.41	6.53	85.80	1.26		100.00
F113.9												
SID 1	6.62	0.58	50.26	1.02		58.47	18.48	1.15	78.76	1.61		100.00
SID 2	5.19	0.35	51.26	1.20		57.99	14.89	0.72	82.44	1.95		100.00
SID 3	6.27	0.72	50.45	1.15		58.59	17.54	1.44	79.20	1.82		100.00
	5.87	0.70	48.99	1.37		56.93	16.93	1.46	79.36	2.25		100.00
SID4	6.09	1.07	49.44	1.21		57.81	17.25	2.18	78.62	1.95		100.00
	6.81	0.93	47.96	1.26		56.95	19.41	1.90	76.66	2.03		100.00
	5.85	1.40	47.86	0.96		56.06	17.07	2.94	78.40	1.59		100.00
F236.7												
SID 1	5.40	2.04	51.48	0.36		59.28	15.02	4.09	80.32	0.57		100.00
	4.58	2.23	51.06	0.22		58.09	13.11	4.58	81.95	0.36		100.00
	3.55	1.26	54.76	0.31		59.88	10.04	2.56	86.91	0.49		100.00
SID 2	3.39	1.10	54.53	0.32		59.33	9.71	2.26	87.52	0.51		100.00
	3.68	1.02	54.44	0.15		59.29	10.50	2.10	87.15	0.25		100.00
SID 3	0.74	2.76	56.50	0.72		60.72	2.11	5.70	91.01	1.18		100.00
SID 4	4.82	5.04	48.42	0.79		59.09	13.35	10.05	75.36	1.24		100.00
	7.22	5.81	44.86	0.61		58.49	19.57	11.31	68.19	0.93		100.00
D164.9*												
SID1	6.10	2.15	43.12	1.58		52.95	18.63	4.72	73.90	2.75		100.00

ANKERITE												
	REPORTED IN OXIDES (%)						REPORTED IN MOLES (%)					
	MgO	CaO	FeO	MnO	SrO	TOTAL	Mg	Ca	Fe	Mn	Sr	TOTAL
W455.6												
ANK 1	11.88	27.20	12.08	0.35	0.00	51.51	30.94	50.90	17.65	0.51	0.00	100.00
	10.73	27.69	13.62	0.38	0.00	52.42	27.88	51.71	19.85	0.56	0.00	100.00
Y566.1												
ANK 1	9.91	28.26	14.51	1.28	0.00	53.96	25.35	51.95	20.83	1.87	0.00	100.00
	10.42	30.25	11.63	0.61	0.00	52.91	26.69	55.70	16.72	0.89	0.00	100.00
	9.02	30.41	13.31	0.92	0.00	53.66	23.20	56.24	19.21	1.35	0.00	100.00
ANK 2	10.34	28.29	15.78	0.93	0.00	55.34	25.82	50.76	22.10	1.31	0.00	100.00
	10.48	26.27	15.29	1.47	0.00	53.51	27.02	48.70	22.13	2.15	0.00	100.00
	6.91	29.41	16.60	1.30	0.00	54.22	18.13	55.49	24.44	1.94	0.00	100.00
Y757.9												
ANK 1	11.38	28.73	12.37	0.43	0.00	52.91	29.01	52.67	17.70	0.62	0.00	100.00
	13.62	29.34	10.67	0.25	0.00	53.88	33.35	51.65	14.66	0.34	0.00	100.00
ANK 2	12.33	29.92	10.87	0.46	0.00	53.58	30.66	53.52	15.17	0.65	0.00	100.00
	12.78	30.37	10.53	0.36	0.00	54.04	31.38	53.62	14.50	0.50	0.00	100.00
ANK 3	11.38	31.07	10.58	0.29	0.00	53.32	28.57	56.09	14.92	0.42	0.00	100.00
	9.94	29.73	11.02	0.80	0.00	51.49	26.19	56.31	16.29	0.21	0.00	100.00

ANKERITE												
	REPORTED IN OXIDES (%)						REPORTED IN MOLES (%)					
	MgO	CaO	FeO	MnO	SrO	TOTAL	Mg	Ca	Fe	Mn	Sr	TOTAL
Z763.8*												
ANK 1	13.42	29.50	11.88	0.50		55.30	32.26	51.02	16.03	0.69		100.00
ANK 2	11.77	28.17	13.45	0.45		53.83	29.55	50.85	18.96	0.64		100.00
ANK 3	12.02	31.97	10.67	0.42		55.08	29.16	55.74	14.52	0.58		100.00
ANK 4	11.36	30.07	12.61	0.55		54.59	28.14	53.56	17.52	0.88		100.00
L406.8*												
ANK 1	10.28	27.48	14.70	0.33		52.79	26.72	51.36	21.44	0.48		100.00
	10.28	27.01	13.95	0.31		51.55	27.26	51.51	20.75	0.48		100.00
ANK 2	9.78	28.19	12.87	0.34		51.19	26.10	54.10	19.28	0.52		100.00
	11.52	27.59	12.78	0.38		52.26	29.73	51.20	18.51	0.56		100.00
ANK 3	10.38	27.80	12.59	0.37		51.13	27.58	53.10	18.76	0.56		100.00
	10.55	27.44	12.88	0.35		51.23	27.98	52.32	19.17	0.53		100.00
L579.2*												
ANK 1	8.90	29.44	14.23	0.48		53.05	23.23	55.22	20.83	0.72		100.00
	9.92	29.20	13.97	0.45		53.53	25.42	53.82	20.10	0.66		100.00
ANK 2	5.60	35.53	9.99	0.95		52.07	15.03	68.49	15.03	1.45		100.00
ANK 3	9.07	29.02	40.18	0.46		52.73	23.76	54.70	20.86	0.68		100.00
	8.96	29.40	14.15	0.43		52.78	23.46	55.09	20.81	0.64		100.00
	9.23	29.22	14.27	0.45		53.18	23.98	54.55	20.80	0.67		100.00
	9.08	28.75	13.95	0.45		52.23	23.99	54.63	20.70	0.68		100.00
ANK 4	9.16	29.00	13.63	0.46		52.25	24.15	54.99	20.17	0.69		100.00
	9.10	29.24	13.56	0.43		52.34	23.96	55.36	20.04	0.64		100.00
	9.19	29.33	13.27	0.49		52.29	24.19	55.48	19.59	0.74		100.00
O637.4												
ANK1	9.08	27.97	14.61	0.33	0.33	52.32	24.07	53.34	21.74	0.50	0.35	100.00
	9.62	27.92	14.82	0.27	0.32	52.95	25.13	52.42	21.72	0.40	0.33	100.00
ANK 2	9.88	26.95	13.58	1.06	0.00	51.46	26.36	51.70	20.33	1.61	0.00	100.00
	10.42	26.53	14.60	0.29	0.04	51.88	27.52	50.37	21.63	0.43	0.05	100.00
ANK 3	8.59	28.62	15.74	1.39	0.02	54.36	22.13	53.04	22.77	2.04	0.02	100.00
	8.79	27.93	15.82	1.47	0.03	54.04	22.78	52.03	23.00	2.16	0.03	100.00
O755.9*												
ANK 1	11.61	28.32	12.22	0.19		52.29	29.82	52.29	17.62	0.27		100.00
	12.68	27.84	11.78	0.21		52.51	32.15	50.79	16.76	0.30		100.00
	12.05	28.46	12.46	0.19		53.17	30.42	51.66	17.65	0.27		100.00
	12.82	27.79	11.60	0.14		52.35	32.54	50.73	16.52	0.21		100.00
	12.98	27.84	12.16	0.23		53.20	32.50	50.10	17.07	0.33		100.00
ANK 2	11.36	30.10	12.56	0.18		54.20	28.30	53.89	17.55	0.26		100.00
	12.16	29.12	11.48	0.21		52.97	30.65	52.80	16.25	0.30		100.00
	11.42	28.54	12.29	0.23		52.48	29.31	52.66	17.70	0.33		100.00
	10.72	28.36	14.05	0.34		53.47	27.25	52.03	20.12	0.50		100.00
ANK 3	13.08	27.28	11.42	0.18		51.97	33.36	50.03	16.34	0.27		100.00
	11.82	28.85	12.24	0.23		53.14	29.87	52.44	17.36	0.33		100.00
	13.19	28.17	12.22	0.21		53.78	32.64	50.10	16.97	0.29		100.00

ANKERITE												
	REPORTED IN OXIDES (%)						REPORTED IN MOLES (%)					
	MgO	CaO	FeO	MnO	SrO	TOTAL	Mg	Ca	Fe	Mn	Sr	TOTAL
B151.7*												
ANK 1	9.71	30.03	11.11	0.98		51.83	25.49	56.68	16.36	1.47		100.00
	9.92	29.98	10.81	0.97		51.68	26.03	56.60	15.93	1.44		100.00
ANK 2	10.76	29.90	10.70	0.34		51.69	27.98	55.90	15.62	0.50		100.00
	11.26	30.37	10.08	0.46		52.16	28.87	55.97	14.49	0.67		100.00
ANK 3	11.55	31.49	11.35	0.40		54.79	28.31	55.51	15.62	0.56		100.00
	12.13	32.67	8.95	0.83		54.58	29.50	57.14	12.21	1.15		100.00
F113.9*												
ANK 1	12.80	30.67	7.50	1.12		52.09	32.24	55.55	10.61	1.60		100.00
	11.19	30.23	10.70	1.12		53.23	28.28	54.93	15.18	1.61		100.00
	13.43	30.82	7.16	1.22		52.63	33.33	54.98	9.97	1.72		100.00
	12.09	30.78	8.72	1.01		52.60	30.47	55.76	12.33	1.44		100.00
ANK 2	12.67	30.75	6.58	1.24		51.23	32.33	56.45	9.42	1.80		100.00
	13.19	30.67	6.75	0.94		51.55	33.35	55.73	9.57	1.35		100.00
F236.7*												
ANK 1	10.98	31.41	9.36	1.09		52.85	27.84	57.27	13.32	1.57		100.00
ANK 2	11.70	31.76	9.34	0.78		53.59	29.10	56.76	13.03	1.11		100.00
ANK 3	11.10	31.86	9.76	1.26		53.97	27.61	56.99	13.62	1.78		100.00
ANK 4	10.44	31.19	9.30	1.07		51.99	26.98	57.96	13.49	1.57		100.00
	10.41	30.90	9.44	1.06		51.81	27.03	57.66	13.75	1.56		100.00
ANK 5	11.26	30.47	9.10	1.01		51.84	28.99	56.39	13.14	1.48		100.00
F751.7*												
ANK 1	12.87	33.68	8.98	0.00		55.53	30.56	57.48	11.96	0.00		100.00
ANK 2	11.52	31.96	9.47	0.14		53.10	28.88	57.60	13.32	0.20		100.00
	11.62	32.94	9.82	0.14		54.51	28.41	57.92	13.47	0.20		100.00
	10.95	32.19	9.73	0.24		53.10	27.59	58.32	13.75	0.34		100.00
	11.40	32.42	9.12	0.00		52.94	28.61	58.53	12.86	0.00		100.00
ANK 3	11.53	33.26	8.47	0.01		53.27	28.68	59.49	11.82	0.01		100.00
	11.51	33.30	8.75	0.00		53.57	28.52	59.31	12.17	0.00		100.00
	11.43	32.68	8.61	0.10		52.82	28.72	59.00	12.14	0.14		100.00
D164.9*												
ANK 1	9.58	30.06	13.91	0.90		54.46	24.25	54.69	19.76	1.30		100.00
ANK 2	8.94	30.86	13.98	0.66		54.43	22.72	56.39	19.94	0.95		100.00
	9.49	30.85	13.27	0.46		54.07	24.10	56.33	19.81	0.66		100.00
ANK 3	8.82	30.62	13.35	0.52		53.32	22.83	57.00	19.40	0.77		100.00
ANK 4	10.58	30.99	12.67	0.83		55.07	26.17	55.09	17.58	1.16		100.00
ANK 5	9.73	30.11	12.00	0.49		52.34	25.34	56.39	17.54	0.73		100.00
H681.3*												
ANK 1	8.14	27.66	8.14	0.34		51.27	38.02	50.00	11.49	0.49		100.00
ANK 2	9.76	24.09	16.56	0.84		51.25	26.48	47.01	25.21	1.30		100.00
FE DOLOMITE												
W455.6												
FE DO1	18.45	28.03	4.71	0.03	0.00	51.22	44.71	48.83	6.41	0.05	0.00	100.00
	19.14	28.15	4.69	0.08	0.00	52.05	45.51	48.13	6.25	0.11	0.00	100.00

CALCITE												
	REPORTED IN OXIDES (%)						REPORTED IN MOLES (%)					
	MgO	CaO	FeO	MnO	SrO	TOTAL	Mg	Ca	Fe	Mn	Sr	TOTAL
B394.4*												
CAL 1	0.18	51.75	0.75	1.48		54.15	0.47	96.27	1.09	2.17		100.00
	0.16	51.45	0.75	1.30		53.66	0.42	96.55	1.10	1.93		100.00
	0.17	50.79	0.67	1.30		52.92	0.44	96.62	0.99	1.95		100.00
CAL 2	0.19	51.67	0.71	1.53		54.09	0.49	96.23	1.03	2.25		100.00
	0.26	50.44	0.93	1.50		53.13	0.69	95.67	1.38	2.26		100.00
L579.2*												
CAL 1	0.29	50.85	1.51	1.80		54.45	0.75	94.42	2.19	2.64		100.00
	0.38	50.38	1.39	1.67		53.81	0.98	94.52	2.03	2.47		100.00
	1.07	48.51	2.68	1.63		53.89	2.78	90.89	3.92	2.41		100.00
	0.35	50.47	1.32	1.81		53.95	0.91	94.48	1.93	2.68		100.00
J514.8*												
CAL 1	0.21	50.59	0.70	2.54		54.03	0.54	94.68	1.02	3.76		100.00
CAL 2	0.18	55.31	0.75	3.82		60.07	0.43	93.47	0.99	5.11		100.00
CAL 3	0.23	56.50	0.81	3.84		61.38	0.53	93.40	1.05	5.02		100.00
CAL 4	0.35	54.37	1.00	3.99		59.72	0.84	92.47	1.33	5.36		100.00
CAL 5	0.31	52.84	0.82	4.00		57.98	0.75	92.58	1.12	5.55		100.00
	0.33	54.82	0.96	4.04		60.15	0.77	92.57	1.27	5.39		100.00
	0.27	53.52	0.94	4.68		59.41	0.66	91.75	1.25	6.34		100.00
J599.9*												
CAL 1	0.12	53.10	0.11	2.49		55.82	0.31	95.98	0.15	3.56		100.00
	0.00	55.43	0.18	3.45		59.06	0.00	95.08	0.24	4.68		100.00
	0.09	56.76	0.24	3.80		60.90	0.20	94.48	0.32	5.00		100.00
	0.17	54.03	0.10	3.30		57.60	0.40	94.88	0.14	4.58		100.00
CAL 2	0.04	53.85	0.11	3.33		57.33	0.10	95.09	0.16	4.65		100.00
	0.26	52.55	0.18	3.01		56.00	0.66	94.79	0.26	4.29		100.00
	0.37	53.24	0.18	2.03		55.82	0.93	95.94	0.25	2.88		100.00
CAL 3	0.27	52.44	0.29	1.96		54.97	0.69	96.05	0.42	2.84		100.00
	0.10	50.85	0.15	2.38		53.48	0.27	95.95	0.22	3.56		100.00
CAL 4	0.46	53.32	0.33	1.61		55.71	1.14	96.11	0.46	2.29		100.00
	0.00	52.84	0.19	2.18		55.22	0.00	96.58	0.27	3.15		100.00
	0.00	53.45	0.06	2.44		55.96	0.00	96.43	0.09	3.48		100.00

Note:

* Sr is not analysed for the sample.

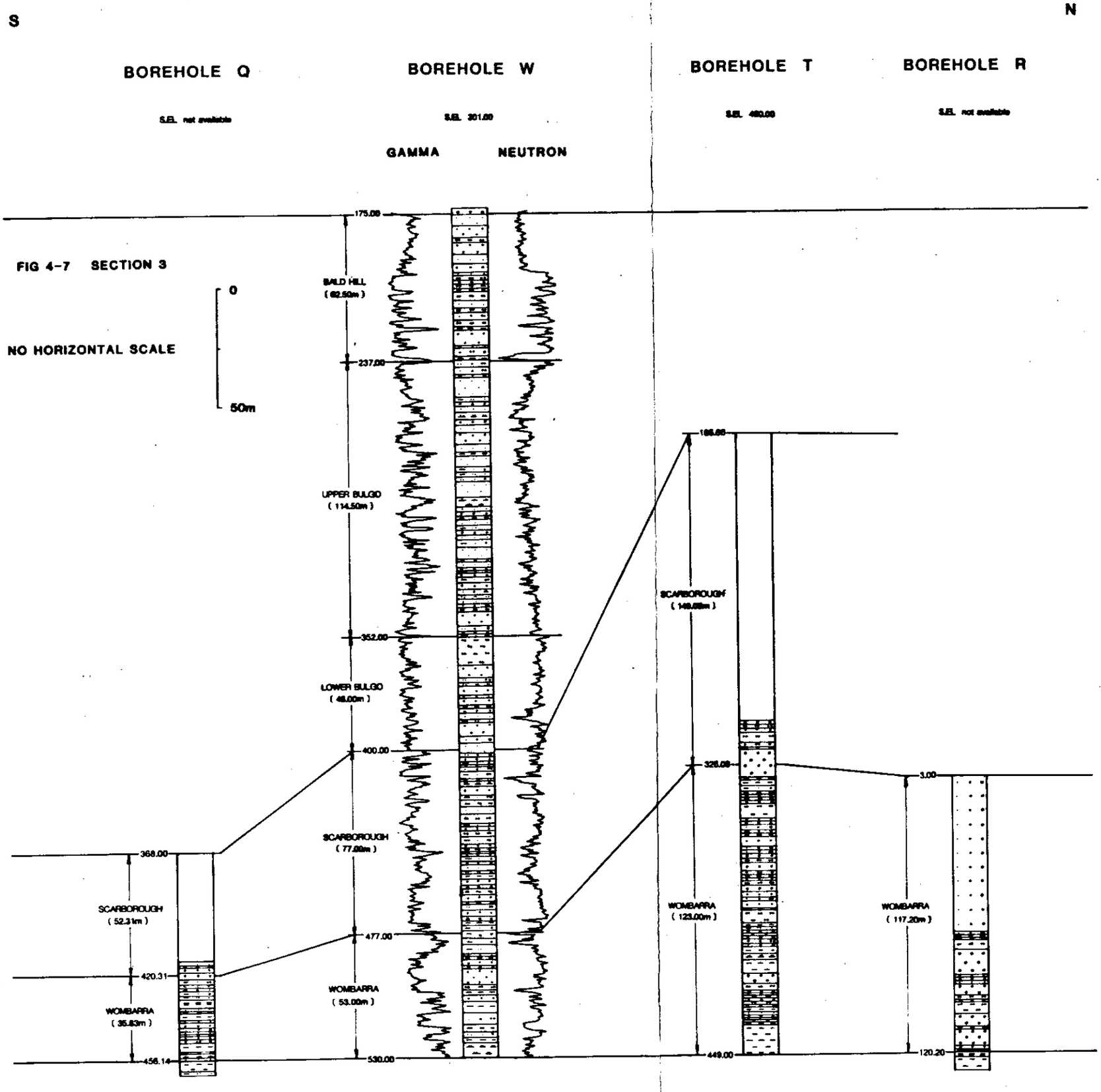
S
N
BOREHOLE Q
S.E.L. not available
BOREHOLE W
S.E.L. 301.00
BOREHOLE T
S.E.L. 460.00
BOREHOLE R
S.E.L. not available
GAMMA
NEUTRON
FIG 4-7 SECTION 3
NO HORIZONTAL SCALE
0
50m
175.00
BALD HILL
(62.50m)
237.00
UPPER BULGO
(114.50m)
352.00
LOWER BULGO
(48.00m)
400.00
SCARBOROUGH
(77.00m)
477.00
WOMBARRA
(53.00m)
530.00
368.00
SCARBOROUGH
(52.31m)
420.31
WOMBARRA
(35.83m)
456.14
185.00
SCARBOROUGH
(148.00m)
326.00
WOMBARRA
(123.00m)
449.00
3.00
WOMBARRA
(117.20m)
120.20

S

N

BOREHOLE A

S.EL 386.00

113.33
BALD HILL (18.33m)
131.72
UPPER BULGO (75.86m)
207.58
LOWER BULGO (36.97m)
244.55
SCARBOROUGH (83.58m)
328.13
WOMBARRA (38.67m)
366.80

BOREHOLE C

S.EL 187.00

UPPER BULGO
74.20
LOWER BULGO (58.20m)
132.40
SCARBOROUGH (72.85m)
205.25
WOMBARRA (59.25m)
264.50

BOREHOLE B

S.EL 217.32

99.00
BALD HILL (20.28m)
119.28
UPPER BULGO (95.72m)
215.00
LOWER BULGO (64.00m)
279.00
SCARBOROUGH (66.00m)
345.00
WOMBARRA (70.00m)
415.00

BOREHOLE L

S.EL 86.00

269.70
BALD HILL (38.30m)
308.00
UPPER BULGO (134.00m)
442.00
LOWER BULGO (82.50m)
524.50
SCARBOROUGH (132.00m)
656.50
WOMBARRA (106.50m)
762.00

BOREHOLE J

S.EL 21.50

390.06
LOWER BULGO (73.00m)
463.00
SCARBOROUGH (134.00m)
597.00
WOMBARRA (86.50m)
683.50

BOREHOLE M

S.EL 67.00

GAMMA NEUTRON

33.53
BALD HILL (56.22m)
98.75
UPPER BULGO (122.06m)
220.83
LOWER BULGO (111.02m)
331.85
SCARBOROUGH (138.40m)
468.25
WOMBARRA (141.45m)
609.70

BOREHOLE I

S.EL 276.79

GAMMA NEUTRON

315.16
BALD HILL (60.45m)
376.61
UPPER BULGO (114.39m)
491.00
LOWER BULGO (128.20m)
619.20
SCARBOROUGH (138.80m)
758.00
WOMBARRA (146.82m)
904.82

BOREHOLE E

S.EL 41.12

GAMMA NEUTRON

100.00
SCARBOROUGH (152.00m)
252.00
WOMBARRA (140.00m)
392.00

FIG 4-9 SECTION 5

NO HORIZONTAL SCALE

0

50m

W

E

BOREHOLE T

S.EL 460.00

BOREHOLE G

S.EL 17.70

BOREHOLE F

S.EL 134.51

GAMMA NEUTRON

BOREHOLE E

S.EL 41.12

GAMMA NEUTRRON

BOREHOLE D

S.EL 51.82

42.00

BALD HILL
(64.00m)

106.00

UPPER BULGO
(157.00m)

263.00

LOWER BULGO
(149.00m)

412.00

186.00

SCARBOROUGH
(140.00m)

326.00

WOMBARRA
(123.00m)

566.00

SCARBOROUGH
(154.00m)

WOMBARRA

595.00

WOMBARRA
(192.00m)

758.00

449.00

100.00

SCARBOROUGH
(152.00m)

252.00

WOMBARRA
(140.00m)

382.00

41.00

SCARBOROUGH
(148.00m)

189.00

WOMBARRA
(119.00m)

308.00

FIG 4-6 SECTION 2

NO HORIZONTAL SCALE

0

50m

S

N

BOREHOLE N

S.E. 781.12

BALD HILL (12.00m)
131.00
143.00
UPPER BULGO (16.35m)
159.35
LOWER BULGO (10.21m)
169.56
SCARBOROUGH (19.69m)
189.25
WOMBARRA (11.21m)
200.46

BOREHOLE P

S.E. 208.79

GAMMA

174.00
BALD HILL (21.00m)
195.00
UPPER BULGO (21.00m)
216.00
LOWER BULGO (84.00m)
300.00
SCARBOROUGH (104.00m)
404.00
WOMBARRA (53.80m)
457.80

BOREHOLE Z

S.E. 121.80

GAMMA NEUTRON

347.46
BALD HILL (43.24m)
390.70
UPPER BULGO (109.44m)
500.14
LOWER BULGO (68.13m)
568.27
SCARBOROUGH (103.41m)
672.68
WOMBARRA (103.32m)
776.00

BOREHOLE O

S.E. 147.00

GAMMA NEUTRON

289.25
BALD HILL (33.59m)
322.84
UPPER BULGO (159.05m)
481.89
LOWER BULGO (64.01m)
545.90
SCARBOROUGH (91.97m)
637.87
WOMBARRA (118.03m)
755.90

BOREHOLE H

S.E. 7.62

GAMMA

62.00
BALD HILL (76.00m)
138.00
UPPER BULGO (184.52m)
322.52
LOWER BULGO (106.48m)
429.00
SCARBOROUGH (89.05m)
581.05
WOMBARRA (185.74m)
703.79

BOREHOLE G

S.E. 17.70

59.45
SCARBOROUGH (132.55m)
192.00
WOMBARRA (162.85m)
354.85

BOREHOLE U

S.E. 99.50

WOMBARRA
595.00

BOREHOLE S

S.E. 155.92

370.00
SCARBOROUGH (181.00m)
551.00
WOMBARRA (106.00m)
657.00

BOREHOLE V

S.E. 177.10

WOMBARRA
67.40

BOREHOLE K

S.E. 148.38

WOMBARRA
118.50

FIG 4-8 SECTION 4

NO HORIZONTAL SCALE

0
50m

W

E

BOREHOLE W

S.E.L. 361.00

GAMMA NEUTRON

175.00

BALD HILL (62.50m)

237.00

UPPER BULGO (114.50m)

352.00

LOWER BULGO (48.00m)

400.00

SCARBOROUGH (77.00m)

477.00

WOMBARRA (53.00m)

530.00

BOREHOLE X

S.E.L. 78.70

GAMMA NEUTRON

275.79

BALD HILL (55.12m)

330.91

UPPER BULGO (117.78m)

448.69

LOWER BULGO (64.84m)

513.53

SCARBOROUGH (92.99m)

606.52

WOMBARRA (86.08m)

692.60

BOREHOLE Y

S.E.L. 94.30

GAMMA NEUTRON

350.00

BALD HILL (37.00m)

387.00

UPPER BULGO (119.00m)

506.00

LOWER BULGO (77.00m)

583.00

SCARBOROUGH (85.00m)

668.00

WOMBARRA (108.00m)

776.00

BOREHOLE Z

S.E.L. 121.00

GAMMA NEUTRON

347.46

BALD HILL (43.24m)

390.70

UPPER BULGO (109.44m)

500.14

LOWER BULGO (69.13m)

569.27

SCARBOROUGH (103.41m)

672.68

WOMBARRA (103.32m)

776.00

BOREHOLE L

S.E.L. 85.00

GAMMA NEUTRON

269.70

BALD HILL (38.30m)

308.00

UPPER BULGO (134.00m)

442.00

LOWER BULGO (82.50m)

524.50

SCARBOROUGH (132.00m)

656.50

WOMBARRA (105.50m)

762.00

BOREHOLE J

S.E.L. 21.50

390.00

LOWER BULGO (73.00m)

463.00

SCARBOROUGH (134.00m)

597.00

WOMBARRA (86.50m)

683.50

FIG 4-5 SECTION 1

NO HORIZONTAL SCALE

0

50m